

ESTIMATION OF POTENTIAL EARTHQUAKE LOSSES FOR
THE EVALUATION OF EARTHQUAKE INSURANCE RISKS

A THESIS SUBMITTED TO
THE GRADUATE SCHOOL OF NATURAL AND APPLIED SCIENCES
OF
MIDDLE EAST TECHNICAL UNIVERSITY

BY
HAKAN KARACA

IN PARTIAL FULFILLMENT OF THE REQUIREMENTS
FOR
THE DEGREE OF DOCTOR OF PHILOSOPHY
IN
CIVIL ENGINEERING

OCTOBER 2014

Approval of the thesis

**ESTIMATION OF POTENTIAL EARTHQUAKE LOSSES FOR
THE EVALUATION OF EARTHQUAKE INSURANCE RISKS**

submitted by **HAKAN KARACA** in partial fulfillment of the requirements for the degree of **Doctor of Philosophy in Civil Engineering Department, Middle East Technical University** by,

Prof. Dr. Gülbin Dural Ünver

Dean, Graduate School of **Natural and Applied Sciences**

Prof. Dr. A. Cevdet Yalçiner

Head of Department, **Civil Engineering**

Prof. Dr. M. Semih Yüccemen

Supervisor, **Civil Engineering Department, METU**

Examining Committee Members:

Assoc. Prof. Dr. Ayşegül Askan Gündoğan

Civil Engineering Department, METU

Prof. Dr. M. Semih Yüccemen

Civil Engineering Department, METU

Prof. Dr. H. Şebnem Düzcün

Mining Engineering Department, METU

Prof. Dr. M. Altuğ Erberik

Civil Engineering Department, METU

Assist. Prof. Dr. F. Kürşat Fırat

Civil Engineering Department, ASU

Date: _____

I hereby declare that all the information in this document has been obtained and presented in accordance with the academic rules and ethical conduct. I also declare that, as required by these rules and conduct, I have fully cited and referenced all material and results that are not original to this work.

Name, Last name: Hakan Karaca

Signature:

ABSTRACT

ESTIMATION OF POTENTIAL EARTHQUAKE LOSSES FOR THE EVALUATION OF EARTHQUAKE INSURANCE RISKS

Karaca, Hakan
Ph.D., Department of Civil Engineering
Supervisor: Prof. Dr. M. Semih Yüçemen

October, 2014, 391 pages

Estimation of extreme seismic losses has been a major concern for the insurance sector. Especially, the recent series of large magnitude earthquakes have forced both the client and the insurance companies to obtain reliable estimates of potential seismic losses. Thus, seismic risk mapping has become a major task for the insurance industry. For seismic risk mapping it is necessary to develop a model which integrates the information on seismic hazard and the information on expected earthquake damage on engineering facilities in a systematic way, yielding to estimates of the seismic risk.

This study aims firstly establishing the most up to date seismic hazard mapping procedure based on the appropriate stochastic models. The conversion of the mapped seismic hazard information into risk metrics requires including data on the vulnerability to damage of the exposure at the location under consideration. Thus the second aim of the study is to establish probabilistic procedures for the estimation of the vulnerability of buildings subjected to earthquakes of different severity. Finally, a risk model will be developed to integrate the probabilistic understanding of the hazard with the exposure and vulnerability to arrive at mapped information on risk costs (i.e. annual expected losses) as well as loss exceedence at a range of return periods. Such an output will be of extreme use to the insurance companies in assessing the risks involved due to future earthquakes.

Keywords: Seismic Hazard, Ground Motion Prediction Equations, Spatially Smoothed Seismicity, Discriminant Analysis, Insurance Premiums

ÖZ

DEPREM SİGORTASI RİSKLERİNİN DEĞERLENDİRİLMESİ İÇİN BEKLENEN DEPREM YİTİMLERİNİN TAHMİNİ

Karaca, Hakan
Doktora, İnşaat Mühendisliği Bölümü
Tez Yöneticisi: Prof. Dr. M. Semih Yüçemen

Ekim 2014, 391 sayfa

Büyük depremlerin sebep olduğu kayıpların tahmini sigortacılık sektöründe çok önemli bir sorun olarak ortaya çıkmaktadır. Özellikle son yıllarda meydana gelen büyük magnitüdü depremler, sigorta şirketleri ile müşterileri, beklenen deprem hasarlarının gerçekçi bir şekilde elde edilmesine zorlamıştır. Dolayısı ile sismik riskin haritalanması sigorta şirketlerinin başlıca görevi olmuştur. Sismik riskin haritalanması için sismik tehlike ile ilgili bilgiyi mühendislik yapılarında beklenen deprem hasarlarına ilişkin bilgi ile sistematik bir şekilde birleştiren bir modelin geliştirilmesi gereklidir.

Bu çalışma ilk olarak, uygun stokastik modellere dayanan en güncel sismik tehlike modelini ortaya koymayı amaçlamaktadır. Haritalanmış sismik tehlike bilgilerini risk ölçütüne dönüştürmek için yapı hasar görülebilirlik verilerinin de işin içine katılması gerekmektedir. Bu nedenle çalışmanın ikinci amacı değişik büyüklükteki deprem etkilerine maruz kaldığında yapıların göreceği hasarların tahmini için olasılıksal yöntemlerin belirlenmesidir. Son olarak da olasılıksal sismik tehlike analizi sonuçlarını sismik tehlikeye maruzluk ve kırılma bilgileri ile birleştirerek beklenen yıllık yitim değerleri ve belirli tekerrür süreleri için yitim aşırıları bilgilerini haritalayacak bir modelin geliştirilmesi amaçlanmaktadır. Geliştirilecek modelin çıktısı sigorta şirketlerinin ileriye dönük deprem risklerini değerlendirmelerine önemli bir katkı getirecektir.

Anahtar Sözcükler: Sismik Tehlike, Yer Hareketi Tahmin Denklemleri, Düzleştirilmiş Sismisite Modeli, Diskriminant Analizi, Sigorta Primleri

To my family

ACKNOWLEDGEMENTS

I would like to express my deepest gratitude to my supervisor Prof. Dr. M. Semih Yüccemen. I also would like to thank the thesis committee members Prof. Dr. H. Şebnem Düzgün, Prof. Dr. A. Murat Erberik, Assoc. Prof. Dr. Ayşegül Askan Gündoğan and Asst. Prof. Dr. F. Kürşat Fırat for serving in my committee and providing valuable suggestions and constructive comments. I would like to acknowledge the technical assistance of MODSIMMER, Tepebaşı and Odunpazarı Municipalities. Finally, I also received support from my close friend Asst. Prof. Dr. Onur Pekcan, who always stood by me during this long journey.

TABLE OF CONTENTS

ABSTRACT	v
ÖZ	vi
ACKNOWLEDGMENTS	viii
TABLE OF CONTENTS	ix
LIST OF FIGURES	xv
LIST OF TABLES	xxvi
LIST OF ABBREVIATIONS	xxx
LIST OF SYMBOLS	xxxiii
1. INTRODUCTION	1
1.1. General	1
1.2. Motivation	2
1.3. Organization of the Study	9
2. GENERAL OVERVIEW OF PROBABILISTIC SEISMIC HAZARD ANALYSIS	13
2.1. Introduction	13
2.2. Types of Seismic Hazard Analysis	13
2.2.1 Deterministic Seismic Hazard Analysis.....	14
2.2.2. Probabilistic Seismic Hazard Analysis	14
2.2.3. Comparison of Deterministic and Probabilistic Seismic Hazard Analysis Methods.....	15
2.2.4. Uncertainties in Probabilistic Seismic Hazard Analysis.....	16
2.3. Determination of Seismic Sources	17
2.3.1. Area Sources	18
2.3.2. Line Sources or Faults.....	19
2.3.2.1. Earthquake Generation Models.....	19
2.3.2.2. Rupture Propagation Paths and Termination Structures	23
2.4. Recurrence Models.....	26
2.4.1. Basic Magnitude-Recurrence Relationship.....	27
2.4.2. Physical Recurrence Models for Fault Sources	29
2.4.2.1. Characteristic Earthquake Model.....	31

2.4.2.2. Total Release or Average Slip Predictable Model	33
2.4.2.3. Yield Threshold or Average Time-Predictable Model.....	34
2.4.3. Statistical Recurrence Models	36
2.4.4. Statistical Recurrence Models for Both Time and Magnitude.....	38
2.4.5. Recurrences Based on Geodetic Measurement of Fault Slip Rates	39
2.5. Data Compilation for Seismic Hazard Analysis	44
2.5.1. Choosing the Catalogue Sources Available for Turkey.....	44
2.5.1.1. Magnitude Conversion	45
2.5.1.2. Catalogue Declustering	46
2.5.1.3. Completeness Tests	47
2.5.2. Determination of Faults and Their Parameters	48
2.5.2.1. Evaluation of Earthquake Recurrences Models of Faults	49
3. GROUND MOTION PREDICTION EQUATIONS	53
3.1. Introduction	53
3.2. Review of GMPE Development Studies	54
3.3. Selection of the Most Appropriate GMPE	55
3.3.1. Details of GMPEs.....	57
3.3.2. Strong Ground Motion Data.....	67
3.3.2.1 Preparation of Raw Data	72
3.3.2.2. Evaluation of Raw Data	72
3.4. Selection Process for the Appropriate GMPE.....	76
3.4.1. Initial Elimination	78
3.5. Regression Analysis	79
3.5.1. Trellis Plots of GMPEs by Using Original and Calibrated Coefficients .	88
3.5.2. Final Selection.....	105
3.5.2.1. Performance of the Selected GMPE.....	106
3.6. Evaluation of Results	108
4. ASSESSMENT OF SEISMIC VULNERABILITY	113
4.1. Introduction	113
4.2. Review of the Selected Lateral Performance Estimation Methods.....	113
4.2.1. Discriminant Analysis by Using Main Structural Parameters	114
4.2.2. Analytical Procedures in Lateral Performance Estimation	116

4.2.2.1. Capacity Spectrum Method.....	117
4.2.2.2. Method of Maximum Interstorey Drift Ratios.....	119
4.2.2.3. Displacement Coefficient Method.....	120
4.2.2.4. Improved Displacement Coefficient Method.....	122
4.2.2.5. Evaluation of Procedures.....	123
4.3. Variables Influencing the Lateral Performance.....	125
4.4. Pushover Analysis for the Estimation of Lateral Performance.....	130
4.4.1. Modal Mass Participation Ratio.....	132
4.4.2. Lateral Load Distributions.....	133
4.5. Proposed Approach and Lateral Performance Prediction Equation.....	135
4.6. Sensitivity Analysis.....	137
4.6.1. Modifications of the Structures.....	137
4.6.1.1. Modification Scheme for the Lateral Strength Index.....	137
4.6.1.2. Modification Scheme for the Soft Storey Index.....	138
4.6.1.3. Modification Scheme for the Lateral Stiffness Index.....	139
4.6.1.4. Modification Scheme for the Number of Storeys.....	140
4.6.1.5. Code Compliance Issues.....	141
4.6.2. Building Stock.....	141
5. CASE STUDY: SEISMIC HAZARD ANALYSIS FOR ESKISEHIR.....	143
5.1. Introduction.....	143
5.2. Regional Tectonic Setting.....	143
5.2.1. Tectonic Structures in the Close Vicinity of Eskisehir.....	144
5.2.2. Delineation of Seismic Sources.....	146
5.2.2.1. Detailed Fault Segmentation Study around Eskisehir.....	146
5.3. Processing the Seismic Data.....	163
5.3.1. Seismic Activity around Eskisehir.....	163
5.3.2. Choosing the Earthquake Catalogs and Processing the Raw Data.....	165
5.3.3. Homogenization and Declustering the Seismic Data.....	168
5.3.4. Completeness Analysis of the Declustered Data.....	168
5.4. Seismic Source Parameters.....	175
5.4.1. Area Sources and Source Parameters.....	175
5.4.2. Fault Source and Parameters.....	178

5.5. Response Spectrum Curves and Hazard Maps Developed for the City of Eskisehir	179
5.6. Spatially Smoothed Seismicity.....	186
5.6.1. Data Preparation.....	188
5.6.2. Analysis.....	189
6. CASE STUDY: VULNERABILITY OF SELECTED BUILDINGS IN ESKISEHIR.....	193
6.1. Introduction	193
6.2. Buildings Modeled for the Analysis.....	194
6.2.2. Modeling Assumptions	195
6.2.2.1. Modeling of Hinges.....	196
6.2.2.2. Shear Wall Modeling	198
6.2.3. Application of Modal Mass Participation Ratio Criterion	199
6.2.4. Basic Structural Properties	200
6.2.5. Multicollinearity in Multiple Regression Analysis	206
6.2.6. The Initial Stress Issue	208
6.2.7. Pushover Curves.....	210
6.3. Scaling of Lateral Performance with Proposed Structural Parameters (Sensitivity Analysis)	213
6.3.1. Detailed Investigation of the Scaling of Lateral Performance with Respect to Structural Parameters	218
6.3.1.1. Dependency on Lateral Strength Index.....	221
6.3.1.2. Dependency on Soft Storey Index.....	223
6.3.1.3. Dependency on Lateral Stiffness Index	224
6.3.1.4. Dependency on Number of Storeys	226
6.3.2. Forming the Lateral Performance Prediction Equation.....	226
6.3.3. Investigation of the Relationship between the Lateral Performances and Proposed Structural Parameters	229
6.3.4. Refinement of the Database for Further Analysis.....	231
6.3.5. Reinvestigation of the Relationship between the Lateral Performances and and Considered Structural Parameters	246

6.4. Investigation of Relationship between Lateral Performance and Structural Parameters by Using Various Methods.....	246
6.4.1. The Procedure of Cross Validation.....	246
6.4.2. Investigation of the Relationship between Lateral Performance and Structural Parameters by the Capacity Spectrum Method	247
6.4.2.1. Obtaining the Performance Points	247
6.4.2.2. The Comparison of Performance Points Obtained by Analysis and Proposed Equation	251
6.4.3. Investigation of the Relationship between Lateral Performance and Structural Parameters by Using Interstorey Drift Ratios	253
6.4.4. Investigation of Relationship between Lateral Performance and Various Structural Parameters by Using Displacement Coefficient Method	254
6.4.5. Investigation of the Relationship between Lateral Response and Structural Parameters by Using Improved Displacement Coefficient Method	259
6.4.5.1. Investigation of the Relationship between the Lateral Response and Structural Parameters According to the Adjusted LPPE.....	269
6.5. Nonlinear Time History Analysis	272
6.5.1. Ground Motion Database	272
6.5.2. Analysis Based on Selected Records	274
6.5.3. Scaling of the Records	276
6.5.4. Regression Analysis.....	278
6.6. Evaluation of the Results	279
6.7. Recommended LPPE for Utilization in the Prediction of Lateral Performances	282
7. LOSS ESTIMATION	285
7.1. Introduction.....	285
7.2. Review of Previous Studies	285
7.3. Damage Limit States, Damage Classes and Damage Ratios	287
7.4. Damage Limit States	291
7.5. Estimation of Seismic Loss.....	292
7.6. Insurance Considerations	295
7.7. Case Study.....	296

7.8. Application of the Developed Scheme.....	300
8. SUMMARY AND CONCLUSIONS.....	303
8.1. Summary	303
8.2. Discussion of Results and Main Conclusions	311
8.3. Recommendations for Future Studies	316
REFERENCES	323
APPENDICES	
A. GROUND MOTION DATABASE.....	337
B. MATLAB PROGRAM DEVELOPED FOR CALIBRATION PROCESS..	349
C. CALIBRATED COEFFICIENTS OF AC10.....	355
D. AREA SOURCE COORDINATES	357
E. FAULT PARAMETERS.....	361
F.FAULT COORDINATES	369
G. FLOWCHART I.....	387
H. FLOWCHART II	389
CURRICULUM VITAE	391

LIST OF FIGURES

FIGURES

Figure 2.1. Example for System of Faults Based on Kutahya Segment System (A Gap and Stepmover Between Segment-I and Segment-II, and a Gap and Intersecting Segment Between Segment-III and Segment-IV are Shown as Illustrative Examples)	21
Figure 2.2. Fault Segmentation Hazard Model Developed by Cramer et al. (2000)	22
Figure 2.3 Types of Barriers That Block Earthquake Rupture Propagation (Upper Left is a Gap Structure, Upper Right is a Stepmover Structure, Lower Left is a Single Bend and Lower Right is a Combination Structure).....	24
Figure 2.4. Two Types of Stepmover Structure: Releasing and Restraining Stepmovers in Strike-Slip Fault Systems (McClay and Bonora, 2001).....	25
Figure 2.5. Two Types of Double Bend Structure: Releasing and Restraining Double Bends in Strike-Slip Fault Systems (McClay and Bonora, 2001).....	25
Figure 2.6. Characteristic and GR Model for Magnitude-Recurrence Relationships as Proposed by Wesnousky, 1994	29
Figure 2.7. Earthquake Recurrence Models Modified from Shimazaki and Nakata (1980).....	30
Figure 2.8. Characteristic Earthquake Model Proposed by Youngs and Coppersmith (1985)	31
Figure 2.9. Slip Rates of West Anatolia by McClusky et al. (2000) with a Fixed Eurasian Frame (Reproduced and Modified from McClusky et al., 2000).....	39
Figure 2.10. Smeared Slip Rates of West Anatolia by Kriging Method with a Fixed Eurasian Frame (Based on McClusky, 2000)	40
Figure 2.11. Smeared Principal Strain Rates of West Anatolia by Kriging Method with a Fixed Eurasian Frame (Based on McClusky, 2000)	41
Figure 2.12. Smeared Principal Strain Rates (With Color Codes of Dilatation) of West Anatolia by Kriging Method with a Fixed Eurasian Frame (Based on McClusky, 2000).....	41
Figure 2.13. Slip Rates of West Anatolia with a Fixed Eurasian Frame (Reproduced and Modified from Ayhan et al. (2002)	42

Figure 2.14. Slip Rates of West Anatolia with a Fixed Anatolian Frame; Rates Shown are Normal to the Measurement Axis (Reproduced and Modified from Flerit et al. (2004))	43
Figure 3.1. The Most Common Distance Measures from the Earthquake Source to the Site (Kaklamanos et al., 2010)	61
Figure 3.2. Distribution of Magnitude and Distance of the Local Database.....	69
Figure 3.3. The Range of Shear Wave Velocities at the Recording Station Sites and Associated Site Classes According to NEHRP, 1994	70
Figure 3.4. The Epicenters of Earthquakes and Locations of Recording Stations.....	71
Figure 3.5. Magnitude Scaling in the Raw Data for PGA.....	72
Figure 3.6. Magnitude Scaling in the Raw Data for Spectral Period of 0.2 s	73
Figure 3.7. Magnitude Scaling in the Raw Data for Spectral Period of 1.0 s	73
Figure 3.8. PGA versus Distance Values Shown Separately for Site Class C and D, and Fitted Curves by Least Squares Method.....	74
Figure 3.9. Spectral Acceleration Values at Spectral Period of 0.2 s versus Distance Values for Class C and D, and Fitted Curves by Least Squares Method.....	74
Figure 3.10. Spectral Acceleration Values at Spectral Period of 1.0 s versus Distance Values for Class C and D, and Fitted Curves by Least Squares Method.....	75
Figure 3.11. Moment versus Distance Values Sorted According to Fault Types	75
Figure 3.12. Residuals of Regression Analysis for AS97, BJF97, SY97 and OB04. 84	
Figure 3.13. Residuals of Regression Analysis for AS08, BA08, CB08 and AC10.. 85	
Figure 3.14. Response Spectrum developed by GMPE Models for $M_w = 7.0$ and $R = 10$ km, depth=20 km (Models are AS97, SY97, OB04 and AC10 with Calibrated Coefficients).....	88
Figure 3.15. Response Spectrum developed by GMPE Models for $M_w = 7.0$ and $R = 10$ km, depth=20 kms (Models are AS97, SY97, OB04 and AC10 with Original Coefficients).....	89
Figure 3.16. Response Spectrum Curve Developed for $M_w = 7.0$ and $R = 50$ km (Models are AS97, SY97, OB04 and AC10 with Calibrated Coefficients).....	90
Figure 3.17. Response Spectrum Developed for $M_w = 7.0$ and $R = 50$ km (NGA Models are AS97, SY97, OB04 and AC10 with Original Coefficients).....	91

Figure 3.18. Response Spectrum developed by NGA Models for $M_w = 7.0$ and $R=10$ km (NGA Models are BA08, AS08, CB08 with Calibrated Coefficients)	92
Figure 3.19. Response Spectrum Curve Developed by NGA Models for	92
$M_w = 7.0$ and $R=10$ km (NGA Models are BA08, AS08, CB08 with Original Coefficients)	92
Figure 3.20. Response Spectrum developed by NGA Models for $M_w = 7.0$ and $R=50$ km (NGA Models are BA08, AS08, CB08 with Calibrated Coefficients)	93
Figure 3.21. Response Spectrum developed by NGA Models for $M_w = 7.0$ and $R=50$ km (NGA Models are BA08, AS08, CB08 with Original Coefficients)	93
Figure 3.22. Average Response Spectrum Obtained by the Average of non-NGA and NGA Models ($M_w=7.0$ and $R=10$ km) with Calibrated Coefficients.....	95
Figure 3.23. Average Response Spectrum Obtained by the Average of non-NGA and NGA Models ($M_w=7.0$ and $R=50$ km) with Calibrated Coefficients.....	96
Figure 3.24. Distance Scaling of Ground Motions Modeled by GMPEs with Calibrated Coefficients.....	99
Figure 3.25. Distance Scaling of Ground Motions Modeled by GMPEs with Original Coefficients	100
Figure 3.26. Distance Scaling of Ground Motions Modeled by GMPEs with Calibrated and Original Coefficients	101
(Performance Curves with Original Coefficients are shown in Gray Color in the Background).....	101
Figure 3.27. Comparison of Recorded Acceleration Values of Kocaeli and Duzce Earthquake Data with the Predicted Values by GMPE'	102
Figure 3.28. Distance and Magnitude Scaling of Ground Motion with Calibrated Coefficients	103
Figure 3.29. Response Spectrum Curves Obtained for $M_w=7.0$ and 6.0 for.....	107
$R=10$ and 50 km Using Calibrated Coefficients for Site Conditions of B/C Boundary, Class C and D According to NEHRP.....	107
Figure 3.30. Residual Analysis with Normal Plots for AC10.....	108
Figure 3.31. The Spectral Acceleration Curves Obtained by Several Different GMPEs for Earthquake of $M_w=7.0$ and at a Distance of 10 km	109

Figure 3.32. The Prediction Errors of the Predicted Accelerations by Using Multi-stage Multiple Regression Analysis with Modified AC10.....	111
Figure 4.1. Equivalent SDOF Representation of an MDOF System (Modified from ATC-40)	118
Figure 4.2. Response of the Structure to the Beam Column Stiffness Ratio	129
Figure 4.3. Bilinear Idealization of the SDOF by Using the Pushover Curve of MDOF System Shown on the Left	131
Figure 4.4. The Transformation of MDOF System to SDOF System.....	131
Figure 4.5. Lateral Strength Index Modification Scheme	137
Figure 4.6. Soft Storey Index Modification Scheme.....	138
Figure 4.7. Lateral Stiffness Index Modification Scheme	140
Figure 4.8. Modification of Height Ratio of the Structures	141
Figure 4.9. Types of Reinforced Concrete Structures with Different Periods of Codes	142
Figure 5.1. The Fault Map Showing the Fault Lines around the City of Eskisehir (Ocakoglu, 2007).....	144
Figure 5.2. The Fault Map Covering a the Circular Area of 300 km Radius Centered at Eskisehir	145
Figure 5.3. The Fault System in the Close Vicinity of Eskisehir and Earthquake Activity ($M_w > 5.0$) (Kocyigit, 2005).....	148
Figure 5.4. The Fault System in the Close Vicinity of Bursa (Kocyigit, 2005).....	150
Figure 5.5. The Fault System in the Close Vicinity of South Marmara Region and Earthquake Activity ($M_w > 5.0$) (Kocyigit, 2005).....	152
Figure 5.6. The Fault System in the Close Vicinity of Sea of Marmara and Earthquake Activity ($M_w > 5.0$) (Kocyigit, 2005, Kalkan et al., 2009)	154
Figure 5.7. The Fault System between Sea of Marmara and Duzce within NAFZ and Earthquake Activity ($M_w > 5.0$) (Kocyigit, 2005, Saroglu, 1992)	156
Figure 5.8. The Fault System in the Central NAFZ.....	157
Figure 5.9. The Fault System between Gerede and Bayramoren Faults within the NAFZ and Earthquake Activity ($M_w > 5.0$) (Saroglu, 1992).....	159
Figure 5.10. The Fault System in the Close Vicinity of Kutahya and Earthquake Activity ($M_w > 5.5$) (Kocyigit, 2005, Saroglu, 1992)	160

Figure 5.11. The Fault System in the Close Vicinity of Isparta Triangle and Earthquake Activity ($M_w > 5.5$) (Kocoyigit, 2005, Saroglu, 1992).....	161
Figure 5.12. Faults and Earthquake Activity in the Close Vicinity of Eskisehir ($M_w \geq 4.0$) (Faults by Ocakoğlu, 2008).....	163
Figure 5.13. Seismicity around Eskisehir within Encircled Area with 300 km Radius Circle Between 1900 and 2010, ($M \geq 3.0$, KOERI, 1900-2005, Faults by Saroglu et al., 1992).....	163
Figure 5.14. Seismicity in Turkey between 1900-2010 by KOERI and GDDA ($M_w \geq 4.0$)	167
Figure 5.15. The Effect of Declustering on the Magnitude Distribution.....	168
Figure 5.16. Earthquakes in Each Decade With Respect to Four Magnitude Ranges (KOERI 1900-2005, GDDA 2005-2010 Combined, Raw Data).....	169
Figure 5.17. Distribution of Earthquakes with Respect to Moment Magnitudes (top) and the Comparison of Magnitude Recurrence Curves for Complete and Incomplete Parts (bottom).....	170
Figure 5.18. Trends of Magnitude Completeness Parameters	173
Figure 5.19. Earthquakes in Each Decade With Respect to Four Magnitude Ranges (Combination of KOERI 1900-2005 and GDDA 2005-2010, Homogenized, Declustered and Completed).....	173
Figure 5.20. The Magnitude Recurrence Relationships after Completeness Analysis Results.....	174
Figure 5.21. Area Sources and Epicenters of Earthquakes Occurred Between 1900 and 2010.....	176
(Earthquakes by KOERI, GDDA, $M_w > 4.0$, Before Declustering)	176
Figure 5.22. Area Sources and Epicenters of Earthquakes for the Period Between 1900 and 2010.....	177
(Earthquakes by KOERI, GDDA, $M_w > 4.0$, Declustered According to Deniz and Yucemen, 2008).....	177
Figure 5.23. Full Characteristic Models Used in This Study.....	179
Figure 5.24. Annual Exceedance Rates of Earthquake Events for PGA, and Spectral Periods of 0.2 s and 1.0 s	180

Figure 5.25. Elastic Response Spectrum Curve Developed for the City of Eskisehir (NEHRP B/C Boundary Site, Response at 5% Damping, GMPE of AC10 with Calibrated Coefficients Used)	180
Figure 5.26. Seismic Hazard Map of Eskisehir and Surrounding Region for Earthquakes with 10%.....	182
Annual Exceedance Rates in 50 Years (PGA, NEHRP B/C Boundary Site, $V_s=760$ m/s, as GMPE AC10 with Calibrated Coefficients is Employed)	182
Figure 5.27. Seismic Hazard Map of Eskisehir and Surrounding Region for Earthquakes with 10%.....	183
Annual Exceedance Rates in 50 Years (Spectral Acceleration Values at 0.2 s, NEHRP B/C Boundary Site, $V_s=760$ m/s, as GMPE AC10 with Calibrated Coefficients is Utilized)	183
Figure 5.28. Official Hazard Map of Eskisehir and Surrounding Region for Earthquakes with 10%.....	184
Annual Exceedance Rates in 50 Years (PGA, Site Class Rock According to GMPE of Joyner and Boore, 1981).....	184
Figure 5.29. Response Spectrum Curve Developed for the City of Eskisehir.....	185
Figure 5.30. Faults Sources Used in the Spatially Smoothed Seismicity Model (Lettis et al. 2002 and Duman et al., 2005)	189
Figure 5.31. Spatial Density $n_i(m_{min})$ of Earthquakes for the Considered Region for Model I.....	190
Figure 5.32. Spatial Density $n_i(m_{min})$ of Earthquakes for the Considered Region for Model II.....	190
Figure 5.33. Seismic Hazard Map Developed for 10% Probability of Exceedance in 50 years for PGA Values (Values are in g, NEHRP B/C Boundary Site)	191
Figure 5.34. Seismic Hazard Map Developed for 10% Probability of Exceedance in 50 years for Spectral Period of 0.2 s (Values are in g, NEHRP B/C Boundary Site)	192
Figure 6.1. Moment/Yield Moment-Rotation Relationships for Plastic Hinges.....	196
Figure 6.2. Pushover Curves for Structures with Default and User Defined Hinges in X-Direction (B01, B17 and B28 in Table 6.1).....	197
Figure 6.3. Frame Model for Shear Walls.....	198

Figure 6.4. Lateral Strength Index of all the Models (Total 37 Points).....	203
Figure 6.5. Lateral Stiffness Index of All the Structures in the Sample (Total 62 Points).....	204
Figure 6.6. Period versus Height Relationship of All the Buildings and Calculated Periods by Using Different Formulations (Total 62 Points).....	205
Figure 6.7. Lateral Drift Profiles of Structures (31 Models in Each Direction)	206
Figure 6.8. The Relationship between the Lateral Strength Index and Lateral Stiffness Index.....	208
Figure 6.9. Pushover Curves of Three Structures Obtained by the Application of Different Loading Types and Initial Stresses.....	209
Figure 6.10. The Translational and Rotational Movement Caused by the Eccentricity and Lateral Loading in Fundamental Mode Shape (CM: Center of Mass, CR: Center of Rigidity, C: Geometric Center).....	210
Figure 6.11. Pushover Curves of Buildings in Both Directions in Base Shear-Roof Displacement Format (Total 62 Structural Models)	211
Figure 6.12. Capacity Curves of Buildings in Both Directions in Base Shear-Roof Displacement Format (Total 62 Structural Models)	212
Figure 6.13. The Pushover Curves with the Original Structural Parameters (Uniform Loading) (Number of Structural Models Varies).....	215
Figure 6.14. The Capacity Curves with the Original Structural Parameters (Uniform Loading) (Number of Structural Models Varies).....	216
Figure 6.15. The Scaling of the Fundamental Period with Respect to Lateral Strength Index.....	219
Figure 6.16. Scaling Characteristic of the Global Drift Ratio with the Lateral Strength Index for 2475-year Return Period Earthquake (Performance of 40 Modified Structural Models are Presented)	223
Figure 6.17. Capacity Curves for Different Values of Lateral Strength Index	225
Figure 6.18. The Results of Sensitivity Analysis for Roof Displacement and Global Drift Ratio	228
Figure 6.19. Variation of the Lateral Performance Values with Respect to the Functions Obtained by Sensitivity Analysis (NEHRP Site Class C, Lateral	

Performances of 62 Structural Models for 475-year Return Period Earthquake are Presented).....	230
Figure 6.20. Variation of Roof Displacement with Fundamental Period (62 structural models).....	234
Figure 6.21. Pushover Curves of Eliminated and Outlier Structures.....	235
Figure 6.22. Capacity Curves of Eliminated and Outlier Structures.....	235
Figure 6.23. Variation of Original and Outlier Periods with Height.....	239
Figure 6.24. Relative Sway Ratios and Fundamental Period Values (Eliminated Structures are Identified with Symbols and Numbers)	240
Figure 6.25. The Post Elastic Lateral Stiffness to Elastic Lateral Stiffness Ratios versus Fundamental Period Values (Eliminated Structures are Identified with Symbols and Numbers)	240
Figure 6.26. Fundamental Periods and Ductility Ratios (Eliminated Structures are Identified with Symbols and Numbers)	241
Figure 6.27. Capacity Curves Transformed into ADRS Format after the Removal of Outliers	243
Figure 6.28. Variation of the Lateral Performance Values with Respect to the Functions Obtained by Sensitivity Analysis (Based on Refined Data, NEHRP Site Class C, (NEHRP Site Class C, Lateral Performances of 35 Structural Models for 475-year Return Period Earthquake are Presented)	245
Figure 6.29. Modified Elastic Response Spectrum Curves for Eskisehir (NEHRP C, $V_s = 560$ m/s).....	248
Figure 6.30. The Performance Values Obtained by the CSM with Different Earthquake Return Periods (35 Models are Presented).....	249
Figure 6.31. Equivalent Fundamental Periods of All Structures for Earthquakes with Different Return Periods	249
Figure 6.32. Effective Damping Ratios of All Structures for Earthquakes with Different Return Periods	250
Figure 6.33. Original and Calculated Performance Points of Buildings for Earthquakes with Different Return Periods (28 points for each return period)	251
Figure 6.34. Calculated and Predicted Performance Points of Structures for Earthquakes with 72,175 and 475-year Return Period.....	252

Figure 6.35. The Actual and Estimated Maximum Interstorey Drift Ratios (56 Models Presented).....	254
Figure 6.36. Correlation Coefficients Computed for the Development and Validation Stages and Overall Significance Test Results in terms of p Values (500 Validation Rounds, 475 year Return Period Earthquake is Considered).....	255
Figure 6.37. Estimated and Predicted Global Drift Ratios for Immediate Occupancy Level Corresponding to Earthquakes with Different Return Periods	257
Figure 6.38. Estimated and Predicted Global Drift Ratios for Immediate Occupancy Level Corresponding to Earthquakes with Different Return Periods	258
Figure 6.39. Significance Test Results of Individual Structural Parameters for Immediate Occupancy Level	258
Figure 6.40. Correlation Coefficients Computed for the Development and Validation Stages and Overall Significance Test Results in terms of p Values (500 Validation Rounds, 475 years Return Period)	259
Figure 6.41. Estimated and Predicted Global Drift Ratios by IDCM Method (Development Stage).....	260
Figure 6.42. Estimated and Predicted Global Drift Ratios by IDCM Method (Validation Stage)	261
Figure 6.43. Significance Test Results of Individual Structural Parameters	262
Figure 6.44. Distribution of Coefficients for Lateral Stiffness Index (Distribution of Values Obtained by 291 Validated Rounds of Cross Validation Scheme out of 500)	263
Figure 6.45. Distribution of the Estimated Global Drift Ratios by IDCM with Respect to Lateral Strength Index	265
Figure 6.46. Distribution of Coefficients of Lateral Strength Index (291 Validated Rounds of Cross Validation Scheme out of 500).....	266
Figure 6.47. Distribution of the Estimated Global Drift Ratios by IDCM with Respect to Soft Storey Index.....	267
Figure 6.48. Distribution of the Estimated Global Drift Ratios by IDCM with Respect to Lateral Stiffness Index.....	267
Figure 6.49. Distribution of the Estimated Global Drift Ratios with Respect to Number of Storeys	268

Figure 6.50. Distribution of Number of Storeys and the Estimated and Predicted Target Displacements	270
Figure 6.51. Significance Test Results of Individual Structural Parameters	271
Figure 6.52. Trellis Plot of Global Drift Ratios Obtained by IDCM for 2475-year Return Period Earthquake	271
Figure 6.53. PGA vs Distance Plot	273
Figure 6.54. Distribution of Moment Magnitude and Site Classification of Recording Stations	274
Figure 6.55. Lateral Response Monitored at the Center of Mass of Roof Level of B01 in X-Direction for the North-South Directional Record of 18.07.1979 Dursunbey Earthquake.....	275
Figure 6.56. Result of the Regression Study of Nonlinear Time History Analysis by Using North-South Directional Record of 18.07.1979 Dursunbey Earthquake.....	275
Figure 6.57. Scaling Procedure Applied for 475-Return Period Response Spectrum Curve	277
Figure 6.58. Result of Rounds of Validation Performed with the Roof Displacements and Structural Parameters.....	278
Figure 6.59. Significance Test Results of the Validation Rounds Conducted for the Derivation of Lateral Performance Prediction Equation for a 475-year Return Period Earthquake.....	279
Figure 6.60. Original and Outlier Capacity Curves	280
Figure 6.61. Displacement Response Spectrum Curves Developed for Eskisehir...	281
Figure 6.62. Narrow Band of Roof Displacements Obtained by IDCM and the Fundamental Period Relationship between 0.35 s and 0.80 s	281
Figure 7.1. Structural Performance and Damage Levels (Ghoborah, 2004).....	289
Figure 7.2. Distribution of Yield and Ultimate Drift Ratios (35 Models are Used)	292
Figure 7.3. Annual Exceedance Rates of Earthquake Events for PGA, and Spectral Periods of 0.2 s and 1.0 s (AC10 is Used as GMPE).....	293
Figure 7.4. Selected Building Plan View and Profile Views (All units are in meters)	297

Figure 7.5. Annual Occurrence Rates and Expected Damage Ratios for the Building Considered in the Case Study and for Earthquakes with Different Occurrence Probabilities in 50 years for Eskisehir 299

Figure 7.6. Loss Exceedance Curve for the Sample Building Considered for Insurance Premium Computation..... 300

LIST OF TABLES

TABLES

Table 2.1. Uncertainties Associated with the Elements of Probabilistic Seismic Hazard Analysis (SSHAC, 1997).....	16
Table 2.2. The Rupture Length and Magnitude Relationship for Faults.....	30
Table 2.3. Space and Time Windows to Identify Secondary Events (After Deniz, 2006)	46
Table 2.4. Recurrence Rates for Fault Sources Developed by Various Researchers.	50
Table 3.1. Comparison of Ground Motion Prediction Equations According to Input Parameters.....	58
Table 3.2. Comparison of Ground Motion Prediction Equations According to Input Parameters.....	64
Table 3.3. Ranges of Applicability of Ground Motion Prediction Equations Prescribed by the Developers	66
Table 3.4. Records Used in the GMPE Analysis (GDDA, 1976-2010).....	68
Table 3.5. The Sigma Values Associated with the Multi-Stage Regression Analysis for PGA and Spectral Periods of 0.2 s and 1.0 s	79
Table 3.6. The Coefficients of Determination Associated with the Regression Analysis (With Original and Calibrated Coefficients).....	81
Table 3.7. Comparison of Calibrated and Original Coefficients.....	107
Table 4.1. Values for C_0 Modification Factor	121
Table 4.2. Values for C_2 Modification Factor	121
Table 4.3. The Most Common Methods Used for the Evaluation of Lateral Performance of Structures	124
Table 4.4. Factors Affecting the Lateral Response of a Structure	128
Table 4.5. Lateral Load Distribution Types	134
Table 5.1. The Faults in the Close Vicinity of Eskisehir	149
Table 5.2. The Faults in the Close Vicinity of Bursa (Kocyigit, 2005)	151
Table 5.3. The Faults in the Close Vicinity of South Marmara Region.....	153
Table 5.4. The Faults in the Close Vicinity of Sea of Marmara (Kocyigit, 2005, Kalkan et al., 2009)	155

Table 5.5. The Faults between Sea of Marmara and Duzce within NAFZ (Kocyigit, 2005, Saroglu, 1992).....	158
Table 5.6. The Faults between Gerece and Bayramoren within the NAFZ (Saroglu, 1992)	159
Table 5.7. The Faults in the Close Vicinity of Kutahya.....	160
(Kocyigit, 2005, Saroglu, 1992).....	160
Table 5.8. The Faults in the Close Vicinity of Isparta Triangle (Kocyigit, 2005, Saroglu, 1992).....	162
Table 5.9. Major Large Magnitude Earthquakes within 300 km Radius Circular Area Centered at Eskisehir between 1900 and 2010	164
Table 5.10. Historical Records Compiled for the City of Eskisehir	164
Table 5.11. Comparison of Earthquake Catalogs Obtained from Different Sources	167
Table 5.12. Number of Earthquakes Classified According to Ten-Year Periods and Four Different Magnitude Ranges (Declustered After Deniz, 2006 and Deniz and Yucemen, 2008	169
Table 5.13. Values of Completeness Parameters for Seismic Database Before and After the Completion Procedure by Using the Methodology of Stepp (1973)	172
Table 5.14. Number of Earthquakes Classified According to Ten-Year Periods and Four Different Magnitude Ranges after Completeness Analysis Results.....	174
Table 5.15. Area Sources and Their Parameters	178
Table 5.16. Models Created for the Spatially Smoothed Analysis	188
Table 5.17. Fault Segments and Their Parameters Used for the Spatially Smoothed Analysis.....	189
Table 6.1. Structural Properties of All the Buildings.....	194
Table 6.2. Moment-Rotation Relationships of Default and User Defined Concrete Moment and Biaxial Hinges.....	197
Table 6.3. Categories of Shear Walls According to Their Aspect Ratios.....	199
Table 6.4. Modal Properties of Buildings for Analysis	199
Table 6.5. Structural Properties of Buildings.....	201
Table 6.6. Period and Stiffness Values of Structures.....	236
Table 6.7. The List of Eliminated Buildings.....	242

Table 6.8. The Structural Parameters of the Remaining Structures that are Compiled for Regression Analysis	244
Table 6.9. Maximum Interstorey Drift Ratio Results.....	253
Table 6.10. Mean and Standard Deviations of Coefficients of Lateral Performance Prediction Equation for Each Response Spectrum Curve (291 Validation Rounds)*	264
Table 6.11. Mean and Standard Deviations of Coefficients of Lateral Performance Prediction Equation for Each Response Spectrum Curve (496 Validation Rounds)	270
Table 6.12. Records Used in the GMPE Analysis (GDDA, 1976-2010).....	272
Table 7.1. ASCE 41 Structural Performance Levels and Overall Damage for Reinforced Concrete Structures (ASCE 2007).....	288
Table 7.2. Descriptions of the Damage States Used by the General Directorate of Disaster Affairs, Ministry of Public Works and Settlement	290
Table 7.3. Damage Ratios Corresponding to Various Damage States (Gurpinar et al., 1978).....	291
Table 7.4. Performance Levels and Damage Limit States with Respect to Global Drift Ratio for Both Directions	292
Table 7.5. Damage Ratios Corresponding to Global Drift Ratios	294
Table 7.6. Relative Earthquake Insurance Scheme with Respect to Seismic Zones and Year of Construction for Reinforced Concrete Buildings in TCIP	296
Table 7.7. Structural Parameters of the Selected Building to be Used with the LPPE	298
Table 7.8. Expected Annual Loss Corresponding to Different Earthquake Occurrence Probabilities.....	299
Table 8.1. Total Number of Eliminated Structures and the Associated Elimination Criteria	315
Table A1. Raw Data Used in the Derivation of Coefficients of Ground Motion Prediction Equations	337
Table CI. Calibrated Coefficients of Ground Motion Prediction Equation Developed by Akkar and Cagnan (2010)	355
Table D1. Area Sources and Their Coordinates (In Degrees).....	357

Table E1. The Parameters of the Faults Identified Around the Close Vicinity of Eskisehir.....	361
Table F1. The Coordinates of The Active Faults Identified In The Close Vicinity of Eskisehir (In Decimal Degrees)	369

LIST OF ABBREVIATIONS

(In alphabetical order)

ADRS	: Acceleration displacement response spectra
APRP	: Annual pure risk premium
ASCE	: American Society of Civil Engineers
ATC	: Applied Technology Council
BF	: Bare frame
C	: Geometric center
CDR	: Central damage ratio
CEI	: Compulsory earthquake insurance
CM	: Center of mass
CR	: Center of rigidity
CSM	: Capacity spectrum method
CP	: Collapse prevention
DC	: Damage cost
DCM	: Displacement coefficient method
EADR	: Expected annual damage ratio
EAF	: East Anatolian fault
EAL	: Expected annual loss
EDR	: Expected damage ratio
EFZ	: Eskisehir fault zone
FEMA	: Federal Emergency Management Agency
GDDA	: General Directorate of Disaster Affairs
GMPE	: Ground motion prediction equation
GPS	: Global positioning system

GR	: Gutenberg Richter
GSHAP	: Global seismic hazard program
HAZUS	: Hazard program developed by FEMA
ICSM	: Improved capacity spectrum method
IDR	: Interstorey drift ratio
IDCM	: Improved displacement coefficient method
ISC	: International Seismological Center
ISS	: International Seismology Summary
KOERI	: Kandilli Observatory and Earthquake Research Center
LF	: Load factor
LP	: Lateral performance
LPPE	: Lateral performance prediction equation
MDOF	: Multi degree of freedom system
MIDR	: Maximum interstorey drift ratio
NAF	: North Anatolian fault
NEHRP	: National earthquake hazards reduction program
NGA	: New generation of attenuation equations
N	: Normal fault
NOAA	: National Oceanographic and Atmospheric Administration
OSN	: Oblique slip normal
PGA	: Peak ground acceleration
PMM	: Axial, biaxial moment in hinge definition
PML	: Probable maximum loss
PSHA	: Probabilistic seismic hazard analysis
RCV	: Replacement cost value

RV	: Reverse fault
SASD	: Spectral acceleration spectral displacement
SD	: Spectral displacement
SDOF	: Single degree of freedom system
SESAME	: Seismo-tectonic and seismic hazard assessment of the Mediterranean basin
SH	: Seismic hazard
SS	: Strike-slip fault
SSHAC	: Senior seismic hazard analysis committee
SW	: Shear wall
TCIP	: Turkish catastrophe insurance pool
TEC	: Turkish earthquake code
TP	: Total premium
UDIM	: The National Earthquake Monitoring Center
USGS	: United States Geological Survey
USGS-PDE	: United States Geological Survey preliminary determination of epicenters
WGCEP	: Working group on California earthquake probabilities

LIST OF SYMBOLS

(In alphabetical order)

- α : The bend angles between two continuous faults
- α : The plastic stiffness to elastic stiffness ratio
- α_1 : The effective mass coefficient of the first mode
- α_i : The mean rate of occurrence of earthquakes
- δ : The stepover distance between two faults
- δ : Storey drift
- δ_{Roof} : Roof drift in capacity spectrum method
- δ_t : Roof drift in displacement coefficient method
- Δt : The interarrival times
- Δt^- : The time needed to accumulate the required moment for fault rupture
- Δ_{ij} : The distance between i^{th} and j^{th} cells in spatially smoothed seismicity
- Δm_c : The difference between the upper and lower bound estimate of characteristic earthquake
- ε : The random error
- Φ^* : The complementary cumulative distribution function
- μ : Ductility
- μ : The shear modulus or rigidity of the crustal plate
- λ : The mean rate of occurrences of earthquakes
- σ : The standard deviation
- σ_{max} : The oncoming stresses to the fault
- $\sigma_{ln(y)}$: The standard deviation of the logarithm of the ground motion amplitude
- σ_{tot} : The total standard deviation in multi-stage regression analysis

- τ : The standard deviation in second stage of regression analysis
- ψ : The angle between the oncoming stresses and the fault line
- ν_m : Activity rates of faults
- a : The logarithm of the number of earthquakes in spatially smoothed seismicity model
- a : Coefficient of moment-rupture length relationship
- a : The site class constant in improved displacement coefficient method
- a_R : The aspect ratio of shear walls
- A : The area of rupture surface
- A_{col} : Total areas of columns in a single storey
- A_{nx} : Lateral strength index in x direction
- A_{ny} : Lateral strength index in y direction
- A_i : The area of the segment sections involved in the rupture
- A_{gf} : The area of ground storey
- A_{sf} : Single floor area
- A_{tr} : The tributary area of a typical column
- $(A_{col})_x$: The areas of the columns about the orthogonal x axis
- $(A_{col})_y$: The areas of the columns about the orthogonal y axis
- $(A_{sw})_x$: The areas of the structural walls about x axis
- $(A_{sw})_y$: The areas of the structural walls about y axis
- b : The slope of the curve which reflects the proportion of large earthquakes to small earthquakes in Gutenberg-Richter relationship
- b : Constant term of moment-rupture length relationship
- c : The correlation distance in spatially smoothed seismicity

- c : The slope of the magnitude-time interval curve
- c_1 : A variable in magnitude terms for ground motion prediction equation
- C_0 : Modification factor relating the roof displacement to spectral displacement
- C_1 : Modification factor that relates the expected maximum inelastic displacement to elastic displacement
- C_2 : Modification factor related to the effect of hysteresis shape on target displacement
- C_3 : Modification factor related to the second order effects on target displacement
- C_{site} : The coefficient of linear site parameter
- D : The average displacement of the fault slip
- D_i : The total slip caused by the event in the neighboring segment
- e : Eccentricity
- $E()$: The function of expected number of exceedences
- $f_i()$: The probability density function
- $f_M()$: The function related to magnitude in GMPE
- $f_R()$: The function related to distance in GMPE
- $f_{M,R}()$: The function related to magnitude and distance in GMPE
- $f_P()$: The function related to site effects in GMPE
- F_{lin} : Linear site parameter term
- F_N : Normal fault type
- F_R : Reverse fault type
- F_y^* : Elastic yield force of the equivalent single degree of freedom (SDOF) system
- g : The gravitational constant

h : The depth term in GMPE
 h : The storey height
 i : The source number in spatially smoothed seismicity analysis
 I_{nx} : The lateral stiffness index in x direction
 I_{col} : Total moment of inertias of columns in a single storey
 I_{ny} : The lateral stiffness index in y direction
 $(I_{col})_x$: The moment of inertias of the columns about the orthogonal x axis
 $(I_{col})_y$: The moment of inertias of the columns about the orthogonal y axis
 $(I_{sw})_x$: The moment of inertias of the structural walls about x axis
 $(I_{sw})_y$: The moment of inertias of the structural walls about y axis
 k : The index for distance increment in spatially smoothed seismicity
 k : Parametric constants
 K^* : Elastic stiffness of the equivalent SDOF system
 K_t : Effective lateral stiffness
 K_i : Elastic lateral stiffness
 K_p : Plastic lateral stiffness
 l : The magnitude increment in spatially smoothed seismicity
 m : Magnitude
 m_o : Lower bound magnitude
 m_{max} : Upper bound magnitude
 m_{ref} : Reference magnitude in spatially smoothed seismicity
 m_l : The size of characteristic earthquake
 m_l : The magnitude increment in spatially smoothed seismicity
 M : The total mass of the building

- M^* : The mass of the equivalent SDOF system
- M_b : Body wave magnitude
- M_d : Duration magnitude
- M_l : Local magnitude
- M_0 : The seismic moment
- M_0' : The seismic moment rate
- M_p : The magnitude in combined time and magnitude recurrence model
- M_s : Surface wave magnitude
- M_w : Moment magnitude scale
- n : The number of storeys
- $n_i(m_0)$: The seismic activity rate counted from earthquake catalog
- $n_i(m_{min})$: The smoothed annual activity rate above minimum magnitude $m \geq m_0$
- n_{fy} : The number of continuous frame lines in x direction
- n_{fy} : The number of continuous frame lines in y direction
- nrr : The normalized redundancy ratio
- nrs : The number of redundancy score
- NM : Normal fault
- $N(m)$: the number of earthquakes having magnitude equal or greater than m in GR
- O : The overhang ratio
- PGA : Peak ground acceleration
- RV/O : Reverse oblique fault
- p_i : The probability density function in spatially smoothed seismicity
- P : Probability
- P_a : Probability of seismic hazard at segment a

$PF_{Roof,1}$: The participation factor of the first mode in roof level

$P_{(seg)}^i$: The single segment seismic hazard probability

$P_{(adj.seg)}^j$: The adjusted segment seismic hazard probability

$P_{(mulseg)}^j$: The probability of multiple segment rupture

r : Distance

r_k : Distance increment in spatially smoothed seismicity

R : Ratio of inelastic demand to the calculated yield strength

RL : The rupture length

RV : Reverse fault

R_{JB} : Joyner-Boore distance

R_{rup} : Rupture distance

R_{seis} : Seismogenic rupture distance

R_x : Horizontal distance from tope edge of rupture

ssi : Soft storey index

S : The slip rate

SA : Spectral acceleration

SS : Strike slip fault

S_a : Spectral acceleration

S_d : Spectral displacement

t : Time

\bar{t} : The best estimate of next occurrence of the event

t_{0_i} : The date of the last event

\bar{t}_0 : The weighted average time of the last events

- \hat{t} : The weighted average of t_i for each segment
- T : The repeat time of earthquakes
- T : The length in time
- T_0 : Characteristic period
- T_i : Elastic fundamental period
- T_e : Effective fundamental period
- T_{eq} : Fundamental period of the equivalent SDOF system
- u_y^* : Elastic yield displacement of the equivalent SDOF system
- V : Base shear
- V : Shear wave velocity
- V_{ref} : Reference shear wave velocity
- V_{s30} : Average shear wave velocity of 30 m soil profile
- v_i : The slip rate
- v_r : Rupture propagation velocity
- W : Weight of the building
- y_o : Ground motion level
- y_{ref} : Reference ground motion level
- Y : The ground motion parameter
- z : Ground motion level

CHAPTER 1

1. INTRODUCTION

1.1. General

In earthquake prone areas, there is an urgent need for quick, easy-to-use and reliable estimation methods to determine the seismic hazard and the vulnerabilities of large numbers of buildings in order to estimate the possible losses in an earthquake, to develop a technical basis for insurance industry, and to plan retrofit programs for existing buildings. Seismic events cannot be prevented; however, with sound knowledge of the geology of the area, past history of earthquakes of the region, and local soil conditions, seismic hazard can be quantified in a realistic way and provide the opportunity to adapt structures so as to minimize damage during an earthquake. The information on the vulnerability of structures, which leads to the assessment of risks, can be quantified within a certain degree of accuracy depending on the design characteristics, material properties and compliance to the codes in practice.

A general review of the literature shows that there is a wide spectrum of subjects in the estimation of urban risk, seismic hazard analysis and vulnerability analysis of structures. Due to the importance of urban risk, which covers both seismic hazard and vulnerability, several studies have been conducted, authorities have initiated large-scale research programs in a wide spectrum of subjects, and several software programs have been developed. Therefore, carefully selected criteria are required to present an accurate literature survey on each related subject, as the aim of the study is to develop an easy, quickly applicable and user-friendly approach for the estimation of losses.

In the organization of this thesis, a literature review of overall risk, insurance, seismic hazard analysis, and vulnerability will be given in the respective chapters. The seismic hazard part of the study contains a review of the related studies and historical developments on the related subjects, such as seismic source model definitions, recurrence rates of the source models in both magnitude and time

dimensions, and seismicity of a region. Selected ground motion prediction equations (GMPEs) are examined and calibrated to develop the most appropriate GMPE for the considered region. The vulnerability section contains the historical background and major breakthroughs in the development of the available methods for the performance evaluation of structures. The sections reserved for the review and prediction of vulnerability summarize the methods in addition to the comparisons. A quick, user friendly and easy to apply evaluation method is proposed for the prediction of vulnerability.

1.2. Motivation

The estimation of the occurrence of a future earthquake is almost impossible with today's technology and knowledge. In other words, our ability to estimate the time, location, and size of a future earthquake is quite limited due to the limited amount of past data, lack of information about the physical setting of the areas of interest, and the insufficient technological equipment to measure underground formations and movements. In addition, the potential losses, whether economic or social, are not foreseeable before an earthquake event occurs. Only after the occurrence of an event, the physical background of that event can be analyzed and the technical reasons of the losses can be explained in terms of structural deficiencies. However, the sole aim of thousands of researchers and professionals working in this field is to be able to estimate all the possible scenarios in terms of seismic events and accurately estimate the incurred losses due to such events. Therefore, every step in advancing the ability to measure and quantify seismic threats and losses is considered very valuable because it strengthens the ability to manipulate the way structures are designed and built. Each step in the process of determining seismic threats and risks must be evaluated in order to seek for the possibilities of improvements from start to end for the local risk investigation. The steps should be reviewed in detail and the latest approaches should be sought. The occurrence pattern of earthquakes should be examined, potential earthquake generation sources must be investigated in detail and the methods of determination of seismic risk must be reviewed. The approaches used in seismic threat determination should be questioned and the suitability of the available models to calculate the local seismic threat must be examined in the light of existing resources.

Within the light of the initial search, the author arrived at the conclusion that seismic hazard estimation could be a complex 3-dimensional stress-strain problem if there is sufficient capacity to model each physical source that is capable of generating earthquakes and if there are specialized instruments to obtain the necessary measurements for the analysis. Only then, would it be possible to estimate the timing, location, and size of future earthquakes. Despite the inability of today's technology in the exact determination of the location and size of future earthquakes, there are close approximations for the timing and location of the seismic event occurrences thanks to the availability of recorded past seismic activity and the limited structural and geometrical information of the physical structures that potentially generate seismic events.

Improvements in the estimation of seismic hazard would only be possible by increasing the knowledge of the earthquake generation sources and the dynamics that create these earthquakes. The faults that are created by previous seismic events provide clues about the relative movements of the plates that cause seismic events. Moreover, localized past seismic activity also provides clues about possible local movements. A more educated guess of the time, location, and size of a future seismic event would be possible if the strains and stresses along these faults could be measured in three dimensions, and the material properties of the moving blocks could be known. Consequently, after necessary measurements are performed at certain locations, a stress-strain analysis must be conducted in order to find out the stresses accumulated along the fault lines. Only after than a relative stress-strain map of the area of interest is obtained. Though a two dimensional strain map would not exactly represent the real stresses on the fault lines, they would still provide two dimensional surface stress contours of the area of interest. One of the subsequent steps of such an analysis is to create the potential failure map of the plate structure to foresee seismic events. However, this analysis is still far from an accurate representation of seismic event occurrences; rather it is an educated estimation of the possible future events. A number of studies and projects must be launched to examine the capabilities of the method. Indeed, it is quite probable that in the near future, methods based on the measurements of the stresses, strains could be realized, and the desire of predicting the future events would not be a fantasy anymore in the

public eye. In this study, though the strain maps of the area of interest are generated by the researcher, to obtain the fault parameters, the latest available and practical models have to be considered for the purposes of application.

A new approach is pursued in the modeling of the earthquake propagation from the location of occurrence to the area of interest. The magnitude of the event, distance from the site to the epicenter or hypocenter, fault type, depth, repeat time, source radiation patterns, directivity and the azimuthal change in the direction of rupture of a fault source, basin and basin edge effects, buried rupture effects, hanging wall, and many other factors affect the propagation of the rupture to the distances. Therefore, when modeling a GMPE, every single record that is used to generate the equation should be considered accordingly.

Most of the GMPEs are derived from the statistical analyses of strong ground motion records and are updated as new records become available. These strong motion records generally include earthquakes from several different regions. Generally, a homogeneous distribution of magnitudes and distances is sought in the compiled databases so that the equation would correctly model the distance and magnitude affects. If there are not enough strong motion records available for a region of interest, the strong ground motion records gathered for other locations are used in the database despite the differences of the propagation dynamics of the regions. Despite the fact that developers often carefully investigate such records from different databases and try to create a uniform database considering the similarities of the geological structures that generated the earthquakes, it is still far more reliable to use only the local data since the local geological structures are very specific to the area of interest.

Therefore, it is clear that for a selected location, not all GMPEs are suitable for seismic hazard calculations. The most suitable GMPE would be a specifically developed one for the location of interest by using the available past seismic data of the same region. The past seismic data must be evaluated with a sensitivity analysis in order to sort the variables that affect the resultant ground motion. The commonly used GMPEs that contain these variables must be selected and calibrated by past seismic data in order to seek the best performance in modeling the propagation of the ground motions in the region of interest. Therefore, rather than including a number of

GMPEs in a logic tree method, the best model must be developed and employed for the seismic hazard analysis.

As significant as GMPE, the time dimension is one of the most important elements in a probabilistic seismic hazard analysis. Because the estimation of seismic hazard can be reduced to a stress-strain problem, there must be a pattern for the accumulation and release mechanism of these stresses and strains, and therefore the time dimension must be involved in the formation of this pattern. The timing of the next event can only be estimated if the stress-strain accumulation and release patterns of the geological structures are known. Indeed, there are already several proposals to model the occurrence patterns of earthquakes in time. These models are readily available for exploitation provided that the necessary seismic parameters are available. By using these models, seismic hazards for a specific location and for specific time can be calculated and updated by the inclusion of seismic events occurring in-between the updates.

As the seismic hazard analysis part of the study offers many opportunities of improvement, the methods that are developed for the determination of vulnerability of the structures also offer many opportunities in terms of improvement. In practice, expert opinions, field studies, and analytical methods are used for the estimation of the vulnerability of buildings. Mostly expert opinions and field studies prove to be highly subjective and relative and therefore analytical studies are preferred for more detailed and precise analysis. These analytical methods rely on nonlinear dynamic or static analysis. Nonlinear dynamic analyses provide the most precise information on how a structure reacts to dynamic lateral forces. Nonlinear static analysis or pushover analysis involves pushing the structure until failure while observing the deflections along the height of the building. Both of these analyses can offer several opportunities for determining the lateral performances of buildings.

The need to find out the behavior of buildings under the effect of lateral loading in the simplest and most accurate way encourages researchers to seek and develop different methods. Moreover, the efficiency, ease of application, and time to reach the desired results are factors, which have influenced the way these methods are developed. In an attempt to develop such a method, the objective of this study is decided as the evaluation of structures in terms of lateral performances without

consuming too much time and effort. In order to fulfill such an objective several studies are reviewed. In a few of these studies, Ozcebe et al. (2003), Yucemen et al. (2004), Yucemen (2005), Yakut et al. (2006) sought a relationship between the various structural parameters and the observed damages of buildings. Their aim was to develop a preliminary evaluation tool for the assessment of the existing structures by using various structural parameters. The proposed structural parameters were regressed with the various damage states that were quantified with scores assigned to each of the damage state. A relationship is derived between the damage states and the proposed structural parameters. In the end, their study succeeded in estimating the right damage state by using the derived equations.

The method that was applied in these studies gave the idea of correlating various structural parameters with different lateral performance variables. Consequently, by using analytical methods, it is planned to develop an equation to model the relationship between different lateral performance variables and various structural parameters. This equation is named as lateral performance prediction equation (LPPE) by the author.

Before attempting to develop a LPPE, the sensitivity of each proposed structural parameters can be derived as it is generally performed in the GMPE development procedure. Initially, structural parameters are selected from amongst the various parameters that could potentially influence the lateral performance. Then, a sensitivity analysis is conducted to confirm the scaling of lateral performance with the proposed structural parameters. After that, an equation is formulated with the selected structural parameters, and a multiple regression analysis is performed as it is done whilst deriving a GMPE. After all the procedures are completed, an equation similar to a GMPE is derived.

In the development of the LPPE, the most appropriate lateral performance variables that correlate with the various structural parameters are sought by considering the fact that all buildings are designed for the best performance and not in accordance with the criteria like highest capacity or minimum deformation. Therefore, the building sections and geometry are optimized to carry and safely transfer the vertical and lateral forces to the ground and satisfy the serviceability standards. Consequently, there is a possibility that different lateral performance variables relate

to the structural parameters in different ways. Therefore, different methods with different lateral performance variables should be assessed with the proposed structural parameters.

The approximations that are employed by the insurance firms in the determination of earthquake insurance premiums, a decision makers approach to the planning of seismic mitigation and any loss estimation required by the planners or property market values are all dependent to the methods that are used in the determination of the lateral performances of buildings. All these fields require this technical information before taking any decision or setting the insurance premiums or property values of a building. The most common methods that are used to assess these buildings can be as simple but subjective as street surveys or complex analytical analysis for different types of buildings that would provide all the required values without field investigations. All of these approximations are based on some assumptions in theory or statistical surveys in the field, and they rely on building classification systems in the estimation of the required values. Although none of these methods claims to be a very specific evaluation tool for a specific building, they are valid tools in the evaluation of a large number of buildings.

In the light of the above explanations, it is obvious that there is a need to evaluate all buildings separately without putting them into subclasses and classifying them according to developed categories. Every building deserves a specific analysis by putting the so-called educated engineering intuition into action so that they are not evaluated under an inappropriate category. Building-specific analysis includes the examination of the basic structural properties of a building by just looking at the plan and profile of the building, doing a simple calculation, and deriving the lateral performance of the building by using the building-specific properties. With such a method available, the building evaluation can be such an easy task that even the owners themselves could evaluate their dwellings and make their own decisions. Moreover, if this method proves to be more precise than any other comparable methods, it would provide a powerful tool for the decision makers, seismic mitigation planners, insurers, and city planners.

As a subject, that combines the seismic hazard and the vulnerability, loss estimation offers many opportunities for improvements. As input, loss estimation requires the

exposed ground motion level, building vulnerability information, and the associated damage ratios at the predefined damage states. In other words, it requires the probability of exceeding a damage state of a building for a ground motion level that the building is subjected to and the damage ratios associated with these damage states. The probabilities of exceeding certain damage states and therefore damage ratios are generally established by using subclasses of buildings. These exceedence probabilities are not calculated for a single building because a structure-specific damage state and damage ratio determination requires more time and effort. Consequently, there is no structure specific formulation; instead, an average value of a subclass of buildings is assigned as average value for each building that belongs to that subclass. The evaluation of a structure in a subclass has drawbacks since it does not provide structure-specific loss estimation. A structure-specific loss estimation scheme could provide a better evaluation and it prevents the punishment of the high quality structures by the existing classification system. Such as currently all the reinforced structures are in the same subclass, which in the end are subjected to the same criteria in the evaluation for insurance purposes. However, if a structure-specific system could be developed, the structures with high quality would be awarded with less insurance premiums since the lateral performance of such structure would be more far better than a structure with poor quality, which is in the same subclass according to the classification system of currently applied system.

Another drawback of the current methods is the assignment of central damage ratios to each damage state. Despite the fact that the real damage ratios could be a continuous function, the current classification systems are based on central damage ratios and there is no chance for interpolating the in-between values of the damage ratios that are associated with the damage states. Therefore, with the different lateral performances, there is likelihood of assigning the same damage ratio to the building. Hence, a new method must be proposed to model a continuous damage function so that the resultant damage ratio can be structure-specific, and there would always be a chance to interpolate between predefined damage ratios at certain levels of damage states to reach the exact damage ratio.

Proposing a continuous damage function with the lateral performance variable as the sole input parameter is not difficult. However, the points where the damage ratios are

associated with the lateral performance variable are not clearly defined. In literature, several different damage ratios are defined with respect to the various levels of lateral performances. The damage ratios that are assigned to the established intervals are very questionable due to the subjectivities involved in creating them. However, deriving such ratios for the associated intervals is not the focus of this study so available assumptions will be applied in establishing the continuous damage function and locally developed damage ratios with respect to varying lateral performances will be employed.

1.3. Organization of the Study

The thesis contains eight chapters. The first chapter, the introduction, presents the objectives, motivations and the organization of the thesis. The improvements required to obtain better results in the related fields are assessed and the main objectives of the study and the methods to fulfill these objectives are briefly explained.

In Chapter 2, the elements of the probabilistic seismic hazard analysis are reviewed in detail. The major studies for each subject of seismic source classification, seismic data handling and earthquake recurrence models are reviewed. The fault strain maps are also given in this section as the fault specific strain rates in terms of the dilatations, contractions and slips are provided by these maps. Comments are also provided considering the geological structures of the region.

Chapter 3 focuses on the subject of GMPEs. Several GMPEs that are commonly used in Turkey and around the world are reviewed. Initial selection of the GMPEs with the suitable functional forms is performed considering the proposed applicability criteria for a specific region. For the application of the adaption scheme to the selected GMPEs, the raw database of strong ground motions within 300 km radius circle centered at Eskisehir is formed. The regression analysis was performed by using the ground motion records of the local database and parameters of commonly used GMPEs in order to find the best performing functional form with the local seismic behavior and propagation patterns. Lastly, the most appropriate functional form of the selected GMPE was selected for the application of the seismic hazard analysis.

In Chapter 4, the information on the vulnerability of the structures, various methods

to estimate the lateral performances proposed by the researchers, details of pushover analysis and the sample preparation scheme for the sensitivity analysis are provided. The discriminant analysis that proposes a relationship between various structural parameters and the performance of the structures, and various analytical procedures are reviewed, followed by an explanation of historical developments, current approaches and evaluation of procedures. The analytical methods are summarized and the most convenient and appropriate methods are explained as the objective of the study is to develop a simple, quickly applicable and easy to use tool for the vulnerability evaluation. The selection criteria, such as user friendliness, efficiency, and reliability issues are investigated for each procedure. Then for the sensitivity analysis, the artificial model generation schemes by modification of various structural parameters are explained. At the end of the chapter, the building stock of the Turkish cities is examined depending on the different periods of practice depending on the imposed codes.

Chapter 5 starts with presenting the regional tectonic setting in the region surrounding Eskisehir and the details of each single fault source that could pose seismic threat to Eskisehir. The region is subdivided into several subregions for the ease of identification of the fault sources. Simple maps providing the orientation and geometry of the faults belonging to these subregions are provided with the basic seismic parameters of the faults presented in a tabular format. After the identification of the fault sources and presenting them in visual and tabular formats, the gathered data for the probabilistic seismic hazard analyses (PSHA), such as catalogue data, the methods applied to solve the completeness and homogeneity issues of the compiled catalogue, the area sources and their seismic parameters are presented. As the results of the PSHA conducted for Eskisehir, the response spectrum curves and the annual exceedence rates of earthquakes with different return periods are provided. A comparison of the seismic hazard map obtained by PSHA and the official map is also presented.

The chapter also offers the brief review of spatially smoothed seismicity, and a case study is presented. The case study is performed to obtain the seismic hazard for the city of Eskisehir. Only two fault sources are modeled in the seismic hazard analysis since the sole aim is to compare the performance of the method in approximating the

hazard values to the ones obtained by EZ-FRISK (Risk Engineering, 2013). The results of the analyses are presented as seismic hazard maps.

In Chapter 6, the compilation of the building database, the results of the sensitivity analysis, the application of various lateral performance estimation methods and the regression analyses that are used to develop the LPPE are presented. Initially, presentation of the basic structural characteristics of the structures in the created sample database is provided in graphical and tabular format. Then, the results of the sensitivity analysis, which provide the type of scaling of the lateral performances with the various structural parameters, are presented. The basic form of the LPPE is obtained by using the results of the sensitivity analysis. This basic form of the equation is utilized in the multiple regression analysis in order to model the lateral performances by using the proposed structural parameters.

After the formation of the basic form of the LPPE, the individual lateral performances of the structures in the sample are estimated by using improved displacement coefficient method. Greatly varied lateral performances were observed for the structures in the sample database. The dispersion of the lateral performances of the structures in the database, initiated a refinement procedure for the elimination of the structures with the outlier performances. The refinement procedure is based on the prescriptions in ATC-40 (1996) and FEMA-440 (2005), which are imposed for the utilization of the lateral performance estimation methods. After the refinement of the database through elimination procedures, multiple regression analysis is conducted with the application of two fold cross validation procedure. The lateral performances obtained by using capacity spectrum method (CSM), displacement coefficient method (DCM), improved displacement coefficient method (IDCM), the method that uses the maximum interstorey drift ratio, are regressed with the structural parameters of the LPPE. Finally, nonlinear time history analysis is performed to verify the validity of the developed LPPE.

Chapter 7 is reserved for loss estimation and insurance calculation schemes. The relation between the damage classes, damage states, damage ratios and the lateral performances are explained. The pure insurance premiums are computed by using the lateral performance values obtained by the proposed equation. The obtained insurance premiums are compared with the insurance premiums of the compulsory

earthquake insurance system of Turkey.

In Chapter 8, the comments on the results and the future prospects of the study are summarized. The validity and the failure of the claims are listed. Reasons for the success and failure of the claims, through a thorough examination of the results are provided. The possible improvements of the procedures are outlined and new ideas for the development of the initial idea of relating the lateral performances to the various structural parameters are proposed.

CHAPTER 2

2. GENERAL OVERVIEW OF PROBABILISTIC SEISMIC HAZARD ANALYSIS

2.1. Introduction

This section covers various subjects related to the elements of the PSHA as the seismic source definitions, proposed models of earthquake occurrences for fault sources, information on the methods used to collect the required seismic data and the processing and preparation procedures of seismic data for the seismic hazard analysis. In order to explain the data collection methods and processing procedures in detail, the elements of a seismic hazard analysis must be identified. A probabilistic seismic hazard analysis (PSHA) requires inclusion of several seismicity parameters, such as the earthquake recurrence models in magnitude terms, timewise behavior of the occurrences and the interconnectedness of the events with existing geophysical structures, and the propagation patterns. Consequently, informative sections are prepared for the explanation of the aforementioned elements of PSHA and a literature review is provided. Among the elements of seismic hazard analysis, the faults are given special attention. Several fault behavior models are presented.

The strain maps are developed by using the global positioning system (GPS) measurements of the earth crust around Eskisehir as presented in this section. Various displacement mapping studies of the region is also provided in order to explain the relative movements that cause seismic events in the region.

2.2. Types of Seismic Hazard Analysis

For the decision makers and insurers, rational solutions are obtained by utilizing the deterministic or probabilistic seismic hazard analysis. A typical deterministic seismic hazard analysis makes use of a single-valued event, or a model to obtain the seismic hazard, while PSHA, which was introduced first by Cornell (1968), allows the consideration of the probability of occurrence of several earthquake scenarios in the analysis. His paper clearly laid the algorithm to integrate the contributions of each seismic source in probabilistic terms in order to determine the total hazard at a site.

After this development, similar studies mainly focused on the development of the method by the refinement of the input parameters of the analysis (Scawthorn, 2006).

2.2.1 Deterministic Seismic Hazard Analysis

Deterministic seismic hazard analysis is useful to identify the worst-case seismic events, such as the largest magnitude event occurring at the closest distance to a location. Since insurance is quantitative and requires analyses that consider all possible events, and decisions are often made on the 250-year or 500-year loss, deterministic method has proven very useful (McGuire, 2001).

The deterministic method is straightforward, and they do not include data uncertainties, unless a large amount of parametric analyses are required. Consequently, there is usually no measure for the uncertainties. The scenarios in deterministic seismic hazard analysis have a clear physical basis. These scenarios are either related to seismic sources identified by geological and seismological investigations or derived from past seismic activity.

This method can be employed for seismic hazard assessment applications with an extended data analysis that provides the frequency of seismic events. Moreover, it provides a reliable and robust design basis for applications such as the design of critical infrastructures like nuclear power plants or dams. In most countries, seismic hazard analysis is still largely based on the deterministic method (Klugel, 2008).

2.2.2. Probabilistic Seismic Hazard Analysis

PSHA is built upon four main elements, namely, determination of possible earthquake sources, determination of recurrence characteristic of events of those sources, determination of site effects based on GMPEs, and finally, combination of all event probabilities to reach a single seismic hazard value at a certain location. This method has its origin in the fundamental work of Cornell (1968). It allows the use of continuous, multi-valued events and models, and may have applications in many areas, the most important of which is the development of seismic hazard maps, followed by infrastructure planning, building-code development, and insurance perspectives.

In the determination of seismic hazard at a site, the effects of all earthquakes of different sizes occurring at different locations at different probabilities of occurrence

are integrated into one curve that shows the probability of exceeding different levels of ground motion at the site during a specified period. This can be written as presented by Cornell (1968):

$$E(Z) = \sum_{i=1}^N \alpha_i \int_{m_0}^{m_u} \int_{r=0} f_i(m) f_r(r) P(Z > z | m, r) dr dm \quad (2.1)$$

where $E(Z)$ is the expected number of exceedence of ground motion level z during a specified time period t , and α_i is the mean rate of occurrence of earthquakes between lower and upper bound magnitudes. $f_i(m)$ is the probability density function of magnitude within the source i , and $f_r(r)$ is the probability density function of epicenter distance between the various locations within source i and the site for which the hazard is being estimated. Moreover, in the equation, $P(Z > z | m, r)$ is the probability for the ground motion level due to a given earthquake of magnitude m and epicenter distance r to exceed z . The possibility that ground motion level at a site might be different for the same magnitude earthquakes with same distance from the source is one of the main contributions of the probabilistic method while the inclusion of all the possible sources either as line or area sources strengthens the method.

2.2.3. Comparison of Deterministic and Probabilistic Seismic Hazard Analysis Methods

In simple terms, the deterministic method is based on a single most critical scenario, whereas the probabilistic method considers all possible scenarios. In the deterministic method, the seismic hazard analysis results in overestimation of total loss, whereas the probabilistic method can model the actual seismicity with more reasonable estimation of the total loss. On the other hand, although the actual seismicity can be reflected more correctly in the PSHA, the calculated seismic hazard strongly depends on the probabilistic models used and it is difficult to evaluate how a given input parameter influences the results, as stated in Reiter (1990). Additionally, the probabilistic analysis relies on the input values of Gutenberg-Richter (GR) equation, which in fact may not be reliable due to incomplete or total lack of data in most cases. Reiter (1990) claims that deterministic approaches would be the best to use in seismic hazard analysis, if the nature of the seismic process and its effects

were well understood; however, the probabilistic approaches would be the best to use, if the uncertainty in the earthquake occurrence was very well known. On the other hand, Wang et al. (2003) argue that a probabilistic seismic hazard analysis leads to the loss of physical meaning in the results since it provides the decision maker with infinite choices for the selection of design basis earthquake. However, currently almost all of the seismic hazard maps are prepared using probabilistic methods, while the use of the deterministic approach is limited to special cases.

Historically elements of earthquake magnitude, frequency and GMPEs were first used in Japan to produce a probabilistic seismic hazard map that was prepared by Kawasumi (1951). The first probabilistic mapping studies using probabilistic method in Turkey started with Hattori (1979). Later developments led the way to more rational approaches involving neo-tectonic movements. Various probabilistic hazard maps were prepared by Yarar et al. (1980), Erdik et al. (1982, 1985) and the most current probabilistic seismic hazard map was prepared by Gulkan et al. (1993). Within the global seismic hazard program (GSHAP) and program that was planned for the seismic hazard assessment of Mediterranean basin (SESAME), seismic hazard maps were prepared (Erdik et al., 1999).

2.2.4. Uncertainties in Probabilistic Seismic Hazard Analysis

There are different types of uncertainties in PSHA as seen in Table 2.1, namely aleatory or inherent uncertainties, such as estimating the exact location of an earthquake as well as epistemic uncertainties, as in the case of determination of fault location and geometry. Indeed the category of each variable in Table 2.1 is arguable, although the classification of uncertainties is clearly defined.

Table 2.1. Uncertainties Associated with the Elements of Probabilistic Seismic Hazard Analysis (SSHAC, 1997)

Aleatory (physical randomness)	Epistemic (insufficient knowledge)
Magnitude of the event	Catalogues
Location of epicenters in areal seismic sources	Fault location and geometry
Depth of earthquakes	Seismic source zones
Recurrence relations (location and magnitude of the next event)	Ground motion propagation model and choosing the best applicable GMPE
Standard deviation of the GMPE	Seismicity rates

Aleatory uncertainty can be quantified but not modified by additional information; however, epistemic uncertainty can be reduced by gathering additional information (Firat, 2007, Firat and Yucemen, 2014). Epistemic uncertainties are traditionally handled with logic trees (discrete values with associated weights) while aleatory uncertainties are often handled with probabilistic distributions for convenience. In reality, both types of uncertainty can be represented by both discrete and continuous distributions.

2.3. Determination of Seismic Sources

As one of the most critical components of the seismic hazard analysis, the first step is the determination of seismic sources. A seismic source is described as a point, line or areal zone which, when activated by tectonic forces, could initiate seismic events with the same annual occurrence rate, and has a certain maximum earthquake value and same propagation behavior (Reiter, 1990). In fact, a seismic source zone can be identified through combination of geological, geophysical and seismic data, such as fault identification through site investigation, historical seismicity, and expert opinion.

In PSHA the seismic sources within a specified distance to the site of interest are identified. This region is generally taken as a circular area with its center at the site of interest. The radius of this circle depends on the importance of the structure, propagation characteristics of the ground motion parameters, and the faults in the region. A radius of 250-300 km is usually recommended. Within this circular area, the region is partitioned into a set of area sources, and fault lines are identified. It is assumed that the seismicity for each fault line and area zone is sufficiently homogeneous so that it can be treated as uniform in the computations.

As mentioned, there are three types of seismic source models, which are point, line, and area sources. When several earthquakes occur in a small and far away region from the site, they can be assumed to originate from a point in space. The point source model is also used in the application of spatially smoothed seismicity model that was developed by Frankel et al., (1995). It is based on the idea that the location of a new earthquake is related to past earthquake locations by a Gaussian probability function. When there are not enough area or line sources in the area of interest, the spatially smoothed seismicity model can be employed.

Area source model is the most common type of source model due to its easy and straightforward nature in the modeling phase. Despite its inherent subjective nature, area sources are generally defined by past historical seismic activities, geological structures, and expert opinions.

Line sources are used if there are well-defined faults and with the assumption that earthquakes occur with equal probability at any point on the fault. Only after then the faults are modeled as line sources. Establishment of the line sources also requires studying of surface morphology and characteristics of fault seismicity, such as a geometrical discontinuities or earthquake rupture segmentations. Following sections provide detailed information on the source models.

2.3.1. Area Sources

Seismic hazard results are sensitive to source modeling whether it is an area source or a line source. If the fault location is known without much uncertainty, and if all the earthquakes could be attributed to the fault sources then only fault sources must be used, however since it is not the case area sources always must be used. It is the most widely accepted and used source model, due to straightforward and easy application. Most of the time area and line sources are used together since there are earthquakes that are both attributed to areal and line sources.

Despite its straightforward nature, the determination of the boundaries of the area sources and dividing the region of interest into areas attracted criticism. In one of the studies that criticize the area source model, Yucemen (1982) pointed out that the delineation of the areal seismic sources depends mostly on subjective judgment and that an extremely detailed area source modeling has no considerable effect in the results for a macro scale seismic hazard analysis. Detailed analyses in the seismic source modeling may bring about difficulty in the numerical computations too. Division of the examined region into a large number of seismic sources will reduce the number of earthquakes belonging to each region and then the magnitude-frequency relationships of such regions would be unreliable. Therefore, increasing the number of seismic sources unnecessarily should be avoided when using the areal sources. Area sources are extensively used in the development of seismic hazard maps around the world and in Turkey. As the most significant work in seismic

hazard analysis for Turkey, Gulkan et al. (1993) prepared the current seismic hazard map by using the area sources. They prepared a very comprehensive earthquake-zoning map by modeling all the possible earthquake sources as area sources. With the consideration of the neotectonic structures, and their intensity, distribution and earthquake generation potentials, source zones are established. In later studies, Erdik et al. (1999) utilized 37 seismic source zones for the seismic hazard analysis conducted for Turkey. An updated and improved version of their seismic source zones is employed by Bommer et al. (2002), in relation with a study carried out for the formation of the Turkish Catastrophe Insurance Pool (TCIP).

2.3.2. Line Sources or Faults

As a very crucial source of input for the PSHA, faults are mostly modeled as line sources. In order to model the faults as line sources, study of the surface morphology and seismicity characteristics of the faults is required. As the important fault characteristics, the geometrical discontinuity, segments involved in an earthquake rupture, and patterns of occurrences should be mentioned. The earthquake generation along a fault is studied in detail by several researchers and several models are proposed to explain the generation of earthquakes. Moreover, the recurrences of the earthquakes on the faults are also investigated as a crucial subject by the researchers.

The faults are investigated and classified according to structural and geometrical properties, the earthquake generation mechanisms, rupture propagation patterns and recurrence characteristics with respect to magnitude and timewise distribution. These fault characteristics are so much intertwined and so much related to each other that, describing each model requires a through classification. In the light of this fact, following sections are prepared to describe the most common models developed for earthquake generation, rupture propagation and recurrence models.

2.3.2.1. Earthquake Generation Models

Due to the stress accumulation along the tectonic plates, from time to time a rupture of the fault occurs that causes the vibration of the whole area of the rupture, which is called an earthquake. Sometimes a single structural segment of the fault ruptures with the whole section of the fault involved in the rupture. Moreover, rarely these faults form a family of a greater fault system and act collectively in an earthquake rupture, hence affecting a large area in the vicinity of the fault system. These groups

of faults that align within a specific geometrical and structural form are called fault segments. So three main models are developed for the describing the generation mechanism of earthquakes as fault rupture, segmentation, and cascade models (Field et al., 2007, WGCEP, 1995, 1999, 2003, 2006, 2007).

The fault rupture model was developed considering the fact that earthquake occurrences along a fault are caused by the sudden release of accumulated energy due to movement of the boundary plates. The theory proposes that the magnitude of an earthquake is proportionally related to the ruptured length or area of the fault. The corresponding empirical equations are derived by using observed data (Youngs and Coppersmith, 1984, Wesnousky et al., 1994).

The segmentation of the faults is mainly based on both structural and geometrical formation of the faults and past earthquakes that were produced by the fault. A segment is part of the fault that ruptures in a single characteristic earthquake event. Based on this criterion, the bend structures and the stepovers along a fault, the geometry of the surface cracks during a characteristic earthquake event, the clustering pattern of the past events along a fault, and most important of all, professional judgment is required to define a segment (Shaw et al., 2007). These segmentation examinations along a fault provide the basis for future earthquake scenarios (WGCEP, 1995).

The boundaries of fault segments are defined as discontinuities in the surface fault trace such as stepovers or gaps, directional shifts in fault geometry, geomorphologic changes along the strike direction, intersection with the nearby faults, or existing fault segments that block the propagation of ruptures. Figure 2.1 presents various boundary types of faults acting as barriers of earthquake propagation.

The segmentation and fault rupture models require the maximum magnitude of the earthquake that occurred along the segment and its return period in order to estimate the probability of occurrence of such events. Both models assume the probability of occurrence of an earthquake event along the fault as constant, which in the end causes a higher probability of occurrence on a relatively quieter segment of a fault. The third model that was developed to describe the earthquake generation mechanism is called cascade model. A simultaneous rupture of several segments that

generates a greater size earthquake along the fault is modeled by the cascade model in WGCEP (1995, 1999).

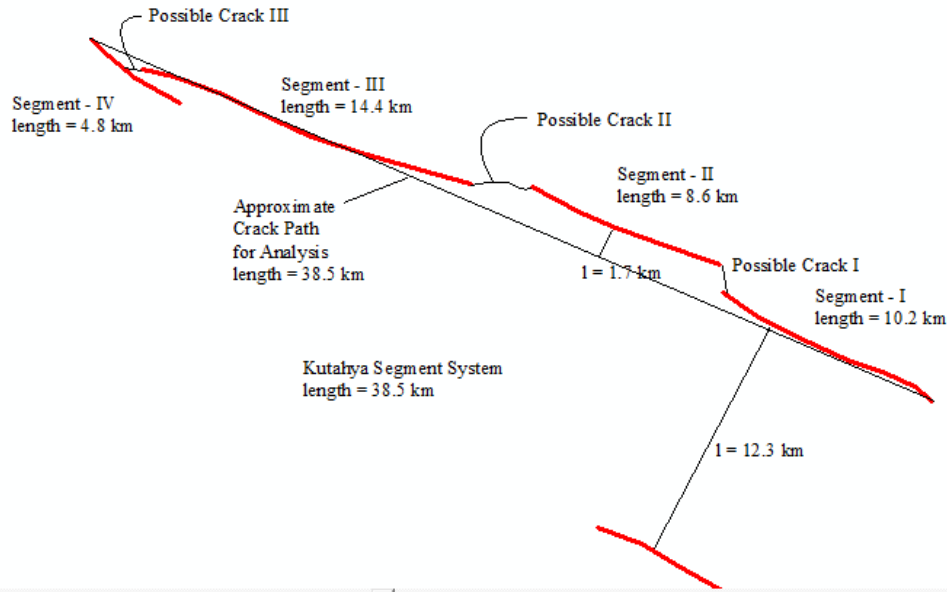


Figure 2.1. Example for System of Faults Based on Kutahya Segment System (A Gap and Stepmover Between Segment-I and Segment-II, and a Gap and Intersecting Segment Between Segment-III and Segment-IV are Shown as Illustrative Examples)

The model is based on the fact that each and every segment has its own recurrence rate and the combination of the segments has a different recurrence rate than each individual segment that forms the segment system. That is, an earthquake might rupture just a single segment or two neighboring segments or a family of segments along the system depending on the magnitude. Consequently, the total probability of occurrence of at least one large earthquake is defined as

$$P = 1 - (1 - P_a)(1 - P_b)(1 - P_c) \dots \quad (2.2)$$

where P_a , P_b and P_c are the probabilities of individual segments with the assumption that the occurrences of earthquakes for each individual fault segment is an independent event.

Cramer et al. (2000) formulated the behavior of segmentation by the equations 2.3 and 2.4, and the model is explained in graphical format as seen in Figure 2.2. The probability of a single segment hazard probability is defined as

$$(1 - P_{(seg)}^i) = (1 - P_{(adjseg)}^j)(1 - P_{(mulseg)}^j) \quad (2.3)$$

$$P_{(adjseg)}^i = 1 - (1 - P_{(seg)}^i)(1 - P_{(mulseg)}^j) \quad (2.4)$$

where $P_{(seg)}^i$ is the single segment hazard probability of the i^{th} segment, $P_{(adj.seg)}^j$ is the adjusted segment probability for each single segment, and $P_{(mulseg)}^j$ is the probability of multiple segment rupture. The equations 2.2, 2.3, and 2.4 are derived with the simple logic that probability of nonoccurrence in a single segment equals the probability of nonoccurrence in multiple segments that include the considered segment, multiplied with the adjusted probability of nonoccurrence in the specified fault segment. By using the equation 2.4, all the adjusted segment probabilities can be calculated.

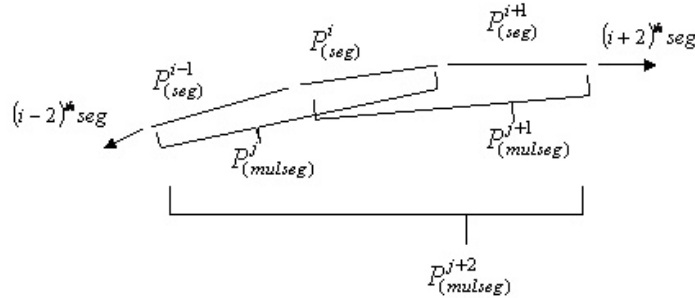


Figure 2.2. Fault Segmentation Hazard Model Developed by Cramer et al. (2000)

Due to the scarcity of data the identification of the segments and obtaining the associated probabilities of earthquake occurrences on the segments are difficult. Because of an incorrect modeling, which is caused by the scarcity of the seismic data, an incorrect seismic hazard might be produced (Field, 2007). Therefore, when using the cascade model, it should be realized that a very accurate and reliable seismic data must be available for the considered fault segments.

Lately, fault segmentation and cascade models have been thoroughly investigated that is based on the assumption that large earthquakes occurring in a zone around a fault segment are likely to belong to the same segment or a homogenous system of fault segments. Moreover, the stress accumulation and releasing mechanism are also investigated in order to find a pattern of behavior along a fault line that is composed of several segments. In order to explain the earthquake generation mechanisms, the stress accumulation and releasing mechanisms must be explained.

Indeed, all the active fault structures are subjected to the stress accumulations and the magnitude of a possible stress-releasing event is dependent on the several factors such as the geometrical alignment and structural features of these faults, already built-up stresses and the rate of stress accumulation. In theory, a path with a large size and no discontinuities allows stresses to build with almost no size restriction. However, a path with several irregularities and discontinuities allows the stress to build up within certain boundaries until the stresses reach a critical level and there is no room left for additional stresses and strains. Then, a releasing earthquake event is initiated at the weakest part of the fault system by breaking off the portions of the segments. Therefore, when referring to a possible rupture propagation path, it must be understood that a possible stress accumulation path is also being referred. Researchers have been studying this relatively new subject to understand the mechanisms of earthquake initiation and propagation (Kase and Kuge, 1998, Oglesby, 2005, Aochi et al., 2005).

The rupture propagation parameters are quite important since the size and location of the future earthquakes are dependent on the possible rupture paths due to the cycle of stress accumulation and releasing scheme. To explain it further in simple terms, the more faults form a family of faults that act together, the more they allow for the accumulation of slip and therefore stresses, so is the larger magnitudes of the earthquakes with the greater return periods. Several researchers, such as Harris et al. (1991), Harris and Day (1999), Cramer et al. (2000), Wesnousky (2006), Field (2007) studied the possible paths of propagation in the system of faults.

Because the size of the earthquake is related to the ruptured area, the segmentation studies provide very crucial information on how an earthquake progresses on the fault segments. The rupture propagation paths can be explained by studying the possible segmentation and rupturing mechanisms of a fault segment system. Therefore, identification of the segments, system of segments that could rupture in a single event, and the boundaries of the segment systems can be considered as the critical components for the seismic hazard analysis.

2.3.2.2. Rupture Propagation Paths and Termination Structures

The rupture propagation follows the weakest path that the energy of the rupture could flow without much resistance. Therefore, if there is a geological structure that could

stop the propagation, at that location the rupture energy could diminish rapidly. These structures are very easy to identify in most cases while a through study is required to model the stopping of the rupture propagation. The rupture propagation stopping structures or barriers are generally stepover structures that act as energy dampening or releasing zones between two near parallel faults that bend structures where the transfer of stresses to the next fault segment becomes very difficult due to the orientation of faults. Moreover, a gap between two aligned faults might also act as a barrier that dissipates the earthquake energy.

Figure 2.3 presents the types of barriers with the representation of the faults as lines, and the geometrical discontinuities between two neighboring faults as gaps and bends. The oncoming stresses are represented by σ_{max} , the angle between the oncoming stresses and the fault line is represented by ψ , the stepover distance between the two faults are shown as δ , and the bend angles between two continuous faults are given as α , and v_r represents the rupture propagation velocity.

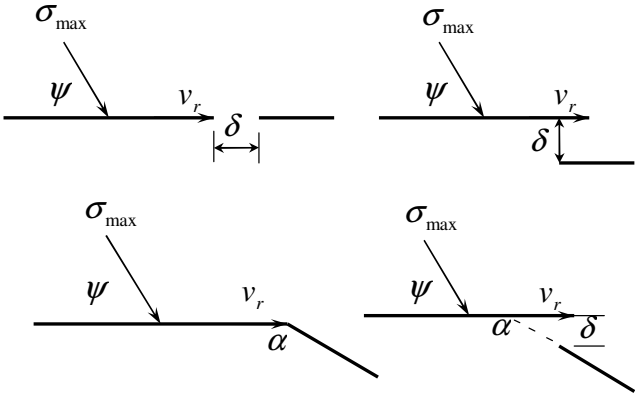


Figure 2.3 Types of Barriers That Block Earthquake Rupture Propagation (Upper Left is a Gap Structure, Upper Right is a Stepmover Structure, Lower Left is a Single Bend and Lower Right is a Combination Structure)

The stepover structures act in two different ways in stopping the rupture propagation, by either dampening the rupturing energy in a compression resisting zone, or by releasing the oncoming stress and energy in a tension dominated pull-apart basin where the energy is dissipated within the basin structure as shown in Figure 2.4.

The ability of a stepover structure to resist the oncoming stresses and energy during the rupture propagation depends on many factors. The magnitude of oncoming stresses, the size of the restraining or releasing stepover zone, the existence of

transfer fault structures within the resisting or releasing stepover zone, and the amount of directivity between the transferring and the transferred fault segments on either sides of the stepover zone influence the performance of the stepover zone.

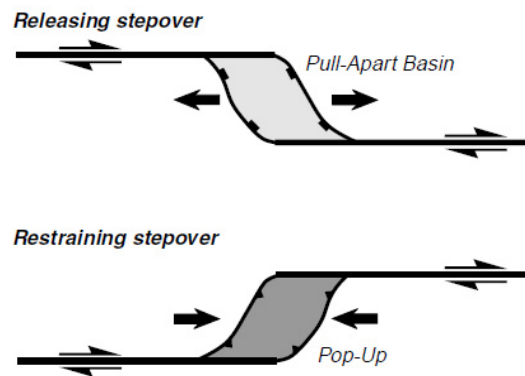


Figure 2.4. Two Types of Stepmover Structure: Releasing and Restraining Stepmovers in Strike-Slip Fault Systems (McClay and Bonora, 2001)

Rupture propagation sometimes encounters fault bends on its way which is either capable of stopping earthquakes or at least dampens the energy of earthquakes more than a continuing fault line. The bend structures as presented in Figure 2.5. Similar to the stepovers, bend structures have releasing and restraining types depending on the configuration of the bend and the oncoming stresses. King and Nabelek (1985) compiled eight earthquakes occurring between 1966 and 1985 for their rupture propagation behavior along the faults and studied the role of bend structures in stopping the rupture. They concluded that all earthquake energy is consumed between the bend structures. They assumed that the rupture could not propagate further when it encounters a bend structure, which was proven wrong by later studies.

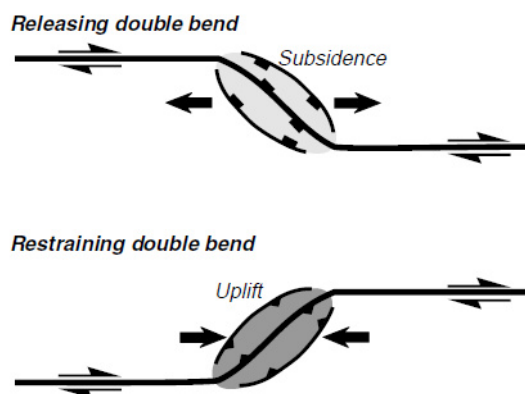


Figure 2.5. Two Types of Double Bend Structure: Releasing and Restraining Double Bends in Strike-Slip Fault Systems (McClay and Bonora, 2001)

As much as fault bends, the stepover structures are also capable of stopping rupture propagation. In fact, it is more difficult for a rupture propagation to jump to a parallel strand of a fault than propagating through a bend structure. A number of studies were initiated to investigate the role of gap structures in stopping the rupture. In one the significant studies, Wesnousky (2006) compiled a catalog of twenty earthquakes with rupture lengths of more than 15 km and with associated rupture maps, in order to analyze the properties of the rupture endpoints. He claimed that the minimum distance between the two parallel fault segments of a stepover structure that can successfully stop the rupture propagation, is 5 km. In a few theoretical studies about this distance, Harris et al. (1991) and Harris and Day (1999) also proposed 5 km as the minimum thickness of the stepover zone between the two parallel fault segments where a rupture propagation might be stopped. However, below 5 km, among the list of earthquakes they compiled; there are cases where the rupture propagation is successfully stopped by the stepover zone, which is a fact that could be explained by other variables of the rupture propagation.

2.4. Recurrence Models

Recurrence models are used to model the magnitude distribution and interval times of the consecutive earthquakes. Both area and fault sources are considered in developing these models. For area sources, mostly basic Gutenberg-Richter (GR) relationship and Poisson model are used for the magnitude and the timewise recurrences respectively. Indeed, for fault sources the magnitude recurrence models vary while Poisson model is generally employed for timewise recurrences due to the practicality and applicability reasons.

Though, the earthquake recurrence models claim a regular pattern of seismicity of the faults, due to several different sources of stress accumulation and the unforeseeable rupture patterns along the fault, it can be claimed that the occurrences could be quite unpredictable. However, there is a large amount of information accumulated in the literature about the recurrence models. It is also promising that with the accumulated data, the exact behavior of the faults could be modeled in the near future. In the mean time, there are already approved models, for the practical use.

As the accumulated information about the fault behavior proves, earthquake events show physical relatedness in their timing and magnitudes, and that this pattern is closely associated with the faults and not to the other seismic sources. The pattern of occurrences is modeled by considering the number of occurrences or by calculating the recurrence of earthquakes with magnitudes above certain values. The magnitude-recurrence relationship and time dependent pattern of behavior can be modeled respectively by using the aforementioned recurrence studies and in the following sections, detailed information is provided about the proposed recurrence models in the related studies.

2.4.1. Basic Magnitude-Recurrence Relationship

Earthquake magnitude and occurrence frequency relationship is valuable to model the seismic activity in an area. The annual number of earthquakes of various sizes that are assigned to each area source or a line source is defined by statistical distributions. Each seismic source is characterized by an earthquake probability distribution or magnitude-recurrence relationship obtained through the probability distribution of earthquake magnitudes.

The magnitude-recurrence relationship is based on relating the magnitude level m , to the total number of events with a magnitude equal to or greater than m . The magnitude-recurrence curve is usually simply presented by a straight line whose ordinate shows the logarithm of the number of earthquakes with a magnitude larger than certain size and whose abscissa shows the magnitude. The recurrence curve has a simple equation, which is generally called the GR magnitude frequency relationship:

$$\log(N(M)) = a - b(m) \quad (2.5)$$

where $N(m)$ represents the number of earthquakes with a magnitude equal or greater than m , a is the logarithm of the number of earthquakes of magnitude zero or greater which are expected to occur during the specified period of time. Moreover, in the equation, b is the slope of the curve, which indicates the proportion of large magnitude earthquakes to small magnitude earthquakes.

In seismic hazard analysis, a lower limit, m_0 , is defined for the minimum magnitude earthquake to be included in the analysis. The magnitude with no structural damage

capacity is usually chosen as the minimum magnitude. Although there is no clearly defined method for choosing the minimum magnitude, a value of $m_0=4.0$ is commonly applied in PSHA.

There is also an upper limit, m_{max} , for earthquake magnitude, generally chosen as equal to the maximum historical earthquake in the earthquake catalog of the region. If it is not applicable, the maximum magnitude is determined by the earthquake generation capacity of the largest fault in the close vicinity. Determination of m_{max} requires serious attention since it has a significant impact on the outcome of the PSHA. Both the values of a and b in equation 2.5 increase with increasing maximum magnitudes within a source zone. Therefore, this parameter should not be based only on recorded seismicity for the fault sources; rather the paleoseismic and historical records must also be evaluated to check whether the area experienced any larger magnitude earthquake before the recording started.

The validity and universality of the GR relationship is questioned by several researchers and as a result, linear, parabolic and bilinear relationships were proposed (Yucemen, 1982). Especially, larger magnitude earthquakes were investigated for their recurrence behavior, in terms of both periodicity and magnitude ranges. One of the challenging studies was conducted by Felzer (2007), who claimed the universality of the Gutenberg-Richter relationship based on both geophysical and statistical features. In her study, in order to test the universality of this relationship, the global catalog of earthquakes was compiled to derive the recurrence relationship for the period 1976-2005. However, while she concluded that there is a linear relationship for the smaller magnitudes, she emphasized the necessity to evaluate the large magnitude earthquakes separately due to the jaggedness of the recurrence relationship at large magnitudes.

In one of the significant studies that proposes different models for large magnitude recurrences, Wesnousky (1994) proposed a classical GR model and characteristic model as shown in Figure 2.6. While the relationship is linear for the smaller magnitude earthquakes, for the larger magnitude earthquakes the relationship exhibits a smoothly truncated behavior for GR model, and smoothly extruded behavior for the characteristic model.

The extruded part in Figure 2.6.b indicates that above certain magnitude, earthquakes occur more than projected by the linear part of the relationship. The reason why there is such a different pattern of occurrences is explained by an earthquake source that consistently generates such earthquakes more than any other magnitude. The physical background of the magnitude recurrences are explained in several studies and several models were proposed associated with the gathered information as provided in the following sections.

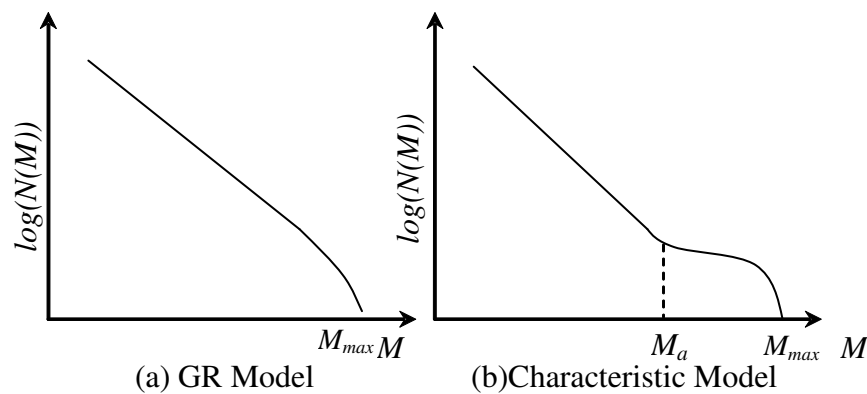


Figure 2.6. Characteristic and GR Model for Magnitude-Recurrence Relationships as Proposed by Wesnousky, 1994

2.4.2. Physical Recurrence Models for Fault Sources

Recurrence models for the fault sources originate from the theory that strain level required to break the rock is the basic requirement for a rupture initiation along a fault. In other words, the recurrence model relies on the periodicity of the accumulation of the strain energy that initiates the sudden release and break of the resisting rock structure. The periodicity, however, is a parameter that is related to the way a fault releases the accumulated strain. There are three models developed to model this behavior of the faults, as given in Figure 2.7. The first model shown in Figure 2.7 is called characteristic earthquake model, which is based on the idea that the amount of slip that causes an earthquake is always the same at each event. Therefore, there is a constant periodicity of slip accumulation and reoccurrence rate. The second basic principle of this model states that all the accumulated energy is released in a single event.

The second model is called time predictable model, which is in agreement with the yield threshold theory explained in Shimazaki and Nakata (1980). The time

predictable model agrees with the characteristic model in defining a threshold strain where the earthquake is initiated, but differs in how the accumulated energy is released. According to the model, there are several possible scenarios of how a strained fault releases energy. The third model, which is called total release model in Shimazaki and Nakata (1980) or slip predictable model, does not propose a certain threshold level as a prerequisite to trigger an event. According to the model when an event occurs, it releases all the strain energy accumulated at that time, whether it is too large for a characteristic event or too small for that specified fault. Time predictable and slip predictable models rely on the previous data and statistical models in order to predict the time interval for the next event while in the characteristic earthquake model; the time interval is accepted to be constant.

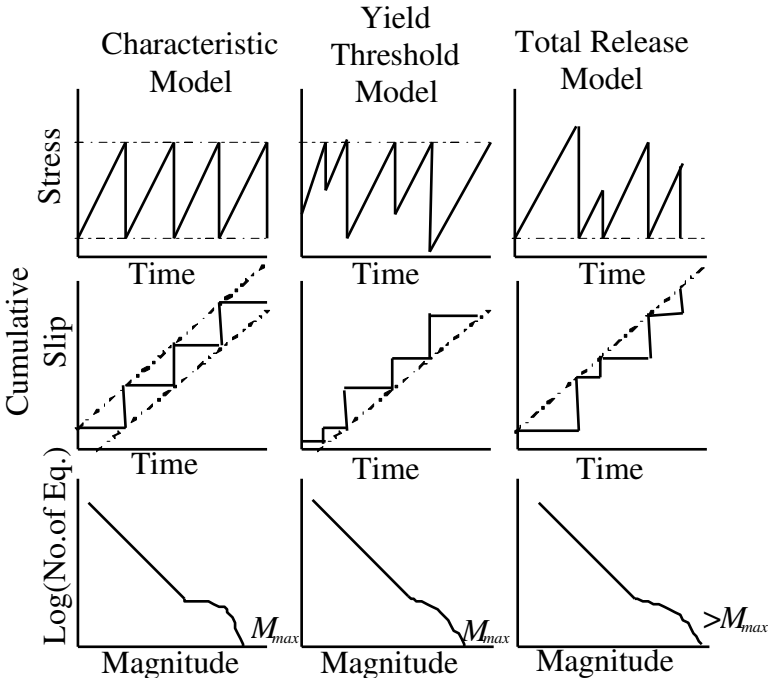


Figure 2.7. Earthquake Recurrence Models Modified from Shimazaki and Nakata (1980)

Table 2.2. The Rupture Length and Magnitude Relationship for Faults

Developer	Equation	Standard Deviation	Fault Type
WC,1984	$\log RL = -3.55 + 0.74M_w$	0.23	Strike-Slip
BML,1984	$\log RL = -4.10 + 0.80M_s$	0.33	Strike-Slip
WC,1984	$\log RL = -2.01 + 0.50M_w$	0.21	Normal
WC,1984	$\log RL = -3.22 + 0.69M_w$	0.22	All
BML,1984	$\log RL = -2.77 + 0.62M_s$	0.29	All

* WC, Wells and Coppersmith, 1984, BML, Bonilla et al., 1984

Among the recurrence models, the characteristic earthquake and yield-threshold model assumptions define a maximum strain level where the fault capacity is reached and the rupturing of the segment starts. Therefore, both models propose a limitation to the maximum magnitude for the earthquakes, which is the largest earthquake obtained from the catalogs increased by some margin. However, if the catalog is not long enough or not reliable enough, then the maximum magnitude is obtained from the rupture length of the fault by the following formula:

$$M = a + b \log RL \quad (2.6)$$

where a and b are the coefficients obtained statistically from the empirical data, M is the magnitude and RL is the rupture length. Various researchers developed this relationship as listed in Table 2.2, which was developed according to the fault types. All the equations are valid for all the faults since the database used in the development of the equation included all the faults from around the world.

2.4.2.1. Characteristic Earthquake Model

According to the characteristic earthquake model, the empirical relationship results in maximum magnitudes of m_1 given the length of the fault. For those values closer to m_1 , an earthquake occurrence model was developed by Schwartz and Coppersmith (1984). Later, Youngs and Coppersmith (1985) derived a density function specifically considering the large magnitudes. In this model, magnitudes are assumed to be exponentially distributed up to the magnitude level $(m_1 - \Delta m_c)$ as shown in Figure 2.8. Above this magnitude, the characteristic earthquakes display a uniform distribution between $(m_1 - \Delta m_c)$ and m_1 , as seen in Figure 2.8.

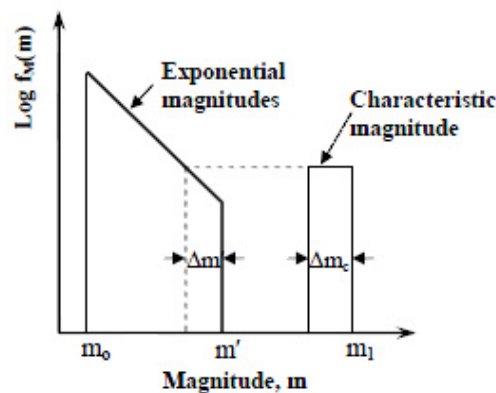


Figure 2.8. Characteristic Earthquake Model Proposed by Youngs and Coppersmith (1985)

Between m_0 and $(m_I - \Delta m_c)$, the coefficients of the equation that models the exponential distribution must be calculated by using the appropriate method, as shown in equation 2.5. After obtaining the coefficients of a and b the values must be evaluated for any discrepancies in source delineation by considering the amount of data used to derive these constants. Since the return periods of characteristic earthquakes with a magnitude greater than $(m_I - \Delta m_c)$ are very large, these earthquakes need special attention.

There are a few models developed for practical purposes within the main model. The simplest form of this model, called the pure characteristic model, uses a single magnitude for the characteristic earthquake. The full characteristic model assumes only large magnitude earthquakes but within an interval generally set between $(m_I - \Delta m_c)$ and m_I .

Considering that there is a lack of information in the catalogs for characteristic earthquakes, both paleo-seismological information about historical earthquake records and the physical relationship of earthquake occurrences and fault length and geometry must be utilized.

The activity rates of the characteristic earthquake generating faults are difficult to obtain because generally, the length of available earthquake catalog is not long enough to predict the frequency of characteristic earthquakes and most of the time paleo-seismicity data is not available for the faults. Consequently, the basic equation about the seismic moment and moment release rates are used to obtain the activity rates. Seismic moment, first introduced by Aki (1966), describes the size of an earthquake with static fault parameters as follows:

$$M_0 = \mu AD \quad (2.7)$$

where M_0 is the seismic moment, μ is the shear modulus or rigidity of the crustal plate, usually taken as 3.0×10^{11} dyne/cm², A is the area of rupture surface, and D is the average displacement of the fault slip. The variables are associated with the slip rate of the fault through the derivation of the above formula with respect to time:

$$M'_0 = \mu AS \quad (2.8)$$

where M'_0 is the seismic moment rate and S is the slip rate. The seismic moment can be obtained through moment magnitude, M_w , from the relation given by Hanks and Kanamori (1979)

$$M_w = 2/3 \log M_0 - 10.70 \quad (2.9)$$

by rewriting the above equation, seismic moment is obtained as

$$\log_{10}(M_0) = 1.5M_w + 16.05 \quad (2.10)$$

and the number of earthquakes above a minimum magnitude becomes

$$N(M_{min}) = \mu AS / \text{mean}(M_0/\text{earthquake}) \quad (2.11)$$

and the activity rate of faults will be

$$v_M = \frac{M'_0}{M_0} = \frac{\mu AS}{10^{1.5M_w + 16.05}} \quad (2.12)$$

The return interval of the characteristic earthquake is accepted as constant according to the above calculations. In the applications, when pure characteristic model of full characteristic model is employed the activity rates are accepted as constant and the rates are generally obtained by expert opinion if there is not a reliable source of information on the slip rates and other fault parameters.

2.4.2.2. Total Release or Average Slip Predictable Model

The average slip predictable model relies on the idea that earthquake occurrence is dependent on the sufficient moment accumulation and the conditions of the fault segment or multiple segments since the occurrence date of the last earthquake.

The next possible event on a fault segment is estimated by including the initial condition of the fault in terms of stresses and strains and by introducing the date of the last event. The accumulated stresses already built up in the segment, the slip rate, the area of the segment, which is exposed to the slip, and the shear modulus that is accepted as constant throughout the segment are employed. The time of occurrence of the next event is best approximated by the equation

$$M_0 = \mu \sum_{t=0}^n v_i A_i (t - t_{o_i}) \quad (2.13)$$

where μ is the shear modulus, v_i is the slip rate, A_i is the area of the segment sections involved in the rupture, \bar{t} is the best estimate time of next occurrence of the event, and t_{0_i} is the date of the last event. Rewriting the equation 2.13 in order to find the next time of occurrence, yields equations 2.14 to 2.17 (WGCEP, 2006).

$$\bar{t} = \frac{M_0 + \mu \sum_{ii=0}^n v_i A_i t_{0_i}}{\mu \sum_{i=0}^n v_i A_i} \quad (2.14)$$

or

$$\bar{t} = \Delta \bar{t} + \bar{t}_0 \quad (2.15)$$

where

$$\Delta \bar{t} = \frac{M_0}{\mu \sum_{i=0}^n v_i A_i} \quad (2.16)$$

and

$$\bar{t}_0 = \frac{\sum_{ii=0}^n v_i A_i t_{0_i}}{\sum_{i=0}^n v_i A_i} \quad (2.17)$$

where $\Delta \bar{t}$ is the time needed to accumulate the required moment and \bar{t}_0 is the weighted average time of the events. The periodicity derived from the above equations does not imply that the model is strictly characteristic; in fact, there are no assumptions for the definite rupture boundaries. Therefore, the multiple segment ruptures can be analyzed by using the above equations (WGCEP, 2006).

The magnitude recurrence rates can be statistically derived for this model, but obviously, a normal distribution is expected at the larger magnitudes since the nature of the occurrences are statistically distributed as the equations 2.14 to 2.17 suggest.

2.4.2.3. Yield Threshold or Average Time-Predictable Model

The average time predictable model is developed to consider the release and restrain produced by the last event, in addition to the strain already built up in the individual

segments. This model considers the fact that there are additional strains developed within a segment due to events occurring in neighboring fault segments as well. The time of the next event is calculated as follows:

$$t_i = \frac{D_i}{v_i} + t_{0_i} \quad (2.18)$$

where t_i is the best estimate of next occurrence of the event, D_i is the total slip caused by the event in the neighboring segment, v_i is the slip rate, and t_{0_i} is the date of the last event. If multiple segment rupture is assumed, a weighted average of t_i for each segment is then calculated by (WGCEP, 2006)

$$\hat{t} = \frac{\sum_{i=0}^n A_i \left(\frac{D_i}{v_i} + t_{0_i} \right)}{\sum_{i=0}^n A_i} \quad (2.19)$$

or

$$\hat{t} = \Delta \hat{t} + \hat{t}_0 \quad (2.20)$$

where

$$\Delta \hat{t} = \frac{\sum_{i=0}^n A_i \frac{D_i}{v_i}}{\sum_{i=0}^n A_i} \quad (2.21)$$

and

$$\hat{t}_0 = \frac{\sum_{i=0}^n A_i t_{0_i}}{\sum_{i=0}^n A_i} \quad (2.22)$$

where, D_i is the slip caused an event in the neighboring segment, v_i is the slip rate, A_i is the area of the segment sections involved in the rupture, \hat{t} is the best estimate of next occurrence of the event, and t_{0_i} is the date of the last event. The last two models differ in handling the initial stresses and strains while they build up with time due to a constant slip on each segment (WGCEP, 2006). The magnitude distribution

is similar to the average slip predictable model as a normal distribution is expected at the larger magnitudes.

2.4.3. Statistical Recurrence Models

The physical magnitude and timewise recurrence relationships are investigated in detail by providing the physical background information about the earthquake generation and the pattern of occurrences with respect to magnitudes and time. There is another recurrence character of earthquake events, which is based on statistical distribution of recurrences in the time dimension. The recurrence models of the earthquakes in time, or simply called renewal models provide the statistical estimation of the time of a future event. Knowing the timing of the future earthquake is as important as knowing the magnitude of the future event, so renewal models are as important as magnitude-recurrence models for a probabilistic seismic hazard analysis.

The most commonly applied renewal model that was developed to model the periodicity of the earthquake events is the Poisson model. For an area or a fault source, earthquake occurrences can be assumed to follow the Poisson model. The Poisson process model provides the probabilities of earthquake occurrences of any magnitude. The basic principle of this model is the assumption that the earthquake occurrences are independent from each other.

If the probability of occurrence of an event is independent from other event occurrences in terms of time and magnitude, then it can be concluded that the event occurrences have no memory and have no dependence to the previous events. Therefore, Poisson model can be utilized to model the occurrence of such events. While the claim of independence of earthquake events is generally in agreement with the observed seismic activity related to moderate and large magnitude earthquakes, temporal dependence is observed in several seismic regions, which raised the issue of correlation among seismic events. The observed correlation is explained by the proportionality of the size of preceding events and the periodicity of the events with similar magnitudes.

The physical interpretation of the time predictability originated from the fact that an earthquake ruptures either the entire segment or some part of the segment of the fault. The rupture of the segment causes the release of the energy accumulated along

the fault segment. Therefore, the process of accumulating strain energy continues until the next earthquake occurs. The cycle of accumulating and releasing the strain energy naturally has a periodicity, whether it is quasi-periodical or perfectly periodical.

Consequently, if an earthquake occurs along a fault segment that initiates the cycle of accumulating energy, the possibility of another earthquake is less likely on the same fault segment than the other fault segment, which is late in its cycle of accumulating energy. In other words, the probability of an earthquake increases with the time elapsed since the last earthquake (Thenhaus and Campbell, 2003). Though the pattern of earthquake occurrences can be explained in physical terms, due to the unknowns and uncertainties involved, the occurrence of the next earthquake event is very hard to predict. Therefore, statistical models are developed in order to model the temporal dependency of the recurrences. The temporal dependency is taken into consideration by the following conditional probability distribution function of inter-event times. The conditional probability $P(t < T \leq t + \Delta t | T > t)$, which is the probability that an earthquake occurs during the next Δt interval given that it has not occurred until time t , is

$$P(\Delta t | t) = \frac{P(t < T \leq t + \Delta t)}{P(T \geq t)} \quad (2.26)$$

in terms of the probability density of T

$$P(t < T \leq t + \Delta t) = \int_t^{t+\Delta t} f(z) dz \quad (2.27)$$

$$P(T \geq t) = \int_t^{\infty} f(z) dz \quad (2.28)$$

then substituting the equations (2.27) and (2.28) the following equation

$$P(\Delta t | t) = \frac{\int_t^{t+\Delta t} f(z) dz}{\int_t^{\infty} f(z) dz} \quad (2.29)$$

is obtained. There are several different probability density models for the distribution

of interarrival times, Δt , such as Gamma, Weibull, and Brownian Passage Time, lognormal and exponential models. Unfortunately, these models require inputs that can only be obtained by expert opinion in almost all cases.

2.4.4. Statistical Recurrence Models for Both Time and Magnitude

Earthquakes have a defined repetition cycle in time and in magnitude according to both the time and slip predictable models. As the size of the earthquake increases, the time to accumulate enough strain is longer and the amount of slip that has to accumulate is greater than that of smaller size earthquakes. Therefore, the time required for a larger earthquake is longer than that of a smaller size earthquake. However, the relationship between the required time and the magnitude of the event might vary from one source to the other depending on the geometry, the loading and unloading pattern of the fault source, the slip rates, stress accumulation paths, and closer triggering sources.

A study conducted by Papazachos and Papaioannou (1993), resulted with a time and magnitude predictable seismicity model developed for a system of faults. This relation of magnitudes and repeat time is defined with the equation

$$\log T = cM_p + a \quad (2.30)$$

where T is the repeat time, c is the slope of the magnitude time interval curve obtained statistically, and a is the constant depending on the source characteristics.

The time and magnitude recurrences of faults and the physical explanations of the recurrence character of the faults are summarized in the preceding sections. The available mathematical models are also provided to quantify the probabilities, the recurrence rates and other quantities. However, there is not enough evidence to show the advantages of one theory over the other due to the lack of enough information about past seismic activity. In addition, there is lack of sufficient physical knowledge that explains the behavior of faults. Despite the fact that no method has been proven to be correct, some of the above procedures are already in practical use due to the necessities and especially expert opinion remains as a very crucial input in the determination of fault specific hazard rates.

2.4.5. Recurrences Based on Geodetic Measurement of Fault Slip Rates

The recurrence rate for a fault largely depends on the stress-strain release mechanism of the fault. The slip along a fault causes the accumulation of stresses. The slip rate of a fault, whether a normal displacement in a normal fault or a lateral displacement of a strike-slip fault, is one of the major indicators of the seismic activity of the considered fault. The constant slip due to interaction of neighboring plates eventually accumulates to a level where the plates are not able to attain the strains further and break, which causes an earthquake event.

Many slip rate estimations are performed especially for the North Anatolian Fault (NAF) system, by using relative displacements or offsets of the geological structures. Barka (1996), Hubert-Ferrari et al. (2002) and Kozacı et al. (2007) conducted slip rate measurement by offset observations of geological structures, such as river valleys and terraces along NAF. Hubert-Ferrari et al. (2002) focused on the total offsets in the river creeks and their study concluded with an estimation of 18 ± 5 mm/year slip rate interpreted by 200 ± 20 m overall offset observation along NAF. Combined with the geodetic measurements, the resultant slip rates from evaluating the relative movement of geological markers provide a more meaningful slip rate for the whole section.

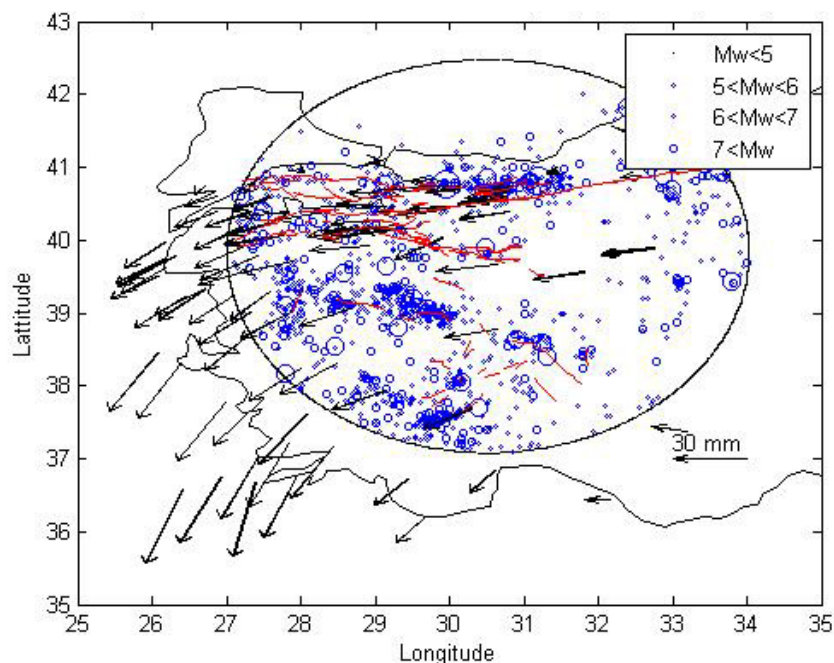


Figure 2.9. Slip Rates of West Anatolia by McClusky et al. (2000) with a Fixed Eurasian Frame (Reproduced and Modified from McClusky et al., 2000)

Oral (1994) conducted a PhD. study on the kinematics of the Anatolian plate and neighboring plate movements through GPS velocity measurements. He obtained a 25 ± 8 mm/yr motion across NAF, and 49 ± 8 mm/yr convergence rate of African and Anatolian plates south of Peloponnese. Straub and Kahle (1994) and Straub (1996) worked on the Marmara Sea region to detect the crustal deformation and infer the strain accumulation in the region. They found that the two western branches of NAF, namely Karamursel-Sapanca and Iznik-Geyve sections have slip rates of 16 mm/yr and 9 mm/yr, respectively.

McClusky et al. (2000) conducted GPS measurements in Western Turkey and the Aegean Sea by using 200 stations over the period covering 1988-1997 with a fixed reference of Eurasian plate, as seen in Figure 2.9. They adopted GPS Euler vectors in order to smear the relative plate motions on the main fault traces while performing the slip rate measurements along the main fault traces. They estimated a 24 ± 1 mm/yr slip on NAF and the smearing of all relative plate motion on the main fault system was justified by the focal mechanisms of the major earthquakes along the fault. According to their study, there is no significant off fault deformation along the western and central sections of NAF. In addition, Western Turkey is extending in north-south direction and central Anatolia is moving with less than 2 mm/yr in alignment with NAF and East Anatolian Fault (EAF).

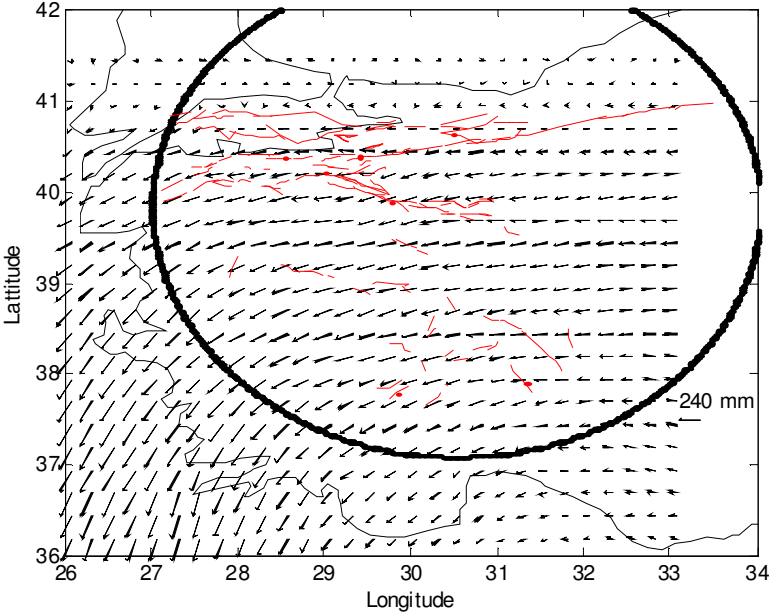


Figure 2.10. Smeared Slip Rates of West Anatolia by Kriging Method with a Fixed Eurasian Frame (Based on McClusky, 2000)

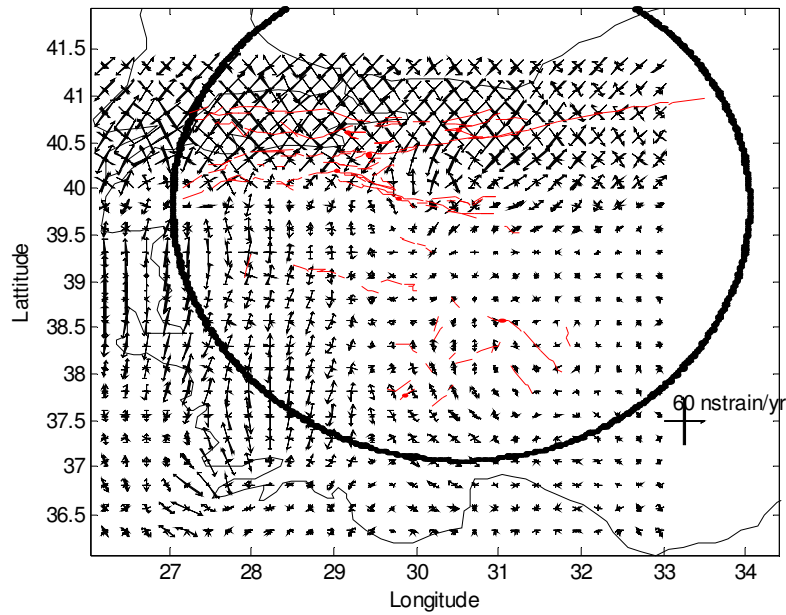


Figure 2.11. Smeared Principal Strain Rates of West Anatolia by Kriging Method with a Fixed Eurasian Frame (Based on McClusky, 2000)

Figures 2.10, 2.11 and 2.12 are generated by using the displacement vectors of McClusky et al. (2000). In the figures, the strain, slip rates and dilatational strain contour maps are presented.

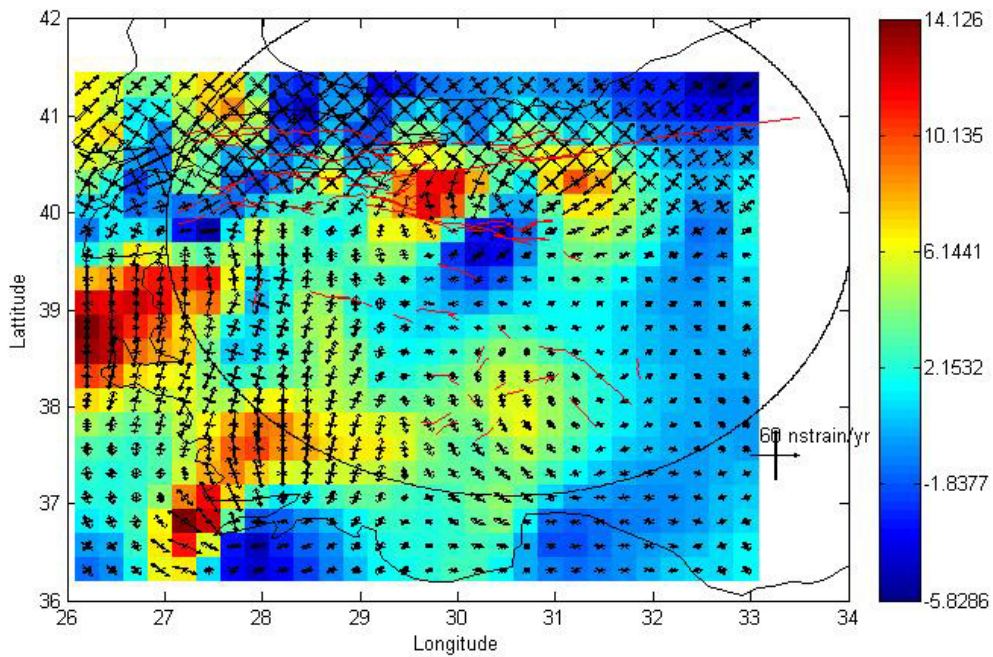


Figure 2.12. Smeared Principal Strain Rates (With Color Codes of Dilatation) of West Anatolia by Kriging Method with a Fixed Eurasian Frame (Based on McClusky, 2000)

Ayhan et al. (2002) compiled the measurements from 136 stations for the period between 1992-1999 and for the region bounded by latitudes between 38° and 42°

north and longitudes between 26^0 and 33^0 east, as seen in Figure 2.13. Their measurement shows varying slip rates along NAF, with 26 mm/yr under the Marmara Sea, 13 mm/yr in the Gulf of Izmit, 11 mm/yr near Izmit, 17 mm/yr near Sapanca Lake, 20 mm/yr in the Duzce Fault, and 17 mm/yr in the Bolu–Gerede area.

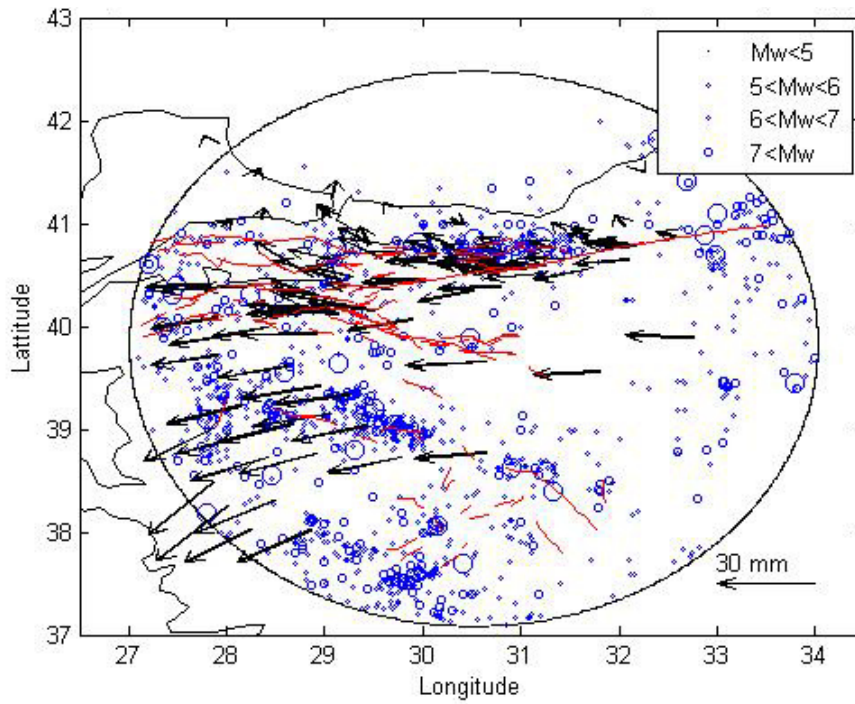


Figure 2.13. Slip Rates of West Anatolia with a Fixed Eurasian Frame (Reproduced and Modified from Ayhan et al. (2002))

Nyst and Thatcher (2004) conducted GPS measurements focusing on entire Greece, Aegean Sea, and Western Anatolia with measurements as early as 1988 and as recent as 2001. The measurements were performed by using 374 stations and by taking a fixed Eurasian frame like its predecessors. According to their measurements, the northern and southern branches of NAF in south Marmara Sea moves 23 mm/yr in pure right lateral strike-slip mode, 11 mm/yr in oblique extension in the southeast of the Sea of Marmara, and 5 mm/yr strike-slip motion on the border of Aegean Sea.

Flerit et al. (2004) investigated the interaction between the western propagating NAF and extending Aegean Sea. To serve the purpose of their study, GPS measurements were performed by taking the Anatolian plate as a fixed reference. As presented in Figure 2.14, the extension pattern of the faults in Western Anatolia with respect to Anatolian plate shows a consistent behavior. The opening in the graben structures in Western Anatolia reaches 8 mm/yr in the western tip and reduces towards the inland.

Reilinger et al. (2006) conducted measurements similar to those of McClusky et al. (2000) as a part of an international project covering a very wide region including the whole Middle East and Eastern Mediterranean in an attempt to update the previous measurements. The measurements were performed between 1988 and 2005 with 440 GPS stations. According to the project, NAF has a slip rate of 24 ± 1 mm/yr.

For Eskisehir, the available GPS data suggests the movement of the Central Anatolian plate with 2 mm/yr according to Reilinger et al. (1997) and McClusky et al. (2000). According to Kahle et al. (1998), the Eskisehir Fault Zone (EFZ) extends closer to Bursa and almost no extension or contraction occurs near Eskisehir. Altunel and Barka (1998) claimed a 1-2 mm/yr movement for the Eskisehir fault zone. Kocyigit et al. (2003) observed a 0.07-0.13 mm/yr extensional slip rate according to field measurements. Due to both the selection of different references for strain rate fields and quantification methods of inter-seismic velocity field, there are discrepancies among the measurements of the researchers. However, with the correction of frame references and derivation of the net slip rates and supporting field measurements, more accurate slip rates can be obtained.

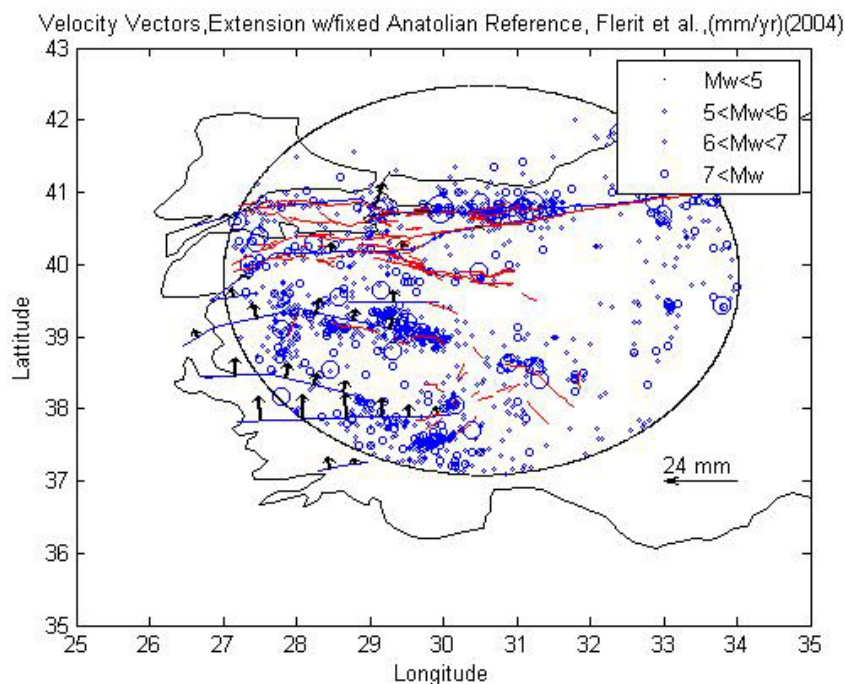


Figure 2.14. Slip Rates of West Anatolia with a Fixed Anatolian Frame; Rates Shown are Normal to the Measurement Axis (Reproduced and Modified from Flerit et al. (2004))

2.5. Data Compilation for Seismic Hazard Analysis

The seismic hazard analysis should be conducted with a serious attention from the selection of the methods to the gathering and processing the raw data. There are inherent uncertainties of the data arising from the incompleteness issues and homogeneity of the catalogs, the magnitude conversion problems, and the assignment of fault parameters. Especially for the fault parameter assignments, certain assumptions and expert opinions are generally used in order to obtain the data. The GMPEs also creates additional uncertainty in the seismic hazard analysis. However, with a probabilistic approach, all of the uncertainties arising from each of the single element of seismic hazard analysis could be modeled and reflected to the results.

2.5.1. Choosing the Catalogue Sources Available for Turkey

One of the first steps in performing PSHA, the compilation of the past seismic activity data, is important in modeling the earthquake occurrences. The seismic activity data, or technically called earthquake catalogues, are crucial sources of seismic activity.

The seismic activity in Anatolia has been documented by researchers since Ergin et al. (1967) who first published the catalog going back as far as 2000 years. Following them, researchers created several catalogs about seismic activity in Turkey. Five large data sets are available for the historical earthquake data of Anatolia. These are provided by the General Directorate of Disaster Affairs of Turkey (GDDA), Kandilli Observatory and Earthquake Research Institute of the Bogazici University (KOERI), International Seismological Centre (ISC), International Seismology Summary (ISS), and the United States Geological Survey (USGS). Among the sources listed above, KOERI of the Bogazici University compiled a catalog covering the period starting from 1900 until today. This catalog includes all of the earthquakes with magnitudes of 3.0 and larger that occurred in Turkey and its surroundings within the region bounded by 32° - 45° north latitudes and 23° - 48° east longitudes. Currently, in the catalog, the number of earthquakes with magnitudes larger than $M \geq 3.0$ is about ~42000 . In addition to the sources listed, Tan et al. (2008) compiled a complete catalog that consists of two datasets. The first one is titled as ‘The historical earthquake catalogue of Turkey’, which includes the earthquakes that occurred

between 2100 B.C. and 1963 A.D. The second dataset is named as ‘The Focal Mechanism Solutions Catalogue of Turkey’ and includes the fault parameters of the destructive earthquakes, which occurred between 1938 and 2004.

These catalogs use different magnitude scales, cover different periods, and keep records of earthquakes with different magnitude ranges. Therefore, to evaluate all the information offered by these different catalogs, a few procedures must be applied to create a uniform database of seismic activity. The main drawback of compiling a unified catalog is the variety of the magnitude scales that are used in keeping the records, such as moment magnitude (M_w), body wave magnitude (M_b), duration magnitude (M_d), local magnitude (M_l), and surface wave magnitude (M_s).

In order to create a catalog with a single magnitude scale, a homogenization is required. Homogenization is performed through magnitude conversion equations that are suitable for the catalog data. After the homogenization, declustering of the catalog is required to remove the secondary or foreshock and aftershock events from the catalogue. These events are removed by using time and space windows. Then, the catalog is subjected to a completeness test and the incomplete parts of the catalog are completed artificially to obtain a homogeneous and complete catalog both in various magnitude and time ranges.

2.5.1.1. Magnitude Conversion

While collecting the catalog data and evaluating for the applicability, the first issue always become the magnitude conversion problem. Consequently, a set of conversion equations are sought which best suits the Turkish catalog data. Amongst the latest works performed on the conversion relationships, Deniz and Yucemen (2008) provided the set of equations that were developed by using a large amount of local data as follows:

$$\begin{aligned}
 M_w &= 2.25M_b - 6.14 \\
 M_w &= 1.27M_d - 1.12 \\
 M_w &= 1.57M_l - 2.66 \\
 M_w &= 0.54M_s + 2.81
 \end{aligned}
 \tag{2.31}$$

These conversion equations are adopted in this study to convert magnitudes recorded in different scales to the moment magnitude scale.

2.5.1.2. Catalogue Declustering

In PSHA, earthquake occurrence can be modeled by using the Poisson model. Since this model assumes independence between earthquake events, secondary events, i.e. foreshocks and aftershocks, should be removed from the earthquake catalog. A number of methods have been developed to obtain the extent of secondary event sequences within a cluster, with respect to the spatial or temporal, or both domains. Several researchers (Stepp, 1973, Gardner and Knopoff, 1974, Savage and Rupp, 2000, Kagan, 2002) used different time and space windows to arrive at a final catalog that is composed of only the main shocks.

Deniz (2006) studied the most common spatial and temporal windows with the Turkish data in order to arrive at a conservative and reasonable time and space window special to Turkey. He proposed a set of spatial windows that envelope the maximum of all the values from Stepp (1973), Gardner and Knopoff (1974), Savage and Rupp (2000) and Kagan (2002) and developed temporal windows by averaging the established temporal windows that were suggested by Gardner and Knopoff (1974), and Savage and Rupp (2000).

**Table 2.3. Space and Time Windows to Identify Secondary Events
(After Deniz, 2006)**

Moment Magnitude (M_w)	Width of Space Window (km)	Width of Time Window (Days)
4.5	35.50	42
5.0	44.50	83
5.5	52.50	155
6.0	63.00	290
6.5	79.40	510
7.0	100.00	790
7.5	125.90	1326
8.0	151.40	2471

In this study, time and space windows proposed by Deniz (2006) will be used. The windows that are given in Table 2.3 are created for earthquakes with moment magnitudes equal or greater than 4.5. For those values that are not listed in Table 2.3, a linear interpolation for space, and log-linear interpolation for the temporal values are utilized.

2.5.1.3. Completeness Tests

The issue of catalogue completeness is a subjective matter based on the requirements of the seismic hazard analysis. In fact, if the complete parts of the catalogs are sufficient for a reliable seismic hazard analysis, then a completion analysis is not required. In other words, the necessity for a longer period of coverage of earthquake activity within the required range of magnitudes is the main motivation of the completion procedure. The required range is determined by selecting the minimum magnitude to be included in the compiled database for seismic hazard analysis. Generally, in engineering applications, the magnitude of an earthquake that has a potential of inflicting damage to the structures is accepted as the minimum magnitude to be included in a seismic hazard analysis. This magnitude is commonly accepted as 4.0 in moment magnitude in practical applications and it is set as the minimum magnitude in this study as well.

The importance of the completion of an incomplete catalog originates from the fact that the result of a seismic hazard analysis is highly dependent on the coefficients of exponential distribution of magnitude of earthquakes. In other words, completeness of the catalog is one of the most crucial subjects of the seismic hazard estimation due to its determining effect on the b values given in equation 2.5.

Among the available completeness tests proposed by Stepp (1973), the entire magnitude range method by Ogata and Katsura (1993), the maximum curvature method and goodness-of-fit test by Weimar and Wyss (2000), and the method proposed by Cao and Gao (2002) are evaluated. After the evaluation, the method proposed by Stepp (1973) is found to be the most suitable and satisfactory for the requirements of this study. Based on the study of Stepp (1973), which depends on the division of the catalog into periods, the statistics of the mean rate per unit time is utilized. Given that earthquake activity is accepted to follow Poisson distribution, the mean rate and variance must remain the same throughout the considered time. If the sample unit time interval is accepted as one, then the mean rate can be calculated as

$$\lambda = \frac{1}{T} \sum_{i=1}^n k_i \quad (2.32)$$

where λ is the mean rate of occurrences, T is the sample length in time, and k

represents the individual occurrence of earthquakes. Since the mean rate is accepted as constant, the standard deviation of the mean must be proportional to the inverse square root of the sample time as in the following equation:

$$\sigma = \sqrt{\frac{\lambda}{T}} \quad (2.33)$$

Therefore, if the time intervals are established short enough to capture the incomplete intervals, and the sample length of the time is long enough to have a stable mean rate, it is more probable to spot the departure of standard deviation from $1/\sqrt{T}$ as the time interval becomes longer starting from the latest date considered. The intervals until the observed departure of standard deviation from $1/\sqrt{T}$ are considered as complete and the rest of the intervals are considered as incomplete.

After finding the incomplete intervals, the completion of the catalogue is performed by means of simple arithmetic until the standard deviation of the mean rate aligns with $1/\sqrt{T}$ together with the complete parts.

2.5.2. Determination of Faults and Their Parameters

The identification of fault sources, especially locating the active faults and the activity rate calculations is mostly questionable and sometimes very subjective. The fault location, geometry, structural properties and the past activities are generally not exactly known in a seismic hazard analysis. Despite the difficulty in the determining of fault parameters, the behavior of the faults is modeled by using the known theories, the observed measurements on the faults and past earthquake activities.

By looking at the past earthquake data, it is suggested that earthquakes that are greater than a certain magnitude level are only generated by large faults and fault segments. It should not imply that smaller size earthquakes are not generated by the same faults. Moreover, if no large magnitude earthquakes have occurred on the existing fault line, it does not mean that there will not be such an event on that fault.

For the purpose of determination of the seismic hazard, each fault is associated with a maximum magnitude earthquake according to its capacity. Moreover, range of earthquake magnitudes is associated with each fault that is capable of producing such earthquakes in that range. In that case, the activity rates are taken into consideration

to classify the faults according to the contribution to the overall seismic hazard.

In addition, if significant seismic activity is observed at locations where there are no large faults or fault segments, then it suggests that there are faults yet unknown or there are other types of sources causing these events. These events are generally modeled by using the background seismicity model or within areal sources.

2.5.2.1. Evaluation of Earthquake Recurrences Models of Faults

In an attempt to evaluate the proposed methods, Table 2.4 was created to list the significant models that claim to describe the fault behavior. Unfortunately, all of these models at times align and occasionally contradict with the observed events.

As for the characteristic earthquake model assumption, it is very strict and straightforward in the definition of the recurrence rate of fault ruptures, which makes the model very simple and easy to use. However, the assumption of a full stress restoration of a fault segment and full discharge of the stresses on the same fault segment at each event is not consistent with the observed events. Such as, after the Izmit earthquake, it was observed that there was a rupture of 125 km on the surface, which indicates the involvement of five different segments, which is contrary to the assumptions of the model.

While the characteristic model is accepted as a satisfactory model with the introduction of the limitation on the magnitude of the earthquake generated by a fault segment, the periodicity of earthquakes still needs to be studied by the available catalog data. The charge and discharge rates of fault segments must be known and they must be compared with the slip rates of each segment or with the available moment rates of faults. The slip rate dependency of the earthquake recurrence rates is modeled by the average slip predictable model. In the establishment of the model, it is assumed that if the last occurrence of the event and the average slip of each segment are known, the next possible event might also be estimated by using equations 2.13 to 2.17. It is very similar to the characteristic earthquake model, however, multiple segment ruptures are allowed in this model, and inclusion of the slip rate provides more rational basis for the calculation of the next event.

The characteristic earthquake and slip-predictable models do not take into account the initial stresses and strains that are induced by a closer event that ruptures a

neighboring segment. In addition, in both models, it is assumed that all the strain is released by the last event, therefore strain built-up starts with the last event with a depleted fault segment in terms of stresses and strains.

While studies already provided enough evidence that the initial stresses are not only dependent on how much of the total accumulated stress is released in the last earthquake, but the activities of the neighboring segments that cause further additional stresses in the segment of interest. Considering the additional stresses that are induced by the seismic activity of the neighboring segments and by introducing the initial stresses in the prediction of the recurrence rates, the average time predictable model is proposed. The inclusion of the initial stresses improves the estimation capability of the model.

The method using the balanced moment rates is proposed to consider the relative contribution of different segments to the overall seismic moment that initiated the earthquake. The different geometry, slip rates, and stress accumulation in different segments in a multi-segment rupture must be considered and a contribution factor for each fault segment must be derived in alignment with the total slip and magnitude of the earthquake. The main issue with this method is the lack of a consistent procedure to derive the balancing constants, especially the requirement of expert opinion for weight of each fault for each event is very subjective and open to criticism.

Table 2.4. Recurrence Rates for Fault Sources Developed by Various Researchers

Model	Advantages	Disadvantages
Characteristic Model	Easy and practical	Limited to single segments and full recharge and discharge of segment is proposed
Average Slip Predictable Model	More realistic in explaining some of the events	Cannot explain recurrence of similar events and triggering effect
Average Time Predictable Model	More realistic in explaining some of the events	Cannot explain recurrence of similar events and triggering effect
Balance of Moments Method	Almost all of the events can be explained with this model	Subjective weights must be assigned to different segments
Segmental Recurrence Rate Derivation	Easy applicability	Many events cannot be explained by this model

According to the balanced moment rate method, the assignment of specific moment rate to each contributing fault segment is required in order to distinguish the contribution of each fault segment to the overall moment that initiated the earthquake. A fault segment might generate smaller earthquakes than a neighboring segment due to the associated slip rate, length, and other geological features. Therefore, while the accumulation of strain on the different segments is distinguished, the release mechanisms of different segments must also be considered. The method is intuitively generated and it claims to model the magnitude of any event by the assignment of different weights to the fault segments that play a role in the generation of a large event. However, it is still far from proven as a fact.

As one of the drawbacks in the modeling of earthquake recurrences, while the recurrence rates of smaller magnitudes are available for several segments on the famous fault systems in the world, catalogs still lack the data for events with large magnitudes. As a result of that, unfortunately the larger magnitude part of the recurrence relationship cannot be precisely modeled. In addition, the pattern of the large magnitude earthquake occurrences of a fault segment might be very different from the smaller magnitude earthquake occurrences and could change from one fault segment to another.

In conclusion, it seems that although different models try to explain fault behavior, they still lack the validation, which could only be performed by the comparison of the modeled behavior with the real fault behavior. Moreover, many other factors influence the fault behavior. Among these factors, the directivity of the strain accumulation, additional normal stresses that build up in almost all cases, stepover or bend structures that help to release the part of the seismic moment should be mentioned. In many cases, though the rupture propagation is blocked by stepover or bend structures, slip resistance decays due to the age, and activity rates of the faults should be considered as a factor that influence the fault behavior. Moreover, possible earthquake locations due to excessive stress accumulation at certain barrier structures are not mentioned at all in any of the models. Finally, the different dipping angles at neighboring segments that would create another obstacle in strain accumulation and releasing scheme are not considered at all.

With all the complexities involved in fault behavior modeling, due to practical reasons and applicability issues, some of the models are preferred to the others. In this study, among the physical earthquake generation models, the fault segmentation is preferred to the other models considering the applicability issues. Moreover as for the magnitude recurrences, characteristic earthquake model is more reliable with the opportunity to use a single magnitude in pure characteristic model or a uniform distribution of higher magnitudes in full characteristic model. Simple Poisson model is selected for temporal recurrences as it is widely accepted model in use. The details of the selection of fault model behavior will be provided in Chapter 5.

CHAPTER 3

3. GROUND MOTION PREDICTION EQUATIONS

3.1. Introduction

Ground motion prediction equations (GMPE) are essential tools in seismic hazard analysis to predict the ground motion amplitude at the site located at a distance from the hypocenter of an earthquake. When an earthquake occurs, the generated waves of the ground motion will propagate and attenuate as it moves away from the hypocenter. The effect of the ground motion at a distance is dependent on several parameters of ground motion and the travel path: the magnitude of the earthquake, the distance, fault type and site conditions are a few of them to name. In a seismic hazard analysis, the most appropriate GMPE must be sought to reflect the real behavior of the ground motion at a distance and obtain the closest ground motion amplitudes for the location of interest.

Due to the crucial role of the GMPE in the seismic hazard analysis, countless number of GMPEs have been developed by the researchers and professionals. Most of these equations are developed to model the ground motion behavior specifically for a region. However, most of the time, in order to develop such an equation, the ground motion records from all over the world is employed regardless of the local seismic behavior which could create a bias in the development process of the equation. Therefore, either an equation must be specifically developed for a region of interest or an equation must be adapted by considering the local seismic behavior. In the adaptation of such an equation, the functional forms of the available GMPEs are employed, as it will be performed in this chapter.

The selection process of the most appropriate form of GMPEs for seismic hazard analysis of Eskisehir is presented in this chapter. Most actively utilized and commonly accepted GMPEs are chosen for adaption of the equations to the local seismic behavior. In order to adapt the selected equations, the coefficients of the equations are calibrated by using the local seismic data. The performances of the

equational forms of GMPEs by original and calibrated coefficients are presented. The distance and magnitude scaling plots are provided for the comparison of accuracy of each form, and the performance of the best-suited form is presented in detail.

3.2. Review of GMPE Development Studies

A GMPE gives a prediction of ground motion amplitude as a function of magnitude, distance from the site, site conditions and other factors including fault type, depth, repeat time, source radiation pattern, directivity and especially for near field regions, the azimuth change in the direction of the rupture of a fault source. Most of the GMPEs are derived from the statistical analyses of the strong ground motion records, and they are updated as new records become available.

The following is a standard form of a GMPE:

$$\ln(y) = f_M(M) + f_R(R) + f_{M,R}(M, R) + f_P(P_i) + \varepsilon \quad (3.1)$$

where $\ln(y)$ is the logarithm of the ground motion amplitude, $f_M(M)$ is a function of the magnitude, $f_R(R)$ is a function of distance, $f_{M,R}(M, R)$ is a function related to magnitude and distance, $f_P(P_i)$ is a parameter related to site effects, and ε represents the random error. In addition to the given parameters in equation 3.1, many other parameters are introduced in order to increase the prediction capability of GMPEs.

Among all the GMPEs that utilize several different ground motion parameters, selection of the appropriate equation for the application of seismic hazard analysis for Eskisehir, requires the review of previous seismic hazard studies that were conducted for Turkey. As a result of the review of previous studies, it is observed that, in various seismic hazard model studies for Turkey, most of the GMPEs that were originally developed for the San Andreas region of USA are used due to the geological similarities between the San Andreas Fault in the USA and the NAF in Turkey. For example, Erdik et al. (1985) and Gulkan et al. (1993) employed the GMPE that was developed by Joyner and Boore (1981, 1988) to develop seismic hazard maps of Turkey. For the TCIP program, the equations of Western US have been found conservative and practical to use due to the similarities between the available Turkish strong motion behavior and Western US data (Bommer et al.,

2002). The aforementioned Western US equations included the equations developed by Abrahamson and Silva (1997), Boore et al. (1997), Campbell (1997), Campbell and Bozorgnia (2003), Sadigh et al. (1993, 1997), Idriss (1991, 2002). Moreover, the next generation ground motion attenuation (NGA) models of Abrahamson and Silva (2008), Boore and Atkinson (2008), Campbell and Bozorgnia (2008), Chiou and Youngs (2008) and Idriss (2008) are developed for Western US applications.

The NGA models are developed within a comprehensive project that was launched in 2002 by five independent teams who had previously developed earlier versions of the equations. The purpose of the project was to increase the accuracy of the seismic hazard studies and incorporate the accumulated seismic data since the development of the previous versions of the NGA equations. The equations were updated through new additions of parameters, and new parametric coefficients were derived by the incorporation of the new data. Later modifications to these equations were added as the new data becomes available.

In addition to the GMPEs that were specifically developed to model the ground motion behavior in Western US, GMPEs specifically developed for Turkey are also employed in seismic hazard studies in Turkey. Various researchers developed GMPEs that are specific to Turkey (Inan et al., 1996, Gulkan and Kalkan, 2002, Kalkan and Gulkan, 2004, Ulutas et al., 2004, Ulusay et al., 2004, Ozbey et al., 2004, Beyaz, 2004). In one of the latest significant studies, Akkar and Cagnan (2010) developed a GMPE similar to Abrahamson and Silva (2008) and Boore and Atkinson (2008).

3.3. Selection of the Most Appropriate GMPE

The reasons of regional dependency of GMPEs and the problems regarding adaption are well documented in Campbell (2003), Scherbaum et al. (2004, 2005) and Douglas (2004, 2007). The crustal structure along the propagation path, the local geology, the topography, radiation pattern, and the faulting mechanism are some of the factors that have an impact on the way a seismic wave propagates. Therefore, significant bias in magnitude, distance, site and fault style scaling could be introduced by employing a GMPE, which is developed for another region. In order to avoid the regional bias in these models, a selection and adaption procedure should be introduced and local seismicity must be utilized in order to test the applicability of

the GMPEs to local seismic hazard studies.

The information about the seismicity of Eskisehir region is not scarce especially if the low magnitude earthquakes are considered. Moreover, with the addition of the records of Kocaeli and Duzce earthquakes to the catalog as the strong motion records in 1999, the number of recordings of large and small size earthquakes became more homogeneous. Therefore, it has become more possible to create a local GMPE or adapt available GMPEs by using the local data. In this study, instead of developing a new GMPE, adjustment and adaption of selected GMPEs to the local seismic behavior is preferred.

The most appropriate GMPEs are selected as candidates from amongst the several GMPEs available in the literature, which are mentioned in 3.2. The geophysical properties of Eskisehir region, characteristics of the seismic activity and the local site conditions are taken into account in the selection of the candidate GMPEs. The international acceptance, well documentation and the similarity of the tectonic regimes of the western US and Eskisehir and surrounding areas automatically led to the inclusion of the NGA models and their predecessors mentioned in section 3.2. In fact, there are studies that were performed to adapt the NGA equations to the European data with both encouraging and discouraging recommendations. Stafford et al. (2008) promoted the use of NGA equation throughout Europe, while Douglas (2004) questioned the validity of the equations since there are evidences of rapid distance scaling in the European data according to his study. Though the validity is still questioned, the GMPEs that were developed for Western US are included in the adaption procedures. The GMPEs developed specifically for Turkey such as Gulkan and Kalkan (2002), Kalkan and Gulkan (2004), Ozbey et al. (2004), and Akkar and Cagnan (2010) are included in reviewing and evaluation study as well.

The initial selection criteria regarding the suitability of the mentioned GMPEs are based on Cotton et al. (2006). The purpose of development, the equational forms, input parameters and the application criteria of these equations are examined. The functional forms are assessed in terms of the modeling of the local data. Especially parameters for magnitude-dependent distance scaling, and saturation effects of magnitude are investigated. In addition, the assumptions on site classes in the development phase of the GMPEs are taken into account.

Since the results of a seismic hazard analysis could be adjusted to the site conditions (Cramer, 2011) after the completion of the analysis, there is no requirement to specify any of the site conditions, therefore the site condition is assumed to be rock considering the calculation convenience. Consequently, the initial selection of the GMPEs is performed accordingly. That is, instead of selecting the GMPE derived for different site conditions, the equations developed for site condition of rock is included in the study.

The final selection criteria are based on the performances of adapted GMPEs with the local data. The ground motion parameters of the local earthquakes are regressed with the amplitudes of the ground motions by using the functional forms of the GMPEs to calibrate the coefficients of the equations. The necessary minor modifications due to local conditions and gathered records are incorporated into the functional forms of GMPEs. If there was not sufficient data for a parameter, or if the parameter was irrelevant, then that parameter is omitted from the equation. After that, the remaining parameters are employed in the regression analysis for that GMPE. In order to correlate the observed and predicted ground motion amplitudes, among the several available statistical methods, classical residual analysis is conducted. The statistical parameters of coefficient of determination, correlation coefficient, standard deviation and significance test results are also employed for the final selection. Analysis of residuals by the methods proposed by Scherbaum et al. (2004) is not preferred, since the performance of the equations are monitored by trellis plots (Stewart et al., 2012) which serve the purpose of this study.

3.3.1. Details of GMPEs

Each equation has varying parameters depending on the purpose of use. While most of the equations require basic variables such as magnitude, distance, fault types and site parameters, the others require very specific information about the local site conditions such as sediment depth, fault mechanisms and detailed geological properties of the earthquake events such as hanging wall and depth to rupture parameters in addition to the basic variables. While some GMPEs have a linear magnitude scaling parameters, some of the GMPEs have parameters related to magnitude scaling with distance and magnitude saturation. Table 3.1 lists and compares the functional forms of the magnitude, distance, site parameters used in the

Table 3.1. Comparison of Ground Motion Prediction Equations According to Input Parameters

GMPE*	Magnitude Parameter	Distance Parameter	Magnitude and Distance Parameter	Site Parameters
AS97	$(M - c_1), (8.5 - M)^2$	$\ln(\sqrt{R_{Rup}^2 + h^2})$	$(M - c_1) \ln(\sqrt{R_{Rup}^2 + h^2})$	$\ln(pga_{Rock})$
BJF97	$(M - 6), (M - 6)^2$	$\ln(\sqrt{R_{JB}^2 + h^2})$	*****	$\ln(Vs30/V)$
SY97	$M, (8.5 - M)^2$	$\ln(R_{Rup} + 2)$	$\ln(R_{Rup} + e^{(c_1+c_2M)})$	**
C97	$M, \tanh(c_1(M - 4.7))$	$R_{SEIS}, \ln(R_{SEIS})$	$MR_{SEIS}, \ln\left(\sqrt{R_{SEIS}^2 + [c_2 e^{(c_3M)}]^2}\right)$	$\ln(R_{SEIS})$
I02	M	$\ln(R_{Rup} + 10)$	$M \ln(R_{Rup} + 10)$	*****
CB03	$M, (8.5 - M)^2$	-	$\ln\left(\sqrt{R_{SEIS}^2 + [c_1 e^{(c_2M+c_3(8.5-M)^2)}]^2}\right)$	**
OB04	$(M - 6), (M - 6)^2$	$\ln(\sqrt{R_{JB}^2 + h^2})$	*****	**
AS08	$(M - c_1), (8.5 - M)^2$	$\ln(\sqrt{R_{Rup}^2 + h^2})$	$(M - c_1) \ln(\sqrt{R_{Rup}^2 + h^2})$	$\ln\left(Vs30/V\right), \ln(pga_{Rock})$

* AS97, Abrahamson and Silva (1997), BJF97, Boore, Joyner and Fumal (1997), SY97, Sadigh et al. (1997), C97, Campbell (1997), I02, Idriss (2002), CB03, Campbell and Bozorgnia (2003) and OB04, Ozbey et al. (2004), AS08, Abrahamson and Silva (2008).

**Different GMPEs were developed for different site classes

***Single linear site parameter is introduced for different site classes

**** No parameter is defined

Table 3.1 Continued

GMPE*	Magnitude Parameter	Distance Parameter	Magnitude and Distance Parameter	Site Parameter
BA08	$(M - c_1), (M - c_1)^2$ $M \leq c_1$ $(M - c_1)$ $M > c_1$	$\ln\left(\frac{R_{JB}}{c_2}\right),$ $(R_{JB} - c_2)$	$(M - c_1) \ln\left(\frac{R_{JB}}{c_2}\right)$	$\ln\left(\frac{V_{s30}}{V}\right), \ln(pga_{Rock})$
CB08	M $M \leq 5.5$ $M, M(-5.5)$ $5.5 < M \leq 6.5$ $M, (M - 5.5), (M - 6.5)$ $M > 6.5$	$\ln(\sqrt{R_{Rup}^2 + h^2})$	$M \ln(\sqrt{R_{Rup}^2 + h^2})$	$\ln\left(\frac{V_{s30}}{V}\right), \ln(y_{ref})$ $e^{Vs30} \ln(y_{ref})$
CY08	$(M - 6), \ln(1 + e^{c_1(c_2 - M)})$	$\ln(\sqrt{R_{Rup}^2 + h^2})$	$\ln(R_{Rup} + c_1 \{c_2 \cosh[c_3] \max(M - c_4, 0)\})$	$\ln\left(\frac{V_{s30}}{V}\right), \ln(y_{ref})$ $e^{Vs30} \ln(y_{ref})$
I08	M	$R_{Rup},$ $\ln(R_{Rup} + 10)$	$M \ln(R_{Rup} + 10)$	_***
AC10	$(M - c_1), (8.5 - M)^2$	$\ln(\sqrt{R_{JB}^2 + h^2})$	$(M - c_1) \ln(\sqrt{R_{JB}^2 + h^2})$	$\ln\left(\frac{V_{s30}}{V}\right), \ln(pga_{Rock})$

* BA08, Boore and Atkinson (2008), CB08, Campbell and Bozorgnia (2008), CY08, Chiou and Youngs (2008), I08, Idriss (2008) and AC10, Akkar and Cagnan (2010)

** No parameter is defined

selected equations. Fault parameters are not included in the table because linear scaling of ground motion amplitudes with fault types is assumed by all the developers. Table 3.2 provides more detail about the types of faults considered in each GMPE. The hanging wall, depth to rupture, large distance and sediment depth effects that are specific to a few GMPEs are not presented in Table 3.1.

In Table 3.1, M stands for magnitude; R_{Rup} , R_{SEIS} , R_{JB} represent the distance parameters of the equations; and c , c_1 , c_2 , c_3 , c_4 , h and V are various parametric constants of the GMPEs. In their original forms, these symbols are assigned with a different scheme; however, for the sake of coherence in presenting the base forms of GMPEs, the simpler symbols are reassigned to avoid confusion. Given in the last column of the table, V_{s30} represents the average shear wave velocity of top 30 m layer of soil, and pga_{rock} is used for the reference ground motion amplitude on rock respectively. In addition, V and y_{ref} are the symbols employed for reference shear wave velocity.

As can be seen in the table, all the magnitude terms are agreeably in moment magnitude scale. In some of the equations, magnitudes are classified into two or three groups, to model large magnitude scaling of ground motions. I02 and I08 have the simplest form of magnitude parameter. Both of the equations propose a linear relationship between the logarithm of the ground motion amplitude and the magnitude. However, both equations consider the magnitudes in three different bins, and therefore three groups of coefficients are derived respectively. CB08 also considers three magnitude bins but with different terms added for each magnitude bin. AS97, AS08 and AC10 have the same forms with two different magnitude bins used to model the magnitude dependency of the ground motion amplitude.

In some of the equations, a quadratic magnitude term is added to model the magnitude scaling of the ground motion except for I02, I08, C97, CB08 and CY08. The same quadratic magnitude term is employed in AS97, SY97, CB03, AS08 and AC10. Among these equations, SY97 provides a different group of coefficients for two magnitude bins, while the others do not propose a different group of coefficients

but introduce different bins for the quadratic terms. C97 and CY08 propose complex parameters for magnitude dependency.

BJF97 proposes two magnitude parameters as a linear and a second-degree quadratic magnitude term. Since OB04 borrowed the basic forms from BJF97, the same magnitude terms are used in the equation. BA08, on the other hand, has two different bins for magnitude scaling, while an additional quadratic term is proposed for smaller magnitudes.

There is a variety of distance terms in the listed GMPEs in Table 3.1. Indeed, a standard GMPE could have various source-distance measures, most common measures being the hypocentral distance, epicenter distance and closest distance to rupture plane. There is no clear-cut functional form to model the scaling of ground motion amplitude with the distance (Figure 3.1). As shown in column three in Table 3.1, the primary distance measure is the rupture distance, which is defined as the closest distance from the site to the rupture plane. When the earthquake source is modeled as point source, the rupture distance is calculated as the closest distance from the site to the hypocenter. BJF97, OB04, BA08 and AC10 use Joyner-Boore distance, R_{JB} , which is the closest horizontal distance from the recording site to the surface projection of the rupture plane. C97 and CB03 use seismogenic rupture distance, R_{SEIS} , and the rest of the equations employ rupture distance, R_{Rup} .

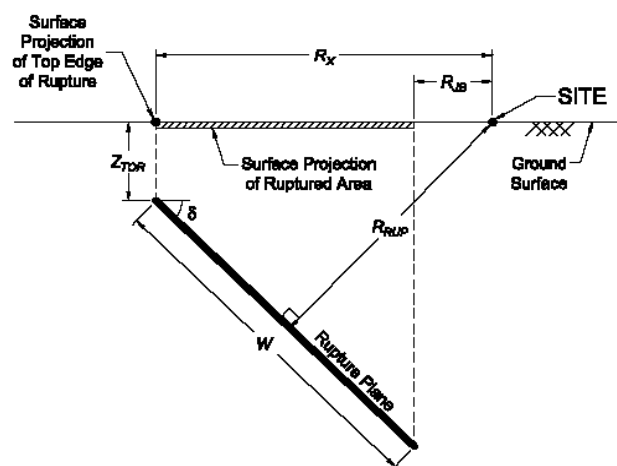


Figure 3.1. The Most Common Distance Measures from the Earthquake Source to the Site (Kaklamanos et al., 2010)

Most of the equations have similar functional forms for the distance parameter, which is expressed as the natural logarithm of the square root of sum of squares of distance with a coefficient. The coefficient is supposed to be obtained through regression analysis. Among the considered GMPEs, the simple log distance scaling is employed by C97, SY97, I02, BA08 and I08. Only CB03 does not include a separate distance term. It should be mentioned that, all the distance terms used in this study will be Joyner-Boore distance.

In AS97, C97, I02, AS08, BA08, CB08, I08 and AC10, the parameter that contains both magnitude and distance terms to model the magnitude dependent distance scaling. These parameters follow a pattern of combining the simple magnitude and distance terms of the equation through multiplication. BJF97 and OB04 do not have such a parameter that models the magnitude dependent distance scaling, while CY08, SY97 and CB03 have forms that are more complex.

The site parameters are probably the most complicated parameters of the GMPEs due to the complex nature of site effects. Most of the equations listed above have site parameters. While the GMPEs that were developed before the development of NGA equations have the parameters in their simplest form, NGA equations and AC10 have them in a complex form. AS97 introduced the term of expected peak acceleration on rock pga_{Rock} to account for the nonlinear site effects. The nonlinear parameter is defined as a function of the peak acceleration on rock that is initially calculated by a regression analysis excluding the site parameter. BJF97 has log-linear parameter that uses V_{s30} to model the site effects. A reference velocity is introduced for scaling the shear wave velocity, V_{s30} , of the considered site. SY97 is developed for rock sites; therefore, it does not contain any site parameters. The creators of SY97 developed a separate GMPE to model the ground motion propagation including the site effects. C97 has site parameter with distance scaling terms, while OB04 and CB03 have a simple site parameter with assignment of coefficients of 1 or 0 to the site parameter depending on the site conditions of the considered location. I02 and I08 do not contain any site parameters. AS08, BA08, CB08, CY08 and AC10 have both linear and nonlinear parameters for modeling the site effects. The linear site effect

parameter is based on V_{s30} , while a few modifications performed in choosing a reference shear wave velocity or a few constants are introduced in the GMPEs to account for the analytical site response analysis (Walling et al., 2008). Equation 3.2 provides the general form of the site parameter that is introduced to model the linear site effects for the mentioned GMPEs.

$$F_{lin} \propto C_{site} \ln\left(\frac{V_{s30}}{V_{ref}}\right) \quad (3.2)$$

In the equation F_{lin} is the linear site response parameter, C_{site} is the constant to be derived by regression analysis and V_{ref} is the reference velocity above which the site response is accepted as linear. Except for CY08, C_{site} includes constants obtained from the site response analysis. In all the GMPEs that propose nonlinear site parameters, the parameters contain both, V_{s30} , and, pga_{Rock} . There are three V_{s30} intervals defined in AS08 and CB08, where the pga_{Rock} is considered with the lowest values of V_{s30} and nonlinearity is not considered with the highest values of V_{s30} . Between these two intervals, the site response is considered as linear. BA08 considers nonlinearity by specifying the V_{s30} dependence for the coefficient and the pga_{Rock} dependence for the function that expresses the nonlinearity. Except for very low levels of ground motion amplitudes on rock, pga_{Rock} is part of the nonlinear site parameter in the entire range of ground motion amplitudes. The amplification is constrained by imposing a limitation on pga_{Rock} values for low levels of ground motion amplitudes on rock. Moreover, a smooth transition is projected through the introduction of different levels of nonlinearity by using different functions and coefficients for different intervals of ground motion amplitudes on rock.

In summary, dependency on pga_{Rock} is excluded below a predefined level of V_{s30} and pga_{Rock} values. Moreover, in AS08, CB08, BA08 and AC10, this dependency is taken into consideration for the entire range of V_{s30} values that are lower than reference velocity. Table 3.2 summarizes and compares the parameters used in the GMPEs in detail. As already mentioned, the magnitude terms are all in moment magnitude scale, and in some equations, magnitudes are classified into two or three bins in order to model the magnitude scaling. Most of the equations include this magnitude

Table 3.2. Comparison of Ground Motion Prediction Equations According to Input Parameters

Equation*	Magnitude	Distance	Fault Mechanism***	Site Conditions	Note
AS97	$M_w > c_1, M_w < c_1$	R_{rup}	R,R/O, Others	Applicable to deep soil and others, reference PGA on rock is employed	Geometric mean of horizontal components, hanging wall term included
BJF97	M_w	R_{JB}	SS,R, and others	No classification provided, V_{s30} scaling assumed	
SY97	$M_w < 6.5, M_w > 6.5$	R_{rup}	SS, R/Thrust	NA**	
C97	M_w	R_{SEIS}	SS and others	Soft and hard rock sites	Depth of basement rock sought, superseded by CB03
I02	M_w	R_{rup}	R,R/O and others	***	
CB03	$M_w \geq 5.5, M_w > 6.5$ $5.5 < M_w \leq 6.5$	R_{SEIS}	SS, R	Firm soil, very firm soil, soft rock, firm rock	
OB04	M_w	R_{JB}	***	Site classes A, B, C and D classified according to V_{s30}	
AS08	$M_w > c_1, M_w < c_1$	R_{rup}, R_{JB}, R_x	R,N, others	Linear parameter is based on V_{s30} , and for nonlinear parameter expected PGA at $V_{s30} = 1100$ m/s is used	Aftershock effect included the effect of hanging wall, basin, large distance, and the depth of rupture introduced.

*AS97, Abrahamson and Silva (1997), BJF97, Boore, Joyner and Fumal (1997), SY97, Sadigh et al. (1997), C97, Campbell (1997), I02, Idriss (2002), OB04, Ozbey et al. (2004) and AS08, Abrahamson and Silva (2008),

** No parameter is defined

***N: Normal fault, SS: Strike-slip fault, R: Reverse fault, R/O: Reverse oblique fault

Table 3.2 Continued

Equation*	Magnitude	Distance	Fault Mechanism**	Site Conditions	Note
BA08	$M_w > M_h$, $M_w < M_h$	R_{JB}	SS, R, N and others	Linear parameter is based on V_{s30} , nonlinearity included by expected acceleration at $V_{s30} = 760$ m/s reference rock velocity	
CB08	$M_w < 5.5$ $5.5 < M_w \leq 6.5$ $6.5 < M_w$	R_{rup} , R_{JB}	R, N and others	Mostly based on AS08, with additional linear scaling parameter based on V_{s30} introduced	Hanging wall and base sediment depth parameters included
CY08	M_w	R_{rup} , R_{JB} , R_x	R, N and others	V_{s30} and reference PGA at $V_{s30} 1130$ m/s is employed	Geometric spreading effects (path scaling), near-source distance effects (magnitude scaling), HW and sediment thickness included
I08	$M_w \leq 6.75$, $M_w > 6.75$	R_{rup}	SS, R and others	V_{s30} is used, , valid for only $450 < V_{s30} < 900$ m/s	Hanging wall and base sediment depth parameters included
AC10	$M_w \leq 6.50$, $M_w > 6.50$	R_{JB} ,	R, N and others	Based on BA08	-

* BA08, Boore and Atkinson (2008), CB08, Campbell and Bozorgnia (2008), CY08, Chiou and Youngs (2008), I08, Idriss (2008) and AC10, and Akkar and Cagnan (2010)

**N: Normal fault, SS: Strike-slip fault, R: Reverse fault, R/O: Reverse oblique fault

dependence of the log distance slope or magnitude scaling and saturation effects of the ground motions at low periods and short distances with quadratic models. The distance parameters are given in column three in the table and the necessary explanations are already provided in Table 3.1. In column four, the styles of faults that are used to model the influence of fault on the ground motion propagation are listed. Except for OB04, all the equations consider the different fault types depending on the development purpose of the equation or the data utilized in the development of the equation.

Table 3.3. Ranges of Applicability of Ground Motion Prediction Equations Prescribed by the Developers

Model	Magnitude	Distance (km)	V_{s30} (m/s)	Other Requirements
AS97	$4.5 \leq M_w$	-	-	-
BJF97	$5.5 \leq M_w \leq 7.5$	$R_{JB} \leq 80$ km	-	Rupture depth < 20 km
SY97	$4.0 \leq M_w$	$R_{rup} \leq 100$ km	-	
C97	$5.0 \leq M_w$		-	Limited to near source distances
I02	$4.5 \leq M_w \leq 8.0$	$R_{rup} \leq 100$ km	$450 \leq V_{s30} \leq 900$	-
CB03	$5.0 \leq M_w$	$R_{SEIS} \leq 80$ km	-	-
OB04	$5.0 \leq M_w$	$R_{JB} \leq 100$ km	-	-
AS08	$4.0 \leq M_w \leq 8.5$	$R_{rup} \leq 200$ km	-	-
BA08	$5.0 \leq M_w \leq 8.0$	$R_{JB} \leq 200$ km	$180 \leq V_{s30} \leq 1300$	-
CB08	$4.0 \leq M_w \leq 7.5$	$R_{rup} \leq 200$ km	$180 \leq V_{s30} \leq 1300$	$Z_{2.5}^* \leq 10$ km $Z_{TOR}^{**} \leq 15$ km
CY08	$4.0 \leq M_w \leq 8.5$	$R_{rup} \leq 200$ km	$180 \leq V_{s30} \leq 1300$	Normal fault (N) and Reverse Fault (R) for - $4.0 \leq M_w \leq 8.0$ Strike-Slip (SS) for $M_w > 8.0$
I08	$4.5 \leq M_w \leq 8.0$	$R_{rup} \leq 200$ km	$450 \leq V_{s30} \leq 900$	-
AC10	$5.0 \leq M_w \leq 7.4$	$R_{JB} \leq 200$ km	-	-

* Shear wave velocity at 2.5 km depth

** Closest point of rupture plane to surface

Fifth column of Table 3.2 provides the site classification schemes of each equation. Except for equations of I02 and I08, all equations include a site parameter. Site classification parameters greatly vary among the equations. For instance, V_{s30} and pga_{Rock} are introduced as site parameters in AS08, CB08, CY08, BA08 and AC10, while simple classification scheme is employed in S97, C97, CB03 and OB04. The additional site effects such as sediment thickness, model basin effect and depth to the 1000 m/s velocity and depth to the 2500 m/s shear wave velocity are also included in the models.

After reviewing the functional forms in detail, the developers' suggestions about the applicability criteria of GMPEs are reviewed. Since each developer compiled a different catalog of earthquakes in the development stage of their equations, the applicability of these equations for the seismic hazard analysis for Eskisehir is examined. Most GMPEs have various applicability constraints suggested by the developers. Table 3.3 lists the range of applicability of the equations with respect to magnitude, distance, shear wave velocity and other parameters. It should be highlighted that some of the GMPEs were developed for magnitudes greater than 5.0 and distances less than 100 km. Therefore, in the selection criteria these applicability limits are considered. It should be mentioned that, in the application of the adaption procedures no applicability criteria are imposed on the GMPEs.

3.3.2. Strong Ground Motion Data

The adaption of the selected GMPEs to conduct a seismic hazard analysis for Eskisehir requires the collection of the past seismic activity data within the circle with the radius of 300 km that centered at Eskisehir. In order to reflect the effects of the travel path of the earthquakes on GMPEs, the geology, local soil conditions, and most importantly, the propagation behavior of the previous events must be known. Although certain constraints of the equations may be weakened due to the limitations of the local data (Strasser et al., 2009), the intrusion of the records from any other site is not allowed. The aim of this restriction is to capture the region specific behavior of the propagation. The scaling of the ground motion with respect to magnitude and distance, the effect of the special fault mechanisms, and the influence of the focal depth are generally specific to the location of interest, therefore the database is strictly limited with the local data.

Table 3.4. Records Used in the GMPE Analysis (GDDA, 1976-2010)

Date of the Event	Name of the Event	Fault Type*	M_w **	Depth (km)	Lat. (deg.)	Long. (deg.)	No of Records
19.08.1976	Denizli	N	5.3	3.0	37.71	29.00	1
18.07.1979	Dursunbey	SS	5.3	5.0	39.66	28.65	1
29.03.1984	Balikesir	SS	4.9	12.0	39.64	27.87	1
01.10.1995	Dinar	N	6.4	5.0	38.11	30.05	5
21.01.1997	Buldan	N	4.8	18.0	38.12	28.92	1
04.04.1998	Dinar	N	4.6	15.0	38.14	30.04	7
17.08.1999	Kocaeli (Izmit)	SS	7.4	18.0	40.70	29.91	20
11.11.1999	Sapanca	SS	5.6	8.9	40.82	30.20	7
12.11.1999	Duzce	SS	7.2	25.0	40.74	31.21	16
23.08.2000	Hendek	SS	5.3	15.3	40.68	30.71	11
04.10.2000	Denizli	N	5.0	8.4	37.91	29.04	3
26.08.2001	Yigilca	SS	5.4	7.8	40.95	31.57	3
03.02.2002	Sultandagi	R	6.5	5.0	38.57	31.27	7
03.04.2002	Burdur	SS	4.2	5.0	37.81	30.26	1
09.03.2003	Akyazi	SS	4.1	4.4	40.73	30.62	2
21.05.2003	Duzce	SS	4.7	7.7	40.87	30.98	2
09.06.2003	Bandirma	SS	4.8	14.7	40.20	27.97	8
23.07.2003	Buldan1	N	5.3	5.0	38.14	28.83	7
26.07.2003	Buldan2	N	5.3	5.0	38.11	28.88	6
26.07.2003	Buldan3	N	5.7	4.3	38.06	28.89	7
26.07.2003	Buldan4	N	5.2	8.5	38.12	28.84	4
24.10.2006	Manyas	N	5.2	7.9	40.42	28.99	30
20.12.2007	Bala1	SS	5.7	0.0	39.42	33.05	9
26.12.2007	Bala2	SS	5.6	0.0	39.41	33.04	11
18.07.2007	Simav1	N	4.5	11.7	39.30	29.31	2
12.03.2008	Cıncık	SS	4.9	24.0	40.63	29.02	18
17.02.2009	Simav2	N	5.2	7.0	39.15	29.04	8

* N: Normal fault, SS: Strike-slip fault, R: Reverse fault

** The magnitudes are obtained from KOERI and GDDA catalogs in different scales and the unification of magnitudes is performed by conversion formulations proposed by Deniz and Yucemen (2008).

The past earthquake data within a circle of 300 km radius centered at Eskisehir is investigated. The catalogs compiled by Kandilli Observatory and Earthquake Research Institute (KOERI), General Directorate of Disaster Affairs (GDDA) (Currently Disaster and Emergency Management Presidency) , Deniz et al. (2008), Tan et al. (2008) and several other catalogs are examined to gather the necessary

earthquake activity information about the area. The catalogues are subjected to further elimination by using engineering judgment to include only the strong motion events with the damage inflicting capability to a nearby settlement. In the formation of the database, the uniformity of magnitude and the distance variables are considered. As presented in Table 3.4, 27 strong ground motion records are gathered from GDDA website. The database is composed of 198 records from 27 earthquakes that occurred between 1976 and 2009. The priority is given to compile a homogeneous earthquake database to reduce the bias such as domination of the database by a few earthquakes.

Especially in terms of magnitude, a uniform distribution is sought in the selection of the records. Despite these intentions due to the reason that the number of local seismic events between the magnitudes of 6 and 7 is quite low, the database has a certain level of bias. However, since the objective is to model the local propagation characteristics with the functional forms of the selected GMPEs, this level of bias is accepted. If the earthquakes of Duzce on November 12, 1999 and Izmit (Kocaeli) on August 17, 1999 are removed from the list of gathered earthquakes, the remaining earthquakes could form a database with uniform distribution.

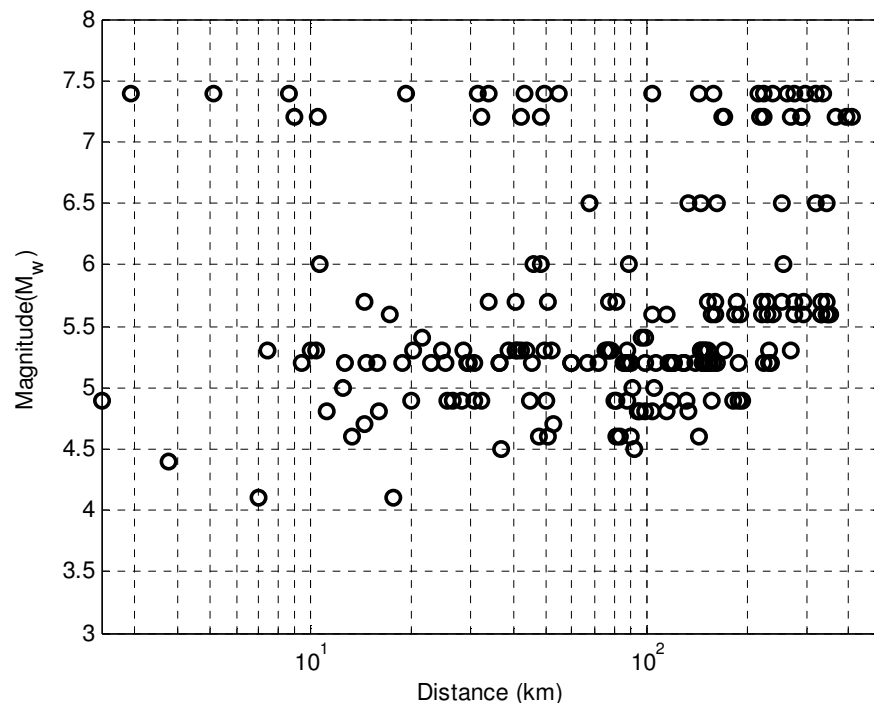


Figure 3.2. Distribution of Magnitude and Distance of the Local Database

However, removing the most important earthquakes from this list and adapting a GMPE by just using smaller size earthquakes would undermine the whole adaption process. Therefore, a compromise in the distribution of magnitudes is tolerated like the other Turkish originated GMPE equations of Ozbey et al. (2004) and Akkar and Cagnan (2010). Even considering the entire Turkish strong motion database, since there are not many earthquakes recorded between the magnitudes of 6.0 and 7.0, the database would be prone to bias at the mentioned magnitude ranges.

In the database, the recording distance varies from 2.4 km to 409 km, and a relatively uniform distribution is provided as can be seen in Figure 3.2. The fault types of the earthquake events reflect the local conditions of the region, which is dominated by the strike-slip faults on the north and normal faults in the south.

The earthquake records of GDDA include two horizontal and one vertical component. The geometric mean of the two horizontal components is used as input acceleration. Earthquake records until 2007 are already processed by Akkar et al. (2010). Therefore, the remaining records are processed by using a 4-pole Butterworth filter with varying low cutoff and high cutoff frequencies and baseline correction method as previously performed by Akkar et al. (2010).

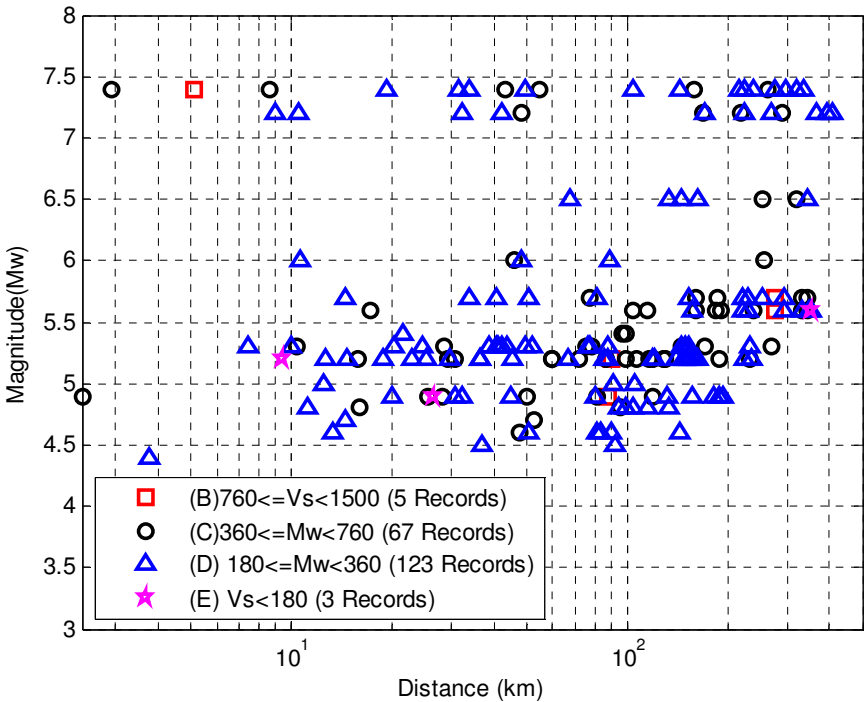


Figure 3.3. The Range of Shear Wave Velocities at the Recording Station Sites and Associated Site Classes According to NEHRP, 1994

Among the several different measurement methods, the closest horizontal distance to the rupture surface, which is called Joyner-Boore distance, is utilized. Below certain magnitude and above certain distance values, the rupture point is accepted as hypocenter and the horizontal distance from the surface projection of the rupture to the recording station is accepted as Joyner-Boore distance. Izmit (1999) and Duzce (1999) earthquakes, which are two earthquakes with a moment magnitude greater than 7.0, caused a large surface rupture. The distances for these two earthquakes are assigned as the closest horizontal distance from the surface projection of the rupture to the recording station.

As the site shear wave velocity, which is a crucial site condition parameter, the shear wave velocities of the uppermost 30 m layer are utilized. The recording site shear wave velocities are gathered from Akkar et al. (2010) and then these velocities are used to classify the recording sites according to NEHRP.

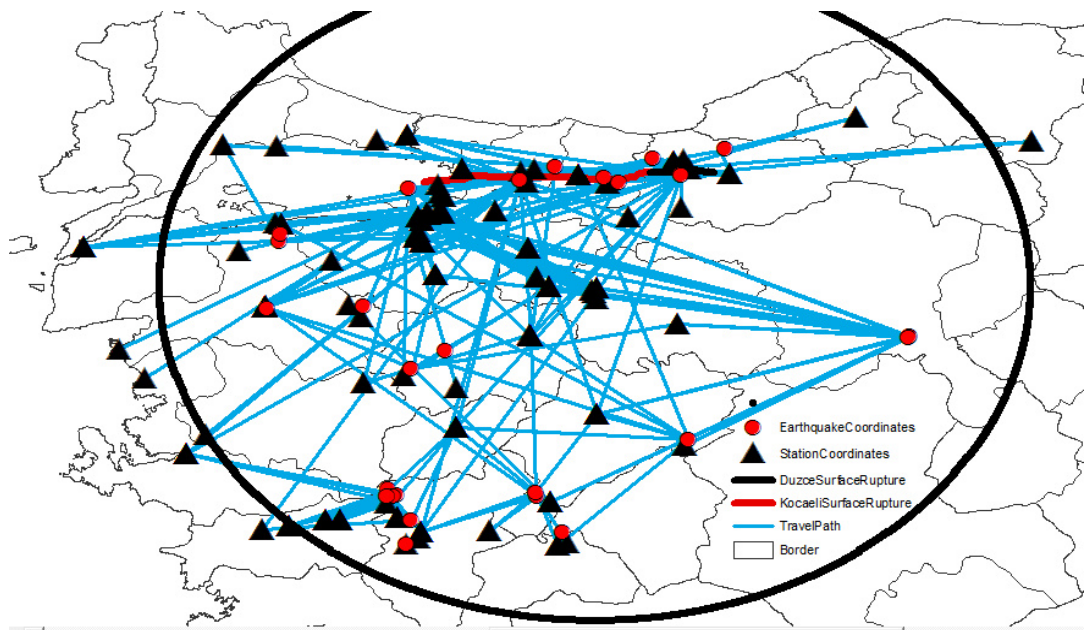


Figure 3.4. The Epicenters of Earthquakes and Locations of Recording Stations

Most of the recording station sites are classified as either C or D as observed in Figure 3.3, which is also a general situation considering the whole recording station sites throughout Turkey (Akkar et al., 2010). The locations of the earthquakes and the recording stations are chosen in such a way that the travelling path is evenly distributed and cover the whole area surrounding Eskisehir as can be seen in Figure 3.4.

3.3.2.1 Preparation of Raw Data

A total of 198 earthquake records are gathered with each record having two directional signals in N-S and E-W directions. The database included every possible record that could be exploited in the proposed GMPE selection and adaptation procedure. The gathered records are processed in order to seek the relative performance of the GMPEs with regard to the local data. The raw ground motion records are gathered from GDDA website and then they are subjected to the filtering procedure by using a 4-pole Butterworth filter. GMPEs require the spectral evaluation of the certain earthquake parameters like spectral acceleration and spectral velocity, so response spectra of each earthquake record must be calculated for each direction. Eventual response spectra are found by calculating the geometric mean of response spectral values in both directions and for each period. After the filtering procedure is completed, then another database is created which is composed of the spectral acceleration values of each record at the predefined periods.

3.3.2.2. Evaluation of Raw Data

One of the basic governing relationships of a GMPE is the scaling characteristics of the ground motion amplitude with the magnitude.

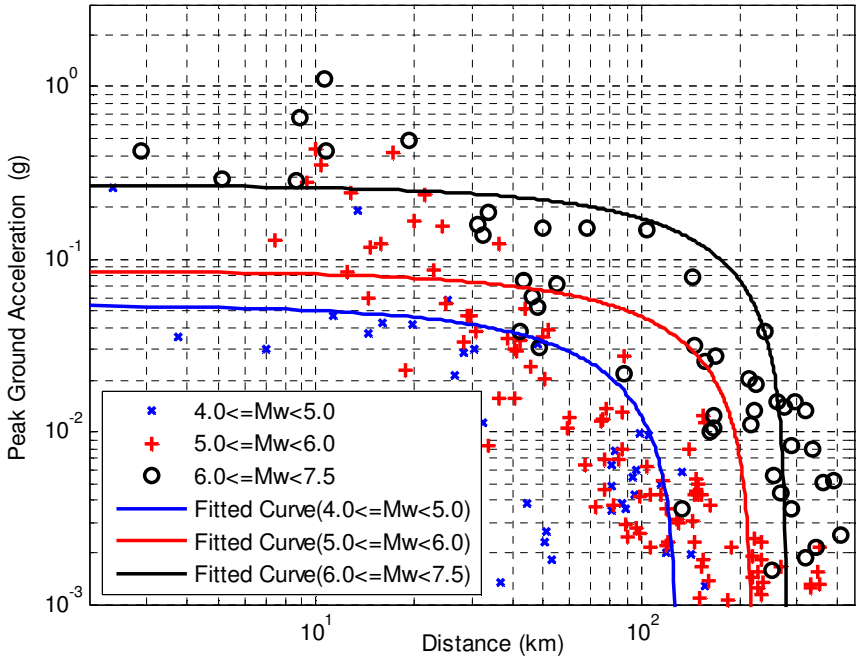


Figure 3.5. Magnitude Scaling in the Raw Data for PGA

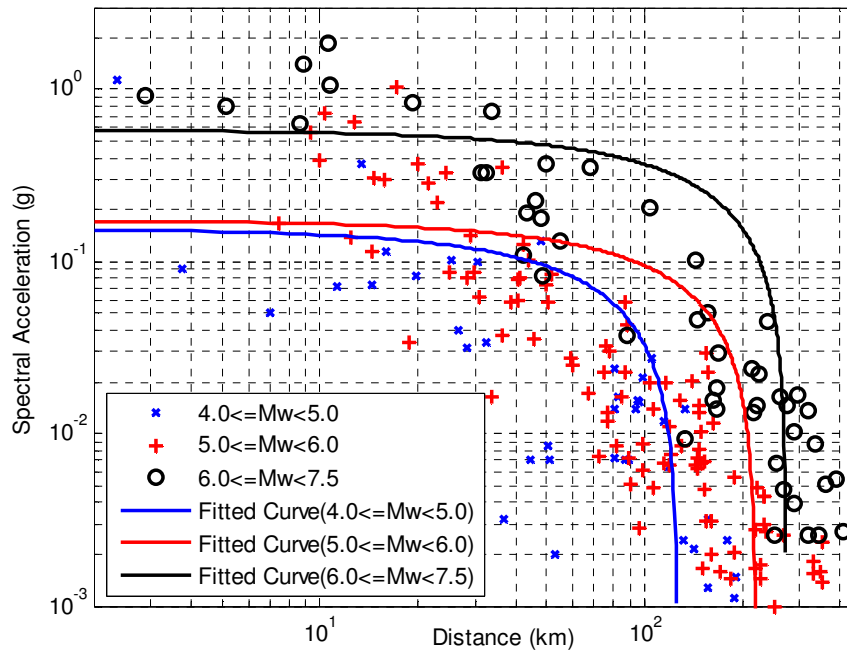


Figure 3.6. Magnitude Scaling in the Raw Data for Spectral Period of 0.2 s

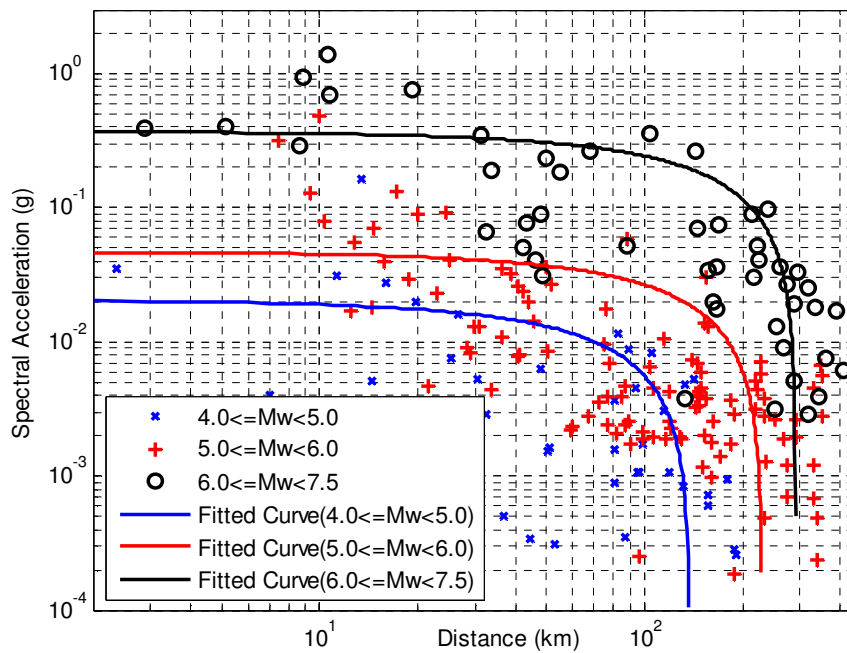


Figure 3.7. Magnitude Scaling in the Raw Data for Spectral Period of 1.0 s

As can be observed by Figures 3.5 to 3.7, there is a complex scaling characteristics that requires higher order terms to model the scaling of magnitude. Especially at larger magnitudes, an additional term could be introduced to model the large magnitude scaling. A similar approach is used in order to observe the dependency of the peak ground acceleration and spectral acceleration values on the local site conditions.

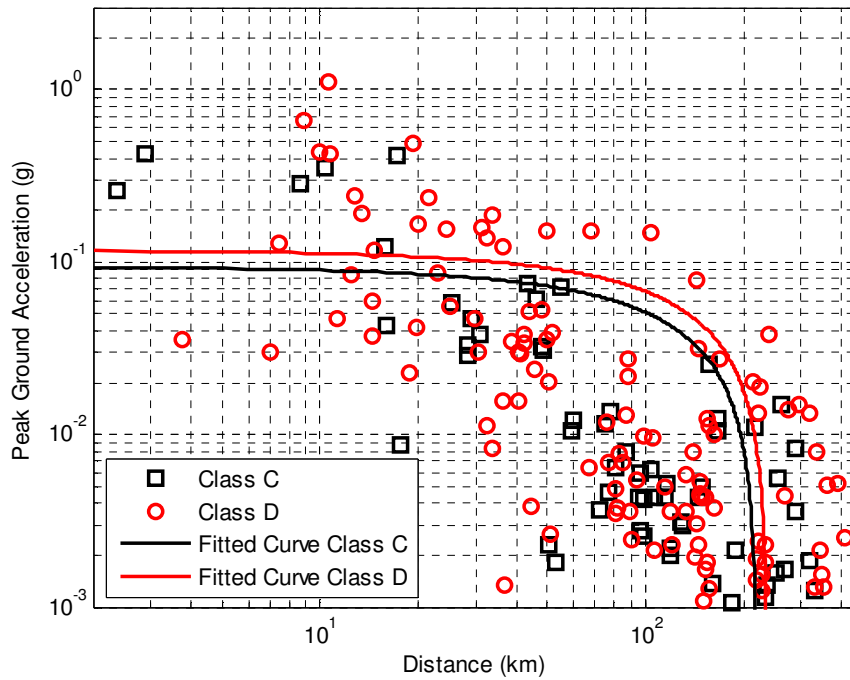


Figure 3.8. PGA versus Distance Values Shown Separately for Site Class C and D, and Fitted Curves by Least Squares Method

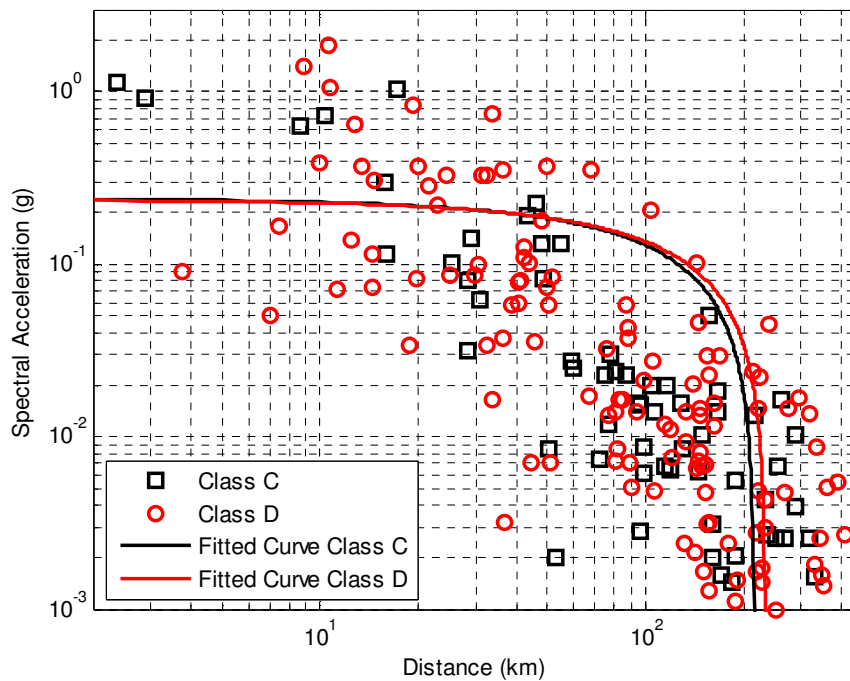


Figure 3.9. Spectral Acceleration Values at Spectral Period of 0.2 s versus Distance Values for Class C and D, and Fitted Curves by Least Squares Method

A series of plots are created for PGA and spectral acceleration at the spectral periods of 0.2 s and 1.0 s and for site conditions of class C and D on NEHRP (1994) scale as seen in Figure 3.8, 3.9 and 3.10. The other site classes are not used in creating these

plots since in the database; there are only 5 records for class B and 3 records for class E on NEHRP (1994) scale.

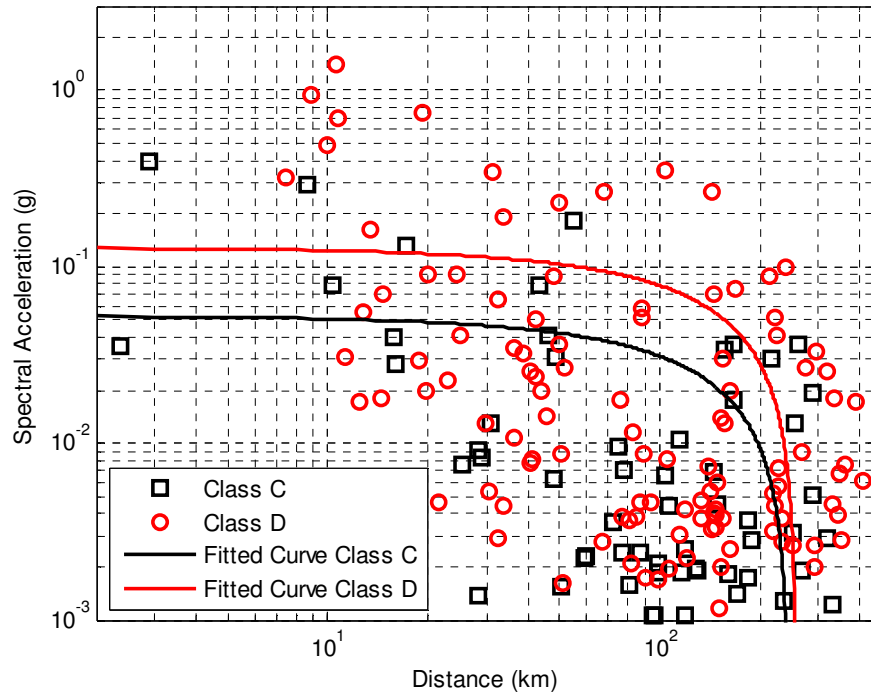


Figure 3.10. Spectral Acceleration Values at Spectral Period of 1.0 s versus Distance Values for Class C and D, and Fitted Curves by Least Squares Method

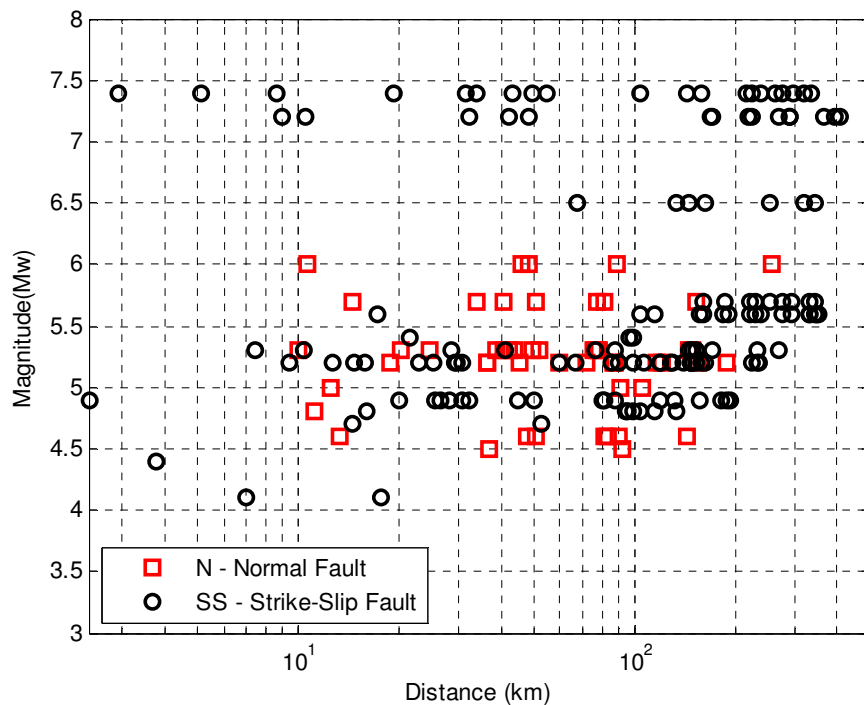


Figure 3.11. Moment versus Distance Values Sorted According to Fault Types

The distribution of earthquakes with respect to fault types is presented in Figure 3.11. As the figure shows, all the earthquakes were generated by either strike slip faults or normal faults due to the tectonic regime of the region.

The dampening of the amplitude of ground motion with the travelled distance is one of the facts of propagation dynamics. The main parameter that models the ground motion decay with the travelled distance is simply called as distance parameter. Generally, the ground motion amplitude is inversely proportional with the travelled distance. Figures 3.5 to 3.10 imply a nonlinear dependency of the ground motion amplitudes to the distances in each of the magnitude ranges and for different site classes.

3.4. Selection Process for the Appropriate GMPE

Indeed, there could be many different forms of equations, which would model the propagation of ground motions within reasonable accuracy. However, with the increasing number of seismic activity within the region, the functional forms and parameters of the equations could be adjusted to reflect the real behavior of the local propagation characteristics and the specifically developed GMPE for the region of interest could be improved. Fortunately, there are already several modeling studies about the earthquake propagation and large amounts of accumulated literature exist. Therefore, instead of creating an entirely new form for an equation, the available equations could be adapted. As a result of this approach, in the present study, several GMPEs are gathered as subjects of adaption procedures before using in a probabilistic seismic hazard analysis.

Since there is not a definitive method to evaluate and compare the performances of GMPEs, it is always difficult to select the most suitable equation. However, statistical tools provide means to evaluate the relative performance of the equations in modeling the local ground motion behavior. The first step in evaluation and comparison of the performance of GMPEs for a region is to compile seismic activity database of the considered region. It is only possible then to adapt the GMPEs by calibrating the coefficients of the equations with the local seismic data and compare the performances of the adapted GMPEs to select the best fitting equation.

The estimation of the coefficients of an equation require multiple linear regression analysis, which is a method used to model the linear relationship between a

dependent variable and several independent variables. Multiple linear regression is based on least squares; the model is adjusted in such a way that the sum-of-squares of differences of observed and predicted values is minimized. Before regression analysis is performed, the raw data has to be arranged in a proper format.

Researchers state that there is a relationship between the number of regressed parameters, the amount of data and the accuracy of the regression analysis. If the necessary amount of data is not provided, unstable regression causes the loss of meaning of the parameters. Therefore, considering the amount of data gathered for this study, GMPEs with high number of parameters are carefully handled and the necessary checks are performed for each parameter's performance.

In this study, the ground motion amplitudes in terms of spectral accelerations at the predefined spectral periods will be used as dependent variable, and the ground motion parameters of the earthquake records will be regressed with the spectral accelerations by using the functional forms of the selected GMPEs. The parametric coefficients of selected GMPEs will be derived and these coefficients will later be used for validation purposes and for the development of site-specific response spectrum curves.

Both single and multiple stage regression techniques will be applied for the calibration of the coefficients of the selected GMPEs. In general, the application of regression analysis in a single stage causes loss of relative dependence information of the data, e.g. dependence on magnitude or distance. Therefore, if the applicability of multistage multiple regression analysis is not found suitable, and an unexpected outcome is observed due to the unstable regression setup resulting from the limited amount of data, then single stage multiple regression analysis is utilized instead of multi stage analysis.

Lastly, the relative performances of the equations will be evaluated by using different statistical tools and various performance plots. The statistical evaluation of the performances with the basic statistical values of coefficient of determination, standard deviation and t-test results are just part of a larger regression and validation scheme. Unfortunately, the highest coefficient of determination values between the observed and predicted ground motion amplitudes are not sufficient for final decision unless the associated residual analysis and trellis plots confirm the statistical results

of the multiple regression analysis. Therefore, as a second step in the validation scheme, residuals or the differences between the observed and predicted ground motion amplitudes are analyzed. Residual analysis is a very powerful tool to observe the relative performances of the equations in modeling the data. The relative spread of the residuals, and the trends and patterns in the residual distribution give clues about the adequacy of the modeling. In the validation of GMPE models, residual analysis is definitely required before using any other tools for the evaluation.

If the residual analysis is not enough for the selection of the best fitting equation to the local propagation patterns, then trellis plots are generated as the last step. These plots are capable of offering the performances of GMPEs with respect to the whole range of distance, magnitude and site class parameters within desired period ranges. The provided information via these plots creates the opportunity to select the best performing functional form of the GMPE with desired performances. Hence, initially the statistical evaluation and residual analysis will be conducted and then trellis plots will be generated if necessary.

3.4.1. Initial Elimination

Before the application of the GMPE selection procedure that involves the multiple regression analysis, the initial selection criteria are applied in order to eliminate the equations with obvious incompatibilities with the local seismic behavior. The selected equations are subjected to the elimination by considering the relevance of the GMPE parameters, the requirements of the necessary parameters to model the magnitude and distance scaling characteristics of the ground motion amplitudes of the earthquakes in the sample and the applicability issues.

Among the listed GMPEs, the applicability criteria seem to be quite limiting to certain values of magnitudes and distances. However, since the aim of the study is to adapt the GMPEs by using the local seismic data, it is thought that most of these GMPEs must be included in the further steps of the evaluation. Therefore, unless an inconvenience is observed, the applicability limits that are imposed on magnitudes and distances are not taken into consideration in the first stage elimination.

Among the listed GMPEs, the equations of I02 and I08 are eliminated due to the lack of moment scaling terms in quadratic forms even though there are three ranges of moment magnitudes defined to model the moment scaling. Additionally, the

boundaries of the site shear wave velocities prescribed by the developer encouraged for the elimination. There is a single linear moment parameter for each defined range in the equations and they were created by using records with shear wave velocities greater than 450 m/s. Therefore, considering the moment scaling observed in the evaluation of the gathered data, and the shear wave velocities of the recording sites that generally stay below 450 m/s with 160 records out of 198, it was decided to eliminate these two equations in the initial elimination stage.

The equations of C97, CB03 and CY08 are eliminated due to existing complex parameters in the equations, which could result in an unreliable regression analysis considering the limited number of records gathered. Moreover, for some of the introduced parameters, no information is available for Eskisehir and the surrounding region.

3.5. Regression Analysis

Both single-stage and multi-stage multiple linear regression analysis are performed with the processed raw data. The site class is accepted as rock for all the GMPEs since the implementation of the multiple regression analysis is more convenient with site class assigned as rock.

Table 3.5. The Sigma Values Associated with the Multi-Stage Regression Analysis for PGA and Spectral Periods of 0.2 s and 1.0 s

GMPE	PGA			T=0.2 s			T=1.0 s		
	σ^{**}	τ^{**}	σ_{tot}^{**}	σ	τ	σ_{tot}	σ	τ	σ_{tot}
AS97	0.63	0.65	0.91	0.74	1.02	1.26	1.27	1.16	1.72
BJF97	1.36	0.73	1.54	1.32	0.95	1.63	2.71	1.28	3.00
SY97	0.67	0.63	0.92	0.76	0.73	1.05	1.19	1.04	1.58
OB04*	0.26	0.13	0.29	0.25	0.16	0.30	0.52	0.23	0.57
AS08	0.57	0.75	0.94	0.70	1.04	1.25	1.06	1.47	1.81
BA08	0.63	0.85	1.06	0.73	0.86	1.13	1.31	1.48	1.98
CB08	0.58	0.74	0.94	0.7	1.17	1.36	1.08	1.37	1.75
AC10*	0.88	0.92	1.27	0.94	1.26	1.57	1.57	1.46	2.14

*Different units are used for ground motion amplitude; therefore standard deviations are in different units.

** σ : first stage standard deviation, τ : second stage standard deviation, σ_{tot} overall standard deviation

Generally, in multi-stage multiple regression analysis, the magnitude and distance parameters are considered separately in two different stages. Sometimes, the site

parameters are also considered in a separate stage in order to eliminate the biases introduced by the site conditions of the different recording stations. However, only two stages are usually sufficient with magnitude and distance biases are minimized. By the introduction of two separate stages for distance and magnitude parameters, the record-to-record and event-to-event variability are captured.

The distance parameters are considered in record-to-record variability while magnitude parameters are considered in event-to-event variability. In the present study, because of the limited number of large magnitude events above 6.5, in multi stage analysis, GMPEs of AS97, AC10, AS08, BA08 and CB08 are modified such that instead of considering separate magnitude scaling parameters, both large and small magnitudes are considered in a single parameter.

In the first stage, the distance parameters are regressed with the ground motion amplitudes of each record and in the second stage, the magnitude parameters are regressed with the newly created parameter derived in the first stage for each event. As shown in Table 3.5, the multi-stage multiple regression analysis yielded high standard deviation values both in the first and second stages. The underlying reason for this high variability is the insufficient number of events for a reliable regression in the second stage, which causes higher variability in the overall regression. Therefore, considering the high sensitivity of the PSHA to the total standard deviations of GMPEs, instead of the results obtained from the multistage regression analysis, single stage analysis will be employed for further use in the study.

In the single stage analysis, the different magnitude bins that were originally developed to model the large magnitude scaling, are employed unlike multistage analysis. Despite event-to-event and record-to-record variability could not be observed, more reasonable statistical results are obtained with single stage analysis. The statistical results of these analyses are provided in Table 3.6 to show the relative performances of original and calibrated coefficients with the local data. Initially, in order to calibrate the coefficients, observed spectral accelerations and the parametric values of magnitude, distance, site shear wave velocity and fault style information gathered from 198 records are regressed in a single stage. Then, the calibrated coefficients are employed to predict the ground motion amplitudes in terms of spectral accelerations. These predicted spectral accelerations are then correlated with

the observed spectral accelerations. In order to compare the relative performance of the calibrated and original coefficients of GMPEs, original coefficients of the selected GMPEs are used with the same parametric values of the ground motions to obtain a different set of predicted spectral acceleration values. The predicted spectral accelerations are correlated with the observed spectral accelerations as it was done previously with the calibrated coefficients.

Both correlation studies resulted in statistical parameters of coefficient of determinations, R^2 , and standard deviations in logarithmic scale, $\sigma_{\ln(y)}$ that are compiled in Table 3.5. The table provides coefficient of determination and standard deviation for PGA, and for spectral periods of 0.2 s and 1.0 s. For all the GMPEs listed in the table, for PGA and spectral periods of 0.2 and 1.0 s, the coefficient of determination values are higher and the standard deviations are lower with the calibrated coefficients. Therefore, it is clearly shown that the calibrated coefficients perform better in modeling the raw data as expected.

Table 3.6. The Coefficients of Determination Associated with the Regression Analysis (With Original and Calibrated Coefficients)

GMPE	PGA				T=0.2 s				T=1.0 s			
	R ²	$\sigma_{\ln(y)}$	R ²	$\sigma_{\ln(y)}$	R ²	$\sigma_{\ln(y)}$	R ²	$\sigma_{\ln(y)}$	R ²	$\sigma_{\ln(y)}$	R ²	$\sigma_{\ln(y)}$
	Coefficients											
	Original		Calibrated		Original		Calibrated		Original		Calibrated	
AS97	0.77	0.83	0.83	0.60	0.67	1.27	0.83	0.69	0.66	1.28	0.68	1.18
BJF97	0.67	1.17	0.84	0.58	0.50	1.94	0.83	0.69	0.58	1.51	0.76	0.92
SY97	0.82	0.64	0.82	0.63	0.81	0.73	0.82	0.72	0.65	1.27	0.68	1.19
OB04*	0.71	0.19	0.83	0.26	0.67	0.24	0.82	0.30	0.57	0.30	0.74	0.44
AS08**	0.78	1.00	0.85	0.55	0.71	1.11	0.83	0.67	0.67	1.19	0.75	0.94
BA08	0.61	0.92	0.72	0.83	0.61	0.91	0.80	0.74	0.62	1.30	0.59	1.26
CB08**	0.81	0.65	0.85	0.55	0.78	0.84	0.83	0.67	0.68	1.14	0.75	0.95
AC10*	0.77	0.79	0.79	0.87	0.72	1.01	0.78	0.95	0.65	1.28	0.66	1.43

* Different units are used for ground motion amplitude; therefore, standard deviations are in different units.

** Nonlinear site terms are excluded.

Significance test was used to test the significance of the overall model and to check the significance of individual coefficients used in the equations. Tests on individual parameters resulted in varying levels of significance. The sensitivity of the t-test to sample size, distribution characteristics of the sample with respect to individual

parameters and even multi-collinearity issues might cause unexpected results in hypothesis testing. Therefore, residual analysis and trellis plots are given priority in evaluating the regression results.

Since the purpose of the study is to evaluate the functional forms of the GMPEs and the adaptability of these forms to the compiled database, some parameters and details of the equations are examined accordingly. In the practice, the original parameters of GMPEs in the modeling of the ground motion propagation are adjusted to reflect the databases used in developing these equations. Therefore, using the same methodology, a similar approach is employed in this study and each equation is subjected to modifications if necessary. The adjusted GMPEs indeed might result a deviation from the original performances, still it would serve the purpose of the study since the study claimed adaption of the best form of the GMPEs with calibrated coefficients. The following paragraphs explain the parameters of each GMPE in detail.

As one of the predecessors of the GMPEs of NGA project, Abrahamson and Silva (1997) developed a GMPE with two magnitude bins and introduced a parameter with distance and magnitude terms to model the large magnitude scaling. The site parameter is represented by values of peak ground acceleration for rock site, which was derived by an initial regression scheme that excludes the site related terms. The strong motion data used by the developers consisted of shallow earthquakes with magnitudes greater than 4.5. In the regression analysis of this study, all the parameters except for the hanging wall parameter is included in the regression analysis. The hanging wall parameter is omitted due to the lack of information in the database. After the analysis, it is verified that the calibrated coefficients for this study show higher performance as approved by the statistical parameters as shown in Table 3.5.

Boore, Joyner and Fumal (1997) developed a model with quadratic magnitude term, a combined magnitude and distance term and a site parameter, which is dependent on the uppermost shear wave velocity of the ground. The equation was developed by using earthquakes with magnitudes greater than 5.0 and distances less than 80 km. The developers also suggested the same limitations for the usage, as the magnitude is limited between 5.0 and 8.5, and the distance values that are less than 80 km is

suggested. The number of records in the database that comply with these requirements are only 24. The low number of records in the database that comply with the prescriptions of the BJK97 might cause a failure in the multiple regression analysis. Therefore, considering the aim of the adaptation procedure, it was decided to include all the earthquake records in the database and the multiple regression analysis is carried on. As shown in Table 3.6, the statistical results of the regression analysis showed a higher coefficient of determination and lower standard deviation values with calibrated coefficients. For Sadigh et al. (1997), among the equations developed for rock and soil sites, the equation that was developed for rock is used. The calibrated coefficients developed for this study have resulted in slightly more correlated spectral acceleration values with the observed values from the records as given in Table 3.6.

Ozbey et al (2004) developed an equation based on Boore, Joyner, and Fumal (1997). Only the site parameter is different in OB04. The database used in developing the equation is quite similar to the database used in the present study, with earthquake records selected only from GDDA sources. The record selection criteria is different from this study as the records from earthquakes with magnitude greater than 5.0 and epicenter to recording station distances of less than 100 kms were selected to develop the equation. Moreover, the focus of OB04 is northwestern Turkey, while in this study a region within 300 km radius circle centered at Eskisehir is considered. The statistical results of the regression analysis are provided in Table 3.6 for the calibrated and original coefficients. As part of the NGA project, the GMPEs AS08, BA08 and CB08 were developed to supersede the equations of AS97, BJK97 and BJK93, and C97 and CB03. Among the five set of NGA equations, I08 and CY08 are excluded from the multiple regression analysis phase due to the applicability issues. The NGA project compiled a large database of earthquakes with magnitudes ranging from 4.0 to 7.9. Employing this database in the derivation of coefficients, AS08 and CB08 set the applicability limit to minimum magnitude of 4.0, while BA08 set this value to 5.0 due to the reasons explained in Boore and Atkinson (2008). Though the database used in developing these equations is the same, the functional forms of the equations are quite different as presented in Tables 3.1 and 3.2. After this brief introduction of the NGA project, each of equation's performance is evaluated separately in the following paragraphs.

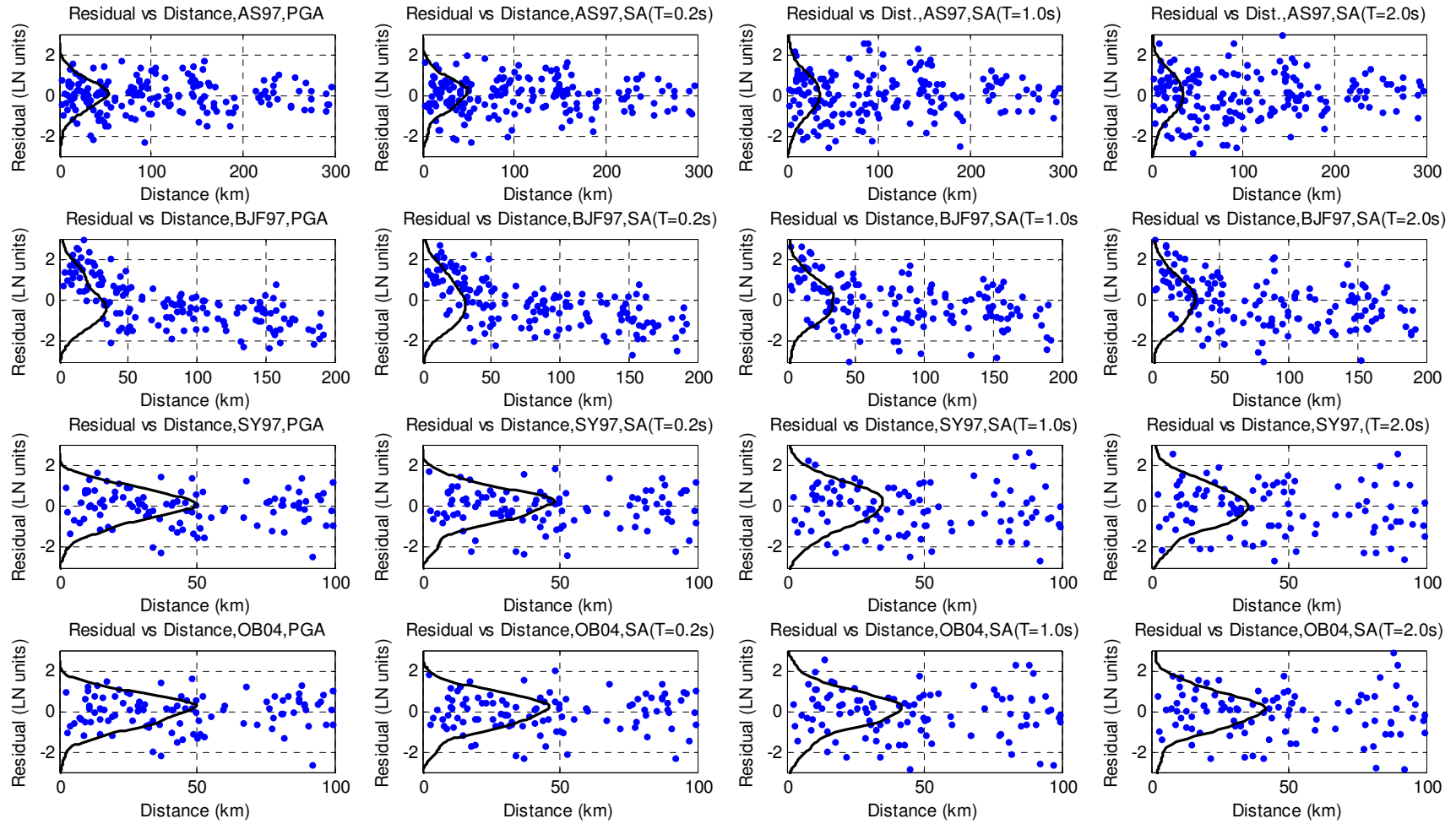


Figure 3.12. Residuals of Regression Analysis for AS97, BJJ97, SY97 and OB04

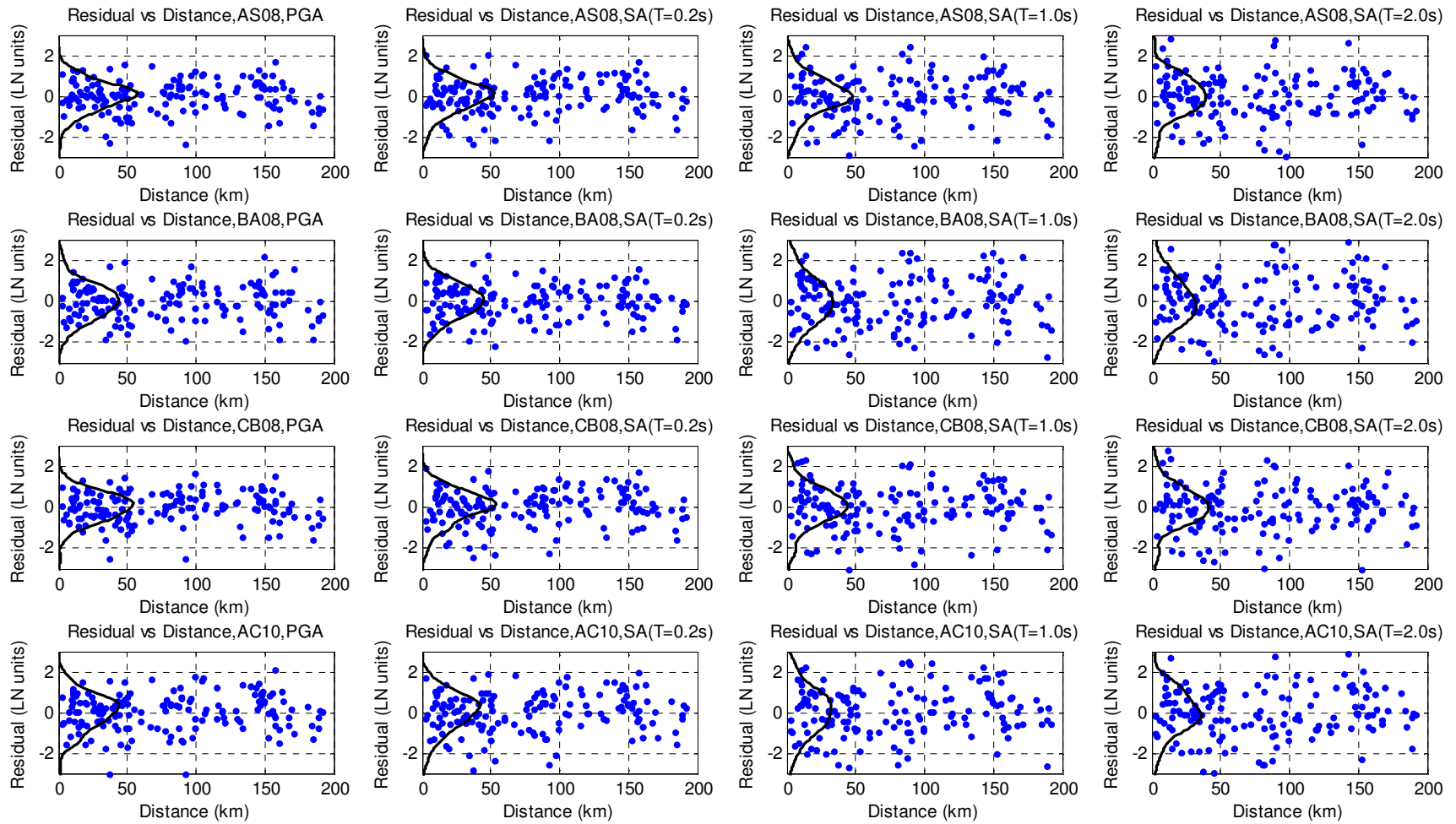


Figure 3.13. Residuals of Regression Analysis for AS08, BA08, CB08 and AC10

As mentioned, Abrahamson and Silva (2008) developed a complex equation within the framework of NGA equation development project, superseding AS97. The linear and nonlinear site parameters, parameters of depth to top rupture, large distance, and soil depth in addition to the factors of hanging wall and peak ground acceleration on rock are included in AS08. Since the site class of rock is assumed for the site parameters and due to the limitation of our knowledge for the target area, the parameters of hanging wall, depth to top rupture, large distance and soil depth are not considered in the evaluation. Nonlinear site effects are also excluded in the calibration procedures. Despite the omission of several parameters, the base model is found to be satisfactory in modeling the data, while the calibrated coefficients developed for this study perform better than the original coefficients of the equation.

Campbell and Bozorgnia (2008) introduced different magnitude terms for each of the three magnitude bins as shown in Table 3.1. In the equation, the fault parameters are introduced for normal and reverse fault types. The site parameters are similar to Abrahamson and Silva (2008). Moreover, hanging wall effects and basin response is introduced to account for the sedimentary thickness. The new terms that are introduced with this equation are the depth to top rupture coseismic plane, the rake angle, dip of the rupture plane, depth to the 2.5 km/s shear wave velocity and basin depth.

Due to the limited data, the mentioned parameters are omitted in addition to the nonlinear site parameters and the regression analysis is performed by using the base form of the equation including the parameters of magnitude, distance, linear site term and fault styles. The resultant statistical parameters are listed in Table 3.6 with both original and calibrated coefficients performing well.

Akkar and Cagnan (2010) developed a model claiming that the local seismicity must be represented well in a GMPE. Their equation is largely based on Abrahamson and Silva (2008) for the distance and magnitude terms and on Boore and Atkinson (2008) for the site response terms. The database that was employed in the derivation of the coefficients was gathered from Turkish strong motion database that was compiled by Akkar et al. (2010) and Sandıkkaya et al. (2010). Therefore, the database gathered for the development of the equation has similar distribution characteristics of the higher magnitudes with only two largest earthquakes of Izmit and Duzce earthquakes

included. It is a large database dominated by earthquakes with magnitudes between 5.0 and 5.8.

Overall comparison of results presented in Table 3.6 reveals that it is more appropriate to adapt the GMPEs to the local seismicity rather than using them with their original coefficients. In other words, the equations that were developed by utilizing the international seismic database or the equations that were developed for a specific region could be successfully adapted to local seismicity by adjusting the equations to the local seismicity and calibrating the coefficients by the local seismic data. Consequently, the GMPEs listed in Table 3.6 are utilized for further study in order to find the best fitting functional form of the GMPEs to the local seismicity.

Residual analysis is performed in order to verify the performances of the GMPEs with the local seismic data. The residuals that are obtained by calculating the difference between the observed and predicted spectral accelerations give the relative deviation of the predicted spectral acceleration from the original values. The residuals could be examined with respect to any parameter of the equation such as distance or magnitude.

In Figures 3.12 and 3.13, the residuals of GMPEs are presented. As shown in the figures, the residuals are clustered around zero except for BJF97, and there is no tendency of accumulation of residuals or no signs of relationship are detected, which is a good indication of the success modeling of local seismic data by the GMPEs. BJF97 residuals are biased with a decreasing trend for distances up to 50 km and there is a sign of nonlinearity of the data in terms of distance scaling. Moreover, normal distribution characteristics of the residuals are observed in all the GMPEs as shown in Figures 3.12 and 3.13 as the distribution functions are presented on the left side of each subplot. The narrower residuals of OB04 and the wider range of residuals observed in AC10 are caused by the different units used for the ground motion amplitude. While not presented here, the residuals with respect to magnitudes also show no sign of relationship. With all the valuable information provided by the residual analysis, it should be admitted that none of the equations could be singled out for the best performance; therefore, trellis plots will be created in order to observe the relative performances of the GMPEs.

3.5.1. Trellis Plots of GMPEs by Using Original and Calibrated Coefficients

Trellis plots provide a powerful visual tool to display the performances of GMPEs in application. These plots could be generated for distance, magnitude, and site class scaling of the ground motion amplitudes. In these plots, generally the behavior of the ground motion amplitude is observed for a number of magnitudes, distance values and site classes.

In order to evaluate and compare the performance of the models with original and calibrated coefficients, an arbitrary earthquake with magnitude of $M_w=7.0$ at distances of 10 and 50 km with site class assumed as rock and hypocentral depth of 20 km's is considered. The hypocenter depth is carefully selected considering the high sensitivity of the expected acceleration to the log distance scaling.

The generated spectral curves for the models using the original and calibrated coefficients are compared. Several plots are created in order to see whether the performances of the generated curves are in agreement with the findings and assumptions about the original and derived coefficients.

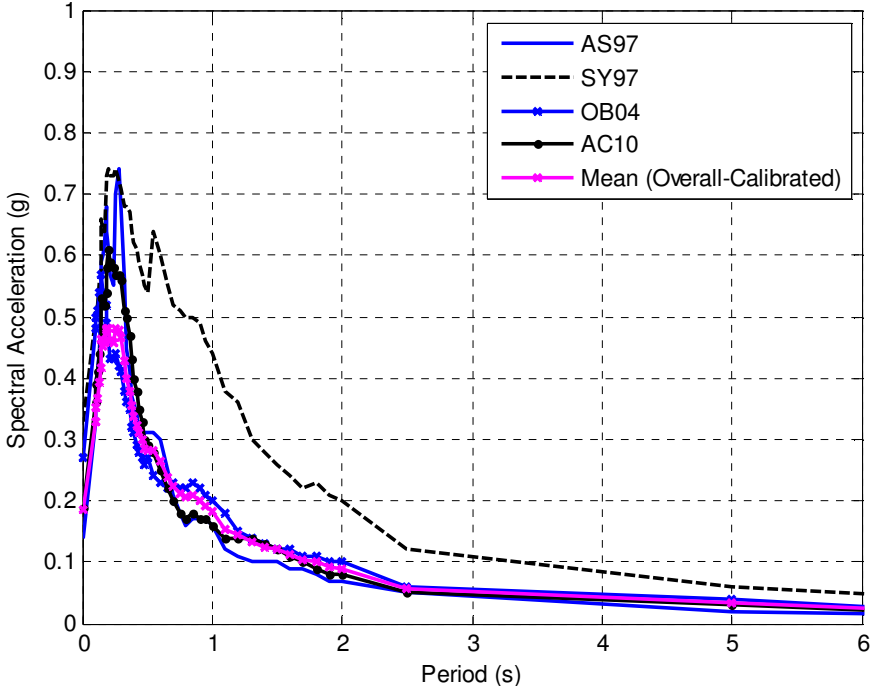


Figure 3.14. Response Spectrum developed by GMPE Models for $M_w = 7.0$ and $R= 10$ km, depth=20 km (Models are AS97, SY97, OB04 and AC10 with Calibrated Coefficients)

Figure 3.14 presents the response spectrum curves developed by using AS97, SY97, OB04 and AC10 with calibrated coefficients. The peak spectral accelerations of the models are in a close range. There are sizable deviations from the overall average curve that is calculated by using all the GMPEs listed in Table 3.6. Starting from the peak spectral acceleration, SY97 takes a different path with higher spectral accelerations. The largest of peak spectral accelerations is around 0.73g for AS97, and the smallest is 0.62g for AC10. Figure 3.15 shows the response spectrum curves plotted for the same models with the original coefficients. The curves are not in general agreement in a wide range of spectral periods since the ranges of spectral accelerations are very different. The values of peak spectral acceleration range from 0.36g to 0.61g. The main differences observed between the models in Figure 3.14 are the range of peak spectral accelerations and the SY97 behavior at large periods. Obviously, the peak spectral acceleration values are larger with the calibrated coefficients.

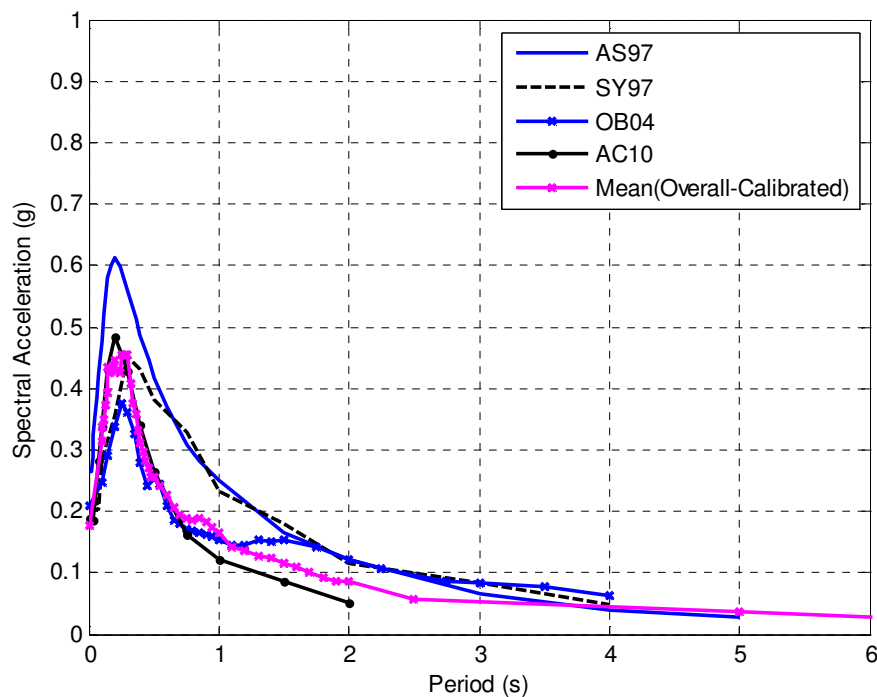


Figure 3.15. Response Spectrum developed by GMPE Models for $M_w = 7.0$ and $R = 10$ km, depth=20 kms (Models are AS97, SY97, OB04 and AC10 with Original Coefficients)

Figure 3.16 demonstrates the performance of the GMPEs with calibrated coefficients for $M_w=7.0$ with a distance of 50 km and with the same site conditions. The peak spectral acceleration values decrease dramatically as is the case with the other

spectral values. The order of GMPEs according to their peak spectral accelerations change when compared with the GMPEs in Figure 3.14. It is obvious that especially SY97 failed to follow the suit when compared with Figure 3.14, while the other three GMPEs have their spectral acceleration values scaled accordingly with the distance. The outlier performance of SY97 could be attributed to its distance parameters, which differs by scaling the ground motion amplitude with two different terms as shown in Table 3.1, while the other equations propose different parameters for the scaling of the ground motion amplitude with the distance.

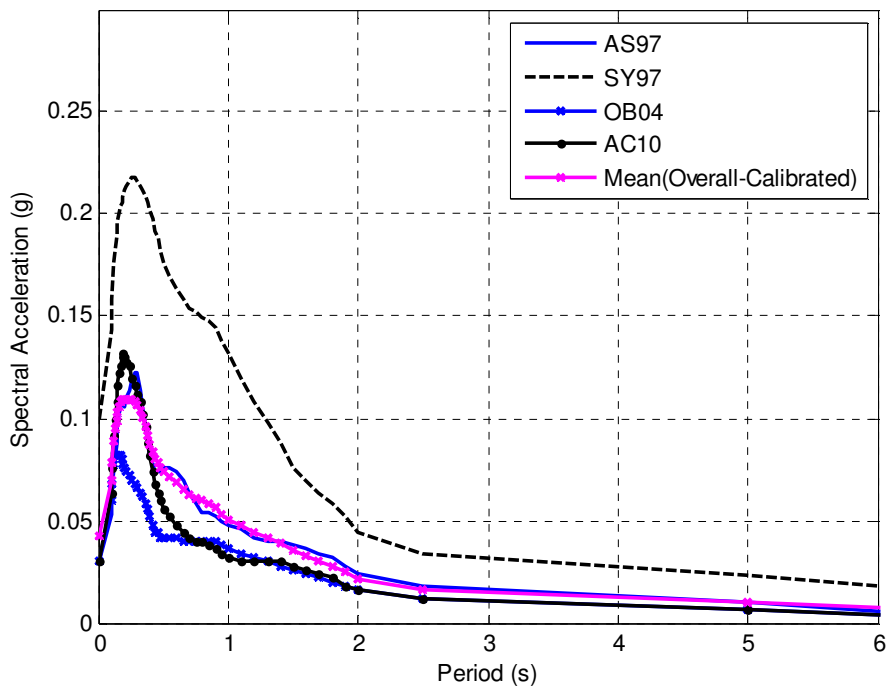


Figure 3.16. Response Spectrum Curve Developed for $M_w = 7.0$ and $R = 50$ km (Models are AS97, SY97, OB04 and AC10 with Calibrated Coefficients)

Figure 3.17 is specially created for the same purpose of comparing the performances of the GMPEs that are equipped with the original coefficients for $M_w=7.0$ with a distance of 50 km. The equations do not align in the same order with respect to their peak spectral acceleration values compared to the values observed in Figure 3.16. Furthermore, the effect of distance scaling on GMPEs clearly distinguishable as the peak acceleration values decrease dramatically for the distance of 50 km. AS97 and SY97 seem to be less affected by the increasing distance compared to AC10 and OB04.

The Figures 3.14 and 3.17 clearly demonstrate the effect of the calibrated coefficients on the outcome of the response spectrum curves. The variation observed in the performances using original coefficients does not seem to fade away with the calibrated coefficients. However, the observed distance scaling using the original coefficients seems to be less than the observed scaling using the calibrated coefficients. This behavior could be attributed to the local seismic activity in that the decaying of the ground motion within shorter distances could be a pattern. Particularly, the decaying of the ground motion with AC10 for both calibrated and original coefficients deserves special attention, since the equation was derived by using the seismic data of Turkey.

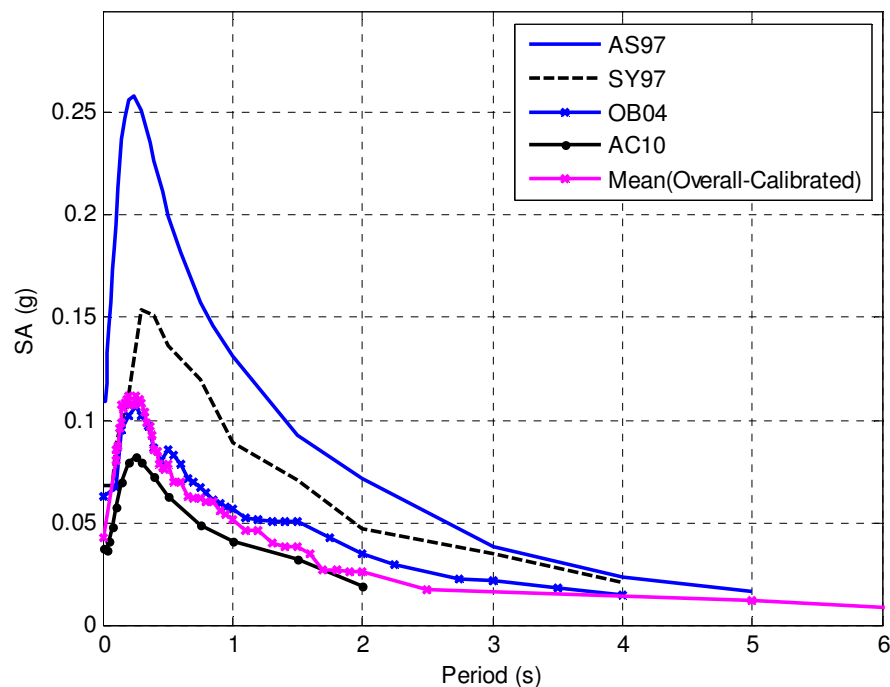


Figure 3.17. Response Spectrum Developed for $M_w = 7.0$ and $R = 50$ km (NGA Models are AS97, SY97, OB04 and AC10 with Original Coefficients)

Figure 3.18 is developed for the purpose of evaluating the new generation GMPEs with the calibrated coefficients. BA08, AS08 and CB08 are selected for the evaluation. The resultant response spectrum curves cover a narrow range of values of peak spectral acceleration, with the smallest one being 0.20g for BA08 and largest one being 0.36g for CB08. Figure 3.19 is created with the same models but with the original coefficients. The models perform in a very different range of peak acceleration values compared to Figure 3.18 with a range of 0.26g to 0.56g.

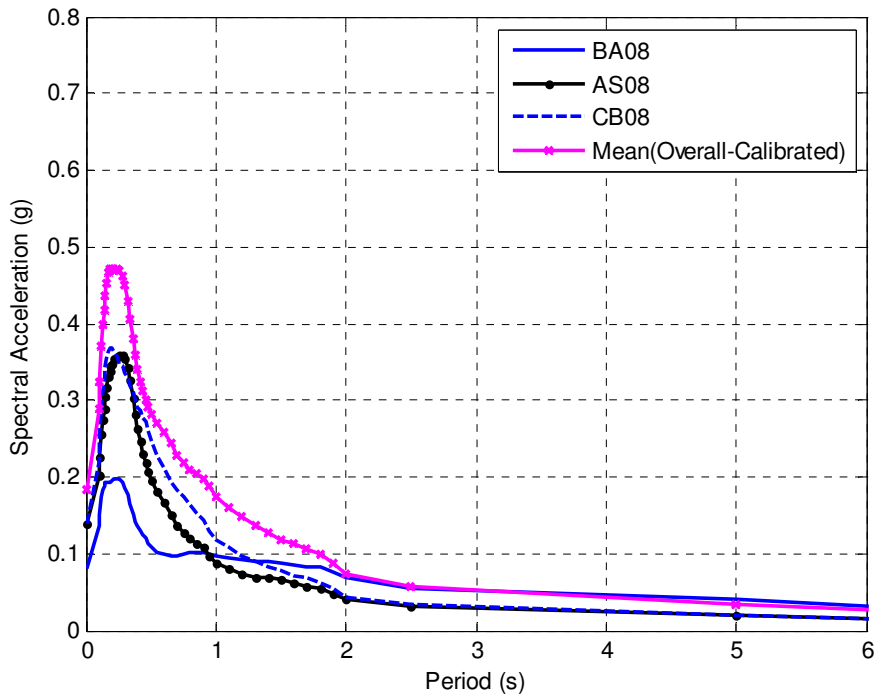


Figure 3.18. Response Spectrum developed by NGA Models for Mw = 7.0 and R= 10 km (NGA Models are BA08, AS08, CB08 with Calibrated Coefficients)

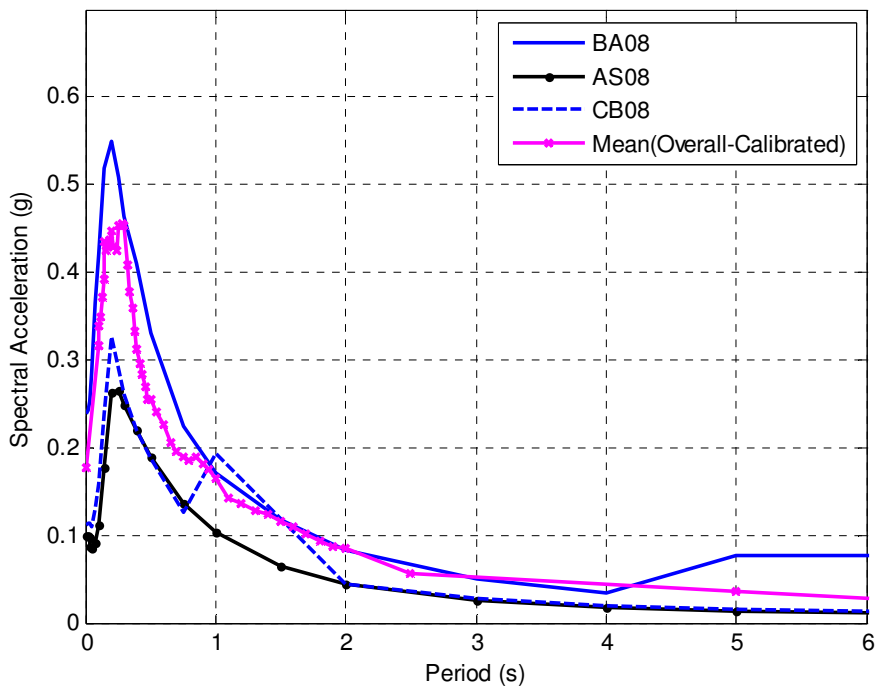


Figure 3.19. Response Spectrum Curve Developed by NGA Models for Mw = 7.0 and R= 10 km (NGA Models are BA08, AS08, CB08 with Original Coefficients)

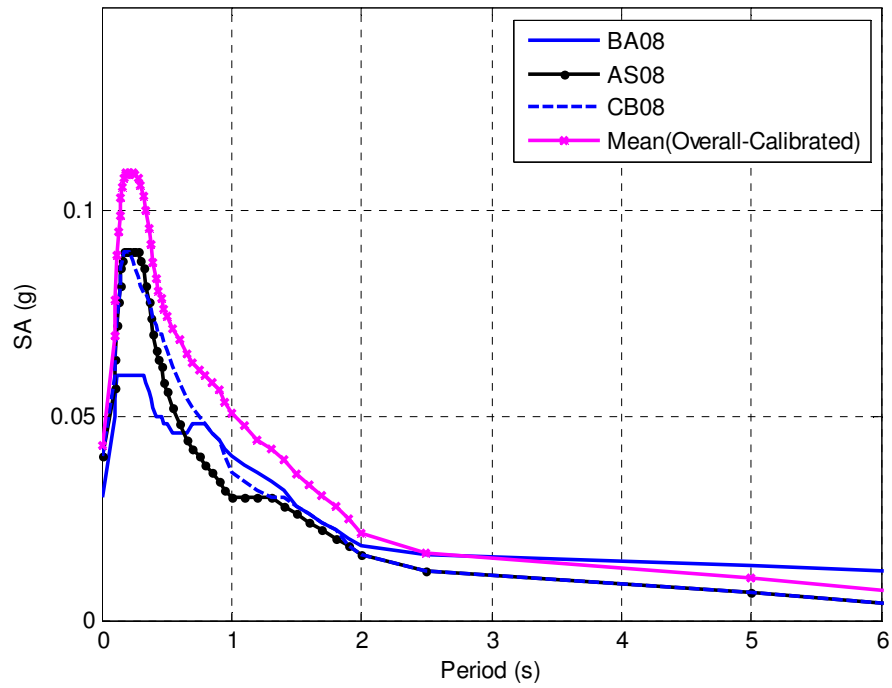


Figure 3.20. Response Spectrum developed by NGA Models for $M_w = 7.0$ and $R = 50$ km (NGA Models are BA08, AS08, CB08 with Calibrated Coefficients)

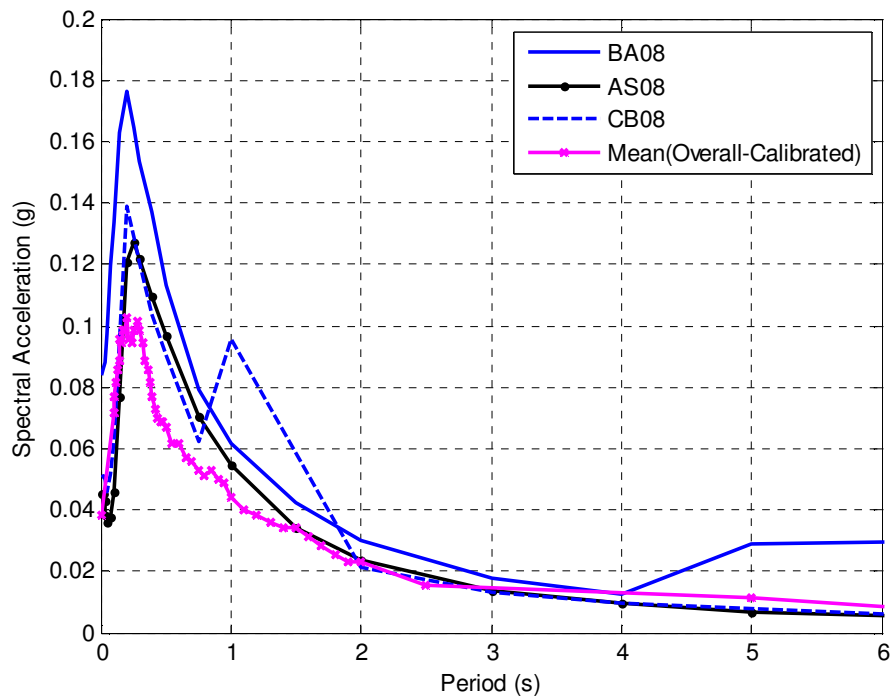


Figure 3.21. Response Spectrum developed by NGA Models for $M_w = 7.0$ and $R = 50$ km (NGA Models are BA08, AS08, CB08 with Original Coefficients)

Figures 3.20 and 3.21 show the behavior of the new generation GMPEs for a distance of 50 km with the $M_w=7.0$ magnitude earthquake. The performance of the GMPEs shows a considerable variation, and no pattern of behavior is observed in

terms of the order of the GMPEs in the values peak spectral acceleration. However, the substantial distance scaling of the ground motions with the calibrated coefficients is clearly observed.

The fact that the response spectrum curves obtained for distance of 10 km with original coefficients remain below the average curve whereas the curves obtained for a 50 km distance with original coefficients stay above the average curve, prove that distance scaling with the original coefficients is less than the scaling observed with the calibrated coefficients. In addition, it is clearly demonstrated that the peak spectral accelerations of BA08, AS08 and CB08 are reduced more with calibrated coefficients compared to the reduction observed with the original coefficients.

The comparison of the performances of GMPEs with the original and calibrated coefficients involved a strong visual evaluation of the GMPEs, while the statistical tools are utilized for each parameter of the equations for their individual performance. As the elimination scheme of the models required a solid statistical analysis such as significance test, the visual representation demonstrated the behavior of the equations in modeling the raw data and development of the response spectrum curve. Figures from 3.14 to 3.21 proved that a big variation exists among the GMPEs in predicting the values of response spectrum curves, given that most of these equations have different ranges of applicability and the database used in their development varies.

After the evaluation of the trellis plots, it is decided to use the calibrated coefficients since it is thought that there could be a local pattern of propagation, which is reflected by the rapid decay of the ground motion, or the magnitude range used in the database is forcing the rapid distance scaling. As the values of coefficient of determination and standard deviations strongly convince in regards to the use of calibrated coefficients, together with the residual analysis supporting this view, the plots given in Figures from 3.14 to 3.21 are also strongly in favor of using calibrated coefficients. The study of the performance comparison of the GMPEs with original and calibrated coefficients yielded an important outcome. A higher decay of the spectral curves is observed with the distance for all the GMPEs with calibrated coefficients, whereas the same decay is not observed with the original coefficients. This special decay suggests the existence of a local propagation pattern, which also

is validated by the behavior of local GMPEs of AC10 and OB04 for both calibrated and original coefficients and points to the magnitude range used in the analysis.

As expected, the equations with calibrated coefficients yielded results that are more successful in statistical terms. Since the database used in the derivation of the calibrated coefficients was also used to predict the ground motion amplitudes with the original coefficients for comparison purposes, the success of the equations with calibrated coefficients is not a surprise. However, it has to be demonstrated that before using a GMPE for a specific area, the local patterns of earthquakes must be known and if necessary a site-specific equation must be derived or a selected GMPE must be adapted. Consequently, the final site-specific response spectrum curves with the given parameters and with the calibrated coefficients are presented in Figures 3.22 and 3.23. The trellis plots or performance plots provided very valuable information on the performance of the GMPEs with original and calibrated coefficients. It is observed that most of the equations are very susceptible to distance parameter and the variance of the performances do not disappear with the calibrated coefficients. This observation, however, is not sufficient to identify the best performing GMPE, therefore additional trellis plots are prepared, which magnitude and distance scaling of the ground motion amplitudes are observed.

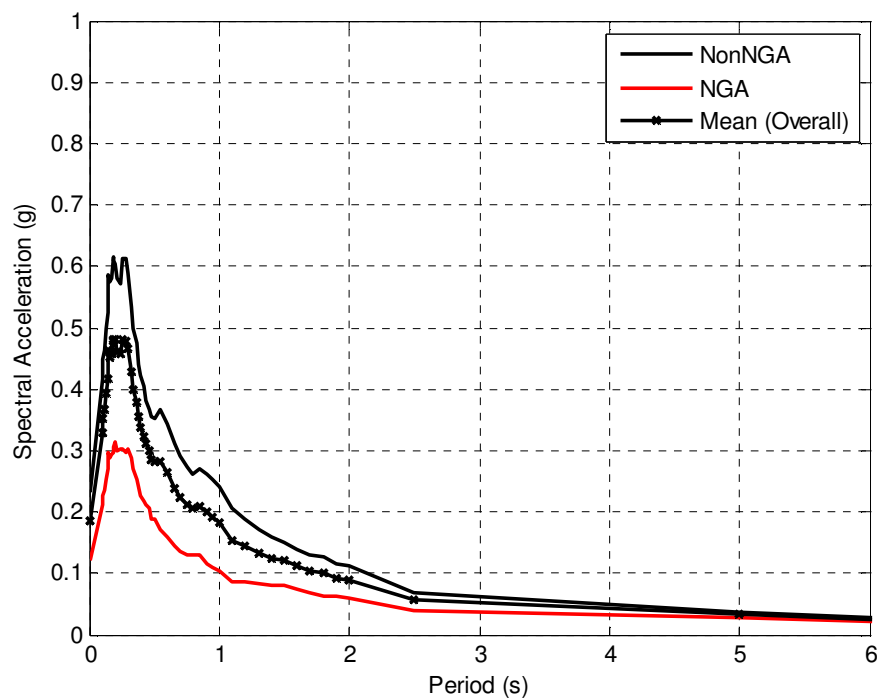


Figure 3.22. Average Response Spectrum Obtained by the Average of non-NGA and NGA Models ($M_w=7.0$ and $R=10$ km) with Calibrated Coefficients

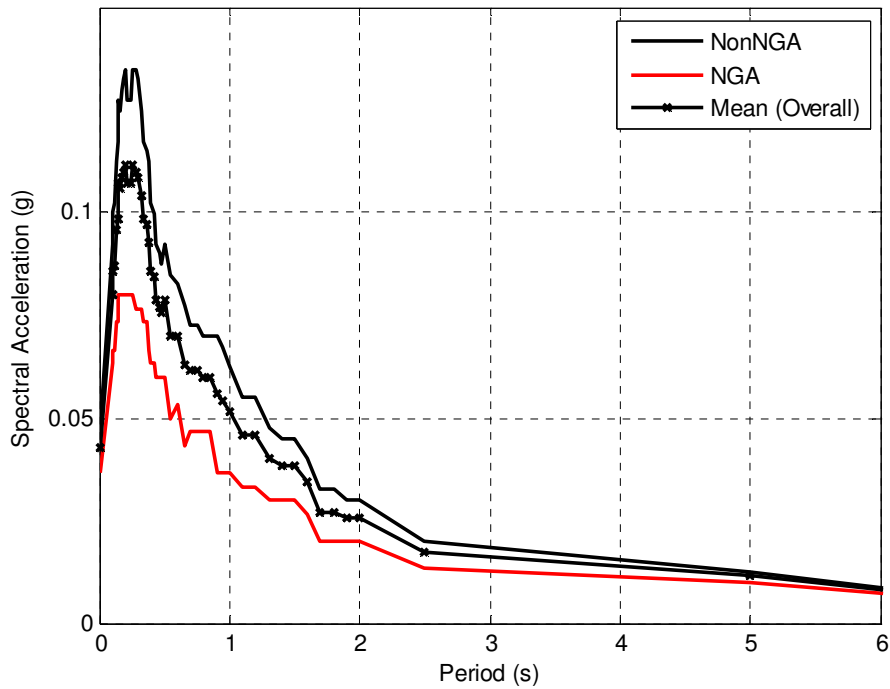


Figure 3.23. Average Response Spectrum Obtained by the Average of non-NGA and NGA Models ($M_w=7.0$ and $R=50$ km) with Calibrated Coefficients

Considering the previous steps for the assessment of the selected GMPEs, out of eight remaining equations, only BKF97 was eliminated due to the observed pattern in the residuals. If Table 3.6 is closely examined, among the GMPEs listed, only BA08 stands out with the lowest values of coefficient of determination and the highest values of standard deviation with calibrated coefficients. The response spectrum plots also did not provide enough information regarding the best performing equation. Therefore, trellis plots with a wider range of magnitudes, distances and spectral periods are created as shown in Figures 3.24 to 3.26 and in Figure 3.28. The hypocentral depth used in rupture distance is accepted as 20 km as previously assumed for trellis plots in Figures 3.14 to 3.21.

Distance scaling can be carefully examined for within a range of magnitude and periods. Confirming the performances of GMPEs in Figures 3.14 to 3.21, SY97 is less susceptible to distance scaling, while OB04 and AC10 is observed to be highly sensitive to the distance parameter as the spectral acceleration values decay more rapidly with the distance than the other GMPEs. Compared to AC10 and OB04, except for the spectral period of 0.2 s with calibrated coefficients, the rest of the equations show a lesser degree of distance scaling both with the calibrated and original coefficients as shown in Figures 3.24, 3.25 and 3.26. In order to find out the

underlying reason of this decay with the distance, the spectral acceleration-distance curves obtained by calibrated and original coefficients are plotted, while the curves obtained by the original coefficients are shown on the background with gray color in Figure 3.26. There is a slightly greater decay of ground motions experienced for all the GMPEs, except for SY97, with the calibrated coefficients.

Initially, the reason of slightly greater decay of the ground motions with the calibrated coefficients is investigated. In fact, a through explanation of the influence of magnitude range of the database on the scaling characteristics of the ground motions is provided in Boore and Atkinson (2008). As stated in their study, depending on the trigger thresholds of the instrumentation, some of the earthquakes are not even recorded at some distances, which in the end would lead to a false assumption that the earthquake waves die out at closer distances. For example, the lack of any record beyond 50 km might give a wrong impression about the behavior of an earthquake of size 6.0 that could potentially be recorded as far as 100 km with the existing instrumentation. In addition, beyond certain distance, it is already difficult to record the earthquake waves due to the technical limitations mentioned. Additionally, another earthquake with the magnitude 7.0, which is recorded at all possible distances before it dies out completely, could create additional problems in the database such that, beyond 50 km, the regressed parameters are provided only for the large magnitude earthquakes. Eventually, if the developed equation is applied for an earthquake with magnitude smaller than 7.0, the predicted behavior of the earthquake would not reflect the real data. Therefore, the amplitude cutoff levels of the instrumentation at the recording stations and consequently the exclusion of the smaller magnitude earthquakes eventually lead to over-prediction of ground motion amplitude. Considering this fact, which is stated in Boore and Atkinson (2008), if the distance scaling of lower magnitude earthquakes was modeled by the GMPE that was developed by the database, which is dominated by larger magnitude earthquakes, the predicted lower magnitude earthquake behavior with the distance would be biased. Therefore, it is concluded that the magnitude range of the compiled database and the associated spectral acceleration values, have strong influence in the modeling of GMPEs. The GMPEs with the original coefficients are obviously weak in the modeling of the local ground motion behavior.

Considering the significant rate of decay in AC10 and OB04 for both original and calibrated coefficients, the higher rate of decay indeed could be attributed to the distribution characteristics of the Turkish strong motion data, which lacks large magnitude records similar to the compiled database in this study. However, it should be noted that both AC10 and OB04 was developed by using the ground motion records of the earthquakes with magnitudes larger than 5.0. Therefore, it is deduced that another mechanism or source could also be reducing the values of spectral accelerations of GMPEs with the calibrated coefficients.

It is identified that, the magnitude distribution of the ground motions in the database with which the GMPEs are developed; cannot be the sole reason for the rapid decay of the ground motions. Therefore, the influence of the local seismic structures is investigated since they seem to play a role in the distance scaling as well. Considering the acceleration-distance plots of Figure 3.26, with almost all the GMPEs with calibrated coefficients showing a relatively faster decay, and the decay of ground motions with AC10 and OB04 for both original and calibrated coefficients, this possibility about the local seismic behavior could be a valid one. As there are findings of rapid distance scaling of European strong motion compared to the strong motions of California (Douglas, 2004), there are also findings about the rapid decay of Turkish strong motion within shorter distances. In order to verify the inherent distance scaling observed in the local database, the measured spectral acceleration values of the two largest magnitude earthquakes are compared against the predicted acceleration values by the GMPEs with original coefficients. The magnitude, distance and site parameters of the recorded earthquakes are used with the original coefficients of the GMPEs and spectral accelerations are predicted. As shown in Figure 3.27, the predicted spectral acceleration values are becoming larger than the measured acceleration values as the distance increases for all GMPEs except for AC10. Therefore, it is concluded that, the cause of the relative distance scaling observed with the calibrated coefficients is not only the magnitude distribution of the database, but also the inherent local behavior of the wave propagation. The reason behind the successful modeling of the rapid decay is the moment and distance terms of the base form of the equations.

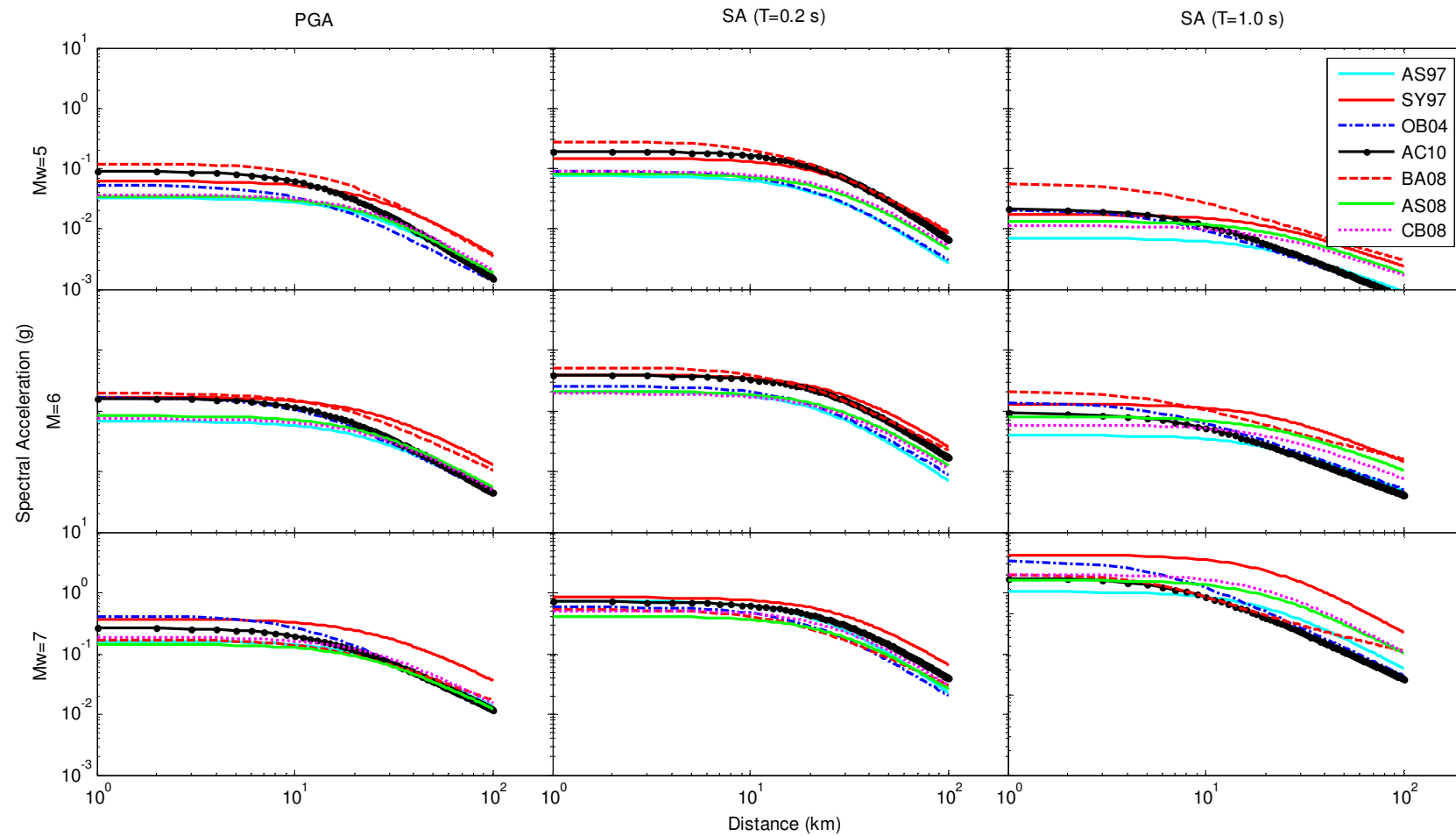


Figure 3.24. Distance Scaling of Ground Motions Modeled by GMPEs with Calibrated Coefficients

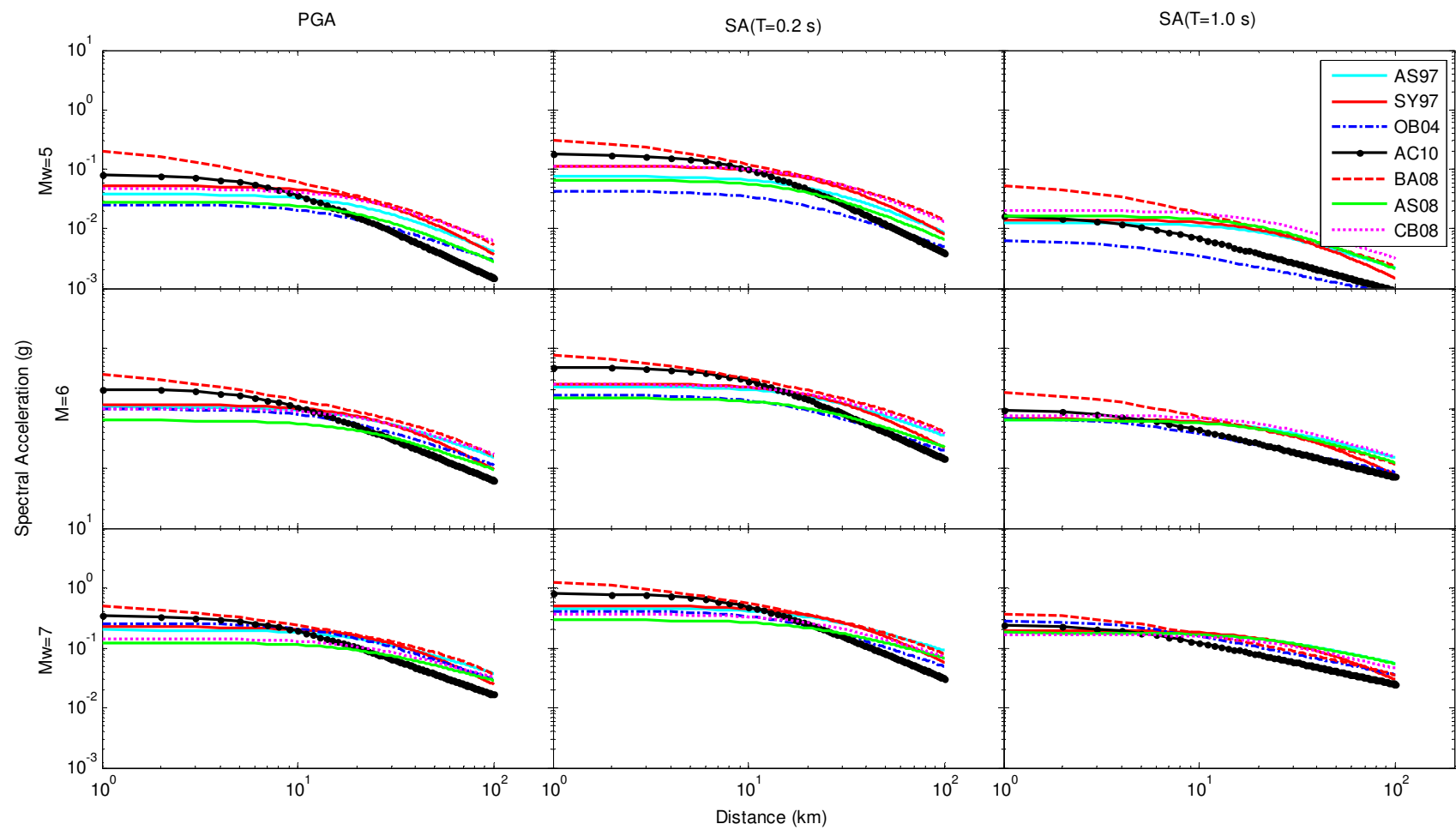


Figure 3.25. Distance Scaling of Ground Motions Modeled by GMPEs with Original Coefficients

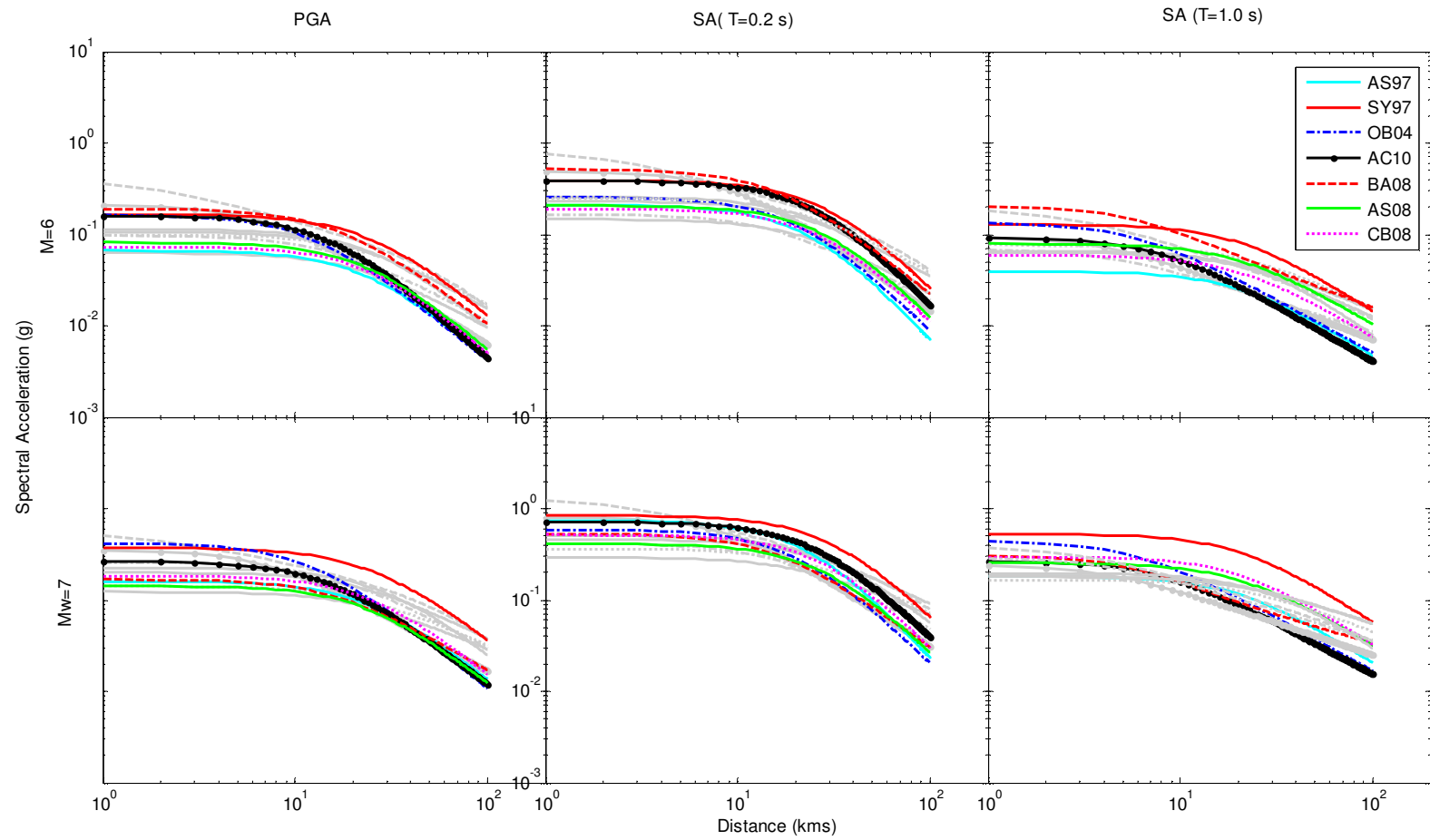


Figure 3.26. Distance Scaling of Ground Motions Modeled by GMPEs with Calibrated and Original Coefficients (Performance Curves with Original Coefficients are shown in Gray Color in the Background)

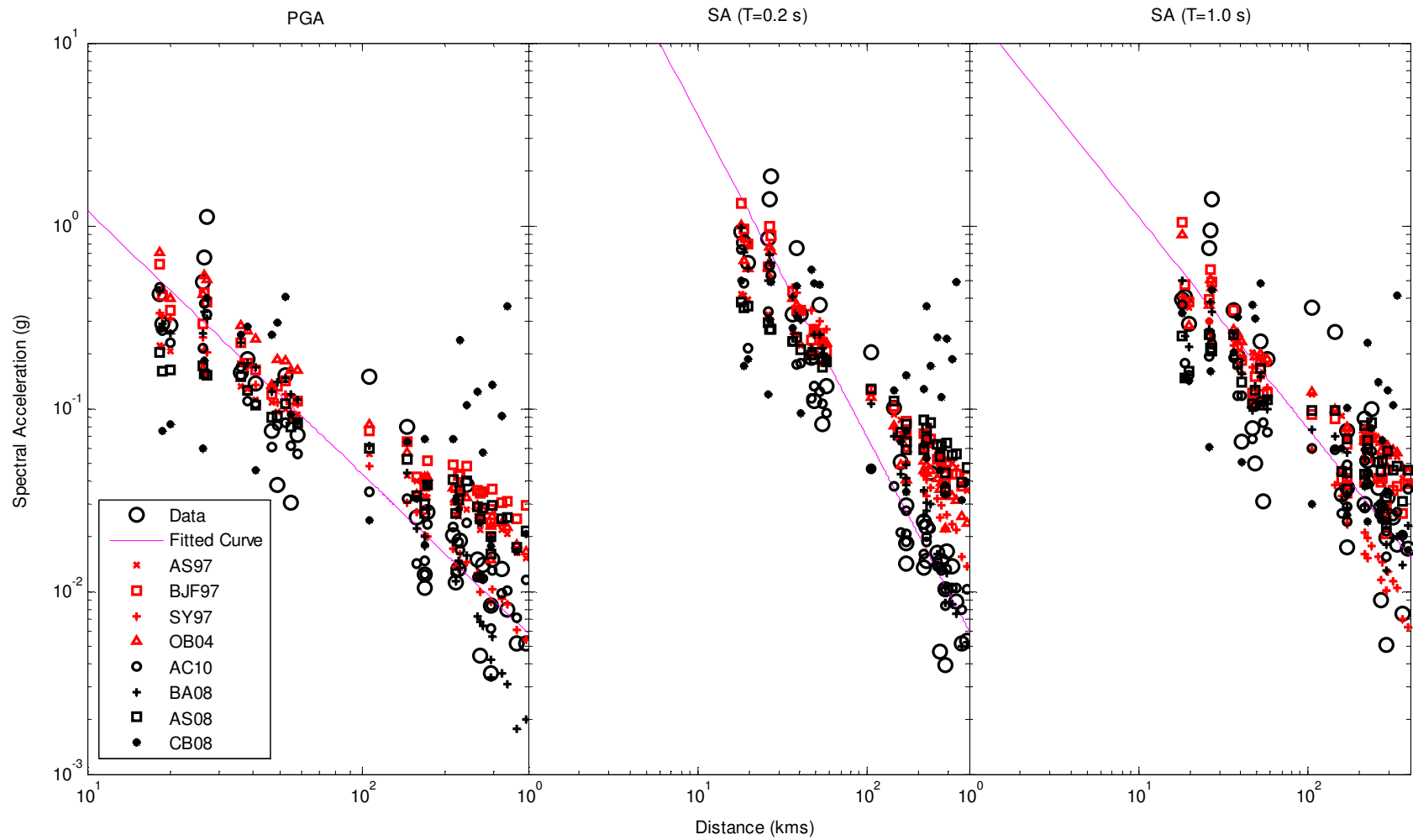


Figure 3.27. Comparison of Recorded Acceleration Values of Kocaeli and Duzce Earthquake Data with the Predicted Values by GMPE'

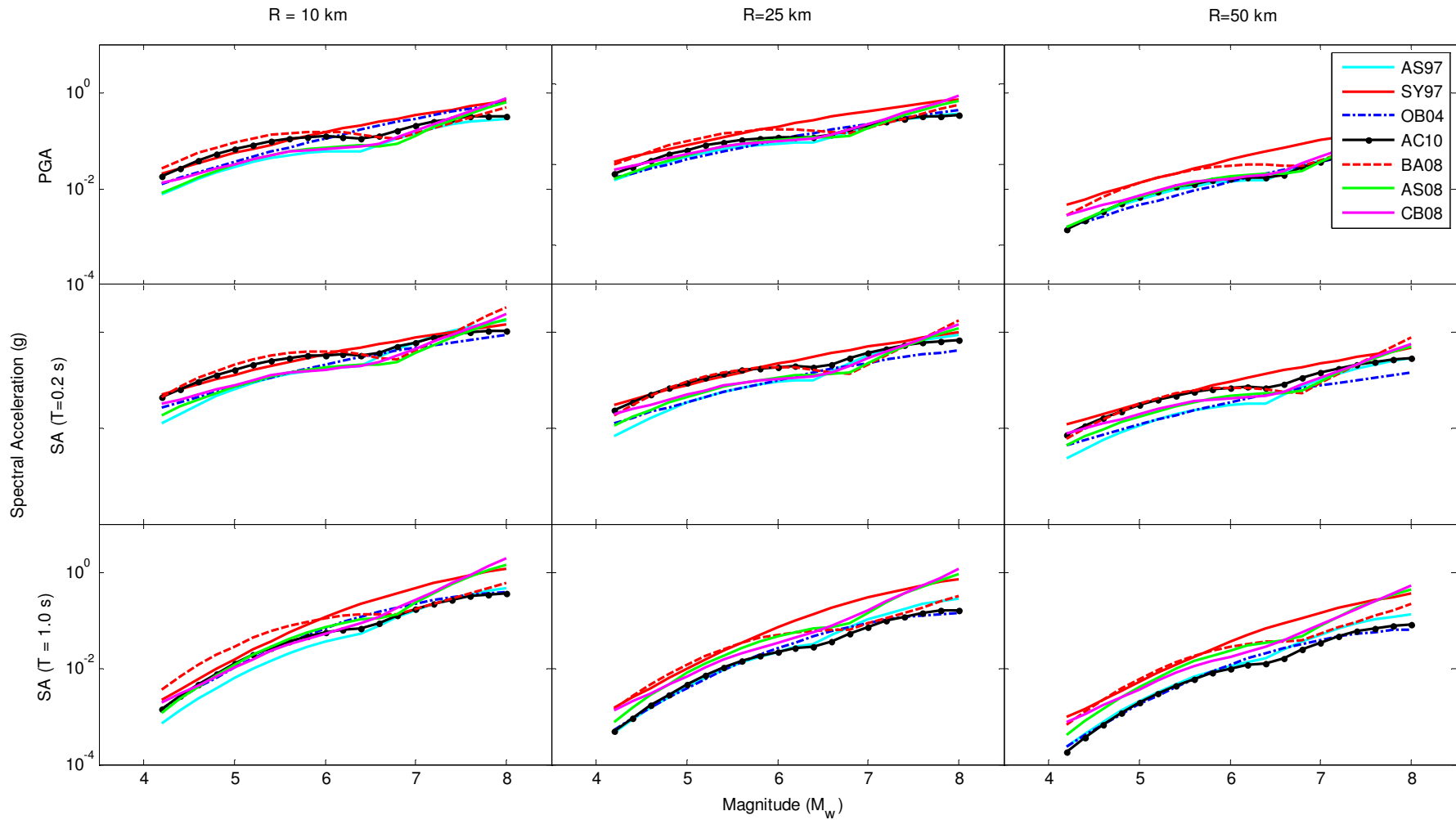


Figure 3.28. Distance and Magnitude Scaling of Ground Motion with Calibrated Coefficients

Comparing the performances of AC10 and AS08, which have the same base form with magnitude and distance terms, it is deduced that, the distance parameter predict higher ground motion scaling if the Joyner-Boore distance is used. Considering the depth term used in the rupture distance, the ground motion is already assumed that it travelled and propagated through a distance which indeed modeled numerically by the depth. Therefore, compared with the distance scaling parameter that contains the Joyner-Boore distance, the ground motion is supposedly travelled through a distance when using the rupture distance term. This phenomenon is already observed in Figures 3.14 to 3.21, as the GMPEs of AC10 and AS08 which have the same base forms with the only difference being the distance terms, the equations with the rupture distance terms do not display the same behavior in distance scaling. Obviously, the rapid decay is captured by the coefficients of the AC10 that are derived by using the Joyner-Boore distance. The MATLAB program for deriving the coefficients of AC10 is given in Appendix B for reference purposes.

Evaluating the equations in Figure 3.24, it is worth mentioning that BA08 seem to have the highest acceleration values for magnitudes of 5.0 and 6.0 for PGA and spectral periods of 0.2 s and 1.0 s, while it stays at lower values of acceleration for $M_w=7.0$. AS97 has a similar pattern of performance with the highest values observed for $M_w=7.0$ at the spectral period of 0.2 s.

For the rest of magnitude and period values, AS97 has quite lower values compared to the rest of the GMPEs. CB08 and AS08 consistently have lower range of spectral acceleration values. SY97 is least affected by the distance decay characteristics of the data, which is understandable considering the distance scaling parameters of the equation. In Figures 3.24, it is clearly observed that OB04 has similar characteristics with AC10 in modeling the rapid decay of the ground motion with the distance whereas; the same distance scaling is not observed with the original coefficients of the equation.

The magnitude scaling plots in Figure 3.28 offers valuable information especially for the equations with more than a single magnitude bin. The behaviors of the GMPEs below and above the magnitude value that splits the equations are distinguished with two separate curves, which indicates the abrupt transformation of the equation with the expression of large magnitude scaling. The split magnitudes are 6.4 for AS97,

6.75 for AS08 and BA08, 6.5 for AC10 and CB08, respectively. At these magnitudes, it is obvious that the performances of the GMPEs change swiftly for AS08, BA08, CB08, AS97 and AC10. Among these equations, AC10 has a smooth transition of spectral acceleration values from one magnitude bin to the other.

The reason for this abrupt change in the GMPEs at the split magnitudes is the local bias introduced by the employment of local earthquakes. While the equations are designed according to the databases gathered by the developers, the split magnitudes and different expressions for different ranges of magnitudes are all introduced by considering the performance of the GMPE. As one of the performance measures, the smooth transitions between the different magnitude bins are also determining factor in the modeling of the equation. The abrupt change at the split magnitudes are also taken into account in the selection of the best performing GMPE.

As a result of the examination about the local seismic behavior specific to the region, and considering the relative performances of the selected GMPEs with the calibrated and original coefficients, without the need for further inquiry, it is concluded that local data must be definitely be used to adapt the GMPEs or to adjust the GMPEs to the local conditions.

3.5.2. Final Selection

Following all the assessments of candidate GMPEs and especially following trellis plots, the determination of the right choice or right choices for the seismic hazard analysis is relatively easy. Among the eight GMPEs listed in Table 3.4, BJF97 was removed from the list due to the observed nonlinearity in the residual analysis, and BA08 was already singled out with the low coefficient of determination and high standard deviation.

When all the NGA equations are considered, it is observed that the distance scaling inherent in the local seismic data is not strongly expressed with the original and calibrated coefficients. Moreover, the moment scaling plots are not smooth enough for AS97, BA08, AS08 and CB08. Therefore, the NGA equations are not found to be suitable for the seismic hazard analysis of Eskisehir. Contrary to AC10 and OB04, SY97 reduces the acceleration values with two separate parameters of the distance; therefore, as given in Figures 3.24 to 3.26, the acceleration values at farther distances

are the highest among all the equations. Hence, it is obvious that SY97 does not serve the purpose of this study either.

Consequently, only AC10 and OB04 are found to be appropriate GMPEs regarding the modeling of the local seismicity. Before finalizing the selection of the most appropriate equation, it should be mentioned that, the fact that the local data was employed for the derivation of the original coefficients already created a bias towards AC10 and OB04. Moreover, the success of OB04 and AC10 in expressing the local seismicity with the originally derived coefficients is a convincing factor in the selection process. Between OB04 and AC10, both of which were developed by using Turkish strong motion database, AC10 is more credible with strong distance and magnitude scaling observed in the Figures of 3.14 to 3.21 and 3.24 to 3.28 and site parameters. Considering the parameters of the equations and the performances, in the end, AC10 was selected as the most appropriate GMPE for the application of seismic hazard analysis for Eskisehir.

3.5.2.1. Performance of the Selected GMPE

The functional form of AC10 is given in the equations 3.3 and 3.4. The site parameters are borrowed from BA08, hence it is not provided for the sake of simplicity.

For $M < c_1$

$$\ln(Y) = a_1 + a_2(M - c_1) + a_4(8.5 - M)^2 + [a_5 + a_6(M - c_1)]\ln(\sqrt{R_{JB}^2 + a_7^2} + a_8F_N + a_9F_R) \quad (3.3)$$

For $M > c_1$

$$\ln(Y) = a_1 + a_3(M - c_1) + a_4(8.5 - M)^2 + [a_5 + a_6(M - c_1)]\ln(\sqrt{R_{JB}^2 + a_7^2} + a_8F_N + a_9F_R) \quad (3.4)$$

where Y is the median spectral acceleration in g for 5% damping, or peak ground acceleration in g's; M is moment magnitude; R_{JB} is the closest horizontal distance to the rupture surface in km; F_N and F_R are the fault type; and c_1 is a variable in magnitude terms and is generally accepted as 6.5. The linear and nonlinear site effects of the site response function that are used in Boore and Atkinson (2008), are also used in AC10 with the same coefficients as well.

Table 3.7. Comparison of Calibrated and Original Coefficients

Spectral Period	Type of Coefficient	a ₁	a ₂	a ₃	a ₄	a ₅	a ₆	a ₇	a ₈
PGA	Calibrated	11.91	-3.49	-1.41	-0.56	-1.75	0.26	15.00	0.02
	Original	8.92	-0.51	-0.70	-0.19	-1.26	0.18	7.34	-0.02
T=0.2	Calibrated	15.14	-3.04	-1.07	-0.53	-2.19	0.17	26.00	-0.04
	Original	10.64	-0.51	-0.70	-0.21	-1.45	0.12	9.61	-0.04
T=1.0	Calibrated	9.65	-2.96	-0.99	-0.7	-1.13	0.12	7.00	0.37
	Original	7.62	-0.51	-0.70	-0.35	-0.76	0.10	4.13	-0.02

Table 3.7 is created for the comparison of calibrated coefficients and the original coefficients. The coefficients of the site parameters are not provided since original coefficients are employed in this study, which are provided in Appendix C together with the calibrated coefficients.

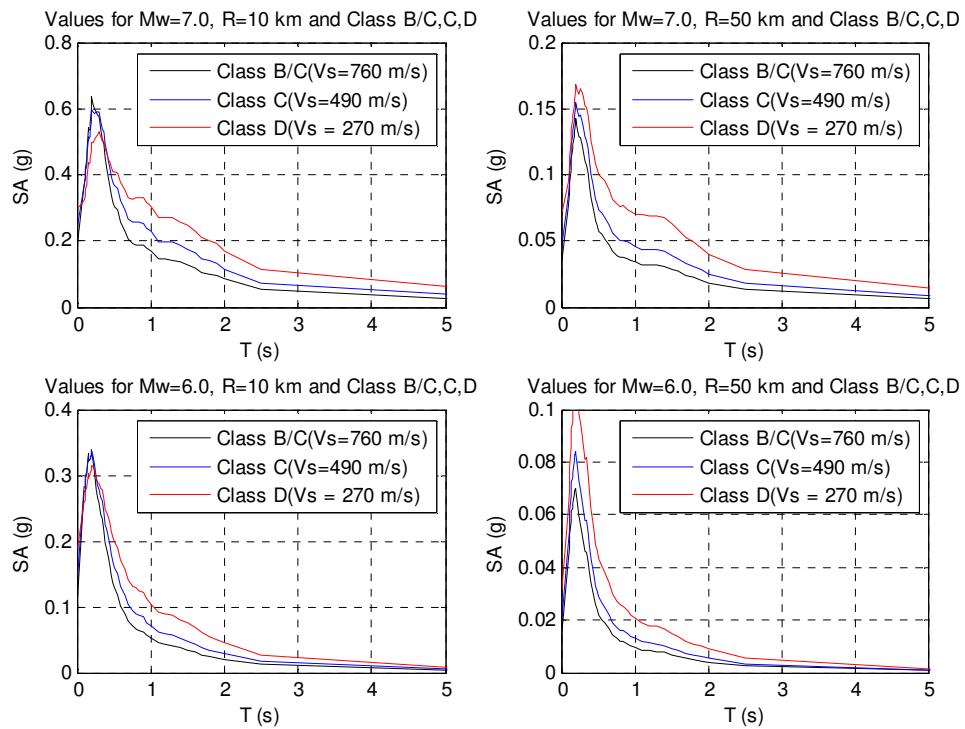


Figure 3.29. Response Spectrum Curves Obtained for M_w=7.0 and 6.0 for R=10 and 50 km Using Calibrated Coefficients for Site Conditions of B/C Boundary, Class C and D According to NEHRP

In order to present the performance of AC10, the plot in Figure 3.29 was prepared for the different cases of earthquake magnitude, distance and site conditions. Moreover, a goodness of fit test that involves normalizing residuals and comparison of residuals

against the calculated values was carried out as seen in Figure 3.30. As shown in the figure, residuals are clustered around zero, with a display of a tendency to scatter without any pattern, which implies the success of the modeling.

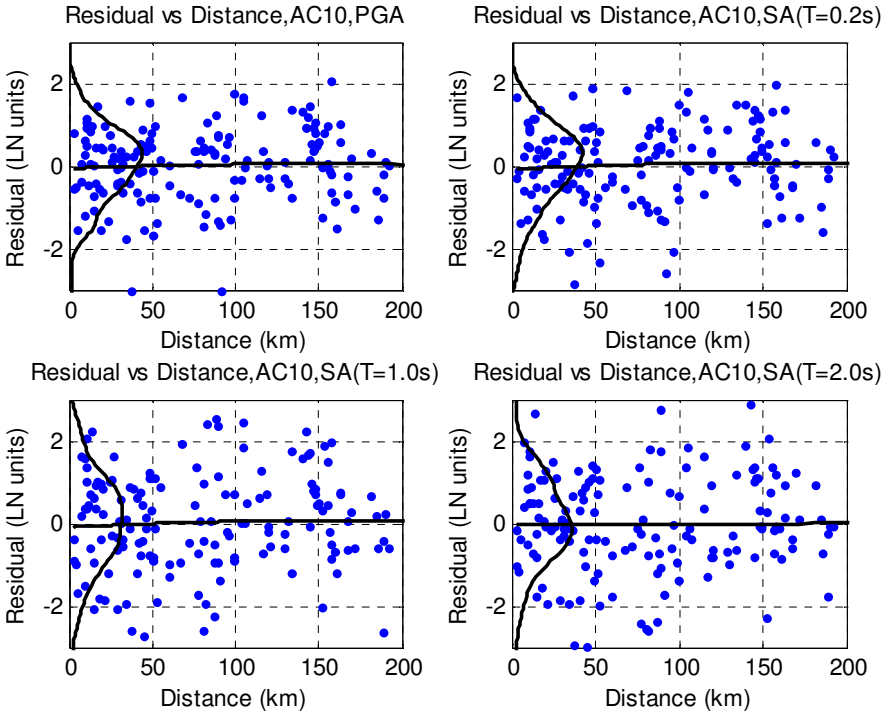


Figure 3.30. Residual Analysis with Normal Plots for AC10

3.6. Evaluation of Results

It is the Figure 3.31, which created confusion in the selection of the right GMPEs for seismic hazard analysis. As one of the classical approaches, a logic tree method could be proposed to average the effects of the selected GMPEs in a seismic hazard analysis. However, the obvious variances among the GMPEs regarding their performance in taking the ground motion amplitude of an earthquake to varying distances led to the development of a new approach. None of the GMPEs in Figure 3.31 is eligible to use in a seismic hazard analysis unless there is a proven fact that single one of them is the more suitable over the others with the condition that it successfully reflects the propagation characteristics of the earthquakes recorded in the area.

A reliable comparison of GMPEs requires a thorough investigation of the earthquakes in the databases that are compiled by the developer of the GMPE. However, a comparative study is not an easy task, and it is not required since the creators of the equations have prescribed different application limitations for the use

of the equations for different magnitudes of earthquakes, site conditions, fault styles and distance ranges. Depending on the database used in their study, there is a possibility of over-predicting or under-predicting the local seismic effects at distances as proven in this study. If the local seismic activity is dominated by different magnitude distribution, then the magnitude scaling, log distance scaling and magnitude saturation parameters could cause a distortion of the local behavior in the modeling.

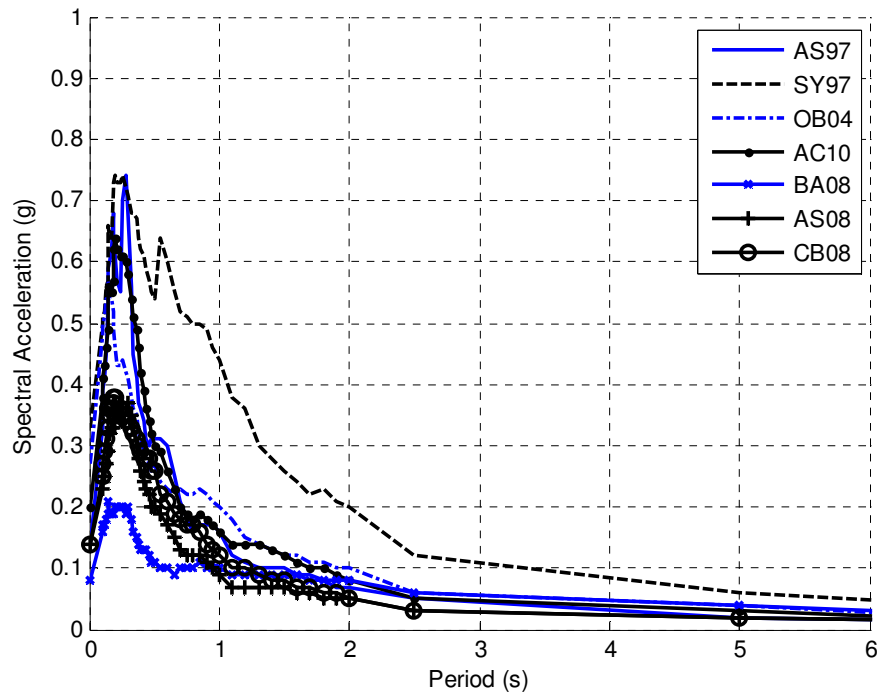


Figure 3.31. The Spectral Acceleration Curves Obtained by Several Different GMPEs for Earthquake of $M_w=7.0$ and at a Distance of 10 km

Therefore, as the first step, the past seismic activity of the surrounding region is studied in order to capture the local seismic patterns and characteristics of earthquake propagation. The seismic activity records are evaluated in order to verify whether there is enough earthquake activity for a reliable evaluation of the GMPEs. Initial evaluation of gathered records showed that there is a homogeneous distribution of earthquakes of magnitude up to 5.8 and distance up to 200 km. The magnitude distribution is not as uniform as the NGA equations due to the consistent local seismic behavior that the local seismic sources consistently produce earthquakes with magnitudes lower than 6.0 throughout Turkey. Naturally, the magnitude distribution is similar to the distributions of AC10 and especially OB04 in terms of magnitude deficiency above 6.0. The site characteristics of the recording stations are within the

typical range for the entire region. Finally, though the local database is not as big as the commonly utilized GMPEs around the world, it is concluded that with the local database, a new GMPE could be developed or an existing GMPE could be adapted to the local conditions.

After gathering the local seismic activity data, the existing coefficients of the GMPEs are calibrated by using the local database. The statistical performances of GMPEs in modeling the propagation characteristics of the ground motions of the database are compared in order to select the best fitting equation to the local data. The comparison of response spectrum curves that are developed by using the original and calibrated coefficients of GMPEs for an earthquake with magnitude $M_w=7.0$ and at distances of 10 and 50 km with rock as site condition, provided crucial information.

The variance of the spectral acceleration values, which is observed by using GMPEs with original coefficients, does not disappear with calibrated coefficients; however, the effect of calibrated coefficients is clearly visible especially for larger distances. The equations yielded smaller spectral accelerations with calibrated coefficients for larger distances, which could be a sign of decay in the ground motion amplitudes of the earthquakes of the database within shorter distances. This distance scaling could be inherent in the local wave propagation characteristics, or could originate from the domination of the smaller magnitude earthquakes in the database. It could also be originated from the exclusion of the smaller magnitude earthquakes at maximum distances as claimed by Boore and Atkinson (2008). According to them, the inclusion of records of higher magnitude earthquakes with larger distances and the absence of records of lower magnitude earthquakes at larger distances are caused by amplitude cutoff values of the instrumentation.

The observed distance scaling is investigated with trellis plots for three different magnitudes and spectral periods in Figures of 3.24 to 3.26 and 3.28. AC10 and OB04 should be highlighted with recognizable distance scaling with the calibrated coefficients. In addition, in all of the assessed GMPEs, relatively higher distance scaling is captured with the calibrated coefficients. Therefore, it is concluded that the observed distance scaling is largely due to the inherent scaling of the ground motion at distance and partially due to the compiled database. Hence, the distance scaling term became the most important parameter in the selection of the most suitable GMPEs.

The multi-stage multiple regression analysis is used for eliminating the bias of magnitude and distance terms. It is performed for the purpose of refining the distance and magnitude scaling dependency of the ground motion amplitude. However, the variability of the predicted and observed acceleration values increased with the multi-stage approach as presented in Figure 3.32. As can be observed in the figure, the predicted acceleration values from AC10 and the measured acceleration values from the records show high variability. Therefore, it is concluded that the database is not suitable for the application of multiple stage multiple regression analysis.

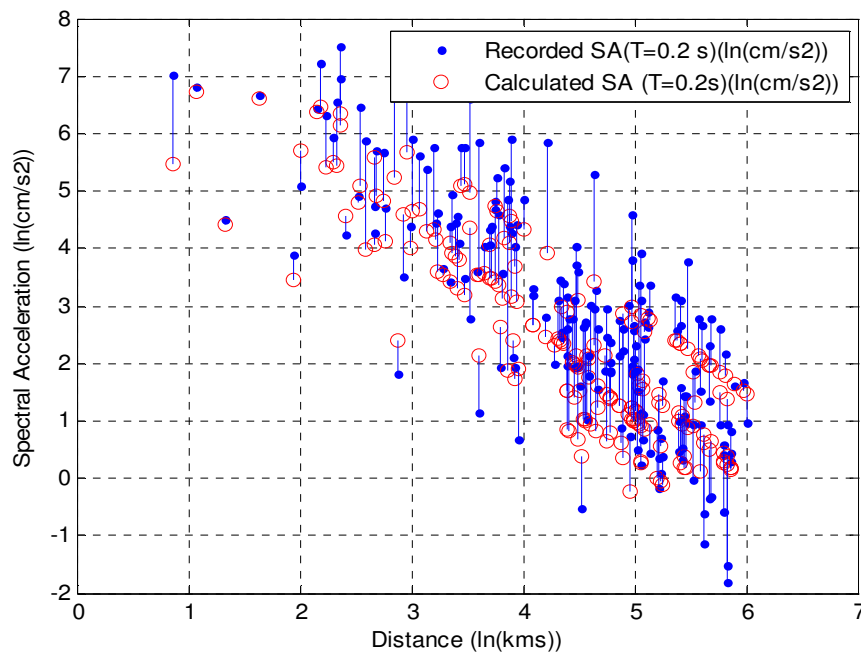


Figure 3.32. The Prediction Errors of the Predicted Accelerations by Using Multi-stage Multiple Regression Analysis with Modified AC10

After several evaluation procedures, the relative performances of GMPEs are assessed, and AC10 is selected to utilize in the seismic hazard analysis. The reasons behind this selection vary. The local database, which is part of a larger database that is used to develop AC10, is one of the reasons of the successful modeling of the local seismic behavior by AC10. Moreover, the equation is also found successful in modeling the inherent distance scaling of the earthquake propagation in the area of interest.

Considering that PSHA is partly dependent on the areal sources, which include coefficients generated by using earthquakes with magnitudes greater than 4.0, the GMPE developed by including similar size earthquakes has a more tendency to

reflect the local seismic behavior. Therefore, in the application part, AC10 is used with the calibrated coefficients. The calibrated coefficients for AC10 are given in Table 3.7 for PGA and spectral periods of $T=0.2$ s and 1.0 s, and in full list in Appendix C.

CHAPTER 4

4. ASSESSMENT OF SEISMIC VULNERABILITY

4.1. Introduction

This section consists of the review of the most commonly applied methods for estimation of lateral performance, structural parameters that influence the lateral performance, important issues in the analytical modeling, the proposed method and the details of the sensitivity analysis that is performed for the derivation of lateral performance scaling with respect to the proposed structural parameters.

As explained in section 1.2 of the first chapter, the motivation of the study is to develop a quick, easy-to-use and reliable tool in order to predict the damageability of the structures by using the basic structural parameters. Unfortunately, the review of the literature for similar studies did not yield a satisfactory outcome. Therefore, this study is mostly based on a few reference studies conducted by Ozcebe et al. (2003), Yucemen et al. (2004), Yucemen (2005) and Yakut et al., (2006). Different from these studies, the present study predicts lateral displacements and drifts by using analytical methods instead of using the expected damage as the estimated parameter. The brief literature review of these analytical methods is provided in the consecutive sections.

After the review of the analytical methods, the structural parameters that play decisive roles in shaping the lateral performance are provided by tables. Following that, the structural modeling issues are summarized, and the related assumptions are explained. Moreover, the modification scheme of the structures are provided, which is performed for the sensitivity analysis.

4.2. Review of the Selected Lateral Performance Estimation Methods

Scaling of the lateral performance and the overall damage with various structural parameters such as ductility, lateral stiffness, and fundamental periods has been implicitly studied throughout the known history of structural analysis. Most of these parameters are abstract and complex parameters in nature that require complicated

analysis. However, simpler and easily determined structural parameters such as sizes of columns, storey heights and number of storeys are not explicitly related with lateral performance. The most distinguished method that relates these simple structural parameters to overall damage is called as discriminant analysis by the aforementioned researchers in section 4.1. The same discriminant method is modified and redeveloped to estimate the lateral performance of structures and verification is sought by using analytical methods. Therefore, it is necessary to explain these methods briefly with the history of development, and with the procedures in the application of the methods.

4.2.1. Discriminant Analysis by Using Main Structural Parameters

In their study, Ozcebe et al. (2003), Yucemen et al. (2004), Yucemen (2005) and Yakut et al. (2006) proposed a discriminant method that is based on relating the basic structural parameters to the observed damage of the structures. These studies provided the main hypothesis of the present study, as the basic structural parameters in this study are based on the proposed parameters in the aforementioned studies. As explained in their method, discriminant functions include number of storeys, minimum normalized lateral stiffness index, minimum normalized lateral strength index, normalized redundancy score, overhang ratio and soft storey index as the discriminating parameters. By using these parameters, the damage states of the structures are predicted.

According to their studies, the minimum normalized lateral stiffness index is based on the minimum ratio of the total moment of inertia of the columns and structural walls to the storey area in a single storey as shown in the following equations:

$$I_{nx} = \frac{\sum(I_{col})_x + \sum(I_{sw})_x}{A_{sf}} \times 1000 \quad (4.1)$$

$$I_{ny} = \frac{\sum(I_{col})_y + \sum(I_{sw})_y}{A_{sf}} \times 1000 \quad (4.2)$$

where $(I_{col})_x$ and $(I_{col})_y$ represent the moment of inertias of the columns about the orthogonal x and y axes, while $(I_{sw})_x$ and $(I_{sw})_y$ represent the moment of inertias of the structural walls about x and y axes.

For the minimum normalized lateral strength index, *mnl_{si}*, the ratio of the areas of columns, shear walls and masonry infill to the total storey area is considered. The minimum value of the two orthogonal indexes is included in the overall equation. Following equations are used to determine the *mnl_{si}*:

$$A_{nx} = \frac{\sum(A_{col})_x + \sum(A_{sw})_x + 0.1\sum(A_{mw})_x}{A_{tf}} \times 1000 \quad (4.3)$$

$$A_{ny} = \frac{\sum(A_{col})_y + \sum(A_{sw})_y + 0.1\sum(A_{mw})_y}{A_{tf}} \times 1000 \quad (4.4)$$

where $(A_{col})_x$ and $(A_{col})_y$ are the total area of the columns, $(A_{sw})_x$ and $(A_{sw})_y$ are the areas of structural walls and $(A_{mw})_x$ and $(A_{mw})_y$ are the areas of unreinforced masonry walls, A_{tf} is the total floor area bounded by the structural frame boundaries of the storey of interest. The normalized redundancy score, *nrs*, is introduced to consider the lateral stiffness discontinuities in the structural system. It is calculated by using normalized redundancy ratio, *nrr*, of the system, which is calculated by using the following expression

$$nrr = \frac{A_{tr}(nf_x - 1)(nf_y - 1)}{A_{gf}} \quad (4.5)$$

where A_{tr} is the tributary area for a typical column, nf_x, nf_y is the number of continuous frame lines, and A_{gf} is the area of the ground storey. If both nf_x and nf_y are greater than 3, than the column tributary area is accepted as 25 m², and for all other cases, it is accepted as 12.5 m². The *nrs* value ranges from 1 to 3 as given in equation 4.6.

$$nrs = \begin{cases} 1 & \text{for } 0 < nrr \leq 0.5 \\ 2 & \text{for } 0.5 < nrr \leq 1.0 \\ 3 & \text{for } 1 < nrr \end{cases} \quad (4.6)$$

The soft storey index is defined as the ratio of the ground storey height to the second storey height. The overhang ratio is calculated by dividing the overhang area that is defined by the extended area beyond the frame boundaries to the ground floor area. The studies of the aforementioned researchers are concluded with positive and encouraging results, which confirm the initial claims that it is possible to predict the

damage level with the basic structural parameters. Therefore, it is thought that, with a refinement and classification criteria based on the types of behavior of the structures and by choosing the right lateral performance variable, a lateral performance prediction equation (LPPE) can be developed.

4.2.2. Analytical Procedures in Lateral Performance Estimation

The most commonly accepted lateral performance estimation methods can be listed as the Capacity Spectrum Method (CSM), Improved Capacity Spectrum Method (ICSM), N2 method, Displacement Coefficient Method (DCM), Improved Displacement Coefficient Method (IDCM) and the modal pushover analysis. CSM was proposed by Freeman et al. (1975), which is based on the spectral representation of the pushover curve in spectral acceleration and spectral displacement (SASD) format, which yield the capacity spectrum curves. In the application, the acceleration displacement response spectrum (ADRS), which is obtained by converting the elastic response spectrum to spectral acceleration and spectral displacement format, is superpositioned with the capacity spectrum curves. Later, the performance point of the structure is derived by an iteration procedure, or engineering judgment is employed to locate the performance point as ATC-40 (1996) suggests.

ICSM, was developed by FEMA (2005) by introducing constant-ductility inelastic design spectra to replace the elastic response spectra. The criterion for the performance point is redefined such that the calculated ductility, μ_{calc} , must be equal to the ductility value obtained for the intersecting demand curve.

N2 method, which was originally proposed by Fajfar and Fischinger (1988), is adopted as a valid method in recent versions of Eurocode 8 (EC8). The aim of the method is to idealize the response spectrum curves more realistically by including the ductility factor, and ductility and period dependent reduction factor for spectral acceleration and spectral displacement curve.

DCM, on the other hand, proposes a different approach in the calculation of the target or roof displacement by using a relationship based on multiplication of the demand spectral displacements by several modification factors. As the updated version of DCM, the IDCM eliminated two of the four displacement modification factors of DCM and updated the remaining coefficients.

The modal pushover analysis was developed by Chopra and Goel (2001, 2002). It involves the calculation of capacity curves for every mode and the determination of the total response demand through the combination of modal responses via an appropriate modal combination procedure.

Nonlinear time history analysis is the most reliable and accurate method to obtain the lateral performances. It is a reference method to develop and validate the lateral performance estimation methods. The most significant drawback of this method is the required time and effort to perform the analysis.

The following sections provide detailed information on the lateral performance estimation methods that are utilized in this study.

4.2.2.1. Capacity Spectrum Method

CSM is a form of equivalent linearization method that is based on the assumption that the response of the structure is at the point where the demand and capacity curves intersect each other with the condition that the effective damping ratio of the structure and demand curve is equal to each other. The method is advantageous since the analysis is easier and simpler.

CSM is developed for evaluation of the structural performance under lateral loading by using the nonlinear static pushover analysis, since then it is widely accepted by practitioners and academics. The methods are incorporated into the codes of practice while it is being updated as the results of the new findings are incorporated. Indeed a new version of the method is already developed to replace the CSM, which is named as Improved Capacity Spectrum Method (ICSM).

The capacity curves obtained from lateral pushover analyses are converted into the SASD format in order to utilize the CSM for the lateral performance evaluation. The base shear coefficient and roof displacement values are converted into the spectral acceleration and spectral displacement via the following equations.

$$S_a = \left(\frac{1}{\alpha_1} \right) \left(\frac{V}{W} \right) \quad (4.7)$$

$$S_d = \frac{\delta_{Roof}}{PF_{Roof,1}} \quad (4.8)$$

where S_a , is spectral acceleration of the equivalent SDOF system, α_1 is the effective mass coefficient of the first mode, V is the base shear, W is the weight of the building and S_d is the spectral displacement of the equivalent SDOF system, δ_{Roof} is the roof displacement, and $PF_{Roof,1}$ is the participation factor of the first mode in the roof level.

While the conversion of the base shear coefficient and roof displacement values into SASD is performed, the elastic response spectrum curve is converted into the ADRS format. The lateral performance point is then calculated by an iteration procedure, which is carried on until the equivalent period, and effective damping values of the structure match with the calculated values.

This method requires remodeling of the structure for the application of the procedure. In Figure 4.1, multiple degree of freedom (MDOF) system, which is shown on the left side with the mass and stiffness values given for each storey, is converted into the single degree of freedom (SDOF) system which is shown on the right side with the mass, M^* and stiffness, K^* . The stiffness of SDOF system is calculated by an appropriate method using the pushover curve, and the equivalent mass, M^* , is calculated by the following equation.

$$M^* = \alpha_1 M \tag{4.9}$$

where M is the total mass of the structure and α_1 is the modal mass participation ratio of the fundamental mode.

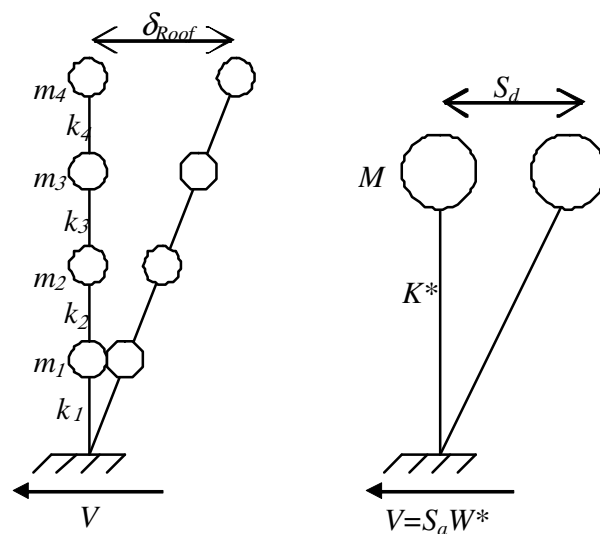


Figure 4.1. Equivalent SDOF Representation of an MDOF System (Modified from ATC-40)

Bilinear representation of the obtained capacity spectrum curves is required to estimate the effective damping ratio and appropriate reduction ratio corresponding to the effective damping ratio of the demand curve. There is not a definitive method for the bilinearization of the capacity spectrum curves in the literature. However, the aim of bilinearization is that the area underneath the curve and the bilinear model are equal to each other. In this study, the assumptions used in the bilinearization procedure developed for DCM is used for convenience.

4.2.2.2. Method of Maximum Interstorey Drift Ratios

The interstorey drift ratio (IDR) is defined as the ratio of the drift along the consecutive floors as expressed in the following equation.

$$IDR = \frac{(\delta_i - \delta_{i-1}) / h_i}{(\delta_{i+1} - \delta_i) / h_{i+1}} \quad (4.10)$$

where IDR is interstorey drift ratio, δ_i is the lateral displacement of the i^{th} floor, and h_i is the height of the i^{th} floor. The maximum of the IDR values that is defined as the maximum interstorey drift ratio (MIDR) is sought along the height of the structure. The interstorey drifts are not conveniently expressed by the response spectrum curves due to the accepted theory behind the formation of the curves. However, recent studies focus more and more on the relative drift of each storey due to the associated damages caused by the relative drift. It was correlated with the overall damage in buildings by several researchers (Sozen, 1983; Moehle, 1984; Qi and Moehle, 1991; Moehle, 1994; Gulkan and Sozen, 1999; Bozorgnia and Bertero, 2001).

Especially after the breakthrough study of Iwan (1997) which introduced a simple measure of drift demands for earthquake ground motion called the drift spectrum, many researchers studied the drift demands by using this approach. In his study, the structure was modeled as a continuous shear beam and the drift spectrum is developed by wave analyses of several models. Chopra and Chintanapakdee (2003), Gulkan and Akkar (2002), Kim and Collins (2002) and Miranda and Akkar (2006) studied and evaluated the applicability of drift spectrum. Especially Miranda and Akkar (2006), in particular, introduced the generalized interstorey drift spectrum,

which is applicable for different kinds of structures with the modeling of combined flexural and shear responses to lateral loads.

4.2.2.3. Displacement Coefficient Method

DCM performs the estimation of the nonlinear displacement of the structure by using the elastic displacement of the equivalent SDOF system by the modification factors. It is based on the statistical analysis of the results obtained by the time history analysis of SDOF oscillators of various types. In other words, the method introduced the modification factors to include the effects of the nonlinearity caused by the geometrical parameters, inelasticity of the materials, the hysteresis shapes and modal participation factors. It is generally proposed as one of the common techniques to estimate the structural performance in the literature. Due to its simplicity and easy applicability, it is preferred to the other methods although there are still questions of the reliability of the method and investigations are being performed for comparison of the relative performance of the methods.

DCM is proposed in FEMA-273 (1997) and adopted in the FEMA-356 (2000) for estimating the target or roof displacement, δ_t . As the name implies, this approach determines δ_t by applying modification factors to the equivalent SDOF elastic displacement by the following equation:

$$\delta_t = C_o C_1 C_2 C_3 S_a \frac{T_e}{4\pi^2} g \quad (4.11)$$

where C_o is the modification factor that relates the roof displacement to the spectral displacement, C_1 is the modification factor that relates the expected maximum inelastic displacement to the elastic displacement calculated by linear methods. Moreover, C_2 is the factor that represents the effect of hysteresis shape on the maximum displacement response and C_3 is the modification factor developed for the second order effects. As the first step of the analysis, the bilinear models of the pushover curves are generated as described in 4.2.2.1. The bilinear models are necessary to derive the elastic, effective and plastic stage stiffness values and these bilinear models lead to the derivation of the effective fundamental period of the structure by using the following equation.

$$T_e = T_i \sqrt{\frac{K_i}{K_e}} \quad (4.12)$$

where T_e is the effective fundamental period, T_i is the elastic fundamental period, K_i is the elastic lateral stiffness of the building, and K_e is the effective lateral stiffness found by the bilinearization process. After the derivation of the effective fundamental period of the building, the modification factors are determined as outlined in ATC-40 (1996) and in FEMA-356 (2000). The modification factor that relates the roof displacement to the spectral displacement, C_0 , is obtained by using Table 4.1. The values in between are found by interpolation.

Table 4.1. Values for C_0 Modification Factor

Number of Storeys	C_0 , Modification Factor
1	1.0
2	1.2
3	1.3
5	1.4
10+	1.5

The C_1 modification factor that relates the expected maximum inelastic displacement to the elastic displacement is found by using the following equation.

$$= \begin{cases} 1.0 & T_e \geq T_0 \\ \frac{[1.0 + (R-1)T_0/T_e]}{R} & T_e < T_0 \\ 2.0 & T_e < 0.1 \end{cases} \quad (4.13)$$

where T_0 is the characteristic period of the response spectrum curve; R is the ratio of the elastic strength demand to the calculated yield strength. C_2 is the factor that represents the effect of hysteresis shape on the maximum displacement response. For C_2 , there are different set of values defined for the immediate occupancy, life safety and collapse prevention level for moment resisting frame structures.

Table 4.2. Values for C_2 Modification Factor

Performance Level	T=1.0		T>T ₀	
	Framing Type 1	Framing Type 2	Framing Type 1	Framing Type 2
Immediate Occupancy	1.0	1.0	1.0	1.0
Life Safety	1.3	1.0	1.1	1.0
Collapse Prevention	1.5	1.0	1.2	1.0

Table 4.2 provides different values of C_2 factor for different type of structures. The modification factor developed for the second order effects is generally taken as unity because of the positive post-yield stiffness observed in most of the structures.

Studies are performed in order to evaluate the performance of the DCM and compare with the other available methods of damage and performance estimation. As part of the project named as ATC-55 (2003), the nonlinear static analysis procedures are subjected to evaluation by using SDOF systems with different period, strength, hysteretic behavior, site conditions and ground motions. The results of the project were published in FEMA 440 (2005) that summarizes and assess the ability of the DCM to estimate the maximum displacement of inelastic structural models. As a conclusion of this study, for the medium and long period structures the method overestimates the target displacement. Various researchers such as Lin et al. (2004) and Gencturk and Elnashai (2008) also concluded that the displacements are overestimated by this method.

4.2.2.4. Improved Displacement Coefficient Method

IDCM was developed by FEMA (2005) following an investigation, which was performed for the assessment of the reliability of the coefficients of DCM. The method eliminated two coefficients from the equation of the DCM: the modification factor that relates the roof displacement to the spectral displacement, C_0 , and the modification factor that represent increased displacements due to dynamic P - Δ effects, C_3 . In addition to these, the modification factor that relates the inelastic displacements to the elastic displacements, C_1 , and the factor that represents the effect of hysteresis shape on the maximum displacement response, C_2 , was updated.

In the IDCM method, the target or roof displacement, δ_t , which represents the displacement at the roof level, is estimated as:

$$\delta_t = C_1 C_2 S_a \frac{T_e}{4\pi^2} g \quad (4.14)$$

where C_1 , is the modification factor that relates the expected maximum inelastic displacement to the elastic displacement, and C_2 , is the factor that represents the effect of hysteresis shape on the maximum displacement response.

The simplified expression for C_1 is:

$$C_1 = 1 + \frac{R-1}{aT_e^2} \quad (4.15)$$

where T_e is the effective fundamental period of the SDOF model of the structure in seconds, and R is the ratio of the inelastic demand to the calculated yield strength. The constant a is equal to 130, 90, and 60 for site classes B, C, and D, respectively. For fundamental periods greater than 1.0 s, C_1 can be taken as 1.0. The hysteretic shape factor, C_2 , is calculated as

$$C_2 = 1 + \frac{1}{800} \left(\frac{R-1}{T} \right)^2 \quad (4.16)$$

For fundamental periods greater than 0.7s, C_2 factor can be taken as 1.0.

4.2.2.5. Evaluation of Procedures

The aforementioned procedures have been studied and tested numerous times by many researchers. To name a few of them, Mahaney(1993), Paret (1996), Gupta and Kunnath (1999), Inel, Tjhin, and Aschheim (2003), Kunnath and John (2000), Lew and Kunnath (2001), Mwafy and Elnashai (2001), Goel and Chopra (2004) and Kalkan and Kunnath (2007) studied and tested the above procedures with different samples having different structural properties. Load patterns, frame types, and analysis methods were all subjected to assessment with the available information.

The reason why there are so many different methods with so many different details of application is that the performance of the structure with varying ground motion could be in a wide range of spectrum. For instance, one of the reasons is the variances in the inertial responses against the overturning and the lateral movement, which indeed determines the type of the lateral performance of the structure. In addition, the inherent modal vibration characteristics complicate the lateral response of structures even more. Therefore, each structure requires a detailed investigation for the determination of its lateral performance. This investigation requires considerable amount of time and effort, which indeed is not practical for the purposes of evaluation. Therefore, for practical reasons, a lateral performance estimation method that encompasses all the structures or at least a group of structures is necessary so that the lateral performances could be quickly estimated for insurance, mitigation and evaluation purposes.

Table 4.3. The Most Common Methods Used for the Evaluation of Lateral Performance of Structures

Name of the Method	Developer	Strengths	Weaknesses
Capacity Spectrum Method	Freeman et al. (1975)	-The capacity and the response spectrum curves on the same plot	- Very unreliable results might be obtained such as performances with associated damping ratios more than 40%
Improved Capacity Spectrum Method	FEMA-440 (2005)	-Constant ductility inelastic spectra that yield a closer approximation are used.	- Conservative predictions due to sensitivity to ductility ratios
N2	Fajfar and Fischinger (1988)	-Period dependent reduction factor for spectral acceleration and displacement curve	-No strength degradation or hardening is assumed
Displacement Coefficient Method	FEMA-274 (1997)	- Uses empirical factors to estimate the demand -Straightforward, easy to use	- Too many approximations are involved
Modal Pushover Analysis	Chopra and Goel (2001, 2002)	-Includes several mode shapes in the performance calculation which is more realistic than using only the first mode shape	- Too many calculations are included, which is costly and time consuming
Improved Displacement Coefficient Method	Ruiz-Garcia and Miranda (2003), Guyader and Iwan (2006) FEMA-440 (2005)	-Site classes are introduced; fewer parameters	-Plastic stage stiffness ratio is not considered; linear dependency of peak inelastic displacement on the spectral acceleration (Akkar and Metin, 2007)
Maximum Interstorey Drift Ratio	Algan 1982, Sozen 1983, Moehle 1984	-The building collapse mechanisms are explained better; associates well with the damage ratios	-Not associated with the response spectrum curves
Time History Analysis	-	-Most accurate results	-Considerable time and effort is spent

In order to serve the purpose of practicality, several lateral performance estimation methods are proposed as listed in the Table 4.3. The name of the method, the developers, strengths and weaknesses of each method are all provided in the table. Regarding the provided weaknesses and strengths of the listed methods, it is obvious that none of the developers of the methods can assure the maximum accuracy in the estimation, and all of the methods require a prescription that defines the limitations of the methods. Moreover, even the listed methods claim the ease of application; all of them require the calculation of the abstract structural parameters as input, which indeed require analysis of structures.

Therefore, for the assessment of the existing structures, either the most proper method must be selected amongst the available methods, or a new method must be developed for the assessment of structures with respect to their lateral performances. Proposing a new lateral performance evaluation method is only possible by proposing new parameters that relates to the lateral performance.

4.3. Variables Influencing the Lateral Performance

Several lateral response variables can define the lateral performance of a structure. The base shear, roof displacement, base shear coefficient, global drift ratios at the yield and ultimate stages, performance spectral acceleration and displacement values obtained by CSM, the target displacements obtained by DCM and IDCM and inter-storey drift ratios are considered as the main lateral performance variables.

Obviously, the lateral performance of a structure cannot be defined by a single variable. In fact, each one of the above variables offers valuable information about the structural performance. In this study, lateral performances in terms of spectral displacements obtained by CSM, maximum inter-storey drift ratios and target displacements obtained by DCM and IDCM are all employed in the development of LPPE. The practicality and reliability are considered in selecting the displacements as lateral response variable in the development of LPPE. Since the displacements can be more closely associated with the lateral performance levels and the proposed structural parameters, it is very practical to use instead of using accelerations. In addition, all the damage classifications are based on displacements and drifts which in the end makes this variable more reliable than accelerations.

Each of the mentioned lateral performance variables have to be associated with the attained levels of damage in order to quantify the inflicted damage. In fact, researchers have been trying to find the most accurate way to estimate the lateral performance and the associated damage levels so that before an event occurs, necessary modifications could be performed and precautions could be taken to prevent failure. Generally, in order to quantify the potential damages under lateral loading, predefined levels of global drift ratios are employed. There are levels of the lateral global drift ratios in a structure which significantly define the behavior and which can be associated with the damage levels. Namely, the yield displacement or yield global drift ratio is generally accepted as the point that forms the transition from elastic to plastic behavior in the pushover analysis. In addition, it also provides a border between the damage limit states of immediate occupancy and the life safety in almost all the classification of damage limit states. The ultimate global drift ratio is also considered as a threshold where the structure reaches its deformation capacity. These two threshold values are used to generate more damage limit states. Such as the global drift ratio at the damage state of life safety is generally assumed as 75% of the ultimate global drift ratio, whereas, the operational level damage limit state is obtained by using global drifts at the yield or assignment of the preset limits determined by a certain ratio of the total height.

The attained lateral forces by the structure at these damage limit states are considered as a crucial part of the evaluation of structure or group of structures. Generally, spectral acceleration is considered as a variable corresponding to the predefined levels of damage states. The spectral acceleration is used to associate the damage levels to the levels of ground motion so that potential damages attained at different ground motion levels could be quantified. Fragility curves, or probability curves of exceeding certain damage states, are employed in order to quantify the damages experienced by structures. Indeed fragility curves provide a very convenient tool to calculate the probabilities of damage states by using the ground motion parameter in terms of peak ground accelerations, spectral accelerations and spectral displacements. Therefore, it is important to obtain the spectral accelerations, base shear coefficients, and lateral performance in terms of spectral acceleration in CSM method at the predefined levels of drifts or displacements.

As it was mentioned in the preceding paragraphs, the lateral performance variables could be associated with the levels of damage by means of assigning predefined levels of displacements with the levels of damage. Moreover, these lateral performance variables could be associated with the basic structural parameters of the structures, which in the end, pave the way of relating the basic structural parameters to the overall damage. In order to prove such a claim, the dependency of the abstract structural parameters of fundamental period, ductility, lateral stiffness and other parameters, to the basic structural parameters are investigated.

The structural response to the lateral loads mainly depends on the lateral resistance of the structure to the attracted forces during the shaking and to the ability of the structure to deform in order to dissipate energy. Technically the mass, lateral stiffness, strength and the ductility of a structure govern the structural response during lateral loading. The mass of the building plays the main role in attracting forces of the shaking. In other words, earthquake forces attracted by the structure increase with the increasing mass. Yield strength of the building affects the structural response in terms of resisting greater lateral loads and increasing yield strength helps a structure withstand larger lateral loads.

Lateral stiffness of the building is defined as the slope of the load-displacement curve. Generally, the base shear and roof displacement relationship provides a measure for the lateral stiffness in a building. The increase in the stiffness means an increase in the ratio of base shears to the roof displacement, while a decrease implies more deformation under smaller lateral loads. The ductility or ratio of ultimate displacement to the yield displacement also influences the lateral performance of the structure. With more ductility, higher inelastic deformation is expected. The inelastic deformation in the structure, which sometimes goes beyond serviceability limits, is a determining factor in the level of attained damages. Similar to the ductility, strength factor is introduced to quantify the elastic strength demand to strength demand at the yield point. Several studies were conducted, methods were suggested and codes were developed to estimate the inelastic lateral displacements and relate them with the equivalent elastic system by using the ductility ratios and strength factors.

Among the main parameters, which shape the lateral response of the structure, stiffness and mass are the main factors that determine the fundamental periods.

Knowing that, the spectral demand in terms of spectral accelerations and spectral displacements are dependent on the fundamental period of the structure, the importance of the mass and stiffness is obvious. Structural response varies with the changing fundamental period of the system due to the inherent characteristics of the lateral response to the ground motions.

Table 4.4. Factors Affecting the Lateral Response of a Structure

Structural Parameter	Main Parameter	Explanation
Vertical uniformity	Strength	The height, column sizes and mass distribution in vertical direction
Horizontal uniformity	Stiffness	Single frame continuity
Total column area ratio	Strength	The total area of columns in a single storey to the total floor area of the storey
Total column stiffness ratio	Stiffness	Total column inertias in a single storey divided by the total floor area of the storey
Total beam to column stiffness ratio	Stiffness	Ratio of the total beam to the column stiffness
First storey to the second storey height ratio	Stiffness	The height ratio of the second storey to the first storey
Hinge mechanism	Ductility	The response type and shape of the hinges
Number of storey	Stiffness	Total number of storey of the buildings
Overhang ratio	Stiffness	The ratio of the extending structure to the main structure
Material	Strength	The concrete and reinforcement strength of the building

The ground motions are sensitive to acceleration, velocity and displacement at different periods of excitation. This natural phenomenon is expressed in the structural response as equal energy or equal displacement principle, both of which govern the response depending on the fundamental period of vibration. For example, if a structure with a fundamental period approaching to the natural period of vibration of the ground motion with higher accelerations, then, a highly amplified response in terms of spectral accelerations could be observed. However, as the fundamental period of the structure moves away from the mentioned natural period

of vibration of the ground motion, obviously the demand spectral acceleration diminishes. The damping ratio is also an important parameter that expresses the inherent energy dissipating capability of the structures. Higher damping ratios lead to quicker dissipation of the oncoming energy, while with lesser damping ratios, the response of the structure is slower in reducing the effects of the ground motion.

The aforementioned abstract parameters are defined to explain the general principles of the structural response under the lateral loads. However, a closer look at the structure is required in order to explain the above parameters, and new non-abstract or explicit structural parameters should be introduced to quantify them. These explicit structural parameters influencing the above abstract parameters of lateral stiffness, yield strength, fundamental period, damping ratio and the ductility are summarized in Table 4.4.

Among parameters given in Table 4.4, the influence of beam to column stiffness ratio on the lateral displacement patterns was investigated by Akkar et al. (2005). They sought a meaningful relationship between the displacement patterns and the beam to column stiffness ratio. This ratio covered a range starting from zero to one, or in structural terms, from full flexural behavior to the shear frame behavior. The study showed that ground storey drifts are more sensitive to this ratio than the roof drifts. The responses of the different type of the structures with changing beam to column stiffness ratios are shown in Figure 4.3. If the beams in a storey are much more rigid than the columns, the structure tends to sway in shear mode as illustrated in (a) in Figure 4.2. If the columns are relatively stronger than the beams, the structure sways in flexural mode, as seen in the illustration (c) in Figure 4.2. Generally, most code conforming structures tend to behave in both flexural and shear type with a different combinations as specified in the Turkish Earthquake Code (2007) (TEC), unless it is designed specifically to behave in a single mode.

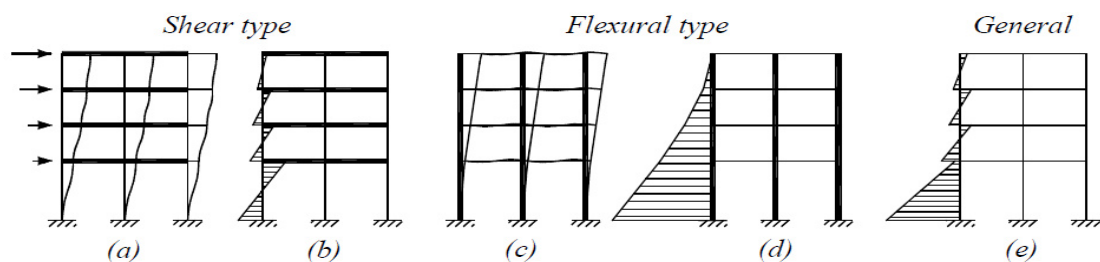


Figure 4.2. Response of the Structure to the Beam Column Stiffness Ratio

Other explicit structural parameters are also the subject of analytical studies mostly with an implicit approach; however, they are not generally evaluated as the prime subject of any study that has wide acceptance.

4.4. Pushover Analysis for the Estimation of Lateral Performance

Pushover analysis is a nonlinear incremental static analysis that produces a pushover curve, which is expressed in terms of base shear and roof displacement. Pushover analysis provides very important information about the lateral behavior of the structure. These curves can be expressed in terms of base shear coefficients and global drift ratios. Although uncertainties exist due to material and geometrical modeling assumptions especially in post-elastic stage, lateral drifts and displacements at predefined levels of ground motion, base shear coefficients at predefined levels of drifts and the associated levels of damage for specified levels of lateral drift provide a measurement tool for the vulnerability evaluation of a structure.

The pushover analysis is based on the idea that the response of the structure to a lateral load is related to the overall lateral performance of the structure. In the analysis, a distributed lateral load is applied to a structural model and the load is incremented until structural failure.

The pushover curve is idealized as bilinear curve by defining elastic and plastic stages of the curve as shown in Figure 4.3. The elastic stiffness is defined as the yield strength divided by yield displacement, and post-elastic stiffness is defined as the ratio of elastic stiffness by introducing strain hardening constant α . To put it in simple terms, the elastic stiffness of the equivalent SDOF is defined by

$$K = \frac{F_y^*}{u_y^*} \quad (4.17)$$

and the initial period of the equivalent system will be

$$T_{eq} = 2\pi \sqrt{\frac{M^*}{K^*}} \quad (4.18)$$

Thus, for simplicity's sake, the MDOF system structure is modeled by an equivalent SDOF system as given in Figure 4.4.

The types of pushover analysis vary depending on the way forces are applied to the structure. There are conventional methods, adaptive method, energy based method and upper bound pushover analysis. The conventional methods assume a constant and time independent loading pattern regardless of the modes involved in the analysis, while adaptive pushover analysis requires a loading pattern that is consistent with the changing structural characteristics of the structure. Energy based analysis is developed in order to eliminate the problems observed in force and displacement controlled nonlinear static analysis, while upper bound pushover analysis differs in the estimation of the load distribution with the shape of combined first mode shape added with factored second mode shape. Since the scope of this study is limited with conventional pushover analysis, adaptive method and methods based on energy are not studied further.

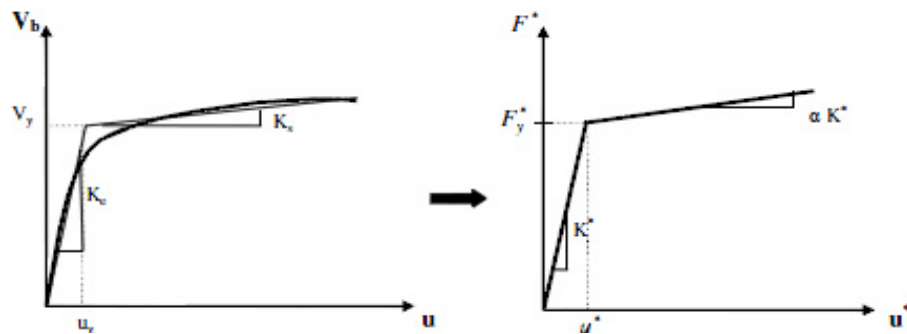


Figure 4.3. Bilinear Idealization of the SDOF by Using the Pushover Curve of MDOF System Shown on the Left

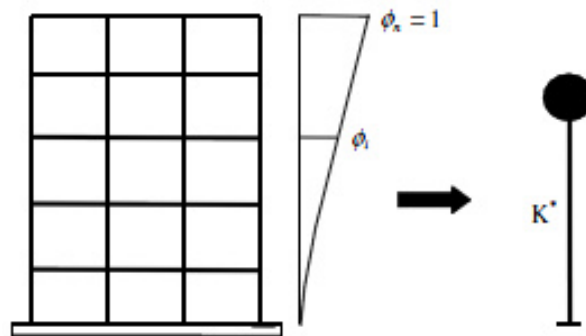


Figure 4.4. The Transformation of MDOF System to SDOF System

There are two main drawbacks of the analysis, which are the assumption about the modal response and the influence of the type of lateral loading on the resultant pushover curve. Firstly, with the assumption that the response of the structure is controlled by the first mode of vibration, instead of using the nonlinear dynamic

analysis, nonlinear static analysis is utilized. Secondly, it should be mentioned that, the sensitivity of the pushover curve to the lateral load patterns could be quite unpredictable. There are several lateral load types simply developed to model the lateral forces that the structures experience in an earthquake. The uniform, inverted triangular, first mode distribution, multi-modal load pattern and FEMA load distribution are the most common loading patterns applied. These two drawbacks, namely the modal mass participation ratios and lateral load distributions are thoroughly explained in the following sections.

4.4.1. Modal Mass Participation Ratio

The main purpose of the pushover analysis is to measure the structural response under the lateral loading. The most important issue to consider in such an analysis is the effect of modal mass participation ratios of the considered modes. Generally, in the pushover analysis, it is assumed that a structure responds in the first mode under lateral loading. Therefore, the lateral load is applied in the first mode shape rather than other mode shapes, meaning that the effects of the other modes in the lateral response is not taken into account. Researchers have already developed methods to include the higher modal effects in the pushover analysis, but a great deal of time and effort is required to conduct such an analysis.

In order to have acceptable and close to real performances with pushover analysis, the higher mass participation of the first mode would be required. In other words, a lower modal mass participation ratio of a structure would mean a compromise from obtaining a reliable lateral response data from the pushover analysis. In the literature, there are not definitive values set for this ratio. The seismic rehabilitation standard of Turkish Regulations on the Design of Buildings set this value as 70%, and FEMA 356 (2000) requires the determination of the significance level of the higher mode effects by comparing the storey shear forces of higher modes to the first mode shear forces of the storey. If the higher mode effects are significant, the standard requires a linear dynamic analysis to support the results of the pushover analysis.

In this study, modal mass participation ratio of 60% is accepted as the limit value. If the structure has modal mass participation ratio less than the limit value then it is eliminated and not included in the following steps of the study. The main reason for setting the mass participation ratio to a comparatively low value was to be able to

include as many structures as possible from the limited database compiled for this study, though it caused a compromise in the accuracy of results due to the lower estimating capability brought by the lower mass participation ratios.

4.4.2. Lateral Load Distributions

Lateral load patterns are one of the critical factors that affect the outcome of pushover analysis. Unless the structure has a very effective higher mode response and a specific type of yielding mechanism, then generally the lateral load types are reasonably satisfactory to a desirable degree for some applications. Several lateral load patterns were proposed to model the behavior of the structure under earthquake loading and it was realized that some of them are more suited for certain type of structures. Due to the inherent difficulty of determination of structural response and the distribution of inertial forces to each storey in an earthquake, no lateral load pattern is claimed to be the right pattern and investigations are still being performed for better modeling of the lateral load.

As mentioned, the main reason behind the existence of several lateral load types is the differences in the inertial responses of different structures. The inertia of the structure is formed according to the resistance to the displacement and rotation of the structure. The beam-column stiffness ratios, storey heights, the masses of storeys, lateral stiffness and various combinations of these parameters shape the lateral response of the structure. Higher order effects are ignored in the distribution of inertial forces with respect to beam-column stiffness ratios, storey heights and masses. Eventually, when all these factors are considered, it becomes very difficult to claim the right lateral loading pattern.

Table 4.5 presents the various lateral load types with the names of developers and information about the type of loading provided consecutively. Among these load patterns, the inverted triangle load pattern is very simple and easy to apply, since the shape is only dependent on the height of each storey from the ground. The load pattern is strong in modeling the overturning moments; however, it is very weak in reflecting the storey shear forces due to the emphasis on the roof level response. The underestimation of the structural capacity due to the smaller lateral loads applied to the lower storey is another shortcoming of the method. Whereas, uniform loading does not exactly reflect the dynamic capacity of the structure due to the strong

emphasis on the storey shear effects and neglecting the inertial responses to overturning effects.

All the other lateral load patterns are developed in order to reflect the two main inertial reflexes of the structures against the overturning and shear in varying degrees as explained in Table 4.5. Elastic first mode method, moment of masses and modified moment of masses are variants of the same group of methods, which strongly consider the overturning inertial responses.

Table 4.5. Lateral Load Distribution Types

Lateral Load Type	Developer	Notes
Inverted Triangle		The lateral load at each storey is based on the height of the storey from the ground to the overall height.
Uniform Load	ATC-40 (1996)	The lateral force at each storey is dependent on the ratio of the mass of that storey to overall mass.
Elastic First Mode		The product of the amplitude of the elastic first mode and mass is proportional to the lateral load in each
Moments of Masses	Various Codes	Loads are distributed based on the mass moments with respect to the ground level.
Modified Moment of Masses	FEMA-273 (1997)	The product of the mass and height of each storey from the ground with a modification factor to include higher
Mode Shape by Secant Stiffness	Eberhard and Sozen (1993)	At each force step, the mode shapes are derived from secant stiffness.
Stiffness Dependent	Bracci et al. (1997)	Load pattern is based on the shear resistance of each storey.
Deflected Shape and Mass	Fajfar and Fischinger (1987)	The deflected shape multiplied by the storey masses is used.
Inclusion of Higher Modes	Chopra and Goel (2000,2001)	Based on creating lateral load patterns for each mode and combining the results

FEMA 356 (2000) suggests using at least two lateral load patterns depending on the modal mass participation ratio, storey shear distributions and fundamental period of the structure, while ATC-40 (1996) suggests the distribution the lateral loads according to the first mode shape for regular buildings.

There are many other different lateral load patterns proposed by different researchers. Eberhard and Sozen (1993) offered the modification of the lateral load shape at each step based on the mode shapes that are derived by secant stiffness method. Moreover, Fajfar and Fischinger (1987) proposed lateral load pattern proportional to the lateral displacement of the structure at each step, and Bracci et al. (1997) calculated the storey shear resistance at each step and used these values to assign proportional values to the lateral forces of the next step.

Most of the lateral load patterns shown in Table 4.5 are very complicated and detailed, also difficult to model and apply. However, regardless of all the details and complicated nature of the models, there is not enough evidence that these lateral load patterns perform better than the basic load patterns. In addition to that, since the focus of the study is not on the issues arising due to the selection of the lateral load type, modal and uniform load pattern is found to be more suitable for the reasons of accuracy and practicality requirements. The buildings are subjected to lateral loads automatically by the SAP2000 program (Computer and Structures, 2011) in acceleration for uniform loading, and lateral loads in the fundamental mode shape. Therefore, among the many types of loadings, lateral loads are distributed according to the mass distribution for uniform loading and in fundamental mode shape for the modal type lateral loading.

4.5. Proposed Approach and Lateral Performance Prediction Equation

A very practical, time-wise, and cost-wise efficient method of analysis which is based on relating the certain structural features of structures to the level of damage is proposed by Ozcebe et al. (2003), Yucemen et al. (2004), Yucemen (2005), Yakut et al., (2006) known as discriminant analysis. The method proposes various structural parameters such as minimum lateral strength and stiffness indexes, soft storey index, number of redundancy score which is determined by the number of continuous frames and the column influence areas and overhang ratio. Among the proposed parameters, the overhang ratio is removed from the proposed equation due to the applicability issues, when considering the area of interest. Moreover, the number of redundancy score is also omitted which depend on assignment of scores and sensitivity of a structure cannot be measured without changing the orientation of a structure, which does not serve the purpose of this study. Minimum lateral strength

and stiffness indexes are renamed as lateral strength index and lateral stiffness index and since each of the transverse directions are used in the evaluation and the vertical uniformity is generally satisfied with the Turkish structures. If the vertical uniformity is not satisfied than the minimum lateral strength and stiffness index of the structure will be applied. The parameters of soft storey index and number of storeys are more straightforward and used in originally intended purpose in the relevant studies.

After the selection and modification of the structural parameters to be used in this study, as an outcome of this idea of relating the structural parameters to the damage, a method is proposed to associate the selected structural parameters with the lateral performance of the structure. For the prediction of the lateral performance of a structure, the following equation is proposed:

$$f(lsiA, ssi, lsiI, n) = f(lsiA) + f(ssi) + f(lsiI) + f(n) + \sigma \quad (4.19)$$

where $f(lsiA, ssi, lsiI, n)$ is the function describing the lateral performance of the structure, $lsiA$, represents the lateral strength index, ssi is the soft storey index, $lsiI$ is the lateral stiffness index, n is the number of storeys and σ represents the standard deviation term.

Due to the reasons explained previously, to be able to associate the lateral performances with the existing damage states, the lateral performances in roof displacements and global drift ratios obtained by DCM and IDCM and the spectral displacements obtained by CSM are used as lateral performance variables. The reason behind the selection of various lateral performance variables is to seek the best-related variable with the structural parameters.

The development of a LPPE is not exactly representative unless large numbers of structures covering whole range of structural parameters and in many different shapes and orientations are utilized in the development stage. However, it is quite difficult to include as many structures in order to develop a general LPPE for all the types of structures. Because of this limitation, the variance of the structural parameters must be minimized for the overall success of the developed LPPE. Accordingly, certain limitations are imposed in the gathering of the sample buildings: The number of storeys will be limited to 4 to 8, and only moment resisting frame and shear walled frame structures will be considered. The flat slab structures,

precast or pre-stressed structures, and cellular reinforced structures are all excluded from the sample. The vertical uniformity of the structures is also required in gathering process.

4.6. Sensitivity Analysis

The sensitivity analysis is conducted to seek the scaling of the lateral performance of a structure with respect to its structural parameters. Parameters of lateral strength and stiffness index, soft storey index and number of storeys are modified for each structural model in each direction.

4.6.1. Modifications of the Structures

4.6.1.1. Modification Scheme for the Lateral Strength Index

The lateral strength index, or the ratio of the total column area to the total floor area in a single storey of the structure is calculated by summing the areas of the columns in a single storey and dividing it to the total floor area defined as the area bounded by the structural frame boundaries. It is quite dependent on the geometry and structural design of the building. In order monitor of the lateral performance of the structure with the varying ratios of lateral strength index, a set of modified structures are generated with lateral strength indexes as shown in equation 4.20. In order to generate structural models with the predefined lateral strength indexes out of a single structure, the column sizes of the original structure are modified by changing the width of the column that is transverse to the direction of loading.

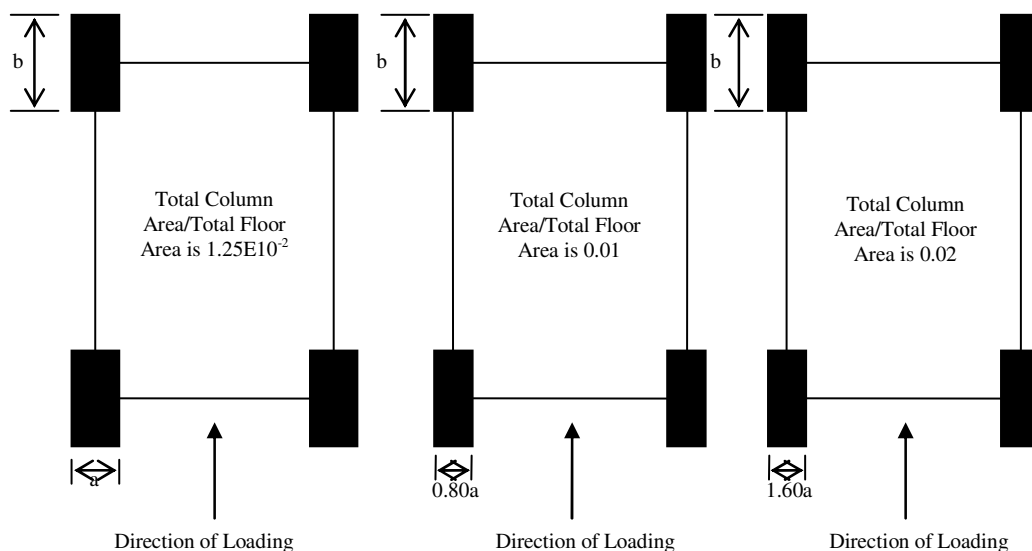


Figure 4.5. Lateral Strength Index Modification Scheme

The scheme can be understood by the pictogram given in Figure 4.5. While the original structure has a ratio of 0.0125, all column widths should be reduced by 20% in order to have a lateral strength index of 0.01. Similarly, the same column areas are increased by 60% to obtain a lateral index of 0.02. Following lateral strength indexes are imposed to the original structure:

$$\frac{\sum(A_{col})}{A_{sf}} = [0.01; 0.02; 0.03; 0.04; 0.05] \tag{4.20}$$

where A_{col} is the total column area in a single storey and A_{sf} is the total floor area of the storey. Since vertical uniformity is required except for the enclosed basement storeys, throughout the height of the structure the lateral strength index is the same for all storeys. Additionally, the reinforcement used in the original structure remained unchanged to isolate the dimension criterion.

4.6.1.2. Modification Scheme for the Soft Storey Index

Soft storey index is defined as the ratio of the first storey height to the second storey height. This index proved to be a strong determining factor in the lateral performances of the structures in earthquakes. If this index is higher, the attained damages are higher too as observed throughout Turkey. It plays an active role both in influencing the structural modes and failure pattern, and therefore, the lateral performance.

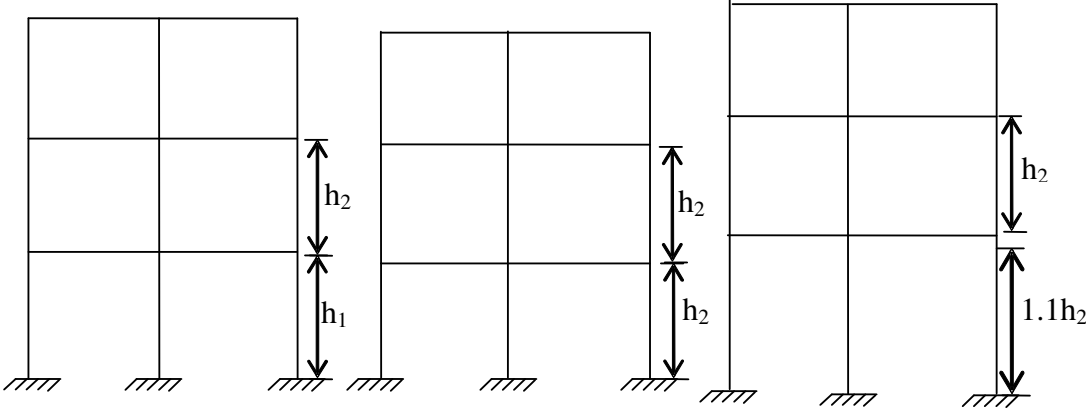


Figure 4.6. Soft Storey Index Modification Scheme

The modification scheme is explained in Figure 4.6, where the original structure has *ssi* ratio of h_1/h_2 , and modification is performed by changing the first storey height to match the second storey height in order to obtain *ssi* value of one. If the structure has

already an index value of one, then no modification is performed to set this index to one. After setting the index value to one, then, the first storey height is modified to match the *ssi* indexes given below.

$$(ssi) = [1.0; 1.1; 1.2; 1.3; 1.4; 1.5] \quad (4.21)$$

Not all the buildings are subjected to modification due to the code compliance issues and due to different geometrical and structural configurations that do not serve the purpose of the modification such as a completely encircling shear walled basement or existing soft storey condition in the second storey.

4.6.1.3. Modification Scheme for the Lateral Stiffness Index

The lateral stiffness index or the ratio of the sum of inertias of columns to the total floor area in a single storey is very clear by definition. It is calculated very easily by summing the column inertias of a single storey and dividing it by the total floor area of the same storey. Similar to the lateral strength index, the vertical uniformity of the structure in term of sizes of columns and floor areas is checked, so that the lateral stiffness index that is calculated for a single storey is valid throughout the structure. This intuitively deduced relationship between the lateral performance and lateral stiffness index has to be proven by modifying the index and monitoring the variance in the lateral performance with respect to the varying index.

The monitoring of the scaling of lateral performances with the varying lateral stiffness indexes requires the establishment of the meaningful index interval that is allowed by the codes. The following lateral stiffness indexes in equation 4.22 are chosen for monitoring and evaluation of the scaling of lateral performances.

$$\frac{\sum(I_{col})}{A_{sf}} \text{ (m}^2\text{)} = [1; 2; 3; 4; 5; 10; 20; 30; 40; 50] \times 10^{-4} \quad (4.22)$$

where I_{col} is the sum of the moment of inertias in a single storey and A_{sf} is the total floor area of a single storey. In order to have structures with the lateral stiffness indexes in 4.22, the modification of the structures are required by changing the sizes of the columns while keeping the other structural parameters constant. The size modification is performed in the direction of the loading, and the sizes of columns are reduced or increased to match with the indexes given above.

As shown in Figure 4.7, to modify a structure with lateral stiffness index of $1.25E-4$ and to obtain a structure with the lateral stiffness index of $1.0E-4$, all the column sizes are reduced by 7.2% in the direction of loading. To obtain a structure with the index of $2.0E-4$, all the columns sizes are increased by 16.9% in the direction of loading. The reinforcement of the columns remains unchanged.

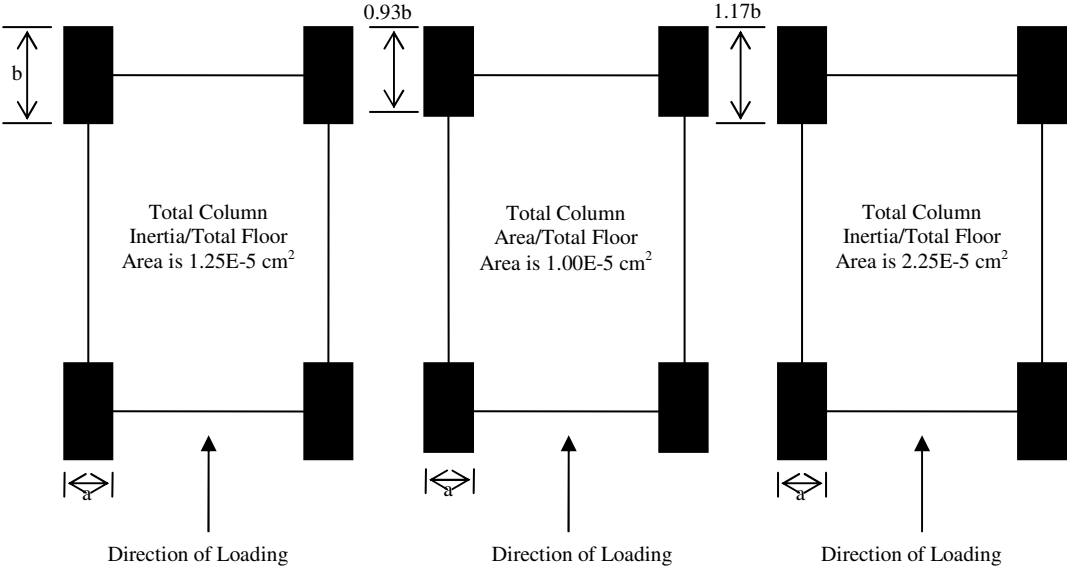


Figure 4.7. Lateral Stiffness Index Modification Scheme

4.6.1.4. Modification Scheme for the Number of Storeys

Number of storeys is a very crucial factor in the shaping of lateral performance together with the other proposed structural parameters. Almost all the studies group the structures according to the number of storeys for lateral performance evaluation purposes.

The database included structures with 4,5,6,7 and 8 storeys that are generally named as medium-rise structures. The evaluation range is automatically set for 4,5,6,7 and 8 storeys. The modification is very straightforward as the number of storeys is increased by adding storeys or decreased by removing storeys to create the structures with the specified number of storeys. Therefore, five set of modified structures are obtained including the original structure. The pictogram given in Figure 4.8 explains the modification scheme for a 6-storey building to create the modified structures with the specified number of storeys. The code compliance issue is checked to see if a structure is capable of carrying the vertical loads when additional storeys are added.



Figure 4.8. Modification of Height Ratio of the Structures

4.6.1.5. Code Compliance Issues

The modification of the structures is necessary in order to figure out whether there is a scaling between the lateral performance of the structure and proposed structural parameters. The column sizes, the first storey height and the number of storeys are subjected to modification by either changing the size of columns, or adding or removing a number of storeys, or increasing and decreasing the first storey height. Consequently, a compliance issue arises even before the structures are considered as eligible for further analysis. Especially in the modification of the column sizes, in some cases column sizes are supposed to be very small to match the index. In such cases, the structure is not included in the analysis since the Turkish code does not allow column sizes smaller than a certain size.

4.6.2. Building Stock

Turkish building stock consists of two main types of structures: buildings with reinforced concrete frames and buildings with stone/brick masonry as the load carrying system. There is already a strong trend in the construction industry that newly built structures are mostly reinforced concrete frame structures both as replacement to the older type of buildings and as new built dwellings. Therefore, when considering a general view of the construction industry and existing building stock, reinforced concrete structures must be dealt carefully and in detail.

Figure 4.9 further explains the types of structures according to the different period of codes. There are a number of periods with different codes of application, which influenced the design approach and caused variability of the structural responses to the same lateral loads. Although the applied code might deeply influence the type of the behavior of a structure, the database is not filtered according to the period of codes since different types of structures provide a wider spectrum of coverage.

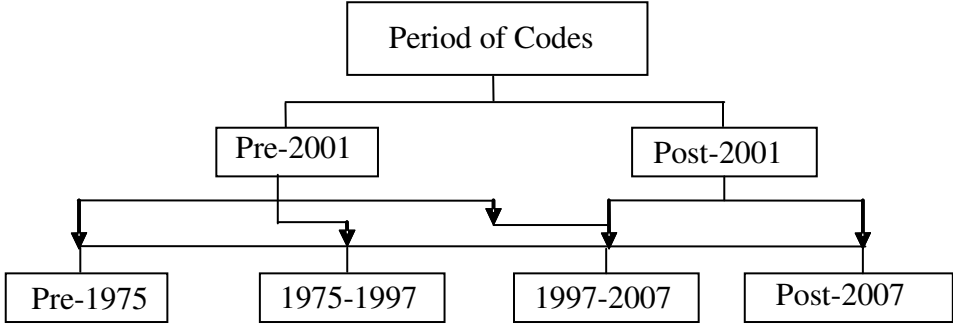


Figure 4.9. Types of Reinforced Concrete Structures with Different Periods of Codes

In this study, no restriction is imposed in gathering of the buildings in terms of applied codes in practice. Therefore, buildings with different design approaches will be evaluated in the same database. The same structures will be employed for the sensitivity analysis, as the structures will be subjected to modifications in terms of the proposed structural parameters as explained in 4.6.1.1 to 4.6.1.4.

Indeed, there are a few geometrical and structural restrictions imposed in gathering the structures. Such as the number of storeys are limited to 4 to 8 storeys, the vertical uniformity of the columns sizes have to be satisfied. The same beam sizes throughout the storeys of the structures are also sought and only moment resisting frame and shear walled frame structures are considered. The flat slab structures, precast or pre-stressed structures, and cellular reinforced structures are all excluded from the sample. Lastly, since this section is prepared to offer the review of the available methods and literature, the proposed method and the sensitivity analysis scheme, the results of the sensitivity analysis will be provided in Chapter 6.

CHAPTER 5

5. CASE STUDY: SEISMIC HAZARD ANALYSIS FOR ESKISEHIR

5.1. Introduction

Previously in Chapter 2, a very detailed literature review was provided about the seismic sources and related parameters and in Chapter 3, the most suitable GMPE was selected through an adaptation procedure. Therefore, the elements of PSHA with large degree of uncertainties are investigated and the GMPE selection was performed. As a continuation of aforementioned chapters, this chapter explains the methods used for the gathering and evaluation of the seismic data, the analysis techniques used for processing the gathered data and presents the results of the seismic hazard analysis performed for Eskisehir and surrounding area. The gathering of regional seismicity and tectonic setting, selection of fault models, the catalog selection, declustering and completion of the catalog data, area source determination, and assignment of fault recurrence rates are all provided in this chapter. Finally, the seismic hazard map of Eskisehir and surrounding area with response spectrum curves for earthquakes with different return periods are presented. In addition, seismic hazard study by using spatially smoothed seismicity model is also provided.

5.2. Regional Tectonic Setting

For the purpose of the study, Eskisehir and its close vicinity is defined as a circular area with a radius of 300 km centered at Eskisehir. The encircled area includes two regions that are identified as the most tectonically active regions, namely the North Anatolian Fault (NAF) zone and Aegean region. NAF is one of the most tectonically active fault systems in the world. This strike-slip fault system follows a line of arch of 1500 km in the Northern part of Anatolia spanning from the east to the west. Since 1939, the NAFZ has produced nine large magnitude earthquakes in a consistently westward-propagating sequence. The only exception to this sequence is the Duzce earthquake that occurred in 1999 to the east of the epicenter of earthquake of Izmit in 1999 (Kalkan et al., 2009). West of Eskisehir, lies the Aegean region, which is one of

the most active extensional regions in the world. This detachment tectonic regime in the region originated from the western movement of the Anatolian block along the NAFZ (Sengor et al., 1985). In addition, the movement on the Hellenic belt causes a counter-clockwise rotation in the region and further causing pressure due to the movement of the African plate towards the north. The movements of these plates caused the north-south directional strain and created grabens that are vertically oriented with respect to the direction of the stress in the region. Buyuk Menderes, Kucuk Menderes, Alasehir, Simav, Gediz, Bergama, and Edremit can be accepted as the typical examples of the grabens mentioned above with general directions are determined to be approximately east to west. However, in addition to these generally east-west extending grabens, other numerous types of faults with different directions exist on the tectonic map of the Aegean region. Large earthquakes sometimes occur in this region, such as the Demirci, 1969 ($M_S=6.0$), Alasehir, 1970 ($M_S=6.6$) and Gediz, 1970 ($M_S=7.0$) earthquakes.

5.2.1. Tectonic Structures in the Close Vicinity of Eskisehir

The northwest to southeast trending group of fault zones extending from Uludag in the west to Kaymaz in the east are named separately as the Inonu-Dodurga fault zone, Eskisehir fault zone (EFZ), and Kaymaz fault zone on the active fault map of Turkey. These three groups of fault zones are generally accepted as EFZ (Sengor et al., 1985). It is located between the strike-slip NAF and the Aegean extensional regime characterized by normal faults.

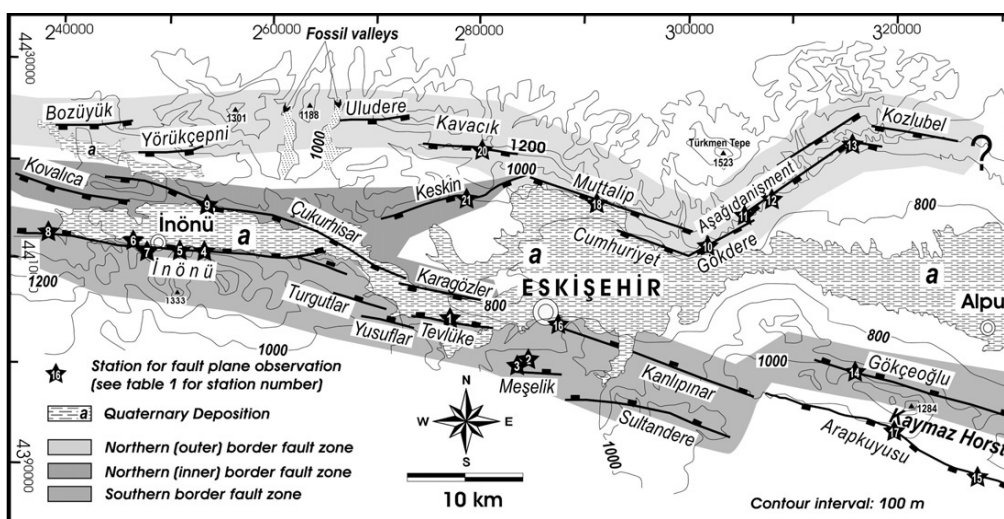


Figure 5.1. The Fault Map Showing the Fault Lines around the City of Eskisehir (Ocakoglu, 2007)

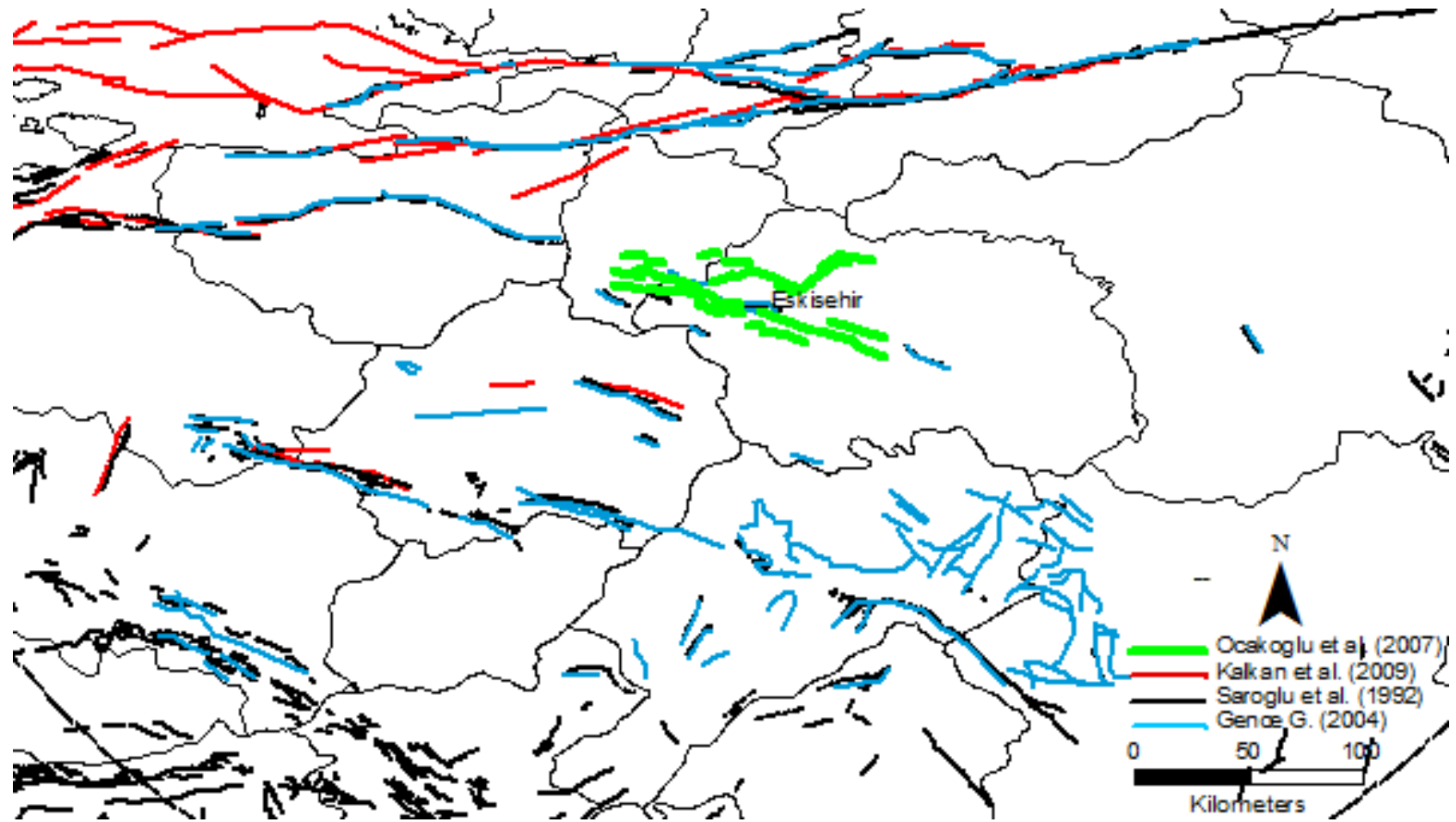


Figure 5.2. The Fault Map Covering a the Circular Area of 300 km Radius Centered at Eskisehir

As shown in Figure 5.1 several fault segments are distinguished within the EFZ that vary from 5 to 25 km in length, while the offset may reach 450 m at most. Being one of the active structures within the Anatolian plate, EFZ is a right-lateral strike-slip fault zone with a normal component (Sengor et al., 1985, Barka et al., 1995 and Saroglu et al., 1992) and it is moving more rapidly in west to southwest direction. Despite the existence of several faults in the EFZ, considering the high earthquake risks in other parts of the country, Eskisehir is relatively less prone to the earthquake risks. The largest magnitude earthquake that occurred over the last 100 years was on 20th February 1956. The earthquake with registered magnitude of $M_s=6.4$, caused a variety of damage in the downtown areas of Eskisehir, Bilecik, and Bozüyük and their vicinities.

5.2.2. Delineation of Seismic Sources

As the first step of determining the seismic sources around Eskisehir province, the fault map of the region and surroundings is investigated. Several fault maps of Turkey were prepared by many researchers, and among them, the most detailed and officially recognized active fault map was prepared by Saroglu et al. (1992). On local scale, the surrounding area, especially the NAFZ, and grabens of the Aegean region were studied in detail for the local geology and seismo-tectonic activities. Ocakoglu (2007) locally investigated the seismicity near Eskisehir and developed a very detailed map of faults in the close vicinity of the city. Figure 5.2 clearly presents the collection of several active fault-mapping studies conducted by Saroglu (1992), Kalkan et al. (2009), and Ocakoglu (2007). Since there is less uncertainty in the mapping of NAF, only the required portions of the NAF are sought. Hence, the recent study by Kalkan et al. (2009) which offered the detailed map of faults in and around Marmara Sea is also included in Figure 5.2. Though not included in the fault mapping study, Kocyigit (2005) was also included in the gathering process of the active faults in the area of interest. Indeed, his study provided crucial information in locating the active faults in and around Bursa.

5.2.2.1. Detailed Fault Segmentation Study around Eskisehir

The main fault zones are already discussed in the previous sections and by using the fault maps shown on Figure 5.2, the potential fault sources that could affect the city of Eskisehir are gathered. The closest faults to Eskisehir are obtained from

Ocakoglu et al. (1997), while the faults within the Sea of Marmara are compiled by using Kalkan et al. (2009). Most of the faults and associated parameters are obtained from Kocyigit (2005), indeed for most of the faults within the surrounding region of Eskisehir, type of the faults, degree of activities and the fault recurrence intervals are gathered from his study. The rest of the faults are obtained by using the official fault map of Turkey and through expert opinion (Kocyigit, 2010). The magnitudes of maximum largest earthquakes that could be generated by the faults are also listed in the related tables as the equations in Table 2.2 are used to calculate the associated maximum sizes of earthquakes. The faults and associated parameters that are listed in the following paragraphs are also provided in Appendix E in a compact form.

The potential fault lines that could influence the city center of Eskisehir are shown in Figure 5.3, which are gathered from the aforementioned sources. As shown in Figure 5.3, the northern part of the EFZ shows an interrupted geometry with sharp bends towards the western end and it extends towards Bursa. The easternmost section includes the Kozlubel and Sepetci (Segments #14 and #13) faults with 13 and 12 km lengths respectively. Then with a bend of 27.3° to the southwest, three parallel fault segments (Segments #15, #16 and #17) extend with varying lengths, with the longest segment intersecting another set of parallel faults with another bend of 53.1° to the northwest. Two faults namely, Muttalip and Cumhuriyet faults (Segment #18 and #19) with 12 and 13 km in length respectively, extend towards the location of the epicenter of the 20th February 1956 earthquake ($M_s=6.4$), which is the largest magnitude earthquake that occurred within the last 100 years, before meeting the largest segment in the region.

As presented in Figure 5.3, the southern branch of the EFZ consists of segments numbered between #2 and #10 with lengths ranging from 10 km to 19 km. The eastern part of the branch is formed by three normal faults, namely Sultandere fault (Segment #6), Altıpatlar (Segment #9) and Karacaoren faults (Segments #7, #8) with lengths of 11 km, 12 km, and 20 km respectively. To the south of these faults, lies the oblique-slip normal Gulpınar fault (Segment #10) with 16 km length and 108° azimuth from the north. To the west lie two parallel strands of oblique-slip normal faults (Yusuflar and Meselik) each with length of 10 km. These two faults extend in the east-west direction and they are separated by only a 1.5 km stepover structure.

Meselik fault (Segment #5) is also separated by a 2.5 km gap structure from Sultandere fault (Segment #6). Satılımısoglu-Karagozler fault (Segment #3), which is a normal fault, extends in the northeast-southwest direction from 1,3 km north of Meselik fault to the west for 14 km before meeting with the Cukurhisar-Hisaronu fault (Segment #2). The Cukurhisar-Hisaronu fault has a length of 19 km and extends in southeast-northwest direction. Segment #22, named as Kaymaz fault, though not shown in Figure 5.3 due to space limitations, is the eastern most segment of EFZ, which indeed is the last fault structure that exists in the east of Eskisehir in Central Anatolian region. Most of the faults in the EFZ are oblique-slip normal faults, with normal faults spreading among these oblique-slip normal faults.

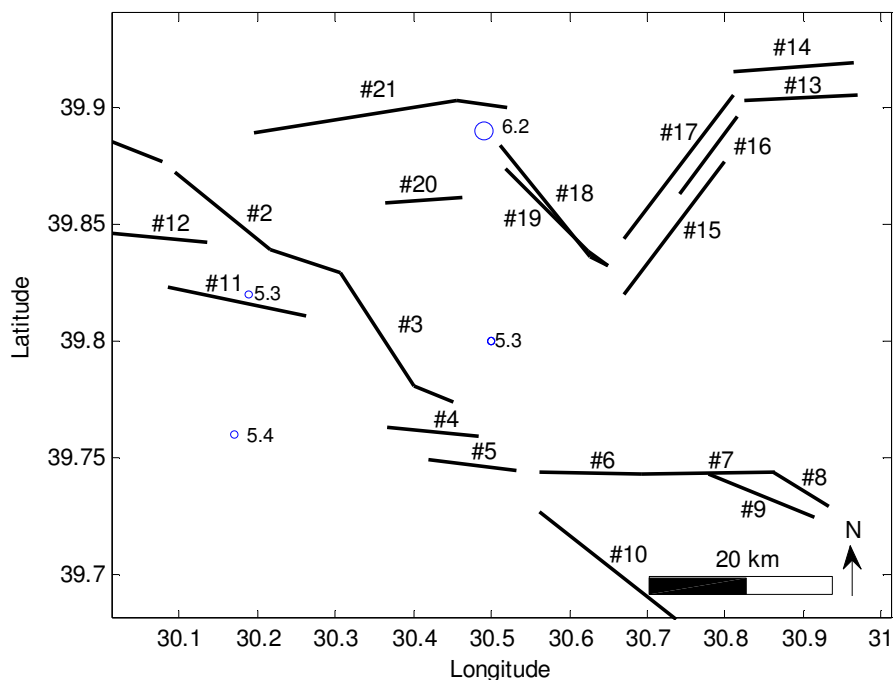


Figure 5.3. The Fault System in the Close Vicinity of Eskisehir and Earthquake Activity ($M_w > 5.0$) (Kocyigit, 2005)

In Figure 5.4, the easternmost segment (Segment #1) called the Kozpinar fault, follows almost a straight path of 39 km with a few bends. South of the Kozpinar fault lies the Dodurga fault (Segment #23) with 10 km length and the Erikli fault (Segments #24, #25 and #26) with 3 segments and 38 km overall length.

The Dodurga fault bends 25° in the middle, and the Erikli fault is composed of three segments with lengths of 13, 13 and 12 km, respectively, with the westernmost segment intersecting the Eskikoy fault (Segments #27, #28) in the north.

Table 5.1. The Faults in the Close Vicinity of Eskisehir

Segment No	Name of Fault	Type*	Length (km)	Degree of activity	M _w **	Return interval (year)
2	Hisaronu+Cukurhisar	N	19	Potentially active	6.5	≥ 1000
3	Satılmışoglu+Karagozler	N	14	Potentially active	6.3	≥ 1000
4	Yusuflar	OSN	10	Potentially active	6.1	≥ 1000
5	Meselik	OSN	10	Potentially active	6.1	≥ 1000
6	Sultandere	N	11	Potentially active	6.2	≥ 1000
7,8	Karacaoren	N	20	Potentially active	6.6	≥ 1000
9	Altıpatlar	N	12	Potentially active	6.2	≥ 1000
10	Gulpınar	OSN	16	Potentially active	6.4	≥ 1000
11	Inonu	OSN	15	Potentially active	6.4	≥ 1000
12	Kovalica	OSN	12	Potentially active	6.2	≥ 1000
13	Sepetci	OSN	12	Potentially active	6.2	≥ 1000
14	Kozlubel	OSN	13	Potentially active	6.3	≥ 1000
15	Gokdere	OSN	13	Potentially active	6.3	≥ 1000
16	Gunduzler	OSN	7	Potentially active	5.9	≥ 1000
17	Kizilcaoren	OSN	14	Potentially active	6.3	≥ 1000
18	Muttalip	N	12	Potentially active	6.5	≥ 1000
19	Kizilyar+Cumhuriyet	N	13	Potentially active	6.3	≥ 1000
20	Keskin	N	8	Potentially active	6.0	≥ 1000
21	ESKKEK*	OSN	28	Active	6.7	~500
22	Kaymaz	N	18	Potentially active	6.6	≥ 1000

* SS:Strike-slip, OSN: Oblique slip normal, N:Normal

** Size of peak earthquake

***ESKKEK is an abbreviation for the collection of the faults Esmekaya, Sogucak, Karaozkuyu, Kavacik, Egrioz, Kozkayi

Segments #27 and #28 form a single fault, however since there is an intersecting fault in the middle from southeast, for the convenience, it is accepted as two segmented faults with 17 km length each.

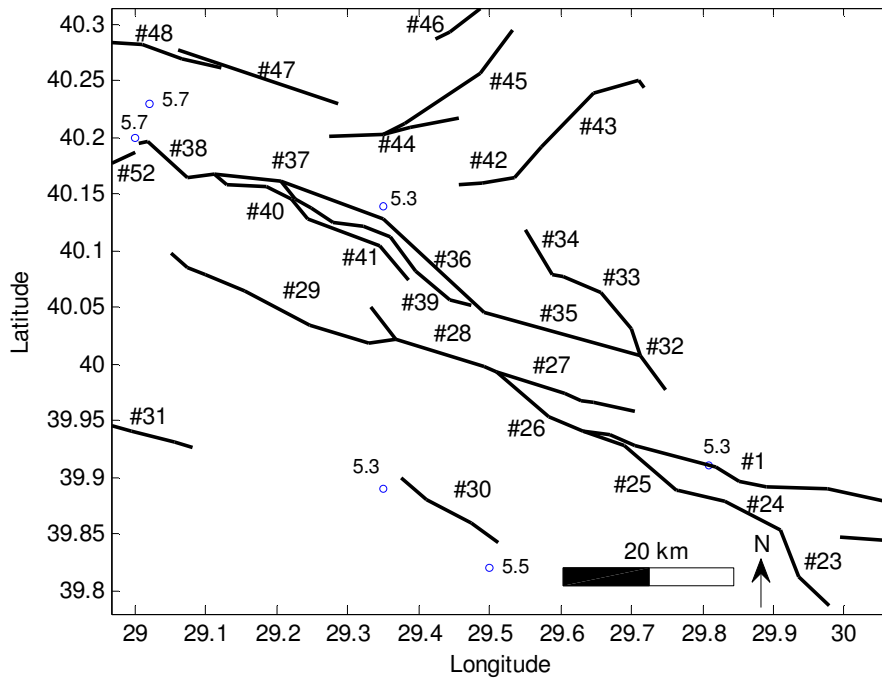


Figure 5.4. The Fault System in the Close Vicinity of Bursa (Kocyyigit, 2005)

The Bursa fault (Segments #35 to #38) lies in the northwest-southeast direction from the city of Bursa in the west to Tozakligol in the east with a total length of 63 km. The westernmost segment (Segment #38) lies 7 km before it bends 43.5° towards the east to segment #37. Segment #37 smoothly bends from east-west direction to southeast direction with two bends of 10° at 3 km starting from the west and 13° at 11 km from the west. The total length of this segment is 24 km. Segments #36 and #35 are the continuation of segment #37 and consist of single segments with 15 km and 19 km lengths as shown in Figure 5.4 and in Table 5.2. Segments #39, which is called the Sayfiye fault, lie just south of the Bursa fault with 27 km total length. The combination of Segment #40 and Segment #41 is called Alacam fault, which lies in the general direction of Bursa fault with a length of 27 km in total. Segments #30 and #31, which are called the Ortaca and Akcabuk faults, lie in northwest-southeast orientation with no association with any fault segments.

As shown in Figures 5.4 and 5.5, Calı fault with segments #52, #53 and #54 lie in a northeast-southwest orientation in the south of the Bursa fault. Segment #52 bends

50⁰ to the southwest from the main Bursa fault and extends 7 km, segment #53 lies 12 km to the west to meet segment #54, which bends 26.5⁰ towards southwest with 10 km length. The rest of the faults are shown with their segment numbers and total lengths in Table 5.2.

Table 5.2. The Faults in the Close Vicinity of Bursa (Kocyigit, 2005)

Segment No	Name of Fault	Type*	Length (km)	Degree of activity	M _w **	Return interval (year)
1	Kozpınar	OSN	39	Potentially active	7.0	≥ 1000
23	Dodurga	OSN	10	Potentially active	6.2	≥ 1000
24-26	Erikli	OSN	38	Potentially active	6.9	≥ 1000
27,28	Eskikoy	OSN	34	Potentially active	6.9	≥ 1000
29	Sogukpınar	OSN	28	Potentially active	6.7	≥ 1000
30	Ortaca	OSN	14	Potentially active	6.3	≥ 1000
31	Akcabuk	SS	20	Potentially active	6.5	≥ 1000
32-34	Eymir	OSN	24	Potentially active	6.6	≥ 1000
35-38	Bursa	OSN	63	Potentially active	7.2	≥ 1000
39	Sayfiye	OSN	27	Potentially active	6.8	≥ 1000
40,41	Alacam	OSN	27	Active	6.7	~500
42,43	Bogazkoy	OSN	26	Potentially active	6.7	≥ 1000
44	Kestel	OSN	16	Potentially active	6.4	≥ 1000
45	Koyunhisar	SS	19	Potentially active	6.6	≥ 1000
47	Karahidir	OSN	20	Potentially active	6.5	≥ 1000
48	Demirtas	OSN	22	Potentially active	6.6	≥ 1000
52-54	Cali	OSN	29	Potentially active	6.8	≥ 1000

- SS: Strike-slip, OSN: Oblique slip-normal ,
- ** Size of peak earthquake

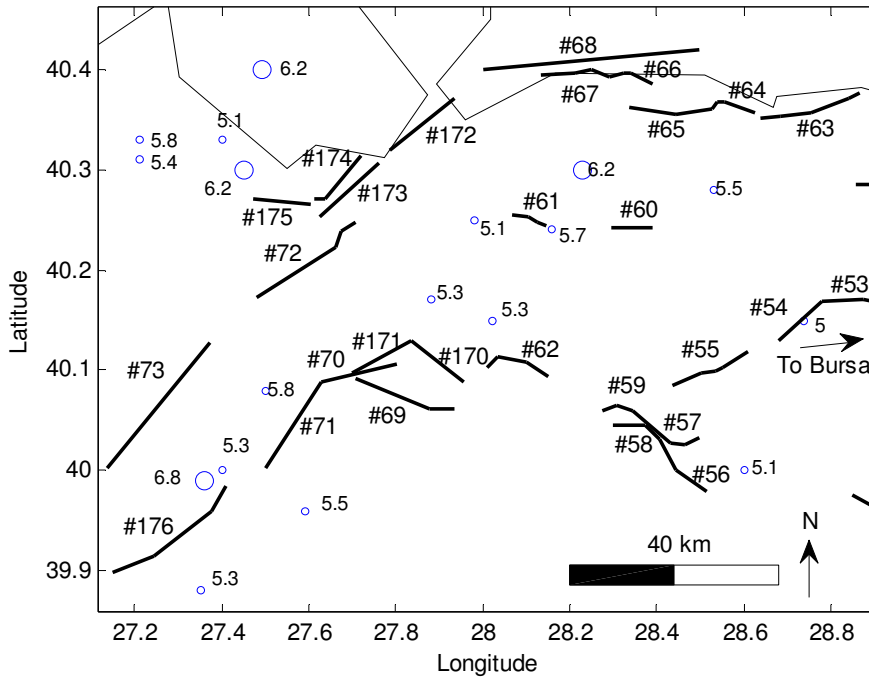


Figure 5.5. The Fault System in the Close Vicinity of South Marmara Region and Earthquake Activity ($M_w > 5.0$) (Kocyigit, 2005)

To the west of Bursa in the south Marmara Region, the southern branch of the NAF passes through the land and then crosses the Biga Peninsula through a set of strike-slip faults. South of this branch extend the oblique normal faults that were created by the northward push of the western Anatolia with its extensional dominated character. As shown in Figure 5.5, the Bandirma fault (Segment #68) extends in east-west direction for about 68 km close to the coast of Marmara. On the coast of Marmara, the Kursunlu fault extends 23 km in east-west direction before a bend of 21.1° towards the southwest to Edincik fault (#172), which is located in the south of Kapıdağ Peninsula. The strike-slip faults in the region are aligned with the Edincik fault, but with large gaps amongst them as shown in Figure 5.5. The normal faults in the region lie from west of Bursa until they intersect the strike-slip faults of the region, which lie in northeast to southwest direction. The Ayaz fault (Segment #55) extends 15 km towards east to the Calı fault with a 6 km gap structure dividing the two segments. Segments #56 to #59 form a different system of faults with their northwest-southeast orientation, and show the distribution of the regional strain pattern. The names of the faults in the close vicinity of south Marmara region, with lengths, activity rates, and return intervals are provided in Table 5.3.

Table 5.3. The Faults in the Close Vicinity of South Marmara Region

Segment No	Name of Fault	Type*	Length (km)	Degree of activity	M _w **	Return interval (year)
55	Ayaz	OSN	15	Potentially active	6.4	≥ 1000
56,59	MKP***	OSN	20	Potentially active	6.5	≥ 1000
57,58	Derecik	OSN	21	Potentially active	6.5	≥ 1000
60	Taslik	OSN	7	Potentially active	6.0	≥ 1000
61	Cavuskoy	OSN	7	Potentially active	6.0	≥ 1000
62	Yenikoy	OSN	12	Potentially active	6.2	≥ 1000
63	Mudanya	SS	20	Active	6.5	~500
64,65	Bogazkoy-Ekinli	SS	25	Active	6.7	~500
66,67	Kursunlu	SS	23	Active	6.6	~500
68	Bandirma	SS	42	Potentially active	7.0	≥1000
69	Tutuncu	N	20	Potentially active	6.5	≥ 1000
70	Gonen	N	15	Potentially active	6.4	≥ 1000
71	Yenice-I	SS	14	Potentially active	6.4	≥ 1000
72	Sarikoy	SS	22	Potentially active	6.6	≥ 1000
73	Sofular	SS	24	Potentially active	6.6	≥ 1000
170,171	Manyas	N	23	Potentially active	6.6	≥ 1000
172	Edincik	SS	14	Potentially active	6.4	≥ 1000
173	Havutca	SS	11	Potentially active	6.2	≥ 1000
174	Gebecinar	SS	11	Potentially active	6.2	≥ 1000
175	Kinalar	SS	11	Potentially active	6.2	≥ 1000
176	Yenice-II	SS	25	Potentially active	6.6	≥ 1000

* SS:Strike-slip, OSN: Oblique slip-normal, N:Normal

** Size of peak earthquake

***Mustafakemalpasa

While there is not enough accumulation of evidence that the fault system is mainly composed of strike-slip faults, the basin of the Sea of Marmara is accepted to have an extensional regime that has strike-slip faults with high normal components (Kalkan et al., 2009). The northern branch of the system consists of strike-slip faults and a single normal fault at segment #100. This fault system starts with segment #99 in the east, which is named as the Darica fault, with a length of 19 km and with a 4.5° bend towards the north of east-west direction. The system continues with the Adalar fault (Segment #100) with a 22.5° bend towards northwest and a length of 32 km. The Adalar fault meets with the strike-slip fault of Yesilkoy at segment #101 with a bend of 33.1° towards southwest. The length of Yesilkoy fault is 42 km, which extends in southwest-northeast direction. These fault triplets are highly important since they are in the close vicinity of Istanbul. Since, a future earthquake event generated by these faults may inflict great damages to the city of Istanbul, a number of investigations were performed (BU-ARC (Bogazici University-American Red Cross), 2002, Erdik et al., 2003, JICA-IMM (Japanese International Cooperation Agency- Istanbul Metropolitan Municipality), 2003, Ozturk, 2007, Oglesby et al., 2008). Among several investigations, Ozturk (2007) studied the possibility of a multi-segmental earthquake event on these three segments in her Ph.D. study. In JICA-IMM (2003), a deterministic approach was used and the maximum earthquake that could be generated by these three segments was considered.

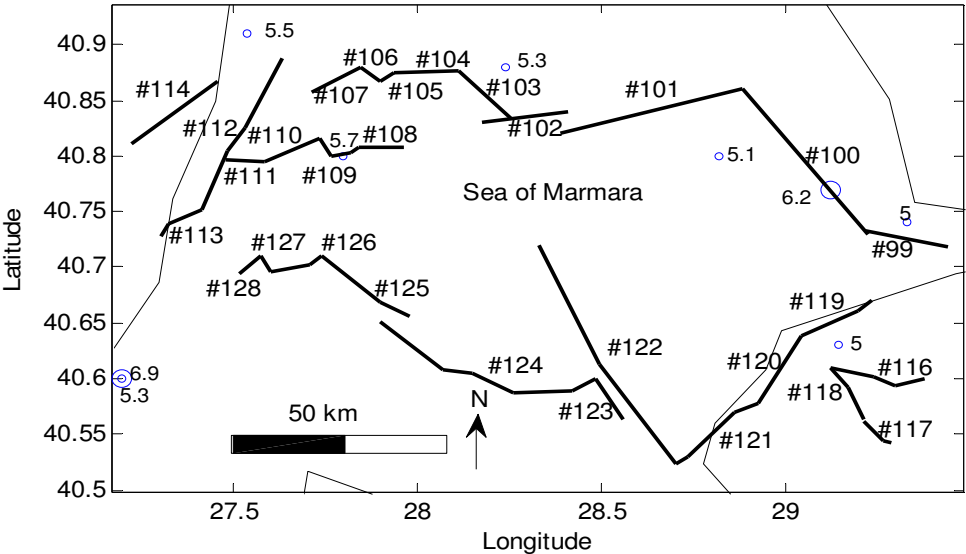


Figure 5.6. The Fault System in the Close Vicinity of Sea of Marmara and Earthquake Activity ($M_w > 5.0$) (Kocuyigit, 2005, Kalkan et al., 2009)

The Southern Marmara branch starts with the 17 km Cınarcık fault (Segment #119) and continues with the Esenkoy fault (Segment #120) with a bend angle of 18⁰ between them. The Armutlu (Segment #121) and Imralı (Segments #122,123) faults follow these segments. Other faults in the region are given with their lengths and related parameters in Figure 5.6 and Table 5.4.

Table 5.4. The Faults in the Close Vicinity of Sea of Marmara (Kocyigit, 2005, Kalkan et al., 2009)

Segment No	Name of Fault	Type*	Length (km)	Degree of activity	Mw**	Return interval (year)
99	Darica	SS	19	Active	6.5	~500
100	Adalar	N	32	Very active	6.9	~250
101	Yesilkoy	SS	42	Very active	7.0	~250
102	Kumruburgaz	SS	18	Very active	6.5	~250
112,113	Ucmakdere	SS	34	Active	6.9	~250
114	Isiklar	SS	20	Active	6.6	~500
115	Orhaniye	SS	19	Active	6.5	~500
116,118	Laledere	SS	21	Active	6.6	~500
117	Kurtkoy-Gokcedere	OSN	16	Very active	6.4	~250
119	Cinarcik	SS	17	Very active	6.5	~250
120	Esenkoy	SS	13	Very active	6.3	~250
121	Armutlu	SS	20	Very active	6.6	~250
122,123	Imrali	SS	45	Potentially active	7.0	≥ 1000
124	Erdek	SS	50	Potentially active	7.1	≥ 1000
125	Asmali	SS	21	Potentially active	6.6	≥ 1000
126-128	Marmara	SS	23	Potentially active	6.6	≥ 1000

* SS:Strike-slip, OSN: Oblique slip normal, N:Normal

** Size of peak earthquake

The central section of the NAF is the most active part of the system that produced several large earthquakes. Especially the 17th August 1999 Izmit earthquake with 7.4 moment magnitude and the 12th November 1999 Duzce earthquake with 7.2 moment magnitude are the largest recorded earthquakes not only in the region but in the country as well. The whole region is dominated by strike-slip faults.

As shown in Figure 5.7, starting from Izmit Bay, the northern branch extends from the coast to the Duzce segment in the east. The fault system starts with the three parallel strands that extend in east-west direction, namely the Karamursel, Korfez, and Golcuk Faults with segment numbers #96, #97, and #98 respectively. The Karamursel fault extends 28 km in northwest-southeast direction with 12° from east-west, the Golcuk fault lies 4° in northwest-southeast direction with a length of 25 km and Korfez Fault extends 16 km in east-west direction. To the east, The Tepetarla fault (Segment #95) lies 18 km in east-west direction, from the coast of Izmit Bay to Sapanca Lake. There is strong evidence that this fault continues under Sapanca Lake but further studies are required to confirm.

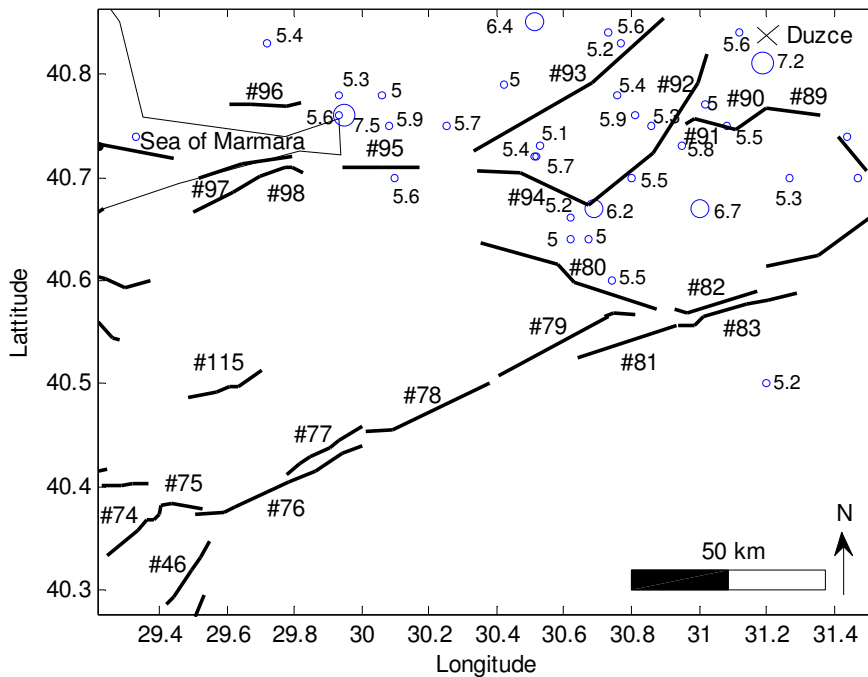


Figure 5.7. The Fault System between Sea of Marmara and Duzce within NAFZ and Earthquake Activity ($M_w > 5.0$) (Kocyigit, 2005, Saroglu, 1992)

The rupture path of the Izmit earthquake provided crucial data in terms of rupture propagation mechanisms and segments involved in the rupture. One of these

segments is the Arifiye fault (Segment #94) which constitutes the continuation of the Tepetarla fault (Segment #95). The bend angle between the two faults' segments is 1° for the first 10 km and 11° for the next 18 km. The total length of the fault is 28 km. The next fault on the rupture of the Izmit earthquake is the Karadere fault (Segment #92), which extends 35 km in northeast-southwest direction with a 15° to the east-west direction.

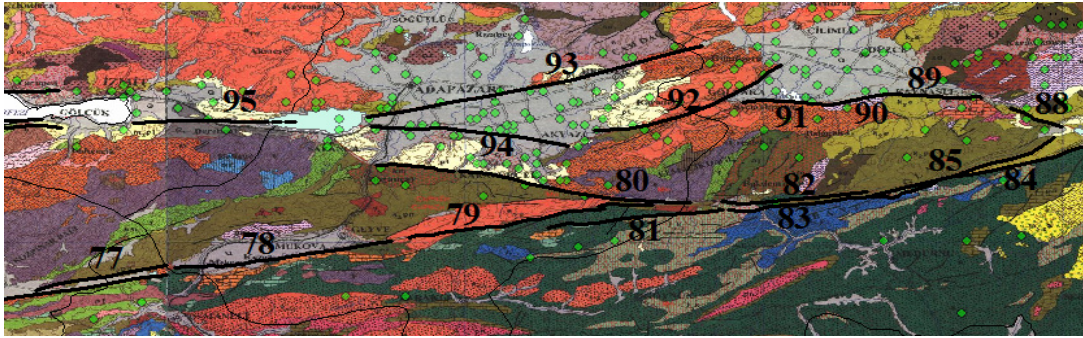


Figure 5.8. The Fault System in the Central NAFZ

There is a gap of 5 km and a bend angle of 25.5° between the Arifiye and Karadere faults, which is called the Akyazı gap. North of the Karadere and Arifiye faults extends the Hendek fault with a length of 50 km and in northeast-southwest orientation. One of the most active faults is the Duzce fault (Segments #89 to #91) with several earthquakes are associated as shown in Figures 5.7 and 5.8 and Table 5.5. The fault generated an earthquake with moment magnitude 7.2 within its own segmental structure. Three segments are defined within the fault, the Eften, Dagdibi and Kaynaslı segments (Segments #89, #90 and #91) (Duman et al., 2005) with 13 km, 6 km and 13 km's length respectively. The eastern fault is called the Bakacak fault (Segment #88), which extends in southeast-northwest direction with a length of 8 km. The gap and bend structure between the Bakacak fault and the Duzce fault system acted as a barrier in stopping the rupture in the 12 November 1999 Duzce earthquake (Duman et al., 2005). Table 5.5 gives the other related information about the faults belonging to the fault system between the Sea of Marmara and Duzce and Figures 5.7 and 5.8 provide the fault map with the surrounding geological structures.

The southern branch of the NAF is composed of several strike-slip fault segments that extend in the same general direction of NAF, starting from Sukriye fault (segment #74) in the east to the westernmost Bayramoren fault (Segment #87) (Figure 5.9). The NAF extends about 340 km in the considered region.

**Table 5.5. The Faults between Sea of Marmara and Duzce within NAFZ
(Kocyigit, 2005, Saroglu, 1992)**

Segment No	Name of Fault*	Type*	Length (km)	Degree of activity	Mw**	Return interval (year)
46	Kavakli	SS	13	Potentially active	6.3	≥ 1000
49	GAK***	SS	21	Active	6.3	~500
50	Gemlik	SS	14	Active	6.4	~500
51	Gurle	SS	12	Active	6.3	~500
74	Sukruye	SS	20	Active	6.5	~500
75	Narlica	SS	10	Active	6.2	~500
76	Camdibi	SS	42	Potentially active	7.0	≥ 1000
77	Karadin	SS	19	Active	6.5	~500
79	Tarakli	SS	28	Active	6.8	~500
80	Karapurcek	SS	43	Very active	7.0	~250
81	Goynuk	SS	32	Active	6.8	~500
82	Mudurnu-I	SS	21	Active	6.6	~500
83	Mudurnu-II	SS	55	Active	7.1	~500
84	Yenicaga-Gerede	SS	92	Active	7.5	~500
88	Bakacak	SS	8	Very active	6.0	~250
89-91	Duzce	SS	34	Very active	7.0	~250
92	Karadere	SS	35	Very active	7.0	~250
93	Hendek	SS	50	Very active	7.1	~250
94	Arifiye	SS	28	Very active	6.9	~250
95	Tepetarla	SS	18	Very active	6.8	~250
96	Körfez	SS	16	Very active	6.4	~250
97	Golcuk	SS	25	Very active	6.7	~250
98	Karamursel	SS	28	Very active	6.7	~250
116-118	Laledere	SS	21	Active	6.6	~500

* SS:Strike-slip,OSN: Oblique slip normal

** Size of peak earthquake

***GAK - Gençali-Altıntaş-Kurşunlu

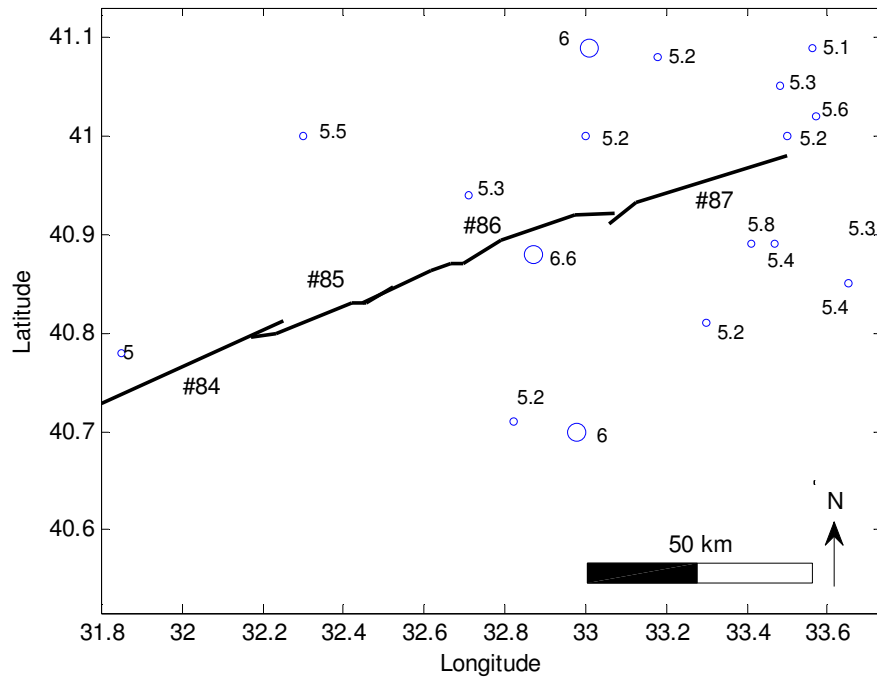


Figure 5.9. The Fault System between Gerede and Bayramoren Faults within the NAFZ and Earthquake Activity ($M_w > 5.0$) (Saroglu, 1992)

Figure 5.9 shows the varying lengths of the Gerede, Ismetpasa and Bayramoren faults (Segments #85, #86 and #87). The properties of the faults are also provided in Table 5.6. The same alignment of Camdibi fault (Segment #76) is almost constantly carried to the Bayramoren fault with only a single degree of difference observed in the direction of alignment.

Table 5.6. The Faults between Gerede and Bayramoren within the NAFZ (Saroglu, 1992)

Segment No	Name of Fault	Type*	Length (km)	Degree of activity	M_w^{**}	Return interval (year)
85	Gerede	SS	31	Active	6.8	~500
86	Ismetpasa	SS	54	Active	7.1	~500
87	Bayramoren	SS	38	Active	6.9	~500

* SS: Strike-slip

** Size of maximum earthquake

Figure 5.10 and Table 5.7 presents the fault system near Kutahya, which is located in the southwest of Eskisehir. The region is dominated by normal faults and the extensional regime of the Aegean region is clearly reflected in the region. There are three main fault systems, namely Kutahya (Segments #129 to #132), Gediz (Segments #133 to #136), and Simav (Segments #138 to #141).

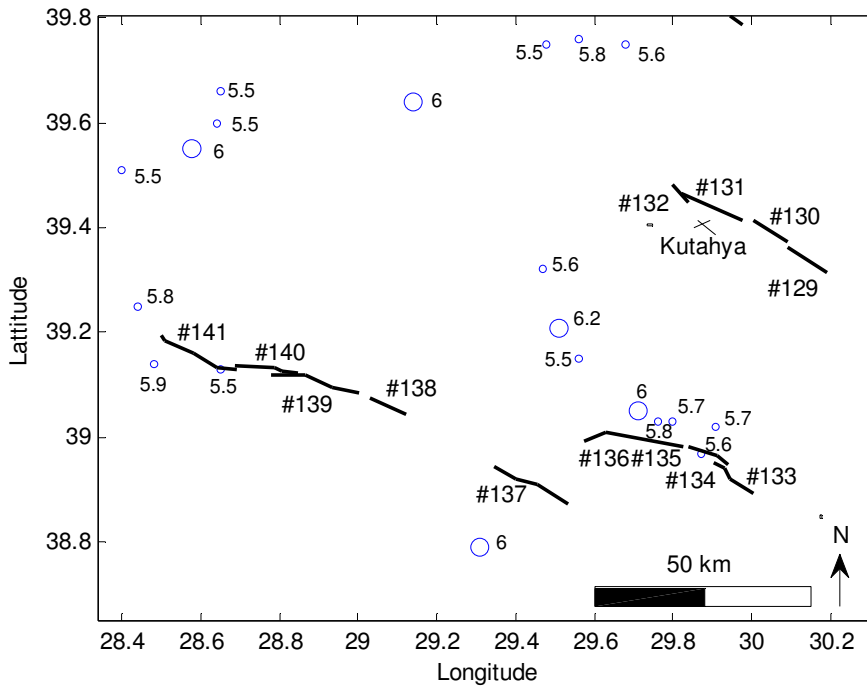


Figure 5.10. The Fault System in the Close Vicinity of Kutahya and Earthquake Activity ($M_w > 5.5$) (Kocyigit, 2005, Saroglu, 1992)

The Kutahya fault lies in southeast-northwest direction with an azimuth of 60° . The fault is composed of four segments with lengths ranging 5 km to 15 km. The Gediz fault is a very active fault that has produced 18 earthquakes with magnitudes greater than 5.0 in the last century. It consists of four segments with lengths ranging from 5 km to 17 km.

Table 5.7. The Faults in the Close Vicinity of Kutahya (Kocyigit, 2005, Saroglu, 1992)

Segment No	Name of Fault	Type*	Length (km)	Degree of activity	M_w **	Return interval (year)
129-132	Kutahya	OSN	41	Potentially active	7.0	≥ 1000
133-136	Dumlupinar	N	72	Potentially active	7.2	≥ 1000
137	Gediz	N	18	Potentially active	6.5	≥ 1000
138-141	Simav	N	59	Potentially active	7.2	≥ 1000

* N: Normal, OSN: Oblique-slip normal

** Size of maximum earthquake

The Simav fault is another fault system in the region with four segments of 9 km to 30 km length. The activity rate is quite homogenous; however, larger magnitude

earthquakes are generated in the western part of the fault. The last region that could pose a seismic threat to Eskisehir is called the Isparta triangle by the experts. This region consists of several normal faults that show the pattern of strain caused by the tectonic movements of the surrounded regions. The faults are presented in Figure 5.11 and the related parameters are given in Table 5.8. The most important fault system in the region are formed by the Cay fault, the Sultandagi fault and Aksehir fault (Segments #145 to #152), which are formed by eight segments that have produced three earthquakes with magnitudes greater than 6.0 in the last century.

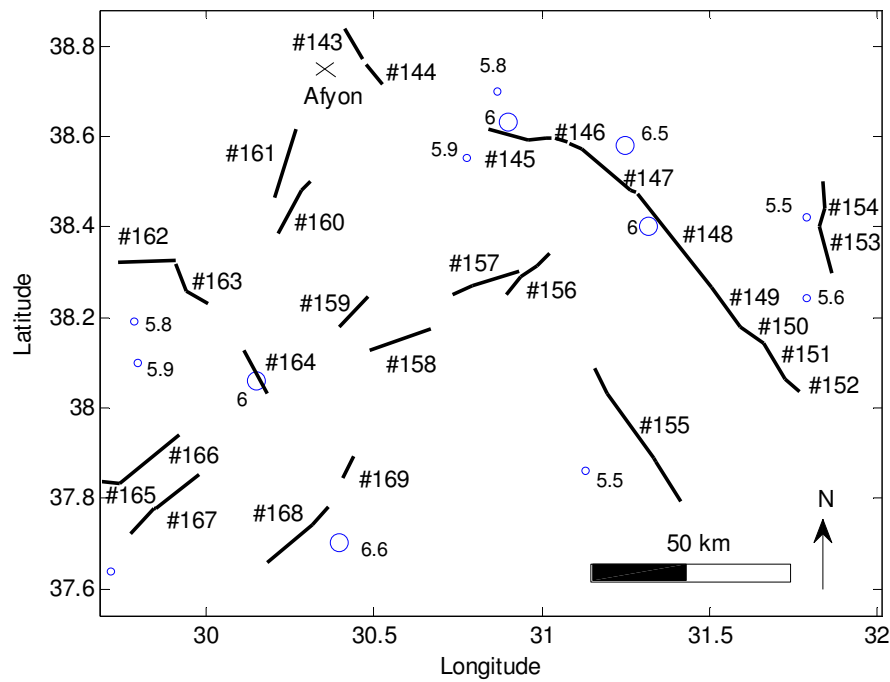


Figure 5.11. The Fault System in the Close Vicinity of Isparta Triangle and Earthquake Activity ($M_w > 5.5$) (Kocigit, 2005, Saroglu, 1992)

The first segment in the mentioned fault system is called the Cay fault (Segment #145). It lies in east-west orientation with a length of 17 km before crossing a gap structure. Following the Cay fault lays the first segment of the Sultandagi fault (Segment #146) which is a very small segment of 3 km length. There is a 2 km gap between segment #146 and the adjacent segments. However, it is highly probable that these segments are a single piece and act together underneath. Following the 2 km gap, segment #147 is encountered, which lies with a 21 km in east-west and northwest-southeast orientation.

**Table 5.8. The Faults in the Close Vicinity of Isparta Triangle
(Kocyigit, 2005, Saroglu, 1992)**

Segment No	Name of Fault	Type*	Length (km)	Degree of activity	M _w **	Return interval (year)
143,144	Afyon	N	17	Potentially active	6.4	≥ 1000
145	Cay	N	15	Active	6.4	~500
146,147	Sultandagi	N	24	Active	6.7	~500
153,154	Ilgin	N	24	Potentially active	6.7	≥ 1000
155	Beysehir	N	42	Potentially active	7.0	≥ 1000
156	Hoyran-I	N	14	Potentially active	6.4	≥ 1000
157	Hoyran-II	N	20	Potentially active	6.6	≥ 1000
158	Senirkent	N	17	Potentially active	6.4	≥ 1000
159	Haydarli	N	16	Potentially active	6.4	≥ 1000
160	Sandikli-I	N	16	Potentially active	6.4	≥ 1000
161	Sandikli-II	N	17	Potentially active	6.4	≥ 1000
162	Isikli-I	N	15	Potentially active	6.4	≥ 1000
163	Isikli-II	N	14	Potentially active	6.4	≥ 1000
164	Dinar	N	13	Potentially active	6.3	≥ 1000
165	Cardak-I	N	11	Potentially active	6.2	≥ 1000
166	Cardak-II	N	19	Potentially active	6.5	≥ 1000
167	Basmakçı	N	23	Potentially active	6.6	≥ 1000
168	Burdur-I	N	21	Potentially active	6.6	≥ 1000
169	Burdur-II	N	5	Potentially active	5.7	≥ 1000
148-152	Aksehir	N	64	Active	7.3	~500

* N: Normal

** Size of maximum earthquake

Segment #147 bends 30° to the south from east-west direction before meeting a 30 km segment (Segment #148) of the Aksehir fault that extends in the same direction. From segment #149 to #152, the segments extend 35 km further in southeast direction in the same alignment with the segments #147 and #148. The remaining faults in the region are shown in Figure 5.11 and in Table 5.8 together with their lengths and activity rates.

5.3. Processing the Seismic Data

5.3.1. Seismic Activity around Eskisehir

Eskisehir is located in a transition region between the Aegean Region and the NAFZ, which are among the most active earthquake regions in the world. While Eskisehir is surrounded by these two active regions, the close vicinity of Eskisehir did not experience very high earthquake activity.

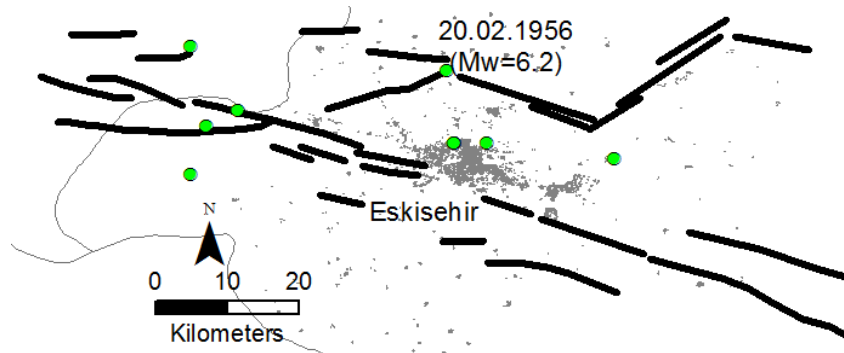


Figure 5.12. Faults and Earthquake Activity in the Close Vicinity of Eskisehir ($M_w \geq 4.0$) (Faults by Ocakoğlu, 2008)

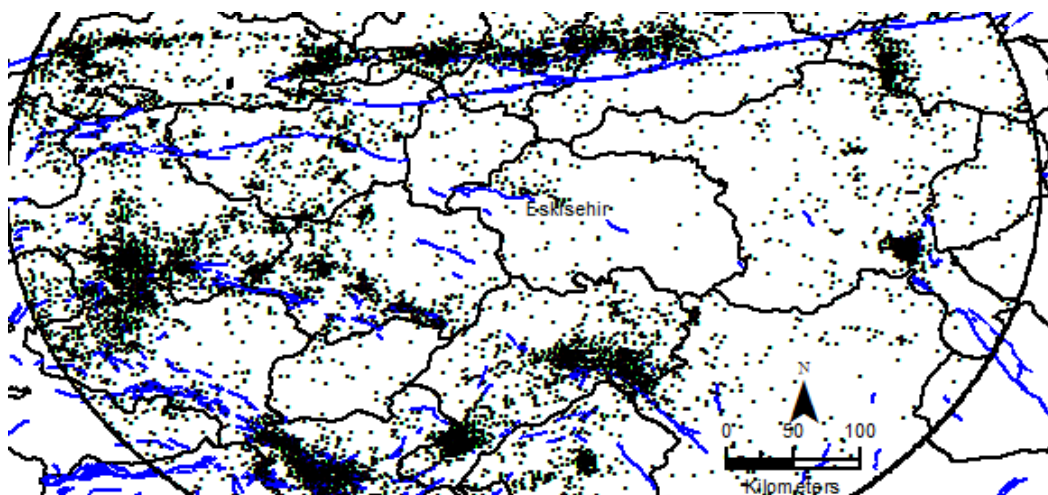


Figure 5.13. Seismicity around Eskisehir within Encircled Area with 300 km Radius Circle Between 1900 and 2010, ($M \geq 3.0$, KOERI, 1900-2005, Faults by Saroglu et al., 1992)

The activity is concentrated on the NAFZ and the Aegean region while the city itself is subject to a substantial local activity. As shown in Table 5.9, within the radius of a 300 km circle centered at Eskisehir, large and medium scale earthquakes have occurred during the period between 1900 and 2010.

Table 5.9. Major Large Magnitude Earthquakes within 300 km Radius Circular Area Centered at Eskisehir between 1900 and 2010

Name of the Event	Date	Longitude (degrees)	Latitude (degrees)	Magnitude (M_w)	Distance from Eskisehir
Eskisehir	20.02.1956	39.89	30.49	6.2	7.89
Cinarcik	18.09.1963	40.77	29.12	6.2	118.62
Sakarya	22.07.1967	40.67	30.69	6.2	62.69
Gediz	28.03.1970	39.21	29.51	6.2	80.23
Dinar	01.10.1995	38.06	30.15	6.0	121.71
Izmit	17.08.1999	40.76	29.95	7.4	78.43
Düzce	12.11.1999	40.81	31.19	7.2	85.01
Sultandagi	15.12.2000	38.40	31.32	6.0	110.35
Cay-Eber	03.02.2002	38.63	30.90	6.5	83.79

The two largest destructive earthquakes, which ruptured the two westernmost segments of the northern branch of the NAFZ occurred on 17th August 1999 (M_w =7.4) and on 12th November 1999 (M_w =7.2). The largest and closest earthquake that occurred in the vicinity of Eskisehir, which is located in the map shown in Figure 5.18 within the period of 1900-2010 is 20th February 1956 earthquake with magnitude M_w =6.2, which inflicted a variety of damage in downtown Eskisehir. Historical earthquakes for the pre-1900 period are provided in Table 5.10, which was prepared according to Ambraseys and Finkel (1991) and Ambraseys (2009).

Table 5.10. Historical Records Compiled for the City of Eskisehir

Date*	Latitude (degrees)	Longitude (degrees)	Magnitude (M_w)	Distance from Eskisehir (km)
10.09.1509	40.90	28.70	6.7	197
10.05.1556	40.30	27.80	6.7	238
30.07.1633	41.00	29.00	6.0	186
1646	41.00	29.00	6.0	186
25.05.1672	41.00	30.00	6.2	142
1674	40.18	29.10	6.0	128
25.05.1719	40.70	29.80	6.8	119

Table 5.10 Continued

Date*	Latitude (degrees)	Longitude (degrees)	Magnitude (M_w)	Distance from Eskisehir (km)
1737	40.10	27.30	6.6	276
1737	41.00	29.00	6.0	186
02.09.1754	40.80	29.20	6.5	159
03.09.1763	41.00	29.00	6.0	186
23.04.1766	40.80	28.20	6.0	226
22.05.1766	40.80	29.00	6.6	171
1767	41.00	29.00	6.0	186
06.10.1841	40.85	29.05	6.1	172
1850	40.10	28.30	6.1	192
1851	40.03	28.40	6.0	182
28.02.1855	40.10	28.60	6.6	167
11.04.1855	40.20	28.90	6.2	145
1863	38.50	30.60	6.4	142
11.05.1875	38.00	29.00	7.1	237
04.05.1875	38.10	30.20	7.4	189
13.05.1876	38.80	30.50	-	109
28.09.1881	40.60	33.60	6.0	278
1886	38.30	29.30	6.0	195
10.07.1894	40.70	29.60	6.8	128
16.04.1896	39.30	29.20	6.0	124

* Some of the dates are not known in detail, therefore only the year of occurrence is given

5.3.2. Choosing the Earthquake Catalogs and Processing the Raw Data

After the identification of faults as possible earthquake generating sources, gathering the information on the previous seismic activity in the region of interest becomes the next issue. In general, seismic activity is classified into two as pre-instrumental (historical) and instrumental period activity. The historical activity contains events with historical accounts and it is mostly based on the evidence of the local geological formations. On the other hand, the instrumental period activity includes the earthquake events that are recorded by special instruments. Instrumental period records provide significant information for the evaluation of seismic hazards, though some of them are incomplete and with inconsistent quality. In the end, regardless of the types of earthquakes, whether historical or instrumentally recorded, all the records are registered in catalogs, for documenting the seismic activity of a considered region.

These catalogs are crucial in understanding the earthquake occurrence patterns for specific locations. In order to compile a reliable catalog for Eskisehir and the surrounding region bounded by a 300 km radius circle centered at Eskisehir, a number of catalogs were gathered, such as Tan et al. (2008), Deniz (2006), KOERI, and GDDA catalogs. Each catalog covers different periods with different magnitude scales.

The catalogs covering the period starting from 1900 are generally compiled from the bulletins of the International Seismology Summary (ISS), the National Oceanographic and Atmospheric Administration - US Geological Survey (NOAA-USGS), the United States Geological Survey Preliminary Determination of Epicenters (USGS-PDE), and the International Seismological Center (ISC) (Deniz, 2006). These catalogs however, lack the earthquake data below certain magnitudes due to lack of instrumentation or the insufficient recording capacity of the instruments below certain magnitudes. Nevertheless, relatively complete instrumental data is available for $M \geq 4.0$ earthquakes since 1965 owing to the fact that recording instruments were improved enough to serve as a reliable source of information. This instrumentation was very effective in recording the significant earthquakes and helped to form several catalogs by different institutions.

Amongst these catalogs, GDDA catalog, catalogs gathered by Tan et al. (2008), Deniz. (2006) and KOERI catalog are evaluated in terms of their coverage period, area of coverage, the magnitude scales, and the minimum magnitudes. As can be seen in Table 5.11, the KOERI compiled a catalog covering the period from 1900 until 2005, which includes more than 41000 earthquakes with magnitudes of 3.0 and larger that occurred in Turkey and its surroundings covering a rectangular area bounded by 32° - 45° north latitude and 23° - 48° east longitudes.

The KOERI catalog provides a more convenient source of information when compared with the other catalogs, since the coverage of period is longer, the coverage area is larger, and the earthquakes are listed in all magnitude scales. Therefore, it is selected as one of the sources to be used in this study. GDDA also has an up to date catalog that provides the earthquake records as well, covering the period starting from 1976. As a final catalog, a combined catalog is created which is composed of KOERI data for the period between 1900 and 2005 and GDDA data

starting from 2006 to 2010. Therefore, a locally specific catalog covering the period between 1900 and 2010 is obtained.

Table 5.11. Comparison of Earthquake Catalogs Obtained from Different Sources

Catalog Source	Number of Data	Coverage Period	Magnitude Scales	Coverage Area (degrees)	Minimum Mag.
KOERI	41609	1900-2005	Various magnitudes: $M_b, M_d, M_l,$ M_s, M_w	32-45 ⁰ N 23-48 ⁰ E	$M \geq 3.0$
Deniz A. (2006)	4752	1900-2004	Moment magnitude: M_w	34-44 ⁰ N 24-47 ⁰ E	$M_w \geq 4.5$
Tan et al. (2008)	12508	-2100-1963 1963-2007 (ISC)	Various magnitudes: $M_s, M_i,$ M_w, M^*	34-43 ⁰ N 25-46 ⁰ E	$M_i \geq 3.5$
GDDA	2556	1976-2010	Various magnitudes: M_L, M_D	35.81 ⁰ -42.10 ⁰ N 25.60 ⁰ -44.82 ⁰ E	$M_i \geq 2.3$

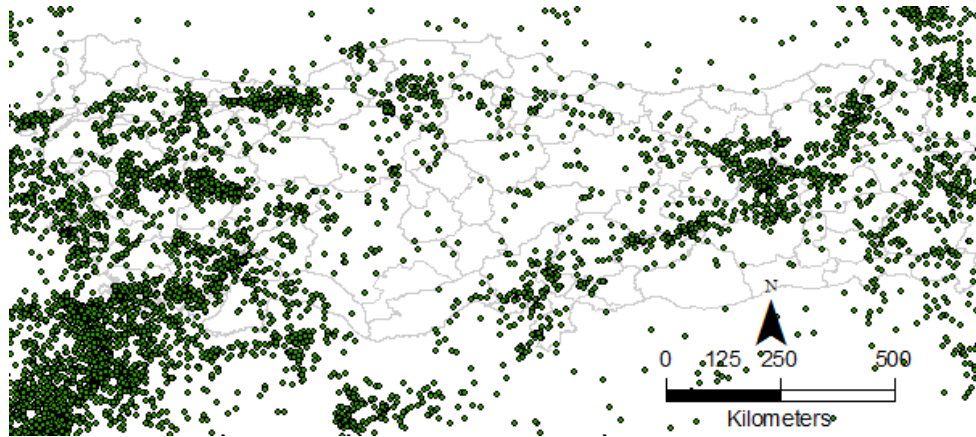


Figure 5.14. Seismicity in Turkey between 1900-2010 by KOERI and GDDA ($M_w \geq 4.0$)

Figure 5.14 shows the earthquake epicenters covering the period of 1900-2010. The combination of the KOERI data covering between 1900 and 2005 and the GDDA data covering the 2006-2010 is utilized to have a complete record of events in Anatolia from 1900 until 2010.

5.3.3. Homogenization and Declustering the Seismic Data

Both the KOERI and GDDA sources contain earthquakes with magnitude registered in different scales as presented in Table 5.11. Nevertheless, the procedures for declustering the catalog and in particular GMPEs require moment magnitude scale since this scale is being widely accepted and used in the recent studies and became a commonly accepted scale in the related investigations. Therefore, initially the catalog is homogenized by unification of magnitude scales into moment magnitude by using the equations in 2.31.

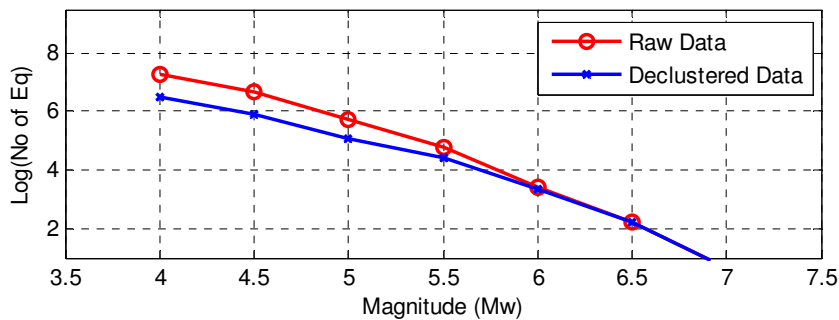


Figure 5.15. The Effect of Declustering on the Magnitude Distribution

Then, the catalog is declustered by using the time and space windows of Deniz (2006), Deniz, and Yucemen (2008) as given in Table 2.3 of section 2.5.1.2. Before the declustering, 1422 earthquake events are identified within the considered region, which is bounded by a 300 km radius circle centered at Eskisehir. After declustering, the number of events decreased to 653, which indicates the existence of a large number of foreshock and aftershock events in the catalogs. Declustering has a considerable effect on earthquake magnitude distribution, especially for smaller magnitude ranges up to 5.0, as presented in Figure 5.15.

5.3.4. Completeness Analysis of the Declustered Data

A comprehensive 110-year catalog of earthquakes that occurred within the area of interest is compiled from two different sources. For the period of 1900-2005, the KOERI catalog is used and the rest of the data until 2010 is gathered from the GDDA catalog. Histogram of the records of this combined catalog is shown in Figure 5.16 in four magnitude ranges.

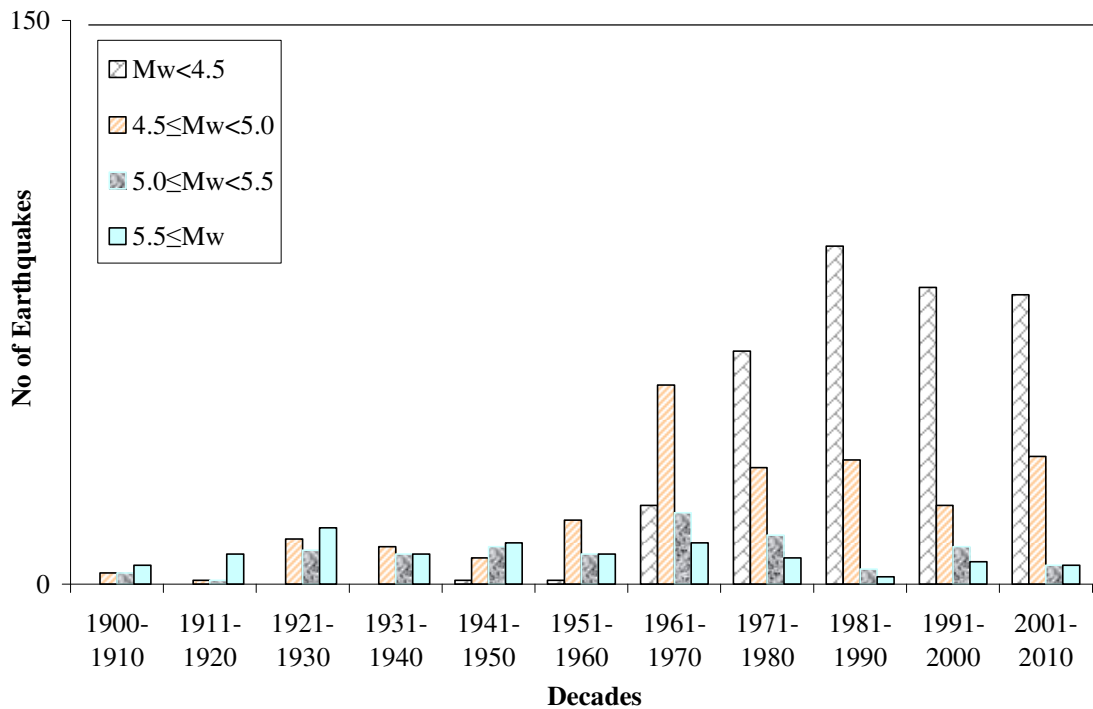


Figure 5.16. Earthquakes in Each Decade With Respect to Four Magnitude Ranges (KOERI 1900-2005, GDDA 2005-2010 Combined, Raw Data)

Table 5.12. Number of Earthquakes Classified According to Ten-Year Periods and Four Different Magnitude Ranges (Declustered After Deniz, 2006 and Deniz and Yucemen, 2008)

DECLUSTERED DATA				
Period	M _w < 4.5	4.5 ≤ M _w < 5.0	5.0 ≤ M _w < 5.5	5.5 ≤ M _w < 6.0
1900-1910	0	3	3	5
1911-1920	0	1	1	8
1921-1930	0	11	8	15
1931-1940	0	9	7	7
1941-1950	0	6	13	11
1951-1960	1	16	7	8
1961-1970	13	45	15	11
1971-1980	59	28	11	6
1981-1990	89	33	4	2
1991-2000	61	15	6	6
2001-2010	71	29	5	4

As shown in Figures 5.16 and Table 5.12, the smaller magnitude earthquakes are very rare for the earlier decades when the instrumentation was not fully spread. In other words, the magnitude distribution is biased especially for the smaller magnitude earthquakes if the whole period between 1900 and 2010 is considered. For magnitudes greater than 5.0, the catalog shows a uniform distribution for the entire period.

Table 5.12 provides detailed information on the distribution characteristics of earthquakes with respect to the recording periods and the magnitude ranges. Regarding the magnitude ranges, four different bins are created after the initial evaluation of the magnitude distribution in Figure 5.17. Although it is already obvious that magnitudes above 5.0 have no recognizable signs of incompleteness, two different bins are created just to suit to the arrangement of magnitude ranges for smaller magnitude earthquakes. In an attempt to explain the influence of incompleteness on the coefficients of the magnitude distribution equation, Figure 5.17 is created. In the upper part of the figure, the yearly distribution of the earthquakes with respect to the magnitudes is presented. As the plot implies, there is a gap of activity between magnitudes 4.0 and 5.0 before the mid-1960s. The high clustering of these events after the mid-1960s is due to the deployment of several seismographs around the country. For magnitudes above 5.0, earthquake events seem to follow a pattern with limited periodical fluctuations.

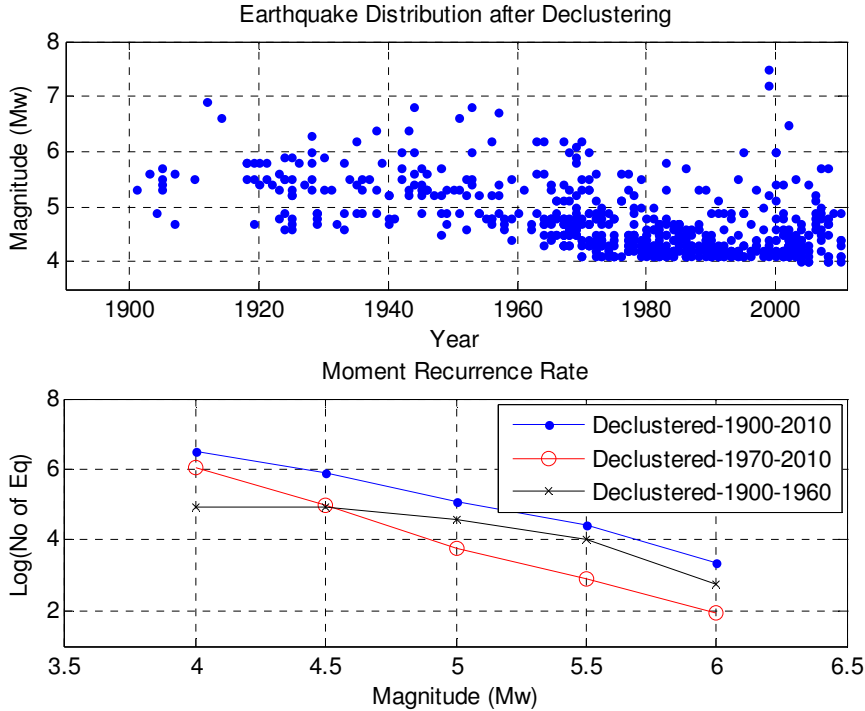


Figure 5.17. Distribution of Earthquakes with Respect to Moment Magnitudes (top) and the Comparison of Magnitude Recurrence Curves for Complete and Incomplete Parts (bottom)

In the lower subplot in Figure 5.17, the magnitude recurrence curves of the declustered seismic database are presented. The magnitude recurrence curves for the

whole database covering the period of 1900 to 2010, and two other recurrence curves for the complete and incomplete parts of the database are presented in the figure. The curve developed for the incomplete part reflects a recognizable decrease at the lower magnitudes, while for the complete period; the magnitude distribution curve seems to be linear. If the whole period is considered, the distribution curve has a downward bend in the lower magnitude ranges.

The subintervals of the catalog where the incomplete reporting is identified by using the Stepp (1973) methodology, which was explained in section 2.5.1.3, are completed artificially by adjusting the number of events in the incomplete intervals to satisfy the requirement of the mentioned methodology.

Table 5.13 presents the completeness analysis results for the catalog. The first column in the table shows the periods of evaluation, with the covered period becoming longer until it covers the whole catalog as shown in the last row. The time intervals and the inverse square of the intervals are provided in the next two columns. The rest of the columns in the table provide values calculated for completeness analysis in four different magnitude ranges. For each magnitude range, the total number of earthquakes belonging to each period, N , is given in the first column. The mean yearly rates of occurrences, λ , that are obtained by dividing the number of earthquakes in each period by the total years covered by the period, are given in the following column. The values of σ that are calculated by using equation 2.33 are provided in the next column.

For each magnitude range, the alignment of standard deviation, σ , and the values with the inverse square root of the time in years is checked. Although it may be rather subjective, the alignment of the σ values with $1/\sqrt{T}$ are observed for different magnitude ranges and the complete years of the catalogue is obtained by observing the alignment of the values.

It was already mentioned that above the moment magnitude of 5.0, the database is accepted as complete and no completion procedure is applied for those magnitude ranges. Below that magnitude, the database is investigated for the incomplete parts and the parameters of completeness according to methodology of Stepp (1973) are derived. The completion process involved increasing the number of earthquakes for

the incomplete reporting years and then checking the stability of the $\sigma-1/\sqrt{T}$ curve until the slope of the curve become stable.

Table 5.13. Values of Completeness Parameters for Seismic Database Before and After the Completion Procedure by Using the Methodology of Stepp (1973)

PERIOD	T(yr)	1/√T	N	λ	σ	N	λ	σ
			INCOMPLETE					
			m _w <4.5			4.5≤m _w <5.0		
2010-2001	10	0.32	71	7.10	0.84	29	2.90	0.54
2010-1991	20	0.22	132	6.60	0.57	44	2.20	0.33
2010-1981	30	0.18	221	7.37	0.50	77	2.57	0.29
2010-1971	40	0.16	280	7.00	0.42	105	2.63	0.26
2010-1961	50	0.14	293	5.86	0.34	150	3.00	0.24
2010-1951	60	0.13	294	4.90	0.29	166	2.77	0.21
2010-1941	70	0.12	294	4.20	0.24	172	2.46	0.19
2010-1931	80	0.11	294	3.68	0.21	181	2.26	0.17
2010-1921	90	0.11	294	3.27	0.19	192	2.13	0.15
2010-1911	100	0.10	294	2.94	0.17	193	1.93	0.14
2010-1901	110	0.10	294	2.67	0.16	196	1.78	0.13
PERIOD	T(yr)	1/√T	N	λ	σ	N	λ	σ
			COMPLETE					
			m _w <4.4			4.5≤m _w <5.0		
2010-2001	10	0.32	71	7.10	0.84	29	2.90	0.54
2010-1991	20	0.22	132	6.60	0.57	44	2.20	0.33
2010-1981	30	0.18	221	7.37	0.50	77	2.57	0.29
2010-1971	40	0.16	280	7.00	0.42	105	2.63	0.26
2010-1961	50	0.14	362	7.24	0.38	150	3.00	0.24
2010-1951	60	0.13	417	6.95	0.34	180	3.00	0.22
2010-1941	70	0.12	503	7.19	0.32	228	3.26	0.22
2010-1931	80	0.11	559	6.99	0.30	256	3.20	0.20
2010-1921	90	0.11	651	7.23	0.28	302	3.36	0.19
2010-1911	100	0.10	687	6.87	0.26	320	3.20	0.18
2010-1901	110	0.10	719	6.54	0.24	336	3.05	0.17

As can be followed in Table 5.13 in the columns reserved for σ and $1/\sqrt{T}$ and in Figure 5.18, for each magnitude class, the time needed to reach the stability of σ and

he deviations from the σ versus $1/\sqrt{T}$ are identified for the considered magnitude ranges. Obviously, the stability of the parameters is gained after 1970 and the number of events before 1970 is adjusted as presented in Table 5.13 until the earlier periods follow the same trend as the period after 1970, as given in Figure 5.18.

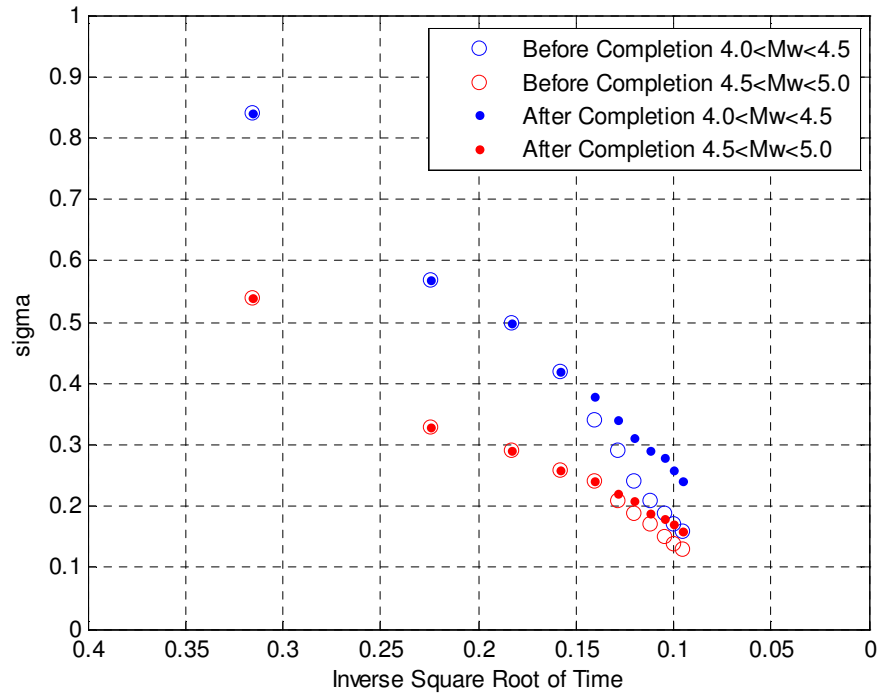


Figure 5.18. Trends of Magnitude Completeness Parameters

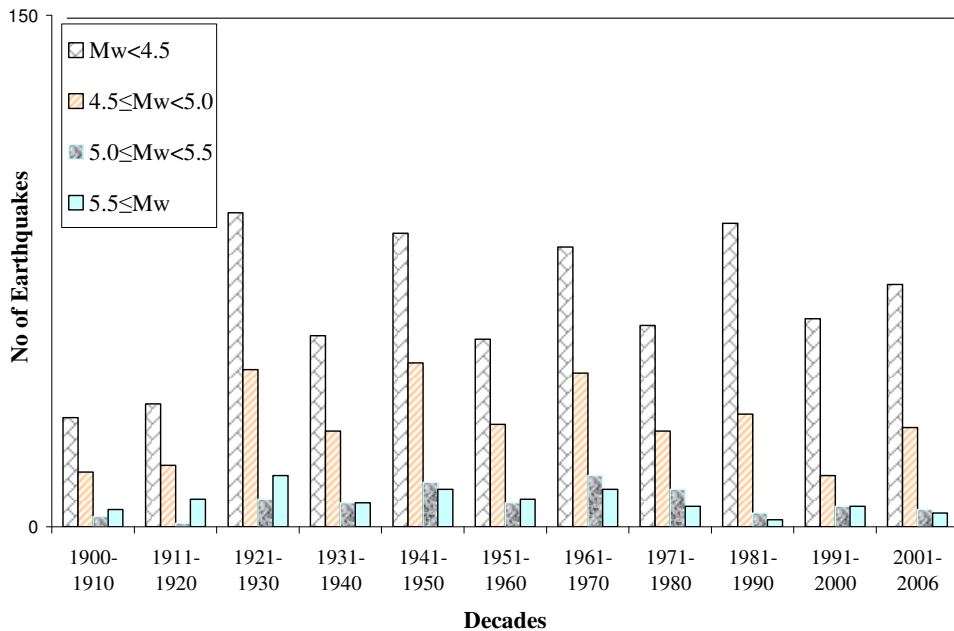


Figure 5.19. Earthquakes in Each Decade With Respect to Four Magnitude Ranges (Combination of KOERI 1900-2005 and GDDA 2005-2010, Homogenized, Declustered and Completed)

The adjustment of the number of events of the incomplete periods is perfectly reflected in Figure 5.19 as the fluctuations of the complete parts of the catalog are well projected onto the incomplete periods. A simpler and clearer representation of the completed database is provided in Table 5.14. The number of events for the magnitude ranges and the periods are also provided in the table.

Table 5.14. Number of Earthquakes Classified According to Ten-Year Periods and Four Different Magnitude Ranges after Completeness Analysis Results

DECLUSTERED and COMPLETED DATA				
Period	$M_w < 4.5$	$4.5 \leq M_w < 5.0$	$5.0 \leq M_w < 5.5$	$5.5 \leq M_w < 6.0$
1900-1910	32	16	3	5
1911-1920	36	18	1	8
1921-1930	92	46	8	15
1931-1940	56	28	7	7
1941-1950	86	48	13	11
1951-1960	55	30	7	8
1961-1970	82	45	15	11
1971-1980	59	28	11	6
1981-1990	89	33	4	2
1991-2000	61	15	6	6
2001-2006	71	29	5	4

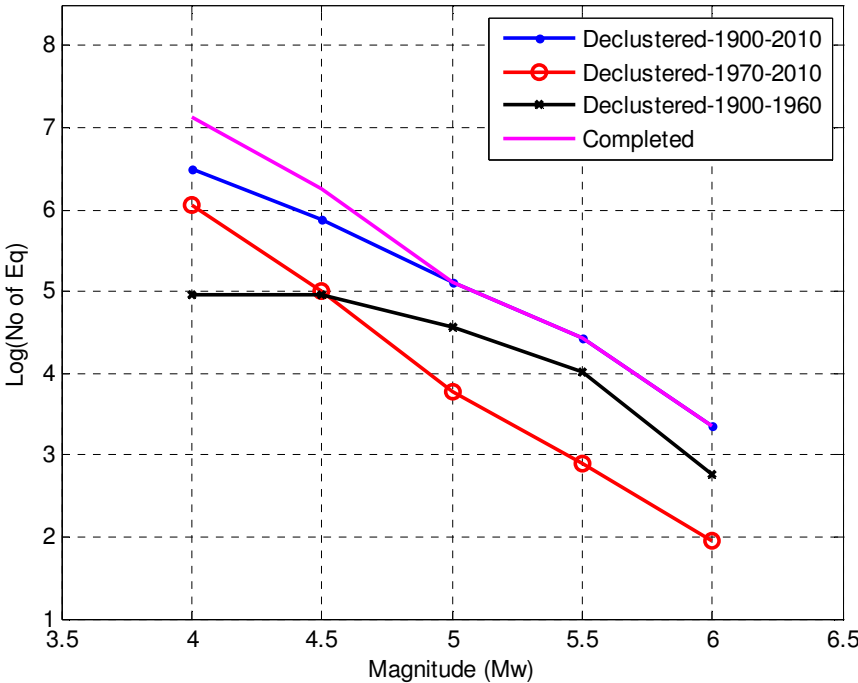


Figure 5.20. The Magnitude Recurrence Relationships after Completeness Analysis Results

Figure 5.20 summarizes the completeness analysis, the constant value of b is 0.90 for the incomplete dataset, but for the completed catalog, b takes the value of 1.03. The completeness periods for each magnitude level are addressed considering every seismic source zone separately. Table 5.14 presents the number of earthquakes after the completion process is performed. It should be mentioned that this completion procedure is quite subjective since it based on trial and error, and due to the subjective decision on the stability of σ versus $1/\sqrt{T}$. However, with a careful application of the procedure as it is done in the present study, it is possible to obtain a better distribution of events that reflects the behavior of the complete part.

5.4. Seismic Source Parameters

5.4.1. Area Sources and Source Parameters

Since the full characteristic earthquake model is used, earthquakes with a magnitude smaller than 6.0 are incorporated into the area sources. In order to establish realistic and reliable area sources, certain criteria must be considered, such as the existence of a group of geophysical structures that are associated with a cluster of events, the clustering and spread of epicenter locations, and maximum magnitude earthquake generated by the earthquake generating sources. In addition, the established sources must contain sufficient number of events to obtain a reliable set of seismic parameters. Figures 5.21 and 5.22 present a delineation study created by evaluating the regional geophysical structures, the clustering of earthquake epicenters over the period of time, the way they are spread over the area of interest and the number of events in a single area. The maximum magnitudes for these areal sources are typically assessed either from the historical seismicity of the region, or from the regional tectonic setting, or from the regional paleoseismological data. It is also limited to maximum magnitude of $M_w=6.0$, due to the fact that above that magnitude earthquakes are considered to be produced by fault sources. Figures 5.21 and 5.22 also show the effects of the declustering which is performed by the time and space windows proposed by Deniz and Yucemen (2008). Random or so-called “floating earthquakes”, or the earthquakes that cannot be associated with any of the seismic sources, are assigned to background sources. The modeling of these background sources is similar to those of area sources, since the same seismic parameters are calculated for these sources as well.

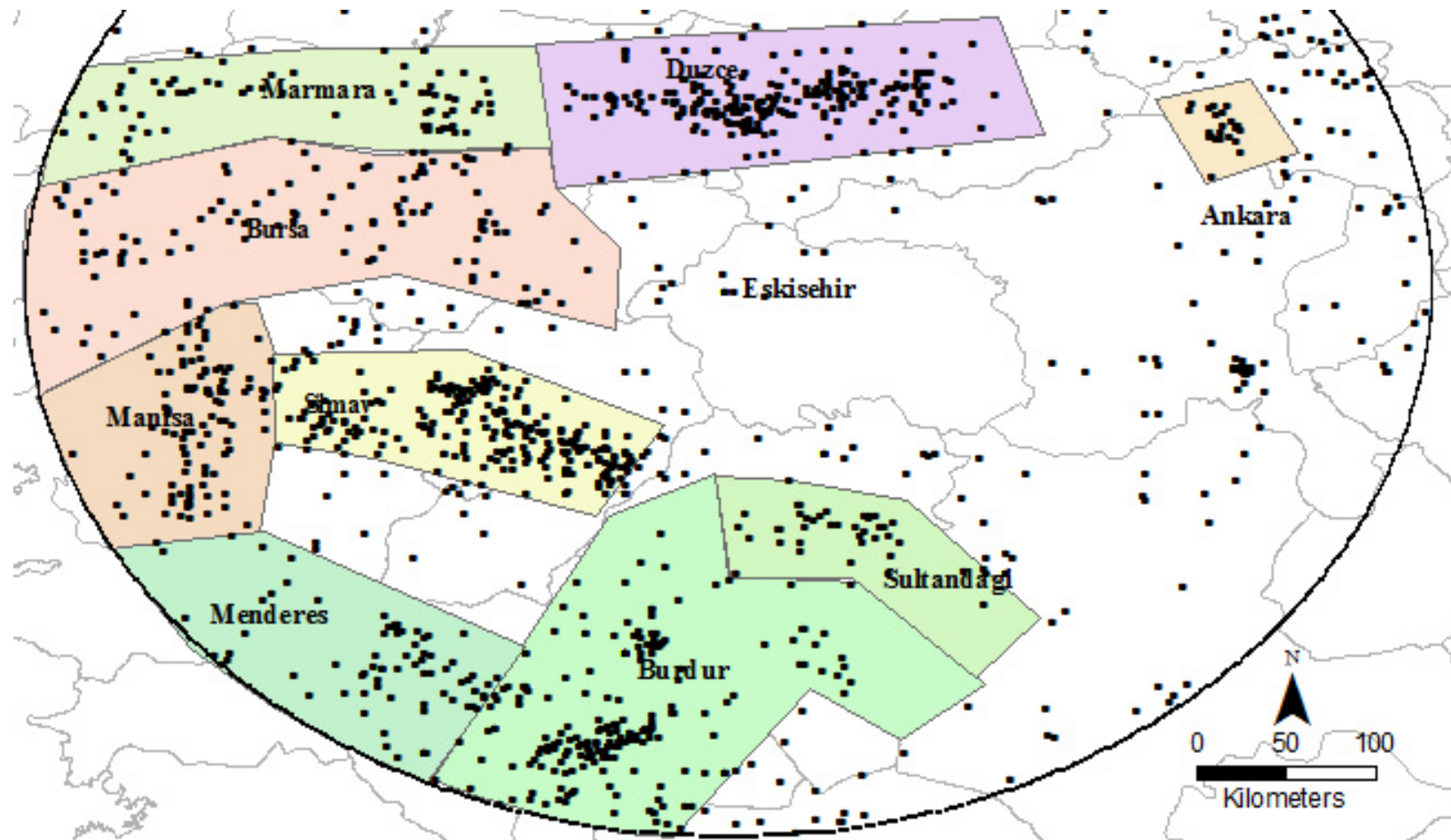


Figure 5.21. Area Sources and Epicenters of Earthquakes Occurred Between 1900 and 2010 (Earthquakes by KOERI, GDDA, $M_w > 4.0$, Before Declustering)

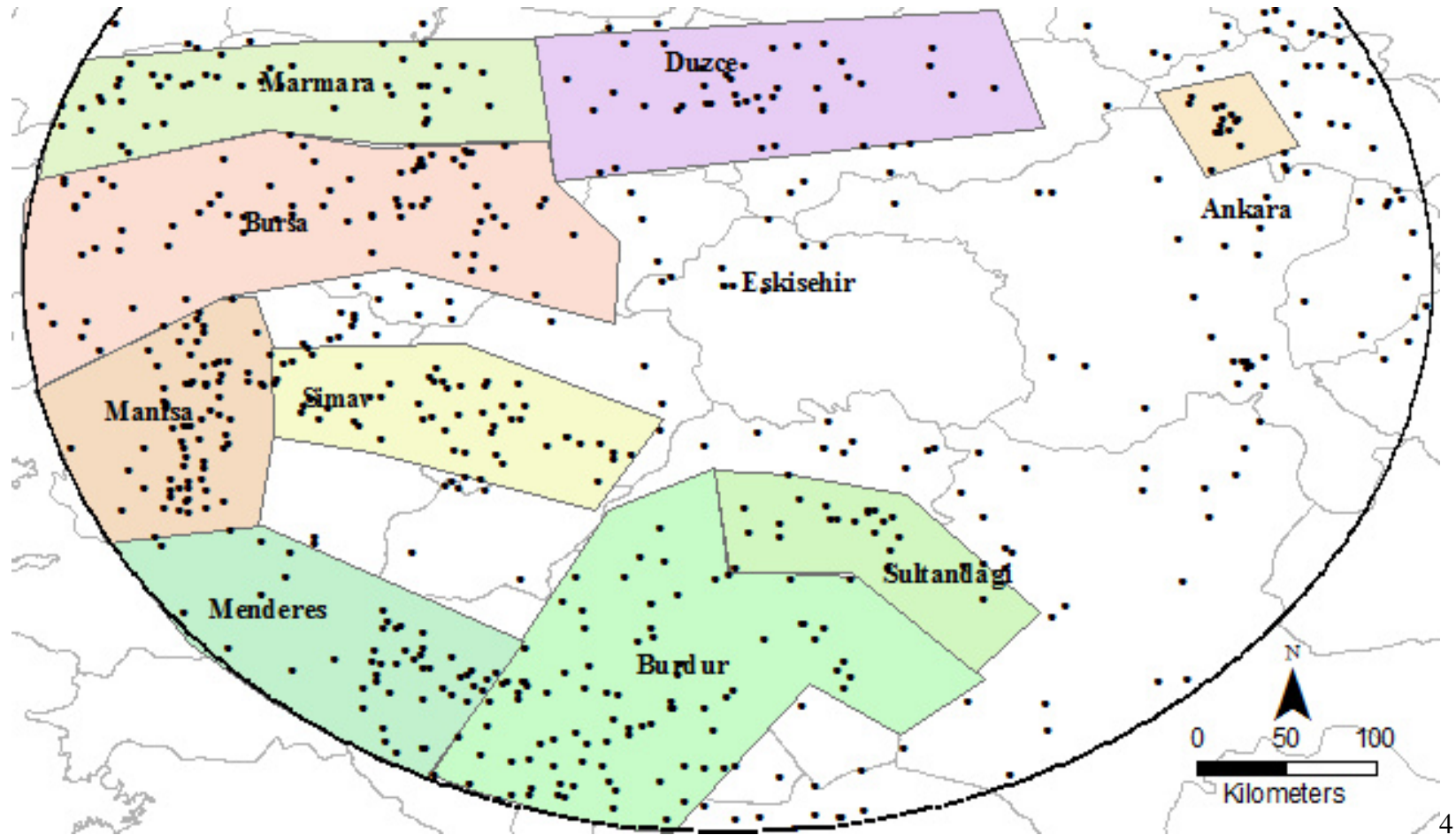


Figure 5.22. Area Sources and Epicenters of Earthquakes for the Period Between 1900 and 2010 (Earthquakes by KOERI, GDDA, $M_w > 4.0$, Declustered According to Deniz and Yucemen, 2008)

Table 5.15 presents the created area sources and the related parameters that are derived after the delineation study. As a common practice, the minimum magnitude is taken as $m_0= 4.0$ and the assigned maximum magnitudes are given in the second column of Table 5.15. The annual rate of occurrences and b values of GR relationships that are specific for each area source is listed for the raw catalog data, declustered data and completed data in the following columns of Table 5.15. The depth values of the source areas are assumed as 20 km for all the area sources. The coordinates of the area sources are provided in Appendix D.

Table 5.15. Area Sources and Their Parameters

Source Name	Max M_w	Raw Data		Data After 1970		Declustered and Completed	
		ν (/year)	b	ν (/year)	b	ν (/year)	b
Ankara	6.0	0.20	1.29	0.13	1.34	0.19	1.02
Burdur	6.0	2.00	0.91	0.55	0.93	1.22	0.93
Bursa	5.8	1.02	0.65	0.45	0.91	1.14	0.84
Düzce	5.6	2.08	0.83	0.24	0.71	0.66	0.74
Marmara	5.7	0.69	0.89	0.32	0.93	0.36	0.89
Manisa	6.0	0.97	0.78	0.52	1.28	0.93	1.04
Menderes	5.8	0.68	0.62	0.28	0.61	0.91	0.74
Simav	6.0	2.34	0.92	0.52	0.96	0.70	0.95
Sultandagi	6.0	0.35	0.59	0.15	1.26	0.41	0.93
Background	6.0	2.61	0.69	1.09	0.96	3.39	0.91
Overall	6.0	12.95	0.78	4.24	0.96	9.91	0.88

5.4.2. Fault Source and Parameters

As mentioned previously, it is assumed that the faults or fault segments have a pattern of releasing the accumulated stresses that rupture the large parts or entire length of the fault segment. The pattern of the events in both time and magnitude has been under thorough investigation, while no sound and reliable method to predict the time and magnitude of the next event has been developed yet. Among the several proposed methods to model the recurrence patterns of fault sources, the characteristic earthquake method is widely accepted and utilized while the other proposed methods receive increasingly more attention. The full characteristic earthquake model is employed for fault sources. The behavior of this model is explained in Figure 5.23 in time and magnitude dimensions. In this model, the exponential part that is associated with the smaller magnitude earthquakes is not taken in to account, as shown in

Figure 5.23. The part of the model that expresses the large magnitude probability distribution is accepted as constant for an interval of $(m_{max}-0.5)$ to m_{max} . Each fault is considered as a different segment and the seismic characteristics of each segment are determined separately. The return intervals of earthquakes are gathered by expert opinion (Kocigit, 2010). These values are used as the activity rate parameter of the fault segments in calculations performed by the EZ-FRISK (Risk Engineering, 2013) program.

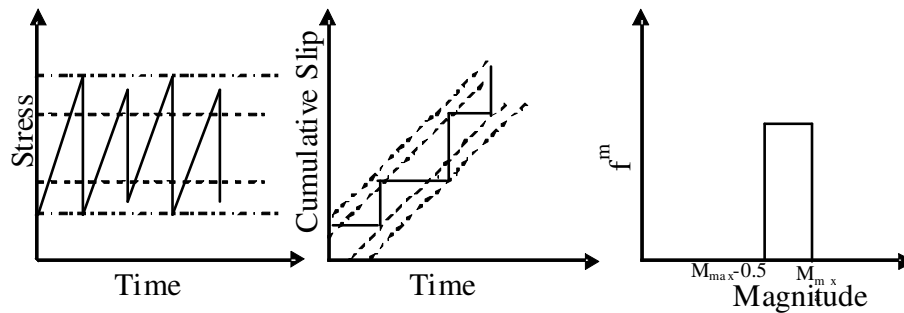


Figure 5.23. Full Characteristic Models Used in This Study

The calculation of the seismic hazard by using the full characteristic earthquake model is not a difficult task. The EZ-FRISK (Risk Engineering, 2013) software program provides an interface which all the related seismic source parameters are loaded to the program easily. The activity rates, lengths and the maximum magnitudes of earthquakes that can be generated by the fault segments are obtained from Tables 5.1 to 5.8. In addition, the depths of faults are assumed 20 km with vertical dipping angles. After gathering of the fault parameters, these parameters are loaded to the EZ-FRISK software to conduct the seismic hazard analysis. The overall tables of all faults with associated seismic parameters are provided in Appendices E and F.

5.5. Response Spectrum Curves and Hazard Maps Developed for the City of Eskisehir

The contributions of all the areas and fault sources are combined into a single seismic hazard for the city of Eskisehir. As an important output of seismic hazard analysis by EZ-FRISK, the annual exceedence rates of earthquake events for PGA and spectral periods of 0.2 and 1.0 s are presented in Figure 5.24. The curves represent the annual exceedence rate versus spectral acceleration values in terms of g . As the most important outcome of the analysis, in addition to the hazard curves,

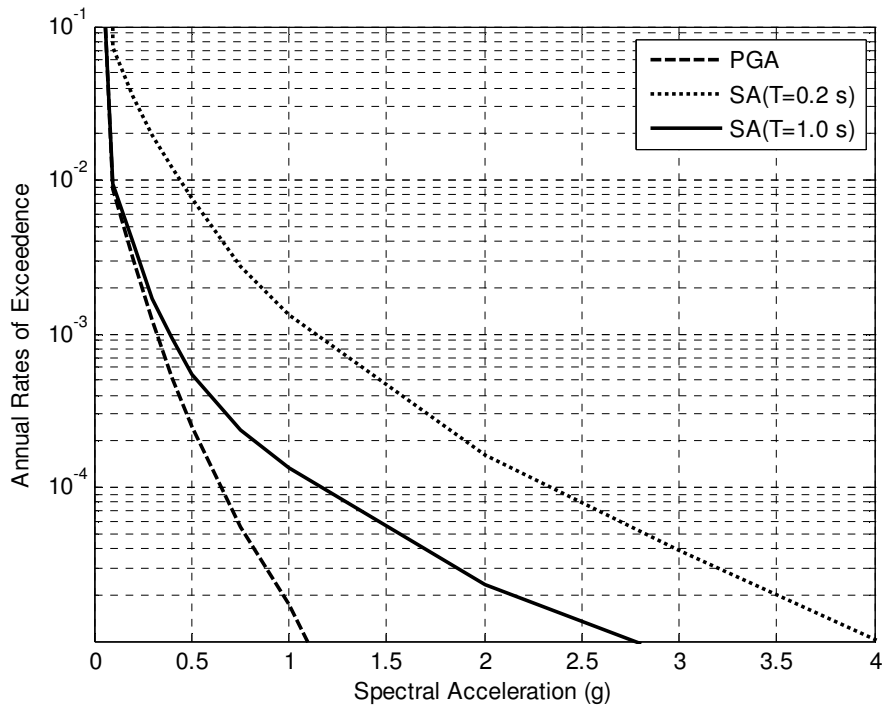


Figure 5.24. Annual Exceedance Rates of Earthquake Events for PGA, and Spectral Periods of 0.2 s and 1.0 s

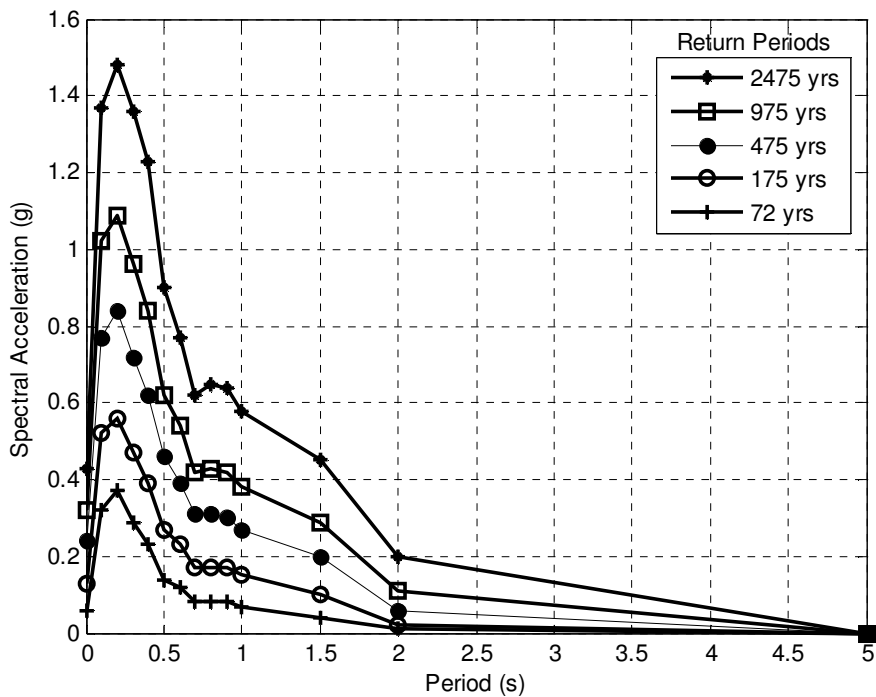


Figure 5.25. Elastic Response Spectrum Curve Developed for the City of Eskisehir (NEHRP B/C Boundary Site, Response at 5% Damping, GMPE of AC10 with Calibrated Coefficients Used)

the elastics response spectrum curves are developed for 5% damping coefficient for the city of Eskisehir as shown in Figure 5.25. The curves are developed for different

annual exceedence rate of earthquake occurrences in 50 years and the site condition is assumed as NEHRP B/C boundary site with $V_s=760$ m/s.

The hazard maps in Figures 5.26 and 5.27 are prepared for an earthquake with 475-year return period and for PGA and spectral period of 0.2 s, respectively. As GMPE AC10 with calibrated coefficients is employed with the site condition is accepted as NEHRP B/C boundary with $V_s=760$ m/s. The reason of selecting this boundary site class is that, the linear and nonlinear site effects can be ignored with the assigned site condition. Therefore, the resultant seismic hazard calculated by using this site class could be accepted as the reference hazard. Similarly official hazard map, which was produced by using the GMPE developed by Joyner and Boore (1981), was created by using a site class of rock, which the resultant hazard value could be used as reference to generate new hazard values upon the obtained ones. In other words, the site effects are accepted as zero in both GMPEs in the calculation of seismic hazard, which lead to creation of comparable seismic hazard maps.

As can be observed from the maps in Figure 5.26 and 5.27, a considerable level of earthquake hazard exists in the southwest and northwest of Eskisehir, where there is a high concentration of midsize earthquake activity. In both maps, to the southwest of Eskisehir, an important source of earthquake activity exists and it must be highlighted as the most critical seismic source for Eskisehir after nearby faults. The faults to the north of Eskisehir in NAFZ are able to generate earthquakes with large magnitudes and with greater return periods. This characteristic of the NAF is very well reflected in the hazard map.

The official seismic hazard map prepared by Gulkan et al. (1993) is presented in Figure 5.28 for comparison purposes. As expected, there are certain regions with similar hazard rates, such as the central section of NAF in the PGA map of this study and the region surrounding the NAF in the official map, should be both emphasized in the maps. To the southwest of Eskisehir, where a significant local earthquake activity exists, the calculated hazard rate is high and likewise, in the official map, the same region is within a larger region with the highest seismic hazard rate.

Eskisehir must be classified as a relatively quiet city with lower values of seismic hazard in the seismic hazard maps in Figure 5.26 and 5.27 and in the official map. The city is located in a wider region with the same PGA and spectral acceleration

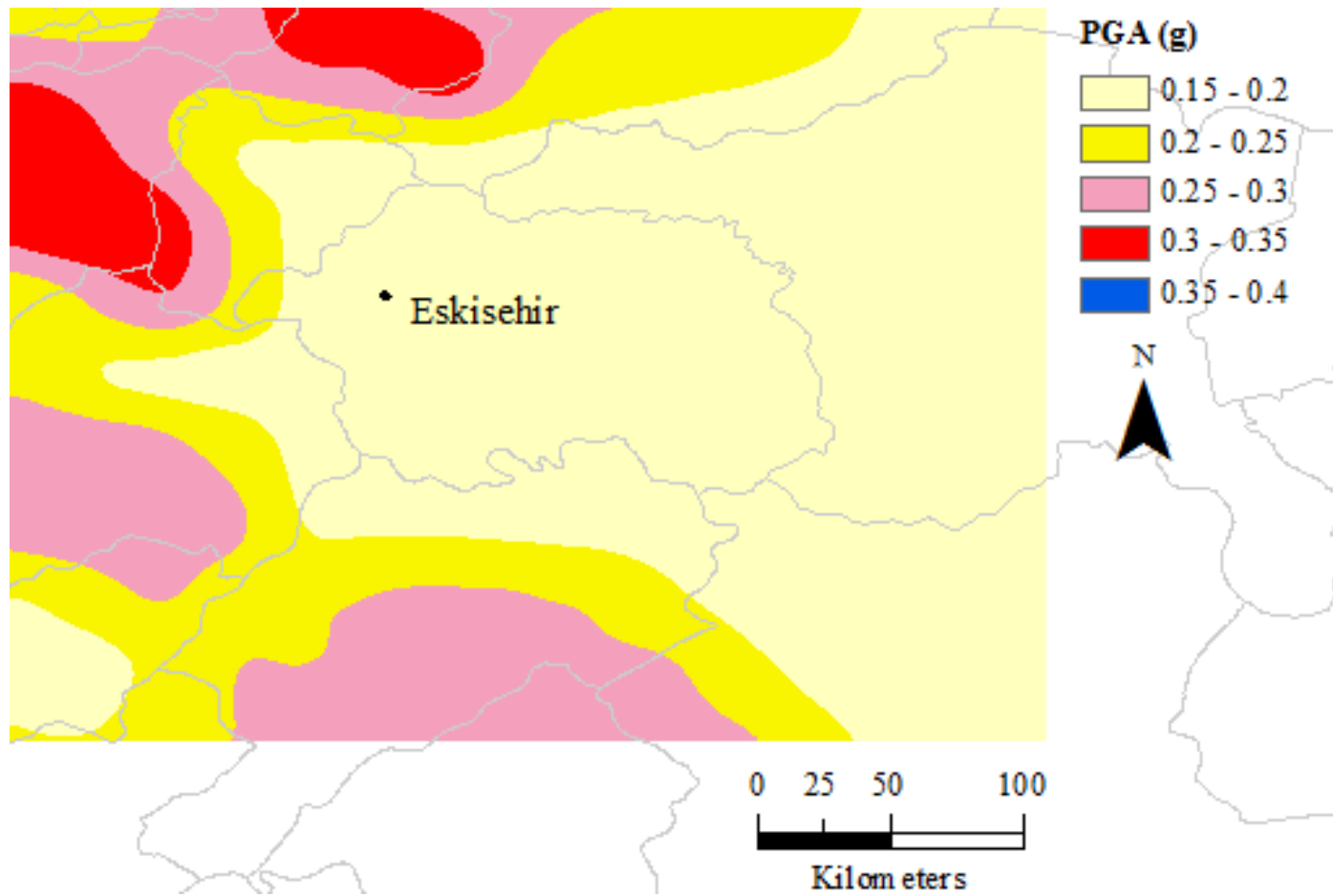


Figure 5.26. Seismic Hazard Map of Eskisehir and Surrounding Region for Earthquakes with 10% Annual Exceedance Rates in 50 Years (PGA, NEHRP B/C Boundary Site, $V_s=760$ m/s, as GMPE AC10 with Calibrated Coefficients is Employed)

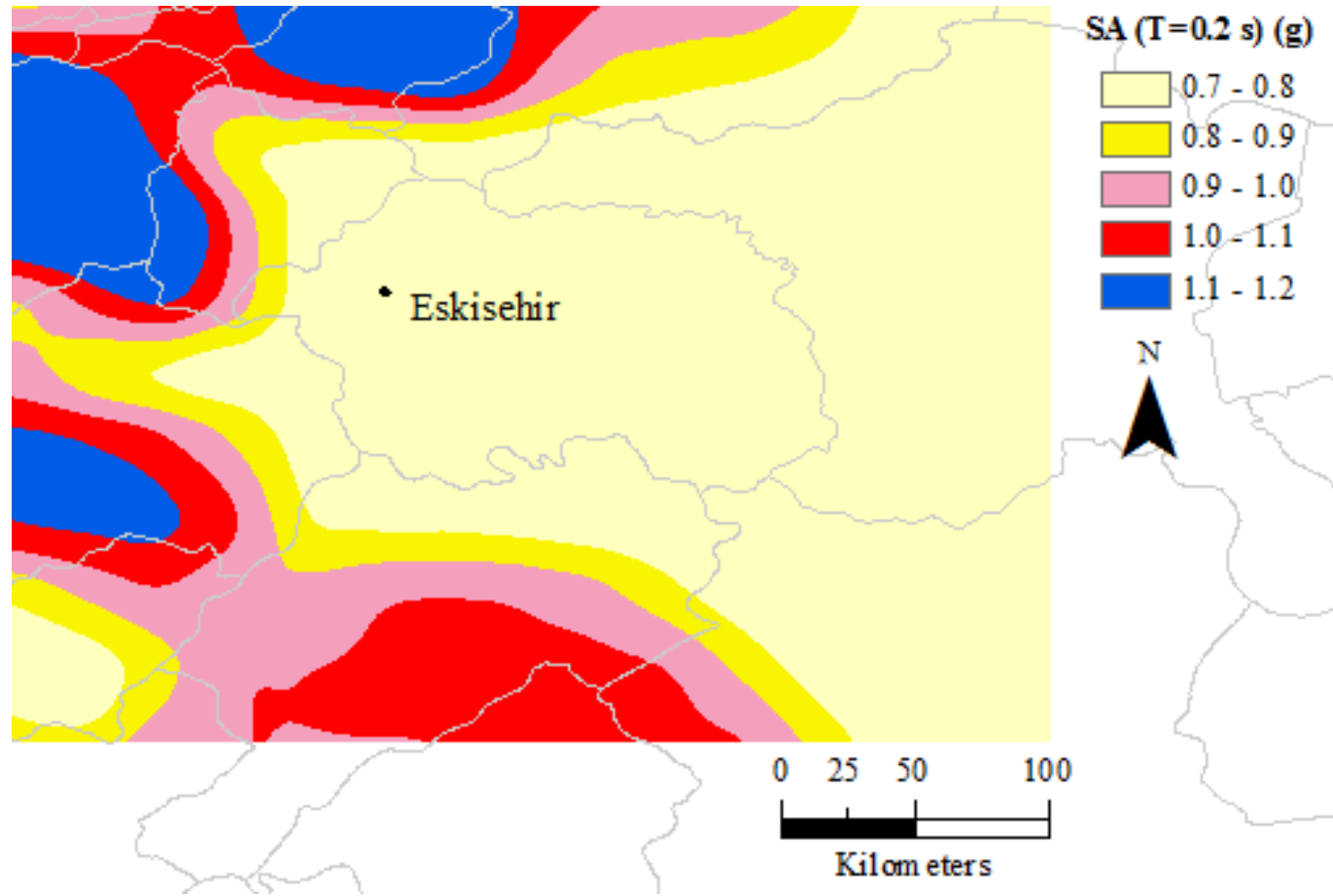


Figure 5.27. Seismic Hazard Map of Eskisehir and Surrounding Region for Earthquakes with 10% Annual Exceedance Rates in 50 Years (Spectral Acceleration Values at 0.2 s, NEHRP B/C Boundary Site, $V_s=760$ m/s, as GMPE AC10 with Calibrated Coefficients is Utilized)

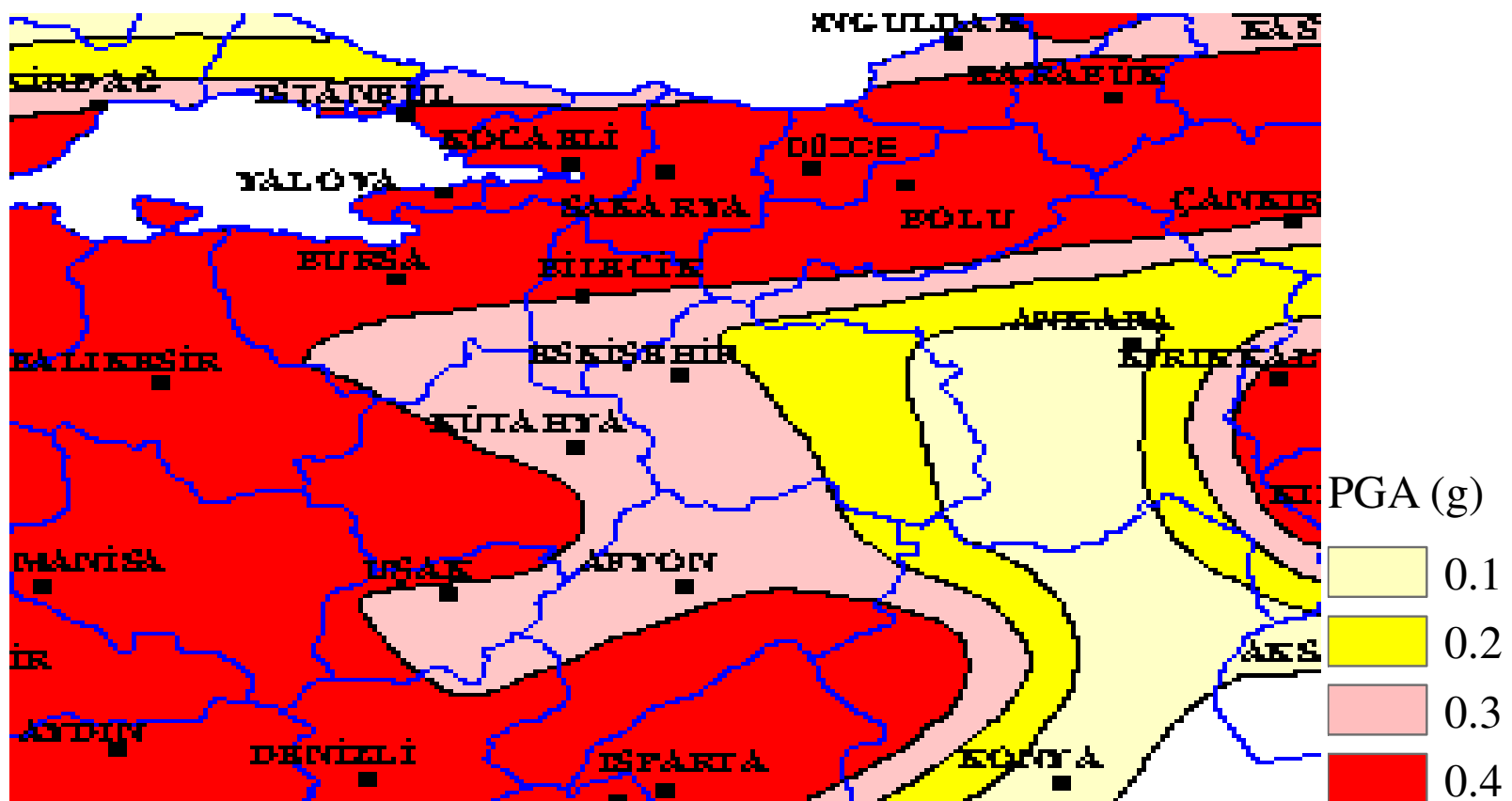


Figure 5.28. Official Hazard Map of Eskişehir and Surrounding Region for Earthquakes with 10% Annual Exceedance Rates in 50 Years (PGA, Site Class Rock According to GMPE of Joyner and Boore, 1981)

values at the spectral period of 0.2 s. In the official map, Eskisehir is located in zone II with the PGA value at 0.3g and in Figure 5.27; it is located in a region with PGA values ranging between 0.15g and 0.2g. Despite the low exposure levels of seismic hazard, it should be mentioned that, since the city itself is located in a transition area where the seismic activity in the vicinity could pose threat, the influence of the seismic activity in the surrounding region must be taken into account. Moreover, the differences in the seismic hazard maps obtained in this study and the official map is found to be acceptable since the official map reflects the country scale hazard while the seismic hazard maps obtained in this study are limited to the local scale. In other words, the area and fault sources considered in the official map is in larger scale compared to the smaller area and fault sources considered in the local seismic hazard analysis.

Considering the response spectrum curves in Figure 5.29, it must be mentioned that the response spectrum curve developed for the present study and the officially calculated curve are almost identical for the initial ramp and up to spectral period of 1.5 s, both curves follow a similar path. After spectral period of 1.5 s, the values of the official response spectrum curves become twice as much as the ones obtained by the PSHA in this study.

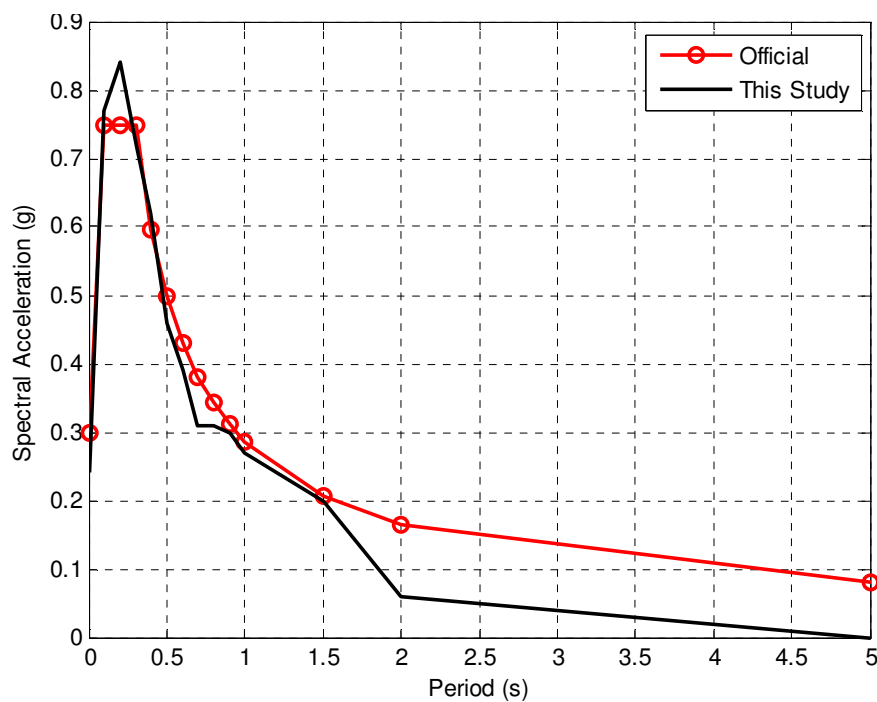


Figure 5.29. Response Spectrum Curve Developed for the City of Eskisehir

5.6. Spatially Smoothed Seismicity

In classical PSHA, the earthquake generating sources are classified as point, line or area sources and earthquakes that cannot be assigned to a source are evaluated in the background seismicity model, which indeed is an area source with uniform seismicity. The lack of detailed knowledge of seismicity in a region causes difficulties in the assignment of earthquakes to the area sources. Because of the fact that creating area sources is a highly subjective method, assumption of uniform seismicity in the entire area already raises concerns over the results of the analysis. On top of that, the limitation of the lack of data causes more concerns, and consequently, other methods are sought for a reliable seismic hazard analysis. In response to the problem stated above and to avoid the classical problems of the probabilistic seismic hazard method, the spatially smoothed seismicity model was developed. Instead of creating areal source zones with uniform seismicity based on subjective judgment, Frankel (1995) used the spatially smoothed seismicity procedure. However, it should be mentioned that, it is accepted as an appropriate procedure to apply for places where there is not enough seismic data.

The spatially smoothed seismicity model claims that, the epicenters of future earthquakes would be in the close vicinity of epicenters of past earthquakes. The future epicenters of the earthquakes are spatially distributed to the grids of locations centered at the epicenter of the past events by using a Gaussian function with a correlation distance c . In the model, the cumulative number of earthquakes, n_i with a magnitude greater than minimum magnitude is counted and the obtained values are converted to incremental values in terms of moment magnitude. These values are spatially smoothed by multiplying them with a Gaussian function with the equation

$$n_i = \frac{\sum_j n_j(m_0) e^{-\left(\frac{\Delta_{ij}}{c}\right)^2}}{\sum_j e^{-\left(\frac{\Delta_{ij}}{c}\right)^2}} \quad (5.2)$$

where c is the correlation distance and Δ_{ij} is the distance between i^{th} and j^{th} cells. In each grid cell i , the seismic activity rate $n_i(m_0)$ is counted from the earthquake catalog. The radius of smoothing equals to $3c$.

Obtaining the \bar{n}_i values quantifies the spatial uncertainty in the future earthquake locations without using line or area sources. To complete a probabilistic seismic hazard calculation, the other elements of the uncertainties must be addressed, and the expected annual rate of exceedence of ground motion level u_0 at a site is calculated using

$$\lambda(y > y_0) = \sum_i n_i(m_{\min}) \int_{m_{\min}}^{m_u} \int_r P[y > y_0 | m, r] p_i(m) p_i(r) dr dm \quad (5.3)$$

where $n_i(m_{\min})$ is the smoothed annual activity rate above minimum magnitude $m_{\min} > m_0$ in a seismic source i . $P[y > y_0 | m, r]$ is the conditional probability that an earthquake of magnitude m at a distance r from the site produces a ground motion level y greater than y_0 . $p_i(m)$ is the probability density function of magnitude within source i , and $p_i(r)$ is the probability density function of distance between the point of source i and the site.

In Frankel (1995), the $n_i(m)$ values are grouped by their distance and magnitude and incremental values of $n_i(m)$ are created, such as the number of events from m_{ref} to $m_{ref} + \Delta m$ and the total of $n_i(m)$ for cells within certain distance increment, r_k , from the site. The annual rate $P[y > y_0 | m, r]$ of exceeding the ground motion level y_0 at a specific site is determined by the following summation.

$$P[y > y_0] = \sum_k \sum_l 10^{\log(n_k / T) - b(m_l - m_{ref})} P[y > y_0 | m_l, r_k] \quad (5.4)$$

where k is the index for distance increment, while l represents the magnitude increment, and T is the time span of the earthquake events. The b value obtained from GR equation is accepted as the same for the whole area of interest.

The probability of exceeding a specified ground motion level, y_0 is calculated by integrating

$$P[y > y_0 | m, r] = \frac{1}{\sqrt{2\pi}\sigma_{\ln y}} \int_{\ln y_0}^{\infty} \exp\left[-\frac{1}{2}\left(\frac{\ln(y) - \ln y(m, r)}{\sigma_{\ln y}}\right)^2\right] d \ln y \quad (5.5)$$

which is actually the cumulative distribution function of a selected ground motion parameter, represented as in the following equation.

$$P[y > y_0 | m, r] = \frac{1}{2} \Phi^* \left(\frac{\ln y_0 - \ln y(m, r)}{\sigma_{\ln y} \sqrt{2}} \right) \quad (5.6)$$

The term $\ln y(m, r)$ represents the GMPE model, and for each ground motion level assumed at certain values, y_0 , the probability in the equation must be calculated. The probability density functions of moment magnitude and distance are quantified by introducing the distance and magnitude increments after dividing the region into small grids and forming the cells.

5.6.1. Data Preparation

For the spatially smoothed seismicity analysis, the available raw data obtained from the catalog assembled for this study are evaluated without any concerns of completeness. Since the completeness procedures cannot provide the necessary data for the spatial density of the incomplete periods for the incomplete magnitude ranges, only the complete parts of the catalogs are considered. Therefore, the catalog data is partitioned into two as presented in Table 5.16, which are named as model I and model II. In model I, the seismic data covering the period of 1900-1969 has 95 records with magnitude above or equal to 5.0, and in model II, the seismic data covering the period of 1970-2010 has 432 records with magnitude above or equal to 4.0. The b values in GR relationship are calculated as 1.38 for model I and 1.25 for model II respectively.

Table 5.16. Models Created for the Spatially Smoothed Analysis

Models	Period	Magnitude Range	b-Values
Model I	1900-1969	$M_w \geq 5.0$	1.38
Model II	1970-2010	$M_w \geq 4.0$	1.25

Faults included in the analysis are selected as the ruptured parts of the NAF during the Izmit, 1999 and Duzce, 1999 earthquakes. These ruptured portions are the closest sections of the NAF to Eskisehir, as can be seen in Figure 5.30. An evaluation of the proximity of the faults and the influence of a large magnitude earthquake at certain distance is also investigated while choosing the fault sources. The pure characteristic

model is applied as the maximum magnitude of $M_w=7.4$ and 7.2 is assigned to the Izmit rupture and Duzce ruptures respectively.

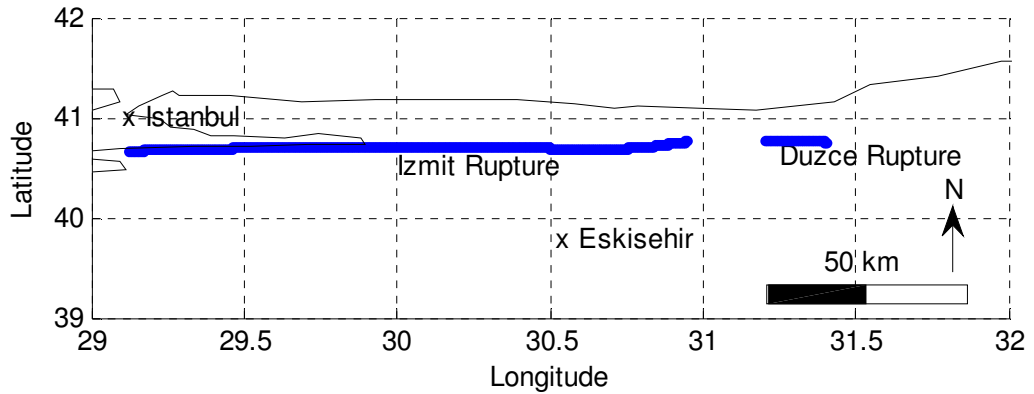


Figure 5.30. Faults Sources Used in the Spatially Smoothed Seismicity Model (Lettis et al. 2002 and Duman et al., 2005)

The return intervals are obtained through personal communication with Kocyyigit (2010). Consecutively, the activity rates are calculated by using the return intervals of the earthquakes. After gathering the necessary fault parameters, then, the probability of occurrence of at least a single event in 475 years is calculated by using the Poisson model.

Table 5.17. Fault Segments and Their Parameters Used for the Spatially Smoothed Analysis

Segment Name	Length (km)	Depth (km)	Characteristic Earthquake Magnitude (M_w)	Return Interval (year)*	Activity Rate
Izmit	130.0	20	7.4	250	0.004
Duzce	14.5	20	7.2	250	0.004

*The return intervals are assumed after personal communication with Kocyyigit (2010)

For the GMPE, the equation developed by Akkar and Cagnan (2010) is utilized with the calibrated coefficients. The performance of the equation is displayed in Figure 3.29 for earthquakes of size $M_w=7.0$ and $M_w=6.0$ for NEHRP B/C, C and D site conditions. The effect of the distance and magnitude on the ground motion decay is also provided in the trellis plots in Section 3.5.1.

5.6.2. Analysis

In spatially smoothed seismicity analysis, the earthquake occurrence is assumed to follow Poisson distribution.

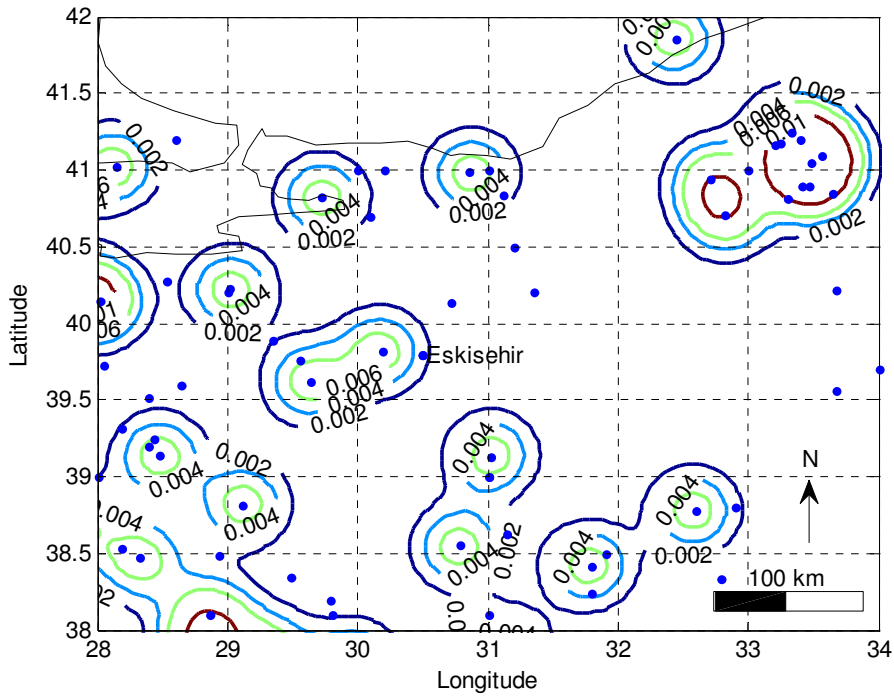


Figure 5.31. Spatial Density $n_i(m_{min})$ of Earthquakes for the Considered Region for Model I

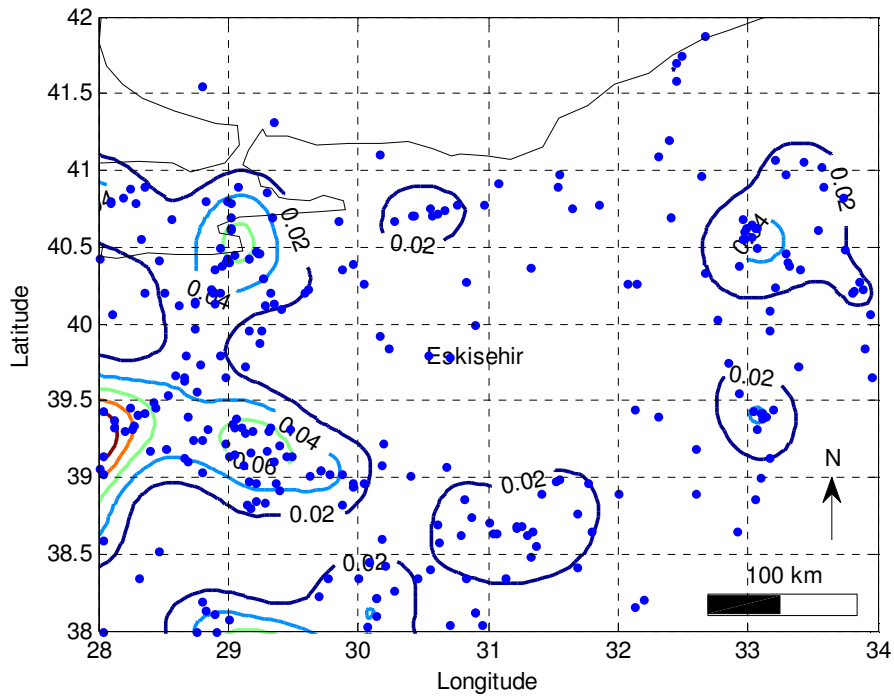


Figure 5.32. Spatial Density $n_i(m_{min})$ of Earthquakes for the Considered Region for Model II

In order to find the desired level of ground motion with certain probability, the ground motion values are interpolated. For example to find the level of ground motion with 10% probability of exceedence in 50 years, the annual probability of

exceedence is calculated as 0.0021 and the calculated ground motion value for that probability is found by interpolation.

Initially, the spatial distribution of the earthquakes is determined with the grid cells set at 0.04° in latitudes and 0.05° longitudes, which corresponds to 4.3 km in both directions for the area covered in this thesis study. The correlation distance is set as 28.7 km, a value selected to justify the existing pattern of occurrences around Eskisehir, where the span of a cluster is usually more than 100 km in diameter. Since larger correlation distances causes the loss of pattern of seismicity by assigning whereas smaller correlation distances concentrates the seismicity to smaller clusters (Frankel, 1995), an average value of 28.7 km is selected to reflect the seismic pattern of the region.

In Figures 5.31 and 5.32, the values of $n_i(m_{\min})$ or spatial distribution of the number of earthquakes or spatial density for each grid cell is shown as contours for northwestern Turkey. These values are also used as the maximum likelihood estimate for the 10^a values of Gutenberg-Richter relationship (Weichert, 1980).

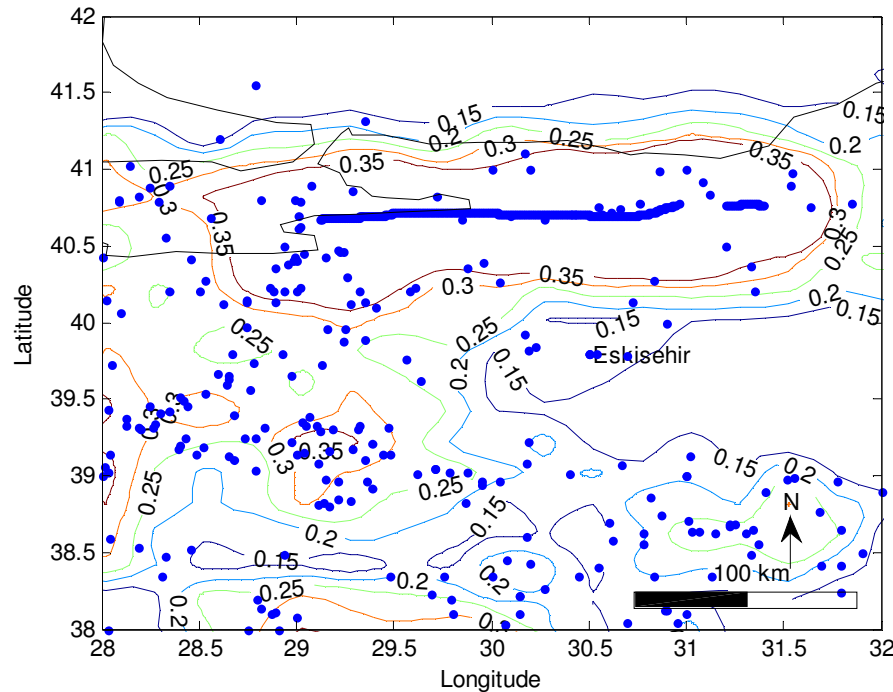


Figure 5.33. Seismic Hazard Map Developed for 10% Probability of Exceedance in 50 years for PGA Values (Values are in g, NEHRP B/C Boundary Site)

The map of peak ground acceleration and spectral acceleration at the spectral period of 0.20 s for 10% of exceedence probability in 50 years with 475 years of return

period are shown in Figures 5.33 and 5.34 respectively. The maps are a combination of seismic hazard obtained by using the weights 0.5 for model I and II and adding the hazard from the faults to the combination. The highest PGA values are observed around the North Anatolian Fault due to the magnitude and the frequency of the characteristic earthquake that occurs in the region. The fault ruptures of the 1999 Izmit earthquake and 1999 Duzce earthquakes were taken as the potential sources of earthquake generation.

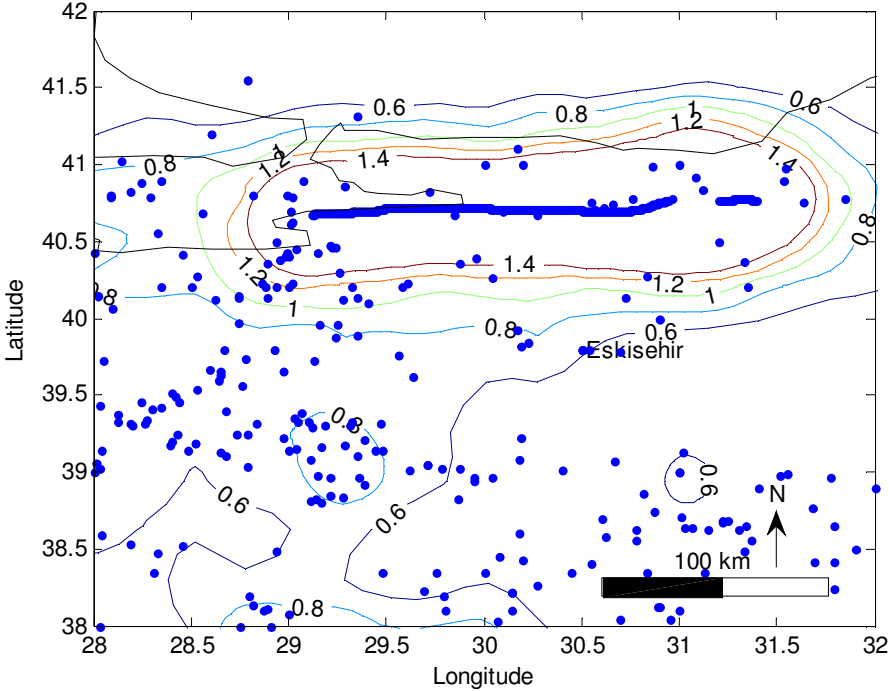


Figure 5.34. Seismic Hazard Map Developed for 10% Probability of Exceedance in 50 years for Spectral Period of 0.2 s (Values are in g, NEHRP B/C Boundary Site)

The reason why these two faults are selected is their proximity and high activity rates. As shown in the figure, the highest concentration of earthquake hazard is observed around the NAF. Moreover, it is clearly observed that Eskisehir is located in a transition region where the seismic hazard increases from southeast to the northwest.

Comparing to the official PGA map and the seismic hazard map obtained by using EZ-FRISK v7.62 (Risk Engineering, 2013) for PGA, the spatially smoothed seismicity model yielded lesser hazard rates than the official map while similar hazard rates are observed with the seismic hazard map developed by using the program.

CHAPTER 6

6. CASE STUDY: VULNERABILITY OF SELECTED BUILDINGS IN ESKISEHIR

6.1. Introduction

In the previous chapter, the exposed levels of seismic hazard are investigated for Eskisehir and the elastic response spectrum curves are developed for earthquakes with different return periods. In addition to elastic response spectrum curves, probabilistic seismic hazard maps are generated. After completion of the seismic hazard component, for the loss estimation, the seismic risk needs to be calculated by using the elastic response spectrum curves developed in Chapter 5. On the other hand, determination of seismic risk requires the determination of the lateral performances and associated damages attained at these performances.

In this chapter, a lateral performance study will be performed. As the aim of the study is to develop a quick, easy-to-use and reliable method, a lateral performance prediction equation (LPPE) will be developed by using the proposed structural parameters, which indeed are very easy to obtain by simple calculations.

Mainly, this section consists of the results of the sensitivity analysis that is conducted to investigate the scaling of lateral performance with the proposed structural parameters, the development of the LPPE by utilizing various lateral performance estimation methods and the verification of LPPE by using the nonlinear time history analysis. The database will be assessed with respect to the proposed structural parameters and important structural characteristics of fundamental period, ductility, ratio of post elastic stiffness to elastic stiffness and height. The emerging patterns of lateral performances will be sought for each elastic response spectrum curve. Then, LPPE will be developed by using a two fold cross validation scheme. Lastly, nonlinear time history analysis will be conducted by using some of the records that were employed for the application of adaptation procedure to selected GMPEs in Chapter 3. Nonlinear time history analysis will be used in order to verify whether there exist a relationship between the lateral performances and proposed structural parameters.

6.2. Buildings Modeled for the Analysis

Initially, a database, which consists of several reinforced concrete structures that are arbitrarily selected from the city of Eskisehir, is gathered.

Table 6.1. Structural Properties of All the Buildings

Building Code	Plot/Parcel No	No of Storeys	Material Strength (MPa)	Design Year	Structural System
B01	(2001)-4	4	C25/S420	2001	BF+SW
B02	(2010)-4	4	C25/S420	2010	BF
B03	10025/1	6	C25/S420	2005	BF
B04	1034/557	6	C25/S420	2008	BF
B05	1077/201	6	C14/S220	1995	BF
B06	1358/5	5	C25/S420	1993	BF
B07	1415/4	5	C25/S420	2006	BF+SW
B08	1519/18	6	C25/S420	2008	BF+SW
B09	152/1	8	C16/S420	1995	BF+SW
B10	205/3	6	C30/S420	2004	BF+SW
B11	2067/107	5	C25/S420	2007	BF+SW
B12	2069/229	7	C25/S420	-***	BF
B13	2073/172	8	C25/S420	2010	BF+SW
B14	2133/218	5	C25/S420/	1996	BF
B15	2571/14	4	C20/S420	2000	BF
B16	2927/1	6	C20/S420	1997	BF+SW
B17	2928/4	5	C25/S420	2008	BF+SW
B18	376/34	6	C25/S420	2004	BF+SW
B19	490/35	5	C25/S420	2007	BF+SW
B20	496/14	5	C16/S420	1996	BF
B21	5541/8	5	C25/S420	2008	BF+SW
B22	557/11	5	C25/S420**	1975	BF
B23	6041/9	5	C20/S420	1994	BF
B24	632/8	5	C20/S420	1980	BF
B25	7768/3	6	C25/S420	2007	BF+SW
B26	876/515	5	C20/S420	2002	BF+SW
B27	890/25	4	C25/S420	2006	BF
B28	(1993)-6	6	C20/S420	1993	BF+SW*
B29	1068/63	7	C25/S420	2010	BF+SW
B30	1547/197	5	C25/S420	2008	BF+SW
B31	2765/3	4	C25/S420	-***	BF+SW
B32	918/12	4	C16/S420	1997	BF
B33	9886/13	5	C25/S420	2006	BF+SW
B34	9918/4	5	C20/S420	2003	BF
B35	(863)-4	6	C20/S420	1993	BF
B36	(944)-4	4	C20/S420	1990	BF
B37	10365/1	5	C25/S420	2007	BF+SW

*BF+SW abbreviation of Bare Frame + Shear Wall

** The assumed material strength due to missing information

*** Missing information

In the selection process, a few restrictions are imposed such as the number of storeys is limited between 4 and 8 storeys, and the vertical uniformity of the storeys are mostly satisfied. Moreover, only moment resisting frame and shear walled frame structures are considered. The flat slab structures, precast or pre-stressed structures, and cellular reinforced structures are all excluded from the sample. Subsequently, only structures with 4 to 8 storeys are gathered, which infact represents a very large portion of the built structures in Eskisehir and in Turkey.

A total of 37 structures are gathered for the development of the LPPE. These structures are arbitrarily chosen to avoid any bias that could arise due to similarities between certain structural parameters. The height, weight, material strength, design year, and type of structural systems are given in Table 6.1.

6.2.2. Modeling Assumptions

As mentioned, all the structures are modeled in three dimensions by using SAP2000 program (Computers and Structures 2011). In the modeling of the structures, conventional beam-column frame modeling assumptions are used. Primary and secondary structural elements are identified, and secondary structural elements such as infill walls are excluded from the models. Primary structural elements of beams, columns, shear walls, and slabs are modeled as line and area elements.

Plastic hinges are assigned to the member ends to model the flexural response in beams and to model the biaxial flexural response under axial loads in columns. Most shear walls are designed to resist high shears and designed to fail first in flexural mode to avoid the undesired consequences in an earthquake, so after necessary checks it is decided that it is reasonable to model these walls only with biaxial flexural hinges. The slabs are modeled as diaphragms that transfer axial loads between the adjacent frames. The interaction of the neighboring frames is allowed with this model, but the in plane and out-of-plane bending is restricted.

The same vertical loads are assigned to all the structures to reduce the variance in lateral performance that could be caused by the different vertical loads. Dead and live loads are assumed as 300 and 200 kg/m², respectively. A wall load of 1050 kg/m is assigned to each beam element. Due to the importance of the hinges in shaping the lateral response of a structure, a thorough explanation is required. The modeling of shear walls is also complicated enough to deserve detailed investigation.

Thus, the following sections present the important issues in hinge and shear wall modeling.

6.2.2.1. Modeling of Hinges

The deformation capacity of the structure is dependent on the nonlinear capacities of its members. Therefore, to monitor the extent of lateral displacement in the structure, the nonlinear properties must be carefully modeled. However, the amount of work to model hinges for each member of a structure is not feasible for most of the cases. Consequently, a modeling simplification is required to include the nonlinearity for each member. Indeed, ATC-40 (1996) and FEMA-273 (1997) already provide characteristic plastic hinges derived by averaging the nonlinear responses of several different types of sections and reinforcement configurations for reinforced concrete members. These hinge models with default characteristics are already built-in in SAP2000 (Computers and Structures, 2011). So, in the analysis, the default force-displacement characteristics of plastic hinges that are based on ATC-40 (1996) and FEMA-273 (1997) criteria are utilized to perform pushover analyses.

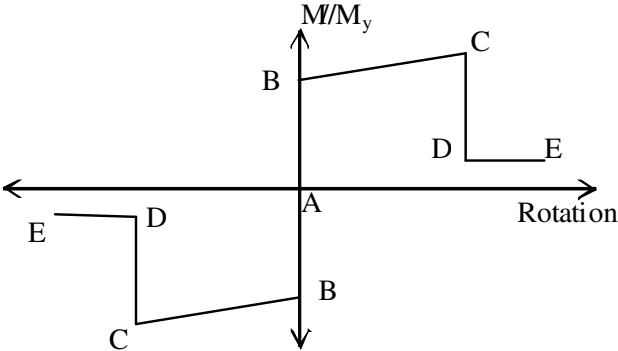


Figure 6.1. Moment/Yield Moment-Rotation Relationships for Plastic Hinges

The beam-end and column-end hinges are located at the member ends since the end moments are assumed as the largest and joints are assumed as the locations where the plastic hinges form. In the structural models, hinges with uncoupled moment force-displacement curves are assigned to the beams and hinges with force-displacement curves based on interaction of axial loads and moments are assigned to the columns. The default and user defined values are assigned to investigate the scaling of lateral performance with the moment-rotation relationship of the hinges. The applied moment-rotation relationship for the hinges is shown in Figure 6.1. The default and

user-defined values of each point in the figure are given in Table 6.2, for the uncoupled moment hinges for beams and biaxial hinges for columns.

Table 6.2. Moment-Rotation Relationships of Default and User Defined Concrete Moment and Biaxial Hinges

Point	Moment/Yield Moment (M/M _y)	Beams (Default)	Beams (User Defined)	Columns (Default)	Columns (User Defined)
		Rotation (radians)			
E-	-0.2	-0.050	-0.040	-0.025	-0.040
D-	-0.2	-0.025	-0.037	-0.015	-0.027
C-	-1.1	-0.025	-0.037	-0.015	-0.027
B-	-1.0	0.000	0.000	0.000	0.000
A	0.0	0.000	0.000	0.000	0.000
B	1.0	0.000	0.000	0.000	0.000
C	1.1	0.025	0.037	0.015	0.027
D	0.2	0.025	0.037	0.015	0.027
E	0.2	0.050	0.040	0.025	0.040

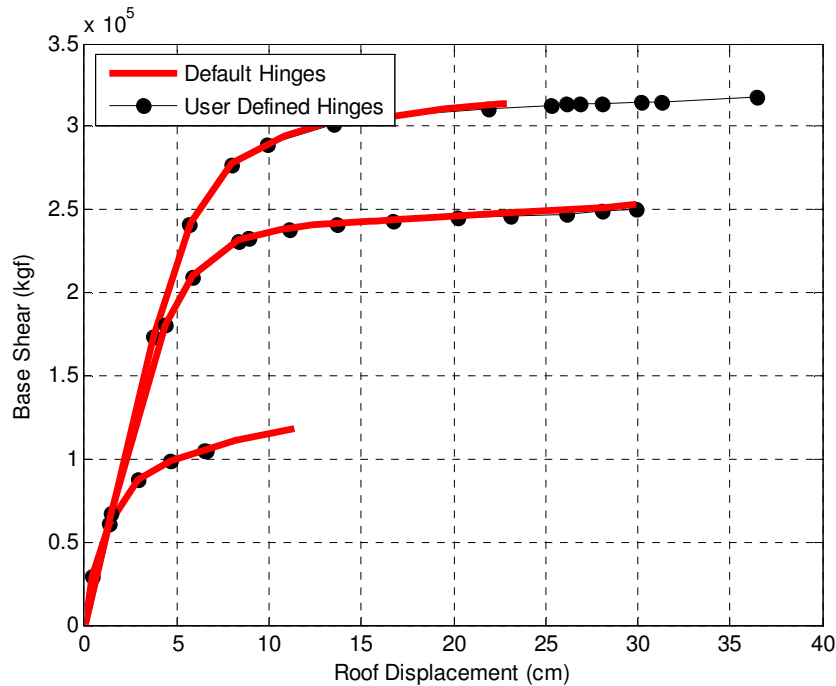


Figure 6.2. Pushover Curves for Structures with Default and User Defined Hinges in X-Direction (B01, B17 and B28 in Table 6.1)

For this purpose, hinges with the default and user-defined moment-rotation relationships are modeled for reinforced concrete columns and beams of the three arbitrarily selected structures. The selected structures, which are labeled as B01, B17, and B28 in Table 6.1, are analyzed in one direction, and the pushover curves are

obtained for both types of hinges as shown in Figure 6.2. The analysis showed that the hinge properties are not a determining factor in the performance levels of structures except that the maximum lateral drift seems to be susceptible to the type of the hinge. When considering the scaling of the lateral performance, it can be safely concluded that as long as the type of hinge is the same, the moment-rotation relationship of a hinge does not influence the lateral performance values and therefore it will not be considered as a structural parameter in the proposed LPPE.

6.2.2.2. Shear Wall Modeling

Shear walls are classified according to the ratio of the wider side to the narrower side. TEC-2007 set this ratio to seven; therefore, any vertical structural element with this ratio greater than seven is classified as a shear wall. These walls are modeled as mid-pier columns, and two rigid beams connected to the neighboring beams as shown in Figure 6.3. The mid-pier element has the same rigidity of the shear wall while the two connecting rigid beams have large enough rigidity to transfer the loads in axial direction without bending. A very important feature that influences the shear wall behavior under lateral loading is the aspect ratio, which is defined as the height to length ratio of the shear wall. Considering the aspect ratios, there are three categories of shear walls, which are listed in Table 6.3.

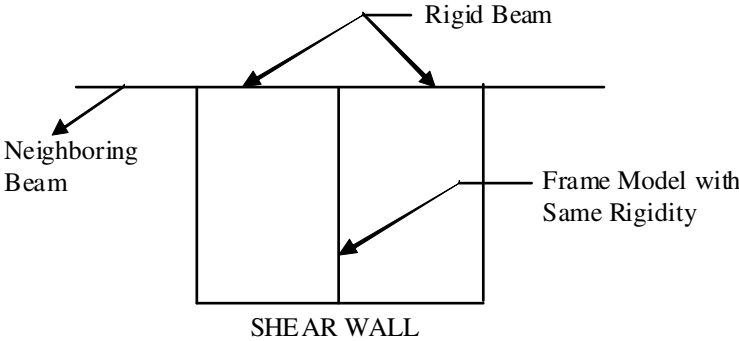


Figure 6.3. Frame Model for Shear Walls

In the first category, the shear walls are tall and slender with dominant failure mode of flexure. The second category shear walls have aspect ratios varying between 1.5 to 3 and these shear walls fail consecutively in flexure and then in shear. Short and wide walls form the third category with a dominant shear type of failure. A pre-evaluation is conducted to classify the gathered structures according to the aspect

ratios of their shear walls. According to the findings of the preevaluation, all the shear walls are classified as category II in terms of the maximum aspect ratios, which imply that the shear walls are vulnerable to flexural failure before the shear failure. Consequently, considering the aspect ratios and the observed performances of the shear walls of Turkish buildings, only axial, biaxial moment (PMM) hinges are assigned.

Table 6.3. Categories of Shear Walls According to Their Aspect Ratios

Category	Aspect Ratio*	Type of Failure	Definition
I	$a_R > 3$	Purely flexure	Tall and slender
II	$1.5 < a_R < 3$	First flexure then shear	Normal
III	$a_R < 1.5$	Purely shear	Short and wide

a_R : Aspect ratio

6.2.3. Application of Modal Mass Participation Ratio Criterion

An important criterion for the successful utilization of the pushover analysis is the modal mass participation ratios of the dominant modes of the structures. Therefore, a modal analysis is performed by using SAP2000 to obtain the modal mass participation ratios (Computers and Structures, 2010), which are summarized in Table 6.4.

Table 6.4. Modal Properties of Buildings for Analysis

Building Code	Plot/ Parcel No	X-Direction		Y-Direction	
		Period (s)	Modal Mass Participation Factor (%)	Period (s)	Modal Mass Participation Factor (%)
B01	(2001)-4	0.38	0.42	0.27	0.70
B02	(2010)-4	0.44	0.69	0.45	0.81
B03	10025/1	0.54	0.70	0.57	0.66
B04	1034/557	0.44	0.67	0.49	0.66
B05	1077/201	0.53	0.81	0.71	0.77
B06	1358/5	0.40	0.73	0.51	0.78
B07	1415/4	0.32	0.69	0.38	0.75
B08	1519/18	0.66	0.53	0.49	0.74
B09	152/1	0.58	0.64	0.61	0.77
B10	205/3	0.84	0.63	1.05	0.73
B11	2067/107	0.35	0.68	0.39	0.69
B12	2069/229	0.65	0.79	0.73	0.82
B13	2073/172	0.64	0.66	1.02	0.55
B14	2133/218	0.53	0.70	0.48	0.64
B15	2571/24	0.58	0.61	0.54	0.78
B16	2927/1	0.90	0.83	1.40	0.63

Table 6.4 Continued

Building Code	Plot/ Parcel No	X-Direction		Y-Direction	
		Period (s)	Modal Mass Participation Factor (%)	Period (s)	Modal Mass Participation Factor (%)
B17	2928/4	0.49	0.78	0.53	0.49
B18	376/34	0.52	0.76	0.49	0.45
B19	490/35	0.43	0.72	0.61	0.78
B20	496/14	0.50	0.72	0.69	0.77
B21	5541/8	1.02	0.60	1.87	0.80
B22	557/11	0.59	0.62	0.56	0.75
B23	6041/9	0.29	0.47	0.41	0.86
B24	632/8	0.69	0.81	0.75	0.60
B25	7768/3	0.88	0.64	0.82	0.81
B26	876/515	0.55	0.78	1.16	0.82
B27	890/25	0.31	0.41	0.44	0.79
B28	(1993)-6	0.63	0.77	0.58	0.77
B29	1068/63	0.72	0.75	0.84	0.42
B30	1547/197	1.95	0.77	1.75	0.68
B31	2765/3	0.24	0.66	0.24	0.44
B32	918/12	0.35	0.75	0.39	0.76
B33	9886/13	0.39	0.74	0.32	0.72
B34	9918/3	1.91	0.86	1.43	0.76
B35	(863)-6	0.46	0.53	0.63	0.77
B36	_(944)-4	0.39	0.76	0.60	0.78
B37	10365/1	0.40	0.78	0.29	0.80

As can be followed from Table 6.4, almost all of the structures satisfy the basic prerequisite of minimum modal mass participation ratio of 60% in both directions, whereas only a small number of the structures satisfy the requirement only in one direction. In total, out of 74 possible models, 62 different structural models comply with the modal mass participation ratio criterion.

6.2.4. Basic Structural Properties

A number of structural parameters are claimed to be the key factors influencing the lateral performance and therefore the overall damage. Considering the compiled database, the utilization of these parameters, namely lateral strength and stiffness indexes, soft storey index and the number of storeys, require a pre-assessment of whether these structural parameters are suitable for the purpose of this study. Therefore, the database is examined for the ranges of the structural parameters and for other main structural indicators such as fundamental periods and total height. Table 6.5 provides all the structural indicators necessary for the evaluation of the

Table 6.5. Structural Properties of Buildings

Bldg. Code	Shear Structure *	Number of Storeys	Height (m)	Weight (t)	Floor Area (m ²)	Floor Column Area (m ²)	ΣI_y (m ⁴)	ΣI_x (m ⁴)	Lateral Strength Index (x10 ⁻²)	Lateral Stiffness Index-y (x10 ⁻⁴ m ²)	Lateral Stiffness Index-x (x10 ⁻⁴ m ²)	ssi	Material Strength (MPa)	X-dir. Period (s)	Y-dir. Period (s)
B01	Yes	4	11.68	325.50	109.90	3.45	0.65	0.53	3.14	59.34	48.25	1.00	25	0.38	0.27
B02	No	4	11.40	253.24	100.86	1.78	0.03	0.03	1.76	3.12	2.56	1.00	25	0.44	0.45
B03	No	6	17.52	917.17	229.44	7.17	0.38	0.37	3.12	16.67	15.93	1.00	25	0.54	0.57
B04	Yes	6	18.00	725.89	135.19	4.85	0.37	0.51	3.59	27.26	37.42	1.00	25	0.44	0.49
B05	No	6	17.10	1391.40	390.98	5.75	0.03	0.12	1.47	0.77	3.06	1.00	14	0.53	0.71
B06	No	5	14.00	323.93	96.04	2.23	0.03	0.07	2.32	2.72	7.10	1.00	25	0.40	0.51
B07	Yes	5	14.75	584.43	154.84	4.75	0.37	0.59	3.07	23.71	38.10	1.00	25	0.32	0.38
B08	Yes	6	18.00	878.79	195.13	4.70	0.56	0.21	2.40	28.36	10.56	1.00	25	0.66	0.49
B09	Yes	8	22.40	2814.25	657.45	15.11	0.62	0.78	2.30	9.38	11.80	1.00	16	0.58	0.61
B10	Yes	6	18.80	610.58	143.08	3.72	0.28	0.32	2.73	20.24	23.37	0.88	30	0.84	1.05
B11	Yes	5	14.60	569.58	155.63	5.06	0.45	0.54	3.25	28.82	34.88	1.00	25	0.35	0.39
B12	No	7	19.60	1890.47	476.97	5.62	0.08	0.21	1.18	1.74	4.47	1.00	25	0.65	0.73
B13	Yes	8	22.70	1014.23	178.00	3.85	0.58	0.61	2.70	40.86	42.71	0.94	25	0.64	1.02
B14	No	5	14.00	246.91	76.72	1.64	0.02	0.02	2.13	3.14	2.47	1.00	25	0.53	0.48
B15	No	4	12.36	402.46	172.14	2.56	0.05	0.04	1.49	2.66	2.14	0.81	20	0.58	0.54
B16	Yes	6	18.70	1114.7	262.23	8.57	0.18	1.10	3.27	6.91	42.07	1.23	20	0.90	1.40
B17	Yes	5	14.50	547.14	186.15	4.03	0.29	0.13	2.16	15.55	6.96	1.00	25	0.49	0.53
B18	Yes	8	22.35	1080.95	217.77	5.93	0.75	0.59	2.80	35.44	27.98	0.98	25	0.52	0.49
B19	Yes	5	14.75	307.52	66.33	2.45	0.05	0.16	3.69	7.37	24.59	1.00	25	0.43	0.61
B20	No	5	14.90	622.84	171.91	2.48	0.02	0.05	1.50	0.94	3.11	0.67	16	0.50	0.69
B21	Yes	5	14.96	498.41	148.65	4.08	0.05	0.78	2.74	3.12	52.23	0.72	25	1.02	1.87
B22	No	5	14.00	237.94	70.00	1.10	0.01	0.01	1.57	1.51	1.47	0.83	16	0.59	0.56
B23	No	5	13.88	322.73	100.70	2.05	0.02	0.04	2.04	1.82	3.76	1.00	20	0.29	0.41

* Depends on the existence of shear walls in the structure

Table 6.5 Continued

Bldg. Code	Shear Structure *	Number of Storeys	Height (m)	Weight (t)	Floor Area (m ²)	Floor Column Area (m ²)	ΣI_y (m ⁴)	ΣI_x (m ⁴)	Lateral Strength Index (x10 ⁻²)	Lateral Stiffness Index-y (x10 ⁻⁴ m ²)	Lateral Stiffness Index-x (x10 ⁻⁴ m ²)	ssi	Material Strength (MPa)	X-dir. Period (s)	Y-dir. Period (s)
B24	No	5	15.93	293.29	84.46	1.42	0.01	0.02	1.68	1.38	1.78	0.76	20	0.69	0.75
B25	Yes	6	18.00	809.27	180.22	5.90	0.37	0.26	3.27	20.30	14.29	1.00	25	0.88	0.82
B26	Yes	5	14.60	476.69	115.31	3.79	0.05	0.48	3.29	4.04	41.92	1.00	20	0.55	1.16
B27	No	4	11.80	346.09	125.62	3.31	0.06	0.16	2.63	4.88	12.78	1.00	25	0.31	0.44
B28	Yes	6	16.80	749.19	221.44	4.25	0.19	0.17	1.92	8.59	7.56	1.00	20	0.63	0.58
B29	Yes	7	20.75	404.97	70.68	2.63	0.21	0.13	3.63	28.94	17.78	1.03	25	0.72	0.84
B30	Yes	5	15.00	1471.49	240.08	6.57	0.62	0.41	2.73	25.64	17.11	1.00	25	1.95	1.75
B31	Yes	4	12.60	1224.78	395.82	13.57	4.58	6.08	3.43	115.59	153.53	0.94	25	0.24	0.24
B32	No	4	11.50	593.08	176.97	3.84	0.07	0.08	2.17	3.85	4.64	0.96	16	0.35	0.39
B33	Yes	5	14.55	658.97	186.41	5.29	0.64	0.30	2.84	34.27	16.35	1.00	25	0.39	0.32
B34	No	5	15.28	731.44	203.84	4.38	0.18	0.05	2.15	8.95	2.58	1.23	20	1.91	1.43
B35	No	7	16.20	645.62	130.13	3.11	0.09	0.16	2.39	6.62	12.03	1.43	20	0.34	0.59
B36	No	4	11.78	302.12	96.25	1.73	0.01	0.02	1.79	1.02	2.40	0.53	20	0.39	0.60
B37	Yes	5	14.60	754.79	208.23	5.31	0.65	0.20	2.83	34.80	10.56	1.00	25	0.40	0.29

* Depends on the existence of shear walls in the structure

structures by considering the proposed method. The number of storeys, the total heights, weights and areas are provided consecutively from third to sixth columns of the table. Total column areas, inertias in both directions and lateral strength and stiffness indexes are provided in the next six columns of the table. Soft storey indexes, material strengths, and fundamental periods in both directions are given in the proceeding columns of the table. Lateral strength and stiffness indexes are examined in detail, as they are crucial parameters in describing the size and distribution of the columns. Both Table 6.5 and Figure 6.4 demonstrate that the lateral strength indexes of all 37 structures are within 0.01 and 0.04. The minimum lateral strength index is observed in B12 with 1.8E-2 and the maximum value is observed in B19. Figure 6.5 shows the range of lateral stiffness indexes in both directions. A clustering is observed at the bottom left of the plot where lateral stiffness index values range between 0.0 and 6E-3 m². Figures 6.4 and 6.5 also present the distribution of single floor areas of the structures, which generally range from 100 to 300 m² with three values above 300 m² and a maximum value well above 500 m².

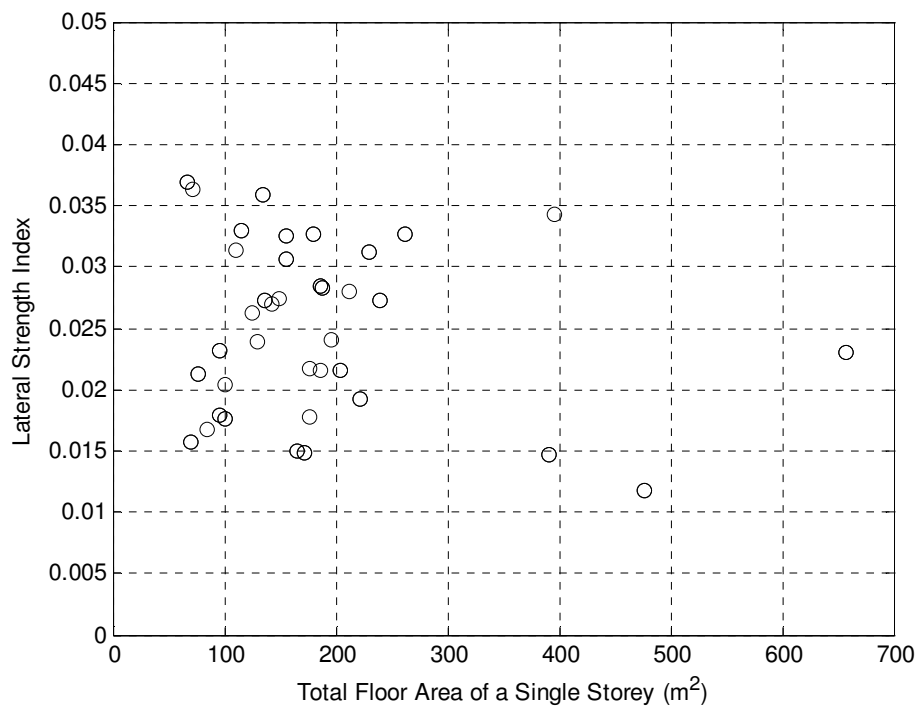


Figure 6.4. Lateral Strength Index of all the Models (Total 37 Points)

The structures listed in Table 6.5 generally show uniform variation in the lateral strength and stiffness indexes and number of storeys. However, the values of soft

storey index have a non-uniform distribution with a clustering pattern at 1.0. Therefore, in the regression analysis, these values will be carefully assessed.

The last two columns of Table 6.5 provide the fundamental periods in both directions. The fundamental period of a structure is one of the most important factors in shaping of the lateral response of a structure. The spectral values of demand acceleration, velocity, and displacement are determined by the fundamental period of the structure. Moreover, increasing or lowering the fundamental periods causes the structure to shift into the different regions of the response spectrum with varying sensitivity to acceleration, velocity, and displacement.

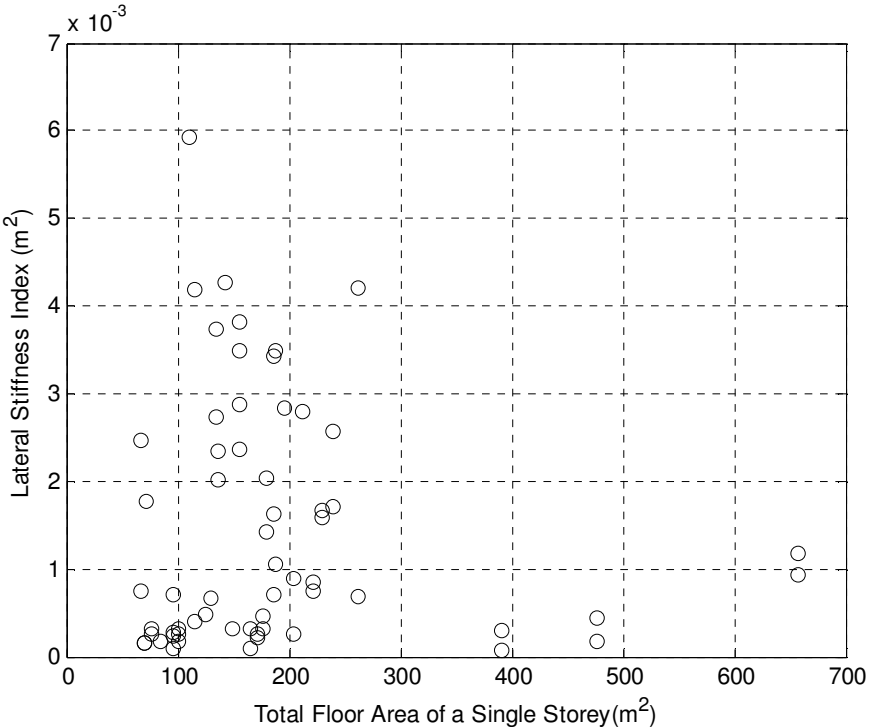


Figure 6.5. Lateral Stiffness Index of All the Structures in the Sample (Total 62 Points)

The structures with high fundamental periods must be closely investigated since the structure moves away from the acceleration sensitive region of the response spectrum curve into the velocity and displacement sensitive regions. In the velocity and displacement sensitive regions, the displacement is equal to the displacement calculated with the elastic parameters of the same system regardless of the type of post-elastic behavior. It is a well-known fact that, the strength reduction ratio and the ductility are equal for this type of behavior. Moreover, as the fundamental period increases, the ductility and strength reduction ratio becomes smaller (Newmark and

Hall, 1982, Vidic, Fajfar and Fishinger, 1994). After a threshold at the fundamental value in the displacement sensitive region, the structure completely sways together with the ground in the reverse direction of the movement. Consequently, it is essential to consider these types of structures separately to accurately predict the displacement by using the structural parameters. Likewise, at very low values of fundamental periods, a similar type of response is observed as the structure moves with the ground but this time in the same direction. Therefore, at very low fundamental periods, a different approach might be required to model the behavior of the structure by using the structural parameters just as in structures with higher fundamental periods. The fundamental period is generally associated with the height of the structure. In order to observe this relationship within the sample, the heights and fundamental periods of the structures in the sample are plotted in Figure 6.6. The figure demonstrates that a pattern of dependency emerges between the height of the structure and the fundamental period if the outliers are excluded. The fundamental periods display an increasing trend with the height as expected. In order to model the relationship between the height and fundamental period and to use as reference, widely used period equations are plotted in the figure (NEHRP, 1994, Eurocode 8, 2004, Goel and Chopra, 1997, 1998).

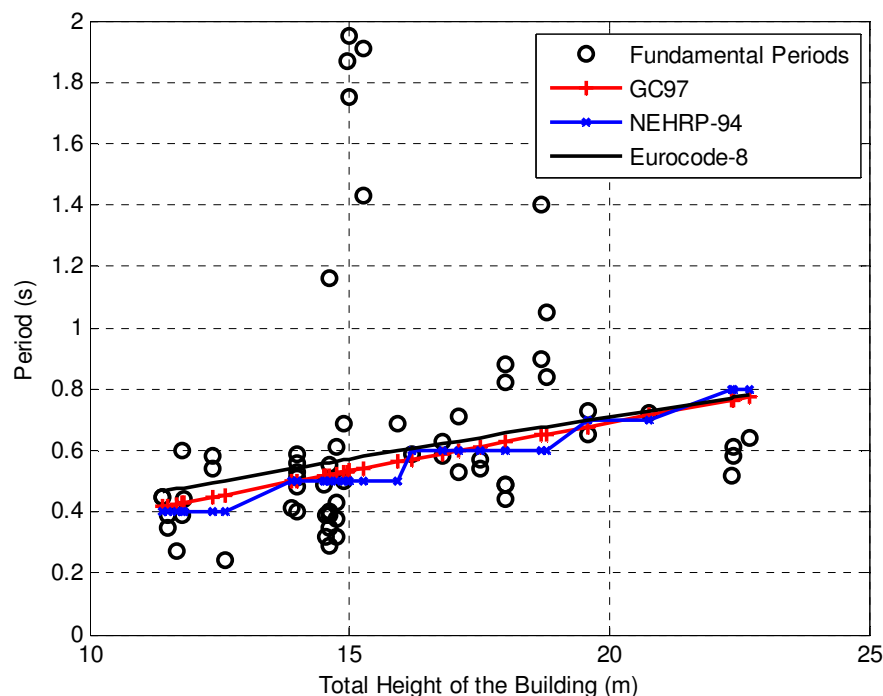


Figure 6.6. Period versus Height Relationship of All the Buildings and Calculated Periods by Using Different Formulations (Total 62 Points)

6.2.5. Multicollinearity in Multiple Regression Analysis

The lateral response is originated from the inertial resistances to lateral push and overturning forces. The inertial responses are composed of flexural or shear forces and with the associated deformations in the members of a structure. This controlling aspect of the structure could be designed in the planning stage of structures and whether shear or flexural response will be dominant could be decided beforehand. Indeed, depending on the distribution of ratios of the column and beam stiffness along the height, the type of the behavior could be predicted as shear or flexural dominated.

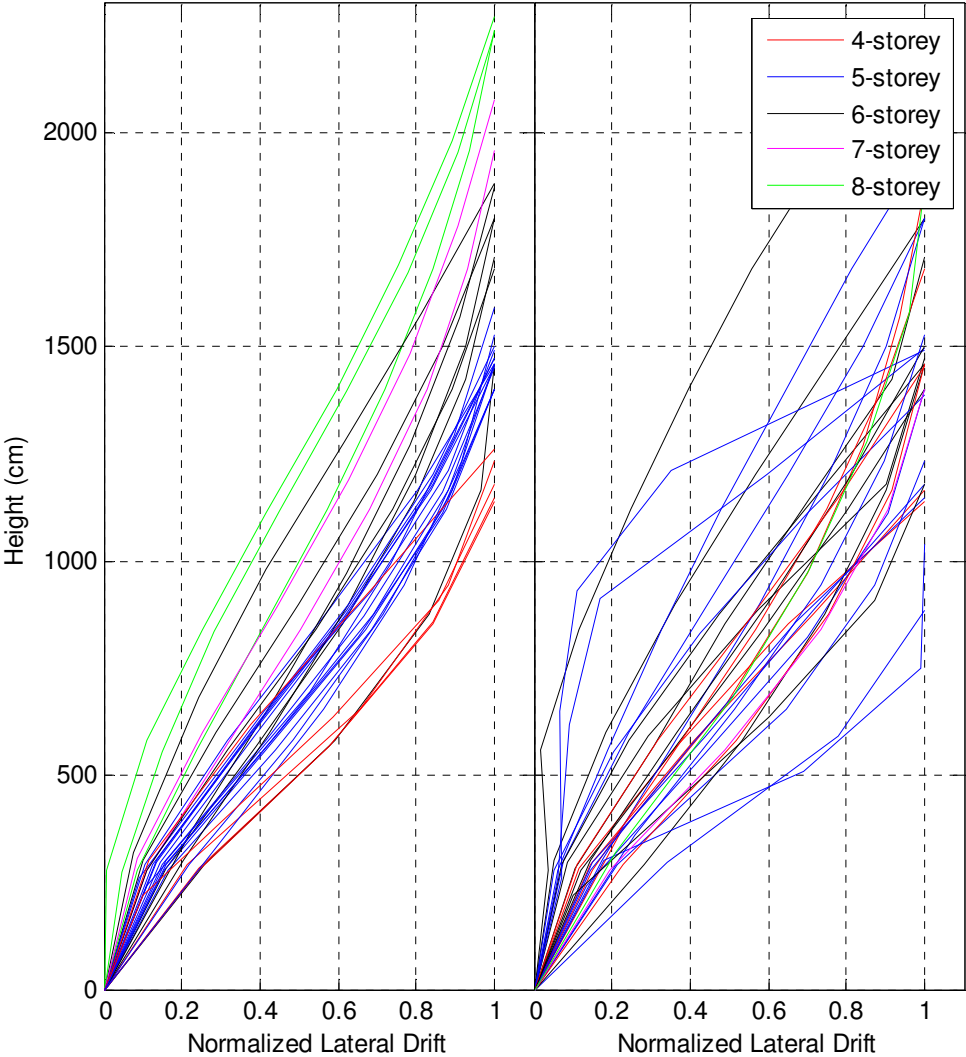


Figure 6.7. Lateral Drift Profiles of Structures (31 Models in Each Direction)

In other words, if the columns are stiffer than the beams in a structure, the type of inertial resistance will be flexure dominated while, with the weaker columns, a shear-

dominated response is more likely to be observed. These two main inertial resistances are expressed in terms of lateral strength and lateral stiffness indexes in this study.

Almost all the structures in the sample, which are gathered for this study, showed flexure dominant lateral responses as presented in Figure 6.7. Shear dominant behavior are also observed especially at the top storeys. Consequently, both lateral strength and stiffness indexes are required to model the lateral response of these structures. However, there is a drawback in employing both of these indexes together in a single equation, since these indexes are related to each other in a certain degree. The lateral stiffness index can be expressed in terms of lateral strength index as follows.

$$lsiI_j = lsiA_j \left(\frac{b_j^2}{12} \right) \quad (6.1)$$

where b_j is the dimension of the j^{th} column in the direction considered. According to the equation, it is obvious that if one of the indexes increases, so does the other index. Figure 6.8 demonstrates that there is a trend of increase in both indexes as the other index increases as the simple arithmetic in equation 6.1 suggests. The phenomenon of dependency of at least two of the predictor variables in a multiple regression analysis is called multi-collinearity.

The multicollinearity, in other words strong correlation between two predictor variables in multiple regression analysis, can severely affect the outcome of the regression analysis. Therefore, unless inclusion of both of the parameters does not negatively influence the regression analysis, a solution must be implemented before progressing with a healthy multiple regression analysis. In most cases, the most straightforward solution to the multicollinearity problem is the elimination of one of the correlated predictor variables.

As Figure 6.7 presents, the lateral performance of the structures is dominated by the flexural stiffness of the structures with local shear dominant behavior observed at the upper storeys. As mentioned previously, the important determining factor in the type of lateral response of a structure, as shear or flexure dominated, is the column-beam stiffness ratios of a structure. In general, the columns are designed to be stiffer than

beams so that the structure would perform in a flexure-dominated response and would not fail in a disastrous fashion. However, depending on the period of design and construction, as the design approach differs, some of the structures do not comply with the aforementioned approach. Therefore, both type of behavior might dominate the lateral response in the compiled sample. Finally, it is concluded that inclusion of both indexes is necessary, as the lateral displacement cannot be modeled with the exclusion of either of the flexural and shear displacements.

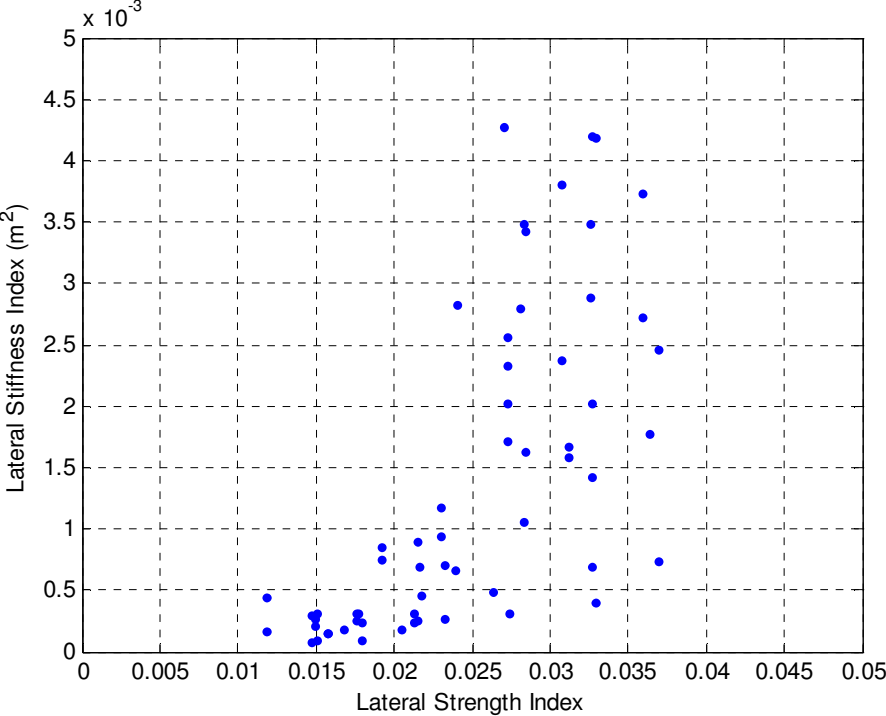


Figure 6.8. The Relationship between the Lateral Strength Index and Lateral Stiffness Index

6.2.6. The Initial Stress Issue

The pushover analysis starts with imposing the vertical loads to the structure and checking for any failures due to the applied vertical loads. A nonlinear analysis is conducted in the vertical direction as the dead and live loads are applied. After checking for the necessary compliance criteria and necessary modifications are performed if necessary, the structure is subjected to the lateral loads for pushover analysis. In other words, if there are any structural failures even before applying lateral loads, the analysis is stopped before proceeding with the pushover analysis. In such a case, it is concluded that the structure must be strengthened before any lateral

load is applied. If the structure successfully performs in this stage, then the analysis continues from the end of the nonlinear case created for vertical loads.

Applying the initial stresses to the structure has some drawbacks considering the purpose of this study. Firstly, the high variability of the vertical loads limits the success of any attempt to correlate the structural parameters with the lateral performance since each structure might display a different lateral performance with varying vertical stresses. Secondly, it is very difficult to foresee the influence of the initial stresses on the lateral performance of the structure, and obviously, there is not a dependency between the proposed structural parameters and the initial stresses. Thus, it is impossible to predict the effect of vertical loading on the lateral performance by using the structural parameters. Consequently, in order to prove the existence of a relationship between the lateral performance and various structural parameters, the potential bias created by the initial stresses must be either removed or reduced.

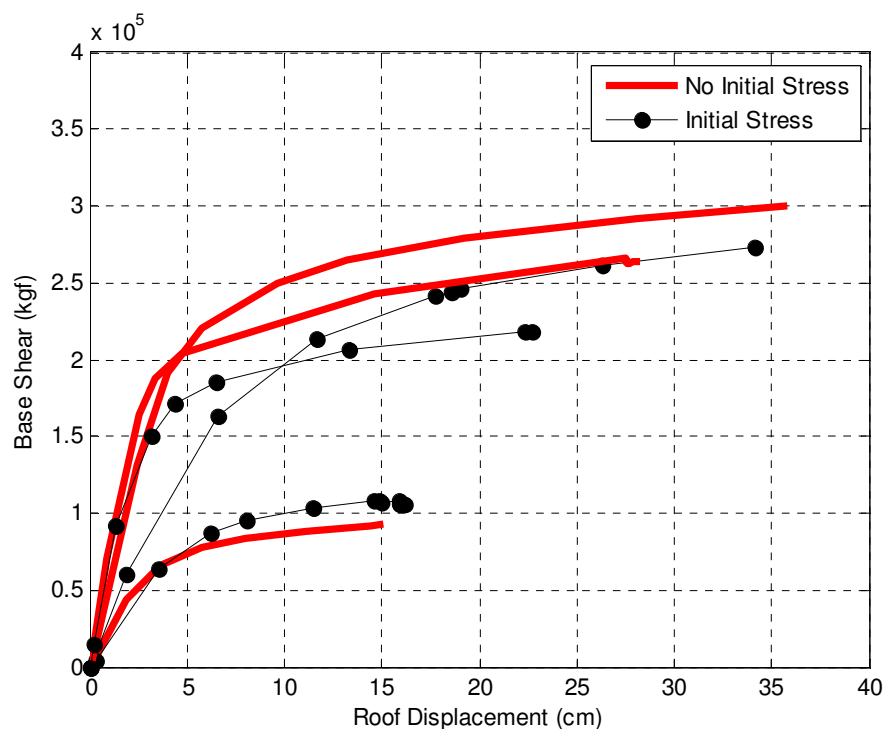


Figure 6.9. Pushover Curves of Three Structures Obtained by the Application of Different Loading Types and Initial Stresses

The variability caused by the initial stresses is clearly observed in Figure 6.9 as the influence of the initial stresses causes a decrease in the base shear values in two of

the pushover curves while causing an increase in one of the curves. Hence, it is concluded that the influence of the initial stresses cannot be predicted by using the pushover curves derived with no initial stresses.

To solve the initial stress problem, the influence of the existing vertical loads on the lateral performance must be investigated. Only then, the influence of vertical loading could be reflected safely to the LPPE. Since the scope of this study is limited, instead of developing an influence factor for the initial stresses, it is decided to apply the same vertical loads to all of the structures as the loading standards of Turkish codes are taken as reference. Another bias in the development of the LPPE, which is p-Δ effect, can be similarly assessed like the initial stresses. However, knowing that the idealistic models cannot provide solutions to the real life problems, instead of ignoring it is also included in the pushover analyses.

6.2.7. Pushover Curves

All the structures are modeled in SAP2000 (Computers and Structures, 2011) as three-dimensional models. The structures are then subjected to lateral loading in the form of dominant mode shape and uniform loading in both directions, and the resultant pushover curves are obtained for both directions.

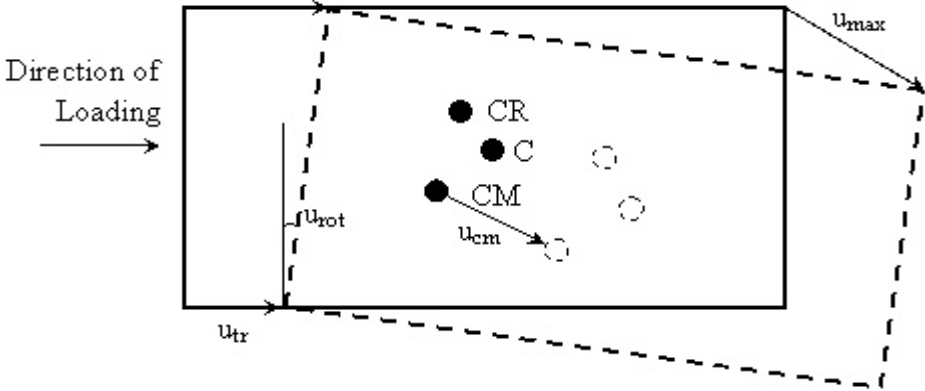


Figure 6.10. The Translational and Rotational Movement Caused by the Eccentricity and Lateral Loading in Fundamental Mode Shape (CM: Center of Mass, CR: Center of Rigidity, C: Geometric Center)

One of the main issues in obtaining the pushover curves in three-dimensional analysis is the determination of the point where the roof displacement is monitored. The location of geometrical center, center of rigidity, and the center of mass could be at varying distances as displayed in the Figure 6.10. In practice, the center of mass of

the storey is selected as reference point to monitor the displacements; however, confusion arises when the displacements over the roof storey greatly vary due to torsion.

The torsion created by the eccentricity between the center of mass and center of rigidity causes the structure to rotate with respect to the center of mass. Therefore, in addition to the translational displacements, the structures are subjected to rotational displacements. Consequently, two types of pushover curves can be considered as translational and rotational pushover curves. The translational curves could be represented by the base shear and translational displacement while the rotational curves could be modeled by the base moment and rotation. The rotation of the structure further complicates the prediction of the lateral performances by the proposed structural parameters since these parameters are not developed to foresee the influences of the torsion. Before a through evaluation is conducted, all the pushover curves are generated by monitoring the displacements at the center of masses of the roof storeys of the structures.

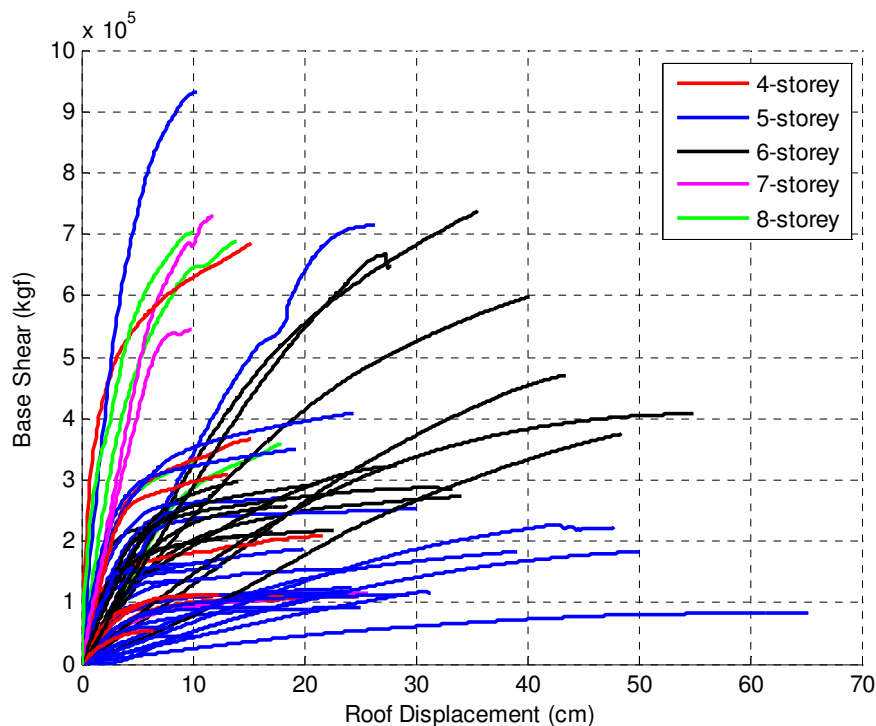


Figure 6.11. Pushover Curves of Buildings in Both Directions in Base Shear-Roof Displacement Format (Total 62 Structural Models)

The generated pushover and capacity curves are plotted as shown in Figure 6.11 and Figure 6.12 consecutively in base shear-roof-displacement format and base shear coefficient-global drift ratio format. In Figure 6.11, the vertical axis represents the base shear values that are defined as the resisting base shear forces, and the lateral axis represents the lateral displacements observed at the centers of masses of the roof levels of the structures. The base shear coefficient and global drift ratio are obtained by dividing the base shear by the weight of the building and roof displacement by the height. The conversion of pushover curves into capacity curves is required since comparing the pushover curves of different structures by introducing weight and height as normalization factors is more relevant.

Both figures contain 62 structural models, and the pushover and capacity curves are classified according to the number of storeys. After reviewing both figures, it can be said that a diverse group of pushover curves is obtained in terms of post elasticity and failure mechanisms. In other words, all the resultant curves followed a divergent pattern in terms of post elastic stiffness and obviously, the structures fail in a brittle and ductile manner though the failure points have a common feature that they take place at the maximum base shear and maximum roof displacement without any strength degradation.

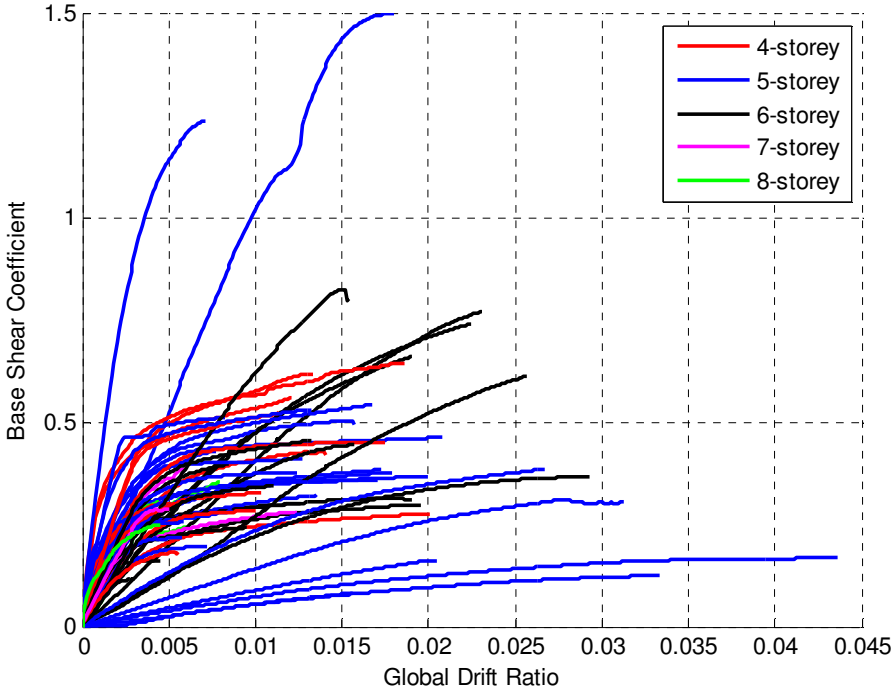


Figure 6.12. Capacity Curves of Buildings in Both Directions in Base Shear-Roof Displacement Format (Total 62 Structural Models)

The present study will be based on these curves in estimating the lateral performances in terms of displacements and drifts. Therefore, detailed investigations will be performed with these curves in order to develop a LPPE.

6.3. Scaling of Lateral Performance with Proposed Structural Parameters (Sensitivity Analysis)

It is clear that the structures are not mainly designed to reach a certain capacity or deformation level but to distribute the vertical and lateral forces safely to the ground, and exhibit displacements within serviceability limit states. As long as the load-carrying mechanism of the structure successfully performs transferring of oncoming loads or energy safely to the ground, it is not the primary issue whether the transfer of loads is performed by elastic or inelastic behavior.

The reasons behind the existence of different types of responses as elastic or inelastic are the different design approaches and applied codes, which impose a certain type of behavior onto the structure. These different approaches and codes contribute to the sizing of structural elements and the shaping of the geometry of the structure. Therefore, the structural system and geometry might show considerable variance from one structure to the other depending on the aforementioned reasons.

It should also be highlighted that, depending on the applied codes in the design and the design approaches used the lateral response of structures in terms of drifts and forces could be highly varied. For example, a structure might be designed to resist the lateral forces within the elastic limits; therefore, instead of exhibiting large lateral drifts, it absorbs and dissipates energy with very small lateral drifts but with considerably large forces carried by the system. Therefore, the drift predictions of such structure would be very different from those of a structure designed to dissipate the earthquake energy by inelastic response. Consequently, it is not easy to estimate the structural response in terms of drifts or any other lateral performance variable with varying column sizes, height distribution characteristics, and number of storeys. In addition, a structural behavior might shift from highly ductile to lesser ductile behavior if the column sizes change, which in turn complicates the matter even more. However, regardless of the design approaches or applied codes, it is intuitively deduced that, with greater size of columns, with more uniform height distribution and higher number of storeys, lateral performance of a structure changes within an

expected pattern. In other words, if a structure is modified to create new models with varying column sizes, height distribution, and number of storeys without changing other parameters, this modification is reflected in the lateral performances in a predictable pattern. The lateral performances like interstorey drift ratio, spectral acceleration and spectral displacement of CSM and ICSM, and target displacement of DCM and IDCM are influenced by the aforementioned modification.

After intuitive reasoning, it is thought that, these lateral performance variables could be subjected to a sensitivity analysis that would lead to the determination of the scaling of the lateral performances with the varying structural parameters. Regardless the complex nature of the structural responses to the modification of various structural parameters, it is anticipated that the sensitivity analysis could unfold the complex nature of lateral response by observing the patterns of responses. Consequently, a sensitivity analysis is conducted in order to measure the response of structures to the varying structural parameters. The modification scheme that is used to create structures with varying structural parameters is provided in section 4.3.2.

All of the 62 structural models are used in the sensitivity analysis. Pushover analyses are performed with uniform lateral loading pattern. Though mode shaped lateral load pattern is more emphasized and used in the development of the LPPE, the pushover curves obtained by the application of uniform lateral loading pattern are preferred since the study proved that high torsional influences exist in the modal loading pattern, which is not desired in the sensitivity analysis. With the uniform loading pattern, the influence of the structural parameters especially soft storey index can be more isolated from the influences of high torsion and varying higher mode participation ratios. Hence, it is not attempted to generate the pushover curves of the modified structures by using mode shape lateral loading pattern.

After deciding on the right loading pattern for the sensitivity analysis, in order to investigate the relationships between the structural parameters and lateral performances in global drift ratios, the pushover curves are converted into base shear coefficient-global drift ratio format. As can be seen in Figure 6.12, there is high variability in the level of base shear coefficients and global drift ratios of different capacity curves. Consequently, with the assumption that the variability of the pushover curves may reduce the chances of obtaining the right scaling of lateral

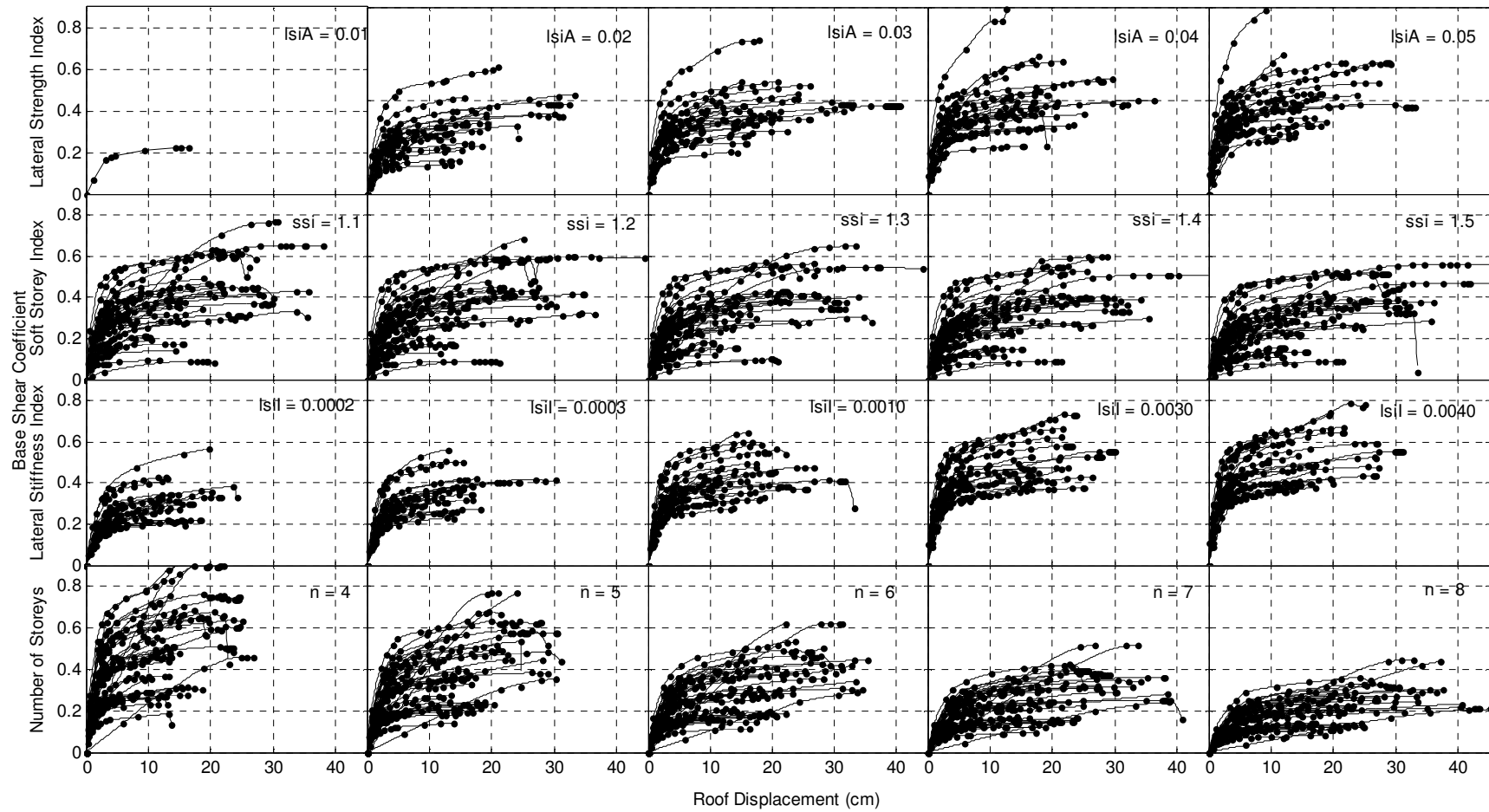


Figure 6.13. The Pushover Curves with the Original Structural Parameters (Uniform Loading) (Number of Structural Models Varies)

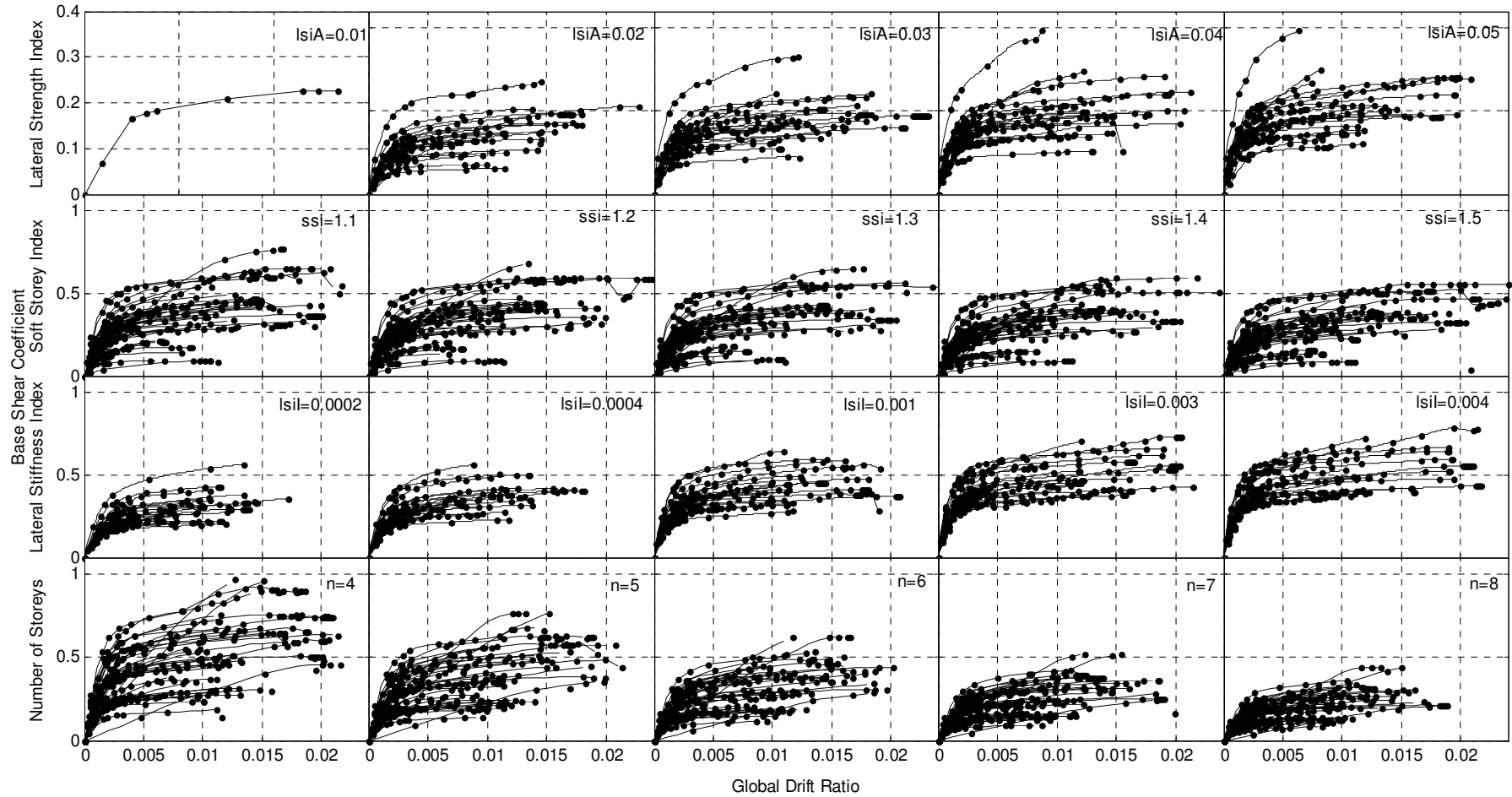


Figure 6.14. The Capacity Curves with the Original Structural Parameters (Uniform Loading) (Number of Structural Models Varies)

performances, a simple elimination scheme is imposed to reduce this variability by introducing thresholds in terms of lateral performance variables. The rationale of this refinement is not based on any technical classification or background. The pushover curves with maximum global drift ratios above $2.3E-2$, maximum base shear coefficients above 0.7, maximum base shear values above $5.0E5$ kgf, and pushover curves with initial slope less than 30 in base shear coefficient and global drift ratio format are removed. All of the pushover curves are subjected to this elimination scheme, and the remaining pushover curves are used to observe the scaling in the lateral performances.

IDCM is selected from among the lateral performance estimation methods to estimate the lateral performances in terms of roof displacements and global drift ratios. CSM is not employed due to the varying and sometimes unrealistic damping ratios required for the estimation of the lateral performance. Since the DCM was already updated by IDCM, it is not used for the sensitivity study either.

Interstorey drift ratios are not considered as the monitored variable in the sensitivity analysis since there are factors such as modal mass participation ratios of higher modes that may influence the interstorey drift ratio, which in the end cause a misrepresentation of the lateral response by the varying structural parameters. In other words, due to the complexities of higher mode participation, the sensitivity analysis might not produce accurate results by using the maximum interstorey drift ratios.

Since the IDCM method requires demand spectral acceleration values for the estimation of the lateral performances in terms of target or roof displacements, the response spectrum curves developed for earthquakes with different return periods as presented in Figure 5.25, are utilized in the sensitivity analysis. Site class C is found to be appropriate as the dominating site class in Eskisehir, therefore the elastic response spectrum curves in Figure 5.25, which are developed for site conditions at the NEHRP B/C boundary, will be modified by using site amplification factors (NEHRP, 1997) to modify the elastic response spectrum curves for site class C. The methods of CSM, DCM and IDCM will be employed by assuming NEHRP site class C as the site condition.

As mentioned, in order to monitor the scaling of roof displacements and global drift ratios of every single structure, the pushover and capacity curves are generated for each varying indexes of the structural parameters. The resultant pushover and capacity curves are presented in Figures 6.13 and 6.14, which display the influence of the modification of the structural parameters on the pushover and capacity curves. It should be mentioned that since the scaling of base shear and base shear coefficients at the performance levels of roof displacements and global drift ratios are not considered as crucial for this study, no investigation is performed to monitor the scaling of base shear values or base shear coefficients. Therefore, for convenience in the presentation, the base shear values in the pushover curves are converted to base shear coefficients in order to observe the scaling of the lateral performances with respect to the roof displacements.

In both figures, the relative shift of pushover curves in both drifts and displacements can be easily followed. In the top rows of Figures 6.13 and Figure 6.14, with lateral strength index as varying structural parameter, significant shifts of base shears are observed in vertical axes, whereas the shifts in the global drift ratios are not visually traceable. Similar to the lateral strength index, the scaling of the lateral performance with the varying soft storey index is not obvious in Figure 6.14, while in Figure 6.13, the scaling can be observed especially in the vertical axis. The scaling of the global drift ratios is not visible at all with varying soft storey index. With the varying lateral stiffness index, the pushover and capacity curves display similar scaling of roof displacements and global drift ratios. As shown in the last row, the number of storeys has a considerable impact on the base shear coefficients whereas the roof displacements and global drift ratios seem to be less influenced. The following sections provide detailed information on the scaling of the lateral performances with the structural parameters.

6.3.1. Detailed Investigation of the Scaling of Lateral Performance with Respect to Structural Parameters

In many studies, among the lateral performance variables that would relate to the overall damage, lateral displacements and drifts are preferred to the accelerations and forces. Similarly, in this study, the displacements and drifts are considered as primary lateral performance variable to predict the damage. Hence, it is decided that, the roof displacements, global drift ratios, maximum interstorey drift ratios, and

spectral displacements of CSM will be regressed with the proposed structural parameters and LPPE will be developed to predict the lateral performances in terms of the mentioned variables. After deciding on the lateral performance variable to be used in LPPE, the physical background of the scaling of the considered lateral performance variables with the proposed structural parameters is investigated. It can be stated that, the scaling of lateral performances with the structural parameters can be deduced intuitively. Generally, the spectral displacement is more associated with the various structural parameters and since global drift ratios and roof displacements are closely related with the spectral displacements, the deductions made by spectral displacements will be valid for the global drift ratios and roof displacements too.

Knowing that the height, fundamental period, mass, lateral stiffness, demand displacements and performance displacements are all related with a physical relationship, a credible deduction is quite probable. This deduction can be based on the elastic demand displacement, which depends on the fundamental period, which in turn depends on the height, mass and stiffness. It should also be noted that with higher modal mass participation ratios, the dependency of the lateral performance on the fundamental period increases.

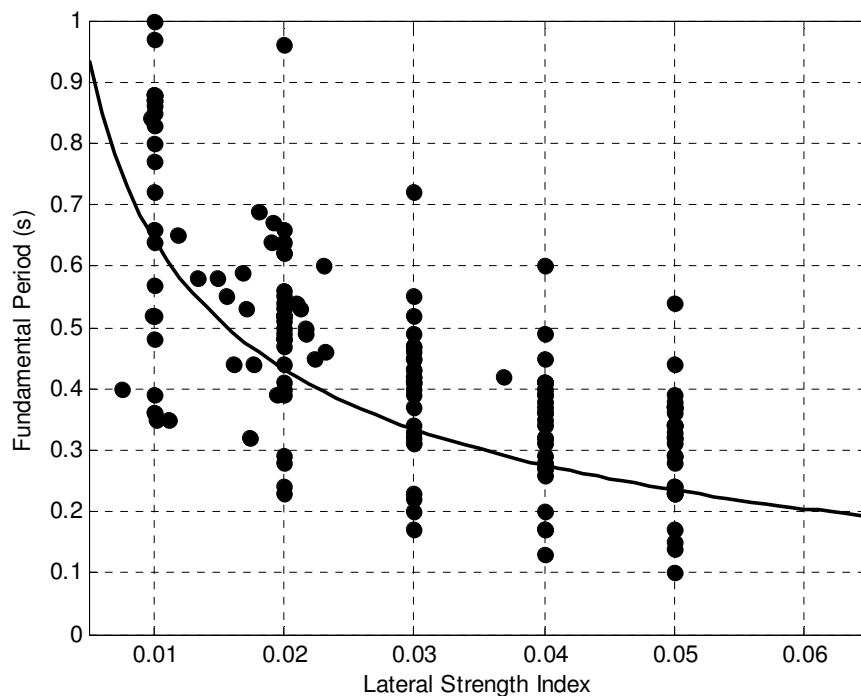


Figure 6.15. The Scaling of the Fundamental Period with Respect to Lateral Strength Index

Since the elastic displacement demand of the structure is dependent on the fundamental period, it can be directly related to the lateral performance. It is already a widely accepted fact that, by introducing displacement modification factors like in DCM and IDCM, final performance displacement could be closely estimated. Conveniently, the fundamental period of a structure can be used as reference, which can give a clue about the lateral performance of the structure in terms of displacements. The influence of the height, mass and stiffness are investigated thoroughly in the following paragraphs to infer the relationship between the displacement and the proposed parameters.

Since total height is one of the most influential parameters that determine the fundamental period of a structure, it is automatically deduced that the proposed structural parameters of soft storey index and number of storeys, which could be expressed in terms of the total height, have highly correlated relationships with the lateral displacement. However, the structures whose fundamental periods are very high or very low, a condition that cannot be expressed by the height of the structures alone, are not rare. They often have unique characteristics that cause the deviation the lateral displacements from displaying the expected pattern of behavior. The different characteristics of these structures should be taken into account when a predictable pattern of behavior is sought among a sample of structures.

In the light of the explanations about the scaling of lateral displacements, it is easily concluded that, the scaling of the lateral performance with respect to the parameters of soft storey index and the number of storeys can be justified by considering the influence of height over the fundamental period of the structure, and on the lateral displacements. Especially with the number of storeys, it is widely known fact that the rate of increase in the displacement response spectrum curve is not as much as the rate of change of the fundamental period. In other words, the demand spectral displacements do not increase as much as the fundamental period and hence scaling between the height and number of storeys with the spectral displacement do not yield a one-to-one linear relationship, but spectral displacements have lower rate of change. Therefore, it is expected that there is a decreasing trend of the global drift ratios and spectral displacements, while an increasing trend exists between the number of storeys and spectral displacements. The same relationship is valid for the soft storey index as well.

Lateral strength and stiffness index has a more complicated influence over the displacement in that increasing both indexes causes a greater increase in the overall lateral stiffness of the structure than that in the total mass of the structure. Therefore, as Figure 6.15 displays, the fundamental period of the structure becomes smaller, which in turn decreases the demand displacement. In addition, decreasing the lateral strength and stiffness index in a structure reduces the ability of the structure to respond within elastic limits and shifts the structural response into the inelastic zone. Hence, the lateral responses in terms of roof displacements might be amplified when lateral strength and stiffness indexes become smaller.

While it is concluded that each structural parameter can be related to the lateral performance by the way of induction, more solid proof can be provided by the sensitivity analysis. The analysis is based on the modification of the structures and application of pushover analysis to the modified structures in order to observe the change in lateral performance with the modified parameter. Following sections offer findings of the sensitivity analysis and more detailed information about the scaling characteristics of lateral performance with each proposed structural parameter.

6.3.1.1. Dependency on Lateral Strength Index

The scaling of the lateral performances with the lateral strength index is investigated by modification of column sizes of the structures in order to adjust the structures to have predefined lateral strength indexes. The column area in each floor is modified by changing the column sizes in the transverse direction of the loading, in order to reset the lateral strength indexes to 0.01, 0.02, 0.03, 0.04 and 0.05. As the modification factors applied and the column sizes are modified, the weight of the building is also modified automatically. The other parameter of the LPPE, the lateral stiffness index, is also subject to change with the change in the sizes of the columns. However, the relative change in the lateral stiffness index is the same as the change in the lateral strength index since only the sides of the columns in the transverse direction of the loading are modified while the sides in the direction of loading remained as the same.

Because not every modification is within the limits of standards and codes, most of the modified structures with lateral strength index of 0.01 are not qualified for further investigation. In other words, to impose the lateral strength index of 0.01, the

modifications required a considerable decrease in the size of columns, which form nonconforming elements; hence, the structure is disqualified from the process.

As mentioned previously in 4.3.2, in order to obtain lateral performances at the specified levels of lateral strength indexes, pushover curves of the modified structures are generated. Then, to obtain the scaling of lateral performances with varying indexes, the lateral performances are calculated by using IDCM. After that, the overall lateral performance values for each lateral strength index are obtained by averaging the lateral performance values obtained for all the structures in the sample at that specific lateral strength index. Figure 6.16 is created to present the lateral performances of the 40 structural models with respect to the global drift ratios. These models are generated by using 8 original structural models. Obviously, the generated structural models that comply with the codes are limited, therefore only 8 original structural models are found suitable in the derivation of the scaling characteristics of the lateral performances with varying lateral strength indexes. The curves in Figure 6.16 are used to obtain an average curve, which is obtained by averaging the values of each curve at each lateral strength index. These average curves are presented in Figure 6.18 for each response spectrum curve that is generated for the earthquakes with different return periods. It is observed that the roof displacements and global drift ratios correlate with the varying lateral strength indexes in an inversely nonlinear manner as expected.

The apparent scaling of the lateral performances with the lateral strength indexes provides a projection capability for the in-between values of lateral strength indexes by interpolation. The values outside of the provided lateral strength indexes, such as those below 0.02, can also be derived by the extrapolation of the fitted equation at those values. Evidently, the scaling of the lateral performance with the varying lateral strength index can be based on the following model:

$$f(lsiA) \propto (lsiA)^{-x} \quad (6.2)$$

where $f(lsiA)$ is the function with lateral strength index as variable, x is the power term introduced to model the nonlinear scaling of lateral performance with the lateral strength index.

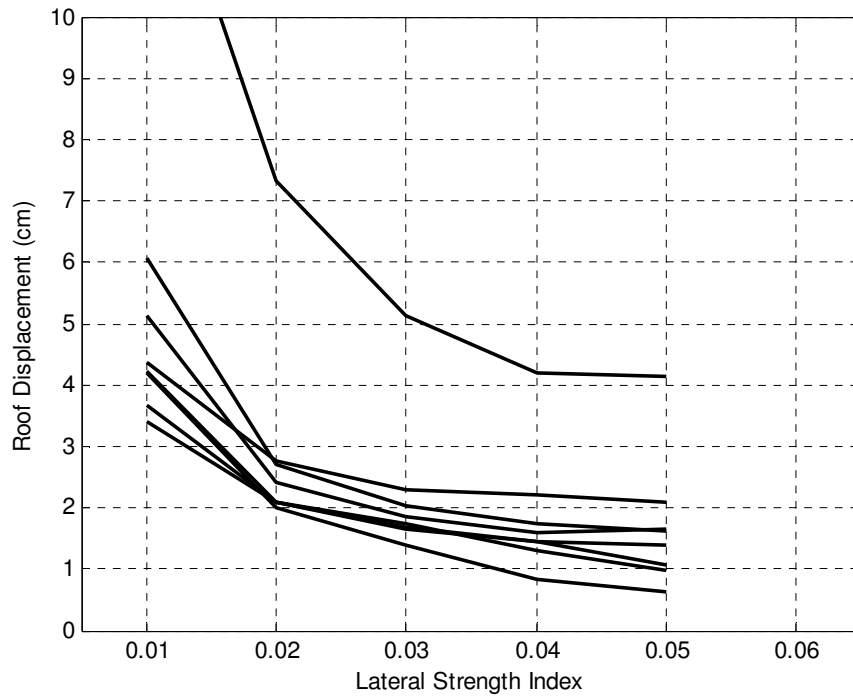


Figure 6.16. Scaling Characteristic of the Global Drift Ratio with the Lateral Strength Index for 2475-year Return Period Earthquake (Performance of 40 Modified Structural Models are Presented)

The coefficients of the equation can be derived for the compiled sample; however, it is more suitable to use the basic scaling model in the LPPE. The power term is difficult to set since it could be dependent on the distribution of the structural models within the sample. Therefore, the coefficients of the power term will be assigned from amongst the best of the predefined range of numbers during the regression analysis.

6.3.1.2. Dependency on Soft Storey Index

Soft storey index or ratio of first storey height to the second storey height has indirect influence over the lateral performances in drifts or displacements in global scale as explained in 6.3.1. Since the lateral performances are predicted in global scale as global drift ratios and roof displacements, the influence of the soft storey index on these global variables could be limited. However, in the first storey, the location where soft storey has direct influence, the local lateral deformation could be amplified which can cause total collapse of the structure. In fact, it is expected that interstorey drift profiles could capture the effects of the soft storey index with greater success. However, since all the methods must be evaluated separately with their

advantages and disadvantages, not only the interstorey drift method but the results of all the methods will be compared.

As part of the modification scheme, all the structures are modified by changing the first storey height in order to set the soft storey index to values ranging from 1.0 to 1.5. The modifications to the structure remained within the limits of the code, and necessary checks are performed before proceeding with the pushover analysis. The analysis results reveal that the global drift ratios and roof displacements linearly scale with the soft storey index. As shown in Figure 6.18, the roof displacement and global drift ratio are positively affected by the soft storey index as they increase with increasing soft storey index. Therefore, the scaling of the lateral performance with the varying soft storey index can be based on the following model

$$f(ssi) \propto (ssi) \quad (6.3)$$

where $f(ssi)$ is the function with soft storey index as variable. Lastly, it should be noted that, the global drift ratio scaling is not noticeably clear, so it could be expected that the sample distribution of the lateral performance and the soft storey index determine that sign of relationship.

6.3.1.3. Dependency on Lateral Stiffness Index

The scaling of the lateral performances with the lateral stiffness index is investigated by a method similar to the one used for the lateral strength index. The inertia of the columns in each storey is modified in the direction of loading to reset the lateral stiffness indexes to the predefined values. As the column size modifications are performed, the weights of the structures are also modified automatically. The lateral strength index of the storey is also subject to change with the change in dimension. The relative change in the lateral strength index of the storey is far less than the lateral stiffness index due to the different sensitivity of the size to the inertia and area in the direction of loading. At some values of lateral stiffness index, the structures are not qualified for the assessment because of the nonconforming elements that are generated during the modification. After the elimination of the pushover curves of these structures, it was realized that the remaining pushover curves are numbered as 7. Therefore, 7 structural models that comply with the code are employed for the derivation of the scaling equation. In Figure 6.17, the pushover curves of one of these

models are generated to present the effect of varying lateral stiffness index on the overall performance. The influence of the lateral stiffness index on the pushover curves can easily be followed in the figure.

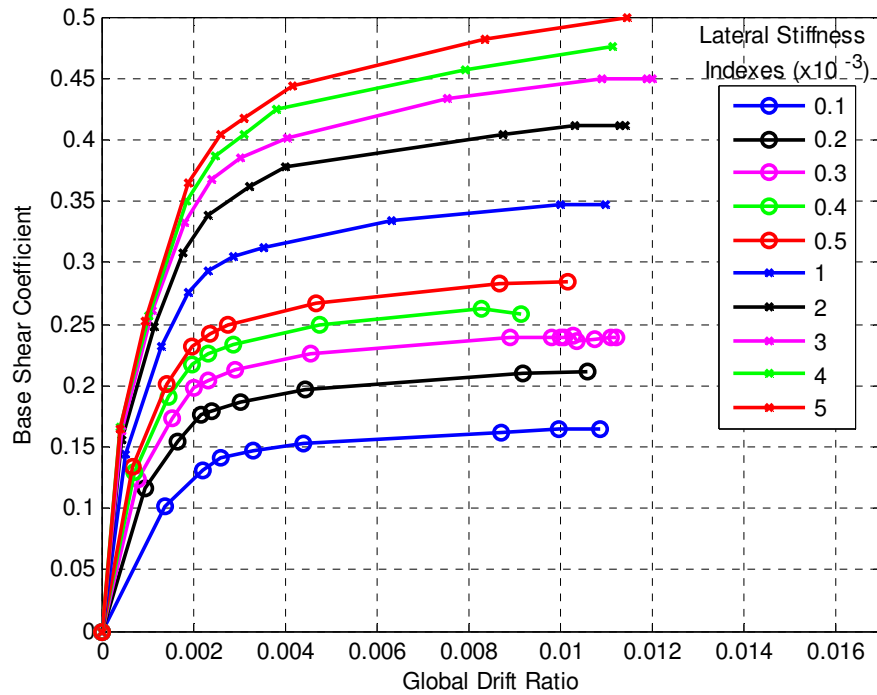


Figure 6.17. Capacity Curves for Different Values of Lateral Strength Index

In order to derive the relation between the lateral performance and lateral stiffness index, the lateral performances of all 7 of the models are calculated at each index and the values obtained at each index was averaged. After the sensitivity analysis, the scaling of the lateral performance with the varying lateral stiffness index can be based on the following model

$$f(lsi) \propto (lsi)^{-x} \quad (6.4)$$

where $f(lsi)$ is the function with lateral strength index as variable and x is the power term introduced to model the nonlinear scaling of lateral performance with the lateral stiffness index.

Considering the fact that almost all the designed structures have lateral stiffness indexes between $1E-4$ and $5E-3 \text{ m}^2$, and lateral strength indexes between 0.01 and 0.05, the above findings about the type of the scaling between the lateral performance and lateral stiffness and strength indexes can be interpolated. However,

it must be admitted that, the coefficients of the equation that models the relationship definitely change with samples of different structures. More generalized equations can be derived by the inclusion of several different types of structures in terms of projected types of behavior and the design standards used.

6.3.1.4. Dependency on Number of Storeys

In the modification scheme, as the other structural parameters remained constant, the number of storeys of each structure is modified by either adding the duplicates of the roof storey or removing storeys from the top to reset the number of storeys to the predefined number of storeys. By adding and removing of the storeys, a family of same-type structures with 4,5,6,7, and 8 storeys is generated. In particular, the ability of the structure to resist the additional loadings due to the added storeys is checked. Especially in the cases of the 4 storey structures, on which additional 4 storeys are added on top of the existing structure, thus exposed to a large amount of dead and live load, the performance of the vertical load carrying mechanisms is carefully checked. After the confirmation of the performance of vertical load carrying mechanism, the sensitivity analysis is conducted as it is performed for the other structural parameters. As the result of sensitivity analysis suggests, as can be observed in Figure 6.18, the scaling of the lateral performance with the varying number of storeys can be based on the functional form given in equation 6.5

$$f(n) \propto (n) \quad (6.5)$$

where $f(n)$ is the function with number of storeys as variable. The global drift ratio scaling is evidently different from the roof displacement since the heights of the structures are involved as parameter. There is a positive linearity of the observed scaling of roof displacements with the number of storeys while the global drift ratio scale negatively linear manner.

6.3.2. Forming the Lateral Performance Prediction Equation

The sensitivity analysis revealed that the lateral performances of the structures in terms of global drift ratios and roof displacements scale with the proposed structural parameters. Regardless of the fact that the proposed parameters may not be sufficient to model the lateral performances, the following functional form is proposed for the prediction of the lateral performances:

$$LP(lsiA,ssi,lsiI,n) = f(lsiA) + f(ssi) + f(lsiI) + f(n) + \sigma \quad (6.6)$$

where LP is the prediction function, f represents the parametric functions, $lsiA$ is the lateral strength index, ssi is the soft storey index, $lsiI$ is the lateral stiffness index, and n is the total number of storeys of the structure and σ is the standard deviation.

Owing to the fact that spectral displacement, roof displacement and global drift ratio are all related, the scaling characteristics are expected to follow the same pattern. Therefore, the functional form of the LPPE could be employed for each of the mentioned lateral performance variables. If the spectral displacements are used as the lateral performance variable then the following LPPE can be formed after rewriting the equations in 6.6.

$$SD(lsiA,ssi,lsiI,n) = f_{SD}(lsiA) + f_{SD}(ssi) + f_{SD}(lsiI) + f_{SD}(n) + \sigma \quad (6.7)$$

where SD represents the performance of the structure in spectral displacements. The above equations can also be modified for the roof displacements that are obtained by the DCM and IDCM. The following equation is written to model this relationship.

$$\delta(lsiA,ssi,lsiI,n) = f_{\delta}(lsiA) + f_{\delta}(ssi) + f_{\delta}(lsiI) + f_{\delta}(n) + \sigma \quad (6.8)$$

where δ represents the target or roof displacement for the considered response spectrum. Finally, the global drift ratio could replace the roof displacement as a lateral performance variable and equation 6.8 could be adjusted.

After establishing the basic functional form of the equation, if the observed scaling are modeled then the final form of LPPE would look like the following equation:

$$LP(lsiA,ssi,lsiI,n) = a_1 + a_2(lsiA)^{a_6} + a_3(ssi) + a_4(lsiI)^{a_7} + a_5(n) + \sigma \quad (6.9)$$

where a_1 , a_2 , a_3 , a_4 and a_5 are the coefficients of LPPE, a_6 and a_7 are the power coefficients to model the nonlinear scaling between the lateral performance and lateral strength and stiffness indexes and σ is the standard deviation. The power coefficients can be selected from a narrow range of values since the sensitivity analysis provides sufficient clues about the degree of nonlinearity.

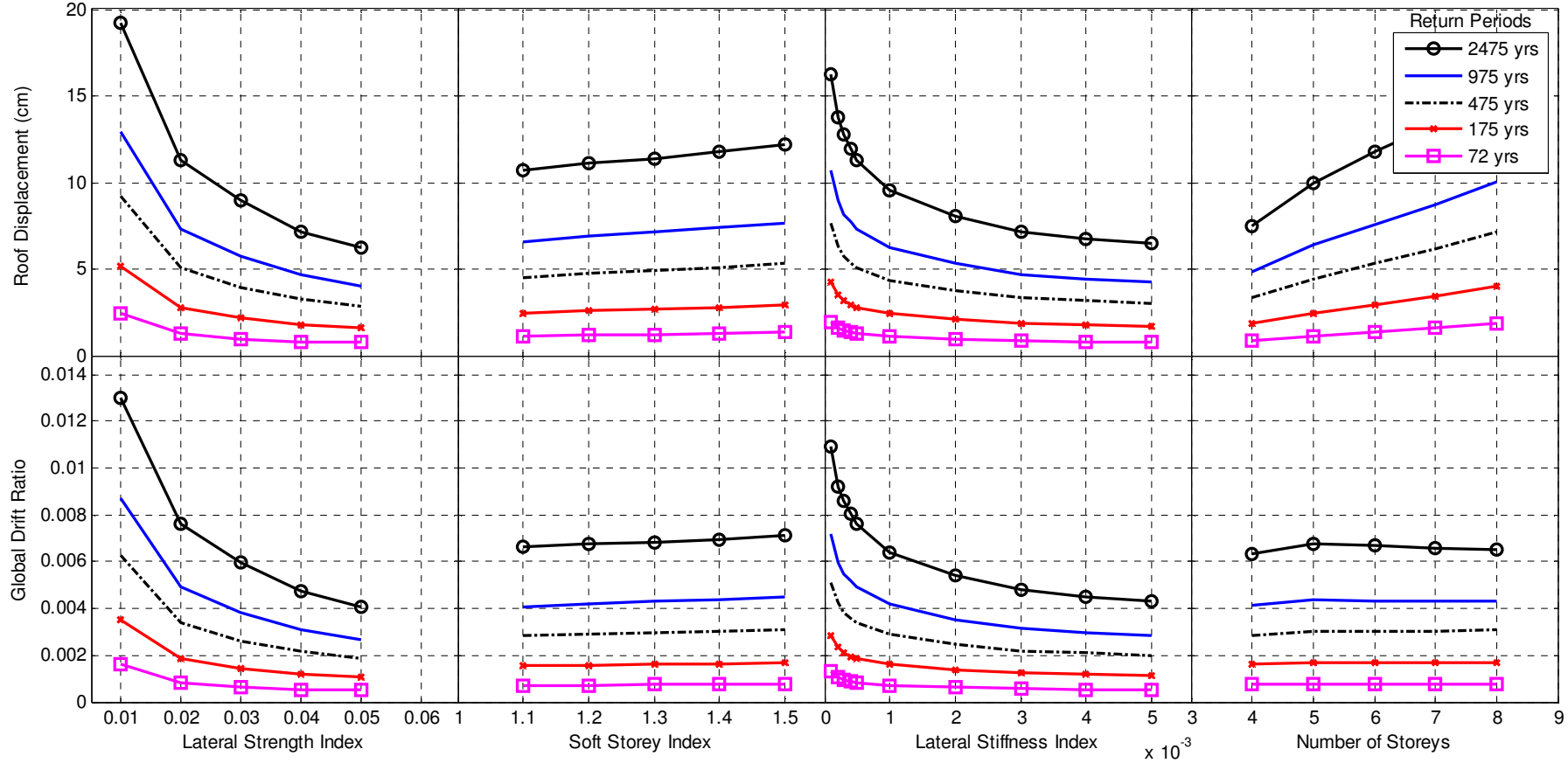


Figure 6.18. The Results of Sensitivity Analysis for Roof Displacement and Global Drift Ratio

After the formation of the basic form of the LPPE, the next step is to determine the right method to derive the coefficients of the LPPE. A simple multiple regression analysis, which is a method used to model the linear relationship between a dependent variable and several independent variables, is selected to be the right method to derive the coefficients of the equation. The nonlinear scaling of the lateral performances is modeled by linearization of the nonlinear model; hence, the linearity assumptions of the multiple regression analysis are correctly utilized.

Moreover, regardless of the fact that DCM and IDCM are based on roof displacements, the utilization of this variable is susceptible to the bias created by the varying heights of the buildings. Consequently, global drift ratio is utilized in the development of LPPE instead of roof displacements that were obtained by DCM and IDCM applications. Converting spectral displacements back to the roof displacements and then to the global drift ratios are not without assumptions that add more complexity to the problem. Hence, instead of converting spectral displacements to global drift ratios, these spectral displacements obtained by CSM are decided to be utilized for the development of LPPE. The interstorey drift ratios do not require such a conversion; therefore, the maximum interstorey drift ratio is employed without requiring a modification. In the end it is decided that the lateral performances obtained by the methods of CSM, DCM, IDCM, and interstorey drift ratios would be employed to develop the LPPE. Nonlinear time history analysis is also decided to be used but not for the purpose of development of an equation but for validation of the existence of such an equation.

The excitement of different modes depending on the frequency content of ground motion that cannot be foreseen by the proposed equation, the torsional effects that might be resonated, and the scaling issues of the raw signals are some of the reasons for such a decision. In addition, considering the wide acceptance of all these methods, it is safely assumed that predicting the estimated lateral performances by any of these methods could be valid.

6.3.3. Investigation of the Relationship between the Lateral Performances and Proposed Structural Parameters

Initially, lateral performances of the structural models are estimated by IDCM to observe if there is a meaningful pattern with the varying structural parameters. To

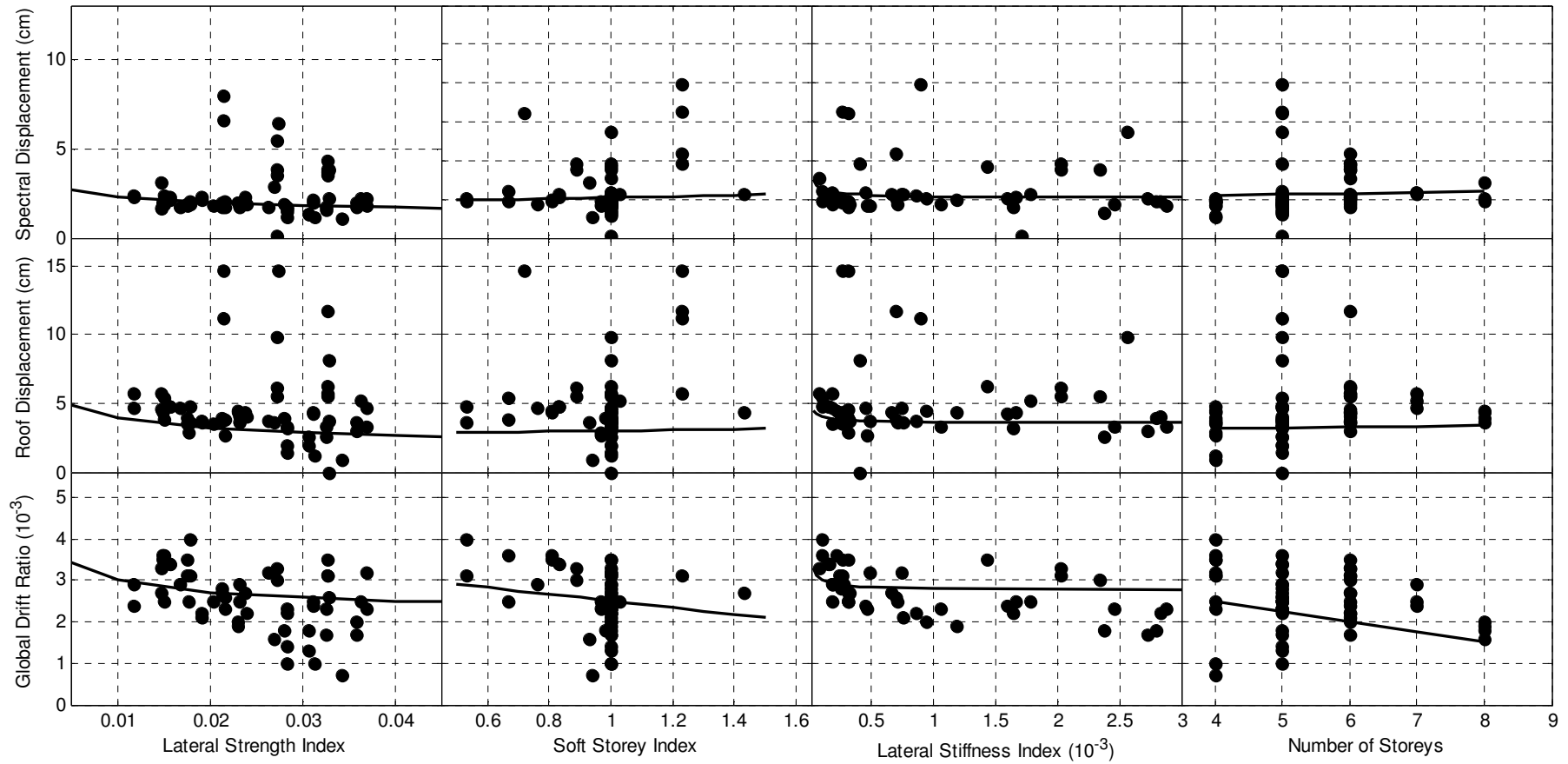


Figure 6.19. Variation of the Lateral Performance Values with Respect to the Functions Obtained by Sensitivity Analysis (NEHRP Site Class C, Lateral Performances of 62 Structural Models for 475-year Return Period Earthquake are Presented)

this end, the roof displacements and global drift ratios are calculated by using the response spectrum curves developed for a 475-year return period earthquake in Eskisehir.

The roof displacements are converted to global drift ratios by normalization of the roof displacements with height to avoid the structure specific bias. In the end, the scaling characteristics of the spectral displacements, roof displacements and global drift ratios with respect to the proposed structural parameters are obtained, which are shown in Figure 6.19. The fitted curves in each subplot are developed to model the lateral performances. These curves are based on the results of the sensitivity analysis, indicating the pattern of lateral performance scaling, which is followed by the spectral displacements, roof displacements and global drift ratios of the structures in the sample. As the first impression, the dispersion of lateral performances is quite noticeable in the plots. The existence of too many outlier values obviously causes a loss of pattern. Therefore, without any further evaluation, a refinement of the database deemed necessary.

6.3.4. Refinement of the Database for Further Analysis

In Figure 6.19, considerable variance and dispersion of the lateral performances as spectral displacements, roof displacements and global drift ratios capture special attention. The potential bias created by the outlier values should be removed in order to seek a pattern of the lateral performance.

In fact, in an attempt to isolate structures with certain characteristics, the structures that cause the dispersion could be eliminated indiscriminately. However, a deep understanding is required for the real causes of the too high and too low response values. In other words, before elimination of any outlier value, the reasons for the dispersion of the lateral responses should be investigated. Therefore, all the structures are subjected to detailed investigation.

The outlier structural models are checked for certain structural features that creates the wide dispersion in the lateral performance distribution. Among the several features the fundamental period, relative sway ratio and ductility are identified as potential source of bias that could create such a dispersion of lateral performances. In addition, knowing the relationship between the fundamental period and performance displacements, the prescriptions of ATC-40 (1996) and FEMA-440 (2005) about the

use of proposed methods of lateral performance estimation are investigated. ATC-40 (1996) suggests the reconsideration of the structures with high relative sways, which is defined as the ratio of the maximum displacement at the roof level to the displacement at the center of mass of roof storey. If this ratio is above 1.2, then the pushover analysis approach needs to be changed by assignment of the loads at the center of mass, and the displacement at the center of mass should be recorded. However, in order to prove the existence of a relationship between the lateral performance of the structures and the structural parameters, the structures should not be prone to the influences of rotational displacements, which is very difficult to foresee by the proposed parameters. Therefore, as the first step of elimination, the structures with high relative sway ratio are excluded.

Another suggestion prescribed in ATC-40 (1996) and FEMA-440 (2005), pertaining to the use of methods of CSM, DCM and IDCM, is related with the fundamental periods of the structures. Both documents tried to set a higher and lower limit value on the fundamental period to prescribe the applicability limits to the displacement estimation methods.

According to ATC-40 (1996), for fundamental periods greater than 1.0 s, the higher modal effects should be included to estimate the roof displacements. Indeed, as a result of this equal displacement rule, which is already mentioned in section 6.1.3, in DCM, the coefficient for the inelastic to elastic displacement ratio is set as 1.0 for structures with fundamental periods higher than 1.0. FEMA-440 (2005) has the same limit value of fundamental period as 1.0 s for the application of the inelastic to elastic displacement ratio, which is more than unity in IDCM. The structures with fundamental periods higher than 1.0 s are considered within the boundaries where equal displacement rule applies. Consequently, the coefficient proposed to estimate the inelastic to elastic displacement ratio is set as 1.0 for the structures with fundamental periods higher than 1.0 s.

Similarly, structures with lower fundamental periods are also considered as a different group that requires attention. Both reports accept the dispersion of the estimated displacement from the equal displacement approximation at shorter periods. ATC-40 (1996) defines the short period range as 0-0.50 s, whereas in FEMA-440 (2005) though the high sensitivity of the target displacement to the low

fundamental periods is mentioned and for the structures with lower than 0.20 s, the use of modification factor that is calculated for 0.20 s is suggested. Therefore, structures with low fundamental periods are evaluated by considering the suggestions of ATC-40 (1996) and FEMA-440 (2005). Moreover, considering the fact that these limits are developed by using a large database of structural models and mostly valid for all types and ranges of structural models, evaluation of the limit values for a specific sample could generate reliable results for that specific sample. In addition, the lower limits are not clearly defined in the related documents, which motivated for in sample investigation for these limiting fundamental period values.

For such an evaluation to define an upper and lower limit fundamental periods a number of structural models are required with very wide range of coverage and the lateral performances of these models must be estimated. In such an attempt, Figure 6.20 was created where the structural models created for this study are used. All the 62 original structural models are used to create Figure 6.20. Obviously, the models have a wide range of fundamental periods and the displayed lateral performances that are estimated by using the IDCM. The response of the roof displacements with respect to the changing fundamental periods provide valuable information in setting the limits of fundamental periods, which a reliable pattern emerges between these limits for the selected structures in the sample.

Knowing that the outliers in terms of fundamental periods could be one of the prime reasons for the dispersion in Figure 6.19, and considering the emerging patterns of lateral performances in Figure 6.20, a lower limit of 0.35 s and an upper limit of 0.80 s is imposed for the elimination of outliers. Only between these two fundamental periods, a pattern emerges for each of the response spectrum curve as shown in Figure 5.25. Actually, for smaller return periods the limits could be extended until the fundamental period of 1.0 s, however for the sake of coherency in the study, it was found appropriate to set the upper limit to 0.80 s. The regions with different pattern of behavior are associated with different regions of the response spectrum curves in Figure 5.25 where the curves display different patterns.

The main disadvantage of limiting the fundamental periods between 0.35 s and 0.80 s is that, the estimated displacements form a narrow band for each response spectrum curve. The estimated roof displacements, and hence the global drift ratios, would

limit the capability of a LPPE that is developed by using these lateral performances. However, these limitations could be imposed as a prescription in the application criteria of the LPPE. Moreover, it should be mentioned that the shape of the elastic response spectrum curves are strong determining factors in the establishment of these limits too. Therefore, the seismic hazard and seismic risk studies must be conducted together in order to set the prescriptions of a developed LPPE for a specific region.

In addition, the ductility ratio distribution is also dependent on the fundamental periods, since it decreases with the increasing fundamental periods. Consequently, with the fundamental period criterion, the ductility ratios of the outlier structural models will be checked too.

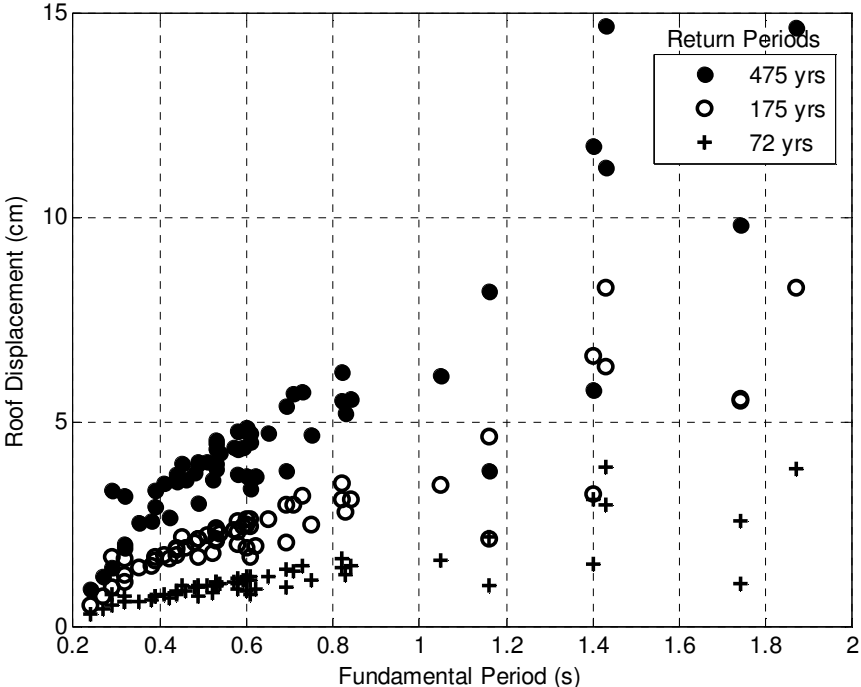


Figure 6.20. Variation of Roof Displacement with Fundamental Period (62 structural models)

Considering the technical background of the prime reasons for the dispersion in Figure 6.19, two-stage elimination was proposed for technical and visual elimination schemes. Technical elimination required the assessment of structures with respect to fundamental periods and relative sway ratios. The ductility ratios and ratios of post elastic stiffness to elastic stiffness of the structures are also investigated in this stage.

Then, visual elimination is performed by removing the outstanding pushover curves with very high values of yield or ultimate global drift ratios, yield or ultimate base

shear coefficients or negative post elastic stiffness. Indeed, the sole purpose of removing the outstanding pushover curves visually is to create more uniformly distributed pushover curves with certain characteristics such as yield drift ratios, plastic to elastic stiffness ratios and ultimate values.

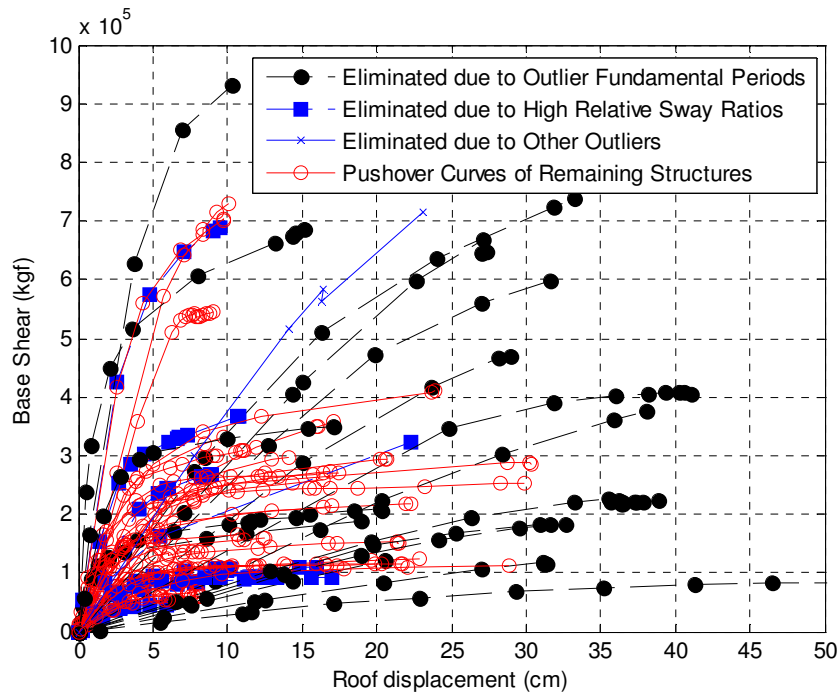


Figure 6.21. Pushover Curves of Eliminated and Outlier Structures

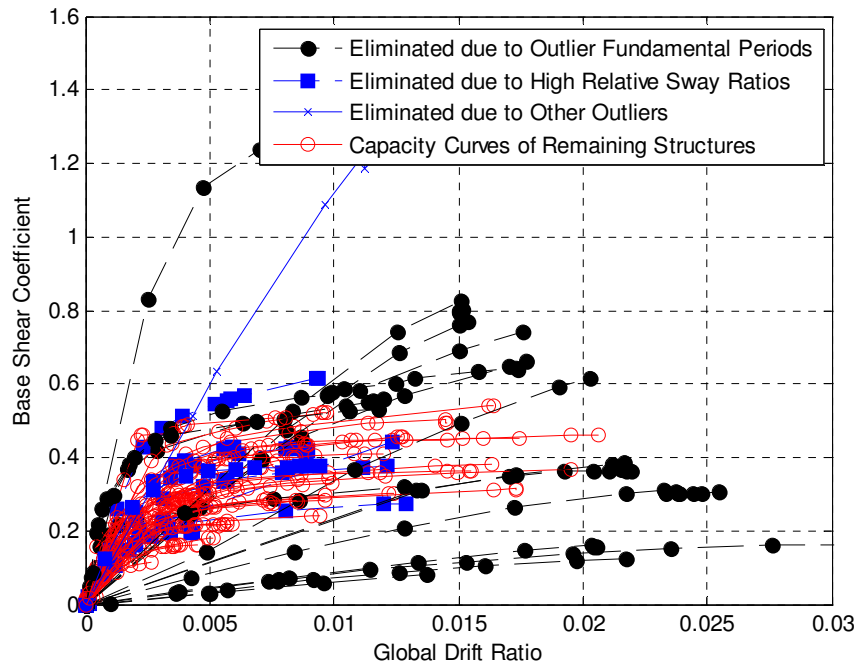


Figure 6.22. Capacity Curves of Eliminated and Outlier Structures

Table 6.6. Period and Stiffness Values of Structures

Direction	Building Code*	Fundamental Periods (s)	K_e** (t/m)	K_p** (t/m)	α** (%)	μ**	e**	
X-Direction	B02 (1)	0.45	0.24	0.02	6.90	3.1	1.59	
	B03	0.54	0.55	0.02	3.08	3.8	1.01	
	B04	0.44	0.71	0.02	2.82	4.5	1.02	
	B05	0.53	0.79	0.02	1.91	7.3	1.00	
	B06	0.40	0.31	0.01	3.68	3.8	1.06	
	B07 (2)	0.32	0.62	0.03	4.37	6.6	1.06	
	B09 (3)	0.58	1.26	0.20	16.05	2.3	1.47	
	B10 (4)	0.84	0.14	0.07	49.86	1.7	1.50	
	B11	0.35	0.63	0.03	5.15	6.2	1.06	
	B12	0.65	0.99	0.07	7.25	3.1	1.17	
	B13	0.64	0.46	0.07	14.43	2.2	1.21	
	B14 (5)	0.53	0.15	0.01	5.93	3.0	1.48	
	B15 (6)	0.58	0.20	0.01	4.90	3.2	1.56	
	B16 (7)	0.90	0.33	0.12	35.06	2.0	1.07	
	B17	0.49	0.54	0.02	3.04	3.8	1.01	
	B18	0.52	0.81	0.11	13.25	2.4	1.03	
	B19	0.43	0.33	0.02	4.96	3.7	1.08	
	B20 (8)	0.50	0.56	0.04	6.80	2.7	1.30	
	B22 (9)	0.59	0.10	0.01	7.14	2.8	1.68	
	B24	0.69	0.15	0.01	3.80	3.3	1.03	
	B25 (10)	0.88	0.18	0.01	4.93	2.5	1.27	
	B26 (11)	0.55	0.36	0.09	25.70	1.8	1.14	
	B28	0.63	0.45	0.03	5.46	3.0	1.00	
	B29	0.72	0.18	0.01	7.34	3.0	1.05	
	B30 (12)	1.95	0.08	0.02	18.87	1.9	1.14	
	B31 (13)	0.24	2.24	0.14	6.23	6.5	1.01	
	B32 (14)	0.35	0.74	0.07	9.01	3.6	1.42	
	B33	0.39	0.77	0.02	2.82	4.1	1.07	
	B34 (15)	1.91	0.06	0.03	49.01	1.4	1.00	
	B36	0.39	0.29	0.01	3.02	6.5	1.04	
	B37	0.40	1.00	0.04	3.67	4.6	1.02	
	Y-Direction	B01 (16)	0.27	0.62	0.02	3.07	6.8	1.08
		B02	0.45	0.31	0.01	4.03	3.4	1.00
		B03	0.57	0.50	0.02	3.07	3.5	1.10
B04 (17)		0.49	0.48	0.06	12.83	4.4	1.27	
B05		0.71	0.43	0.03	6.01	4.2	1.05	
B06		0.51	0.27	0.01	4.46	3.3	1.10	
B07		0.38	0.52	0.01	2.74	7.0	1.00	
B08		0.49	0.61	0.02	3.73	6.5	1.01	

*The numbers in parenthesis next to the buildings codes are assigned to the identify the eliminated structures

**K_e: Elastic lateral stiffness, K_p: Post yield elastic lateral stiffness, α: Ratio of post yield lateral stiffness to elastic lateral stiffness, μ: Ductility ratio, e: Relative sway ratio

Table 6.6 Continued

Y Direction	Building Code*	Fundamental Periods (s)	K_e^{**} (t/m)	K_p^{**} (t/m)	α^{**} (%)	μ^{**}	e^{**}
	B09	0.61	1.53	0.09	5.88	3.4	1.04
	B10 (18)	1.05	0.11	0.06	52.91	1.7	1.27
	B11	0.39	0.52	0.02	3.98	4.7	1.02
	B12	0.73	0.85	0.07	7.79	3.3	1.10
	B14 (19)	0.48	0.20	0.01	5.28	2.9	1.32
	B15	0.54	0.32	0.01	3.76	3.5	1.05
	B16 (20)	1.40	0.09	0.01	8.38	2.4	1.34
	B19	0.61	0.22	0.01	4.53	3.9	1.02
	B20	0.69	0.30	0.02	6.50	2.6	1.06
	B21 (21)	1.87	0.03	0.01	24.83	1.7	1.16
	B22	0.56	0.17	0.01	7.67	2.9	1.01
	B23	0.41	0.49	0.03	5.25	3.4	1.08
	B25 (22)	0.82	0.29	0.10	34.88	1.8	1.02
	B26 (23)	1.16	0.07	0.01	12.54	2.6	1.24
	B27	0.44	0.37	0.01	3.71	3.2	1.05
	B28	0.58	0.47	0.05	10.04	2.6	1.13
	B30 (24)	1.75	0.07	0.01	15.66	2.4	1.53
	B32	0.39	0.76	0.06	8.21	3.4	1.19
	B33 (25)	0.32	0.95	0.04	3.91	4.4	1.13
	B34 (26)	1.43	0.08	0.03	39.95	1.5	1.23
	B35	0.59	0.42	0.05	10.71	2.5	1.04
	B36	0.60	0.17	0.01	3.59	4.0	1.08
	B37 (27)	0.29	1.94	0.29	15.09	2.1	1.02

* The numbers in parenthesis next to the buildings codes are assigned to the identify the eliminated structures

** K_e : Elastic lateral stiffness, K_p : Post yield elastic lateral stiffness, α : Ratio of post yield lateral stiffness to elastic lateral stiffness, μ : Ductility ratio, e : Relative sway ratio

Figures 6.21 and 6.22 are created to illustrate and justify the elimination scheme. A closer look at these figures is necessary for a thorough understanding of dispersion of the lateral performances. Regarding the outlier lateral performance values in Figure 6.19, the eliminated structures are identified as one of the main causes of the dispersion and variance.

The evaluation of the pushover and capacity curves justifies the established elimination scheme, which removes the structures with very high and low periods, mostly accompanied by low or high ductility ratios, and structures with high relative sway ratios from the sample to create more refined database.

Table 6.6 lists all the structures in the sample with the related structural properties provided. The numbers in parenthesis next to the building codes in the second column show the structures eliminated by one of the aforementioned criteria. In the table, the fundamental periods, elastic and post yield stiffness values and ratio of post elastic stiffness to elastic stiffness values, ductility ratios and relative sway ratios are provided in the consecutive columns.

Three main groups are identified within the eliminated structures: the structural models with high or low fundamental periods, the structural models with high relative sway ratios, and structures with other outlier values. The third group contains only one structure labeled as B26 in x -direction, and labeled as 11 in the list of eliminated structures. The sole reason for this elimination is to have a uniform distribution of ultimate base shear coefficients as can be followed in Figures of 6.11 and 6.22.

The first group is identified with high or low fundamental period values that are above 0.8 s and below 0.35 s. These structures are generally identified with highly post-elastic to elastic stiffness ratios. The ductility ratios are also low for these structures as higher fundamental periods shift the structures into the velocity and displacement sensitive zone of the response spectrum curve, where equal displacement rule governs the response. Structures with low fundamental periods follow the equal energy rule, which forces more inelastic displacement to dissipate the same amount of energy that of the equivalent elastic model. Moreover, lower fundamental periods shift the structural sensitivity towards the acceleration sensitive zone, where the accelerations are amplified, compared to the rest of the response spectrum zones. Therefore, with higher fundamental periods low ductility ratios are expected while with lower fundamental periods high ductility ratios are expected.

Figure 6.23 presents a comparison between the distinct fundamental period values of the structural models with outlier lateral performances and the fundamental periods of the rest of the models in the sample. Moreover, in order to evaluate the fundamental period values of all the models, the most common period equations developed by NEHRP (1994), Eurocode-8 (CEN, 2004) and Goel and Chopra (1997) is plotted within the same figure. It is obvious that most of the fundamental period values of the structural models with outlier performances are easily distinguishable

as they are markedly higher or lower than the calculated fundamental periods with the presented models of period estimation.

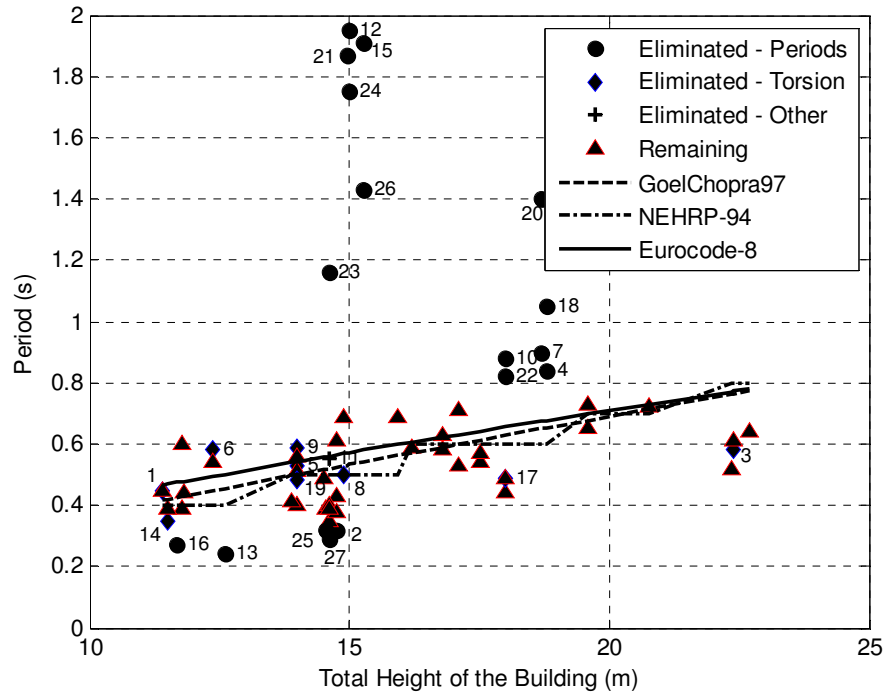


Figure 6.23. Variation of Original and Outlier Periods with Height

A graphical figure is prepared in order to better display the high and low fundamental periods together with the higher relative sway ratios of the outlier models. Figure 6.24, in which the outlier models are clearly distinguishable, describes the reasoning behind the elimination process. Evidently, most of the structures with high fundamental periods are accompanied by higher relative sway ratios, which can be attributed to torsion.

The high fundamental periods are also associated with high post-elastic to elastic stiffness ratios and low ductility ratios as can be followed from Figures 6.25 and 6.26. In order to express the level of inelastic performance of the structures, ductility ratios are used. The structures are categorized according to the level of ductility for examination. Since the prediction of lateral drift and displacement and the associated damage is the focus of this study, the knowledge of inelastic structural behavior under lateral loading is crucial. Structures with too high or too low ductility could challenge the validity of the proposed LPPE. Hence, all the structures are evaluated with respect to the ductility ratios.

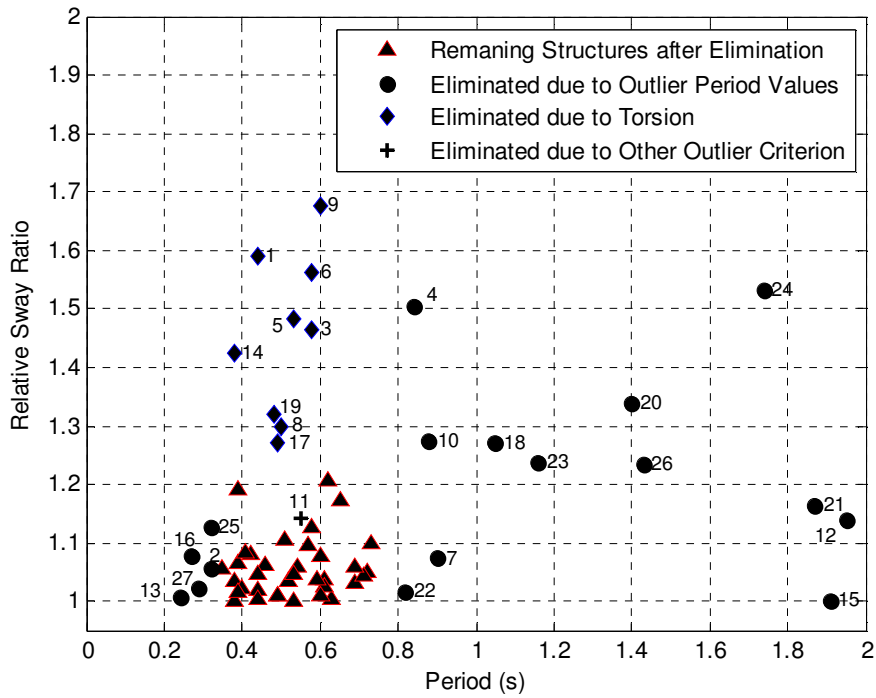


Figure 6.24. Relative Sway Ratios and Fundamental Period Values (Eliminated Structures are Identified with Symbols and Numbers)

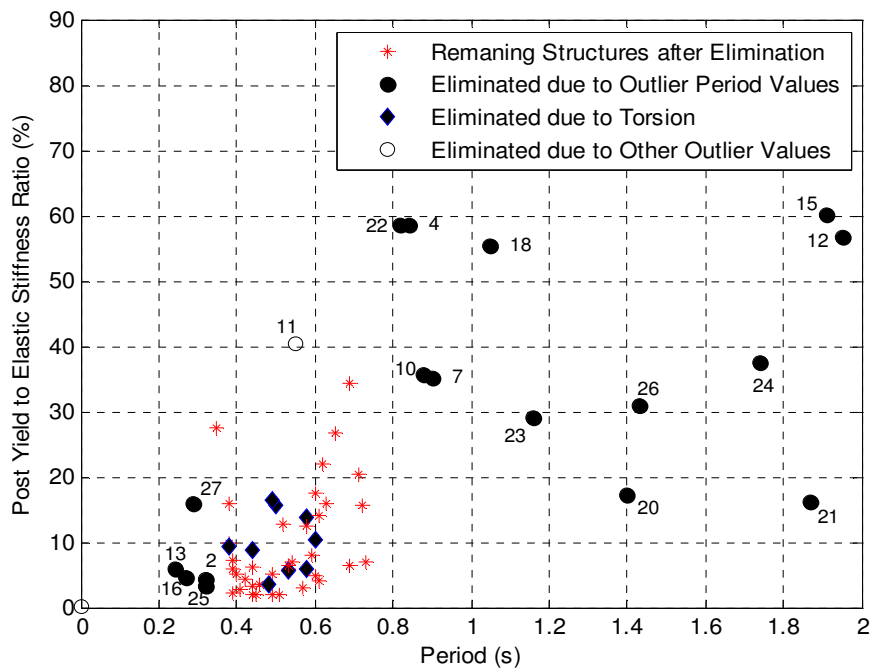


Figure 6.25. The Post Elastic Lateral Stiffness to Elastic Lateral Stiffness Ratios versus Fundamental Period Values (Eliminated Structures are Identified with Symbols and Numbers)

It is already mentioned that the high fundamental periods are accompanied by the low ductility ratios as expected. As shown in Figure 6.26, the cluster on the lower right corner is composed of the structures with high fundamental periods. The figure

also helps to explain the structures designed by very high ductility ratios, which are accompanied by the low fundamental period. It should be mentioned that, the structural models with high relative sway ratios are not significantly different from the rest of the remaining models in the fundamental period and ductility ratio distribution. These structural models indeed are in the cluster of remaining structural models in Figure 6.25 as well. As a clarification about both Figures of 6.25 and 6.26, the numbers assigned next to the dots are related to the numbers in Table 6.7.

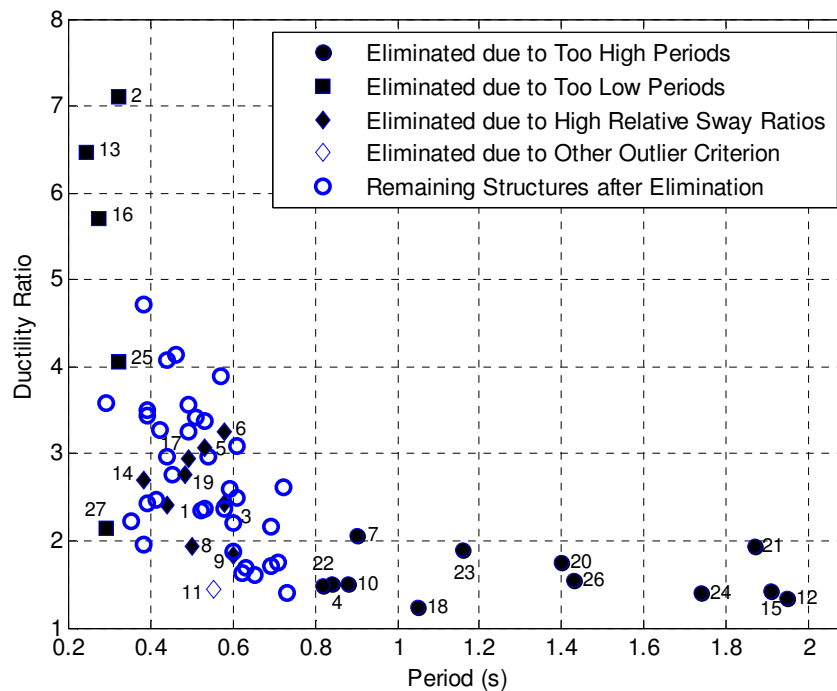


Figure 6.26. Fundamental Periods and Ductility Ratios (Eliminated Structures are Identified with Symbols and Numbers)

A summary of eliminated structures and the reasons for the elimination is prepared and is given in Table 6.7. The structural systems are also listed as bare frame or shear walled. It should be highlighted that, most of the structures that are eliminated due to high or low fundamental periods have shear walled structural systems. In addition, these structural models perform with low ductility ratios depending on several factors including fundamental periods and elastic and plastic stage stiffness. After the elimination stage is completed, a uniform set of pushover curves is obtained, as seen in Figure 6.27. The global drift ratios at yield points seem to merge although the base shear coefficients at these points vary. A very clear transition from the elastic to post-elastic stage is observed for each pushover curve. Additionally, the elastic and the

plastic stage of all the curves follow a general pattern, and variance of the post elastic to elastic stiffness ratios seems to be minimized.

Table 6.7. The List of Eliminated Buildings

Direction	Building No	Plot/Parcel No	Period (s)	Relative Sway Ratio	Reason of Elimination	Structural System
X-Direction	B02 (1)	(2010)-4	0.45	1.59	Sway Ratio>1.2	BF
	B07 (2)	1415/4	0.32	1.06	Period<0.35 s	BF+SW
	B09 (3)	152/1	0.58	1.47	Sway Ratio>1.2	BF+SW
	B10 (4)	205/3	0.84	1.50	Period>0.80 s, Sway Ratio>1.2	BF+SW
	B14 (5)	2133/218	0.53	1.48	Sway Ratio>1.2	BF
	B15 (6)	2571/14	0.58	1.56	Sway Ratio>1.2	BF
	B16 (7)	2927/1	0.90	1.07	Period>0.80 s	BF+SW
	B20 (8)	496/14	0.50	1.30	Sway Ratio>1.2	BF
X-Direction	B22 (9)	557/11	0.59	1.68	Sway Ratio>1.2	BF
	B25 (10)	7768/3	0.88	1.27	Period>0.80 s, Sway Ratio>1.2	BF+SW
	B26 (11)	876/515	0.55	1.14	High ultimate base shear coefficient	BF+SW
	B30 (12)	1547/197	1.95	1.14	Period>0.80 s	BF+SW
	B31 (13)	2765/3	0.24	1.01	Period<0.35 s	BF+SW
	B32 (14)	918/12	0.35	1.42	Sway Ratio>1.2	BF
	B34 (15)	9918/4	1.91	1.00	Period>0.80 s	BF
Y-Direction	B01 (16)	(2001)-4	0.27	1.08	Period<0.35 s	BF+SW
	B04 (17)	1034/557	0.49	1.27	Sway Ratio>1.2	BF
	B10 (18)	205/3	1.05	1.27	Period>0.80 s, Sway Ratio>1.2	BF+SW
	B14 (19)	2133/218	0.48	1.32	Sway Ratio>1.2	BF
	B16 (20)	2927/1	1.40	1.34	Period>0.80 s, Sway Ratio>1.2	BF+SW

Table 6.7 Continued

Direction	Building No	Plot/Parcel No	Period (s)	Relative Sway Ratio	Reason of Elimination	Structural System
Y-Direction	B21 (21)	5541/8	1.87	1.16	Period>0.80 s	BF+SW
	B25 (22)	7768/3	0.82	1.02	Period>0.80 s	BF+SW
	B26 (23)	876/515	1.16	1.24	Period>0.80 s, Sway Ratio>1.2	BF+SW
	B30 (24)	1547/197	1.75	1.53	Period>0.80 s, Sway Ratio>1.2	BF+SW
	B33 (25)	9886/13	0.32	1.13	Period<0.35 s	BF+SW
	B34 (26)	9918/4	1.43	1.23	Period>0.80 s, Sway Ratio>1.2	BF
	B37 (27)	10365/1	0.29	1.02	Period<0.35 s	BF+SW

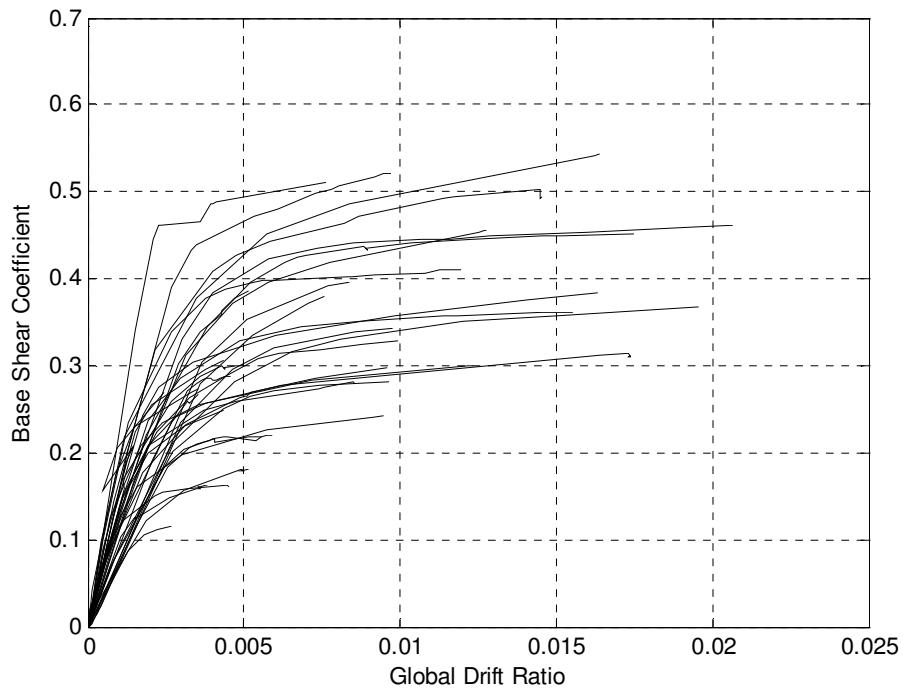


Figure 6.27. Capacity Curves Transformed into ADRS Format after the Removal of Outliers

At the end of the elimination process, the analysis proceeded with the remaining structural models given in Table 6.8. The structural parameters listed in the table are used for multiple regression analysis. In summary, out of 62 models, 27 structural models are eliminated by the technical and visual elimination scheme.

Table 6.8. The Structural Parameters of the Remaining Structures that are Compiled for Regression Analysis

Direction	Bldg. No	Plot/Parcel No	Lateral Strength Index (I_{SA}) (%)	Soft Storey Index (SSI)	Lateral Stiffness Index (I_{SI}) (m²x10⁻⁴)	Number of Storeys (n)
X-Direction	B03	10025/1	2.09	1.00	12.00	6
	B04	1034/557	1.61	1.00	5.10	6
	B05	1077/201	1.71	1.00	3.80	6
	B06	1358/5	2.32	1.00	7.10	5
	B11	2067/107	1.02	1.00	7.40	5
	B12	2069/229	1.18	1.00	4.50	7
	B13	2073/172	1.91	0.93	34.40	8
	B17	2928/4	2.16	1.00	7.00	5
	B18	376/34	0.99	0.98	2.80	8
	B19	490/35	3.69	1.00	24.60	5
	B24	632/8	1.81	0.76	2.20	5
	B28	(1993)-6	1.92	1.00	7.60	6
	B29	1068/63	3.63	1.03	17.80	7
	B33	9886/13	1.95	1.00	3.10	5
	B36	_(944)-4	2.31	0.53	5.30	4
B37	10365/1	0.76	1.00	2.80	5	
Y-Direction	B02	(2010)-4	1.76	1.00	3.10	4
	B03	10025/1	2.09	1.00	5.10	6
	B05	1077/201	1.71	1.00	2.00	6
	B06	1358/5	2.32	1.00	2.70	5
	B07	1415/4	1.74	1.00	1.80	5
	B08	1519/18	1.15	1.00	2.10	6
	B09	152/1	1.34	1.00	1.70	8
	B11	2067/107	1.02	1.00	0.90	5
	B12	2069/229	1.18	1.00	1.70	7
	B15	2571/24	1.49	0.81	2.70	4
	B19	490/35	3.69	1.00	7.40	5
	B20	496/14	2.16	0.67	1.60	5
	B22	557/11	1.68	0.83	1.70	5
	B23	6041/9	2.04	1.00	1.80	5
	B27	890/25	2.63	1.00	4.90	4
	B28	(1993)-6	1.92	1.00	8.60	6
B32	918/12	1.11	0.96	1.70	4	
B35	_(863)-6	2.24	1.43	6.60	6	
B36	_(944)-4	2.31	0.53	1.40	4	

Among the eliminated structural models, 26 of them are eliminated due to the technical reasons and only one of them is eliminated by the visual elimination scheme. The common features of all the eliminated structures are too high or low

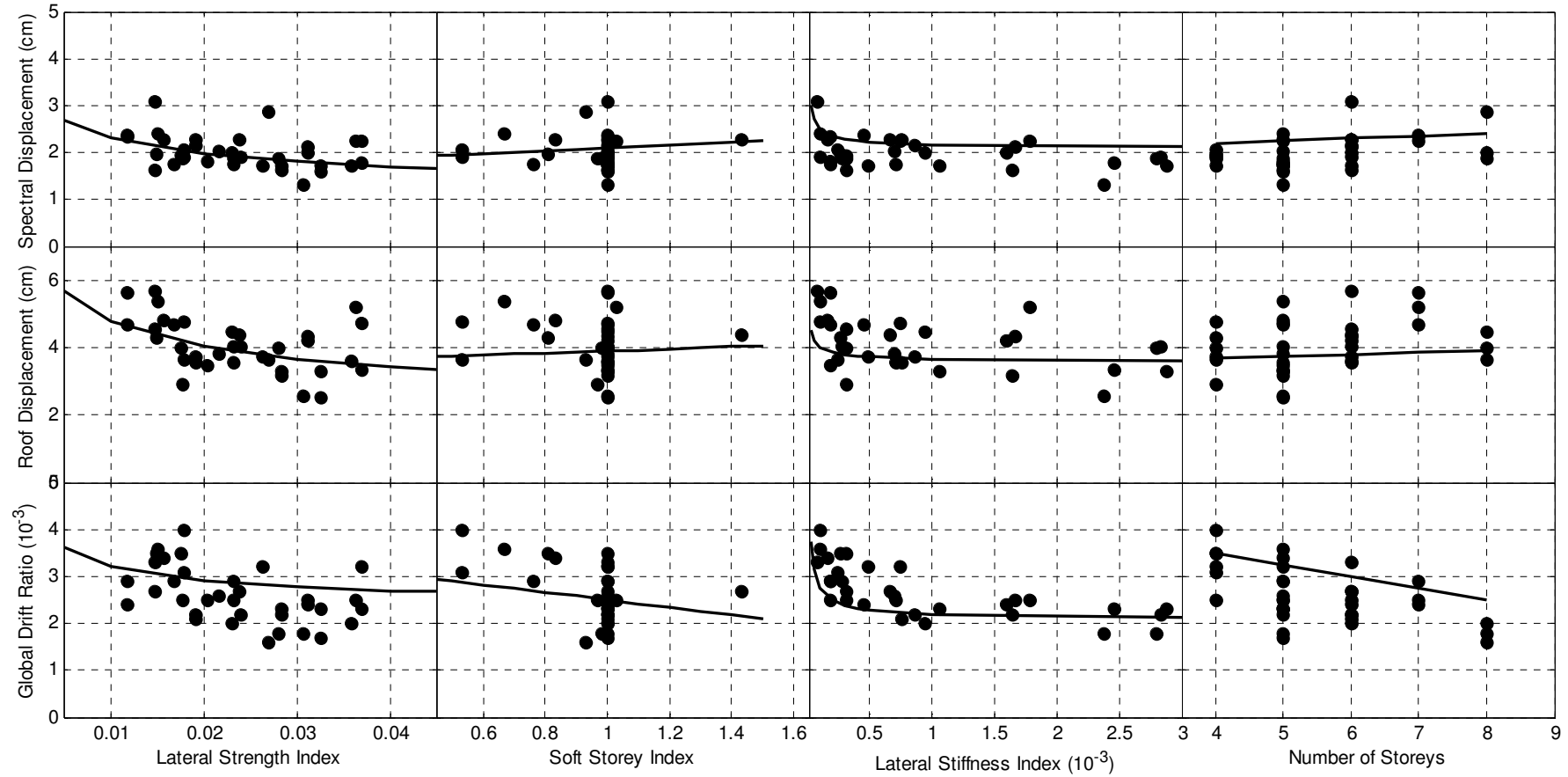


Figure 6.28. Variation of the Lateral Performance Values with Respect to the Functions Obtained by Sensitivity Analysis (Based on Refined Data, NEHRP Site Class C, (NEHRP Site Class C, Lateral Performances of 35 Structural Models for 475-year Return Period Earthquake are Presented)

fundamental periods that are generally accompanied by low ductility and high relative sway ratios within the roof floor due to the eccentric movements.

6.3.5. Reinvestigation of the Relationship between the Lateral Performances and Considered Structural Parameters

After the elimination of outliers, the relationship between the lateral performances of the actual structures and the structural parameters are reinvestigated. Obviously, the variances of the lateral performance values are largely reduced while the outliers are almost fully removed from the database as shown in Figure 6.28. After comparing the scaling of the roof displacement and global drift ratio obtained from sensitivity analysis and the observed scaling in Figure 6.28, it is clearly revealed that the scaling observed in the sensitivity analysis is verified with the scaling of the lateral performances of the sample data. In other words, as Figure 6.28 proves, the scaling characteristics of the roof displacement and global drift ratio of the sample data with the varying lateral stiffness and strength indexes, soft storey index and number of storeys is verified as the same by the sensitivity analysis. The variation of the lateral performances with respect to the spectral displacement is also provided in the figure.

Like roof displacement, the inversely nonlinear scaling is also observed for the global drift ratio for lateral strength and stiffness indexes. However, lateral performances in terms of global drift ratio are susceptible to the height for both parameters of soft storey index and number of storeys. While the positive scaling of roof displacement with the soft storey index and number of storey is observed, the global drift ratio negatively scales with the mentioned parameters.

6.4. Investigation of Relationship between Lateral Performance and Structural Parameters by Using Various Methods

6.4.1. The Procedure of Cross Validation

The refinement procedure is followed by the establishment of the cross validation scheme that would provide sound statistical results for the verification of the scaling of lateral performances. A two fold cross validation scheme is employed, which out of 35 structures, 28 are randomly selected as training sample to develop the LPPE and the remaining 7 structures are used for validation. The analyses conducted based on these two groups of structures are referred to as development and validation stages in the following sections. The selection of structures for training and

validation samples is performed randomly with a MATLAB program developed specifically for this study. Therefore, producing thousands of possible selection scenarios is possible for the cross validation scheme. The coefficients of the structural parameters will be determined by the development stage of the cross validation rounds while the power coefficients will be determined by a trial procedure due to the limited amount of data. Since the nonlinear scaling characteristics of lateral strength and stiffness indexes are easily identifiable and can be easily modeled, the range of power coefficients will be within a narrow range. For the sake of clarity and more vivid illustration, an incidence of this regression and validation scheme will be presented in the following sections.

The final coefficients of equations are obtained from several incidences of statistically acceptable cross validation rounds. For each structural parameter in the LPPE, 95% confidence interval is required for statistically acceptable coefficients. Then, final coefficients of LPPE will be determined by using the average of the coefficients that are obtained from the successful cross validation rounds. Detailed explanations are presented in the related sections.

6.4.2. Investigation of the Relationship between Lateral Performance and Structural Parameters by the Capacity Spectrum Method

CSM, as one of the commonly accepted lateral performance estimation method, estimates the lateral performances as spectral accelerations and spectral displacements at the considered ground motion level. In this study, lateral performances are calculated by using the procedure B of ATC-40 (1996).

6.4.2.1. Obtaining the Performance Points

Initially, the elastic response spectrum curves developed by PSHA procedures are modified to adapt these curves to the CSM procedures. The adaptation procedure largely depends on the site conditions and as ATC-40 (1996) prescribes, the conversion of elastic response spectrum is required in order to apply the methods presented in the document. Originally, in the development of the elastic response spectrum curves given in Figure 5.25, NEHRP B/C boundary condition is accepted as site condition. Therefore, considering the ATC-40 (1996) prescriptions for the use of site-specific seismic hazard maps, the elastic response spectrum curves developed for Eskisehir are modified with the application of site amplification factors to comply

with the requirements and reflect the effect of the site conditions, which is accepted as site class C.

The modification of the original response spectrum curves are performed by using the seismic coefficients of C_A and C_V , wherein C_A is defined by the acceleration of the ground at 0.30 s, and C_V is accepted as equal to the spectral acceleration value at the period of 1.00 s (ATC-40, 1996). Hence, the simplification of the elastic response spectrum curves is carried out by using two spectral acceleration values that are obtained for each response spectrum curve. As shown in Figure 6.29, the modified elastic response spectrum curves, which originally are generated for Eskisehir with the damping ratio of 5%, and associated with earthquakes that have 2%, 5%, 10%, 25% and 50% exceeding rates in 50 years, are presented. In the figure, the original elastic response spectrum curves are also presented in the background in light color.

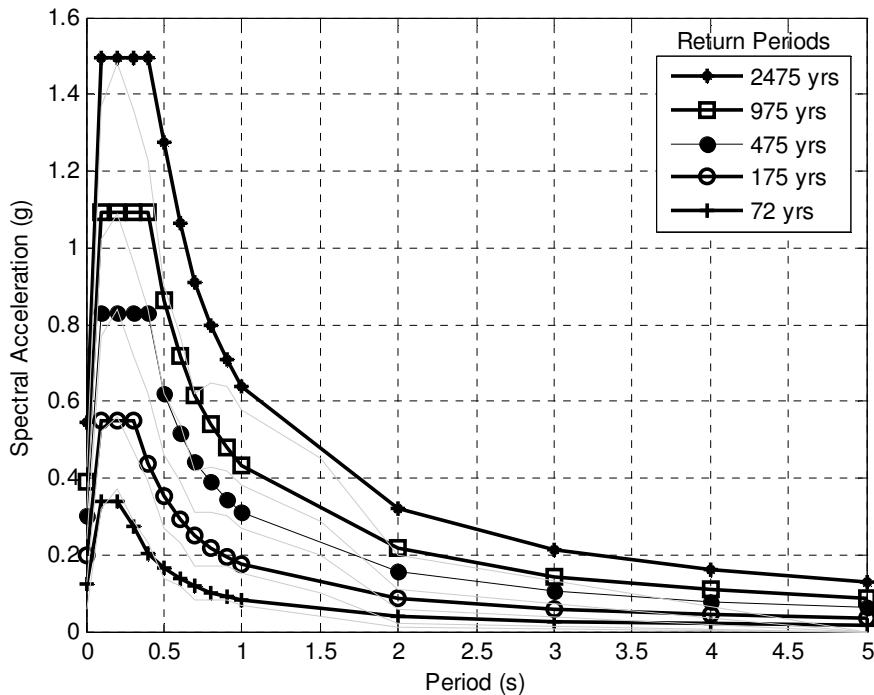


Figure 6.29. Modified Elastic Response Spectrum Curves for Eskisehir (NEHRP C, $V_s = 560$ m/s)

According to the procedure B of ATC-40 (1997), an iteration scheme is applied in order to find the performance point. The iterations are carried out to find the intersection point of the response spectrum curve and the capacity spectrum curves where the effective damping coefficients and the equivalent fundamental periods found by the procedure and the real values match.

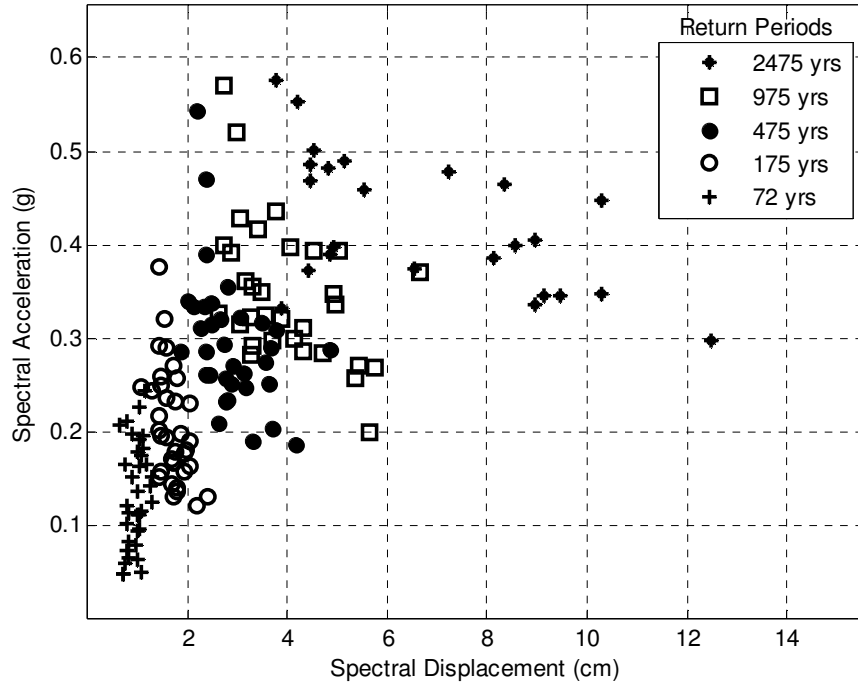


Figure 6.30. The Performance Values Obtained by the CSM with Different Earthquake Return Periods (35 Models are Presented)

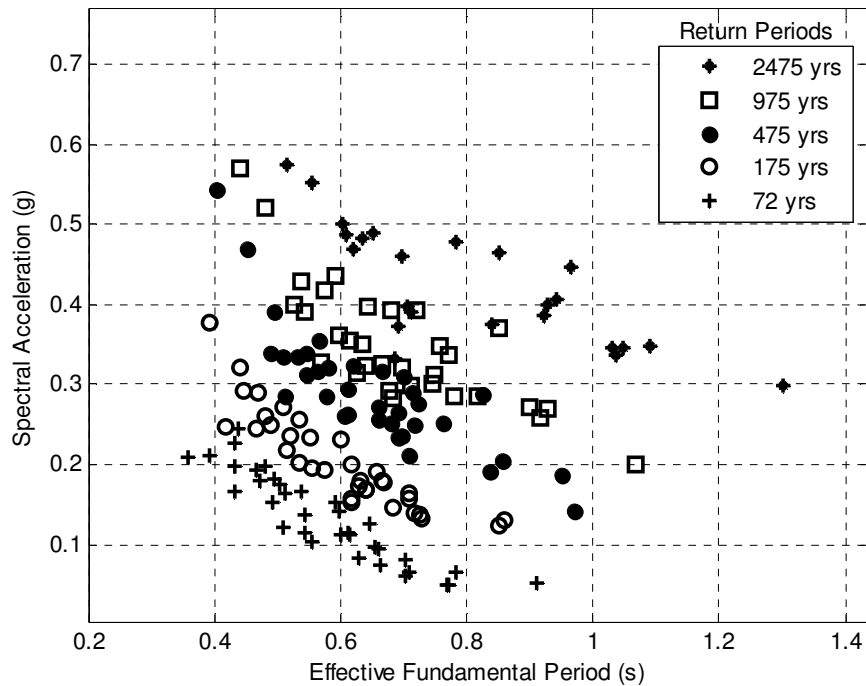


Figure 6.31. Equivalent Fundamental Periods of All Structures for Earthquakes with Different Return Periods

The lateral performances of the structures in terms of spectral accelerations, spectral displacement, equivalent period and effective damping ratios are generated by using

a MATLAB program, which was obtained from a research website (http://peer.berkeley.edu/~yang/ATC55_website, 2012).

After the analysis, different sets of data are obtained for each lateral response variable and for each response spectrum curve. As seen in Figure 6.30, the performance points for earthquakes with different return periods follow a recognizable pattern. In Figure 6.31, the distribution of the performance points with varying equivalent fundamental periods is provided. The performance points seem to cluster with the shorter return period of earthquakes, and the dispersion of values is observed as the return periods of the earthquakes increase.

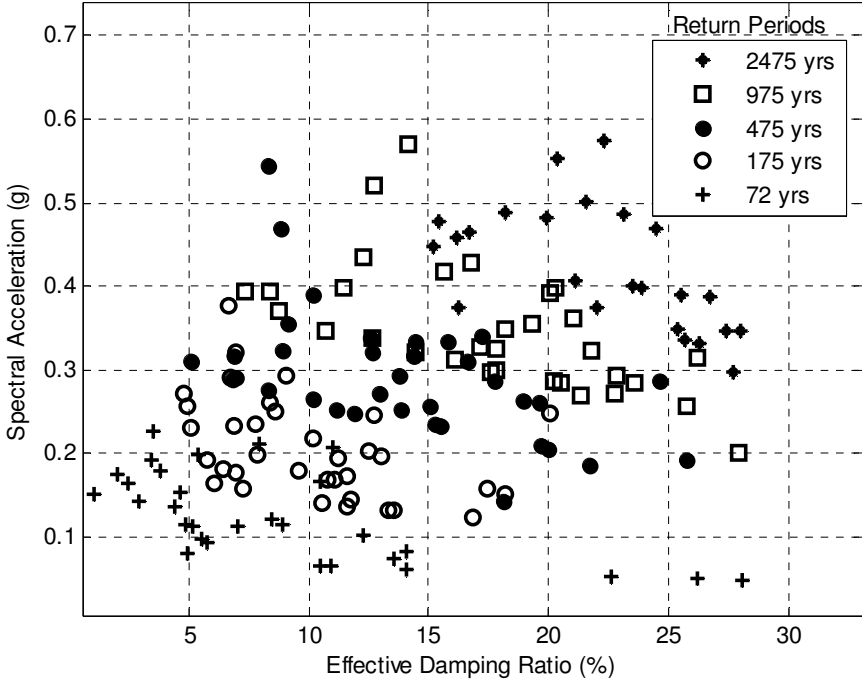


Figure 6.32. Effective Damping Ratios of All Structures for Earthquakes with Different Return Periods

Figure 6.32 presents the effective damping ratios with the lateral performance values of spectral acceleration. The effective damping ratios show a large variance for all the return periods. In the figures, it should be mentioned that, since there are a few number of performance points with unacceptable levels of damping ratios, the performance points with the elastic response spectrum curves of 2475-year return period earthquake are lesser than the performance points obtained for other earthquakes with lesser return periods.

6.4.2.2. The Comparison of Performance Points Obtained by Analysis and Proposed Equation

A statistically meaningful relationship is sought between the lateral performances as spectral displacements and the proposed structural parameters. To this end, several cross validation rounds are carried out as the different coefficients of LPPE are derived and validated for each single round. The values of lateral strength and stiffness indexes, soft storey index and the number of storeys of the randomly selected structures are regressed with the estimated spectral displacements by CSM and a LPPE is developed for that cross validation round. In the validation stage, the values of proposed parameters are used with the developed LPPE and the performance spectral displacements are predicted, and then these predicted spectral displacement values are compared with the performance spectral displacements of the same structures obtained by CSM. This cross validation procedure is repeated several hundred times. The application of the cross validation rounds yielded statistical quantities as correlation coefficients and significance test results at each of the single round.

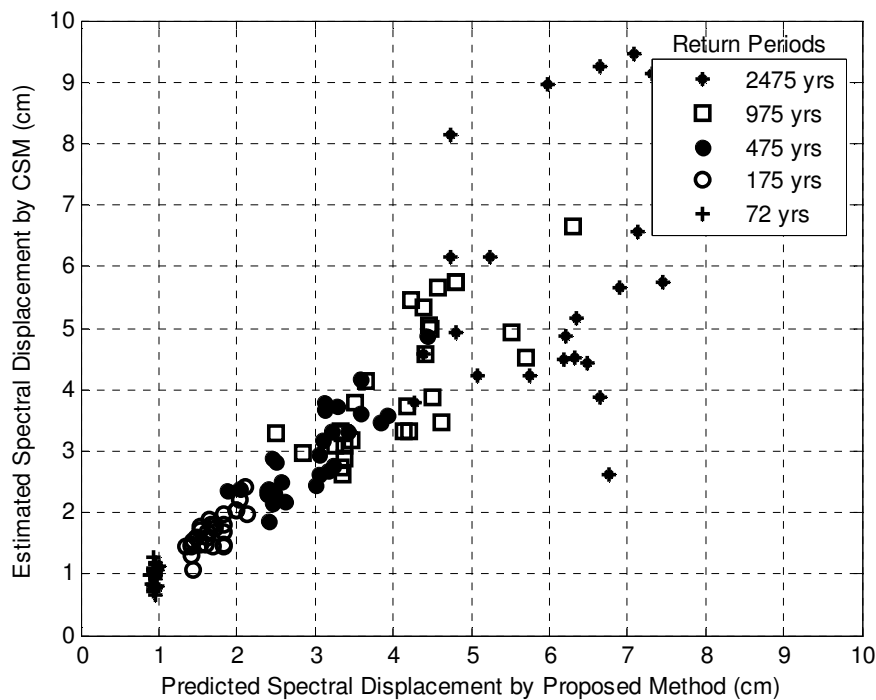


Figure 6.33. Original and Calculated Performance Points of Buildings for Earthquakes with Different Return Periods (28 points for each return period)

Figure 6.33 is the outcome of a randomly selected single round amongst the several cross validation rounds. The lateral performances in the figure show more than 84%

correlation between the estimated and predicted performance spectral displacements for response spectrum curve developed for 475-year return period earthquake. Similarly, for the rest of the performance points obtained by earthquakes with different return periods also show a pattern between the estimated and predicted spectral displacements. In addition, as presented in the upper subplot of Figure 6.34, the correlation values do not display acceptable level of relatedness for none of the considered earthquakes with different return periods.

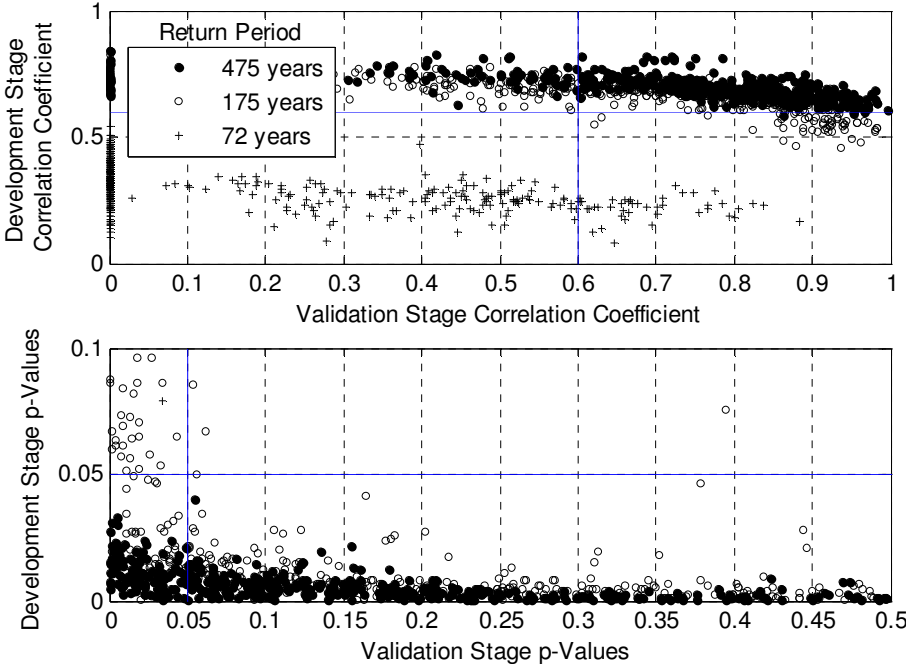


Figure 6.34. Calculated and Predicted Performance Points of Structures for Earthquakes with 72,175 and 475-year Return Period

Each dot in the figure represents a single round of cross validation, hence it should be mentioned that the figure contains results of 500 cross validation rounds, with each round representing a cross validation scheme with 28 structural models are randomly selected as training sample to develop LPPE and remaining 7 are used for validation. Despite the observed high correlation coefficients and acceptable significance results for 475-year and 175-year return period earthquakes, it is concluded that the lateral performance in terms of spectral displacements obtained by CSM cannot be predicted by using the proposed structural parameters of lateral strength and stiffness indexes, soft storey index, and the number of storeys. Due to the unsatisfactory results, further investigation is not performed by using the procedures outlined in this section.

6.4.3. Investigation of the Relationship between Lateral Performance and Structural Parameters by Using Interstorey Drift Ratios

The structures are subjected to lateral loads with dominant modal shape, and the pushover curves are generated. As expected, most of the structures responded in the dominant mode shape because of the higher modal mass participation ratios at these modes. All the structures showed a continuously increasing displacement from the base to the roof level regardless of whether shear or flexural type of displacement is dominant in the response. A few exceptions are observed that do not follow the same pattern, which could be explained by the sudden stiffness change in the consecutive storeys that occasionally exists between the basement and first storey.

Table 6.9. Maximum Interstorey Drift Ratio Results

Building Code	No of Storeys	X		Building Code	No of Storeys	Y	
		Max. Drift Ratio	Storey			Max. Drift Ratio	Storey
B02	4	0.76	1	B01	4	1.51	1
B03	6	1.60	1	B02	4	0.81	1
B04	6	1.09	1	B03	6	1.26	1
B05	6	0.99	2	B04	6	1.53	1
B06	5	1.27	1	B06	5	1.52	1
B09	8	1.19	2	B07	5	1.95	1
B10	6	1.30	3	B08	6	1.19	2
B11	5	1.50	1	B09	8	1.08	2
B12	7	1.31	1	B11	5	1.78	1
B13	8	1.43	2	B14	5	0.80	2
B14	5	0.81	2	B15	4	0.77	5
B15	4	0.63	2	B19	5	1.40	1
B16	6	0.89	2	B23	5	0.79	2
B17	5	1.38	1	B25	6	0.97	2
B18	6	1.46	2	B27	4	1.17	1
B19	5	1.43	1	B28	6	1.41	1
B20	5	1.35	2	B32	4	0.94	2
B24	5	0.63	3	B33	5	1.48	1
B26	5	0.86	4	B34	5	0.89	1
B28	6	1.71	1	B35	6	1.08	1
B31	4	1.53	1	B37	5	1.05	1
B32	4	0.70	2				
B33	5	1.60	1				
B36	4	0.74	2				
B37	5	1.47	1				

Table 6.9 presents the maximum interstorey drift ratios in both directions and the storey where the maximum drift is observed. The drift ratios are generally less than 1.5% except for a few outliers.

The cross validation procedure is applied by using all the maximum interstorey drift ratios. The same form of equation developed by the sensitivity analysis is employed in the cross validation procedure. The calculated and the predicted interstorey drift ratios are plotted for the assessment as shown in Figure 6.35. In the figure, it is clearly shown that the attempt to correlate the structural parameters with the maximum interstorey drift ratios is not successful. Thus, it is, concluded that lateral performance in terms of maximum interstorey drift ratios cannot be modeled with the proposed structural parameters. As a result, no further inquiry is launched in relating the maximum interstorey drifts to the structural parameters.

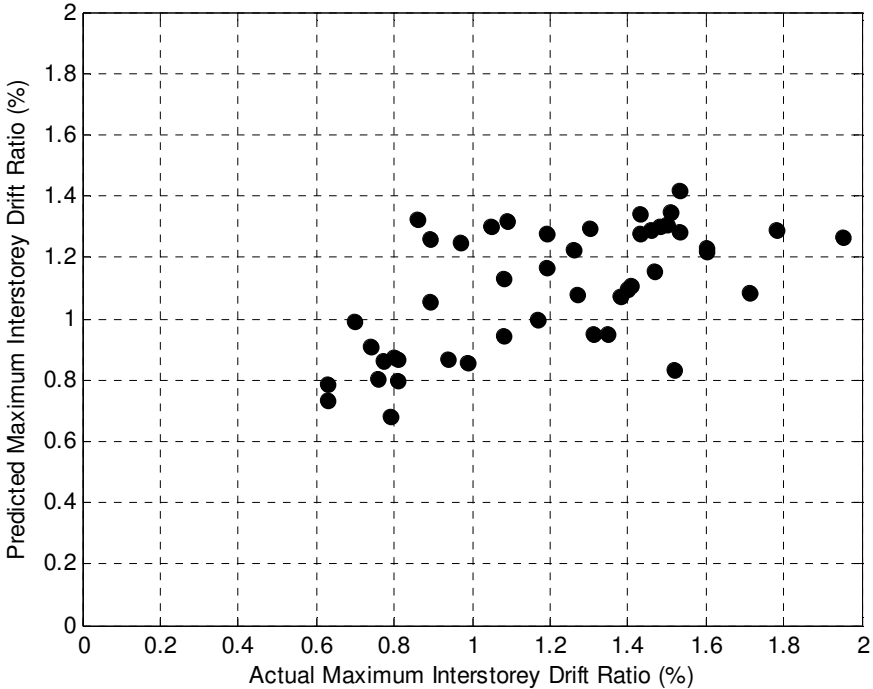
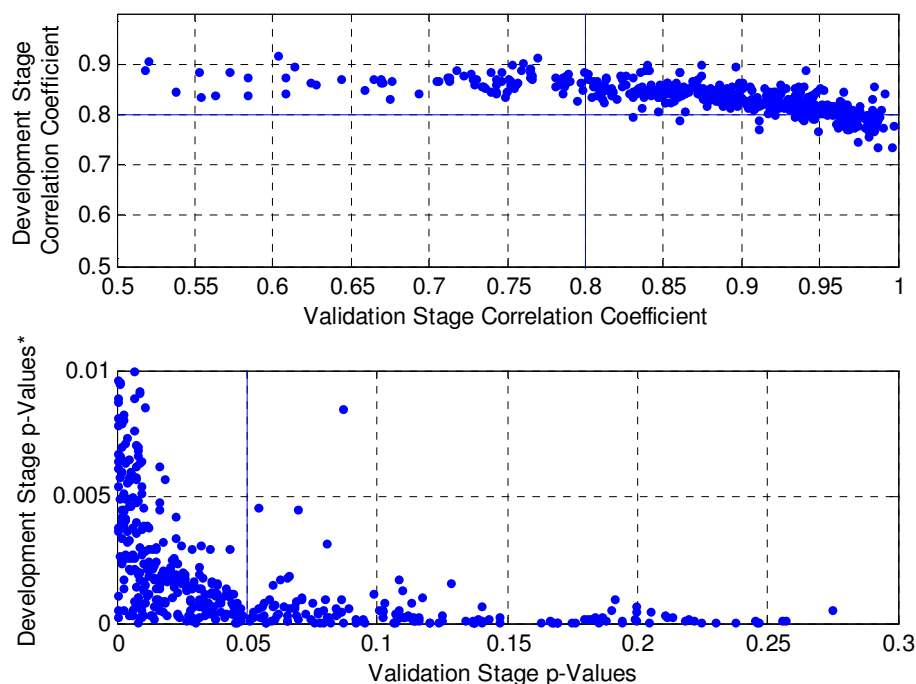


Figure 6.35. The Actual and Estimated Maximum Interstorey Drift Ratios (56 Models Presented)

6.4.4. Investigation of Relationship between Lateral Performance and Various Structural Parameters by Using Displacement Coefficient Method

The DCM is used to obtain the target or roof displacements. The calculations are performed by using adapted MATLAB programs that were obtained from a research website (http://peer.berkeley.edu/~yang/ATC55_website, 2102). The roof

displacements are calculated by using the elastic response spectrum curves developed for earthquakes of 2%, 5%, 10%, 25%, and 50% probability of exceeding in 50 years and for immediate occupancy, life safety, and collapse prevention limit states. The elastic response spectrum curves developed in chapter 5 are modified by using the suggested site amplification factors in order to amplify the ground motion amplitudes for site class C and these adjusted elastic response spectrum curves are used to estimate the roof displacements. These roof displacements are then converted to the global drift ratios and then the procedures of cross validation are repeated. As a result of cross validation, sets of correlation coefficients and significance test results are obtained. For earthquakes with return periods of 2475 and 975 years, some of the structures failed before reaching to the computed roof displacements. Hence, only roof displacements calculated by using response spectrum curves developed for earthquakes with return periods of 475, 175 and 72 years.



* Due to very low t-test results, p values are scaled to display t-test results of validation stage

Figure 6.36. Correlation Coefficients Computed for the Development and Validation Stages and Overall Significance Test Results in terms of p Values (500 Validation Rounds, 475 year Return Period Earthquake is Considered)

The concentration of the correlation coefficients of development and validation stages is clearly identified in Figure 6.36, which was created by using the results of cross validation rounds applied to develop a relationship between the structural

parameters and global drift ratios obtained for 475-year return period earthquake. Almost all the correlation coefficients are above 0.80 for the development stage with an insignificant number of correlation coefficients staying below 0.8. In the figure, the concentrated area of correlation coefficients at the right side of the upper plot is bending towards lower values while the validation stage coefficients are getting higher. This phenomenon could be explained by the likelihood of selecting the best-correlated structures of the sample in the validation stage thus lowering the chances of forming a more correlated group for the development stage. The significance tests are conducted automatically by the MATLAB program for each round of cross validation. The distribution of significance test results is presented in the bottom plot of Figure 6.36. The clustering of the significance test results within the desired levels is evidence to the existence of a relationship between the global drift ratios and the proposed structural parameters. Consequently, the assumptions about the relationship between the lateral performances and the structural parameters are verified. The same calculations are repeated for life safety and collapse prevention cases for earthquakes with different return periods. The analysis for life safety and collapse prevention cases yielded different parametric coefficients but with almost the same degree of correlation and significance test results. The results are not shown for space limitations.

Figure 6.37 presents a single round of cross validation by using the lateral performances in global drift ratios estimated by DCM and the predicted drift ratios by the proposed equation for earthquakes with different return periods. For the selected round, the correlation coefficient between the estimated and predicted target displacements for the development stage stood above 0.80 with p values well below 0.01 for each return period earthquake. In the same round of cross validation, the validation is performed by comparing the estimated global drift ratios by DCM and the predicted global drift ratios by the proposed method. The estimated and predicted global drift ratios for the validation stage are presented in Figure 6.38. The high correlation coefficients, which stood above 0.90 accompanied by the low significance test results, which are below 0.05, encourage for further investigation. Considering the statistical results obtained in Figure 6.36, the fact that a relationship exists between at least one of the structural parameters and lateral performances is

not enough by itself to prove the validity of a relationship. The significance of individual parameters must be investigated for each validation round. Therefore, in each validation round the individual parameters are subjected to the significance tests, which yielded the p values obtained by significance tests performed at each round.

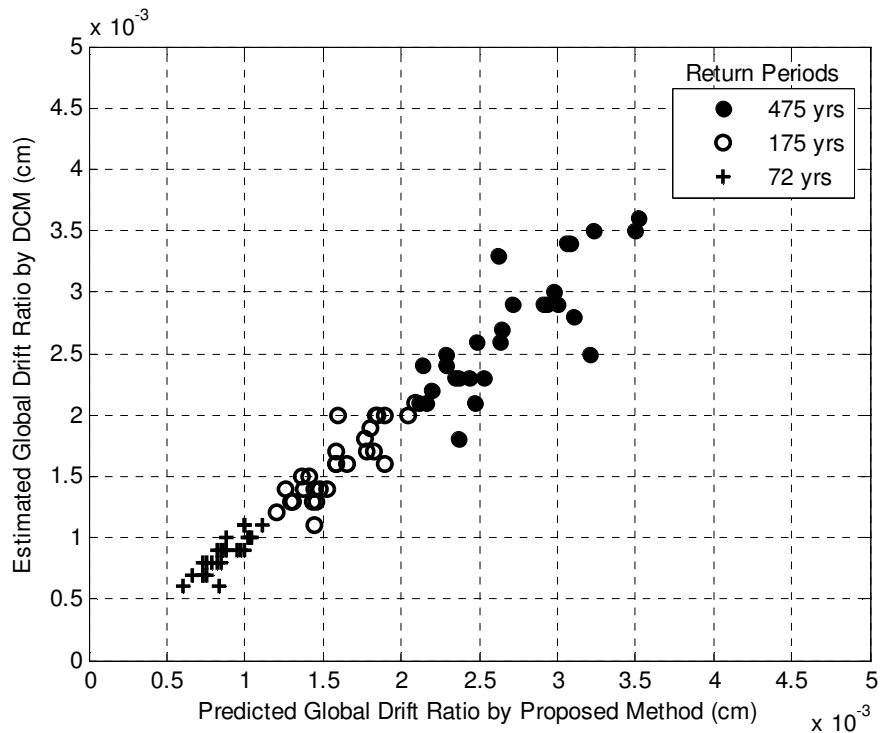


Figure 6.37. Estimated and Predicted Global Drift Ratios for Immediate Occupancy Level Corresponding to Earthquakes with Different Return Periods

In Figure 6.39, the results are provided for each response spectrum curve developed for Eskisehir, and each parameter is shown on the lateral axes. Obviously, lateral strength index and soft storey index performed poorly in significance test while other parameters perform within the desired limits of significance tests. Despite the undesired results of the significance tests, it should be mentioned that, it is a well-known fact that the statistical parameters are automatically influenced by the sample size; therefore; the significance test results could be improved by increasing the size of the sample. Moreover, the refinement procedure of the database could be reviewed for better formation of a more uniform sample. In conclusion, it is confirmed that there is a relationship between the global drift ratios and at least one the proposed structural parameters with several prospects for the improvements.

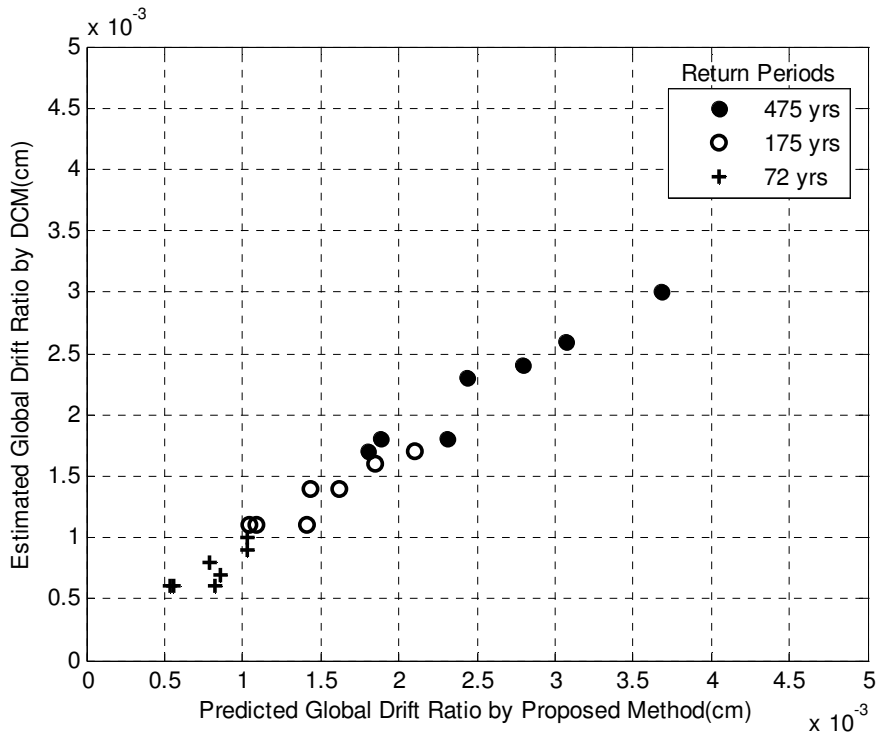
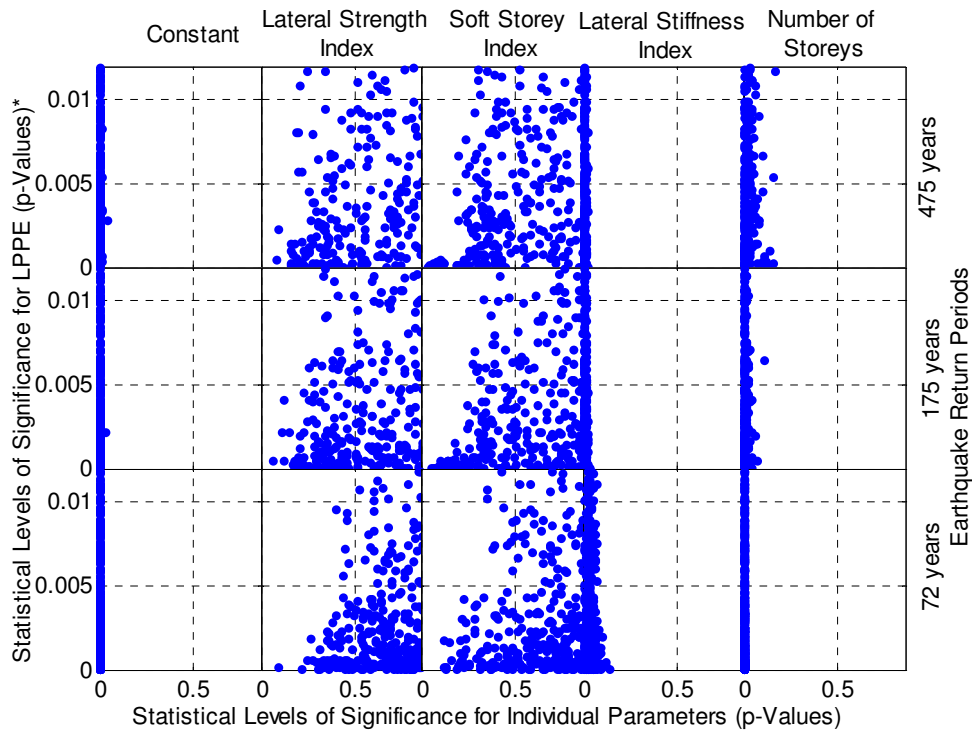


Figure 6.38. Estimated and Predicted Global Drift Ratios for Immediate Occupancy Level Corresponding to Earthquakes with Different Return Periods



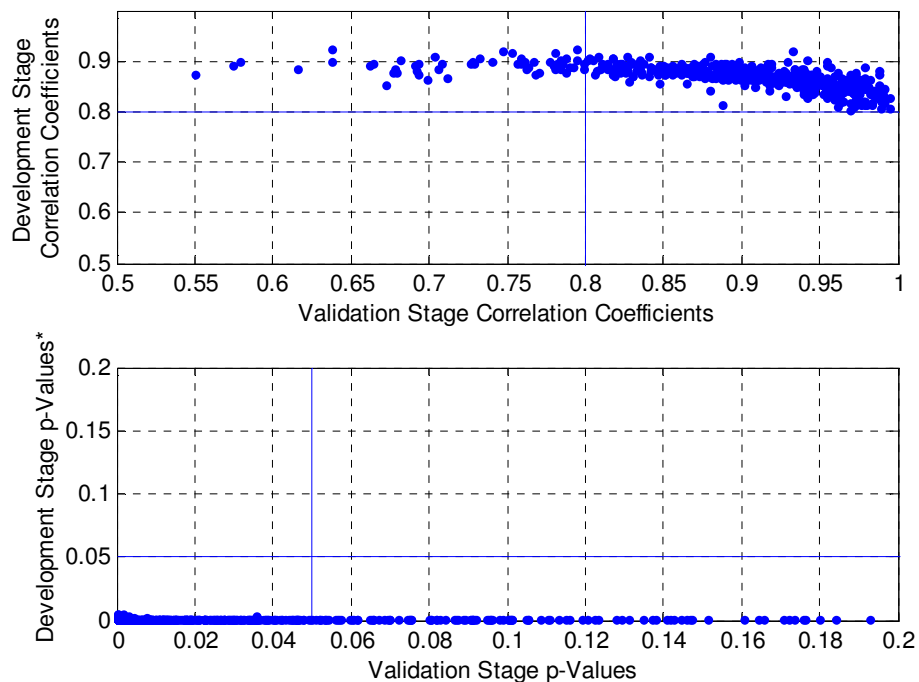
* Due to very low t-test results, p values are scaled to display t-test results of individual parameters

Figure 6.39. Significance Test Results of Individual Structural Parameters for Immediate Occupancy Level

Moreover, knowing that a relationship exists between the structural parameters and the lateral performance, with the support of the physical background of the claims and the emerging patterns after the sensitivity analysis, the distribution of the significance test results could be investigated.

6.4.5. Investigation of the Relationship between Lateral Response and Structural Parameters by Using Improved Displacement Coefficient Method

IDCM, or displacement modification method, is proposed by FEMA-440 (2005) to replace the DCM. The coefficients of DCM are revised, and site conditions are added to the estimation function, which are detailed in 4.5.4. By using the response spectrum curves developed for Eskisehir and the structures listed in Table 6.6, the performance global drift ratios are calculated. The site class is accepted as C according to NEHRP specifications and the corresponding site amplification factors are applied to obtain the elastic response spectrum curves for NEHRP C site class.



* Due to very low t-test results, p values are scaled to display t-test results of validation stage

Figure 6.40. Correlation Coefficients Computed for the Development and Validation Stages and Overall Significance Test Results in terms of p Values (500 Validation Rounds, 475 years Return Period)

The calculated roof displacements by using response spectrum curves developed for earthquakes with 2475 and 975-year return periods are bigger than the ultimate displacements obtained by the structural analysis. Therefore, only, roof

displacements calculated by using response spectrum curves developed for earthquakes with return periods of 475, 175 and 72 years are considered.

After global drift ratios are obtained for each structural model and for each response spectrum curve, cross validation scheme is applied as explained in 6.4.1. The procedure of cross validation is repeated for five hundred times in order to verify the validity of the claims. In addition, the procedure is applied for each response spectrum curve that is developed for earthquakes with different return periods. The results of these cross validation rounds are presented in Figure 6.40 for 475-year return period earthquake, as correlation coefficients for development and validation stages are provided in the upper plot while the significance test results of these rounds are given in the bottom plot. The coefficients of the LPPE are derived by averaging the coefficients obtained by the statistically acceptable cross validation rounds with complying correlation coefficients and acceptable significance test results.

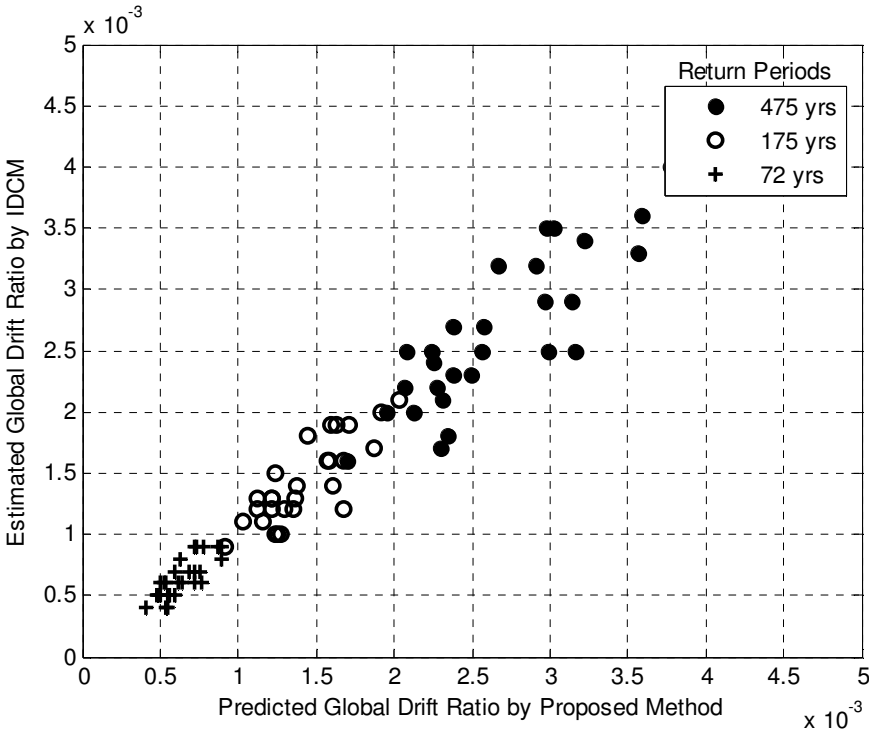


Figure 6.41. Estimated and Predicted Global Drift Ratios by IDCM Method (Development Stage)

Figures 6.41 and 6.42 present the estimated and predicted global drift ratios of a single round of cross validation that is randomly selected among the validation rounds.

The global drift ratios estimated by the IDCM and predicted by the developed LPPE for each round of the development stage is given in Figure 6.41. In the development stage, the coefficient of correlation between the estimated and predicted global drift ratios for 475-year return period earthquake is calculated as 0.85 with associated significance test result less than 0.01. As the development stage regression analysis indicates a relationship, the validation stage results confirm the relationship with the correlation coefficient higher than 0.90 and with significance test result less than 0.01. Figure 6.42 was prepared to present the estimated and predicted global drift ratios in the validation stage.

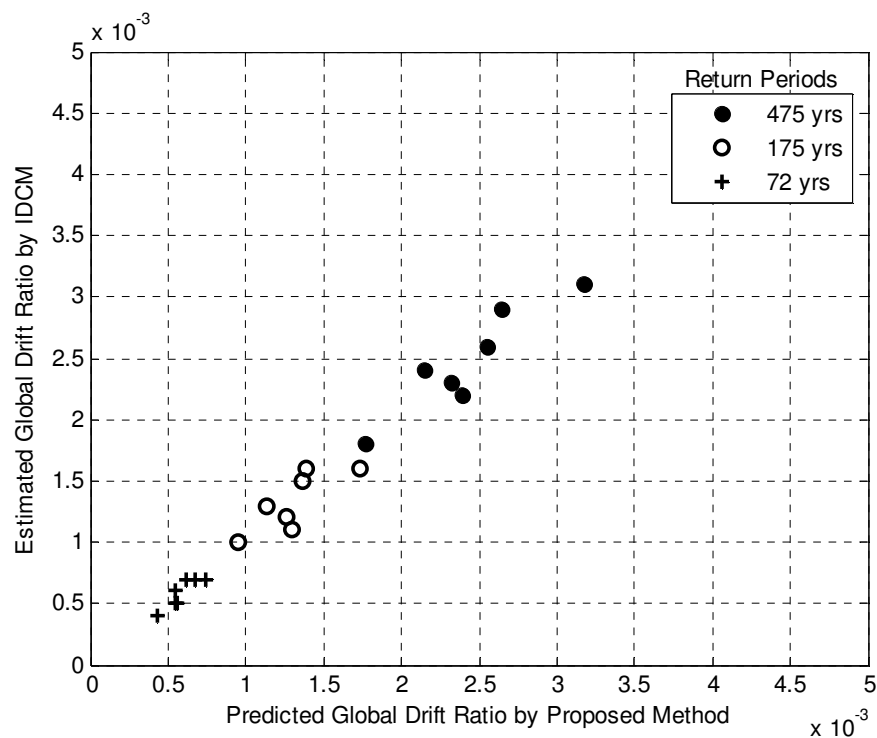
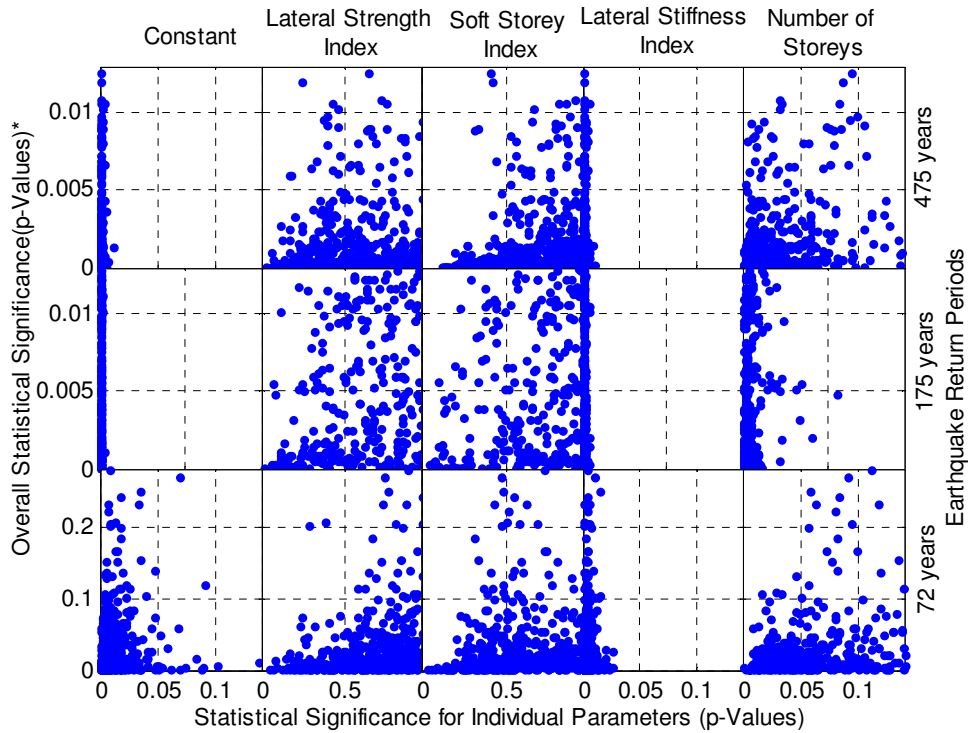


Figure 6.42. Estimated and Predicted Global Drift Ratios by IDCM Method (Validation Stage)

One of the prerequisites of the effectiveness of the proposed method is to conduct significance tests of each parameter. Figure 6.43 verifies whether each coefficient of the LPPE is statistically meaningful. The test results for the p values are clustered between 0 and 0.05 with the parameters of constant term of the equation, lateral strength index, the number of storeys for each considered earthquake. The p values of lateral strength index and soft storey index vary for the considered earthquakes.



* Due to very low t-test results, p values are scale to display t-test results of individual parameters

Figure 6.43. Significance Test Results of Individual Structural Parameters

Knowing the physical background of the claims and the emerging patterns after the sensitivity analysis and together with the performance of the structural models with the scaling characteristics obtained by sensitivity analysis, the distribution of the significance test results could be questioned for both IDCM and DCM results. Since multi-collinearity is an issue in the regression analysis, and the significance test results are very prone to the mentioned issue, the significance test results of each individual parameter might be attributed to this issue. Moreover, knowing that the results of the significance tests could be improved by increasing the sample size, the same significance test results of each individual parameter could also be attributed to the small sample size. In the end, it is decided to adopt the developed LPPE for further use.

As the proposed method proved to be promising, the selection of the coefficients from amongst the several set of coefficients generated by the validation rounds remains an issue. Generally, when a two fold cross validation scheme is applied, the coefficients of the validation round with the highest correlation coefficient are selected. However, it is a fact that the most statistically meaningful validation rounds with highest correlation coefficients might not be associated with the most successful

development stage correlation coefficients. This is clearly observed in the validation rounds as presented in Figure 6.40. In the figure, the validation stages with higher correlation coefficients are not associated with the highest development stage correlation coefficients.

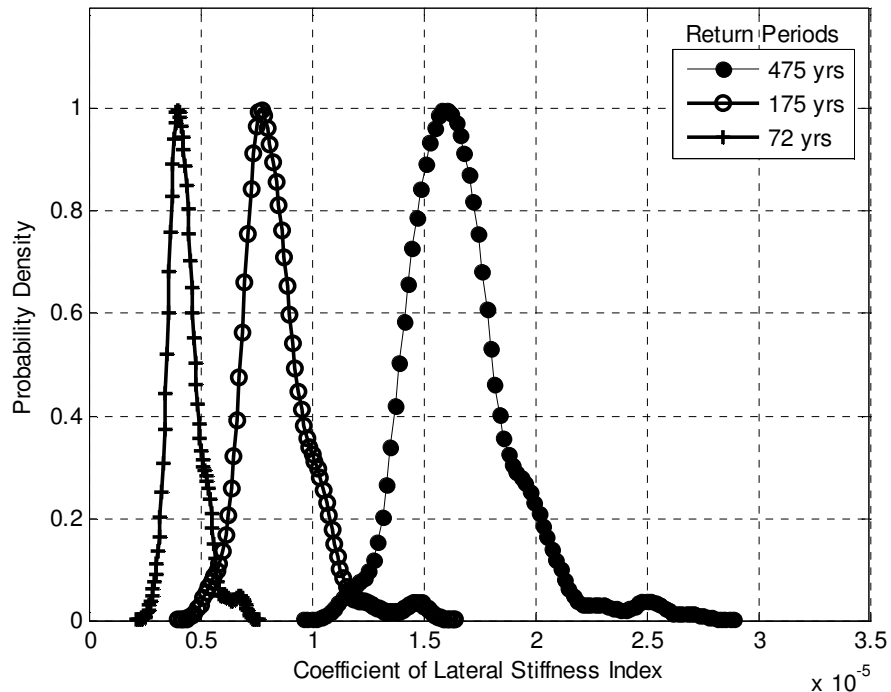


Figure 6.44. Distribution of Coefficients for Lateral Stiffness Index (Distribution of Values Obtained by 291 Validated Rounds of Cross Validation Scheme out of 500)

Therefore, for the selection of the coefficients of the LPPE, firstly, the distribution characteristics of the coefficients of the successful rounds must be investigated. Figure 6.44 illustrates the distribution of the coefficients that are derived for the lateral stiffness index. The coefficients are derived for each response spectrum curve that was developed by using earthquakes with different return periods. Hence, for each structural parameter, five sets of coefficients are derived for each response spectrum curve. Considering the characteristics of the distribution of all the coefficients, which are similar to the distributions in Figure 6.44, the mean of the coefficients that are obtained by the successful cross validation rounds is preferred to the coefficients obtained by only a single round. Hence, by the introduction of distribution characteristics of the computed coefficients, the variability of the coefficients in terms of standard deviation could be incorporated into the LPPE too.

Consequently, the mean of the coefficients of statistically acceptable cross validation rounds are assigned to form the LPPE. The resultant mean and standard deviations of the coefficients for each response spectrum curve are compiled in Table 6.10. The standard deviations could be employed in the LPPE to set ranges of lateral performances if desired. Out of 500 validation rounds performed for the cross validation, 291 statistically validated rounds are used to derive the mean and standard deviation of the coefficients of LPPE.

The type of scaling of the global drift ratios with each individual parameter is crucial for the verification of the reliability of coefficients in reflecting the real physical behavior. A close examination of the coefficients in Table 6.10 reveal that the lateral performance in terms of global drift ratio correlates positively with the parameter of the lateral stiffness index while it does so negatively with the parameters of lateral strength index, the number of storeys and soft storey index. According to the sensitivity analysis, the global drift ratios negatively scale with the parameters of number of storeys and soft storey index while positively scale with lateral stiffness index as expected. However, with lateral strength index, the global drift ratios negatively scale which is not consistent with the sensitivity analysis results. This inconsistency between the scaling of global drift ratios must be explained in order to prove the validity of the proposed LPPE.

Table 6.10. Mean and Standard Deviations of Coefficients of Lateral Performance Prediction Equation for Each Response Spectrum Curve (291 Validation Rounds)*

Return Period**	a ₁	σ _{a1}	a ₂	σ _{a2}	a ₃	σ _{a3}	a ₄	σ _{a4}	a ₅	σ _{a5}	σ _{all}
	(x10 ⁻⁵)										
475	301.17	30.58	-4.21	4.37	-5.32	23.16	1.66	0.23	-15.07	2.86	0.01
175	160.56	19.74	-1.70	2.84	-4.20	15.82	0.84	0.15	-7.99	1.54	0.00
72	58.19	8.35	-0.37	1.34	6.35	6.83	0.43	0.07	-3.46	0.86	0.00

* a₆ and a₇ is obtained as -0.5 by trial and error method
 ** Return periods of the considered earthquake in the derivation of the coefficients

To investigate this inconsistency, the values of lateral strength index, lateral stiffness index, soft storey index and number of storeys are classified into subintervals and the lateral performances estimated by IDCM for an earthquake with 475-year return period are plotted with respect to the mentioned structural parameters.

Since the distribution of the lateral strength index and the estimated displacements have a very significant effect on the outcome of the regression analysis, the distribution of the lateral performances with respect to the lateral strength indexes of

the structures in the sample is examined. As a result of examination of the distribution characteristics of the estimated global drift ratios in Figure 6.45, it is observed that, there is a strong tendency that the global drift ratios decrease with increasing lateral strength index. However, it should be known that, randomly selected values might not yield the expected scaling characteristics. Adding on top of that, the existence of a parameter that models the inverse nonlinear scaling of the lateral performance values complicates the regression analysis more.

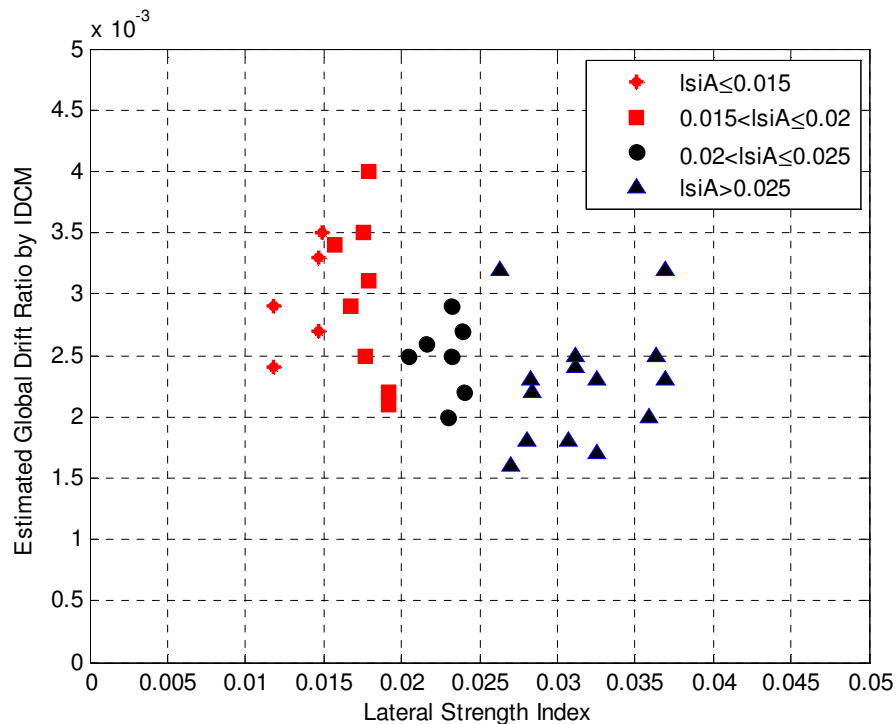


Figure 6.45. Distribution of the Estimated Global Drift Ratios by IDCM with Respect to Lateral Strength Index

The aforementioned issues in the regression analysis challenged the development of LPPE and have a potential to create a bias in the coefficient estimations. These issues also strongly influence the derived coefficients for lateral strength index. As shown in Figure 6.46, the distribution of the derived coefficients for lateral strength index display varying mean and standard deviations. Both negative and positive coefficients are obtained as a reflection of the aforementioned issues.

Similarly, the relationship between the soft storey index and the global drift ratios is evaluated. The distribution of soft storey indexes and the lateral performance might follow the expected pattern as shown in Figure 6.47. It can be clearly concluded from the figure that as the soft storey index increases the estimated drifts by IDCM

decreases. Hence, the LPPE successfully reflects the type of scaling of lateral performances with the soft storey index.

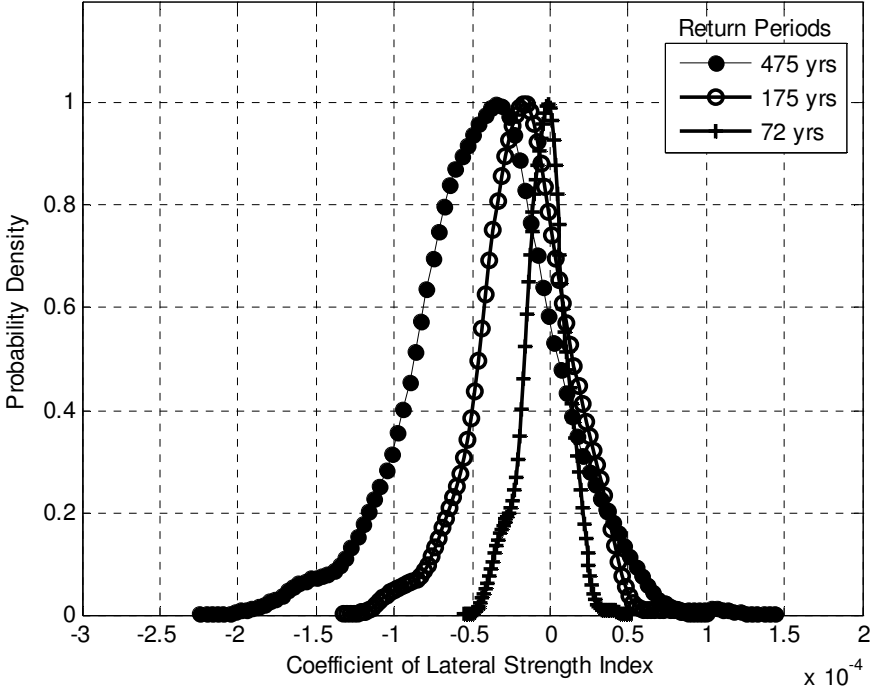


Figure 6.46. Distribution of Coefficients of Lateral Strength Index (291 Validated Rounds of Cross Validation Scheme out of 500)

Similar to the lateral strength index, modifying lateral stiffness index of a structure causes a significant shift in the fundamental period. A decrease in the lateral displacements and drifts are expected when the lateral stiffness index increases as shown in Figure 6.48. The relationship between the lateral stiffness index and the nonlinear scaling of the global drift ratios captures attention in Figure 6.48. Obviously, a pattern emerges between the lateral stiffness index and the estimated global drift ratios, which justifies the obtained scaling characteristics in the sensitivity analysis. It is strongly expected that, with the increasing number of storeys, the target or roof displacements automatically increase since the height increases proportionally with the number of storeys. Even with a few cases where this assumption is not true, the distribution of the number of storeys with the estimated and predicted target displacements follow this assumption. However, as presented in Figure 6.49, the global drift consistently decreases as the number of storey increases, which indicates that the slope of roof displacement versus the number of storeys is less than unity as expected.

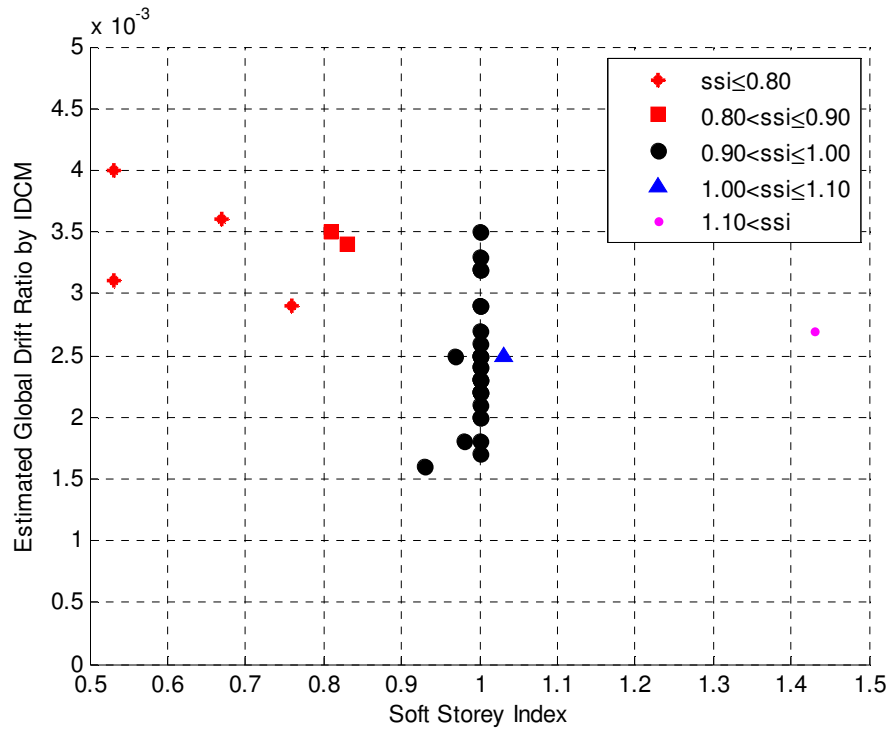


Figure 6.47. Distribution of the Estimated Global Drift Ratios by IDCM with Respect to Soft Storey Index

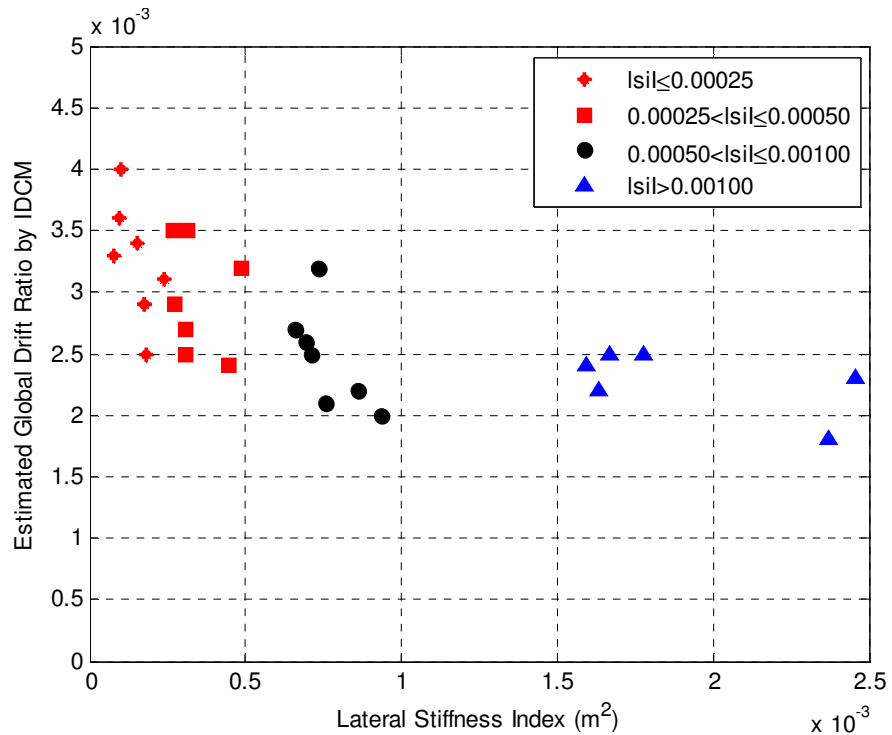


Figure 6.48. Distribution of the Estimated Global Drift Ratios by IDCM with Respect to Lateral Stiffness Index

In the end, it is concluded that the distribution characteristics of the estimated global drift ratios with respect to the structural parameters are determining factors in the development of LPPE. Except for the lateral strength index, the scaling of the structural parameters with the lateral performance is very well reflected in the LPPE.

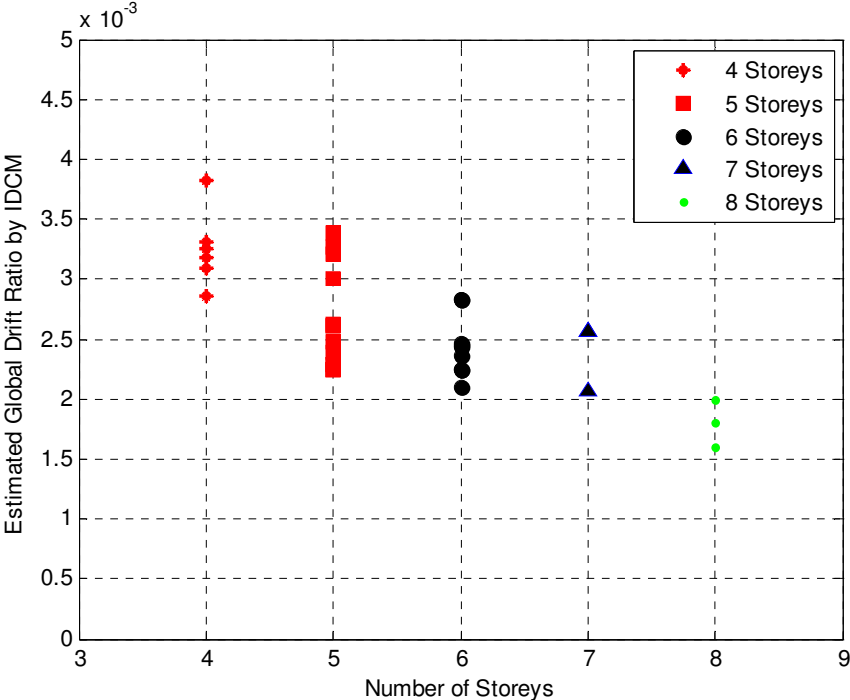


Figure 6.49. Distribution of the Estimated Global Drift Ratios with Respect to Number of Storeys

The issue of scaling of global drift ratio with respect to the lateral strength index, which also could be originated from the multicollinearity issue must be emphasized in addition to the low significance test results of lateral strength index and soft storey index. However, considering the physical background information that explains the scaling of the global drift ratio with respect to the lateral strength index and the results of the sensitivity analysis, which strongly indicates the relationship, the developed LPPE could be a valid one. It should be noted that the complex relationship between the lateral strength and stiffness indexes could yield different results with a different sample, which is dominated by either of the structural parameters in response.

6.4.5.1. Investigation of the Relationship between the Lateral Response and Structural Parameters According to the Adjusted LPPE

In section 6.1.5, the multicollinearity issue is briefly discussed and the potential undesirable effects are listed. It is mentioned that correlation between the parameters of developed equation generally cause a loss of meaning in the significance tests and the sign of the coefficients of the parameters would be usually opposite. This observation is proven true in the case study performed to develop a LPPE. Moreover, the soft storey index is also removed from the equation since the significance test results are not satisfactory. Consequently, the equation 6.9 could be rewritten to model this relationship.

$$\delta_{GDR}(lsiI, n) = f(lsiI) + f(n) + \sigma \quad (6.10)$$

where δ_{GDR} represents the performance global drift ratio for the considered response spectrum. In the open form the equation 6.10 could be rewritten as

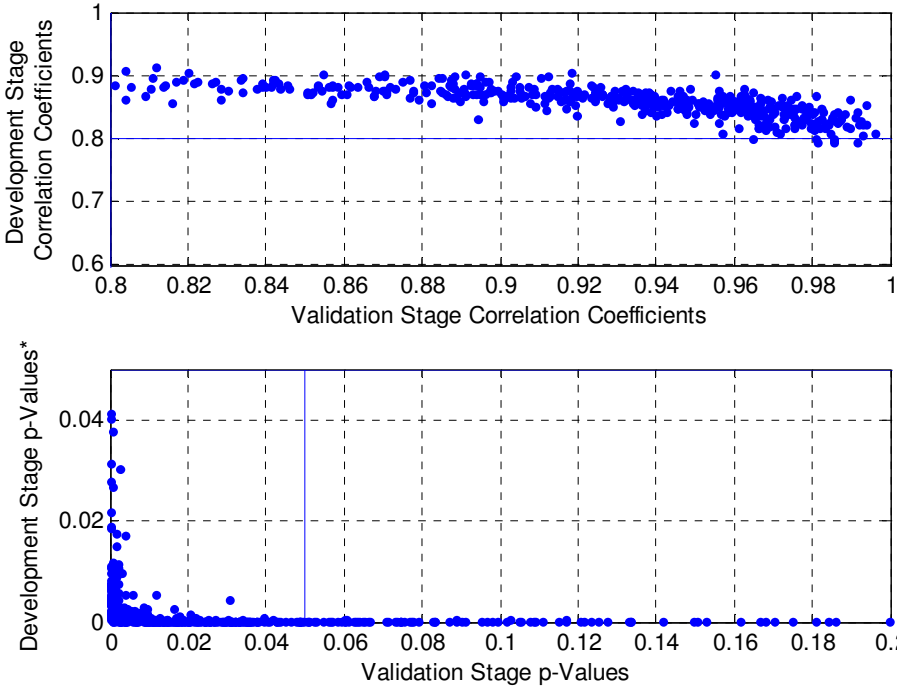
$$\delta_{GDR}(lsiI, n) = a_1 + a_4 lsiI^{a_7} + a_5 n + \sigma \quad (6.11)$$

As expected, the high correlation coefficients associated with the very low significance test results (p values) in Figure 6.50, indicate the existence of a very strong relationship between the lateral performances and the structural parameters in equation 6.10, namely lateral stiffness index and number of storeys. It also proves the success of the adjusted LPPE in modeling the sample data.

Moreover, the significance test result for individual structural parameters in Figure 6.51, also support the success of this adjustment. It can be clearly claimed that both the parameters of lateral stiffness index and number of storeys are highly correlated with the estimated global drift ratios. However, this doesn't mean that the lateral performance of the structures can be predicted by just using these two parameters. It was stated earlier that if the sample size is increased, a definite improvement of the significance test results could be observed. Moreover, with improvements in the formation of LPPE, which might contain both lateral stiffness and lateral strength indexes without creating a multicollinearity issue, might perform better in modeling the lateral performance of the structures.

The coefficients of the LPPE are derived with the application of the same procedures as the mean and standard deviation of the statistically successful cross validation rounds are assigned as the coefficients. The presented coefficients of the adjusted

LPPE display consistent behavior with the results of the sensitivity analysis and the scaling of lateral performances of original structures in the sample.



* Due to very low t-test results, p values are scaled to display t-test results of validation stage

Figure 6.50. Distribution of Number of Storeys and the Estimated and Predicted Target Displacements

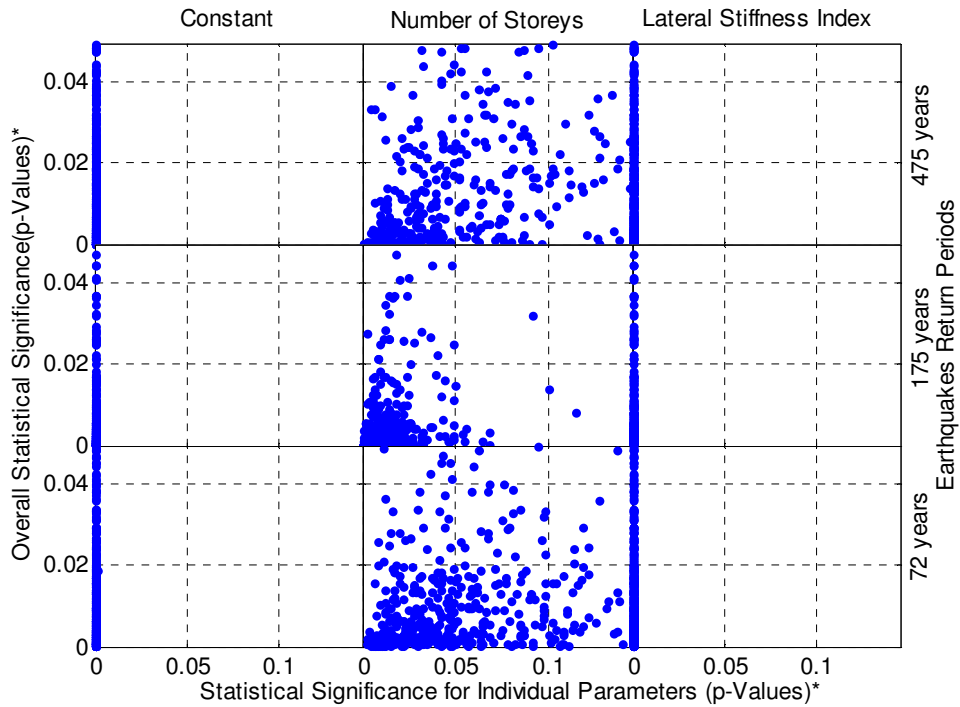
Table 6.11. Mean and Standard Deviations of Coefficients of Lateral Performance Prediction Equation for Each Response Spectrum Curve (496 Validation Rounds)

Return Period*	a_1 ($\times 10^{-5}$)	σ_{a1} ($\times 10^{-5}$)	a_4 ($\times 10^{-5}$)	σ_{a4} ($\times 10^{-5}$)	a_5 ($\times 10^{-5}$)	σ_{a5} ($\times 10^{-5}$)	a_{7**}	σ_{all}
475	281.35	15.97	-16.45	2.20	1.53	0.11	-0.5	0.01
175	150.61	8.81	-8.58	1.18	0.80	0.07	-0.5	0.00
72	62.63	4.69	-3.38	0.66	0.41	0.03	-0.5	0.00

* Return periods of the considered earthquake in the derivation of the coefficients

** Obtained by trial and error

When the coefficients of Table 6.11 are compared with the coefficients in Table 6.10, a similar pattern is observed for the constant term. The weight of the constant term is higher than any other term that forms the lateral performance. In fact as the nature of regression imposes, this phenomenon is also observed in the coefficients of various GMPEs. If the trellis plot in Figure 6.52 and the coefficients provided in Table 6.11 are examined closely, the weight of the constant term could be better understood.



* Due to very low t-test results, p values are scaled to display t-test results of individual parameters

Figure 6.51. Significance Test Results of Individual Structural Parameters

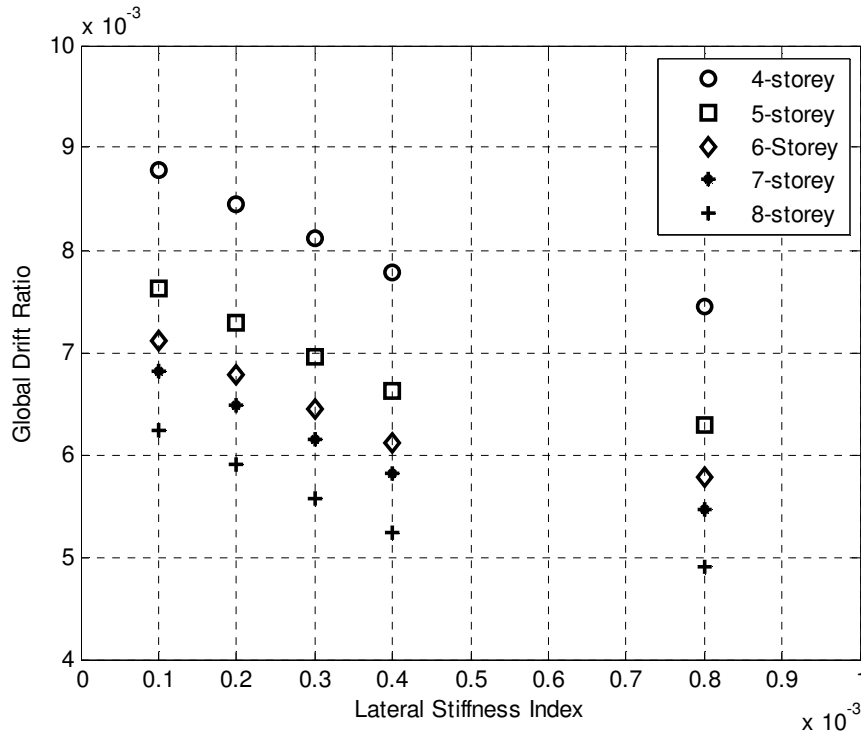


Figure 6.52. Trellis Plot of Global Drift Ratios Obtained by IDCM for 2475-year Return Period Earthquake

The performance of the derived LPPE is best observed in trellis plots. Both the lateral stiffness index and number of storeys are assigned with a range of values.

After that, and the lateral performances are derived by using the developed LPPE for the assigned range of values. Figure 6.52 is a product of such study as the scaling of the lateral performance with the lateral stiffness index is clearly presented in the figure.

6.5. Nonlinear Time History Analysis

After tuning the structures into a predictable pattern by prescriptions of the ATC-40 (1996) and FEMA-440 (2005), the proposed claims can be tested by the nonlinear time history analyses of these structures. The same three-dimensional models with the same nonlinear material properties are used for the nonlinear time history analyses. The earthquake records employed in the analysis are selected from the database gathered for the GMPE adaption process in Chapter 3.

6.5.1. Ground Motion Database

A total of 24 earthquakes with 81 ground motion records are selected from the same database compiled for the adaption study of GMPEs. All the records are obtained from GDDA website, as Table 6.12 lists all the earthquakes used for the nonlinear time history analysis. The epicenters of the earthquakes are within the 300 km radius circle centered at Eskişehir, and the oldest record belongs to Denizli earthquake. A more detailed list about each record can be found in Appendix A.

Table 6.12. Records Used in the GMPE Analysis (GDDA, 1976-2010)

No	Date of the Event	Name of the Event	M_w^*	Lat. (degrees)	Long. (degrees)	No of Records
1	19.08.1976	Denizli	5.3	37.71	29.00	1
2	18.07.1979	Dursunbey	5.3	39.66	28.65	1
3	29.03.1984	Balikesir	4.5	39.64	27.87	1
4	01.10.1995	Dinar	6.4	38.11	30.05	4
5	21.01.1997	Buldan	4.8	38.12	28.92	1
6	04.04.1998	Dinar	4.6	38.14	30.04	3
7	17.08.1999	Kocaeli	7.4	40.70	29.91	18
8	11.11.1999	Sapanca	5.7	40.81	30.20	1
9	12.11.1999	Duzce	7.2	40.74	31.21	7
10	23.08.2000	Hendek	5.3	40.68	30.71	4
11	04.10.2000	Denizli	4.7	37.91	29.04	1
12	26.08.2001	Yigilca	5.4	40.95	31.57	1
13	03.02.2002	Sultandagi	6.5	38.57	31.27	2

Table 6.12 Continued

No	Date of the Event	Name of the Event	M_w^*	Lat. (degrees)	Long. (degrees)	No of Records
14	03.04.2002	Burdur	4.2	37.81	30.26	1
15	09.03.2003	Akyazi	4.0	40.73	30.59	1
16	21.05.2003	Duzce	4.7	40.87	30.98	1
17	09.06.2003	Bandirma	4.0	40.20	27.97	1
18	23.07.2003	Buldan1	5.5	38.17	28.85	4
19	26.07.2003	Buldan2	5.3	38.11	28.88	4
20	26.07.2003	Buldan3	5.7	38.11	28.89	3
21	26.07.2003	Buldan4	5.2	38.11	28.84	3
22	24.10.2006	Manyas	5.2	40.25	27.98	10
23	12.03.2008	Cınarcik	4.9	40.63	29.02	6
24	17.02.2009	Simav	5.2	39.15	29.04	1

*The magnitudes are obtained from KOERI catalog, missing values in the catalog are calculated by Deniz and Yucemen (2008)

Each record is composed of three components: two horizontal components recorded in north-south and east-west direction, and one vertical component. The horizontal components are processed by using a 4-pole Butterworth filter with varying low cutoff and high cutoff frequencies, and baseline correction is applied as previously performed by Akkar et al. (2010).

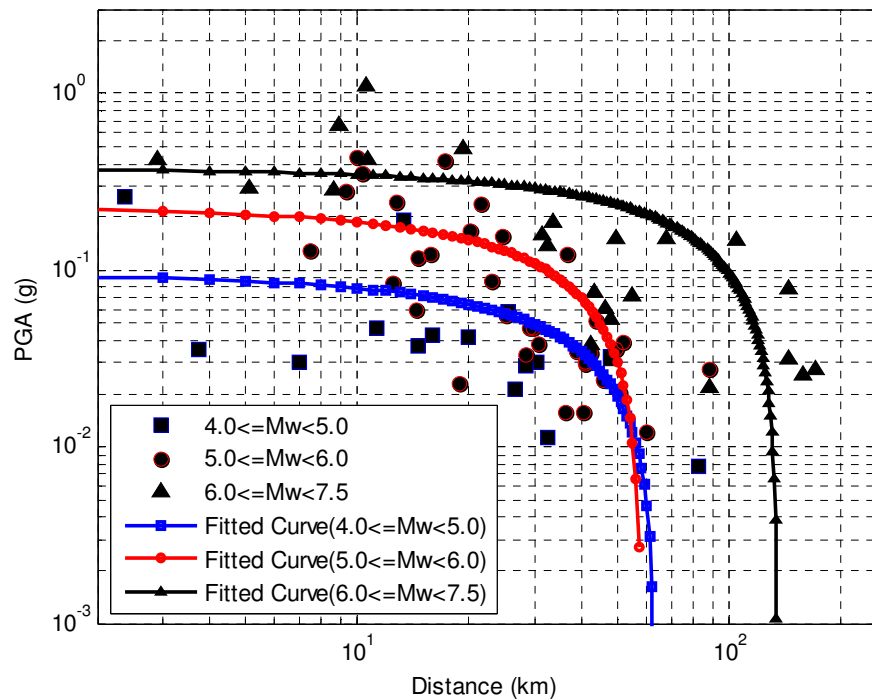


Figure 6.53. PGA vs Distance Plot

Figure 6.53 presents the PGA and distance distribution of the gathered records. The distance between the earthquake hypocenter and the record station is calculated by using the closest horizontal distance to the rupture surface, which is called Joyner-Boore distance. For the largest earthquakes with moment magnitude greater than 7.0, Izmit, 1999 and Duzce, 1999 earthquakes, the distance is measured from the closest distance of the surface projection of the rupture to the recording station.

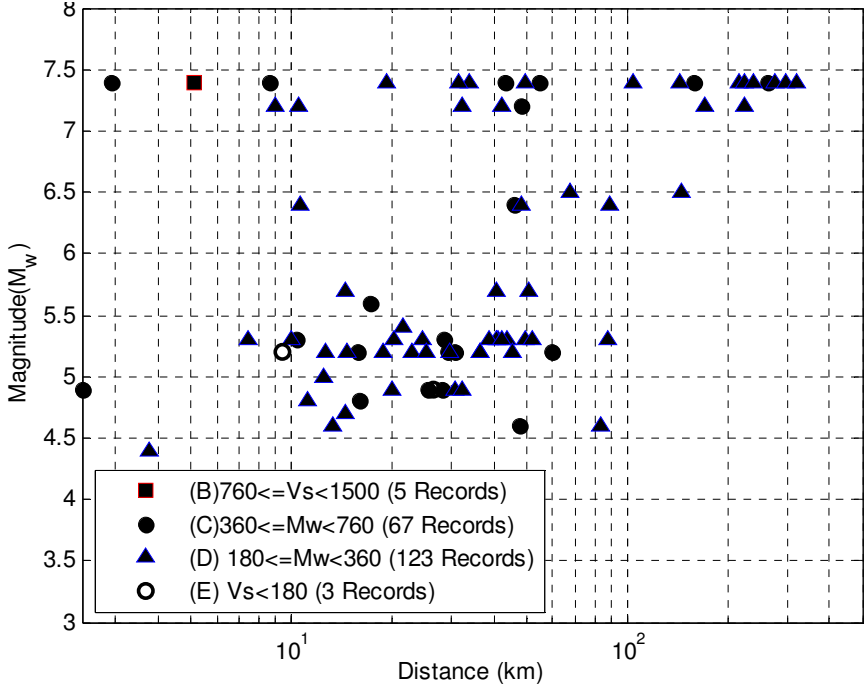


Figure 6.54. Distribution of Moment Magnitude and Site Classification of Recording Stations

The shear wave velocities of the uppermost 30 m layer that are obtained from Akkar et al. (2010) are used as the site condition parameter. The values of shear wave velocity of the station sites are classified according to NEHRP (1994). Most of the recording station sites are classified as either C or D as seen in Figure 6.54, which is also a general situation considering the all of the recording station sites throughout Turkey (Akkar et al., 2010).

6.5.2. Analysis Based on Selected Records

Nonlinear time history analysis is conducted as the load combination of the Turkish design code is imposed by creating a combination of dead and live loads in addition to the ground accelerations. Both north-south and east-west components of each record are utilized for the analysis in both transverse directions of the structures.

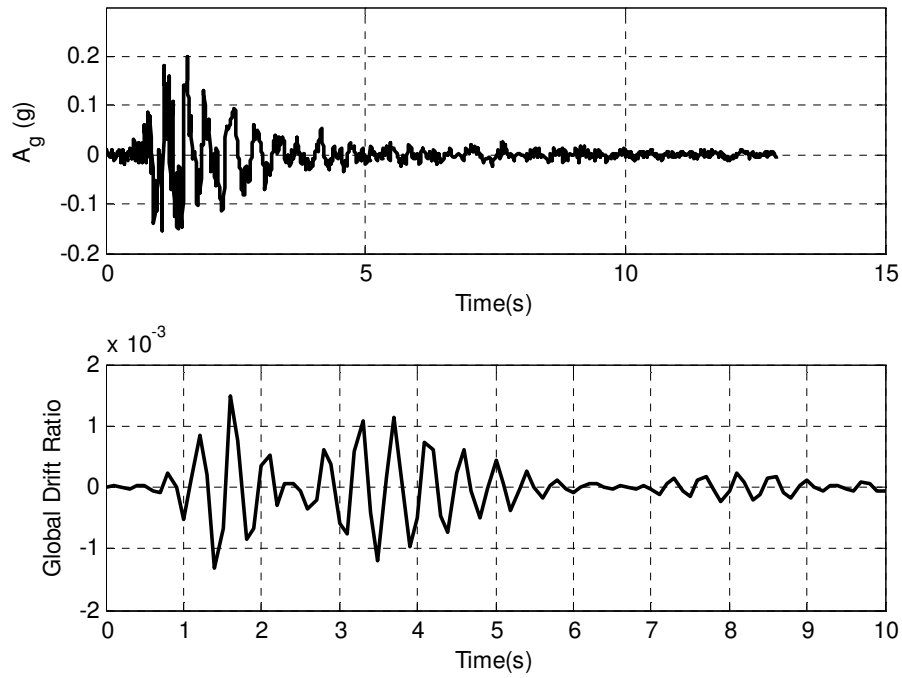


Figure 6.55. Lateral Response Monitored at the Center of Mass of Roof Level of B01 in X-Direction for the North-South Directional Record of 18.07.1979 Dursunbey Earthquake

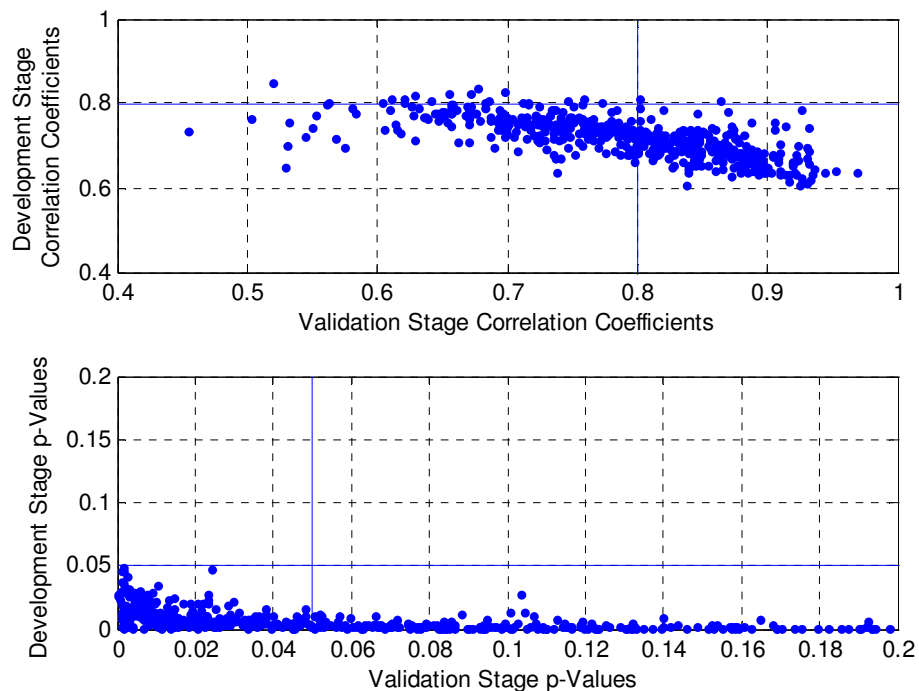


Figure 6.56. Result of the Regression Study of Nonlinear Time History Analysis by Using North-South Directional Record of 18.07.1979 Dursunbey Earthquake

The database obtained after the refinement procedures in 6.3.4 is also employed for the nonlinear time history analysis. 81 records with two horizontal components and

with 35 structural models are employed which total the number of analysis to 5670. A single instance out of 5670 analysis is provided in Figure 6.55, with the original record of north-south component of the ground motion record of 1979 Dursunbey earthquake is provided in the upper subplot and the response of the model B01 at the center of mass at roof level is shown in the bottom subplot.

The results of the nonlinear time history analysis are composed of two groups with the two directional signals of each record are applied in both transverse directions. The resultant performances of the structures in both directions are compiled and then regressed with the structural parameters in both directions. Consequently, 162 separate regression studies are conducted. In each regression analysis, 500 rounds of cross validation are performed with 35 structural models. Due to the space limitations, the results of a single regression analysis are shown Figure 6.56. The regression study is conducted with the global drift ratios obtained by using the north-south directional record of 18.07.1979 Dursunbey earthquake. As shown in the figure, the correlation coefficients for development and validation stages are above 0.60 with most of the p values below 0.05. Though not provided here, most of the results of 162 regression studies showed promising performances; hence, further utilization of nonlinear time history analysis is decided.

6.5.3. Scaling of the Records

In order to obtain the lateral performances, which are comparable with the estimated lateral performances of CSM, DCM and IDCM by the utilization of nonlinear time history analysis requires the scaling of the records. Scaling is a procedure that has certain assumptions that could reduce the precision of the calculated lateral performances. However, it is commonly used in order to reduce the dispersion of structural performances due to the highly varied ground motion levels in different ground motion records, to observe the performances in incremental dynamic analysis and to match the exposed level of seismic hazard in seismic risk calculations.

In the application of the scaling procedure, each value of the ground motion record is multiplied by a scaling coefficient. This coefficient is calculated by using the response spectrum curves that are obtained for the predetermined levels of ground motion, which in this case, are the curves shown in Figure 5.25.

Then each single record is subjected to scaling by using the ratio of the response spectrum values of the developed curves and the response spectrum value obtained by using the record at the equivalent fundamental period. The procedure can be followed in Figure 6.57, as the upper subplot shows the original record and the bottom subplot shows the response spectrum curve of the same record together with the response spectrum curve developed specifically for the city of Eskisehir for earthquake with 475-year return period.

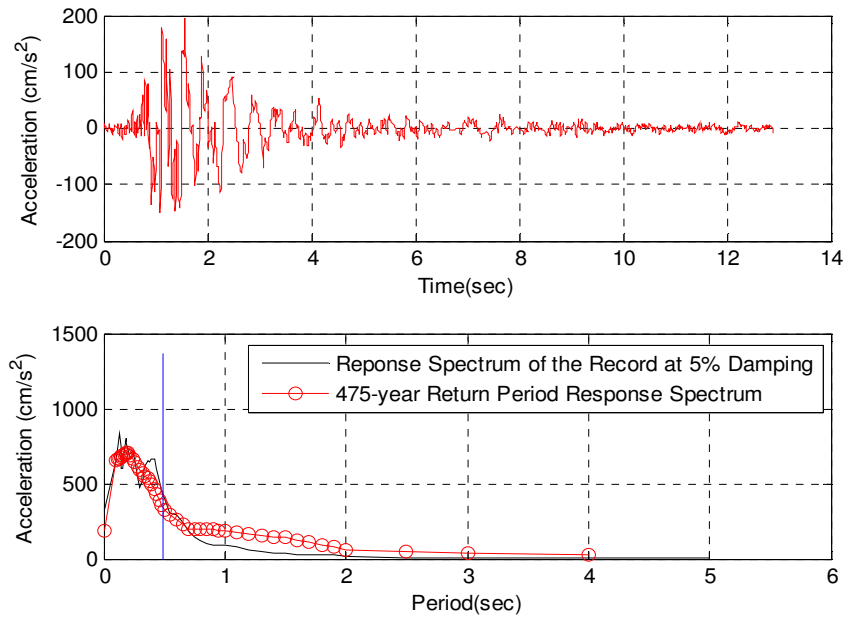


Figure 6.57. Scaling Procedure Applied for 475-Return Period Response Spectrum Curve

The equivalent period is obtained at the performance points obtained by using CSM procedure. Then the acceleration values at the equivalent fundamental period are calculated and a scaling ratio is derived by using the ratio of these acceleration values. This ratio is then used to multiply each value of the record to scale the record. After the application of the scaling to each record, the scaled records are used as input in SAP2000 (Computers and Structures, 2011) and the three-dimensional structural models are analyzed to obtain the roof displacements at the center of masses of the roof level. The scaling is applied only for the north-south directional signal of the ground motion record of Dursunbey, 1979 earthquake since one of the most successful cross validation performances are obtained by using this ground motion.

6.5.4. Regression Analysis

After the scaling procedure is performed, the cross validation procedure is applied as explained in section 6.3 to develop an LPPE equation. It is shown that, the influence of the scaling of the records obviously had negative effects on some of the structures as the lateral displacements are amplified. Only after the removal of distinctly performing models of B05 in y-direction and B13 in x-direction from the list of the structures, the cross validation rounds are concluded with reasonably acceptable results as given in Figure 6.58. The associated significance test results show varying levels of confidence for the individual parameters of LPPE. The test results are not promising as can be followed by Figures 6.59. Especially with respect to lateral strength and stiffness indexes, the resultant p values seem to fail to comply with the limits of the significance tests, which require p values less than 0.05.

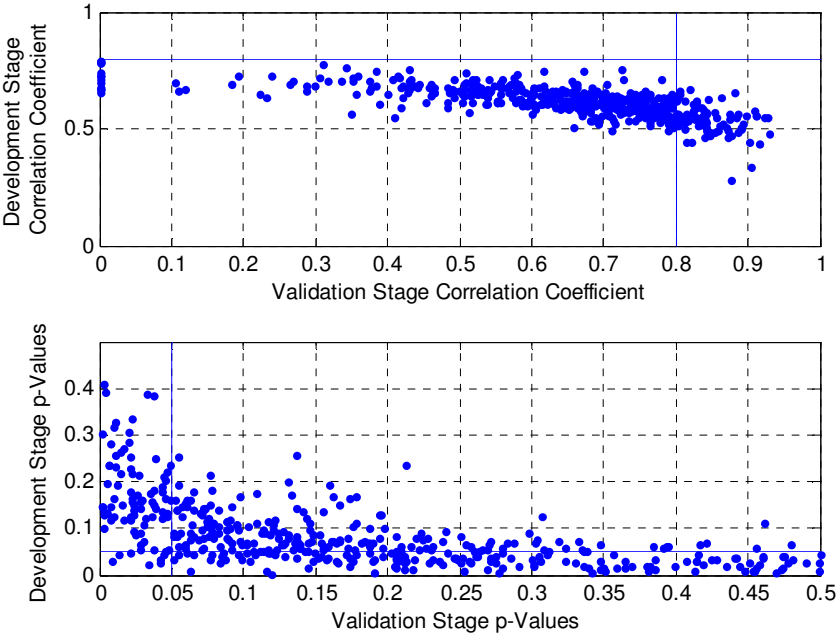


Figure 6.58. Result of Rounds of Validation Performed with the Roof Displacements and Structural Parameters

Unfortunately, the scaling procedure is not less flawless than DCM or IDCM considering the assumptions involved. Therefore, the results of the nonlinear time history analysis conducted by using the scaled ground motions should be treated carefully. The performance period calculation, the calculation of the scaling ratios by using the response spectrum curves and the application of the scaled records in nonlinear time history analysis could result in unexpected lateral responses.

Therefore, nonlinear time history analysis is only used for the verification of the existence of relationship between the lateral performances and proposed structural parameters.

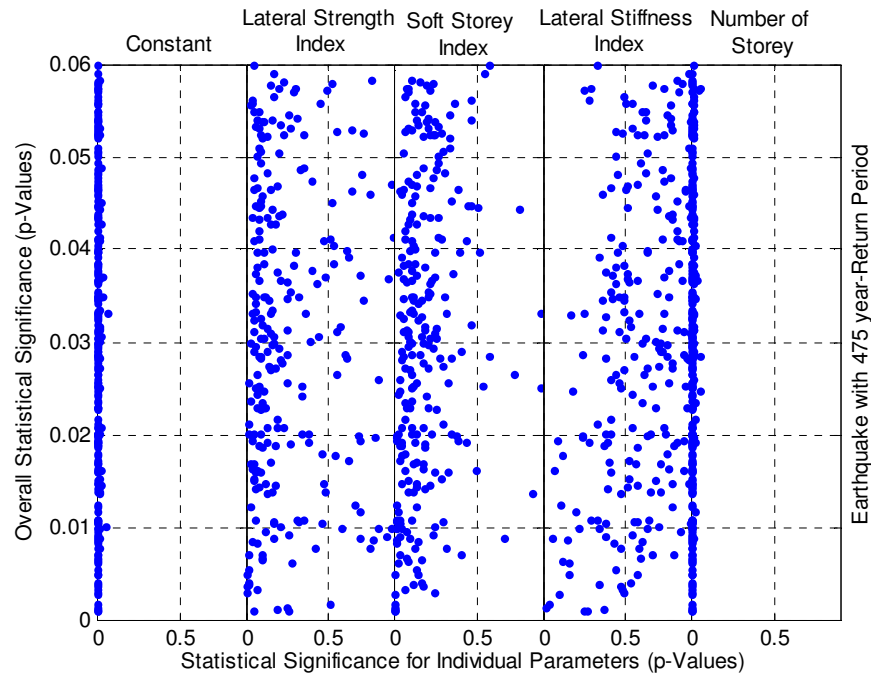


Figure 6.59. Significance Test Results of the Validation Rounds Conducted for the Derivation of Lateral Performance Prediction Equation for a 475-year Return Period Earthquake

6.6. Evaluation of the Results

37 structures in both transverse directions are subjected to a number of compliance criteria and procedures for the development and validation of LPPE. Due to the criteria of modal mass participation ratio, fundamental period and relative sway ratio, 39 structural models out of 74 models were disqualified for further analysis. It should be mentioned that, only a single structural model was eliminated due to visual elimination criteria, while the rest of the models are eliminated due to the imposed technical criteria. Total number of eliminated structural models in order to reach a predictable pattern of performance displacements raises concerns about the applicability of the LPPE to real life problems. Since the aforementioned elements of elimination criteria cannot be known beforehand unless a three dimensional analysis is performed, the practicality of LPPE is questioned. At least it is clear that a generalized LPPE has to be developed to cover whole range of structures.

Several criteria of elimination are imposed to be able to have a predictable pattern of lateral performances in order to serve the purpose of the study. It is not surprising that, the pattern of lateral performances obtained by IDCM is similar to the fundamental period patterns. The similarity is justified by through investigation of the basic relationships of fundamental period, demanded spectral displacement, height, mass and lateral stiffness of the structures. The influence of the basic structural properties on the lateral performances is clearly identified in the application of elimination procedures of 6.3.4. These basic structural properties are also reflected strongly to the pushover and capacity curves and the outlier performances are clearly identified by using these lateral performance curves.

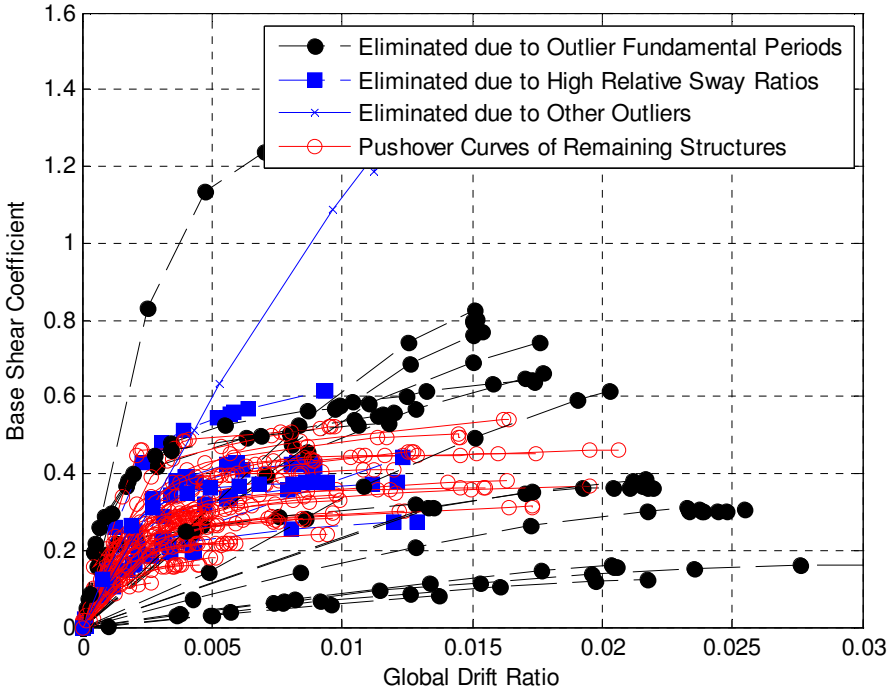


Figure 6.60. Original and Outlier Capacity Curves

The eliminated and remaining pushover curves are presented in Figure 6.60. It should be mentioned that fundamental period has a very strong influence over the type of behavior of the structures, as the capacity curves with the most distinct patterns of behavior in Figure 6.60 is associated with very high or low fundamental periods as they are eliminated due to the distinct pattern of behavior. The high relative sway ratio is also another factor, which cannot be foreseen by using the proposed structural parameters; hence, structures with high relative sway ratios are also removed.

Obviously, there is a requirement of tuning the lateral performances into a predictable pattern with the application of several criteria. In order to obtain a predictable pattern of lateral performances, the elastic response spectrum curves as well as the pushover analysis of the models must be investigated.

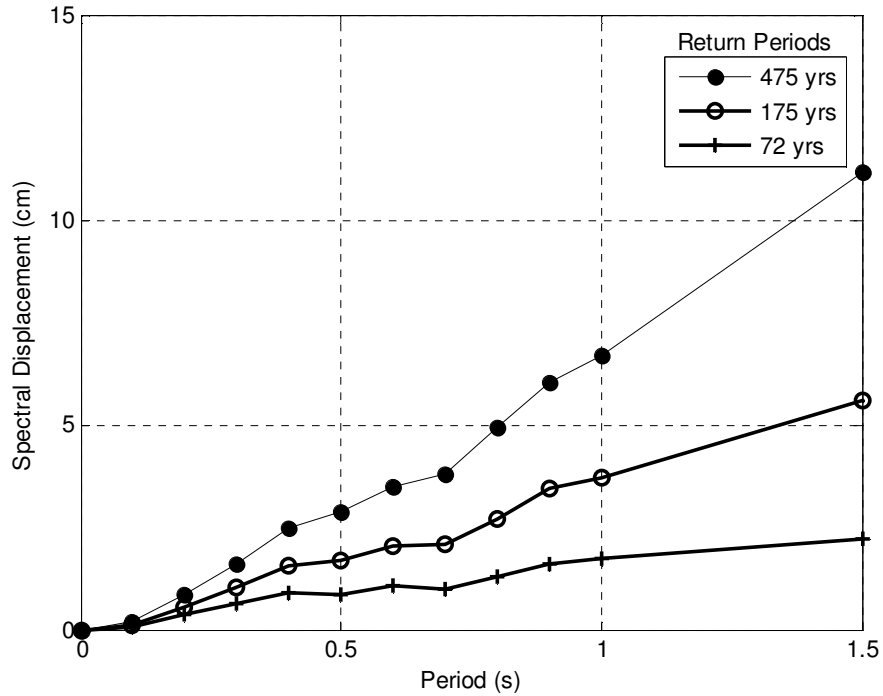


Figure 6.61. Displacement Response Spectrum Curves Developed for Eskisehir

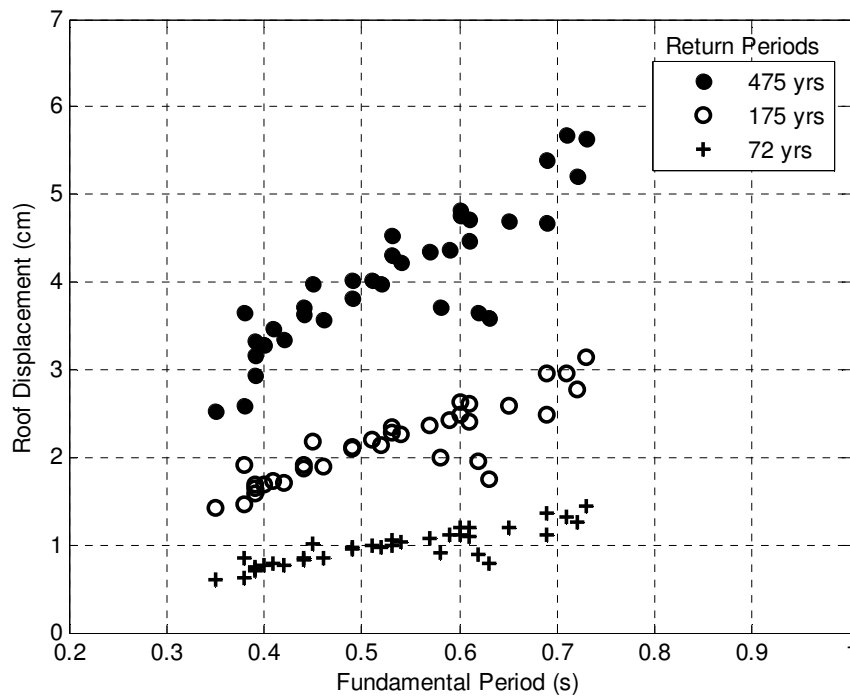


Figure 6.62. Narrow Band of Roof Displacements Obtained by IDCM and the Fundamental Period Relationship between 0.35 s and 0.80 s

If the elastic response spectrum curves allow a smoother pattern, then there is more chance of obtaining more uniformly distributed lateral performances with demand spectral displacements are within a predictable pattern. Unfortunately, the displacement response spectrum curves that were developed for Eskisehir do not allow such a uniform behavior for the interested period ranges. Indeed, between 0.35 s and 0.80 s seems to be hardly justified considering the variance in the displacement response spectrum curves in Figure 6.61.

Moreover, the prerequisites in ATC-40 (1996) and FEMA-440 (2005) helped to create a uniform set of structures with a predictable pattern of behavior. The pattern of behavior could be perfectly followed by Figure 6.62, which presents the scaling of the roof displacements by the fundamental periods. The strong dependence of the estimated roof displacements on the fundamental period of the structures in the refined database, imply that there is a strong connection between the proposed structural parameters and the lateral performance considering the height, mass and lateral stiffness dependence of the fundamental periods.

Obviously imposing a limitation on the fundamental periods limits the capability of the LPPE. However, it should be known that, if the performance of LPPE would be successful in the prediction of the lateral performances for a certain range of fundamental period, than it is induced that, the capability of LPPE could be extended to cover the whole range of periods of the response spectrum curve.

Considering the statistics of the multiple regression analysis, the regression correlation coefficients of DCM and IDCM methods are the highest, while CSM failed to produce such a high correlation. When the DCM and IDCM methods were compared by using significance test results of each individual parameter and the residual analysis, it is decided that the IDCM method should be chosen as the best choice for the development of LPPE.

6.7. Recommended LPPE for Utilization in the Prediction of Lateral Performances

After several stages of obtaining a valid LPPE, two equations are proposed. If the statistical concepts are taken into consideration, only equation 6.11 should be employed with the coefficients provided in Table 6.11. However, if structural concepts are also taken into consideration, equation 6.9 should be employed with the coefficients given in Table 6.10. Following equations provide expanded forms of

equation 6.11, which include lateral stiffness index and number of storeys as parameters.

$$\delta_{GDR}(475) = (281.35 + 1.53lsiI^{-0.5} - 16.45n \pm 0.01) \times 10^{-5} \quad (6.12.a)$$

$$\delta_{GDR}(175) = (150.61 + 0.80lsiI^{-0.5} - 8.58n \pm 0.00) \times 10^{-5} \quad (6.12.b)$$

$$\delta_{GDR}(72) = (62.63 + 0.41lsiI^{-0.5} - 3.38n \pm 0.00) \times 10^{-5} \quad (6.12.c)$$

However, if the equation 6.9 is preferred, which is the case in this study, following forms of equations with the coefficients, should be employed:

$$\delta_{GDR}(475) = (301 - 4.21lsiA^{-0.5} - 5.32ssi + 1.66lsiI^{-0.5} - 15.07n \pm 0.01) \times 10^{-5} \quad (6.13.d)$$

$$\delta_{GDR}(175) = (1606 - 1.70lsiA^{-0.5} - 4.20ssi + 0.84lsiI^{-0.5} - 7.99n \pm 0.00) \times 10^{-5} \quad (6.13.e)$$

$$\delta_{GDR}(72) = (58.19 - 0.37lsiA^{-0.5} + 6.35ssi + 0.43lsiI^{-0.5} - 3.46n \pm 0.00) \times 10^{-5} \quad (6.13.f)$$

The equations are developed considering the different return periods. So the discrete lateral performances in terms of global drift ratios can be interpolated to obtain the lateral performances for the earthquakes with return periods other than the ones employed in this study.

CHAPTER 7

7. LOSS ESTIMATION

7.1. Introduction

This section consists of the loss estimation study of the structures. After obtaining the seismic hazard and lateral performance components of the loss estimation in Chapters 5 and 6, the estimation of the loss becomes easier. The only issue remains to estimate the loss is the association of the lateral performances that are calculated by the developed LPPE in Chapter 6, with the damage ratios and cost of damage. Obviously, the damage and the lateral performances are related, but how much damage will be attained at varying levels of lateral performance has to be known. In the literature, various damage ratios are proposed at the various levels of lateral performances and since none of the established schemes is widely accepted, a local damage ratio study will be used. Therefore, the most suitable damage classification scheme that was specifically developed for Turkey is selected from among the various schemes available in the literature. Then, the relationship between the global drift ratios, the damage limit states, damage classes and damage ratios is established. Lastly, the insurance premiums are calculated. Only the direct physical damage to the building was taken into account in the insurance calculations whereas economic losses due to the damage to the contents of building, or other economic losses and social losses are not considered.

7.2. Review of Previous Studies

The review of the past studies on the subject yielded different approaches that are proposed for reliable and accurate loss estimation. These studies are generally different in their classification scheme of structures, the considered lateral performance variables, and the damage ratios at the selected lateral performance levels. Some of them are worth mentioning in the literature review and deserve greater attention due to the wide acceptance.

The estimation of the loss starts with the determination of the exposed seismic hazard. Deterministic and probabilistic approaches are assumed depending on the

requirements. Then, the potential damage experienced by the structure at the exposed ground motion level is calculated by using damage probability matrices (DPM), reliability based methods, expert opinion, discriminant functions or analytically developed force based or displacement based procedures. All of the mentioned methods are receiving more and more attention in accordance with the requirements of the field. In one of the significant studies, Askan and Yucemen (2010) employed DPMs, reliability based methods and discriminant analysis for estimation of the loss and compared the outcome of these three methods. It should also be mentioned that loss estimation is a widely required tool for many purposes and several projects are implemented, computer simulations are developed, and programs are launched to estimate the loss accurately. Consequently, comprehensive damage scenarios and seismic hazard analysis, including GIS-based evaluation tools, have been developed and proposed as parts of major international programs, e.g. HAZUS (1999); RADIUS (1999), Risk-UE (2004), MIRISK (2007), MAEviz (2008). Several software programs have been developed for the same purpose, such as KOERILOSS, SELENA, ESCENARIS, SIGEDPC and DBELA to name a few of them.

In Turkey one of the most detailed studies in loss estimation was performed by Erdik et al. (2003) sponsored by BU-ARC-Munich-Re. Their study involved all the elements of risk: casualties, buildings, lifeline systems, and additional damages due to earthquake induced hazards such as fire. JICA-IMM (2003) provided a similar loss model for Istanbul. These two projects led to the creation of Earthquake Master Plan for Istanbul. Another loss estimation program, HAZTURK, based on MAEviz of Mid-America Earthquake Research Center (MAERC), was developed by Istanbul Technical University (ITU) in cooperation with the MAERC (Sahin et al., 2006, Karaman et al., 2008). Duzgun and Yucemen (2007) developed an integrated risk model in GIS platform for the city of Eskisehir. In their study, a spatial urban disaster risk model is proposed, which uses socio-economic and building vulnerability, infrastructure and economical losses, as well as accessibility to critical services. A study involving street survey and two level discriminant analyses of thousands of buildings in Zeytinburnu district of Istanbul was conducted in an attempt to quickly classify buildings and propose a solution to the urban risk in Istanbul (Yakut et al., 2003, Ozcebe et al., 2003, Ozcebe et al., 2006). All these studies proposed different approaches for the estimation of the potential losses and for the determination of the

exposed risk. The variety of the methods and procedures employed in many studies imply that, none of the methods can claim more accurate and reliable results than the other methods. Therefore, in any loss estimation study, the most appropriate methods and procedures must be selected from amongst the available ones. In order to explain the elements and procedures of loss estimation, following sections are created.

As the important outcome of the loss estimation, the current insurance premiums of Turkish Catastrophe Insurance Pool (TCIP), developed by the technical input of Bommer et al. (2002) are later examined by a number of studies. Yucemen (2005) performed a study by using the damage probability matrix to reach the earthquake insurance premiums. After review, it is concluded that, there are not many studies in order to calculate the insurance premiums. In this study, the performance of the current insurance system of TCIP will be examined and the results of a case study will be compared.

7.3. Damage Limit States, Damage Classes and Damage Ratios

There are different approaches in the classification of structural damage with respect to the attained damage of the structure during a shaking. The basic behavior of the structures can be classified in terms of certain thresholds as elastic and inelastic behavior. These distinct types of responses are so significantly different that various damage limit states and damage classes could be defined for these basic categories of responses. In practice, additional damage limit states and classes are proposed within the elastic and inelastic part of the response, and different threshold levels of these damage limit states and classes are created. One important damage threshold is defined at the point where the structural steel in a member of the structure starts yielding.

The structural behavior changes at this point from elastic to inelastic where the drift increases without causing dramatic increase in the lateral loading. In the elastic region, the damages are repairable because the structure returns to its original shape when the load is removed. On the other hand, the structural damage occurring in the inelastic region is irreparable because the structure does not return to its original shape when the load is removed.

Table 7.1. ASCE 41 Structural Performance Levels and Overall Damage for Reinforced Concrete Structures (ASCE 2007)

	Collapse Prevention	Life Safety	Immediate Occupancy	Operational Level
Overall Damage	Severe	Moderate	Light	Very Light
Damage Description	Little residual stiffness and strength, but load bearing columns and walls function. Large permanent drifts. Some exits blocked. Infills and unbraced parapets failed or incipient failure. Building is near collapse.	Some residual strength and stiffness left in all storeys. Gravity-loadbearing elements function. No out-of plane failure of walls or tipping of parapets. Some permanent drift. Damage to partitions. Building may be beyond economic repair.	No permanent drift. Structure substantially retains original strength and stiffness. Minor cracking of facades, partitions, and ceilings well as structural elements. Elevators can be restarted. Fire protection operable.	No permanent drift. Structure substantially retains original strength and stiffness. Minor cracking of facades, partitions, and ceilings as well as structural elements. All systems important to normal operation are functional.
Non-Structural Components	Extensive damage	Falling hazards mitigated but many architectural, mechanical, and electrical systems are damaged.	Equipment and contents are generally secure, but may not operate due to mechanical failure or lack of utilities.	Negligible damage occurs. Power and other utilities are available, possibly from standby sources.

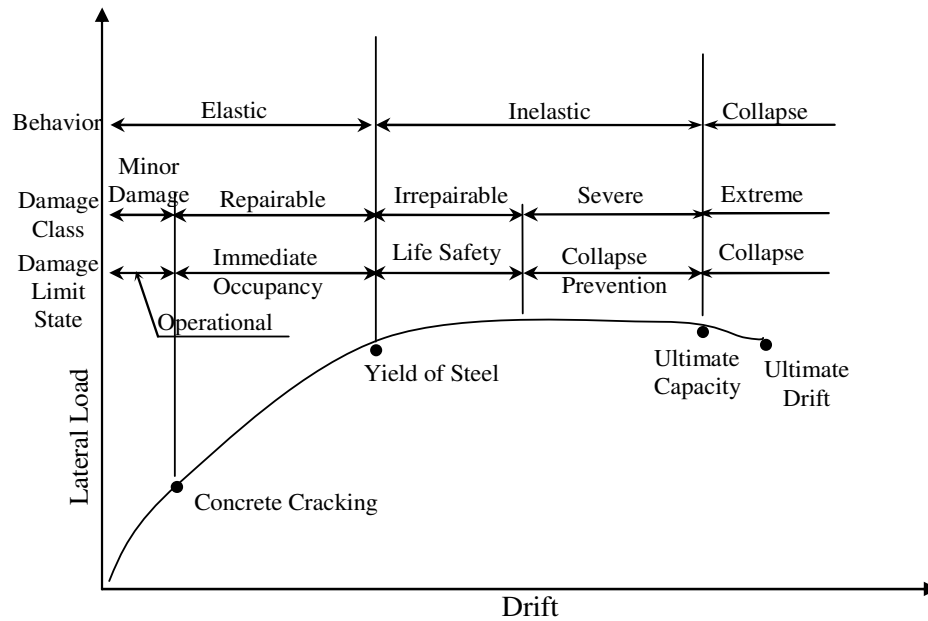


Figure 7.1. Structural Performance and Damage Levels (Ghoborah, 2004)

The types of behavior and associated damage limit states and damage classification, are presented in Figure 7.1 for illustrative purposes. As shown in this figure, two more damage limit states and damage classes are introduced at points within the elastic and inelastic region. The first damage limit state is defined at the point where the concrete starts to crack. As the lateral load increases, the structure experiences initial cracking of the concrete in the elastic region. In this damage state, the damage is quite limited, thus classified as minor damage. The damage state stays at operational level where the structure can be repaired easily. In the inelastic region, which extends from the first yielding of the steel to the total collapse of the structure, there are two distinct regions of damage thresholds named as irrepairable and severe, and two damage limit states named as life safety and collapse prevention. The irrepairable damage class can be identified by the yielding of the steel and cracking in beams and columns.

Associating the lateral response of structure to the damage and eventually the cost of repair does not provide an exact solution to the loss estimation problem. The structural system, the distribution of the damage, failure mode selection, and the earthquake characteristics influence the loss in an event (Ghoborah, 2004). Although this classification of damage limit states and damage classes do not exactly reflect the true nature of the structural response, indeed the structural response under lateral

loading needs to be assessed. Moreover, it provides a reasonably successful tool in the estimation of damages and classifies the building according to the expected damages.

Therefore, since the damage has to be quantified for practical reasons, a close to real solution must be accepted. The existence of so many different damage classification systems raises concerns in the selection of the most suitable system for a study. It is a fact that none of the damage classification systems is better than the other systems and this fact encourages the selection of the local classification systems that are developed by using the local data. Hence, for the present study, widely accepted damage state classification system of General Directorate of Disaster Affairs (GDDA) (Currently Disaster and Emergency Management Agency) will be employed. Table 7.2 provides the damage classes and the description of associated damage in detail according to GDDA classification system. The damage classes are classified as four groups: no damage, light damage, moderate damage, and heavy damage/collapse classes.

Table 7.2. Descriptions of the Damage States Used by the General Directorate of Disaster Affairs, Ministry of Public Works and Settlement

Damage Class(DC)	Description
No damage (N)	Building with no damage as a result of the natural disaster
Light damage (L)	Thin plaster cracks, plaster fall out, 1-4 mm thin cracks in the walls, partial fall out and cracks up to 10 mm in the infill and gable walls.
Moderate damage (M)	Significant cracks in the load bearing walls up to 5-10 mm, partial collapse and disintegration in the partition, infill and gable walls.
Heavy damage / Collapse (H/C)	Frequent shear cracks wider than 10 mm in load bearing walls, disintegration and crushing at the building corners, conical fall outs, horizontal displacements, partial or full collapse in the partition, infill and gable walls. Partial or full collapse in the load carrying system and roof of the building

Though damage classes are defined literally in detail, in order to evaluate the damage in terms of economic loss, these damage classes must be quantified. In terms of structural damage ratio, which is defined as the cost of repair of earthquake induced damage to the replacement cost of the building. In literature, the damage ratios (DR) are generally provided in certain ranges for each damage limit state or damage class and central damage ratios (CDR) are introduced for each damage class. Table 7.3 provides the damage ratios and central damage ratio for each damage class proposed by Gurpinar et al., (1978). Five different damage ratios could be associated with the damage classes as provided in the second column of the table. The central damage ratios are given in the last column of the table.

Table 7.3. Damage Ratios Corresponding to Various Damage States (Gurpinar et al., 1978)

Damage Class	Damage Ratio (%)	Central Damage Ratio (%)
None	0-1	0
Light	1-10	5
Moderate	10-50	30
Heavy	50-90	70
Collapse	90-100	100

7.4. Damage Limit States

The limit states are defined by associating the average yield and ultimate lateral drifts with the predefined damage limit states of immediate occupancy, life safety, and collapse prevention. The average yield lateral drift ratios are associated with the damage limit state of immediate occupancy, while the ultimate lateral drift ratios are used to determine the life safety and collapse prevention limit states.

The average values of yield and ultimate lateral drifts are approximately calculated by using the bilinear models of the pushover curves. The distribution characteristics of these lateral drift values are evaluated in Figure 7.2. A very narrow range of distribution is obtained for the lateral drifts at yielding of structures while a wide range of values are observed for the ultimate drift values. The ultimate drift ratio is used to establish the life safety and collapse prevention limit states, as the 75% of the average ultimate drift ratio is assigned to the damage limit state value for life safety. Moreover, to establish the global drift ratio for operational level, which is accepted as the level where structural concrete starts cracking, 1/1000 of building height is

accepted as limit state. Although this ratio is not very common in the literature on the lateral drift limits for serviceability or elastic limits, it is safe to use such a ratio to be conservative. All the values of the global drift ratios at each limit state are provided in Table 7.4.

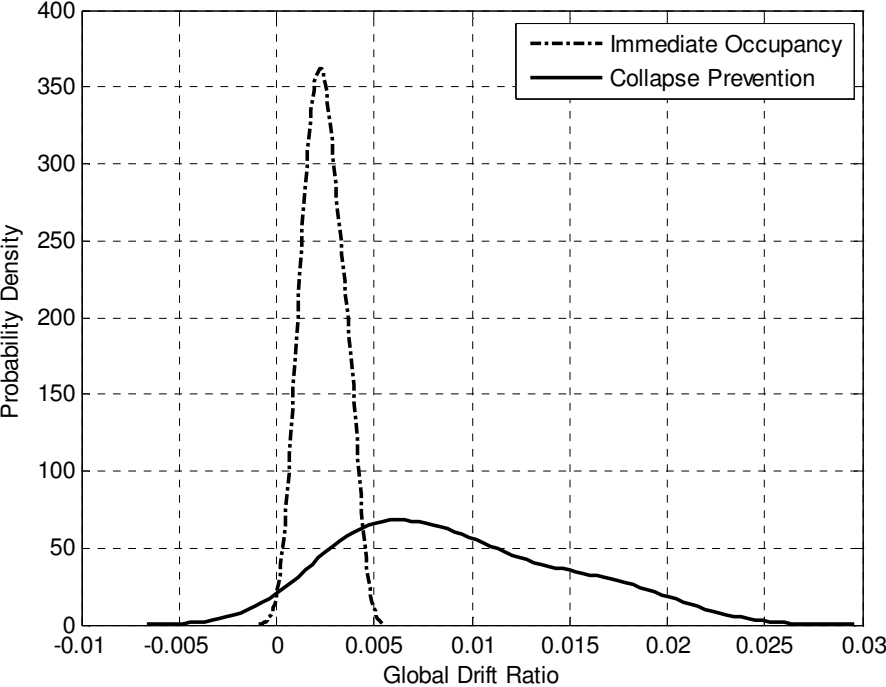


Figure 7.2. Distribution of Yield and Ultimate Drift Ratios (35 Models are Used)

Table 7.4. Performance Levels and Damage Limit States with Respect to Global Drift Ratio for Both Directions

Limit State	Operational Level	Immediate Occupancy	Life Safety	Collapse Prevention
Drift (%)	0.10	0.24	0.69	0.93

7.5. Estimation of Seismic Loss

Two main approaches in the estimation of the loss are considered for insurance purposes. In one of these approaches, the probable maximum loss (PML) or loss associated with the maximum seismic event is considered for the site under consideration. The second approach uses expected annual loss (EAL) and takes a more probabilistic approach by considering the probability of all the seismic event occurrences for the site. Deterministic seismic hazard analysis is used to estimate the PML, whereas PSHA is employed for the calculation of EAL.

The PML estimate could be highly unrealistic due to the very long return period of the largest seismic event, and therefore, considering the lifetime of the building, the

estimate might be unfeasible. However, EAL estimates the yearly occurrence rates of all the seismic events and associates these events with the damage ratios in order to estimate the expected annual loss. Moreover, because PML is based on scenario estimation, the financial reflection of this scenario is not meaningful and cannot be included in the pricing of the building or cost determination of a seismic mitigation program (Porter et al., 2004). On the other hand, EAL offers loss estimation on a yearly basis that could be useful in the financial analysis of insurances, seismic mitigation, or pricing of a building. In this thesis study, EAL is preferred due to the aforementioned disadvantages of the PML estimation.

The average yearly amount of loss or expected annual loss is calculated as follows

$$EAL = RCV \int_0^{\infty} y(s)v(s)ds \quad (7.1)$$

where, RCV denotes replacement cost value, $y(s)$ is the damage function, and $v(s)$ is the seismic hazard function and s represents seismic intensity measure.

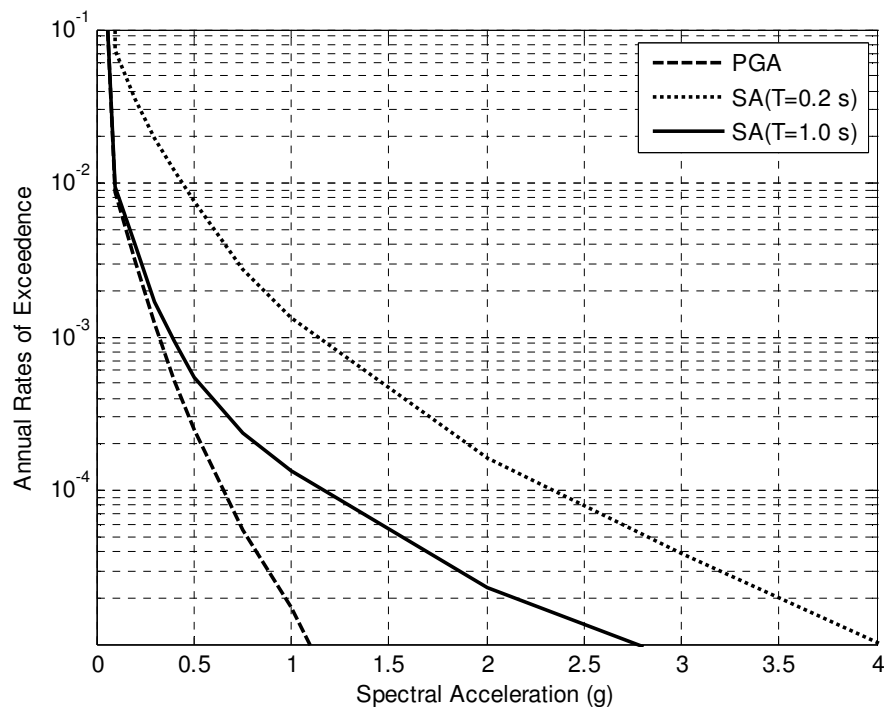


Figure 7.3. Annual Exceedance Rates of Earthquake Events for PGA, and Spectral Periods of 0.2 s and 1.0 s (AC10 is Used as GMPE)

As the first part of the estimation of the expected annual loss, the seismic hazard should be expressed in terms of annual exceedance rates of spectral acceleration as shown in Figure 7.3. By using this figure, hazard values of spectral acceleration at

PGA, and at periods of 0.2 s and 1.0 s can be obtained for earthquakes with different return periods.

The second part of loss estimation involves the determination of lateral performance at various levels of ground motion and the damages attained by the structure at the determined lateral performances. The lateral performance has to be quantified in terms of selected lateral performance variable, which is global drift ratio for this study. After that, the corresponding damage ratios associated with the global drift ratios must be established. Obtaining the damage ratios requires establishment of the damage ratio-global drift ratio relationship, a prerequisite that must be studied carefully.

As mentioned, there are clear performance thresholds such as yield and ultimate levels that cause the structure to attain different damages. Therefore, it is necessary to classify the lateral performance of structure in terms of damages attained by the structure at predefined levels. For this purpose, the damage limit states are established at predefined levels of global drift ratios and at those values of drift, the lateral performance of structure and damage ratio is sought in terms global drift ratio.

Table 7.5. Damage Ratios Corresponding to Global Drift Ratios

Damage Class	Damage Ratio (%)	Central Damage Ratio (%)	Global Drift Ratios	Damage Limit States	Significant Structural Threshold
None	0-1	0	0-0.0010	Operational	Concrete Cracking
Light	1-10	5	0.0010-0.0024	Immediate Occupancy	Yield of Reinforcement Steel
Moderate	10-50	30	0.0024-0,0069	Life Safety	More Yielding
Heavy	50-90	70	0.0069-0.0093	Collapse Prevention	Ultimate Capacity
Collapse	90-100	100	>0.0093	Collapse	Ultimate Drift

Associating the damage limit states with the global drift ratios is a difficult task, and though all of them are established by using statistical observations or reliable assumptions, it is mostly highly subjective since the level of knowledge is quiet limited. Though a relationship between the drift and damage definitely exists, the

damage cannot be estimated by the drift only since there are other building characteristics such as irregular geometry and localized weaknesses. However, there is a growing demand for estimation of accurate damage ratios, therefore reliable functions are required to estimate the damage ratios as a function of global drift ratios. Moreover, most of the gathered structures in the database have regular geometry with uniform height distribution, which could lead to expectable damage ratio estimations.

Several relationships are proposed in the literature for damage ratio-lateral drift relationship and for the damage limit states and associated lateral performance levels (Whitman, 1973, Gurpinar et al., 1978, ATC-13, 1985, FEMA 273, 1997, HAZUS99, 1999, Rossetto and Elnashai, 2003, RISK-UE, 2004). Despite a number of accomplished studies, it is quite difficult to evaluate and compare these proposed relationships because of the variability of data used to create them. The general building characteristics changes from one location to the other, and thus, the type of raw data used to create these relationships is the only determining factor in the evaluation of these relationships prior to application. Considering the aforementioned concerns in the selection of damage limit state definitions, damage classes, and the locally developed damage ratios, established relationships by Gurpinar et al. (1978) are employed for this study. Table 7.5 is created to associate the damage limit states and damage ratios to the global drift ratios and corresponding significant structural thresholds.

7.6. Insurance Considerations

Combination of the two main components of the loss estimation procedure yields to expected loss. Then the expected loss is employed for insurance considerations. The expected annual loss is used as pure premium in the determination of insurance premiums. However, the real earthquake risk insurance premiums can be several times higher than the annual expected loss due to the start-up costs, operational expenses, and the cost of equity capital or cost of bearing the risk in the insurance business. Because earthquake insurance is not as diversifiable as the other type of insurances and because many policyholders are affected by a single event, the cost of equity capital is much higher than the other types of insurance. Therefore, the insurance premium becomes much higher than the pure premium or annual expected loss (Cummings and Mahul, 2009).

In Turkey, the Turkish government established the Turkish Catastrophe Insurance Pool (TCIP) in 2000 to compensate for the earthquake induced losses and introduced the Compulsory Earthquake Insurance (CEI) system. All of the privately owned residential buildings within municipality borders must participate in the insurance scheme that is formed to replace the obligations of the government in disasters of at least up to certain cost. Reinsurance and state obligations still take an important part in the disaster compensation of the induced losses above certain level.

The insurance premiums are calculated according to the location of the property, the period (year) of the construction, and type of the structure. The information about the location is required to classify the building according to the seismic hazard zones; the construction period is necessary since different regulations were enforced in different periods. Moreover, depending on the type of material, there are three types of structures in the classification system of TCIP, namely adobe brick, reinforced concrete or steel frame structures, and others. Most of the buildings in Turkey fall into the category of reinforced concrete or adobe brick structures. According to this classification scheme, the list of scaled premiums for different periods and for different seismic zones for reinforced concrete buildings is given in Table 7.6.

Table 7.6. Relative Earthquake Insurance Scheme with Respect to Seismic Zones and Year of Construction for Reinforced Concrete Buildings in TCIP

Seismic Zone	Pre 1975	1976-1996	1997-1999	1999-2007	2007-
I	100.00	100.00	100.00	100.00	90.61
II	72.26	72.26	72.26	72.26	65.64
III	41.52	41.52	41.52	41.52	37.98
IV	29.57	29.57	29.57	29.57	27.23
V	24.88	24.88	24.88	24.88	23.00

7.7. Case Study

For the case study, a hypothetical 5-year old, 4-storey reinforced concrete moment-resisting frame building with the basic geometric properties given in Figure 7.4 is considered. One part of the building is skewed as shown in the plan view with single floor area of 116.23 m². The total height is 11.35 m, and the height of the storeys is the same except for the first storey as shown in plan view A in Figure 7.4. The

building is assumed to be located in the city center of Eskisehir with soil conditions corresponding to class C.

The buildings fundamental period is 0.44 s in the considered direction, and the modal mass participation ratio is 80%, which satisfies the requirements. The building value is calculated as 302198.00 TL by using the building's total area of 464.92 m² and the unit cost of the building, which is 650.00 TL/m² (The Ministry of Environment and Urbanization, 2014).

In order to calculate the global drift values expected for earthquakes with different return periods, the structural parameters of the building in Table 7.7 are used with the developed LPPE in equations 6.13.a to 6.13.e yielding to the corresponding global drift ratio (GDR).

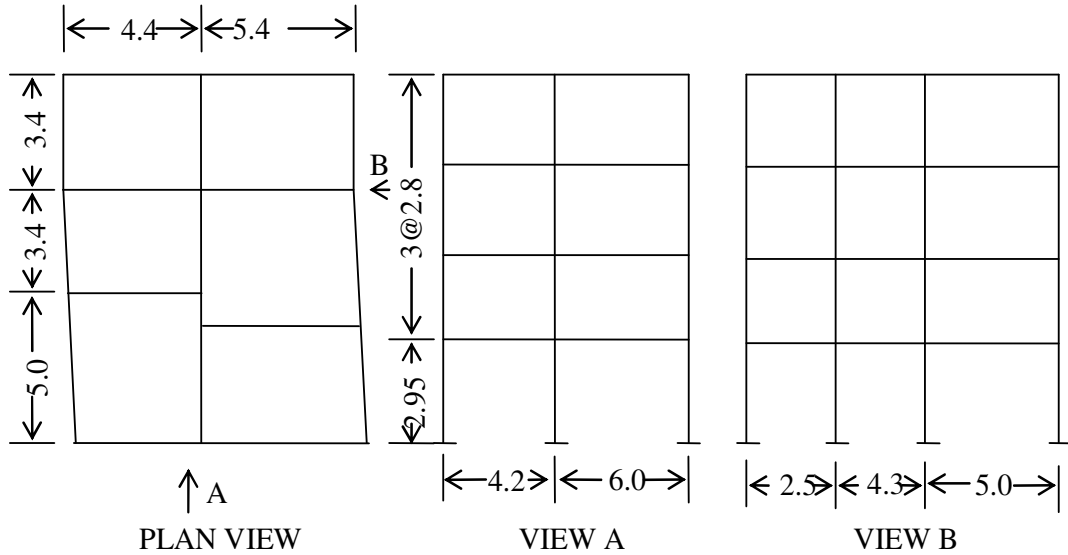


Figure 7.4. Selected Building Plan View and Profile Views (All units are in meters)

This GDR value is then converted to the expected damage ratio (EDR) by using the information presented in Table 7.5. The expected annual damage ratio (EADR) associated with the seismic hazard at the site is computed from the following relationship:

$$EADR = \sum_s EDR_s \times SH_s \quad (7.2)$$

where, $EADR$ is the expected annual damage ratio, EDR_s is the expected damage ratio corresponding to s , SH_s is the seismic hazard associated with s , and s is the

seismic intensity measure. The annual pure risk premium (APRP) can be obtained by multiplying EADR by the replacement cost value (RCV) of the building:

$$APRP = EADR \times RCV \tag{7.3}$$

The above equation gives the computation of annual pure risk premium in a discrete form. However, it is more appropriate to conduct this computation by using continuous functions for damage and seismic hazard. In this case, equation 7.1 will be used where EAL , $y(s)$ and $v(s)$ correspond to $APRP$, EDR_s and SH_s in equations 7.2 and 7.3. The total earthquake insurance premium is computed by introducing a load factor, which is used to account for the financial cost of the insurance as shown in the following:

$$TP = APRP / (1 - LF) \tag{7.4}$$

where TP is the total insurance premium, LF is the load factor to account for the various administration expenses, taxes, profit and hidden uncertainties.

Table 7.7. Structural Parameters of the Selected Building to be Used with the LPPE

Lateral Strength Index ($\times 10^{-2}$)	Soft Storey Index	Lateral Stiffness Index ($\times 10^{-5} \text{ m}^2$)	Number of Storeys
1.82	1.05	38.10	4

Table 7.7 provides the values of the structural parameters of the hypothetical structure. These values are used with the LPPEs listed in equations 6.13.d to 6.13.f to obtain the global drift ratios. The expected damage ratio is calculated for each global drift ratio by interpolation. Then, the cost of damage is found by using these expected damage ratios and the replacement value of the building. After that, the yearly occurrence probabilities of the earthquakes are multiplied by the expected cost of damage, and the expected annual losses are calculated. By using the discrete annual loss values given in Table 7.8, it is possible to create a continuous cost function for each earthquake with different occurrence probability. With varying earthquake occurrence probabilities, the change in the expected damage ratios and the annual occurrence rates can be modeled by interpolation. The generated curves for the expected damage ratios and annual exceedence rates are presented in Figure 7.5. As the severity of earthquake decreases, reflected by the increased occurrence probability, the expected damage cost decreases exponentially. In Table 7.8, the

lateral performances, the associated expected damage ratios and expected annual loss are lumped at 3 different points. Each value of the mentioned parameters are calculated for different earthquake occurrence probabilities in 50 years as given in the first column of the table.

Table 7.8. Expected Annual Loss Corresponding to Different Earthquake Occurrence Probabilities

Earthquake Occurrence Probabilities in 50 Years	Yearly Occurrence Rate	Global Drift Ratio*	Expected Damage Ratio (%)	Expected Cost of Damage (TL)	Expected Annual Loss (TL)
%10	0.002107	0.0029	14.44	43650.80	91.97
%25	0.005754	0.0016	4.21	12722.50	73.20
%50	0.013863	0.0007	0.70	2115.40	29.32

*LPPEs in equations 6.13.d to 6.13.f are used to obtain these values

After the calculations, annual expected loss is found to be 458.47 TL for a 4-storey reinforced concrete structure with a total area of 464.92 m². The coverage includes the structural and nonstructural elements of the building, which are worth 302198.00 TL. If the load factor is accepted as 0.40 then, then the total (commercial) insurance premium could be set to 764.12 TL.

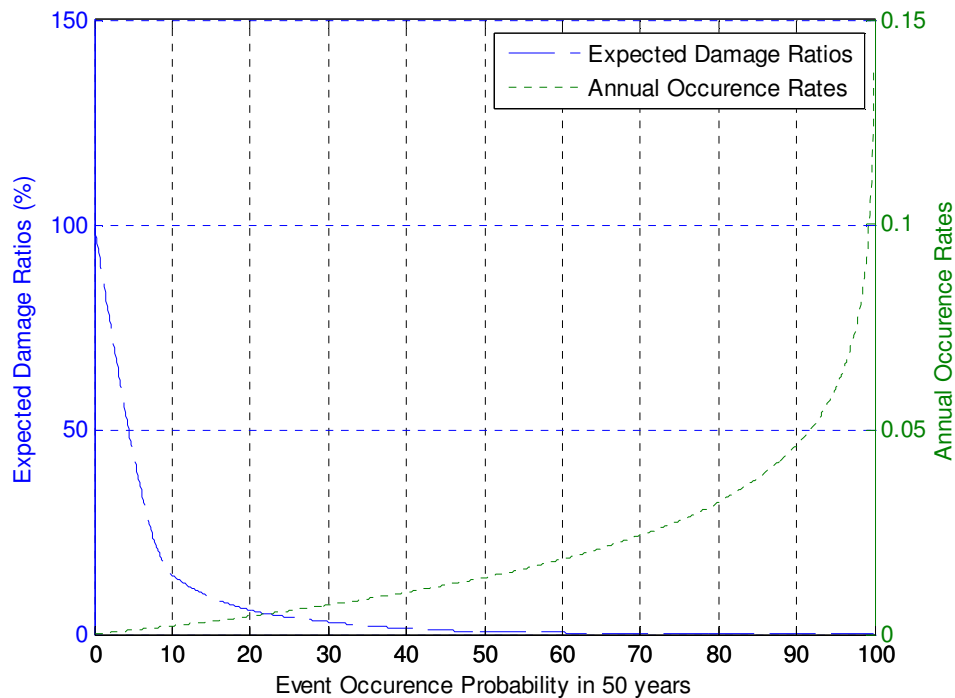


Figure 7.5. Annual Occurrence Rates and Expected Damage Ratios for the Building Considered in the Case Study and for Earthquakes with Different Occurrence Probabilities in 50 years for Eskisehir

When the building is evaluated by the TCIP system of Turkey, the yearly insurance premium is calculated as 123.27 TL for a single storey, with the covered amount is computed as 81.200 TL. The total insurance premium for the building would be 493.08 TL, which yield to 1.06 TL/m².

Considering that the insurance premium obtained with this study is 1.64 TL/m², obviously this study resulted in higher insurance premiums to premiums obtained by TCIP. Lastly, it should be mentioned that, the insurance premiums follow a very similar pattern of global drift ratio scaling with respect to the varying structural parameters in Figure 6.18.

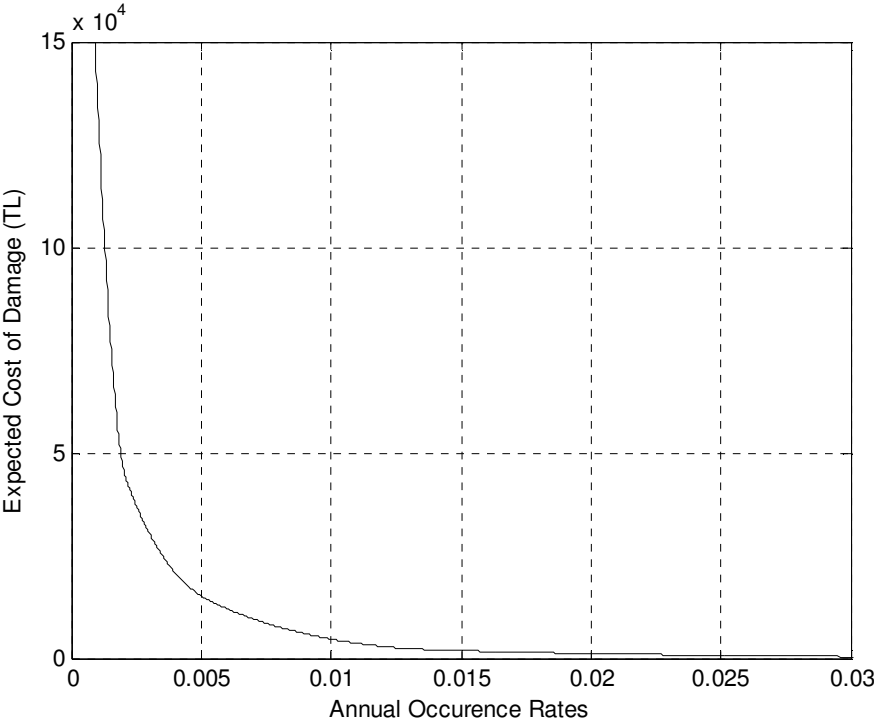


Figure 7.6. Loss Exceedance Curve for the Sample Building Considered for Insurance Premium Computation

7.8. Application of the Developed Scheme

The APRP is computed by using the two elements of the annual loss function given in equation 7.1, namely as the seismic hazard and damage. The seismic hazard is obtained by the application of the procedures given in Chapter 5.

It requires gathering of the seismic activity information, the seismic sources and selecting the most suitable GMPE for the region of interest. The significant uncertainty arises due to the application of various GMPEs with their original

coefficients. Therefore, the locally developed GMPE or a GMPE adapted to the local seismic patterns must be employed for the seismic hazard analysis, which is the case in this study as the GMPE developed by Akkar and Cagnan (2010) is utilized.

For the damage estimation of a structure, which could be a reinforced concrete moment frame or shear walled structure with 4 to 8 storeys, initially the lateral performances in terms of global drift ratios must be obtained by using the equations 6.13.d to 6.13.f. The corresponding damage ratios are found by interpolation of predefined damage ratios corresponding to global drift ratios presented in Table 7.5. Then the discrete values of expected damage ratios and seismic hazard values are converted to continuous form and equation 7.1 is used to obtain the ARPR. The ARPR is then used to obtain the total insurance premium by introducing a load factor to account for the financial cost of the insurance as shown in equation 7.4.

CHAPTER 8

8. SUMMARY AND CONCLUSIONS

8.1. Summary

Since, the purpose of the study is to develop a simple and easy-to-use tool for computing the insurance premiums, every aspect of technical information that is required for insurance calculations are subjected to assessment. The elements of the PSHA, the lateral performance at the exposed level of ground motion and the associated damage ratio of the structures are investigated in detail. The possible improvements are sought in each element of PSHA.

As the first subject of interest, the PSHA is investigated to lay out a more precise way of calculating the seismic hazard by probabilistic approach. The study focused mainly on the most important and controlling aspects of the PSHA that involves large degree of uncertainties. Amongst the several elements of PSHA, GMPE and fault specific recurrence rates are investigated thoroughly, since these elements are open to development and still need improvement. The magnitude conversion, delineation of seismic sources and catalogue completeness issues are examined too since they have been considered as crucial. A flowchart is presented in Appendix G to display the steps of seismic hazard analysis in an organized format.

One of the key elements in PSHA, the GMPEs have a very important role in modeling the propagation of the ground motions to varying distances. In the present study, an adaption procedure is applied to use the forms of the most commonly accepted and widely used GMPEs, instead of developing an original GMPE specific to Eskisehir, or simply borrowing GMPEs with their original coefficients. In fact a local-specific GMPE could be developed but comparison of several forms of different GMPEs has certain advantages since it gives the opportunity to observe the best performing form with the local ground motion database. Moreover, there are already readily available local GMPEs that were developed specifically for Turkey by using the local ground motion database. Hence, the adaption procedure is selected

as the best procedure for the determination of the most suitable GMPE for the application of PSHA for Eskisehir.

After the evaluation of the methods to determine the most suitable GMPE for PSHA, the selected GMPEs are subjected to the adaption procedure by using the ground motion database gathered specifically for the city of Eskisehir, Turkey. All the available ground motion records within the 300 km radius circle centered at Eskisehir are gathered to create the ground motion database. The records are compiled by using different catalogues that cover different periods with different magnitude ranges. Therefore, unification of the magnitudes deemed necessary to obtain a homogeneous catalog in terms of magnitude scales. The magnitude conversion problems are overcome by using the conversion equations developed specifically by using Turkish ground motion data. Lastly, a homogeneous distribution of the magnitude and distance is achieved by careful selection of ground motions in the database.

After the preparation of the ground motion database, adaption of the selected GMPEs is performed by calibrating the coefficients with the local ground motion parameters. In the calibration process, the ground motion amplitudes, the magnitude, distance and other local ground motion parameters are regressed by using the GMPEs to derive the coefficients at the predefined periods. Both multi-stage and single stage regression analysis is employed to derive the coefficients, whereas only the results of single stage multiple regression analysis is utilized due to reliability issues. After the application of the calibration procedure, to reassure the validity of the calibrated coefficients and for the statistical evaluation of the parameters, residual analysis is performed. For further evaluation of the relative performance of the GMPEs in modeling the local ground motion behavior, performances are displayed visually through trellis plots. For the regression analysis, statistical evaluation and for development of the trellis plots, several MATLAB programs are developed and performance comparison of the models is carried out by using these programs.

After the thorough evaluation of the GMPEs for the adaptability to the local seismic pattern of behavior of the region, the best performing GMPE is selected in order to proceed with the PSHA. Then, in order to perform the PSHA for the city of Eskisehir, the earthquake generation sources are identified as area and fault sources,

and the related seismic parameters are quantified. Though very subjective in nature, the area sources are relatively easy to create and related seismic parameters are easy to obtain. Whereas, the fault sources are difficult to identify and the fault parameter derivation is very difficult due to lack of sufficient information. Considering the lack of information and the difficulty in modeling the fault behavior, firstly, the faults surrounding Eskisehir are thoroughly investigated. Then knowing the fact that, a fault line is a complex structure that continuously interacts with the neighboring geological structures, a detailed literature review study is launched to gather information on the fault behavior models.

Owing to the extensive literature review, sizable information about the fault behaviors is gathered. In the literature, the fault behavior is generally modeled by using stress-strain accumulation and releasing patterns. These models form the basic ingredients in developing the physical models to define faults, models of earthquake generation, the rupture propagation models and various timewise and magnitudewise recurrence models.

The models that express both the physical properties and earthquake generation mechanisms are explained by the fault rupture, segmentation and cascade models. Depending on the physical models, geological stress-strain accumulation and release mechanisms that may play an important role in blocking or propagating a rupture are also explained. In addition, various segmentation models and associated recurrence models are also provided in the review. The methods are reviewed and explained for the calculation of fault specific magnitudewise and timewise recurrence rates.

Although there are several models proposed by researchers on earthquake generation, rupture propagation and recurrences in magnitude and time, no single model can explain the complex behavior of the faults, since there are cases both prove the validity of each model and cases proving the contrary. Then the problem became the selection of the most convenient and successful model for the application in PSHA study. Consequently, to be conservative in the hazard analysis, the segmentation model as the physical model and as the earthquake generation model is employed. Then, since all the earthquakes with moment magnitudes above 6.0 are attributed to the faults, the selection of the most suitable magnitude recurrence model for the faults became an important issue. Considering the gathered information about the

seismicity of the various faults and issues of applicability of various models, full characteristic earthquake model, which proposes a uniform distribution of magnitude recurrences above a fault specific magnitude, is utilized.

Timewise recurrence rates of the fault sources have become a subject of investigation due to the importance of these rates in the assessment of seismic hazard. Accordingly, time predictable models and renewal models are reviewed and compared. In the literature, it has been highlighted that without the probability of occurrences in time, a PSHA is not complete. In order to model the earthquake occurrences in time, past seismic activity must be known. However, due to lack of information about the past seismicity, expert opinion is consulted for the timewise recurrences of the fault-generated earthquakes. After the assessment of the models, Possion model is employed with the recurrence rates provided by the expert.

Upon reviewing the fault behavior models and deciding on the most suitable models for PSHA, a specific study is launched about the fault movements. The study involved the estimation of the fault slips and stresses by using satellite measurements in terms of displacements of the selected points on the ground. The satellite measurements at different locations are utilized to create stress-strain maps of the region. Though some parts of the map is questionable in terms of precision because of the fact that it relied on the number of measurements and homogeneous distribution of the measurements in the area, the prepared strain map showed that the dilatational strains in the Eskisehir region signed a contraction, which is also claimed by the researchers. In the end, it is concluded that, the slip measurements specific to the region can improve both the stress-strain calculations for the region and the estimation of a seismic event before the occurrence.

After reviewing the main elements of the PSHA, and seismic data collection and application of procedures on the seismic data for the preparation of PSHA, an earthquake hazard map is obtained by using EZ-FRISK program. The response spectrum curves for earthquakes with different return periods are generated for the city of Eskisehir.

In a specific study independent from the PSHA study, the spatially smoothed seismicity is implemented to develop the seismic hazard map of Eskisehir and the surrounding region. For the application of the method, only two fault sections along

the NAF that generated two large earthquakes of Izmit and Duzce, are modeled as fault sources. The seismic hazard produced by the floating earthquakes and the faults is then combined in a single hazard map. It is shown that unlike the seismic hazard map generated by using EZ-FRISK program, the faults had more impact on the final seismic hazard map.

The second phase of the study is composed of the study of the lateral performance of structures under lateral loads. The main objective in this phase is to develop a Lateral Performance Prediction Equation (LPPE) to predict the lateral performance of the structures, which leads to the determination of the damage ratios and insurance premiums in the end. The proposed structural parameters, which are lateral strength index, soft storey index, lateral stiffness index and number of storeys of the structures in the database, are regressed with the lateral performance indicators in order to develop a simple, easy-to-use, and quickly applicable LPPE. A flowchart is provided in Appendix H that summarizes the followed steps in the development of LPPE.

In order to associate the performance levels with the proposed structural parameters, initially, the scaling (correlation) of lateral performance with the mentioned parameters is investigated. For the determination of the type of scaling of the lateral performance of the structures with the proposed structural parameters, the structures are subjected to modifications by changing the aforementioned structural parameters within certain ranges. Pushover analysis is repeated for the modified structures to be able to monitor the scaling in the lateral performance with respect to the varying structural parameters.

After the derivation of the type of scaling, the original structures are subjected to investigation whether the lateral performances of the original structures are distributed according to the type of scaling observed in the sensitivity analysis. At first, due to the dispersion of the estimated lateral performances, observing the scaling of the lateral performances with respect to the structural parameters was difficult. Therefore, a refinement procedure is developed to remove the outliers in accordance with the procedures of ATC-40 (1996), FEMA-440 (2005) and according to the basic principles of structural behavior under lateral loading. After removing the outliers, the scaling of the lateral performances became more visible.

As one of the crucial criterion of the refinement procedure, it has been observed that the fundamental periods of structures considerably influence the outcome of the lateral performances obtained by CSM, DCM and IDCM. According to the ATC-40 (1996), higher modal effects must be included in the lateral performance analysis to model the exact lateral behavior of the structures with high fundamental periods. However, since the scope of the present study was limited, it was decided to remove all the structural models (buildings) with high fundamental periods. Moreover, structural models with the lower fundamental periods are also subjected to elimination due to the behavioral shifts that the models are exposed with the low fundamental periods. As the second important criterion of refinement procedure, the relative sways at the roof floor due to the torsional influences are monitored. ATC-40 (1996) suggests consideration of the torsional influences in terms of rotational displacements, for the structures with relative sway ratio greater than 1.2. However, since the aim is to identify the scaling characteristics of the lateral performances, the rotational displacements are not considered as the subject matter of this study. Consequently, for the sake of simplicity, the structures with relative sway ratios greater than 1.2 are removed from the list in order to have a more homogeneous database so that the scaling of lateral responses could be better observed. In the application of the refinement procedure, it has been observed that the shear walls are the distinguishing characteristics of the most of the eliminated models due to the high fundamental period criterion.

After the refinement of the database, CSM, the method using the maximum interstorey drift ratios, DCM, IDCM and nonlinear time history analysis are employed to seek a relationship between the proposed structural parameters and the lateral performance of the structures in terms of performance displacements and drifts. In other words, by using the lateral performances estimated by various methods, the validity of the proposed LPPE is investigated. For that purpose, the structural parameters are regressed with the lateral performances in terms of performance spectral displacements obtained by CSM, maximum interstorey drift ratios and performance drifts obtained by DCM and IDCM. Nonlinear time history analysis is performed for the confirmation of the proposed method. Several earthquake records are employed in the analyses, and the lateral performances are then regressed with the proposed structural parameters to confirm the validity of the

scaling between the lateral performance and the proposed parameters and the methods applied to develop the LPPE.

The derivation of the coefficients of the LPPE is performed by using the multiple regression analysis. The database is divided into two since the cross validation of the equation is performed by the arbitrarily selected structures for training and validation stages. Therefore, randomly selected structures or the training sample is used for the development of the equation, and the remaining structures or the validation sample is used to validate the equation. This procedure is repeated several times, and the statistical evaluation of the cross validation stages is performed. If the training and validation stage analysis yielded more than 80% correlation coefficient and the overall significance test p value is less than 0.05 for both training and validation stages, the coefficients of the equations are considered as acceptable. To finalize the determination of the coefficients of the equation, all the statistically valid coefficients are averaged.

After the application of the cross validation procedures, it is concluded that, the LPPE developed by using global drift ratios estimated by IDCM is successful in predicting these global drift ratios by using the proposed structural parameters. Therefore, the global drift ratios are then utilized as lateral performance variable for the nonlinear time history analysis, which is utilized for the validation of the claims about the scaling of lateral performance of structures with the proposed structural parameters. In the application of nonlinear time history analysis, 24 ground motions with 81 records in both east-west and north-south directions are selected from the ground motion database initially compiled for the GMPE adaption procedure. The global drift ratios obtained by the nonlinear time history analysis are regressed with the proposed structural parameters. In general, these regression analyses yielded results that are in general agreement with the claims of this study.

Then, for the purpose of development of LPPE by using the nonlinear time history analysis, a single record, which yielded promising results with the regression analysis, is scaled to create records that represent the earthquakes with the same exceedence probabilities as those used in the development of response spectrum curves. The structures in the database are analyzed with the scaled records, and performance global drift ratios are obtained. Then, these global drift ratios are

regressed with the proposed structural parameters. Unfortunately, the regression analysis with the lateral drifts obtained by using the scaled record did not yield successful results. Therefore, no further scaling is performed with the rest of the ground motion records and no further LPPE development procedure is attempted by using nonlinear time history analysis. However, considering the overall results of the regression analysis with the unscaled records, the claim about the scaling of lateral performances with the proposed structural parameters is validated.

After showing that the lateral performances of the structures can be predicted by using the proposed structural parameters of the buildings, it became clear that these values could be employed for the determination of damage levels and then pure insurance premiums. Initially, lateral response parameters are associated with the damage ratios and cost of damage values. Then, by relating these cost values to the probabilities of the corresponding seismic events, the loss exceedence curves are obtained. After then, it is straightforward to compute the insurance premiums. Following these calculations, the resulting insurance premiums are compared with those of the Turkish Catastrophe Insurance Pool (TCIP) system.

In loss estimation, expert based central damage ratios that were specifically developed for Turkey are utilized. In fact, a procedure relating the damage ratios to the lateral performance variables could be developed just like what has been performed to develop LPPE or to adapt a GMPE. The damage ratios at the performance points could be quantified by using the output of SAP2000 (Computers and Structures, 2011) program. However, this quantification procedure would attract many criticisms since it would be based on calculation of the number of hinges in different level of damage states. Moreover, there is a large degree of uncertainty exists with the accuracy of the modeling of damage, in addition to the subjectivity involved in the damage ratio estimation in the field. Consequently, instead of developing a damage function, it was decided to use expert based damage ratios, just like what has been done in fault parameter assignment.

Another issue in using the expert based damage ratio is that, since it is not based on a continuous function, an interpolation is suggested for the in-between values of damage ratios and global drift ratios. Though none of the developer suggested such a utilization scheme of creating a continuous damage function out of central damage

ratios, it was the necessity that motivated the utilization of damage ratios at certain global drift ratios to obtain a continuous damage function. A continuous function allowed the integration of the damage ratios over a range of damage states and global drift ratios, which in the end supplied the necessary input to insurance calculations.

8.2. Discussion of Results and Main Conclusions

In this section, the results obtained from the case studies are briefly discussed, and based on these results the main conclusions are presented.

- It is observed that there is a large variability in the performance of various GMPEs with varying distance and magnitude ranges. This variability originates from the parameters of the GMPEs and the databases used to derive the coefficients of these parameters. For example, it is observed that using different distance terms whether rupture or Joyner-Boore distance, has significant impact on the outcome of the ground motion at a distance. On the other hand, since the complex parameters of some GMPEs require very specific information that cannot be obtained for Eskisehir, the performances of these GMPEs could be slightly undermined. However, knowing that the weight of these complex parameters could be insignificant, the observed large variability is a valid one.
- As one of the main sources of the uncertainty in seismic hazard analysis, a special attention has to be given to the selection of the right GMPE. The parameters of the right GMPE has to reflect the local seismic behavior and successfully model the local propagation characteristics. In fact, in the present study, it is the significant variation observed in the performance of the selected GMPEs, which automatically led to the idea of adaption procedure. Considering the variation of the performances of various GMPEs, it is concluded that the least could be performed is a pre-evaluation of the readily available GMPEs in order to determine the most suitable GMPE for a local seismic hazard analysis. Otherwise, any averaging method or a logic tree method could lead to inaccurate or even incorrect hazard analysis. However, it should be accepted that, assigning weights to different types of GMPEs and calculating the overall hazard by using different GMPEs with different weights is a valid method when there are not statistically meaningful reasons

to use a single equation. But Eskisehir region had adequate seismic information that gave an opportunity to adapt a GMPE

- In this study, adaption procedure is applied for the selection of the best performing GMPE with the local seismic data. The GMPE coefficients are calibrated by using the ground motion records of the earthquakes and then the most successful GMPE in modeling the local earthquake propagation patterns is selected by using various statistical tools and trellis plots. The statistical evaluation of performances of GMPEs did not yield a conclusive result in the selection; however, trellis plots clearly showed the existence of higher decay of ground motion amplitudes with the distance inherent in the local seismic data and the ability of various GMPEs in modeling the observed behavior. Consequently, it is concluded that, the trellis plots of the various GMPEs are very useful in the selection of the best GMPE in modeling the local propagation patterns.
- Using a database composed of earthquakes with magnitudes above 4.0 in modeling of a GMPE, might cause more decay with the distance compared to employing a database composed of earthquakes above magnitude 5.0 as explained in this study. Despite this fact, there is a consistently higher distance scaling of AC10 and OB04, which were developed by using Turkish ground motions with magnitude greater than 5.0, similar to the rest of the equations. In addition, the poor performance of all GMPEs, except for AC10, to model the distance scaling of earthquakes of Izmit and Duzce as presented in Figure 3.29, gave clues about the inherent distance scaling in Turkish ground motions. Thus, it can be concluded that there is inherent distance scaling in the Turkish ground motions. Furthermore, it may be concluded that before employing a GMPE for a location, the local patterns of behavior of the ground motions must be carefully investigated and the relative performance of the GMPEs with respect to the local data must be checked.
- The seismic hazard map produced for Eskisehir by using the seismic activity data of the region and the fault sources modeled for the surrounding area, reflect the existing seismic threats. Especially around the faults, there is a high concentration of seismic hazard, while the hazard fades away as the

distance from the fault sources increases. A few areas generate more seismic threats than any other source including the faults, which is a sign of high clustering of earthquake generation sources in and around that area. Compared to the official seismic hazard map of Turkey, in the official map, there are not any localized areas of highly concentrated seismic hazard, which implies that the official map may require a revision to reflect the up-to-date seismic activity data compiled for the city of Eskisehir.

- The dependency of lateral performance on the proposed structural parameters of lateral strength index, soft storey index, lateral stiffness index and number of storeys is clearly shown by the sensitivity analysis. As one of the main highlights of this study, it is proved that the lateral performance in terms of drifts and displacements are inversely and nonlinearly dependent on the lateral strength and stiffness indexes both for the shear and for the flexural type of response. The type of relationship is demonstrated to be linear with the soft storey index and number of storeys.
- The relationships obtained via the sensitivity analysis are violated by a group of outliers that have significant deviations from the main sample with their outlier lateral performances. These structural models also have significantly higher and lower fundamental periods and high relative sway ratios, which also happen to be outside the limitations prescribed by ATC-40 (1996) and FEMA-440 (2005) for the utilization of CSM, DCM and IDCM. According to these limitations, structures with fundamental periods higher than 1.0 s and relative sway ratios higher than 1.2 require special treatment if the lateral performance of these structures are to be found. Within the present study, these limitations are extended further by imposing a lower bound for the fundamental period as 0.35 s and an upper bound as 0.80 s, while relative sway ratio limit remained as mentioned. The extension of the limitation is justified by the different regions that were formed in the displacement spectrum curves in Figure 5.25 and the lateral performance distribution of the samples in the database, which also are largely based on the response spectrum curves. Due to the dependency of the lateral performance on the fundamental period and on the height and number of storeys of the

structures, the imposition of upper and lower bounds for the fundamental periods is reasonable with a justified physical background.

- The main disadvantage of the imposing of the limits on the fundamental period is that, the narrow band of estimated roof displacements as shown in Figure 6.20. For the considered region of the fundamental periods, the roof displacements and global drift ratios show a pattern of behavior with lesser variation. This behavior is very well reflected in the development of the LPPE and the coefficients are derived accordingly. Unfortunately, the prediction capability of the developed LPPE is also limited with the sample lateral performances since the regressed lateral performance values display a narrow range of values.
- Out of 27 structural models that are eliminated due to the fundamental period and relative sway ratio criteria, 15 of them are shear walled structures. These structural models also have lower strength and ductility ratios, which are accompanied by higher fundamental periods. However, despite the fact that almost half of the remaining structures have shear walled structural systems, it is proved that the lateral performance of a sample of structures can be related to the structural parameters regardless of the type of structural system in the sample. Therefore, it can be concluded that the classification criteria of the sample database must not rely on the structural system, but on fundamental periods and relative sway ratios if a predictable pattern of behavior is sought with respect to the proposed parameters.
- As one of the aims of the study is to develop a simple and easy to use tool for calculating the lateral performance of a structure, the proposed method proved to be promisingly satisfactory in terms of predicting the lateral performance. However, during the evaluation of the structural models in the database, it is realized that not all the structures perform in a predictable pattern or in general trend with the most of the structures in the database. Therefore, elimination criteria had to imposed, which reduced the number of structural models from 74 to 35. The overall number of eliminated structural models is 39, including the 12 models that are eliminated due to the low modal mass participation ratio.

Consequently, in order to reach a predictable pattern of behavior in terms of roof displacements and global drift ratios, out of 74 structural models, 39 structures, or more than half of them had to be removed. Table 8.1 lists the number of eliminated structural models and the associated elimination criterion.

Table 8.1. Total Number of Eliminated Structures and the Associated Elimination Criteria

Number of Eliminated Models	Elimination Classification	Elimination Criterion
12	Technical	Modal mass participation
10	Technical	Fundamental period
7	Technical	Fundamental period and relative sway ratio
9	Technical	Relative sway ratio
1	Visual	Ultimate base shear coefficient

Considering the purpose of the study, which is to develop a simple and easy-to-use tool for calculating the insurance premiums, it is understood that, procedure like the one proposed in this study is very challenging. The elimination criteria listed in Table 8.1, which are modal mass participation ratio, fundamental period and relative sway ratio are impossible to obtain unless a 3-dimensional model of the structure is analyzed.

Since one cannot know the modal mass participation ratio, fundamental period and relative sway ratio of a structure by just checking physically, a strategy must be developed to create a more generalized LPPE to cover whole range of structures. However, it should be admitted that only development of a successful LPPE that is developed for a specific response spectrum curve and specific group of structures would lead to development of a generalized LPPE that covers wider spectrum of structures. In other words, if groups of structures, which have the structural characteristics of the eliminated structures, could be assembled, according to the results obtained by the sensitivity analysis, a LPPE could be developed specific to the assembled database. Therefore, the promising results in this study would eventually pave the way to improve the LPPE to cover whole range of structures

Considering the above facts, the priority is given to develop a LPPE for the response spectrum curves developed for Eskisehir and specific group of structures with certain limits in terms of fundamental periods and sway ratios. Moreover, it is deduced that, the proposed LPPE could be modified for more successful modeling and the coverage spectrum could be extended to include wider spectrum of structures.

- The loss estimation study showed that the computed insurance premium is significantly higher than those applied by the TCIP system. Therefore, it is concluded that a local specific study should be initiated to evaluate the current insurance system and the possible variations due to the local characteristics of the structures and local seismicity must be reflected to the insurance scheme. In addition, since a structure specific evaluation tool is more appealing for the evaluation of each insurance policy holder, the proposed method gives the opportunity to the policyholders in the evaluation of their property by knowing the lateral performance of their property. Therefore, instead of using a classification scheme that groups the structures with a simple classification system, the proposed procedures offer a structure specific insurance scheme, which enable a better evaluation system. Therefore, structures with a sound quality, which is punished by the poorly performing structures in the TCIP system just because both structures belong to the same group, have a better chance of being evaluated fairly. Therefore, with the proposed system, structures with a better quality are awarded by charging them with low insurance premiums.

8.3. Recommendations for Future Studies

Obviously, there is an urgent need to improve the calculation methods of the seismic hazard and associated risk in order to have more accurate loss estimation. All the elements of seismic hazard and risk calculations offer many improvement opportunities.

As one of the elements of seismic hazard calculation, in order to quantify the occurrence probability of the earthquakes, it is required to know all the dynamics that govern the plate behavior. With today's technology and knowledge, it cannot be realized. However, there is continuous progress on the subject, which creates more

opportunities to understand the real behavior of geological structures. Consequently, the possibility of calculating the real seismic hazard increases day by day.

Until all the unknowns are solved about the real behavior of faults, closest behavior models must be developed in order to model the seismic data of the past and today. Together with satellite measurements, local measurements of the plate movements and ground profiling studies, the behavior of a fault system could be explained as close as possible and characteristics of future earthquakes can be estimated more precisely. Moreover, there should be procedures that are developed to employ this information in order to model the occurrence of the earthquakes in the near future. In fact, it was the author's intention to develop such a program by integrating the past earthquake history on a fault system with the current stress-strain contour of the same system. This kind of calculations would provide the most realistic explanations of the possible earthquake event in terms of occurrence location, occurrence time and the magnitude. However, since it would be a shift from the focus of the study, only the stress-strain contours of the whole region were generated and the fault recurrence rates were obtained through expert opinion. In addition, it was clarified that, eventually, there should be studies that consider the existing stress and strains on a fault, the movements on the fault and the seismic history of the fault so that more physically fitting models could be developed for faults or fault systems.

Accordingly, a more consistent and realistic model must be developed in order to explain the earthquake recurrences. An ideal model must include segmentation, slip rates of the segments, stress accumulation schemes, segment boundary conditions, probabilities of rupture propagation paths, initial stress conditions of the fault segments and its effects in rupture propagation to explain the occurrences of events and future projections

Together with the selection of the fault behavior models and assignment of fault parameters, GMPE selection or the development of a new GMPE is identified as one of the elements of PSHA that requires special attention. It is always difficult to decide on the right GMPE for a location. A study simply and specifically based on the comparison of the various GMPEs according to the intention of development and database characteristics and the performances with the varying parameters could provide a beforehand evaluation according to the needs of the user. Moreover, local

seismic characteristics change from one location to the other, therefore, another study could focus on the local propagation characteristics of several different locations in order to stress the significance of the subject and show the variation of propagation in different locations.

Despite the fact that the renewal models of earthquake occurrences in probabilistic seismic analysis are very crucial, Poisson distribution of earthquake occurrence was taken into consideration for the fault sources. The reason why the renewal models are not employed is the lack of necessary seismic parameters and the applicability limitations. A study must include the time dimension of the seismic hazard analysis by chronologically listing all the known significant events according to the occurrence dates and the associated faults that generated the events. Then, a renewal model must be developed by using the available data that could be completed through expert opinion if necessary. Next, the present-day seismic hazard map, which could be periodically updated, should be prepared. A further improvement in such a map would be to include the stress-strain contours on the map as background to see the stress patterns along the faults.

The study also suggests that there is an opportunity for development of lateral performance-structural parameter relationships. Several structural parameters could be included for a more precise prediction of the lateral performance. The structural parameters such as the hinge characteristics, column longitudinal reinforcement ratio, the ratio of total column inertias to the total beam inertias in a single floor, and the width to height ratio of a building could be added to the proposed structural parameters to see if there is a stronger relationship than it is found in this study. Especially, while the type of hinges does not determine the shape of the pushover curve, technically speaking, it determines how much lateral drift can be observed at the ultimate limit state. Therefore, the type of hinges and the lateral response dependency must be investigated in detail as a subject of another study.

Different lateral performance variables offer different information about the structures and therefore must be evaluated separately. The spectral accelerations and displacements at yields and ultimate drift ratios, base shear or base shear coefficient, global drift ratios, interstorey drift ratios and their relation to the structural parameters could be investigated. Further investigation is required to relate these

lateral performance variables to the fundamental periods of structures.

Minimum modal mass participation ratio is set to 60% for the elimination scheme of structures that are employed in the study. Indeed, the higher the modal mass participation ratio means the closer the pushover analysis results to the real performance of the structure by default. In other words, there is more chance of success of deriving the proposed relationship by using the structures with the higher ratios of modal mass participation. Therefore, a future study must aim to set the minimum modal mass participation ratio as high as possible.

Ignoring the initial stresses in the pushover analysis could yield to the better association of the lateral performances with the structural parameters. Consequently, both sensitivity analysis and the development of LPPE could be performed with the structural models that have no initial stresses. Moreover, the influence of the initial stresses can be measured by comparing the results that are obtained by the analyses with the initial stresses.

Lateral load shapes determine the structural behavior and reflect the characteristics of the load distribution in the global displacements and drifts. While the uniform loading pattern accounts for the inertia forces in the horizontal direction only, load pattern with inverse triangular shape considers mostly the overturning inertial forces. However, the real behavior might be in between these two extreme cases of inertial responses. Therefore, the lateral response dependency on the lateral load patterns must be known better in order to decide on the best lateral load pattern. If the composition of the structures with respect to the type of response is known then the right load patterns could be applied. In this study, a modal shape lateral load pattern is applied to account for the combined shear and flexural responses. However, the same procedures in the development of LPPE could be repeated by using different load patterns and the relative performance of LPPE could be measured.

Another improvement in the development of LPPE would be the inclusion of many types of buildings in terms of structural responses. Obviously, structures with low modal mass participation ratios, very low or very high fundamental periods and high relative sway ratios have different pattern of lateral performances. Consequently, it is concluded that a more inclusive model have to developed by considering the different pattern of behavior of structures with respect to the listed technical criteria

of elimination in Table 8.1. In a new study, in addition to the criteria in this table, especially ductility ratios, the ratios of post elastic stiffness to elastic stage stiffness and strength reduction factors must be thoroughly investigated in establishing a sample with a predictable pattern of behavior. In addition, the proposed LPPE must be modified in order to consider the influence of the mentioned criteria of elimination on the lateral performance of the structures.

The influence of the shear wall on the lateral performances of structures was shown in the application of refinement procedures in Chapter 6. Most of the eliminated structures due to high fundamental period criterion are shear walled. Though half of the refined database was composed of shear walled systems, which means that shear walls might not create such an outlier performance, the degree of influence of shear walls could be investigated. Therefore, before performing a study to evaluate the lateral performance of structures, a classification could be imposed according to their structural systems as heavily shear walled, lightly shear walled or simple frame structures. The group of structures formed with respect to their structural systems could be analyzed separately and the LPPE could be developed accordingly.

For the loss estimation part of the study, the year of construction, the type of the structure according to material and the structural system could be reconsidered. The reinforced concrete structures belong to the same group and evaluated within the single group, however there are structures with very high or low quality considering the lateral performances. Therefore, a structure-specific system of this study could be improved such that groups of structures can be evaluated with a different classification scheme in terms of quality. As a result of new classification system the structures with high performances could be awarded with lower insurance premiums, in opposition to the structures with lower performance which could be penalized by higher insurance premiums.

The establishment of damage limit states by using the average yield and ultimate global drift ratios should also be reviewed to obtain a generalized relationship between the global drift ratio-damage limit state relationships specific to each structure. In other words, similar to the procedures applied in the development of LPPE, an equation could be developed to associate the yield and ultimate global drift ratios with the structural parameters. In addition, base shear coefficients and base

shear at the yield and ultimate stages could be associated with the proposed structural parameters too. The damageability of the structures could be analytically modeled with the consideration of assigned hinges and the associated performance levels of these hinges and the proposed structural parameters could be regressed with the number of hinges in various levels of performances. Hence, a damage prediction function could also be developed just like developing LPPE, which predicts the lateral performance in terms of performance drifts.

The damage ratios corresponding to each damage state and the lateral performance variable must be studied so that continuous damage functions can be derived. Indeed, the possibility of restoring the structures to the original shape and functionality must be considered in the creation of a damage function, since beyond certain percentage of damage, instead of repairing the structure, demolishing could be more feasible.

Finally, to be able to modify the premiums for pre-2007 periods, the weight of the construction periods in setting the premiums could be adjusted by adding an adjustment factor after a detailed investigation. These premiums could further be modified via a more precise geographical variation rather than seismic hazard zones to take the differences associated with different soil conditions and practices of construction into account.

REFERENCES

- Abrahamson N.A. and Silva W.J. (1997). Empirical Response Spectral Attenuation Relations for Shallow Crustal Earthquakes, *Seismological Research Letters*, Vol. 68, No. 1, pp. 94-127.
- Abrahamson N.A. and Silva W.J. (2008). Summary of the Abrahamson and Silva Ground-Motion Relations, *Earthquake Spectra*, Vol. 24, Issue I., pp. 67-97.
- Aki K. (1966). Generation and Propagation of G-waves from the Niigata Earthquake of June 16,1964, *Bulletin of Earthquake Research Institute*, Vol. 44, pp. 23-88.
- Akkar S., Yazgan U., Gulkan P. (2005). Drift Estimates in Frame Buildings Subjected to Near-Fault Ground Motions, *ASCE Journal of Structural Engineering*, pp.1014-1024.
- Akkar S. and Bommer J.J. (2007). Prediction of Elastic Displacement Response Spectra in Europe and the Middle East, *Earthquake Engineering and Structural Dynamics*, Vol. 36. pp.1275-1301.
- Akkar S. and Metin A. (2007). Assessment of Nonlinear Static Procedures In FEMA-440, *Journal of Structural Engineering, ASCE*, Vol. 133 No. 9, pp. 1237-1246.
- Akkar S. and Bommer J.J. (2010). Empirical Equations for the Prediction of PGA, PGV, and Spectral Accelerations in Europe, the Mediterranean Region, and the Middle East, *Seismological Research Letters*, Vol.81, pp. 195-206.
- Akkar S. and Cagnan Z. (2010). A Local Ground Motion Predictive Model For Turkey And Its Comparison With Other Regional And Global Ground-Motion Models, *Bulletin of the Seismological Society of America*, Vol.100, pp. 2978-2995.
- Akkar S., Cagnan Z., Yenier E., Erdogan E., Sandikkaya M.A., Gulkan P., (2010). The Recently Compiled Turkish Strong-Motion Database: Preliminary Investigation For Seismological Parameters, *Journal of Seismology*, Vol.14, pp. 457-479.
- Algan B. B. (1982). *Drift And Damage Considerations In Earthquake Resistant Design Of Reinforced Concrete Buildings*, Ph.D. thesis, Univ.of Illinois, Urbana-Champaign, Ill.
- Altunel E. and Barka A. (1998). Neotectonic activity of Eskisehir fault zone between Inonu and Sultandere, *Geological Bulletin of Turkey*, Vol.41, No.2, pp. 41-52.
- Ambraseys N.N. and Finkel, C.F. (1991). *Long-Term Seismicity Of Istanbul And Of The Marmara Region*, *Engineering Seismology*, Earthquake Report, 91/8, Imperial College.
- Ambraseys N.N. and Finkel, C.F. (1995). *The Seismicity of Turkey and Adjacent Areas*. Eren Yayıncılık, Istanbul, Turkey.
- Ambraseys N. (2009). *Earthquakes in the Mediterranean and Middle East: A Multidisciplinary Study of Seismicity up to 1900*, Cambridge University Press.
- Aochi H., Scotti O., Berge-Thierry C. (2005). Dynamic Transfer Of Rupture Across Differently Oriented Segments In A Complex 3-D Fault System, *Geophysical Research Letters*, Vol 32, L21304

- Askan A. and Yucemen M.S. (2010). Probabilistic Methods for the Estimation of Potential Seismic Damage: Application to Reinforced Concrete Buildings in Turkey, *Structural Safety*, Vol. 32, pp.262-271
- ATC-13 (1985), *Earthquake Damage Evaluation Data for California*, Applied Technology Council, California, USA
- ATC-40 (1996), *Seismic Evaluation and Retrofit Of Concrete Buildings*, Applied Technology Council, California, USA
- ATC-55 (2003), *Improvement of Inelastic Seismic Analysis Procedures*, Applied Technology Council, California, USA
- Ayhan M.E., Demir C., Lenk O., Kılıçoğlu A., Altıner Y., Reilinger R., Barka A., Ergintav S., Ozener H. (2002). Interseismic Strain Accumulation in the Marmara Region, *Bulletin of the Seismological Society of America*, Vol. 92, No.1, pp. 216-229
- Barka A., Reilinger, R., Saroglu, F., Sengor, A.M.C. (1995). *The Isparta angle: its importance in the neotectonics of the eastern Mediterranean region*, Piskin O., Ergun M., Savascın M.Y., Tarcan G. (ed.). IESCA-1995 Proceedings, 3-17.
- Barka A. (1996). Slip Distribution along the North Anatolian Fault Associated with the Large Earthquakes of the Period 1939-1967, *Bulletin of the Seismological Society of America* Vol 86, pp.1238-1254.
- Beyaz T. (2004). *Zemin Etkisinden Arındırılmış Deprem Kayıtlarına Göre Türkiye İçin Yeni Bir Deprem Enerjisi Azalım Bağantısının Gelistirilmesi*, Ph.D. Thesis, Ankara, Turkey (In Turkish)
- Bommer J., Spence R., Erdik M., Tabuchi S., Aydınoglu N., Booth E., del Re D., Peterken O. (2002). Development of an Earthquake Loss Model for Turkish Catastrophe Insurance, *Journal of Seismology*. Vol. 6, pp. 431-446.
- Bonilla M.G., Mark R.K., Lienkaemper J.J. (1984). Statistical Relations Among Earthquake Magnitude, Surface Rupture Length, and Surface Fault Displacement, *Bulletin of the Seismological Society of America*, Vol.74, No.6, pp. 2379-2411.
- Boore D. M. and Atkinson G. (2008). Ground Motion Prediction Equations for the Average Horizontal Component of PGA, PGV, and 5%-damped PSA at Spectral Periods between 0.01 s and 10.0 s, *Earthquake Spectra* Vol.24, No.1, pp. 99–138.
- Boore D.M., Joyner W.B., and Fumal T.E. (1997). Equations for Estimating Horizontal Response Spectra and Peak Acceleration from Western North American Earthquakes: A summary of Recent Work, *Seismological Research Letters* Vol.68, No.1, pp. 128–153.
- Bozorgnia Y. and Bertero V.V. (2001). Improved Shaking and Damage Parameters for Post-earthquake Applications, *Proceedings, SMIP01 Seminar on Utilization of Strong-Motion Data, California Division of Mines and Geology*, Los Angeles, pp. 1–22.
- Bracci J.M., Kunnath S.K., Reinhorn A.M. (1997). Seismic Performance and Retrofit Evaluation Of Reinforced Concrete Structures, *Journal of Structural Engineering-ASCE*, Vol.. 123, No.1, pp. 3-10.

- BU-ARC (2002), *Earthquake Risk Assessment for Istanbul Metropolitan Area, Project Report*, BU Publications. (<http://www.koeri.boun.edu.tr/depremmuh>, 2012)
- Campbell K.W. (1997). Empirical Near-Source Attenuation Relationships for Horizontal and Vertical Components of Peak Ground Acceleration, Peak Ground Velocity, and Pseudo-Absolute Acceleration Response Spectra, *Seismological Research Letters*, Vol. 68, No.1, pp.154 -179.
- Campbell K.W. and Bozorgnia Y. (2003). Updated Near-Source Ground Motion (Attenuation) Relations For The Horizontal And Vertical Components Of Peak Ground Acceleration And Acceleration Response Spectra, *Bulletin of the Seismological Society of America*, Vol.93. No.1, pp.314 -331.
- Campbell K.W. (2003). Prediction of Strong Ground Motion Using the Hybrid Empirical Method and Its Use in the Development of Ground-Motion (Attenuation) Relations in Eastern North America, *Bulletin of the Seismological Society of America*, Vol. 93, pp.1012–1033.
- Campbell K.W. (2004). Erratum: Prediction of Strong Ground Motion Using the Hybrid Empirical Method and Its Use in the Development of Ground-Motion (Attenuation) Relations in Eastern North America, *Bulletin of the Seismological Society of America*, Vol. 94, No.6, 2418.
- Campbell K.W. (2007). *Validation and Update of Hybrid Empirical Ground Motion (Attenuation) Relations for the CEUS*, U.S. Geological Survey
- Campbell K., and Bozorgnia Y. (2008). NGA Ground Motion Model for The Geometric Mean Horizontal Component of PGA, PGV, PGD and 5% Damped Linear Elastic Response Spectra for Periods Ranging from 0.01 s to 10 s, *Earthquake Spectra*, Vol.24, No.1, pp. 139–171.
- Cao A.M. and Gao S.S. (2002). Temporal Variations of Seismic b-values Beneath Northeastern Japan island Arc, *Geophysical Research Letters*, Vol.29, No.9, pp.1-48.
- CEN (2004). *Eurocode 8: Design of Structures for Earthquake Resistance. Part 1: General Rules, Seismic Actions and Rules for Buildings, European Standard EN 1998-1:2004*, Comité Européen de Normalisation, Brussels, Belgium.
- Chiou, B. and Youngs R (2008). An NGA Model for the Average Horizontal Component of Peak Ground Motion and Response Spectra, *Earthquake Spectra*, Vol. 24, No.1, pp. 173–215.
- Chopra, A.K. and Goel, R.K. (2001). *A Modal Pushover Analysis Procedure to Estimate Seismic Demands for Buildings: Theory and Preliminary Evaluation*, Report No. PEER 2001/03, Pacific Earthquake Engineering Research Center, University of California, Berkeley, California.
- Chopra A.K. and Goel R.K. (2002). A Modal Pushover Analysis Procedure For Estimating Seismic Demands For Buildings, *Earthquake. Engineering and. Structural Dynamics*, Vol. 31, No.3, pp. 561–582.
- Chopra A.K. and Goel R.K. (2003). *A Modal Pushover Analysis Procedure to Estimate Seismic Demands for Buildings: Summary and Evaluation*. 5th National Conference on Earthquake Engineering, Istanbul, Turkey.

- Chopra A.K., Goel R.K., Chintanapakdee C. (2003). Statistics of Single-degree-of freedom Estimate of Displacement for Pushover Analysis of Buildings, *ASCE, Journal of Structural Engineering*, Vol. 119, pp. 459-469.
- Chopra A.K., Goel R.K., Chintanapakdee C. (2004). Evaluation of a Modified MPA Procedure Assuming Higher Modes as Elastic to Estimate Seismic Demands, *Earthquake Spectra*, Vol. 20, pp. 757-778.
- Computers and Structures, Inc. (2000). *SAP 2000 Version 15*, Structural Analysis Program, Berkeley, CA.
- Cornell C.A. (1968). Engineering Seismic Risk Analysis, *Bulletin of Seismological Society of America*, Vol. 58, pp. 1583-1606.
- Cornell C.A. and Vanmarcke E.H., (1969) The Major Influences On Seismic Risk. *Proceedings of the Fourth World Conference on Earthquake Engineering*, Santiago, Chile. A-1, pp. 69-93.
- Cramer C.H. Petersen M.D., Cao T., Topozada T.R., Reichle M.S. (2000). A Time-Dependent Probabilistic Seismic-Hazard Model for California, *Bulletin of the Seismological Society of America*, Vol.90, pp.1–21.
- Cummins, J.D., and Mahul O. (2009). *Catastrophe Risk Financing in Developing Countries: Principles for Public Intervention*. The World Bank. Washington, DC.
- Deniz A. (2006). *Estimation of Earthquake Insurance Premium Rates for Turkey*, M.Sc. Thesis, Dept. of Civil Engineering, METU, Ankara
- Deniz A. and Yucemen M.S. (2008). *Processing Earthquake Catalog Data for Seismic Hazard Analysis*, 8th International Congress on Advances in Civil Engineering, North Cyprus
- Douglas J. (2004). An Investigation of Analysis of Variance as a Tool for Exploring Regional Differences in Strong Ground Motions, *Journal of Seismology*, Vol.8, pp.485-486
- Douglas J. (2004). *Use of Analysis of Variance for the Investigation of Regional Dependence of Strong Ground Motions*, Proceedings of Thirteenth World Conference on Earthquake Engineering. Paper no. 29.
- Douglas J. (2007). On The Regional Dependence of Earthquake Response Spectra, *ISET Journal of Earthquake Technology*, Vol. 44, No.1, pp. 71–99.
- Duman Y.T., Emre O., Dogan A., Ozalp S. (2005). Steepland and Bend Structures along the 1999 Duzce Earthquake Surface Rupture, North Anatolian Fault, Turkey. *Bulletin of Seismological Society of America*, Vol. 95 No.4, pp. 1250–1262.
- Duzgun H.S. and Yucemen M.S. (2007). *Kentsel Alanlarda Bütünleşik Deprem Riski Modeli: Eskişehir Örneği*, TMMOB Afet Sempozyumu, s.201-211 (In Turkish)
- Eberhard M.O. and Sozen M.A. (1993). Behavior-based Method to Determine Design Shear in Earthquake-resistant Walls, *Journal of Structural Division*, Vol. 119, No. 2, pp. 619-640.
- Erdik M., Doyuran V., Yucemen S.M., Gulkan P., Akkas N. (1985). *A Probabilistic Assessment of The Seismic Hazard in Turkey for Long Return Periods*, Proceedings of 3rd International Earthquake Microzonation Conference, Seattle, Washington, pp.1261-1272.

- Erdik M., Doyuran V., Akkas N., Gulkan P. (1985). A Probabilistic Assessment Of The Seismic Hazard In Turkey, *Tectonophysics*, Vol. 117, pp. 295-344.
- Erdik M., Biro Y., Onur T., Sesetyan K., Birgoren G. (1999). Assessment of Earthquake Hazard in Turkey and Neighboring Regions – GSHAP, *Annali di Geofisica*, Vol. 42, No.6. pp. 1125-1138.
- Erdik M., Aydinoglu N., Fahjan Y., Sesetyan K., Demircioglu M., Siyahi B., Durukal E., Ozbey C., Biro Y., Akman H., Yuzugullu O. (2003). Earthquake Risk Assessment for Istanbul Metropolitan Area. *Earthquake Engineering Engineering Vibrations* Vol.2, No.1:pp.1–25
- Ergin K., Güçlü U., Uz Z. (1967). *Türkiye Ve Civarının Deprem Kataloğu (Milattan Sonra 11 Yılından 1964 Sonuna Kadar)*. İ.T.Ü., Maden Fakültesi Arz Fiziği Yayınları (In Turkish)
- Fajfar P. and Fischinger M. (1988). *N2-A Method For Nonlinear Seismic Analysis Of Regular Building*, Proceedings 9th World Conference of Earthquake Engineering, Tokyo, Vol.5 pp.111-116.
- Felzer K. (2007). *Universality of Gutenberg-Richter Relationship*, U.S. Geological Survey, Pasadena, California, USA
- FEMA-273 (1997). NEHRP Guidelines for Seismic Rehabilitation Of Buildings. *Federal Emergency Management Agency Report: FEMA 273*. Washington D.C.,USA
- FEMA-274 (1997). Commentary on the Guidelines for Seismic Rehabilitation of Buildings. *Federal Emergency Management Agency Report: FEMA 273*. Washington D.C.,USA
- FEMA-356 (2000). *Prestandard and Commentary for the Seismic Rehabilitation of Buildings*, Washington D.C.,USA
- FEMA-440 (2005). Improvement of Nonlinear Static Seismic Analysis Procedures, *Federal Emergency Management Agency Report, FEMA.440*, Washington D.C., USA.
- Field E.H. (2007). Special Issue: Regional Earthquake Likelihood Models. *Seismological Research Letters* Vol. 78, No.1, pp.7-16
- Firat, F.K. (2007). *Development of Load and Resistance Factors for Reinforced Concrete Structures in Turkey*, Ph.D. Thesis, 293 pp., METU, Ankara, Turkey
- Firat, F.K. and Yucemen, M.S. (2014). Determination of Reliability Based New Load and Resistance Factors for Reinforced Concrete Structural Members. *Tek. Dergi*, Vol. 420, pp. 6805-6829
- Flerit F., Armijo R., King G., Meyer B. (2004). The Mechanical Interaction Between the Propagating North Anatolian Fault and the Back-arc Extension in the Aegean. *Science Letters*, Vol. 224 No.3-4, pp.347-362.
- Frankel A. (1995). Mapping Seismic Hazard in the Central and Eastern United States, *Seismological Research Letters*, Vol. 66, No. 4,pp. 8–21.
- Freeman S.A., Nicoletti J.P., Tyrell J.V. (1975). *Evaluations of Existing Buildings for Seismic Risk—A Case Study of Puget Sound Naval Shipyard, Bremerton*,

Washington. Proceedings of the 1st US National Conference on Earthquake Engineering, Oakland, California, pp. 113–122.

Gardner J.K. and Knopoff L. (1974). Is the Sequence of Earthquakes in Southern California, with Aftershocks Removed, *Bulletin of the Seismological Society of America*, Vol. 64, pp.1363-1367.

Genç G. (2004). *Probabilistic Seismic Hazard Assessment for Eskisehir*, M.Sc. Thesis, Geological Engineering Department, METU

Gençturk B. and Elnashai A.S. (2008). Development and Application of an Advanced Capacity Spectrum Method, *Engineering Structures*, Vol. 30, pp. 3345-3354.

Ghobarah A. (2004). *On Drift Limits With Different Damage Levels*. In: Proceedings of International Workshop on Performance-based Seismic Design Concepts and Implementation, Bled, Slovenia

Goel R.K. and Chopra A.K. (1997). Period Formulas for Moment-resisting Frame Buildings, *Journal of Structural Engineering*, ASCE 123 Vol.11, pp.1454–1461.

Goel R.K. and Chopra A.K. (1998) Period Formulas for Concrete Shear Wall Buildings, *Journal of Structural Engineering*, ASCE, Vol.4, pp. 426-433.

Goel R.K. and Chopra A.K. (2004). Evaluation of Modal and FEMA Pushover Analysis: SAC Buildings, *Earthquake Spectra*, Vol.20, No. 1, pp. 225-254.

Gulkan P., Kocyigit A., Yucemen M.S., Doyuran V., Basoz N. (1993). *En Son Verilere Göre Hazırlanan Türkiye Deprem Bölgeleri Haritası*. Ortadoğu Teknik Üniversitesi İnşaat Mühendisliği Bölümü, Rapor no. 93-01 (In Turkish).

Gulkan P. and Sozen M. A. (1999). Procedure for Determining Seismic Vulnerability of Building Structures, *ACI Structural Journal*, Vol. 96, No.3, pp. 336–342.

Gulkan P. and Akkar S. (2002). A Simple Replacement for the Drift Spectrum, *Engineering Structures*, Vol. 24, No.11, pp. 1477–1484.

Gulkan P. and Kalkan E. (2002). Attenuation Modeling of Recent Earthquakes in Turkey. *Journal of Seismology*, Vol. 6, pp. 397-409.

Gupta B. and Kunnath S.K. (1999). *Pushover Analysis of Isolated Flexural Reinforced Concrete Walls*. Structural Engineering in the 21st Century, Proceeding of Structures Congress, New Orleans, USA

Gurpinar A., Abalı M., Yucemen M.S., Yesilcay Y. (1978). *Feasibility of Mandatory Earthquake Insurance in Turkey*. Earthquake Engineering Research Center, Report No. 78-05, Middle East Technical University, Ankara (In Turkish).

Guyader A.C. and Iwan W.D. (2006). Determining Equivalent Linear Parameters for Use in a Capacity Spectrum Method of Analysis., *Journal of Structural Engineering*, Vol 132., No.1, pp.59-67.

Harris R.A., Archuleta R.J., Day S.M. (1991). Fault Steps and the Dynamic Rupture Process: 2-D Numerical Simulations of a Spontaneously Propagating Shear Fracture, *Geophysical Research Letters*, Vol. 18, pp.893-896.

Harris R.A., Day S.M. (1999). Dynamic 3D Simulations of Earthquake on an Echelon Fault, *Geophysical Research Letters*, Vol 26, pp.2089-2092.

- Hanks T.C. and Kanamori H. (1979). A Moment Magnitude Scale, *Journal of Geophysical Research*, Vol. 84, pp. 2348-2350.
- Hattori S. (1979). Seismic Hazard Maps in the World, *Bulletin of International Seismology. Earthquake Eng.*, Vol. 17, pp. 33-96.
- HAZUS (1999). HAZUS User and Technical Manuals. *Federal Emergency Management Agency Report*, Vol. 7. Washington D.C.,USA
- Hubert-Ferrari A., Armijo R., King G.C.P., Meyer B., Barka A. (2002). Morphology, Displacement and Slip Rates along the North Anatolian Fault (Turkey). *Journal of Geophysical Research*, ETG 9-1:ETG 9:33
- Idriss I.M. (1991). *Earthquake Ground Motions at Soft Soil Site*, Proceedings of Second conference in Recent Advances in Geotechnical Earthquake Engineering and Soil Dynamics, Vol 3, pp.2265-2272.
- Idriss I.M. (2007). *Empirical Model for Estimating the Average Horizontal Values of Pseudo-Absolute Spectral Accelerations Generated by Crustal Earthquakes*, Vol 1, Sites with VS30 =450 to 900 m/s, Report to the Pacific Earthquake Engineering Research Center, Berkeley, California, USA
- Idriss I.M. (2008). A NGA Empirical Model for Estimating the Horizontal Spectral Values Generated by Shallow Crustal Earthquakes, *Earthquake Spectra*, Vol. 24, pp. 217-242.
- Inan E., Colakoglu Z., Koc N., Bayülke N., Coruh E., (1996). *Earthquake Catalogs with Acceleration Records from 1976 to1996*. General Directorate of Disaster Affairs, Earthquake Research Department, Ankara, Turkey. 98 pp. (in Turkish).
- Inel M., Tjhin T., Aschheim A. (2003). *The Significance of Lateral Load Pattern in Pushover Analysis*. Fifth National Conference on Earthquake Engineering, Istanbul, Turkey, Paper AE-009.
- Iwan W.D. (1997). Drift Spectrum: Measure of Demand for Earthquake Ground Motions. *Journal of Structural Engineering*, Vol.123, No.4, pp. 397–404.
- JICA-IMM (2003) *The Study on a Disaster Prevention / Mitigation Basic Plan in Istanbul Including Seismic Microzonation in the Republic of Turkey*, Japan International Cooperation Agency and Istanbul Metropolitan Municipality
- Joyner W.B. and Boore D.M. (1993). Methods for the Regression Analysis of Strong-Motion Data. *Bulletin Seismological Society of America* Vol. 83, pp.469–487.
- Joyner W.B. and Boore D.M. (1981). Peak Horizontal Acceleration and Velocity from Strong Motion Records, Including Records from the 1979 Imperial Valley, California Earthquake: *Bulletin Seismological Society of America*, Vol. 71, No.6, pp. 2011-2038.
- Kagan, Y. Y. (2002). Aftershock Zone Scaling, *Bulletin of the Seismological Society of America*, Vol. 92, No. 2, 641-655.
- Kahle H.G., Straub C., Relinger R., McClusky S., King R., Hurst K., Kastens K., Cross P. (1998). The Strain Rate Field in the Eastern Mediterranean Region, Estimated by Repeated GPS measurements, *Tectonophysics*, Vol. 294, pp.237-252

- Kaklamanos J., Baise L.G., Boore D.M. (2011). A Framework for Estimating Unknown Input Parameters when Implementing the NGA Ground Motion Prediction Equations in Engineering Practice. *Earthquake Spectra*, Vol.27, No.4, pp.1219-1235
- Kalkan E. and Kunnath S.K. (2007). Assessment of Current Nonlinear Static Procedures for Seismic Evaluation of Buildings, *Engineering Structures*, Vol.29, pp.305-316.
- Kalkan E., Gulkan P., Yilmaz N., Celebi M. (2009). Reassessment of Probabilistic Seismic Hazard in the Marmara Region, *Bulletin of the Seismological Society of America*, Vol. 99, No. 4, pp. 2127–2146.
- Kalkan E. and Gulkan P. (2004). Site-dependent Spectra Derived from Ground Motion Records in Turkey, *Earthquake Spectra*, Vol.20, No. 4, pp. 1111–1138.
- Karaman H., Sahin M., Elnashai A.S. (2008). Earthquake Loss Assessment Features of Maeviz-Istanbul (Hazturk), *Journal of Earthquake Engineering*, Vol. 12, No. Supp, pp.175-186.
- Kase Y. and Kuge K. (1998). Numerical Simulation of Spontaneous Rupture Processes on Two Non-coplanar Faults: the Effect of Geometry on Fault Interaction, *Geophysical Journal International*, Vol.135, pp.911–922.
- Kawasumi H. (1951). Measures of Earthquake Danger and Expectancy of Maximum Intensity Throughout Japan as Inferred from Seismic Activity in Historical Times, *Bulletin of Earthquake Research Institute.*, University of Tokyo, Vol. 29, pp. 469-482.
- Kim J. and Collins K. R. (2002). Closer Look at the Drift Demand Spectrum, *Journal of Structural Engineering*, Vol. 128, No.7, pp. 942–945.
- King G., and Nabelek J. (1985). Role of Fault Bends in the Initiation and Termination of Earthquake Rupture, *Science*, Vol. 228, pp. 984– 987.
- Klügel J.U. (2008). Seismic Hazard Analysis-Quo vadis?, *Earth-Science Reviews* Vol.88, pp.1-32.
- Kocyigit, A. (2003). Orta Anadolu'nun Genel Neotektonik Özellikleri ve Depremselliği. *Türkiye Petrol Jeologları Bülteni Özel Sayı*, s. 1-24.
- Kocyigit A. (2005). *Active Fault Investigation in Pilot Municipalities and Their Neighbourhood: Eskisehir, Gemlik, Bandirma, Tekirdag And Korfez*, Final Report, Project: MEER-A3 Microzonation and Hazard Vulnerability Studies For Disaster Mitigation in Pilot Municipalities, 17 pp. (In Turkish)
- Kocyigit A. (2010). Personal Communication, Department of Geological Engineering, METU, Ankara.
- KOERI (2011), Earthquake Catalog, <http://www.koeri.boun.edu.tr/sismo/>
- Kozacı O., Dolan J., Finkel R., and Hartleb R. (2007). Late Holocene Slip Rate for the North Anatolian fault, Turkey, From Cosmogenic ³⁶Cl Geochronology: Implications for the Constancy of Fault Loading and Strain Release Rates: *Geology*, Vol. 35, pp. 867–870.
- Kunnath S.K., John A.Jr. (2000), *Validity of Static Procedures in Performance-based Seismic Design*, in Proceedings of ASCE Structures Congress, Philadelphia, USA

- Lettis W., Bachhuber J., Witter R., Brankman C., Randolph C. E., Barka A., Page W.D. & Kaya A. (2002). Influence of Releasing Steppovers on Surface Fault Rupture and Fault Segmentation: Examples from the 17 August 1999 Izmit earthquake on the North Anatolian Fault, Turkey, *Bulletin of the Seismological Society of America* Vol. 92, pp.19–42.
- Lew H.S., Kunnath S.K. (2001). *Evaluation of Nonlinear Static Procedures for Seismic Design of Buildings*, Presented at the 33rd Joint Meeting of the UJNR Panel on Wind and Seismic Effects, pp. 1-17.
- Lin Y.Y., Chang K.C., Wang Y.L. (2004). Comparison of Displacement Coefficient Method and Capacity Spectrum Method with Experimental Results of Reinforced Concrete Columns, *Earthquake Engineering and Structural Dynamics*, Vol.33, No.1, pp. 35-48.
- Mahaney J.A., Paret T.F., Kehoe B.E., Freeman S.A. (1993). *The Capacity Spectrum Method for Evaluating Structural Response during the Loma Prieta Earthquake* in Earthquake Hazard Reduction in the Central and Eastern United States: A Time for Examination and Action, Proceedings of 1993 National Earthquake Conference, Earthquake Engineering Research Institute, Oakland, CA, U.S.A., pp. 501-510.
- McClay K. and Bonora M. (2001). Analog Models of Restraining Steppovers in Strike-Slip Fault Systems, *AAPG Bulletin*, Vol. 85, No.2, pp. 233-260.
- McClusky S., Balassanian S., Barka A., Demir C., Ergintav S., Georgiev I., Gurkan O., Hamburger M., Hurst K., Kahle H., Kastens K., Kekelidze G., King R., Kotzev V., Lenk O., Mahmoud S., Mishin A., Nadariya M., Ouzounis A., Paradissis D., Peter Y., Prilepin M., Reilinger R., Sanli I., Seeger H., Tealeb A., Toksoz M.N., and Veis G. (2000). Global Positioning System Constraints on Plate Kinematics and Dynamics in the eastern Mediterranean and Caucasus, *Journal of Geophysical Research*. Vol. 105, No. 3, pp. 5695–5719.
- McGuire R.K. (2004). *MNO-10 Seismic Hazard and Risk Analysis*, Earthquake Engineering Research Institute, 240 p.
- Miranda E. and Akkar S. (2006). Generalized Interstorey Drift Spectrum, *Journal of Structural Engineering*, Vol. 132, No.6, pp. 840-852.
- Moehle J.P. (1984). Strong Motion Drift Estimates for Reinforced Concrete Structures, *Journal of Structural Engineering*, Vol. 110, No.9, pp. 1988–2001.
- Moehle J. P. (1994). Seismic Drift and Its Role in Design, *Proceedings, 5th U.S.–Japan Workshop on the Improvement of Building Structural Design and Construction Practices*, San Diego, USA, pp. 65–78.
- Mwafy A.M., Elnashai A.S. (2001) Static Pushover versus Dynamic Collapse Analysis of RC Buildings, *Journal of Engineering Structures*, Vol. 23, pp. 407-424.
- NEHRP (2003). *Recommended Provisions for New Buildings and Other Structures, FEMA-450*, prepared by the Building Seismic Safety Council for the Federal Emergency Management Agency, Washington, D.C., USA
- NEHRP (1994). *Recommended Provisions for the Development of Seismic Regulations for New Buildings*. by the. Building Seismic Safety Council, Washington, D. C., USA

- NEHRP (1997). *Recommended Provisions for Seismic Regulations for New Buildings and other Structures, FEMA-303*, Prepared by the Building Seismic Safety Council for the Federal Emergency Management Agency, Washington, DC.
- Newmark N.M. and Hall W.J. (1982). *Earthquake Spectra and Design, Monograph*, Earthquake Engineering Research Institute (EERI): Oakland, California, USA
- Nyst M. and Thatcher W. (2004). New Constraints on the Active Tectonic Deformation of the Aegean, *Journal of Geophysical Research* Vol. 109:B11, pp. 406-430.
- Ocakoglu F. (2007). A Re-evaluation of the Eskisehir Fault Zone as a Recent Extensional Structure in NW Turkey, *Journal of Asian Earth Sciences*, Vol. 31, pp. 91–103.
- Ogata Y. and Katsura K. (1993). Analysis of Temporal and Spatial Heterogeneity of Magnitude Frequency Distribution Inferred from Earthquake Catalogues, *Geophysical. Journal International*, Vol. 113, pp. 727-738.
- Oglesby D.D. (2005). The Dynamics of Strike-slip Stepovers with Linking Dip-slip Faults, *Bulletin of Seismological Society of America*, Vol. 95, No.5, pp.1604–1622.
- Oglesby D., Mai P.M., Kuvvet A., Pucci S. (2008). Dynamic Models of Earthquakes on the North Anatolian Fault Zone under the Sea of Marmara: Effect of Hypocenter Location, *Geophysical Research Letters*, Vol. 35
- Oral M. B. (1994) *Global Positioning System (GPS) Measurements in Turkey (1988-1992): Kinematics of the Africa-Arabia-Eurasia Plate Collision Zone*, Ph.D. thesis, 344 pp., MIT, Boston, USA
- Ozbey C., Sarı A., Manuel L., Erdik M., Fahjan Y. (2004). An Empirical Attenuation Relationship for Northwestern Turkey, Ground Motion Using a Random Effects Approach. *Soil Dynamics and Earthquake Engineering*, Vol. 24, pp. 115–125.
- Ozcebe G., Yucemen M.S., Aydogan V., Yakut A. (2003). *Preliminary Seismic Vulnerability Assessment of Existing Reinforced Concrete Buildings in Turkey- Part I: Statistical Model Based on Structural Characteristics*, in: Seismic Assessment and Rehabilitation of Existing Buildings, edited by Wasti S.T. and Ozcebe G., Kluwer Academic Publishers-KAP,Doortrecht, pp. 29-42.
- Ozcebe G., Yucemen M.S., Aydogan V. (2004). Assessment of Seismic Vulnerability of Existing Reinforced Concrete Buildings, *Journal of Earthquake Engineering*; Vol.8. No.5, pp.749-773
- Ozcebe G., Sucuoglu H., Yucemen M.S., Yakut A. (2006). *In defense of Zeytinburnu*, *Advances in Earthquake Engineering for Urban Risk Reduction*, edited by Wasti S.T. and Ozcebe G., Springer, pp. 95-116.
- Ozturk N., (2007). *Probabilistic Seismic Hazard Analysis: A Sensitivity Study with Respect to Different Models*, Ph.D. Thesis, METU, Ankara, Turkey
- Papazachos B.C., Papaioannou C.A. (1993). A Time and Magnitude Predictable Model for Strong Earthquakes and its Application for Long Term Earthquake Prediction in the Aegean Area, Proc. 2nd Congress of the Hellenic Geophysical Union, Florina, Greece, Vol 1, pp. 39-60.

- Paret T.F., Sasaki K.K., Eilbeck D.H., Freeman S.A. (1996). *Approximate Inelastic Procedures to Identify Failure Mechanisms from Higher Mode Effects*, Proceedings of 11th World Conference on Earthquake Engineering, Paper No. 966.
- Porter K.A., Beck J.L., Shaikhutdinov R.V. (2004). Simplified Performance-based Earthquake Engineering Estimation of Economic Risk for Buildings, *Earthquake Spectra*, Vol .20 No.4, pp.1239-1263.
- Qi X. and Moehle J. P. (1991). *Displacement Design Approach for Reinforced Concrete Structures Subjected to Earthquakes*, Report EERC/ UCB-91/02, Earthquake Engineering Research Center, Univ. of California at Berkeley, Berkeley, California, USA
- RADIUS (1999). *Risk Assessment Tools for Diagnosis of Urban Areas against Seismic Disasters*, United Nations Initiative towards Earthquake Safe Cities
- Reilinger, R.E., McClusky, S.C., Oral, M.B. (1997). Global Positioning System Measurements of Present-day Crustal Movements in the Arabia-Africa-Eurasia Plate Collision Zone, *Journal of Geophysical Research*, Vol. 102, pp. 9983–9999.
- Reilinger, R.E., McClusky, S.C., Vernant, P., Lawrence, S., Ergintav, S., Cakmak, R., Nadariya, M., Hahubia, G., Mahmoud, S., Sakr, K., Arrajehi, A., Paradissis, D., Al-Aydrus, A., Prilepin, M., Guseva, T., Evren, E., Dmitritsa, A., Filikov, S.V., Gomes, F., Al-Ghazzi, R., and Karam, G. (2006). GPS Constraints on Continental Deformation in the Africa-Arabia-Eurasia Continental Collision Zone and Implications for the Dynamics of Plate Interactions, *Journal of Geophysical Research*, Vol. 111, p. V05411
- Reiter L. (1990). *Earthquake Hazard Analysis: Issues and Insights*, Columbia University Press, New York.
- Risk Engineering Inc. (2013). *EZ-FRISK: Version 7.62*, Seismic Hazard Analysis Program, Boulder, Colorado, USA
- RISK-EU (2004) *The European Risk-Use Project: An Advanced Approach to Earthquake Risk Scenarios*,(2001-2004) www.risk-ue.net
- Rossetto T. and Elnashai A. (2003). Derivation of Vulnerability Functions for European-type RC Structures Based on Observational Data. *Elsevier, Journal of Engineering Structures*, Vol. 25, pp.1241-1263.
- Ruiz-Garcia J. and Miranda E. (2003). Inelastic Displacement Ratio for Evaluation of Existing Structures, *Earthquake Engineering and Structural Dynamics*, Vol.32, No.8, pp. 1237-1258
- Sadigh K., Chang C.Y., Abrahamson N.A., Chiou S.J., Power M. (1993). Specification of Long Period Motions: Updated Attenuation Relations for Rock Site Conditions and Adjustment Factors for Near Fault Effects, *Proc. ATC 17-1*, pp. 59-70.
- Sadigh K, Chang C.Y., Egan J.A., Makdisi F., Youngs R.R. (1997). Attenuation Relationships for Shallow Crustal Earthquakes Based on California Strong Motion Data, *Seismological Research Letters*, Vol. 68 No.1, pp. 180-189.
- Sahin M. and Karaman H. (2006). *Development An Earthquake Loss Estimation Program for Turkey*. *Advances In Global Emergency Management*, TIEMS 13th Annual Conference, Seoul, Korea

- Saroglu F., Emre O., Boray A. (1992). *1:1 000 000 Türkiye Diri Fay Haritası*, MTA, Ankara.
- Savage M.K., Rupp S.H. (2000). Foreshock Probabilities in New Zealand, *New Zealand Journal of Geology and Geophysics* Vol. 43, pp.461-469.
- Scherbaum F., Cotton F., Smit P. (2004). On The Use of Response Spectral Reference Data for the Selection and Ranking of Ground Motion Models for Seismic Hazard Analysis in Regions of Moderate Seismicity: The Case of Rock Motion, *Bulletin of Seismological Society of America*, Vol. 94, No. 6, pp. 2164–2185.
- Scherbaum F., Bommer J.J., Bungum H., Cotton F., Abrahamson N.A. (2005). Composite Ground-motion Models and Logic Trees: Methodology, Sensitivities and Uncertainties, *Bulletin of Seismological Society of America*, Vol. 95, No.5, pp.1575–1593.
- Schwartz D.P. and Coppersmith K.J. (1984). Fault Behavior and Characteristic Earthquakes: Examples from The Wasatch and San Andreas Fault Zones, *Journal of Geophysical Research*, Vol. 89, No. B7, pp. 5681-5698.
- Sengor A.M.C., Gorur N., Saroglu F. (1985). Strike-Slip Faulting and Related Basin Formation In Zones of Tectonic Escape: Turkey As a Case Study. In: Strike-Slip Deformation, Basin Formation and Sedimentation, *Society of Economic Paleontologists and Mineralogists Spec. Publ.*, Vol. 37, pp. 227-264.
- Shaw B.E., and Dieterich J.H. (2007). Probabilities for Jumping Fault Segment Steppers, *Geophysical Research Letters*, Vol. 34, L01307
- Shimazaki K and Nakata T. (1980). Time-predictable Recurrence Model or Large Earthquakes, *Geophysical Research Letters*, Vol 7, pp. 279–282.
- Sozen M. A. (1983). Lateral Drift of Reinforced Concrete Structures Subjected to Strong Ground Motion, *Bulletin of New Zealand National Society of Earthquake Engineering*, Vol.16.,No.2, pp. 107–122.
- SSHAC (1997) *Recommendations for Probabilistic Seismic Hazard Analysis: Guidance on Uncertainty and Use of Experts*, US Nuclear Regulatory Commission report CR-6372, Washington DC.,USA
- Stafford P.J., Strasser F.O., Bommer J.J. (2008). An Evaluation of the Applicability of the NGA Models to Ground-Motion Prediction in the Euro-Mediterranean Region, *Bulletin of Earthquake Engineering*, Vol 6., pp.149-177
- Stepp J. C. (1973). *Analysis of Completeness of the Earthquake Sample in the Puget Sound Area*, Contributions to Seismic Zoning: U.S. National Oceanic and Atmospheric Administration Technical Report ERL 267-ESL 30, pp. 16-28.
- Stewart J.P., Douglas J., Alessandro C.D., Bozorgnia Y., Abrahamson N., Boore D.M., Campbell K.W., Delavaud E., Erdik M., Stafford P.J. (2012). *Selection of a Global Set of GMPEs for the GEM-PEER Global GMPEs Project*, 15th World Conference on Earthquake Engineering, Lisbon
- Straub C. (1996). Recent Crustal Deformation and Strain Accumulation in the Marmara Sea Region, N.W. Anatolia, Inferred from GPS Measurements, *Institute of Geodesy and Photogrammetry, E. THZ Mitt.*, 58, 123 pp.

- Straub C. and Kable H.G. (1994). Global Positioning System (GPS) Estimates of Crustal Deformation in the Marmara Sea Region, Northwestern Anatolia, *Earth and Planetary Science Letters.*, Vol. 121, pp. 495-502.
- Tan, O., Tapırdamaz M.C., Yoruk A. (2008). The Earthquake Catalogues for Turkey, *Turkish Journal of Earth Sciences*, Vol.17, No.2, pp.405-418.
- Thenhaus P.C. and Campbell K.W. (2003). *Seismic Hazard Analysis*, Chapter 8, Earthquake Engineering Hand Book, Chen W. and Schawthorn C. (editors), CRC Press.
- Ulusay R., Tuncay E., Sonmez H., Gokceoglu C. (2004). An Attenuation Relationship Based on Turkish Strong Motion Data and Iso-acceleration Map of Turkey, *Engineering Geology* Vol. 74 No.3-4, pp. 265-291.
- Ulutas E., Guven T., Irmak T. S., Sertcel F, Tunc K. B., Cetinol T., Caka D., Ozer M. F., Kenar O. (2003). *Dogu Marmara Bölgesi için Deneysel en Büyük Yatay Ivme Uzaklık Azalim İlişkisi ve Kocaeli'nin Probabilistik Deprem Tehlikesi*, Kocaeli 2003 Deprem Sempozyumu Tam Metin Kitabı, s.14-26 (In Turkish)
- Vidic, T., Fajfar, P., Fischinger M. (1994). Consistent Inelastic Design Spectra: Strength and Displacement, *Earthquake Engineering and Structural Dynamics*, Vol. 23, No.5, pp. 507-521.
- Wang Z., Woolery E., Shi B., Kiefer J. (2003). Communicating with Uncertainty: A Critical Issue with Probabilistic Seismic Hazard Analysis, *Eos Transactions of the American Geophysical Union*, Vol. 84, 501, 506, 508.
- Weichert D.H. (1980). Estimation of the Earthquake Recurrence Parameters for unequal Observation Periods for Different Magnitudes, *Bulletin of Seismological Society of America*, Vol. 70, pp. 1337-1346.
- Wells D.L. and Coppersmith K.J. (1984). New Empirical Relationships Among Magnitude, Rupture Length, Rupture Width, Rupture Area and Surface Displacement, *Bulletin of the Seismological Society of America*, Vol. 84, No. 4, pp. 974-1002.
- Wesnousky S. G. (1994). The Gutenberg-Richter or Characteristic Earthquake Distribution Which is it?, *Bulletin of Seismological Society of America*, Vol. 84, pp. 1940-1959.
- Wesnousky S. G. (2006). Predicting the Endpoints of Earthquake Ruptures, *Nature*, Vol. 444, pp.358-360.
- WGCEP (Jackson, D. D. Aki, K. Cornell, C. A. Dieterich, J. H. Henyey, T. L. Mahdyiar, M. Schwartz, D. Ward, S. N.) (1995). Seismic Hazards in Southern California: Probable Earthquakes, 1994-2024, *Bulletin of Seismological Society of America*, Vol. 85, pp. 379-439.
- WGCEP (1999). *Earthquake Probabilities in the San Francisco Bay Region: 2000-2030, A Summary of Findings*, Open-File Report 99-517, U.S. Geological Survey
- WGCEP (2003). *Earthquake Probabilities in the San Francisco Bay Region*, Open File Report 03-214, U.S. Geological Survey
- WGCEP (2006). *The Uniform California Earthquake Rupture Forecast and San Andreas Fault Assessment*, USC-SCEC/CEA Technical Report #1,

- WGCEP (2007). *The Uniform California Earthquake Rupture Forecast, Version 2 (UCERF 2)*, Open File Report 07–1437, U.S. Geological Survey
- Whitman R.V. (1973). *Damage Probability Matrices for Prototype Buildings. Structures* publication 380. Boston: MIT
- Wiemer S. and Wyss M. (2000). Minimum Magnitude of Complete Reporting in Earthquake Catalogs: Examples from Alaska, the Western United States, and Japan, *Bulletin of Seismological Society of America*, Vol. 90, pp. 859-869.
- Yakut A., Aydogan V., Ozcebe G., Yucemen M.S. (2003). Preliminary Seismic Vulnerability Assessment of Existing Reinforced Concrete Buildings in Turkey -Part II: Inclusion of Site Characteristics, in: *Seismic Assessment and Rehabilitation of Existing Buildings*, edited by S.T. Wasti and G. Ozcebe, KAP, Dordrecht, pp. 43-58. Federal Emergency Management Agency, Washington, D.C., USA
- Yakut A., Ozcebe, G., Yucemen M. S. (2006). Seismic Vulnerability Assessment Using Regional Empirical Data. *Earthquake Engineering and Structural Dynamics*, Vol.35, pp.1187–1202.
- Yarar R., Ergunay O., Erdik M., Gulkan P. (1980). *A Preliminary Probabilistic Assessment of the Seismic Hazard in Turkey*, Proceedings of 7th World Conference on Earthquake Engineering, Istanbul, pp.309-316
- Youngs R.R. and Coppersmith K.J. (1985). Implications of Fault Slip Rates and Earthquake Recurrence Models to Probabilistic Seismic Hazard Estimates, *Bulletin of the Seismological Society of America*, Vol. 75, No. 4, pp. 939-964.
- Yucemen M.S. (1982). *Seismic Risk Analysis*, METU Publication, Ankara
- Yucemen M.S., Ozcebe G, Pay A.C. (2004). Prediction of Potential Damage due to Severe Earthquakes. *Structural Safety*, Vol. 26, No.3, pp. 349–366.
- Yucemen M.S. (2005). Probabilistic Assessment of Earthquake Insurance Rates for Turkey, *Natural Hazards*, Vol. 35. pp. 291–313.
- Yucemen M.S. (2005). *Prediction of Potential Earthquake Damage: A Discriminant Analysis Approach*, 9th, International Conference on Structural Safety and Reliability, Rome, Italy

Table A1. Raw Data Used in the Derivation of Coefficients of Ground Motion Prediction Equations

Event ID	Name of the Event	Date	Station Latitude (degrees)	Station Longitude (degrees)	Fault Type	M _w	Depth	Epicenter Latitude (degrees)	Epicenter Longitude (degrees)	PGA N-S (cm/s ²)	PGA E-W (cm/s ²)
1	Denizli	19.08.1976	37.76	29.09	N	5.3	3.0	37.71	29.00	348.53	290.36
2	Dursunbey	18.07.1979	39.60	28.63	SS	5.3	5.0	39.66	28.65	232.29	288.25
3	Balıkesir	29.03.1984	39.66	27.86	SS	4.9	12	39.64	27.87	223.89	128.97
4	Dinar	01.10.1995	39.66	27.86	N	6.4	15	38.11	30.05	4.50	3.00
5	Dinar	01.10.1995	37.72	30.29	N	6.4	15	38.11	30.05	41.61	43.92
6	Dinar	01.10.1995	37.83	29.67	N	6.4	15	38.11	30.05	65.07	61.30
7	Dinar	01.10.1995	38.06	30.15	N	6.4	15	38.11	30.05	281.63	329.72
8	Dinar	01.10.1995	37.81	29.11	N	6.4	15	38.11	30.05	16.00	14.50
9	Buldan	21.01.1997	38.05	28.83	N	4.8	18	38.12	28.92	24.37	38.51
10	Dinar	04.04.1998	38.78	30.53	N	4.6	15	38.14	30.04	7.00	5.50
11	Dinar	04.04.1998	37.83	29.67	N	4.6	15	38.14	30.04	24.49	28.88
12	Dinar	04.04.1998	37.70	30.22	N	4.6	15	38.14	30.04	1.89	1.77
13	Dinar	04.04.1998	38.06	30.15	N	4.6	15	38.14	30.04	134.73	130.90
14	Dinar	04.04.1998	37.81	29.11	N	4.6	15	38.14	30.04	2.38	2.56
15	Dinar	04.04.1998	39.42	30.00	N	4.6	15	38.14	30.04	1.46	1.07
16	Dinar	04.04.1998	38.67	29.40	N	4.6	15	38.14	30.04	2.44	2.35
17	Kocaeli	17.08.1999	41.03	28.76	SS	7.4	18	40.70	29.91	118.03	89.61

Table A1 Continued

Event ID	Name of the Event	Date	Station Latitude (degrees)	Station Longitude (degrees)	Fault Type	M _w	Depth	Epicenter Latitude (degrees)	Epicenter Longitude (degrees)	PGA N-S (cm/s ²)	PGA E-W (cm/s ²)
18	Kocaeli	17.08.1999	40.84	31.15	SS	7.4	18	40.70	29.91	373.76	314.88
19	Kocaeli	17.08.1999	37.81	29.11	SS	7.4	18	40.70	29.91	5.92	11.69
20	Kocaeli	17.08.1999	40.79	29.45	SS	7.4	18	40.70	29.91	264.82	141.45
21	Kocaeli	17.08.1999	40.40	30.78	SS	7.4	18	40.70	29.91	117.90	137.69
22	Kocaeli	17.08.1999	40.44	29.72	SS	7.4	18	40.70	29.91	91.89	123.32
23	Kocaeli	17.08.1999	40.77	29.92	SS	7.4	18	40.70	29.91	171.17	224.91
24	Kocaeli	17.08.1999	38.61	27.38	SS	7.4	18	40.70	29.91	12.50	6.50
25	Kocaeli	17.08.1999	40.74	30.38	SS	7.4	18	40.70	29.91	0.21	407.04
26	Kocaeli	17.08.1999	38.78	30.53	SS	7.4	18	40.70	29.91	13.50	15.00
27	Kocaeli	17.08.1999	38.46	27.23	SS	7.4	18	40.70	29.91	9.89	10.80
28	Kocaeli	17.08.1999	40.14	26.40	SS	7.4	18	40.70	29.91	24.57	28.63
29	Kocaeli	17.08.1999	41.06	29.01	SS	7.4	18	40.70	29.91	60.67	42.66
30	Kocaeli	17.08.1999	39.42	30.00	SS	7.4	18	40.70	29.91	50.05	59.66
31	Kocaeli	17.08.1999	41.01	34.04	SS	7.4	18	40.70	29.91	11.69	8.91
32	Kocaeli	17.08.1999	38.67	29.40	SS	7.4	18	40.70	29.91	11.20	14.31
33	Kocaeli	17.08.1999	37.84	27.84	SS	7.4	18	40.70	29.91	5.98	5.25
34	Kocaeli	17.08.1999	40.18	29.13	SS	7.4	18	40.70	29.91	54.32	45.81
35	Kocaeli	17.08.1999	39.65	27.86	SS	7.4	18	40.70	29.91	17.76	18.19
36	Kocaeli	17.08.1999	40.97	27.95	SS	7.4	18	40.70	29.91	90.36	101.36

Table A1 Continued

Event ID	Name of the Event	Date	Station Latitude (degrees)	Station Longitude (degrees)	Fault Type	M _w	Depth	Epicenter Latitude (degrees)	Epicenter Longitude (degrees)	PGA N-S (cm/s ²)	PGA E-W (cm/s ²)
37	Sapanca	11.11.1999	40.18	29.13	SS	5.6	8.9	40.82	30.20	3.05	3.02
38	Sapanca	11.11.1999	41.06	29.01	SS	5.6	8.9	40.82	30.20	4.52	4.33
39	Sapanca	11.11.1999	40.14	26.40	SS	5.6	8.9	40.82	30.20	0.95	0.89
40	Sapanca	11.11.1999	39.42	30.00	SS	5.6	8.9	40.82	30.20	10.01	6.81
41	Sapanca	11.11.1999	40.74	30.38	SS	5.6	8.9	40.82	30.20	946.38	749.70
42	Sapanca	11.11.1999	39.65	27.86	SS	5.6	8.9	40.82	30.20	1.22	0.64
43	Sapanca	11.11.1999	40.97	27.95	SS	5.6	8.9	40.82	30.20	1.59	1.31
44	Duzce	12.11.1999	40.98	27.52	SS	7.2	25.0	40.74	31.21	5.71	6.10
45	Duzce	12.11.1999	39.42	30.00	SS	7.2	25.0	40.74	31.21	17.12	20.69
46	Duzce	12.11.1999	40.74	30.38	SS	7.2	25.0	40.74	31.21	17.33	24.72
47	Duzce	12.11.1999	38.78	30.53	SS	7.2	25.0	40.74	31.21	8.00	10.00
48	Duzce	12.11.1999	40.18	29.13	SS	7.2	25.0	40.74	31.21	9.31	8.00
49	Duzce	12.11.1999	40.14	26.40	SS	7.2	25.0	40.74	31.21	3.94	3.33
50	Duzce	12.11.1999	37.81	29.11	SS	7.2	25.0	40.74	31.21	3.69	3.48
51	Duzce	12.11.1999	40.40	30.78	SS	7.2	25.0	40.74	31.21	24.82	27.89
52	Duzce	12.11.1999	40.47	31.21	SS	7.2	25.0	40.74	31.21	58.34	120.99
53	Duzce	12.11.1999	39.65	27.86	SS	7.2	25.0	40.74	31.21	2.72	2.38
54	Duzce	12.11.1999	38.46	27.23	SS	7.2	25.0	40.74	31.21	1.59	1.86
55	Duzce	12.11.1999	41.01	34.04	SS	7.2	25.0	40.74	31.21	7.93	7.63

Table A1 Continued

Event ID	Name of the Event	Date	Station Latitude (degrees)	Station Longitude (degrees)	Fault Type	M _w	Depth	Epicenter Latitude (degrees)	Epicenter Longitude (degrees)	PGA N-S (cm/s ²)	PGA E-W (cm/s ²)
56	Duzce	12.11.1999	38.67	29.40	SS	7.2	25.0	40.74	31.21	3.05	3.08
57	Duzce	12.11.1999	40.84	31.15	SS	7.2	25.0	40.74	31.21	513.78	407.69
58	Duzce	12.11.1999	41.06	29.01	SS	7.2	25.0	40.74	31.21	8.97	5.25
59	Duzce	12.11.1999	40.75	31.61	SS	7.2	25.0	40.74	31.21	739.51	805.88
60	Hendek	23.08.2000	40.75	31.61	SS	5.3	15.3	40.68	30.71	9.62	6.49
61	Hendek	23.08.2000	40.84	31.15	SS	5.3	15.3	40.68	30.71	23.29	17.55
62	Hendek	23.08.2000	40.44	29.72	SS	5.3	15.3	40.68	30.71	21.69	16.21
63	Hendek	23.08.2000	40.74	30.38	SS	5.3	15.3	40.68	30.71	20.84	27.47
64	Hendek	23.08.2000	39.65	27.86	SS	5.3	15.3	40.68	30.71	0.92	1.37
65	Hendek	23.08.2000	40.33	28.00	SS	5.3	15.3	40.68	30.71	1.19	1.43
66	Hendek	23.08.2000	40.18	29.13	SS	5.3	15.3	40.68	30.71	2.87	3.17
67	Hendek	23.08.2000	41.20	32.62	SS	5.3	15.3	40.68	30.71	0.81	0.53
68	Hendek	23.08.2000	39.42	30.00	SS	5.3	15.3	40.68	30.71	3.20	2.84
69	Hendek	23.08.2000	40.67	30.62	SS	5.3	15.3	40.68	30.71	79.01	96.69
70	Hendek	23.08.2000	41.06	29.01	SS	5.3	15.3	40.68	30.71	2.81	4.09
71	Denizli	04.10.2000	37.84	27.84	N	5.0	8.4	37.91	29.04	1.40	1.59
72	Denizli	04.10.2000	37.81	29.11	N	5.0	8.4	37.91	29.04	49.13	66.38
73	Denizli	04.10.2000	38.67	29.40	N	5.0	8.4	37.91	29.04	1.92	1.50
74	Yigilca	26.08.2001	40.75	31.61	SS	5.4	7.8	40.93	31.53	189.07	131.64

Table A1 Continued

Event ID	Name of the Event	Date	Station Latitude (degrees)	Station Longitude (degrees)	Fault Type	M _w	Depth	Epicenter Latitude (degrees)	Epicenter Longitude (degrees)	PGA N-S (cm/s ²)	PGA E-W (cm/s ²)
75	Yigilca	26.08.2001	41.20	32.62	SS	5.4	7.8	40.93	31.53	7.81	7.79
76	Yigilca	26.08.2001	40.74	30.38	SS	5.4	7.8	40.93	31.53	1.37	2.14
77	Sultandagi	03.02.2002	40.33	28.00	R	6.5	5.0	38.57	31.27	1.62	1.59
78	Sultandagi	03.02.2002	38.67	29.40	R	6.5	5.0	38.57	31.27	7.66	6.17
79	Sultandagi	03.02.2002	38.78	30.53	R	6.5	5.0	38.57	31.27	113.50	94.00
80	Sultandagi	03.02.2002	37.70	30.22	R	6.5	5.0	38.57	31.27	2.59	2.44
81	Sultandagi	03.02.2002	39.42	30.00	R	6.5	5.0	38.57	31.27	23.13	20.78
82	Sultandagi	03.02.2002	40.74	30.38	R	6.5	5.0	38.57	31.27	1.04	1.19
83	Sultandagi	03.02.2002	39.65	27.86	R	6.5	5.0	38.57	31.27	1.62	0.89
84	Burdur	03.04.2002	37.70	30.22	SS	4.2	5.0	37.71	30.26	28.93	21.30
85	Akyazı	09.03.2003	40.67	30.62	SS	4.1	4.4	40.73	30.62	19.17	23.13
86	Akyazı	09.03.2003	40.74	30.38	SS	4.1	4.4	40.73	30.62	3.57	7.93
87	Duzce	21.05.2003	40.84	31.15	SS	4.7	7.7	40.87	30.98	17.82	31.86
88	Duzce	21.05.2003	40.74	30.38	SS	4.7	7.7	40.87	30.98	1.37	1.28
89	Bandirma	09.06.2003	40.42	29.29	SS	4.8	14.7	40.20	27.97	3.27	3.66
90	Bandirma	09.06.2003	40.36	29.12	SS	4.8	14.7	40.20	27.97	5.74	7.59
91	Bandirma	09.06.2003	40.43	29.17	SS	4.8	14.7	40.20	27.97	7.17	6.17
92	Bandirma	09.06.2003	40.14	26.40	SS	4.8	14.7	40.20	27.97	3.08	4.88
93	Bandirma	09.06.2003	40.34	27.94	SS	4.8	14.7	40.20	27.97	35.64	22.86

Table A1 Continued

Event ID	Name of the Event	Date	Station Latitude (degrees)	Station Longitude (degrees)	Fault Type	M _w	Depth	Epicenter Latitude (degrees)	Epicenter Longitude (degrees)	PGA N-S (cm/s ²)	PGA E-W (cm/s ²)
94	Bandirma	09.06.2003	40.23	29.08	SS	4.8	14.7	40.20	27.97	3.42	4.12
95	Bandirma	09.06.2003	40.27	29.10	SS	4.8	14.7	40.20	27.97	4.84	3.26
96	Bandirma	09.06.2003	40.98	27.52	SS	4.8	14.7	40.20	27.97	2.47	3.36
97	Buldan1	23.07.2003	37.91	28.47	N	5.3	5.0	38.14	28.83	21.73	19.90
98	Buldan1	23.07.2003	37.93	28.92	N	5.3	5.0	38.14	28.83	90.16	123.23
99	Buldan1	23.07.2003	37.91	28.34	N	5.3	5.0	38.14	28.83	23.07	25.94
100	Buldan1	23.07.2003	37.86	28.05	N	5.3	5.0	38.14	28.83	7.69	8.34
101	Buldan1	23.07.2003	37.81	29.11	N	5.3	5.0	38.14	28.83	22.19	45.84
102	Buldan1	23.07.2003	38.67	29.40	N	5.3	5.0	38.14	28.83	4.15	5.28
103	Buldan1	23.07.2003	38.46	27.23	N	5.3	5.0	38.14	28.83	2.23	2.04
104	Buldan2	26.07.2003	37.93	28.92	N	5.3	5.0	38.11	28.88	47.54	34.46
105	Buldan2	26.07.2003	38.46	27.23	N	5.3	5.0	38.11	28.88	0.82	0.67
106	Buldan2	26.07.2003	37.91	28.47	N	5.3	5.0	38.11	28.88	10.53	11.22
107	Buldan2	26.07.2003	37.81	29.11	N	5.3	5.0	38.11	28.88	5.31	6.16
108	Buldan2	26.07.2003	37.91	28.34	N	5.3	5.0	38.11	28.88	10.23	16.83
109	Buldan2	26.07.2003	37.86	28.05	N	5.3	5.0	38.11	28.88	3.04	3.35
110	Buldan3	26.07.2003	37.86	28.05	N	5.7	4.3	38.06	28.89	10.45	8.48
111	Buldan3	26.07.2003	38.67	29.40	N	5.7	4.3	38.06	28.89	6.07	6.56
112	Buldan3	26.07.2003	37.93	28.92	N	5.7	4.3	38.06	28.89	107.51	121.12

Table A1 Continued

Event ID	Name of the Event	Date	Station Latitude (degrees)	Station Longitude (degrees)	Fault Type	M _w	Depth	Epicenter Latitude (degrees)	Epicenter Longitude (degrees)	PGA N-S (cm/s ²)	PGA E-W (cm/s ²)
113	Buldan3	26.07.2003	37.81	29.11	N	5.7	4.3	38.06	28.89	23.74	25.79
114	Buldan3	26.07.2003	38.46	27.23	N	5.7	4.3	38.06	28.89	2.87	3.17
115	Buldan3	26.07.2003	37.91	28.47	N	5.7	4.3	38.06	28.89	26.29	19.94
116	Buldan3	26.07.2003	37.91	28.34	N	5.7	4.3	38.06	28.89	26.97	27.16
117	Buldan4	26.07.2003	37.93	28.92	N	5.2	8.5	38.12	28.84	14.32	17.32
118	Buldan4	26.07.2003	37.91	28.47	N	5.2	8.5	38.12	28.84	9.18	12.52
119	Buldan4	26.07.2003	37.91	28.34	N	5.2	8.5	38.12	28.84	14.67	18.41
120	Buldan4	26.07.2003	37.86	28.05	N	5.2	8.5	38.12	28.84	2.60	2.45
121	Manyas	24.10.2006	40.36	29.12	SS	5.2	7.9	40.42	29.00	159.25	179.77
122	Manyas	24.10.2006	40.03	28.39	SS	5.2	7.9	40.42	28.99	4.25	4.70
123	Manyas	24.10.2006	40.14	26.40	SS	5.2	7.9	40.42	28.99	1.69	1.62
124	Manyas	24.10.2006	40.14	29.98	SS	5.2	7.9	40.42	28.99	1.92	2.14
125	Manyas	24.10.2006	39.82	30.15	SS	5.2	7.9	40.42	28.99	2.49	2.46
126	Manyas	24.10.2006	39.43	29.99	SS	5.2	7.9	40.42	28.99	4.72	6.18
127	Manyas	24.10.2006	39.09	28.98	SS	5.2	7.9	40.42	28.99	3.79	2.44
128	Manyas	24.10.2006	39.65	27.86	SS	5.2	7.9	40.42	28.99	2.17	1.92
129	Manyas	24.10.2006	39.77	30.51	SS	5.2	7.9	40.42	28.99	3.11	3.08
130	Manyas	24.10.2006	39.79	30.50	SS	5.2	7.9	40.42	28.99	1.73	1.45
131	Manyas	24.10.2006	39.31	26.69	SS	5.2	7.9	40.42	28.99	0.88	0.68

Table A1 Continued

Event ID	Name of the Event	Date	Station Latitude (degrees)	Station Longitude (degrees)	Fault Type	M _w	Depth	Epicenter Latitude (degrees)	Epicenter Longitude (degrees)	PGA N-S (cm/s ²)	PGA E-W (cm/s ²)
132	Manyas	24.10.2006	39.66	27.86	SS	5.2	7.9	40.42	28.99	1.95	2.36
133	Manyas	24.10.2006	39.90	30.05	SS	5.2	7.9	40.42	28.99	3.10	2.92
134	Manyas	24.10.2006	40.18	29.13	SS	5.2	7.9	40.42	28.99	36.56	28.38
135	Manyas	24.10.2006	40.23	29.08	SS	5.2	7.9	40.42	28.99	77.39	37.00
136	Manyas	24.10.2006	40.39	29.10	SS	5.2	7.9	40.42	28.99	177.14	206.19
137	Manyas	24.10.2006	40.41	29.18	SS	5.2	7.9	40.42	28.99	69.54	100.42
138	Manyas	24.10.2006	40.43	29.17	SS	5.2	7.9	40.42	28.99	65.95	95.34
139	Manyas	24.10.2006	40.42	29.29	SS	5.2	7.9	40.42	28.99	29.86	45.24
140	Manyas	24.10.2006	40.56	29.31	SS	5.2	7.9	40.42	28.99	28.46	29.33
141	Manyas	24.10.2006	40.59	29.27	SS	5.2	7.9	40.42	28.99	37.78	25.66
142	Manyas	24.10.2006	39.07	26.89	SS	5.2	7.9	40.42	28.99	1.89	1.29
143	Manyas	24.10.2006	39.04	28.65	SS	5.2	7.9	40.42	28.99	8.66	6.83
144	Manyas	24.10.2006	39.58	28.63	SS	5.2	7.9	40.42	28.99	2.63	3.22
145	Manyas	24.10.2006	39.72	30.53	SS	5.2	7.9	40.42	28.99	1.09	2.02
146	Manyas	24.10.2006	38.99	29.40	SS	5.2	7.9	40.42	28.99	2.21	2.96
147	Manyas	24.10.2006	40.33	28.00	SS	5.2	7.9	40.42	28.99	5.59	3.97
148	Manyas	24.10.2006	40.11	27.64	SS	5.2	7.9	40.42	28.99	1.65	1.39

Table A1 Continued

Event ID	Name of the Event	Date	Station Latitude (degrees)	Station Longitude (degrees)	Fault Type	M _w	Depth	Epicenter Latitude (degrees)	Epicenter Longitude (degrees)	PGA N-S (cm/s ²)	PGA E-W (cm/s ²)
149	Manyas	24.10.2006	39.92	29.23	SS	5.2	7.9	40.42	28.99	10.05	6.68
150	Manyas	24.10.2006	39.81	30.53	SS	5.2	7.9	40.42	28.99	3.20	4.06
151	Bala	20.12.2007	38.06	30.15	SS	5.7	0.0	39.42	33.05	0.52	0.51
152	Bala	20.12.2007	40.14	29.98	SS	5.7	0.0	39.42	33.05	0.25	0.17
153	Bala	20.12.2007	38.53	31.24	SS	5.7	0.0	39.42	33.05	0.45	0.40
154	Bala	20.12.2007	38.78	30.53	SS	5.7	0.0	39.42	33.05	0.94	0.78
155	Bala	20.12.2007	40.79	29.45	SS	5.7	0.0	39.42	33.05	0.09	0.08
156	Bala	20.12.2007	39.82	30.15	SS	5.7	0.0	39.42	33.05	0.50	0.79
157	Bala	20.12.2007	39.92	29.23	SS	5.7	0.0	39.42	33.05	0.35	0.33
158	Bala	20.12.2007	39.52	31.18	SS	5.7	0.0	39.42	33.05	0.61	0.43
159	Bala	20.12.2007	39.81	30.53	SS	5.7	0.0	39.42	33.05	0.96	1.07
160	Bala	26.12.2007	39.81	30.53	SS	5.6	0.0	39.41	33.04	1.28	1.36
161	Bala	26.12.2007	40.23	29.08	SS	5.6	0.0	39.41	33.04	1.00	0.83
162	Bala	26.12.2007	40.39	29.10	SS	5.6	0.0	39.41	33.04	1.41	1.56
163	Bala	26.12.2007	38.06	30.15	SS	5.6	0.0	39.41	33.04	0.49	0.46
164	Bala	26.12.2007	40.14	29.98	SS	5.6	0.0	39.41	33.04	0.31	0.30
165	Bala	26.12.2007	39.92	29.23	SS	5.6	0.0	39.41	33.04	0.82	0.88
166	Bala	26.12.2007	40.79	29.45	SS	5.6	0.0	39.41	33.04	0.16	0.11

Table A1 Continued

Event ID	Name of the Event	Date	Station Latitude (degrees)	Station Longitude (degrees)	Fault Type	M _w	Depth	Epicenter Latitude (degrees)	Epicenter Longitude (degrees)	PGA N-S (cm/s ²)	PGA E-W (cm/s ²)
167	Bala	26.12.2007	38.53	31.24	SS	5.6	0.0	39.41	33.04	0.66	0.82
168	Bala	26.12.2007	39.52	31.18	SS	5.6	0.0	39.41	33.04	1.11	0.78
169	Bala	26.12.2007	40.43	29.17	SS	5.6	0.0	39.41	33.04	1.12	1.00
170	Bala	26.12.2007	38.78	30.53	SS	5.6	0.0	39.41	33.04	1.03	1.10
171	Simav	18.07.2007	39.09	28.98	N	4.5	11.7	39.30	29.31	1.13	0.70
172	Simav	18.07.2007	39.82	30.15	N	4.5	11.7	39.30	29.31	0.13	0.14
173	Cinarcik	12.03.2008	40.23	29.08	SS	4.9	24.0	40.63	29.02	2.55	2.78
174	Cinarcik	12.03.2008	40.18	29.13	SS	4.9	24.0	40.63	29.02	1.86	1.28
175	Cinarcik	12.03.2008	40.36	29.12	SS	4.9	24.0	40.63	29.02	17.97	22.90
176	Cinarcik	12.03.2008	40.39	29.10	SS	4.9	24.0	40.63	29.02	16.08	13.17
177	Cinarcik	12.03.2008	40.42	29.29	SS	4.9	24.0	40.63	29.02	8.25	7.43
178	Cinarcik	12.03.2008	40.45	29.26	SS	4.9	24.0	40.63	29.02	14.43	24.32
179	Cinarcik	12.03.2008	40.56	29.31	SS	4.9	24.0	40.63	29.02	37.34	45.00
180	Cinarcik	12.03.2008	40.66	29.25	SS	4.9	24.0	40.63	29.02	31.26	26.27
181	Cinarcik	12.03.2008	40.79	30.03	SS	4.9	24.0	40.63	29.02	2.55	2.78
182	Cinarcik	12.03.2008	40.67	29.97	SS	4.9	24.0	40.63	29.02	3.35	3.42
183	Cinarcik	12.03.2008	39.90	30.05	SS	4.9	24.0	40.63	29.02	1.38	1.42
184	Cinarcik	12.03.2008	39.82	30.15	SS	4.9	24.0	40.63	29.02	0.54	0.57
185	Cinarcik	12.03.2008	39.92	29.23	SS	4.9	24.0	40.63	29.02	4.85	4.23

Table A1 Continued

Event ID	Name of the Event	Date	Station Latitude (degrees)	Station Longitude (degrees)	Fault Type	M _w	Depth	Epicenter Latitude (degrees)	Epicenter Longitude (degrees)	PGA N-S (cm/s ²)	PGA E-W (cm/s ²)
186	Cinarcik	12.03.2008	39.81	30.53	SS	4.9	24.0	40.63	29.02	1.04	0.69
187	Cinarcik	12.03.2008	40.86	31.23	SS	4.9	24.0	40.63	29.02	0.25	0.31
188	Cinarcik	12.03.2008	40.79	31.28	SS	4.9	24.0	40.63	29.02	0.31	0.37
189	Cinarcik	12.03.2008	39.79	30.50	SS	4.9	24.0	40.63	29.02	0.43	0.62
190	Cinarcik	12.03.2008	40.84	31.14	SS	4.9	24.0	40.63	29.02	0.52	0.54
191	Simav	17.02.2009	39.04	28.65	N	5.2	7.0	39.15	29.04	94.87	72.44
192	Simav	17.02.2009	39.58	28.63	N	5.2	7.0	39.15	29.04	8.38	5.87
193	Simav	17.02.2009	39.92	29.23	N	5.2	7.0	39.15	29.04	5.69	5.19
194	Simav	17.02.2009	39.43	29.99	N	5.2	7.0	39.15	29.04	10.32	7.28
195	Simav	17.02.2009	39.82	30.15	N	5.2	7.0	39.15	29.04	1.36	1.76
196	Simav	17.02.2009	39.66	27.86	N	5.2	7.0	39.15	29.04	3.41	4.01
197	Simav	17.02.2009	38.06	30.15	N	5.2	7.0	39.15	29.04	1.30	1.22
198	Simav	17.02.2009	39.52	31.18	N	5.2	7.0	39.15	29.04	0.52	0.37

APPENDIX B

B. MATLAB PROGRAM DEVELOPED FOR CALIBRATION PROCESS

The MATLAB Program Developed to Calibrate the Coefficients of AC10

```
[no, eqN,eqD,eqLat, eqLon, f, m, dep, sLat,sLon,
pNS,pEW,st,d,Vs,dRup, pgaRock] = ...
    textread('D:\DOKTORA\Attenuation -
VI\AttenuationRecordsRaw_MATLAB.txt','%d %s %s %f %f %s %f %f %f %f
%f %f %d %f %d %f %f');
[spec] = textread('D:\DOKTORA\Attenuation -
VI\RespSpecDamp(199)005(acc)MATLAB.txt');

[tVal,bLin, b1, b2] = textread('D:\DOKTORA\Attenuation -
VI\BA08\SiteCoeffMATLAB.txt','%f %f %f %f');
fid = fopen('D:\DOKTORA\Attenuation - VI\AC10\outputAC10.txt',
'wt');

for i = 1:50
    if(i == 1)
        T(i) = 0.00001;
    elseif( i<13)
        T(i) = ( 0.08+0.01*i);
    elseif( i<28)
        T(i)= T(i-1) +0.02;
    elseif(i<38)
        T(i) = T(i-1) +0.05;
    elseif(i<48)
        T(i) = T(i-1) +0.1;
    elseif (i<49)
        T(i) = T(i-1) +0.5;
    elseif(i<=50)
        T(i) = T(i-1) +2.5;
    end
end

Vref = 760.0;
a1s = 29.43;
a2s = 88.29;
pga_low = 58.86;
V1 = 180;
V2 = 300;
Vs30C = 490;
Vs30D = 270;
Vs30R = 760;
for j=1:50

H=0;
minR(j) = 0;
for Hcount=1:30
    H=H+1;
    k=1;
    for i = 1: size(eqLat,1)
```

```

        % c(k) = log(spec(i, j));
        c(i, j) = log(spec(i, j));
        cRec(i, j) = log(spec(i, j));
        X(k, 1) = 1;
    if m(i) < 6.5
        X(k, 2) = m(i)-6.5;
        X(k, 3) = 0;
    else
        X(k, 2)=0;
        X(k, 3) = m(i)-6.5;
    end
        X(k, 4) = (8.5 - m(i)) ^ 2;
        X(k, 5) = log(sqrt(dRup(i) ^ 2 + H ^ 2));
        X(k, 6) = (m(i) - 6.5) * log(sqrt(dRup(i) ^ 2 + H ^
2));

    if f{i} == 'N'

        X(k, 7) = 1;
    else
        X(k, 7) = 0;
    end
    k=k+1;

    end

[b, bint, r, rint, stats] = regress((c(:, j)), X, 0.05);

if stats(1) > minR(j)
    minR(j) = stats(1);
    a1R(j) = b(1);
    a2R(j) = b(2);
    a3R(j) = b(3);
    a4R(j) = b(4); %
    a5R(j) = b(5);
    a6R(j) = b(6);
    a8R(j) = b(7);
    hOptR(j) = H;

    % specN(:, j) = exp(c' - r);
else
    minR(j) = minR(j);
end

end
for i = 1: size(eqLat, 1)
    if m(i) < 6.5
        specN(i, j) = exp(a1R(j) + a2R(j) * (m(i) - 6.5) + a4R(j) *
(8.5 - m(i)) ^ 2 + a5R(j) * log(sqrt(dRup(i) ^ 2 + hOptR(j) ^ 2)) +
...
        a6R(j) * (m(i) - 6.5) * log(sqrt(dRup(i) ^ 2 + hOptR(j)
^ 2))) ;
    else

```

```

        specN(i,j) = exp(a1R(j) + a3R(j) * (m(i) - 6.5) + a4R(j) *
(8.5 - m(i)) ^ 2 + a5R(j) * log(sqrt(dRup(i) ^ 2 + hOptR(j) ^ 2)) +
...
        a6R(j) * (m(i) - 6.5) * log(sqrt(dRup(i) ^ 2 + hOptR(j)
^ 2))) ;

    end
    end
    end
    tPass = k;

%
*****
***
% % ***** Non-Linear Site Effects Shall be
%*****Computed by the Following
% ***** Lines
*****

for j=1:50

for i=1:size(eqLat)

    FLin(i,j) = bLin(j)*log(Vs(i)/Vref);
    if Vs(i) <= V1
        bNonlin = b1(j);
    elseif Vs(i)>=V2 && Vs(i) > V1
        bNonlin = (b1(j) - b2(j))* log(Vs(i)/V2)/log(V1/V2) +
b2(j);
    elseif Vs(i) > V2 && Vs(i) <= Vref
        bNonlin = b2(j) * log(Vs(i) / Vref) / log(V2 / Vref);
    elseif Vs(i) > Vref
        bNonlin = 0;
    end

    dx = log(a2s / als);
    dy = bNonlin * log(a2s / pga_low);
    cdx = (3 * dy - bNonlin * dx) / dx ^ 2;
    ddx = -(2 * dy - bNonlin * dx) / dx ^ 3;
    FNonLin(k,j)=0;
    if (specN(i,j)) <= als
        FNonLin(i, j) = bNonlin * 1.773;
    elseif (specN(i,j)) < a2s && (specN(i,j)) > als
        FNonLin(i, j) = 1.773 * bNonlin + cdx *
log((specN(i,j)) / als) ^ 2 + ddx * log((specN(i,j)) / als) ^ 3;
    elseif (specN(i,j)) > a2s
        FNonLin(i, j) = bNonlin * log((specN(i,j)) /
0.1/981);
    end
    FSite(i, j) = FLin(i, j) + FNonLin(i, j);
    c(i,j) = c(i,j) - FSite(i,j);

end

end

```

```

for j=1:50
H=0;
minR(j) = 0;
for Hcount=1:30
H=H+1;

    for i = 1: size(eqLat,1)

        X(i,1) = 1;
        if m(i) < 6.5
            X(i,2) = m(i)-6.5;
            X(i,3) = 0;
        else
            X(i,2)=0;
            X(i,3) = m(i)-6.5;
        end
        X(i,4) = (8.5 - m(i)) ^ 2;
        X(i,5) = log(sqrt(dRup(i) ^ 2 + H ^ 2));
        X(i,6) = (m(i) - 6.5) * log(sqrt(dRup(i) ^ 2 + H ^
2));
        if f{i} == 'N'
            X(i,7) = 1;
        else
            X(i,7) = 0;
        end

        end

        [b,bint,r,rint,stats] = regress(c(:,j),X,0.05);
        stats1(:,j) = regstats(c(:,j),X,'linear');
        if stats(1)>minR(j)
            minR(j)=stats(1);
            sigma(j) = stats(4);
            a1(j) = b(1);
            a2(j) = b(2);
            a3(j) = b(3);
            a4(j) = b(4);
            a5(j) = b(5);
            a6(j) = b(6);
            a8(j) = b(7);
            hOpt(j)=H;

            for p=1:size(r)
                Res(p,j) = r(p);
            end
        else
            minR(j)=minR(j);
        end

    end

end

end

for j=1:50

```



```

fprintf(fid, '%2.2f %2.2f %2.2f %2.2f %2.2f %2.2f %2.2f %2.2f %2.2f
%2.2f %2.2f %2.2f %2.2f %2.2f %2.2f %2.2f %2.2f %2.2f %2.2f
%2.2f %2.2f\n', tVal(j),minR(j),sigma(j),a1(j), ...
a2(j), a3(j), a4(j), a5(j),a6(j), hOpt(j),
LN710(j),LN750(j),LN610(j),LN650(j),
LN710D(j),LN750D(j),LN610D(j),LN650D(j),
LN710R(j),LN750R(j),LN610R(j),LN650R(j));

end

dlmwrite('outputAC10-Res.txt',m, 'delimiter', ' ');
dlmwrite('outputAC10-Res.txt',dRup, '-append', 'roffset',
1, 'delimiter', ' ', 'newline', 'pc');
dlmwrite('outputAC10-Res.txt',Res(:, :), '-append', 'delimiter',
' ', 'newline', 'pc');

fclose(fid);

```


APPENDIX C

C. CALIBRATED COEFFICIENTS OF AC10

Table CI. Calibrated Coefficients of Ground Motion Prediction Equation Developed by Akkar and Cagnan (2010)

Period (s)	a ₁	a ₂	a ₃	a ₄	a ₅	a ₆	a ₇	a ₈	σ _{ln(Y)}
PGA	11.91	-3.49	-1.41	-0.56	-1.75	0.26	15	0.02	0.87
0.10	14.49	-4.54	-2.11	-0.62	-2.12	0.36	22	0.05	0.94
0.11	14.61	-4.21	-1.88	-0.59	-2.15	0.33	23	0.07	0.92
0.12	14.73	-4.06	-1.85	-0.57	-2.17	0.33	24	0.06	0.91
0.13	14.85	-3.85	-1.75	-0.54	-2.19	0.31	25	0.04	0.89
0.14	14.97	-3.56	-1.60	-0.52	-2.21	0.28	26	0.05	0.88
0.15	14.98	-3.40	-1.45	-0.53	-2.19	0.25	25	0.05	0.88
0.16	15.06	-3.38	-1.43	-0.53	-2.20	0.24	26	0.05	0.88
0.17	15.23	-3.40	-1.44	-0.54	-2.22	0.23	27	0.01	0.89
0.18	15.32	-3.50	-1.38	-0.57	-2.21	0.21	27	-0.01	0.89
0.19	15.23	-3.36	-1.25	-0.57	-2.19	0.19	26	-0.03	0.91
0.20	15.14	-3.04	-1.07	-0.53	-2.19	0.17	26	-0.04	0.95
0.22	14.73	-3.01	-1.06	-0.54	-2.11	0.16	24	-0.03	0.99
0.24	14.42	-2.89	-0.94	-0.53	-2.07	0.15	23	0.01	1.00
0.25	14.13	-2.49	-0.72	-0.47	-2.04	0.13	23	0.02	1.03
0.26	13.65	-1.91	-0.48	-0.40	-2.00	0.11	22	0.02	1.04
0.28	13.35	-1.63	-0.38	-0.37	-1.96	0.10	21	0.07	1.07
0.30	13.24	-1.87	-0.48	-0.41	-1.91	0.10	21	0.07	1.14
0.32	13.26	-2.25	-0.75	-0.48	-1.86	0.11	20	0.08	1.20
0.34	13.31	-2.5	-0.83	-0.53	-1.84	0.10	20	0.08	1.23
0.36	12.77	-2.53	-0.75	-0.54	-1.74	0.09	18	0.15	1.21
0.38	12.63	-2.81	-0.91	-0.59	-1.69	0.10	17	0.19	1.23
0.40	12.28	-2.91	-1.01	-0.6	-1.61	0.11	15	0.24	1.25
0.42	12.02	-2.97	-1.03	-0.61	-1.56	0.11	14	0.28	1.23
0.44	11.82	-3.12	-1.05	-0.64	-1.51	0.11	13	0.33	1.23
0.46	11.73	-3.17	-1.09	-0.65	-1.50	0.12	13	0.35	1.24
0.48	11.59	-3.05	-0.99	-0.64	-1.49	0.11	13	0.35	1.23
0.50	11.19	-2.61	-0.86	-0.58	-1.44	0.10	12	0.33	1.27
0.60	10.95	-3.16	-1.11	-0.68	-1.35	0.11	11	0.35	1.28
0.70	10.61	-3.62	-1.17	-0.77	-1.25	0.10	9	0.40	1.28
0.80	10.33	-3.11	-1.15	-0.71	-1.22	0.11	8	0.39	1.33
0.90	10.07	-2.94	-0.96	-0.70	-1.20	0.10	8	0.37	1.39
1.00	9.65	-2.96	-0.99	-0.70	-1.13	0.12	7	0.37	1.43
1.50	8.70	-1.64	-0.66	-0.55	-1.05	0.10	6	0.22	1.48
2.00	7.54	-1.53	-0.46	-0.55	-0.96	0.11	4	0.31	1.45

APPENDIX D

D. AREA SOURCE COORDINATES

Table D1. Area Sources and Their Coordinates (In Degrees)

Source Name	Latitude	Longitude
Ankara	32.90	40.34
	33.38	40.49
	33.12	40.86
	32.64	40.76
Menderes	38.51	27.44
	38.06	27.85
	37.65	28.40
	37.36	29.00
	38.04	29.48
Manisa	38.61	28.20
	38.51	27.44
	39.05	28.25
	39.50	28.24
	39.75	28.16
	39.74	27.99
Simav	39.28	27.07
	39.49	28.24
	39.51	29.21
	39.14	30.19
	38.68	29.85
	38.97	28.73
Burdur	39.05	28.25
	29.00	37.36
	29.91	38.68
	30.44	38.89
	30.51	38.39
	31.18	38.35
	31.80	37.85
	31.37	37.56
	30.92	37.82
30.24	37.09	
29.54	37.20	

Table D1 Continued

Source Name	Latitude	Longitude
Sultandagi	37.85	31.80
	38.35	31.18
	38.39	30.51
	38.89	30.44
	38.86	30.87
	38.76	31.40
	38.17	32.08
Duzce	40.33	29.64
	40.59	32.10
	41.18	31.87
	41.03	29.55
Bursa	39.65	29.95
	40.02	29.96
	40.33	29.64
	40.51	29.62
	40.50	28.76
	40.58	28.22
	40.33	27.07
Marmara	40.51	29.62
	40.50	28.76
	40.53	28.22
	40.33	27.07
	40.68	27.17
	40.93	27.32
	41.03	29.55

Table D1 Continued

Source Name	Latitude	Longitude
Background	39.91	31.04
	40.02	29.96
	40.33	29.64
	40.59	32.10
	41.18	31.87
	40.93	27.32
	41.69	28.00
	42.00	32.53
	41.64	33.08
	41.09	33.62
	40.20	33.99
	39.49	34.00
	37.95	33.06
	37.46	32.28
	37.16	31.34
	37.09	30.24
	37.82	30.92
	37.56	31.37
	37.85	31.80
	38.17	32.08
	38.76	31.40
	38.89	30.44
	38.68	29.91
	38.04	29.48
	38.61	28.20
	39.05	28.25
	38.68	29.85
	39.14	30.19
	39.51	29.21
	39.49	28.24
39.75	28.16	
39.90	28.62	
39.50	30.30	

APPENDIX E

E. FAULT PARAMETERS

Table E1. The Parameters of the Faults Identified Around the Close Vicinity of Eskisehir

Segment No	Name of Fault	Type	L* (km)	Degree of activity	Size of peak earthquake (M _w)	Return interval (year)
1	Kozpinar	Oblique-Slip Normal	39	Potentially active	7.0	≥ 1000
2	Hisaronu+Cukurhisar	Normal	19	Potentially active	6.5	≥ 1000
3	SK**	Normal	14	Potentially active	6.3	≥ 1000
4	Yusuflar	Oblique-Slip Normal	10	Potentially active	6.1	≥ 1000
5	Meselik	Oblique-Slip Normal	10	Potentially active	6.1	≥ 1000
6	Sultandere	Normal	11	Potentially active	6.2	≥ 1000
7,8	Karacaoren	Normal	20	Potentially active	6.6	≥ 1000
9	Altıpatlar	Normal	12	Potentially active	6.2	≥ 1000
10	Gulpınar	Oblique-Slip Normal	16	Potentially active	6.4	≥ 1000
11	Inonu	Oblique-Slip Normal	15	Potentially active	6.4	≥ 1000
12	Kovalica	Oblique-Slip Normal	12	Potentially active	6.2	≥ 1000
13	Sepetci	Oblique-Slip Normal	12	Potentially active	6.2	≥ 1000
14	Kozlubel	Oblique-Slip Normal	13	Potentially active	6.3	≥ 1000
15	Gokdere	Oblique-Slip Normal	13	Potentially active	6.3	≥ 1000

* Length

**SK is an abbreviation for the collection of the faults Satilmisoglu and Karagozler

Table E1 Continued

Segment No	Name of Fault	Type	L* (km)	Degree of activity	Size of peak earthquake (M_w)	Return interval (year)
16	Gunduzler	Oblique-Slip Normal	7	Potentially active	5.9	≥ 1000
17	Kizilcaoren	Oblique-Slip Normal	14	Potentially active	6.3	≥ 1000
18	Muttalip	Normal	12	Potentially active	6.3	≥ 1000
19	Kizilyar+ Cumhuriyet	Normal	13	Potentially active	6.3	≥ 1000
20	Keskin	Normal	8	Potentially active	6.0	≥ 1000
21	ESKKEK**	Oblique-Slip Normal	28	Active	6.7	~500
22	Kaymaz	Normal	18	Potentially active	6.6	≥ 1000
23	Dodurga	Oblique-Slip Normal	10	Potentially active	6.2	≥ 1000
24-26	Erikli	Oblique-Slip Normal	38	Potentially active	6.9	≥ 1000
27,28	Eskikoy	Oblique-Slip Normal	34	Potentially active	6.9	≥ 1000
29	Sogukpinar	Oblique-Slip Normal	28	Potentially active	6.7	≥ 1000
30	Ortaca	Oblique-Slip Normal	14	Potentially active	6.3	≥ 1000
31	Akcabuk	Strike-Slip	20	Potentially active	6.5	≥ 1000
32-34	Eymir	Oblique-Slip Normal	24	Potentially active	6.6	≥ 1000
35-38	Bursa	Oblique-Slip Normal	63	Potentially active	7.2	≥ 1000
39	Sayfiye	Oblique-Slip Normal	27	Potentially active	6.8	≥ 1000
40,41	Alacam	Oblique-Slip Normal	27	Active	6.7	~500

* Length

**ESKEK is an abbreviation for the collection of the faults Esmekaya, Sogucak, Karaozkuyu, Kavacık, Egrioz, Kozkayi

Table E1 Continued

Segment No	Name of Fault	Type	L* (km)	Degree of activity	Size of peak earthquake (M_w)	Return interval (year)
42,43	Bogazkoy	Oblique-Slip Normal	26	Potentially active	6.7	≥ 1000
44	Kestel	Oblique-Slip Normal	16	Potentially active	6.4	≥ 1000
45	Koyunhisar	Strike-Slip	19	Potentially active	6.6	≥ 1000
46	Kavakli	Strike-Slip	13	Potentially active	6.3	≥ 1000
47	Karahidir	Oblique-Slip Normal	20	Potentially active	6.5	≥ 1000
48	Demirtas	Oblique-Slip Normal	22	Potentially active	6.6	≥ 1000
49	Gencali-Altıntas-Kursunlu	Strike-Slip	21	Active	6.3	~500
50	Gemlik	Strike-Slip	14	Active	6.4	~500
51	Gurle	Strike-Slip	12	Active	6.3	~500
52-54	Cali	Oblique-Slip Normal	29	Potentially active	6.8	≥ 1000
55	Ayaz	Oblique-Slip Normal	15	Potentially active	6.4	≥1000
57,58	Derecik	Oblique-Slip Normal	21	Potentially active	6.5	≥1000
56,59	MKP**	Oblique-Slip Normal	20	Potentially active	6.5	≥1000
60	Taslik	Oblique-Slip Normal	7	Potentially active	6.0	≥1000
61	Cavuskoy	Oblique-Slip Normal	7	Potentially active	6.0	≥1000
62	Yenikoy	Oblique-Slip Normal	12	Potentially active	6.2	≥1000
63	Mudanya	Strike-Slip	20	Active	6.5	~500
64,65	Bogazkoy-Ekinli	Strike-Slip	25	Active	6.7	~500
66,67	Kursunlu	Strike-Slip	23	Active	6.6	~500
68	Bandirma	Strike-Slip	42	Potentially active	7.0	≥1000

* Length

** Mustafakemalpasa

Table E1 Continued

Segment No	Name of Fault	Type	L* (km)	Degree of activity	Size of peak earthquake (M_w)	Return interval (year)
69	Tutuncu	Normal	20	Potentially active	6.5	≥1000
70	Gonen	Normal	15	Potentially active	6.4	≥1000
71	Yenice-I	Strike-Slip	14	Potentially active	6.4	≥1000
72	Sarikoy	Strike-Slip	22	Potentially active	6.6	≥1000
73	Sofular	Strike-Slip	24	Potentially active	6.6	≥1000
74	Sukruye	Strike-Slip	20	active	6.5	~500
75	Narlıca	Strike-Slip	10	active	6.2	~500
76	Camdibi	Strike-Slip	42	Potentially active	7.0	≥1000
77	Karadin	Strike-Slip	19	Active	6.5	~500
78	Geyve	Strike-Slip	31	Active	6.8	~500
79	Tarakli	Strike-Slip	28	Active	6.8	~500
80	Karapurcek	Strike-Slip	43	Very active	7.0	~250
81	Goynuk	Strike-Slip	32	Active	6.8	~500
82	Mudurnu-I	Strike-Slip	21	Active	6.6	~500
83	Mudurnu-II	Strike-Slip	55	Active	7.1	~500
84	Yenicaga-Gerede	Strike-Slip	92	Active	7.5	~500
85	Gerede	Strike-Slip	31	Active	6.8	~500
86	Ismetpasa	Strike-Slip	54	Active	7.1	~500
87	Bayramoren	Strike-Slip	38	Active	6.9	~500
88	Bakacak	Strike-Slip	8	Very Active	6.0	~250
89-91	Duzce	Strike-Slip	34	Very active	7.0	~250
92	Karadere	Strike-Slip	35	Very active	7.0	~250
93	Hendek	Strike-Slip	50	Very active	7.1	~250
94	Arifiye	Strike-Slip	28	Very active	6.9	~250
95	Tepetarla	Strike-Slip	18	Very active	6.8	~250
96	Korfez	Strike-Slip	16	Very active	6.4	~250
97	Golcuk	Strike-Slip	25	Very active	6.7	~250

* Length

Table E1 Continued

Segment No	Name of Fault	Type	L* (km)	Degree of activity	Size of peak earthquake (M_w)	Return interval (year)
98	Karamursel	Strike-Slip	28	Very active	6.7	~250
99	Darıca	Strike-Slip	19	Active	6.5	~500
100	Adalar	Normal	32	Very active	6.9	~250
101	Yesilkoy	Strike-Slip	42	Very active	7.0	~250
102	Kumruburgaz	Strike-Slip	18	Very active	6.5	~250
103-107	Central	Strike-Slip	52	Active	7.1	~500
108-111	Kumbagi	Strike-Slip	43	Very active	7.0	~250
112,113	Ucmakdere	Strike-Slip	34	Active	6.9	~250
114	Isiklar	Strike-Slip	20	Active	6.6	~500
115	Orhaniye	Strike-Slip	19	Active	6.5	~500
116-118	Laledere	Strike-Slip	21	Active	6.6	~500
117	Kurtkoy-Gokcedere	Oblique-Slip Normal	16	Very active	6.4	~500
119	Cinarcik	Strike-Slip	17	Very active	6.5	~250
120	Esenkoy	Strike-Slip	13	Very active	6.3	~250
121	Armutlu	Strike-Slip	20	Very active	6.6	~250
122,123	Imrali	Strike-Slip	45	Potentially active	7.0	≥1000
124	Erdek	Strike-Slip	50	Potentially active	7.1	≥1000
125	Asmali	Strike-Slip	21	Potentially active	6.6	≥1000
126-128	Marmara	Strike-Slip	23	Potentially active	6.6	≥1000
129-132	Kutahya	Oblique slip normal	41	Potentially active	7.0	≥1000
133-136	Dumlupınar	Normal	72	Potentially active	7.2	≥1000
137	Gediz	Normal	18	Potentially active	6.5	≥ 1000
138-141	Simav	Normal	59	Potentially active	7.2	≥ 1000

* Length

Table E1 Continued

Segment No	Name of Fault	Type	L* (km)	Degree of activity	Size of peak earthquake (M_w)	Return interval (year)
142	Akhisar	Normal	28	Potentially active	6.7	≥1000
143,144	Afyon	Normal	17	Potentially active	6.4	≥1000
145	Cay	Normal	15	Active	6.4	~500
146,147	Sultandagi	Normal	24	Active	6.7	~500
148-152	Aksehir	Normal	64	Active	7.3	~500
153,154	Ilgin	Normal	24	Potentially active	6.7	≥1000
155	Beysehir	Normal	42	Potentially active	7.0	≥1000
156	Hoyran-I	Normal	14	Potentially active	6.4	≥1000
157	Hoyran-II	Normal	20	Potentially active	6.6	≥1000
158	Senirkent	Normal	17	Potentially active	6.4	≥1000
159	Haydarli	Normal	16	Potentially active	6.4	≥1000
160	Sandikli-I	Normal	16	Potentially active	6.4	≥1000
161	Sandikli-II	Normal	17	Potentially active	6.4	≥1000
162	Isikli-I	Normal	15	Potentially active	6.4	≥1000
163	Isikli-II	Normal	14	Potentially active	6.4	≥1000
164	Dinar	Normal	13	Potentially active	6.3	≥1000
165	Cardak-I	Normal	11	Potentially active	6.2	≥1000

* Length

Table E1 Continued

Segment No	Name of Fault	Type	L* (km)	Degree of activity	Size of peak earthquake (M_w)	Return interval (year)
166	Cardak-II	Normal	19	Potentially active	6.5	≥1000
167	Basmakci	Normal	23	Potentially active	6.6	≥1000
168	Burdur-I	Normal	21	Potentially active	6.6	≥1000
169	Burdur-II	Normal	5	Potentially active	5.7	≥1000
170,171	Manyas	Normal	23	Potentially active	6.6	≥1000
172	Edincik	Strike-Slip	14	Potentially active	6.4	≥1000
173	Havutca	Strike-Slip	11	Potentially active	6.2	≥1000
174	Gebecinar	Strike-Slip	11	Potentially active	6.2	≥1000
175	Kinalar	Strike-Slip	11	Potentially active	6.2	≥1000
176	Yenice-II	Strike-Slip	25	Potentially active	6.7	≥1000

* Length

APPENDIX F

F. FAULT COORDINATES

Table F1. The Coordinates of The Active Faults Identified In The Close Vicinity of Eskisehir (In Decimal Degrees)

Fault Name	No	Latitude	Longitude
Bursa	35	40.01	29.71
		40.05	29.49
	36	40.05	29.49
		40.13	29.35
	37	40.13	29.35
		40.16	29.21
		40.17	29.11
		40.16	29.07
	38	40.16	29.07
		40.20	29.02
40.20		29.01	
Alacam	41	40.07	29.39
		40.11	29.34
		40.13	29.24
	40	40.13	29.24
		40.15	29.22
		40.16	29.18
		40.16	29.13
40.17	29.11		
Sayfiye	39	40.05	29.47
		40.06	29.45
		40.08	29.40
		40.11	29.36
		40.12	29.32
		40.12	29.28
		40.14	29.25
		40.15	29.23
		40.16	29.21
Sogukpinar	29	40.02	29.37
		40.02	29.33
		40.03	29.25
		40.07	29.16
		40.08	29.10
		40.09	29.07
		40.10	29.05

Table F1 Continued

Fault Name	No	Latitude	Longitude
Cali	52	40.19	29.00
		40.17	28.93
	53	40.17	28.93
		40.17	28.88
		40.17	28.78
	54	40.17	28.78
40.13		28.68	
Kestel	44	40.22	29.46
		40.21	29.39
		40.20	29.35
		40.20	29.28
M. Kemalpaşa	59	40.03	28.50
		40.03	28.47
		40.03	28.43
		40.06	28.34
		40.06	28.31
		40.06	28.27
	56	39.98	28.52
		40.00	28.44
Derecik	57	40.00	28.44
		40.03	28.41
		40.05	28.37
	58	40.05	28.37
		40.05	28.30
Yenikoy	62	40.09	28.15
		40.11	28.10
		40.11	28.04
		40.10	28.01
Cavuskoy	61	40.24	28.15
		40.25	28.12
		40.25	28.10
		40.25	28.07
Taslik	60	40.24	28.39
		40.24	28.29

Table F1 Continued

Fault Name	No	Latitude	Longitude
Ayaz	55	40.12	28.61
		40.10	28.55
		40.10	28.53
		40.10	28.50
		40.09	28.44
Ortaca	30	39.84	29.51
		39.86	29.47
		39.88	29.41
		39.90	29.37
Akcabuk	31	39.93	29.08
		39.93	29.06
		39.94	28.99
		39.95	28.96
		39.96	28.90
Tutuncu	69	40.06	27.94
		40.06	27.88
		40.09	27.71
Gonen	70	40.11	27.80
		40.09	27.63
Yenice-I	71	40.09	27.63
		40.00	27.50
Sarikoy	72	40.25	27.71
		40.24	27.68
		40.22	27.66
		40.17	27.48
Sofular	73	40.13	27.37
		40.00	27.14
Manyas	170	40.09	27.96
		40.13	27.84
	171	40.13	27.84
Edincik	172	40.10	27.70
		40.37	27.93
Havutca	173	40.32	27.79
		40.31	27.76
		40.25	27.62

Table F1 Continued

Fault Name	No	Latitude	Longitude
Gebecinar	174	40.31	27.72
		40.27	27.64
		40.27	27.61
Kinalar	175	40.27	27.60
		40.27	27.47
Yenice-II	176	39.99	27.41
		39.96	27.38
		39.91	27.24
		39.90	27.15
Demirtas	48	40.26	29.12
		40.27	29.07
		40.28	29.01
		40.29	28.86
Karahidir	47	40.23	29.29
		40.28	29.06
Eymir	32	39.98	29.75
		40.01	29.71
		40.03	29.70
		40.06	29.66
	33	40.06	29.66
		40.08	29.60
		40.08	29.59
	34	40.08	29.59
40.12		29.55	
Bogazkoy	43	40.24	29.72
		40.25	29.71
		40.24	29.65
		40.19	29.57
		40.16	29.53
	42	40.16	29.53
		40.16	29.49
		40.16	29.46

Table F1 Continued

Fault Name	No	Latitude	Longitude
Eskikoy	27	39.96	29.71
		39.97	29.65
		39.97	29.63
		39.97	29.60
		39.99	29.51
	28	39.99	29.51
		40.00	29.49
		40.02	29.37
		40.05	29.33
Kozpinar	1	39.88	30.08
		39.89	29.98
		39.89	29.89
		39.90	29.85
		39.91	29.82
		39.93	29.71
		39.94	29.67
		39.94	29.63
Erikli	24	39.85	29.91
		39.88	29.83
		39.89	29.77
	25	39.89	29.77
		39.89	29.76
		39.93	29.69
		39.94	29.63
	26	39.94	29.63
		39.95	29.58
39.99		29.51	
Dodurga	23	39.79	29.98
		39.81	29.94
		39.85	29.91
Gemlik	50	40.42	29.25
		40.41	29.19
		40.41	29.14
		40.41	29.08
Gurle	51	40.40	29.37
		40.40	29.32
		40.40	29.29
		40.40	29.23

Table F1 Continued

Fault Name	No	Latitude	Longitude
Bandirma	68	40.40	28.00
		40.42	28.50
Gencali and Altintas-Kursunlu	49	40.37	29.20
		40.37	29.15
		40.37	29.07
		40.35	29.04
		40.35	29.01
		40.35	29.00
		40.35	28.97
Narlica	75	40.38	29.53
		40.38	29.44
		40.38	29.41
Sukruye	74	40.38	29.41
		40.37	29.40
		40.37	29.38
		40.37	29.37
		40.36	29.34
		40.33	29.25
Camdibi	76	40.44	30.00
		40.43	29.95
		40.41	29.86
		40.40	29.78
		40.38	29.62
		40.37	29.59
		40.37	29.51
Karadin	77	40.46	30.00
		40.44	29.93
		40.44	29.91
		40.43	29.85
		40.42	29.81
		40.41	29.78

Table F1 Continued

Fault Name	No	Latitude	Longitude
Koyunhisar	45	40.29	29.53
		40.26	29.49
		40.21	29.38
		40.20	29.35
Kavakli	46	40.35	29.55
		40.33	29.52
		40.32	29.49
		40.29	29.45
		40.29	29.42
Mudanya	63	40.38	28.87
		40.37	28.84
		40.36	28.75
		40.35	28.68
		40.35	28.64
Bogazkoy-Ekinli	64	40.36	28.63
		40.37	28.56
		40.37	28.54
	65	40.37	28.54
		40.36	28.53
		40.36	28.45
		40.36	28.34
Kursunlu	66	40.38	28.39
		40.40	28.34
		40.40	28.32
		40.39	28.29
	67	40.39	28.29
		40.40	28.25
		40.40	28.21
		40.39	28.13

Table F1 Continued

Fault Name	No	Latitude	Longitude
Karamursel	98	40.70	29.82
		40.71	29.79
		40.71	29.77
		40.70	29.70
		40.68	29.62
		40.67	29.50
Golcuk	97	40.72	29.79
		40.71	29.65
		40.70	29.52
Korfez	96	40.77	29.82
		40.77	29.78
		40.77	29.67
		40.77	29.61
Tepetarla	95	40.71	29.94
		40.71	30.06
		40.71	30.17
Arifiye	94	40.71	30.34
		40.70	30.47
		40.67	30.67
Hendek	93	40.73	30.33
		40.79	30.68
		40.85	30.90
Karadere	92	40.67	30.67
		40.72	30.87
		40.79	31.00
		40.82	31.03
Duzce	91	40.75	30.96
		40.76	30.99
		40.75	31.11
	90	40.75	31.11
		40.77	31.20
	89	40.77	31.20
40.76		31.36	

Table F1 Continued

Fault Name	No	Latitude	Longitude
Yenicaga-Gerede	84	40.61	31.20
		40.62	31.36
		40.71	31.72
		40.81	32.25
Gerede	85	40.80	32.17
		40.80	32.23
		40.83	32.42
		40.83	32.46
		40.85	32.53
Ismetpasa	86	40.83	32.45
		40.86	32.62
		40.87	32.66
		40.87	32.70
		40.89	32.79
		40.92	32.97
		40.92	33.07
Bayramoren	87	40.91	33.06
		40.93	33.12
		40.98	33.50
Bakacak	88	40.74	31.41
		40.71	31.50
Mudurnu-I	82	40.57	30.93
		40.57	30.96
		40.59	31.17
Mudurnu-II	83	40.56	30.94
		40.56	30.99
		40.56	31.02
		40.58	31.14
		40.58	31.21
		40.59	31.29
Arifiye	94	40.64	30.35
		40.64	30.39
		40.63	30.48
		40.63	30.49
		40.63	30.52
		40.61	30.58
		40.53	30.77
		40.57	30.88

Table F1 Continued

Fault Name	No	Latitude	Longitude
Geyve	78	40.45	30.01
		40.46	30.09
		40.50	30.38
Tarakli	79	40.51	30.41
		40.58	30.94
Karapurcek	80	40.69	30.29
		40.65	30.35
		40.59	30.75
Goynuk	81	40.52	30.64
		40.56	30.93
Darica	99	40.73	29.22
		40.72	29.44
Adalar	100	40.86	28.88
		40.73	29.22
Yesilkoy	101	40.82	28.39
		40.86	28.88
Kumruburgaz	102	40.84	28.41
		40.83	28.18
Central	103	40.83	28.26
		40.88	28.12
	104	40.88	28.12
		40.88	27.94
	105	40.88	27.94
		40.87	27.90
	106	40.87	27.90
		40.88	27.85
	107	40.88	27.85
		40.86	27.72
Kumbagi	108	40.81	27.96
		40.81	27.84
		40.80	27.82
	109	40.80	27.82
		40.80	27.77
	110	40.80	27.77
		40.82	27.74
	111	40.82	27.74
		40.80	27.59
		40.80	27.48

Table F1 Continued

Fault Name	No	Latitude	Longitude
Ucmakdere	112	40.89	27.63
		40.83	27.54
		40.80	27.49
		40.75	27.42
	113	40.75	27.42
		40.74	27.33
40.73		27.31	
Isiklar	114	40.87	27.46
		40.81	27.23
Orhaniye	115	40.51	29.70
		40.50	29.63
		40.50	29.60
		40.49	29.57
		40.49	29.49
Laledere	116,118	40.60	29.37
		40.59	29.30
		40.60	29.24
		40.61	29.12
		40.56	29.21
		40.59	29.17
		40.61	29.14
Kurtkoy-Gokcedere	117	40.54	29.28
		40.55	29.26
		40.56	29.21
Cinarcik	119	40.67	29.24
		40.66	29.20
		40.64	29.04
Esenkoy	120	40.64	29.04
		40.58	28.93
Armutlu	121	40.58	28.93
		40.57	28.86
		40.53	28.73
		40.52	28.70

Table F1 Continued

Fault Name	No	Latitude	Longitude
Imrali	122	40.52	28.70
		40.61	28.49
		40.72	28.33
	123	40.56	28.56
		40.60	28.49
Erdek	124	40.60	28.49
		40.59	28.42
		40.59	28.26
		40.60	28.15
		40.61	28.07
		40.65	27.90
Asmali	125	40.66	27.98
		40.67	27.90
		40.71	27.74
Marmara	126	40.71	27.74
		40.70	27.71
		40.70	27.60
	127	40.70	27.60
		40.71	27.58
	128	40.71	27.58
		40.69	27.52
Kovalica	12	39.85	29.99
		39.84	30.14
Inonu	11	39.82	30.09
		39.81	30.26
Hisaronu + Cukurhisar	2	39.87	30.09
		39.84	30.22
		39.83	30.31
Satilmisoglu + Karagozler	3	39.83	30.31
		39.78	30.40
		39.77	30.45
Yusuflar	4	39.76	30.37
		39.76	30.48
Meselik	5	39.75	30.42
		39.75	30.53
Keskin	20	39.86	30.37
		39.86	30.46

Table F1 Continued

Fault Name	No	Latitude	Longitude
Kizilyar+ Cumhuriyet	19	39.88	30.51
		39.84	30.63
		39.83	30.65
Muttalip	18	39.87	30.52
		39.84	30.63
		39.83	30.65
Kizilcaoren	17	39.84	30.67
		39.91	30.81
Gokdere	15	39.82	30.67
		39.88	30.80
Gunduzler	16	39.86	30.74
		39.90	30.82
Kozlubel	14	39.92	30.81
		39.92	30.97
Sepetci	13	39.90	30.82
		39.91	30.97
Altıpatlar	9	39.74	30.78
		39.73	30.92
Karacaoren	7,8	39.74	30.69
		39.74	30.86
		39.73	30.93
Gulpınar	10	39.73	30.56
		39.68	30.74
Sultandere	6	39.74	30.56
		39.74	30.69
ESKKEK*	21	39.89	30.20
		39.90	30.46
		39.90	30.52
Beyşehir	155	38.09	31.16
		38.03	31.20
		37.89	31.33
		37.88	31.34
		37.80	31.42

*ESKEK is an abbreviation for the collection of the faults Esmekaya, Sogucak, Karaozkuyu, Kavacık, Egrioz, Kozkayı

Table F1 Continued

Fault Name	No	Latitude	Longitude
Ilgın	153	38.30	31.86
		38.40	31.83
	154	38.40	31.83
		38.44	31.84
		38.50	31.84
Sandikli -II	161	38.62	30.27
		38.47	30.21
Sandikli- I	160	38.39	30.22
		38.48	30.28
		38.50	30.31
Akşehir	152	38.03	31.77
		38.06	31.72
	151	38.06	31.72
		34.14	31.66
	150	34.14	31.66
		38.18	31.59
	149	38.18	31.59
		38.27	31.50
	148	38.27	31.50
		38.47	31.29
Sultandagi	146	38.60	31.04
		38.59	31.08
	147	38.48	31.28
		38.48	31.26
		38.57	31.12
Cay	145	38.58	31.09
		38.59	31.03
		38.60	31.01
		38.59	30.96
Isikli-I	162	38.62	30.84
		38.32	29.74
Isikli-II	163	38.33	29.91
		38.32	29.91
		38.26	29.94
		38.23	30.01

Table F1 Continued

Fault Name	No	Latitude	Longitude
Haydarli	159	38.18	30.40
		38.25	30.49
Senirkent	158	38.13	30.49
		38.17	30.67
Dinar	164	38.13	30.12
		38.03	30.18
Burdur -I	168	37.66	30.18
		37.74	30.32
		37.78	30.36
Burdur-II	169	37.84	30.41
		37.89	30.44
Basmakci	167	37.72	29.78
		37.78	29.85
		37.78	29.85
		37.85	29.98
Cardak -I	165	37.84	29.63
		37.83	29.75
Cardak-II	166	37.83	29.75
		37.94	29.92
Kaymaz	22	39.60	31.09
		39.58	31.11
		39.55	31.14
		39.54	31.18
		39.51	31.26
Kutahya	129	39.31	30.19
		39.36	30.09
	130	39.37	30.09
		39.41	30.00
	131	39.41	29.98
		39.47	29.82
	132	39.45	29.84
		39.48	29.80

Table F1 Continued

Fault Name	No	Latitude	Longitude
Dumlupınar	133	38.89	30.00
		38.92	29.95
		38.94	29.93
		38.95	29.90
	134	38.95	29.94
		38.97	29.91
		38.98	29.84
	135	38.98	29.83
		39.01	29.63
	136	39.01	29.63
38.99		29.57	
Gediz	137	38.87	29.53
		38.91	29.46
		38.92	29.40
		38.95	29.35
Simav	138	39.04	29.12
		39.08	29.03
	139	39.08	29.00
		39.10	28.94
		39.12	28.87
		39.12	28.78
	140	39.12	28.85
		39.13	28.81
		39.13	28.79
		39.14	28.69
	141	39.13	28.69
		39.13	28.64
		39.16	28.58
		39.19	28.51
		39.19	28.50
Akhisar	142	39.04	27.90
		39.15	27.94
		39.29	28.00

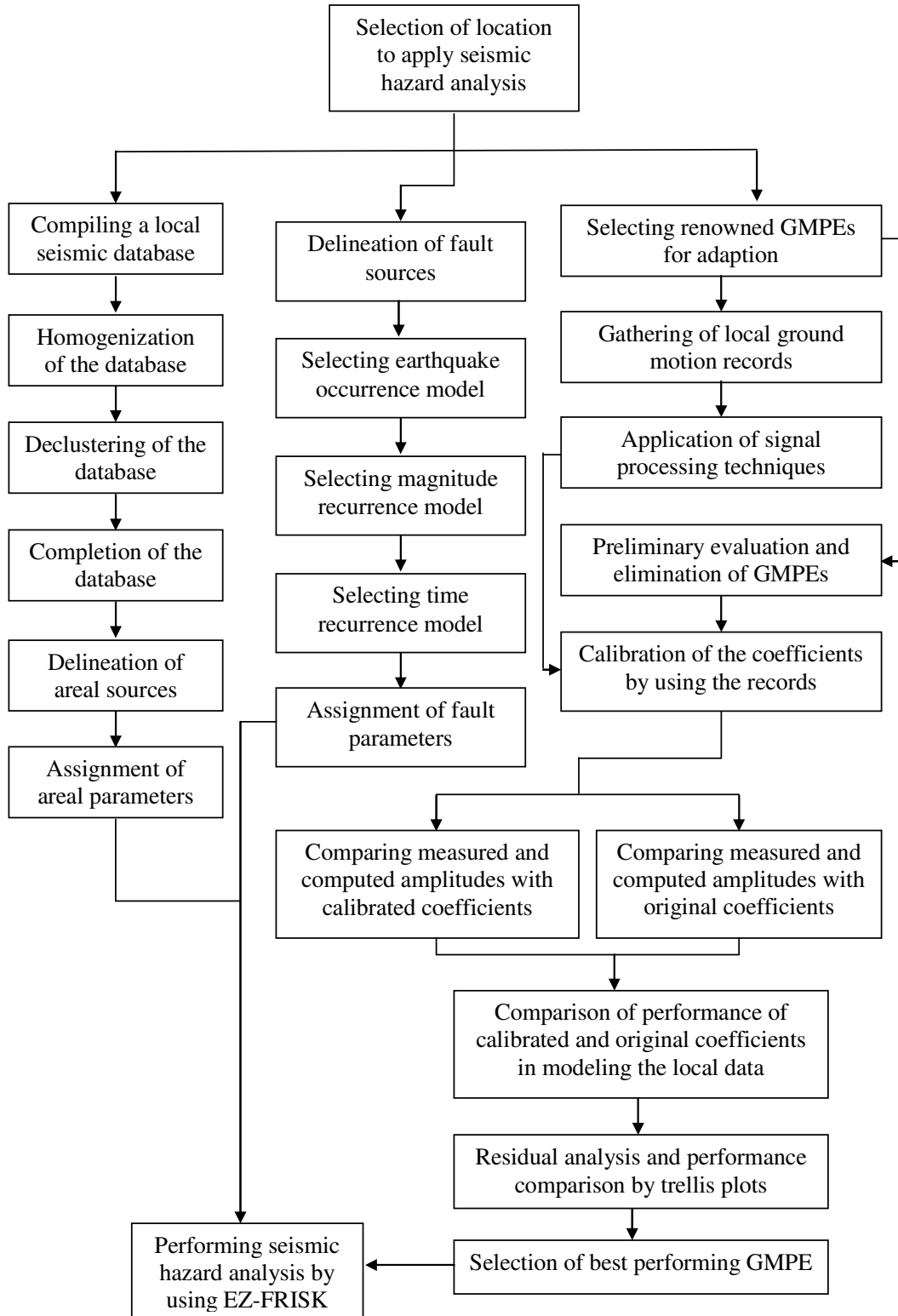
Table F1 Continued

Fault Name	No	Latitude	Longitude
Afyon	143	38.84	30.42
		38.77	30.47
	144	38.76	30.48
		38.71	30.53
Hoyran-I	156	38.25	30.90
		38.29	30.94
		38.31	30.99
		38.34	31.02
Hoyran-II	157	38.25	30.73
		38.27	30.80
		38.30	30.93

APPENDIX G

G. FLOWCHART I

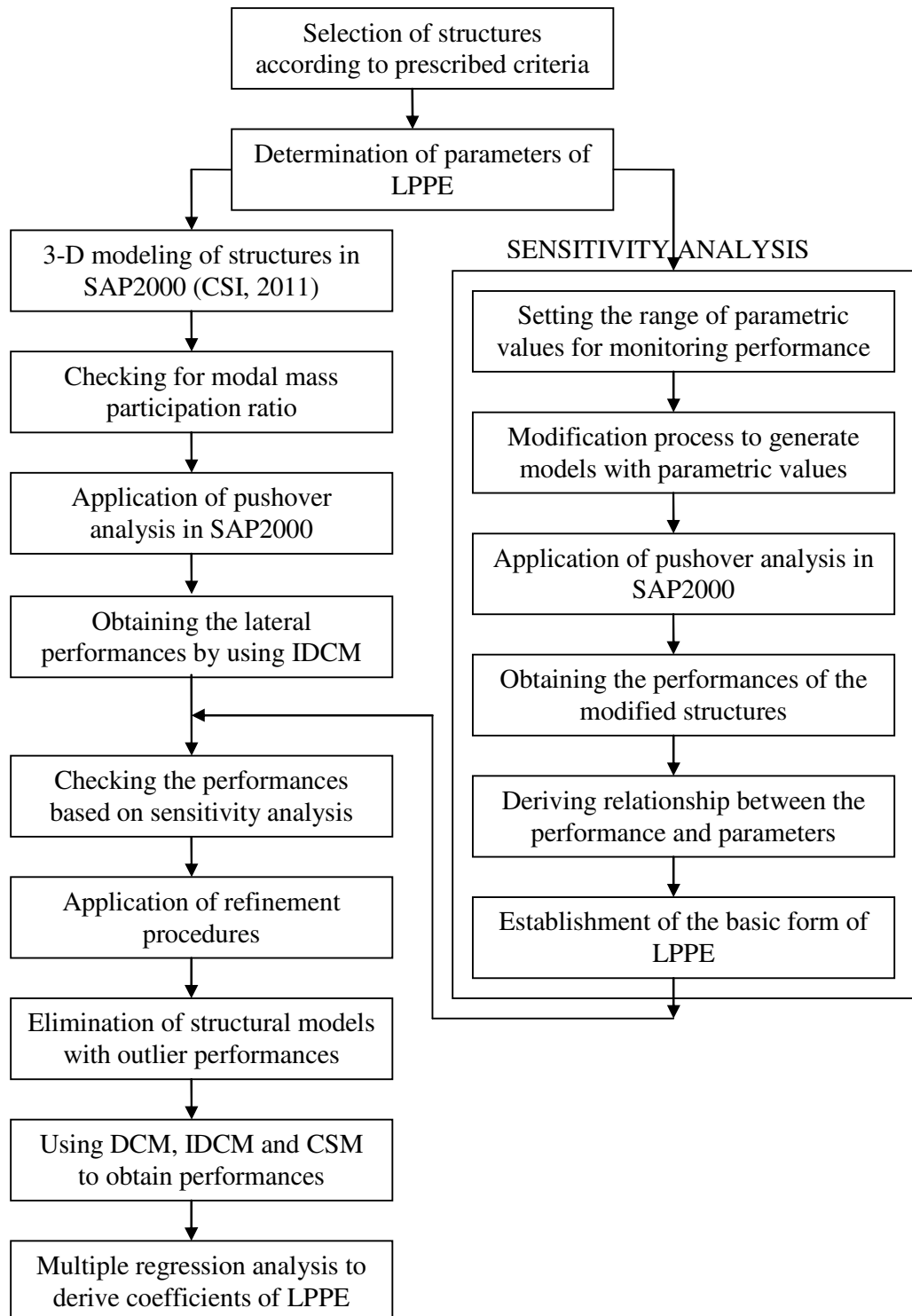
Flowchart for Seismic Hazard Analysis



APPENDIX H

H. FLOWCHART II

Flowchart Describing the Development of Lateral Performance Prediction Equation (LPPE)



CURRICULUM VITAE

PERSONAL INFORMATION

Surname, Name: Karaca, Hakan
Nationality: Turkish (TC)
Date and Place of Birth: 12 February 1977, Ankara
Marital Status: Married
Phone: +90 388 233 25 13
Fax: +90 312 232 34 17
email: karaca26@hotmail.com

EDUCATION

Degree Graduation	Institution	Year of
MS	WSU Civil and Environmental Engineering	2001
BS	METU Civil Engineering	1999
High School	Ankara Science High School, Ankara	1994

WORK EXPERIENCE

Year	Place	Enrollment
2008 – Present -	MEUP	Civil Engineer
2006 -2007	Yuksel Project	Civil Engineer
2002 -2005	PBQD, USA	Civil Engineer
2001 -2002	KISKA Corp. USA	Civil Engineer
1999 -2001	WSU Civil and Environmental Eng.	Research Assistant

FOREIGN LANGUAGES

Advanced English